Mission-Oriented Seismic Research Program

Annual Report

2004

M-OSRP

University of Houston

Sponsors and Advisory Board representatives

Tier I

Amerada Hess ..... Jacques Leveille
Anadarko ..... John Logel
BP ..... Scott Michell
ChevronTexaco ..... Debbie Bones, Joseph Higginbotham
ConocoPhillips ..... Douglas Foster, Robert Stolt
ENI-Agip ..... Michele Buia
ExxonMobil ..... Peter Traynin
Geotrace Technologies ..... Jaime Stein
GX Technology ..... Nick Bernitsas
Petrobras ..... Jurandyr Schmidt
PGS ..... Ruben Martinez
Shell ..... Jonathan Sheiman
Statoil ..... Lasse Amundsen
Unocal ..... Phil Schultz
WesternGeco ..... Luis Canales

Tier II

Panorama Technologies ..... Bee Bednar
Stochastic Systems ..... Suresh Thadani

M-OSRP Personnel

Faculty

Douglas J. Foster (ConocoPhillips) ..... Adjunct Professor (Physics)
Kristopher A. Innanen ..... Research Assistant Professor (Physics)[1]
Robert G. Keys (ExxonMobil) ..... Adjunct Professor (Physics)
Jacques Leveille (Amerada Hess) ..... Adjunct Professor (Physics)
Ken H. Matson (BP) ..... Adjunct Associate Professor (Physics)
Bogdan Nita ..... Research Assistant Professor (Physics)
Jon Sheiman (Shell) ..... Adjunct Professor (Physics)
Robert H. Stolt ..... Adjunct Professor (Physics)
T. Hing Tan (Shell) ..... Adjunct Professor (Physics)
Arthur B. Weglein ..... Cullen Distinguished Professor (Physics)
Daniel Whitmore (ConocoPhillips) ..... Adjunct Professor (Physics)

[1] Postdoctoral Fellow, University of British Columbia

Ph.D. Students

Walter Kessinger ..... Geosciences
Fang Liu ..... Physics[5]
Einar Otnes ..... Petroleum Engineering and Applied Geophysics[3]
Sameera Rajapakshe ..... Physics
Adrianna Citlali Ramirez ..... Physics
Simon A. Shaw ..... Geosciences[4]
Haiyan Zhang ..... Physics[5]
Jingfeng Zhang ..... Physics
Blake (Shaoqing) Zhang ..... Physics
Tao Han ..... Physics
Thang Nguyen ..... Physics

Recent Alumni

Zhiqiang Guo ..... Geosciences
Francisco Miranda ..... Physics

Administrative Support

Jennifer Chin-Davis ..... Business Administrator
Nguyen Tranh ..... Program Coordinator
Andrew Fritz, Jimy Chang ..... Computer/IT Support
Alex Garbino ..... Webmaster

[3]Norwegian University of Science and Technology, Statoil Fellow
[4]ConocoPhillips Fellow 2003-04
[5]ConocoPhillips Fellow 2004-05

Table of Contents

Introduction and Technical Overview, Consortium Strategy and Summary of Progress and Plans: MOSRP04

This has been a positive year for M-OSRP, with significant progress on projects and milestones to report. The central purpose of M-OSRP is to provide seismic methods and algorithms to directly address the current biggest challenges to seismic exploration and production effectiveness. High on the prioritized impediment list is the inability to provide, or adequately estimate, a velocity model and/or the delineation of the boundary of interfaces where velocity and other properties change, especially under complex geologic circumstances such as can occur e.g.,with targets beneath salt, basalt and karsted sediments.

MULTIPLES

In our pre-UH M-OSRP history, we (along with our students and colleagues) developed methods for eliminating free surface multiples and attenuating internal multiples, that require absolutely no subsurface information. That earlier campaign and development was motivated by: (1) the need for multiple removal methods to work in deep water, and (2) the need to provide multiple removal methods that did not depend upon velocity information, move-out differences, periodicity, picking events or any subsurface information or interpretive intervention, whatsoever. Hence, they directly addressed the removal of multiples in the complex geologic circumstances mentioned above, e.g., salt, basalt and sub karsted plays. The methods that evolved from that earlier work were at that earlier time, and remain today, the most physically complete, comprehensive and accommodating methods for removing free surface multiples and attenuating internal multiples. We require that capability to reside within M-OSRP for our research purposes, and we initiated an effort this past year to provide those codes for M-OSRP purposes. These free surface and internal de-multiple algorithms are more complete and capable than the algorithms distributed by all other consortia; and, hence, we anticipate that some of our sponsors might have an interest in them, as well.

ASSUMPTIONS BEHIND THE WAVE THEORETIC INVERSE SCATTERING INTERNAL MULTIPLE METHOD: LOWER HIGHER LOWER DIAGRAMS, IN DEPTH AND WATER SPEED PSEUDO-DEPTH

There has been a recent heightened interest in the inverse scattering internal multiple attenuation method in the literature and in other industry supported consortia, and in exploring possible ways to extend and advance beyond current capability. To that end it is natural that those interested in that pursuit would undertake an examination of the assumptions behind the inverse scattering

internal multiple attenuator. However, in that undertaking some researchers concluded and then published that an assumption behind the algorithm is a requirement that total travel time of primary events must be a monotonic function of the depth of the reflectors where the primaries experienced their upward reflection. B. Nita and A. Weglein examine that published claim in this report, and conclude that no such assumption is ever required, assumed or called-upon in the inverse scattering internal multiple attenuator. The fly in the ointment of those travel time monotonicity arguments resides in an asymptotic analysis of the wave theory inverse scattering de-multiple algorithm, leading to a total travel time condition. Asymptotic analysis is in fact not an analysis of the algorithm, or of an equivalent algorithm, as one derives from adding the number one to both sides of an original formula. That addition of one to both sides of an equation keeps the original algorithm's logic, requirements, assumptions and deliverables intact. Asymptotic analysis is is fact two steps:(1) an asymptotic approximation and then (2) analysis, and conclusions reached by that set of steps, although often useful, are never equivalent to or shared by the original form. The very reason for performing asymptotic approximation is to alter algorithms, their underlying assumptions and properties and requirements. The inverse scattering internal multiple attenuator is applied as it stands, and as it was originally published by Weglein et al in 1997, and is not in its meaning or application applied or calling for having an asymptotic makeover performed on itself with resulting total travel time conditions. Furthermore, there is much analysis of that actual original algorithm in the published literature, that doesn't require asymptotic approximation to gain insights and understanding.

The useful and relevant migration theory analog is that asymptotic analysis and subsequent reduction of prestack FK migration will lead to Kirchoff migration, and results in total travel time arguments, and travel time tables. Those Kirchoff total time candidate reflector arguments are not assumptions behind the non- asymptotic wave theory FK migration.

A form of prestack FK migration, with water speed, is the engine in the inverse scattering internal de-multiple algorithm. Hence, the actual requirement behind the inverse scattering attenuation algorithm is an assumption that the pseudodepth from imaging reflections with water speed have the same relative relationship as the actual depths of the actual reflectors, that generate the internal multiple , with a lower higher lower assumed relationship, for both actual and pseudo depths. Thus, the assumption behind the algorithm is a conserved relative pseudo depth to actual depth relationship or equivalently pseudo depth or vertical travel time monotonicity, as a function of depth. The latter vertical time monotonicity is a much less restrictive and accommodating of internal multiple condition, than asymptotic travel time monotonicity would allow, and examples which violate the erroneous claimed travel time condition but satisfy the actual vertical time condition are provided in this report, along with detailed analysis, taking the data from those examples step-by-step through the multiple prediction algorithm. An example that violates the vertical travel time condition is also described, and a suggestion provided for accommodating that class of events, a suggestion which of course will not require knowing the velocity, since it also derives from the inverse scattering series.

Wave theory and asymptotic approximations of wave theory are distinct in the: (1) assumptions behind methods,and their physical completeness and appropriateness, (2) required input and resulting quality and properties of output, and (3) regimes of useful practical impact. Both are obviously useful, and there are methods that represent combined aspects of both views. The inverse scattering internal multiple attenuator is a wave theory based method and algorithm. As with all useful scientific enterprise it has pushed the boundary of what we can accommodate and attenuate in the

world of internal multiples, and the boundary is defined by the assumptions behind the method.

Separately, on the issue of the effectiveness of the attenuator, within the confines of assumptions in the last paragraph, A.C. Ramirez and A. B. Weglein extend an earlier simpler analysis of the amplitude and time predictive properties of the internal multiple attenuator for 1d layered media. The travel time prediction is exact and the difference between elimination and attenuation resides in too much transmission coefficient in the prediction, compared to the actual multiple, but only with transmission coefficients down to and including the internal multiple's shallowest downward reflection. For example, an internal multiple having its shallowest downward reflection at the water bottom only has an error in its prediction of the transmission coefficients at the water bottom, totally and completely independent of how many layers and how deep into the earth the multiple travels below the water bottom.

CODES and M-OSRP

Kris Innanen, Sam Kaplan and Einar Otnes were involved in the 2D inverse scattering internal de-multiple coding which began in July 2004. A discovery this past year by these researchers that leads to a very significant speed-up of the algorithm is described in this report, and consists of a multidimensional nested integral being replaced by a product of 1D integrals. In general, when these codes reach a level of development, testing and documentation that satisfy our internal criteria and standard for efficacy and transparency as a research prototype, they will be made available and distributed to our sponsors. It is important to clearly state and communicate that the central M-OSRP driver and motivation of code development is and will remain our internal research need and requirement. However, we are delighted to also simultaneously share those research prototype codes with our sponsors. At our meeting on April 20-21 2005, there will be a video presentation of a multiples overview by Ken Matson (BP) and M-OSRP (UH Physics Dept.) where among other important, insightful and practical observations are the distinct and explicit differences between the original inverse scattering internal multiple attenuator, and algorithms available elsewhere today in terms of ability to accommodate and remove multiples and types of multiples.

PRE-REQUISITES FOR MULTIPLE REMOVAL

While these inverse scattering de-multiple methods remove requirements about the subsurface, they do place stringent requirements on estimating the wavelet, deghosting and completeness of data collection and/or reconstruction. The current method for estimating the wavelet, the energy minimizing adaptive subtraction, is often useful. However, it tends to fail precisely under the very complex circumstances where the underlying de-multiple methods have their greatest strengths, e.g, interfering events and multiples of different orders proximal to primaries. In response, we have projects to provide prerequisite satisfaction that are as physically complete and consistent with rather than something less and compromising of the multiple methods they are meant to serve. Hence, satisfying this high bar of prerequisite satisfaction results in the multiple removal methods that depend upon them having the opportunity to reach their potential. The potential of those de-multiple methods are currently not close to being realized in practise. Zhiqiang Guo and Jingfeng Zhang have pioneered and developed new robust methods for wavelet estimation and deghosting, respectively. We expect the new wavelet estimation, deghosting and 2D inverse scattering internal

de-multiple codes to be available around May 31, 2005. Several months later we will have a 2D Free-Surface multiple elimination code, and then a 3D Free-Surface code, without the typical obliquity factor omission, and receiver only deghosting that especially and frequently compromises the de-multiple effectiveness at long offsets. Meetings have been held with the IBM Blue Gene team to determine whether the Blue Gene architecture and/or the internal de-multiple code might need to be altered to accommodate a 3D inverse scattering internal de-multiple application on field data. We anticipate that a committee of our sponsors will provide an important interface and communication channel with IBM, and perhaps others, on that computational issue. M-OSRP does not plan to get distracted and too heavily involved in that end of things. We will remain faithful to our purpose of developing new concepts and "what" needs to be computed to achieve those step change seismic capabilities, and will only be tangentially involved with questions of "how" to compute.

BEYOND ATTENUATION OF INTERNAL MULTIPLES

We have launched a new project this year to incorporate more than the current leading term attenuator from the inverse scattering subseries that eliminates internal multiples. Adriana C. Ramirez and A. B. Weglein extend previous ideas and propose new concepts to identify those terms taking attenuation towards elimination. A new method and algorithm is presented and the 1D initial tests are very encouraging. This method would aim to reduce residual internal multiples where the magnitude of the residual can be significant, as e.g., in converted wave internal multiples, or when a small residual multiple is proximal to, or interfering with, a small primary, as can occur in subsalt plays.

ASSUMPTIONS BEHIND ALL SEISMIC ALGORITHMS DERIVED FROM THE INVERSE SCATTERING SERIES

The inverse scattering series promises to directly produce inverse objectives, (order by order in the measured data) and tasks associated with those objectives, directly in terms of the measured data and reference propagation, never assumed to be the actual nor ever moved or altered towards the actual. There are a series of assumptions in the steps that follow afterwards that are worth explicitly listing. Tasks and terms used and adopted to determine objectives of those tasks are appropriately defined by those whose problems we are seeking to address: exploration and production seismologists. Consequently, definitions of terms like events, multiples and primaries relate to an interface model of the earth where rapid property changes occur, and with constant or slowly or continuously varying properties between those boundaries of rapid change. Definitions of primaries and multiples relate to that model and furthermore often have either ray theoretical or 1D advertent and/or inadvertent assumptions. The definitions of primary and multiple and suggestions for generalization are provided in A. Weglein and B. Dragoset (2005). Within any definition of a multiple certain events are accommodated and others excluded. That definition is then viewed as capturing a set of events we are interested in eliminating; and, assumptions are made on how the forward series would construct those events and how the inverse series would remove those events, in terms of only the measured data and water speed. In seeking to possibly improve and expand the set of events accommodated by an algorithm, each of these distinct assumptions and definitions require examination and generalization as appropriate for your desired increase in inclusiveness.

Sometimes there are positive unanticipated surprises: As when the original inverse scattering internal de-multiple algorithm, which had rather simple ideas behind its thinking, has in fact been shown to accommodate multiples with head-wave subevents. Please see B. Nita and A. Weglein (2005), and our work in this report.

PROCESSING PRIMARIES

Our flagship and vanguard efforts today aim to provide to the processing of primaries the same capability we earlier brought to the removal of multiples. Multiple removal can occur today without subsurface information, whereas, primaries remain captured by the need to provide subsurface information for the goals of depth imaging and inversion. Our purpose is to put them on an equal footing, and the inverse scattering series views processing multiples and primaries in precisely that manner. Since the inverse scattering series is non-linear in measured data, I thought it useful to say a word about non-linear, and its fundamentally different types and the distinct inverse series response and properties regarding those issues.

NON-LINEAR: Intrinsic and Situational

The word non-linear inversion often appears in our papers, presentations and in this report. In an inverse sense, non-linear in the data refers to an objective that requires the multiplication of the data by itself, some number of times, or sums of such data products. In contrast a linear inverse process would require at most a sum over your data, and no data products. There are two types of nonlinearity that occur in inverse problems, one is innate and intrinsic, and the other is situational. An example of the former is the non-linear relationship between a reflection coefficient and the change in any quantity across the interface, and the relationship between the change in physical property and the reflection coefficient. The relationship between the wavefield on the surface and the wavefield at depth is linear when the velocity is known, and non-linear when the velocity is unknown. The latter data on the surface and data at depth relationship is an example of a situational non-linearity. The inverse scattering series automatically accommodates both the intrinsic and situational type of non-linearity. Furthermore, the inverse scattering series can determine, from the non-linear data communication itself, whether the situational non-linearity activity is required, and only acts when a-priori information is determined as inadequate for inverse task specific objectives by standards the data itself establishes. Hence, the situational non-linear inverse activity only activates when the situation warrants and requires an intervention of those terms in the judgement of the data; hence, it is the epitome of purposeful perturbation. That situational activity doesn't, for example, wander aimlessly around perturbation land finally concluding that your original estimate was adequate. It decides that adequacy question while preparing to compute the very first step beyond linear. The intrinsic non-linear activity in the inverse series is always active and can be ignored by the user but is rarely ignorable. Both types on nonlinearity are part of the direct inversion machine that the inverse scattering series represents. There are terms in the inverse series that are addressing a combination of intrinsic and situational non-linearity, e.g., parameter estimation at a target when the data decides the overburden information is less than adequate. These ideas and resulting algorithms are examined and exemplified in the succession of imaging and inversion work of e.g., Simon Shaw, Doug Foster, Ken Matson, Haiyan Zhang, Fang Liu, Kris Innanen and Bogdan Nita.

The "direct" label of direct inverse methods is not to be underestimated, and implies algorithmic purposefulness, in distinction with indirect search methods of model matching and cost function minimization. The inverse scattering series method is the only known direct multi-D inverse seismic method. And isolated task separated concepts allows pinpointing and extracting that purpose for useful algorithms and impactful application.

MODEL TYPE AND INVERSE PROCESSES

The ultimate objective of inverse problems is to determine medium and target properties from measurements external to the object under investigation. At the very first moment of problem definition, there is a immediate requirement and unavoidable expectation, that the model type of the medium be specified. In that step of model type specification, the number and type of parameters and dimension of spatial variation of those parameters are given, and carefully prescribed, and in that way you provide the inverse problem with clarity and meaning. Among the different model types used in exploration seismology are, e.g., acoustic, elastic, heterogeneous, anisotropic, and anelastic, and perhaps most important, the dimension of variability of the properties associated with these model types. In this report we describe the different tasks associated with primaries as we increase the number of spatial dimensions and number of parameters increase, from one parameter acoustic, two parameter acoustic to three parameter elastic. One type of increase is taken with a given study, e.g, we take one parameter from 1D to 2D while another project takes two and then three parameters into a one D elastic world. Each forward research step in our program isolates one single new issue, understands how the inverse series responds to those new challenges and then combines the response to different issues, as appropriate. Hence, H. Zhang and A. Weglein keep increasing number of parameters from acoustic to elastic in 1D, while simultaneously, F. Lui et al. take a single parameter into a multi-D world. Multi-parameter issues are separated from multi-dimensional issues, before combining. Another step taken here represents a direct response to another of the impenetrable current seismic challenges: Q-compensation. A new effort by K. Innanen and A. Weglein, reported here, describes the inverse scattering series response to data smoothed by some process of intrinsic attenuation. In other words, we consider Q compensation in a world of unknown or inadequate Q. They take a normal incidence wave on a 1D acoustic medium where the reference medium is assumed to be free of absorption, i.e., $Q=\infty$, and where only the absorption is assumed to be unknown and never to be determined, but the output is Q compensated. Once again, the plan is to isolate the problem being addressed before combining with other issues for field data application.

One would reasonably expect that the details of methods and algorithms for inversion objectives associated with primaries, and any tasks associated with achieving those ultimate objectives, would overall and each separately depend upon that starting assumption on model type, beginning with the dimension of assumed spatial variation . Once again, it remains an amazing fact that for removing free and attenuating internal multiples that the inverse scattering series algorithms calls only upon you to specify the dimension of earth variation and then the same algorithm only has different numbers of integrals and different dimensions of data, for any of 1D or 2D or 3D, and is totally independent of earth model type, and the properties of the subsurface parameters within any of these models.

INVERSION IN STAGES, ACHIEVING ISOLATED TASKS AND THEN REDEFINING AND RESTARTING THE PROBLEM: A STRATEGY FOR INTERVENING WITH THE INVERSE SERIES FOR PRACTICAL IMPACTFUL SEISMIC OBJECTIVES

The ultimate objective of seismic inversion has never been achieved in practise in a straight ahead single step manner directly from reflection data, and that lack of success has not been due to a lack of compute power.

The indirect model matching procedures of "all (at once) or nothing at all" have had more of the latter and little of former, especially in the applications to a multi-dimensional complex earth, where it is rare to have a reasonable proximal starting model, and bandwidth limitations of field data can seriously impede any usefulness. And those complex ill-defined geologic circumstances are the biggest impediments and challenges to current exploration and production seismic imaging and inversion.

The only direct multi-dimensional inversion procedure for seismic application is the inverse scattering series, and as a series is by definition not a one step method. However, it does not require a proximal starting model, and equally important allows the series to be examined for its inner working parts and to isolate terms into task specific subseries for separate and useful purposes. That staged approach with intermediate objectives of: (1) removing free surface multiples, (2) removing internal multiples, (3) imaging primaries to their correct spatial location, and finally (4) determining medium properties, has provided the most effective methods to-date for removing multiples (see, e.g. Weglein et al , 2003). The latter Topical Review demonstrates that the two distinct multiple attenuation tasks operate with the same identical algorithms independent of whether the earth model is e.g., acoustic, elastic or anelastic. These algorithms only depend upon the dimension of variability of properties in the earth, and knowledge of the source signature in water.

The inverse scattering series has recently progressed to the tasks associated with primaries: depth accurate structure maps and earth property determination. M-OSRP has been the center and driving force behind that new campaign. Although the removal of multiples without knowledge or determination of the propagation properties of waves in the subsurface was far from simple, and taking internal multiples from attenuated towards eliminated is one of our current project objectives (see, e.g., A.C. Ramirez and A.B. Weglein, 2005) never-the-less those methods begin and end as traces in time. Our research into primaries start with traces in the time domain, and output in the spatial domain, the domain of discomfort for inverse methods. Furthermore, there is full expectation that tasks and algorithms associated with primaries will have a closer interest in model type, and e.g. that there is no way to even imagine that medium property identification can take place without reference to a specific model type. Tasks and issues associated with structural determination, without knowing the medium, are also vastly different depending on the dimension of variation and number and types of velocities that are required for imaging reflection data. Hence, a staged approach and isolation of tasks philosophy is essential in this yet tougher neighborhood, and even more in demand for achieving insights, and then practical algorithms for these more complicated and daunting objectives. We adopt that staged and isolation of tasks and issues approach for primaries. We will now proceed to explain the current program activity on primaries, and the logic behind the different parts separately and how they tie together, and how progress within this isolated issue context ultimately contributes to the overall purpose and strategy, and how each interfaces with other initiatives within the program and our projects and plans.

The isolated task achievement plan can often spin-off incomplete but useful distinct intermediate objectives. The test and standard of progress and positive impact here, is not necessarily solely based on how complete the method is in some mathematical and physics sense, but always keeps our eye on the target: Does the method improve upon current best practise.

The stages within the strategy for primaries include the following: (1) 1D earth, with one parameter, velocity as a function of depth, and a normal incidence wave, Simon Shaw et al., (2) 1D earth with a one parameter subsurface and offset data, one shot record; Simon Shaw et al., (3) 2D earth with one parameter, velocity, varying in x and z, and a suite of shot records, Fang Lui et al., (4) 1D acoustic earth with two parameters varying, velocity and density, one propagation velocity, and one shot record of PP data, Haiyan Zhang et al., (5) 1D elastic earth, two elastic isotropic parameters and density, and two wave speeds, for p and s waves, and PP, PS, SP, and SS shot records data collected, Haiyan Zhang et al., (6) a 1D anelastic earth, with acoustic reference, for Q compensation without knowing or determining Q, Kris Innanen et al. Each of these six stages build on previous stages and progress only tackling one specific issue at a time. Then when the separate lessons of how and where any specific isolated issue is addressed within the inverse series is understood, analyzed and tested , then we are in a position to perhaps combine issues into a progression of potentially practical impactful algorithms. Studying combinations of issues as the first step makes the deciphering of multi-dimensional multi-parameter inverse activity extremely difficult, at best. Understanding velocity independent depth imaging in 1D was invaluable for extensions to multi-D where the inverse series has more than an inaccurate depth to address. Understanding acoustic multi-parameter depth imaging where there is one unknown P velocity was invaluable in understanding the elastic depth imaging problem, with unknown P and S velocities, in which, starting with several different erroneous (PP, PS, ...) images, one accurate depth image is created. As one moves from a one parameter, 1D model to a multi parameter multi-dimensional heterogeneous elastic or anelastic medium, a sequence of ever more complex issues are confronted and addressed by the corresponding inverse series. And always starting with the assumption that you don't know, or ever determine, the actual material properties that govern wave propagation in the earth.

The inverse issues that arise in each of the stages in this drive into the world of primaries are separate and distinct, and ever more complex, and their isolation gives some hope of navigating towards practical algorithms.

Among the specific highlights on primaries:

Fang Lui et al. have progressed the velocity independent depth imaging to ever more complex 2D acoustic models and capturing within his progression of algorithms more and more of the imaging capability within the series as its response to those larger contrast and complexity challenges. His input is a water speed FK migration and the algorithm is a closed form in terms of that input. Issues and steps between this fundamentally new robust velocity independent depth imaging algorithmic development and a first field field data test, will be discussed at the meeting.

Haiyan Zhang et al. have provided the first direct non-linear inversion for elastic waves and processing primaries. It accommodates both the intrinsic and situational non-linearity due to an unknown overburden and a non linear relationship between the sought after elastic property changes and density and recorded PP, PS, SP and SS data. Haiyan has then isolated the case of only having the latter AVO issue to address and further provides an approximate method that finds encouraging results using only PP data as input. Six models were provided by Bob Keys of Exxon Mobil for

testing. With PP data only the non-linear approximate method always produced the correct sign of changes in density, in contrast to the linear and standard AVO inverse method that produced the wrong sign of density change for several of the models tested. The overall conclusion is that PP, PS, SP and SS data (in 1D and 2D) would be more effective and accurate in this first ever direct nonlinear elastic prediction algorithm, but never-the-less useful added value results derive from the approximate PP data, in comparison with current standard linear methods. There is absolutely no model matching or cost function minimizing search mechanism here. The method is a direct algorithm and the extension to complex corrugated, non specular and diffractive targets are accommodated within the formalism, waiting for the next steps of staged progress. 4D and reservoir monitoring, with e.g, fluid fingering are far from appropriate for Zoeppritz and Bortfeld methods and ready made for this multi-D target machinery, and within our future plans.

SUMMARY

The biggest issue behind challenges to current imaging beneath complex ill-defined media is actually well-known: the inability to determine an adequate velocity and boundary and interfaces of the overburden velocity model. We communicated this year on a disconnect between the consistently excellent results often shown at the SEG and EAGE imaging sessions with current leading edge imaging algorithms, on synthetic data modeling of, e.g., salt, where either the velocity model is given precisely, or where the sample rate of the modeling algorithm actually smoothed over rapid velocity changes and corrugated boundaries (and thereby lost the very complexity in their model it was seeking and expecting to capture in the modeled data), and the reality of, e.g., an intolerable deep water dry hole drilling rate. Workshops to define the problem are popular and interesting and probably a useful exercise. However, that central complex imaging problem is in fact a well-defined and very well-known issue in every oil and service company, but is often neither acknowledged, nor clearly stated and rarely well-communicated by the experts. In fact it is difficult to locate a single mention of it in the literature, and yet we always hear about it from people in the petroleum industry.

This M-OSRP program is a direct response to that actual challenge. Fundamental new thinking to either significantly improve the velocity or avoid needing it is required. The latter approach is behind our current campaign, and significant progress is being reported here on all fronts. In our history, we provided methods for removing multiples without knowing or determining the velocity, and that thinking is being extended to depth accurate imaging and inversion of primaries. There is one comprehensive theory for removing multiples and processing primaries without knowing or determining the velocity model: The inverse scattering series.

The question most often asked today is “given the exact or adequate velocity model in this geologic setting, what migration strategy gives the best result: Kirchhoff, Beam, Higher order asymptotics, wave theory...?”. The relevant question that in our view needs to be asked is, “Given the fact that our biggest seismic challenges don’t allow an adequate velocity, what should then be our depth imaging response and strategy?” The M-OSRP program is asking and responding to the relevant question. That remains our plan.

The inverse scattering series is being mined for depth imaging and non-linear direct multi-D AVO benefit, and moving internal multiple attenuation towards elimination. The practical prerequisites

of wavelet estimation and de-ghosting are provided by innovative new methods based on the extinction theorem. We expect further progress next year on internal multiple removal methods, prerequisite satisfaction, code development and imaging and inversion of primaries.

Thank you for your constant encouragement, and strong support.

Arthur B. Weglein

University of Houston
20 April, 2005.

Wavelet estimation from towed-streamer pressure measurements

Zhiqiang Guo, Arthur B. Weglein, and Tik H. Tan

Abstract

Seismic processing seeks to extract sub-surface information from the wavefield recorded on a measurement surface. This wavefield contains seismic events that have not experienced the earth, and hence it is necessary to identify and separate them from the ones that have. In addition, scattered seismic waves depend on both earth properties and the character of the wavelet that leaves the source. The separation of the portion that only depends on earth properties (wavelet deconvolution) is a required step in many processing procedures. Furthermore, inverse scattering subseries methods for removing multiples and for imaging and inverting primaries without knowledge of the subsurface, place a high-bar on the pre-processing steps including estimation of the source signature. The current method for estimating the wavelet, the energy minimizing adaptive subtraction, is often useful. However, it tends to fail precisely under the very complex circumstances where the inverse scattering methods have their greatest strengths, e.g., in the case of free surface or internal multiple algorithms, with interfering events and multiples of different orders proximal to primaries. In this paper we present a new approach to addressing this challenge, which combines, extends and alters two previous wave theoretical methods, to find a good approximation to the source wavelet. The algorithm can be interpreted as navigating between two published versions of the extinction theorem and the triangle equality. The triangle relates the pressure along the cable, the normal derivative of the pressure along the cable and the source signature in water. An altered form of one of those two triangle relations provides two independent of a "nearby problem" and allows the subsequent elimination of the normal derivative and solution for the "nearby wavelet" in terms of only the towed streamer data. The central frequency of the incident wavelet determines the alteration of one of the two equations that will allow a good stable wavelet estimate to the actual. Empirical tests indicate that the new method presented in this paper produces an accurate and stable source wavelet. A comparison with the current industry standard, energy minimization adaptive subtraction procedure, is also shown in terms of efficacy for free surface multiple removal. The conclusion of these tests are positive and encouraging. This is the first direct source signature method, for amplitude and phase, directly in terms of pressure measurements along the cable.

1 Introduction

Wavelet estimation is one of the classic and central issues in seismic data processing. These are different methods that address this challenge and objectives that interface and overlap with the purposes of seismic inversion and resolution.

A rejuvenated interest in multiples caused by the industry trend to deep water and exploring beneath complex geologic formations, and new non-linear resides methods that responded to those challenges brought a new heightened interest in the requirements to allow these methods to reach their potential. The intrinsic strengths of these methods, e.g., Carvalho et al. (1), Weglein et al. (7) and Weglein et al. (6), Verschuur et al. (4), reduced or eliminated entirely any required subsurface

information for these algorithms to provide to deep water and complex geological conditions. However, the methods have other requisites in the definition and completeness of the seismic experiment. Among the former requirements is the no-true of the wave that leaves the source, i.e., the source signature or wavelet in water, and in the latter category, these methods share with wave theory processing (e.g., wave imaging methods). A heightened need to collect/extrapolate/interpolate the approximate dimension of surface data that corresponds with the dimension of subsurface variation.

There are two aspects of predicting multiples: amplitude and phase (time). The most serious error in a prediction algorithm is an error in timing of the event, and an incorrect dimension of data acquisition can impact that most serious issue. With recent published results from Shell, Statoil, PGS/Delft on full or close to full 3-D data for free surface multiple removal methods, issues of amplitude properties in prediction use in significance and practical moment. This means that amplitude effects, e.g., obliquity, wavelet, and deghosting are all now high priority. Results of the research in this paper directly address one of these key amplitude requirements. If the requirements of these free-surface and interval multiple methods are satisfied, they can surgically remove multiples without damaging proximal or interfering primaries.

A key requirement for amplitude prediction is the wavelet, i.e., the source signature in water. The underlying physics behind the new free-surface and internal demultiple algorithms do not suffer in the slightest from the presence of interfering events, multiples of different orders and any other difficulties that derive from data from a complex geological subsurface. However, the current industry standard for determining the wavelet, the energy minimization adaptive subtraction, e.g., Verschuur et al. (4), and Carvalho et al. (1), while many times useful, can precisely fail when the multiple removal methods they are meant to serve have their greatest intrinsic strengths.

This fact derives and motivates the search for a wavelet estimation methods that avoids the pitfalls and limitations of the current best practice and rests on as from a wave theoretical basis/foundation as the multiple removal methods they are meant to serve. The new method presented in this paper is the first practical approach that can predict a wavelet directly from measurement of the total field along the towed cable. The new procedure presented here is particularly well-suited for a towed streamer at about 6 m below the free surface.

Weglein and Secrest (9) present a method for computing the scattered wavefield between the cable surface and the free surface, and the reference wavefield below the cable surface, given both the pressure and its normal derivative along the cable. Tan (3) and Osen et al. (2) show that the wavelet due to an isotropic source can be determined from pressure on the measurement surface and an extra hydrophone between the measurement surface and the free surface. Tan (3) observes that in practice it is possible to well-estimate the wavefield above a single towed streamer for points not directly under the source. Using this wavefield prediction formula, the wavelet can in principle be estimated from only a single cable acquisition (8). However, the integral computed for wavelet estimation requires data along the cable including the region excluded by Tan's prediction. The purpose of the research described here is to develop and test a new source wavelet estimation algorithm that requires only the pressure on the cable. In the following, we : (1) first derive the wavelet estimation formula; (2) show how to predict normal derivatives of the wavefield above the cable; (3) then use these ingredients to provide a new way to estimate the source wavelet; and (4) provide numerical examples that exemplify the wavelet estimation and its use and added value for free-surface multiple removal.

2 Wavelet estimation

In this section, we present a wavelet estimation method that does not require any a prior assumption about the earth or the wavelet. It is based on the acoustic wave equation and it only requires the pressure measured along the cable, i.e., no borehole measurements, extra hydrophones or dual streamers. We start with the wave equation for the pressure, $\mathbf{P}(\vec{r}', \vec{r}_s, \omega)$ in the actual medium with variable velocity and constant density in the frequency domain

$$\nabla^2 \mathbf{P}(\vec{r}', \vec{r}_s, \omega) + \frac{\omega^2}{c^2(\vec{r}')} \mathbf{P}(\vec{r}', \vec{r}_s, \omega) = A(\omega)\delta(\vec{r}' - \vec{r}_s), \tag{1}$$

where $\vec{r}'$ is any point in a half space below the free surface, $\vec{r}_s$ is the source location (see Figure 1), $A(\omega)$ is the source signature, that is, the quantity we seek to determine. ω is the angular frequency, and $c(\vec{r}')$ is the actual velocity at position $\vec{r}'$. $\mathbf{P}(\vec{r}', \vec{r}_s, \omega)$ is the total pressure wavefield.

Characterizing the actual medium velocity $c(\vec{r})$ in terms of the reference wave speed c_0 and the variation in the index of refraction (Figure 2)

$$\frac{1}{c^2(\vec{r})} = \frac{1}{c_0^2}[1 - \alpha(\vec{r})], \tag{2}$$

where $\alpha(\vec{r})$ is used to characterize the difference between the actual and reference media. Now we introduce the Green's function $\mathbf{G}_0^D(\vec{r}, \vec{r}', \omega)$, in a homogeneous medium bounded by a free surface with an impulsive source $\delta(\vec{r} - \vec{r}')$. The Green's function satisfies the differential equation (3), and boundary condition (4) at the free surface

$$\nabla^2 \mathbf{G}_0^D(\vec{r}, \vec{r}', \omega) + \frac{\omega^2}{c_0^2} \mathbf{G}_0^D(\vec{r}, \vec{r}', \omega) = \delta(\vec{r} - \vec{r}'), \tag{3}$$

$$\mathbf{G}_0^D(\vec{r}, \vec{r}', \omega)|_{r=F.S.} = 0. \tag{4}$$

We define

$$\mathbf{G}_0^D(\vec{r}, \vec{r}', \omega) = \mathbf{G}_0^d(\vec{r}, \vec{r}', \omega) + \mathbf{G}_0^{FS}(\vec{r}, \vec{r}', \omega),$$

Where $\mathbf{G}_0^d(\vec{r}, \vec{r}', \omega)$ is the direct propagating, whole-space Green's function in water, and $\mathbf{G}_0^{FS}(\vec{r}, \vec{r}', \omega)$ is the additional part of the Green's function due to the presence of the free surface, see Figure (3). All Green's functions are causal.

$$\iiint_V d\vec{r}' \left[\mathbf{P}(\vec{r}', \vec{r}_s, \omega)\nabla^2 \mathbf{G}_0^{DD}(\vec{r}, \vec{r}', \omega) - \mathbf{G}_0^{DD}(\vec{r}, \vec{r}', \omega)\nabla^2 \mathbf{P}(\vec{r}', \vec{r}_s, \omega)\right] =$$
$$\iint_S ds' \left[\mathbf{P}(\vec{r}', \vec{r}_s, \omega)\frac{\partial}{\partial n}\mathbf{G}_0^{DD}(\vec{r}, \vec{r}', \omega) - \mathbf{G}_0^{DD}(\vec{r}, \vec{r}', \omega)\frac{\partial}{\partial n}\mathbf{P}(\vec{r}', \vec{r}_s, \omega)\right], \tag{5}$$

where integral surface S is the enclosed surface of volume V.

Substituting the wavefield $\mathbf{P}(\vec{r}', \vec{r}_s, \omega)$ from equation (1) and the Green's function $\mathbf{G}_0^D(\vec{r}, \vec{r}', \omega)$ into Green's theorem (5), characterizing $c(\vec{r}')$ in terms of c_0 and the perturbation $\alpha(\vec{r}')$ as expressed

in equation (2), we have

$$\begin{aligned}\iiint_V d\vec{r}' \left[\mathbf{P}(\vec{r}',\vec{r}_s,\omega)\nabla^2\mathbf{G}_0^D(\vec{r},\vec{r}',\omega) - \mathbf{G}_0^D(\vec{r},\vec{r}',\omega)\nabla^2\mathbf{P}(\vec{r}',\vec{r}_s,\omega)\right] \\ = \iiint_V d\vec{r}' \left[\mathbf{P}(\vec{r}',\vec{r}_s,\omega)\delta(\vec{r}-\vec{r}') - \frac{\omega^2}{c_0^2}\mathbf{G}_0^D(\vec{r},\vec{r}',\omega)\alpha(\vec{r}')\mathbf{P}(\vec{r}',\vec{r}_s,\omega)\right] \\ - \iiint_V d\vec{r}' \left[A(\omega)\mathbf{G}_0^D(\vec{r},\vec{r}',\omega)\delta(\vec{r}'-\vec{r}_s)\right]. \qquad (6)\end{aligned}$$

We choose the integral volume V to be the region between the free surface (F.S.) and the measurement surface (M.S.) (Figure 1). Furthermore, notice that the second term on the right-hand side of equation (6) will be zero, since all the scattering points $\alpha(\vec{r}')$ are outside of the integral volume V. The first term on the right-hand side of equation (6) is zero because we choose $\vec{r} = \vec{r}_b$ below the towed streamer (and $\vec{r}$ is outside V as well).

Representing the volume integral by the surface integral from Green's theorem (5) and replacing $\vec{r}$ with $\vec{r}_b$ yields

$$-A(\omega)\mathbf{G}_0^D(\vec{r}_b,\vec{r}_s,\omega) = \iint_S d\vec{s}' \left[\mathbf{P}(\vec{r}',\vec{r}_s,\omega)\frac{\partial}{\partial n}\mathbf{G}_0^D(\vec{r}_b,\vec{r}',\omega) - \mathbf{G}_0^D(\vec{r}_b,\vec{r}',\omega)\frac{\partial}{\partial n}\mathbf{P}(\vec{r}',\vec{r}_s,\omega)\right]. \qquad (7)$$

Since the Green's function $\mathbf{G}_0^D(\vec{r},\vec{r}',\omega)$ is zero on the free surface, and since we assume that the total field $\mathbf{P}(\vec{r},\vec{r}_s,\omega)$ will vanish on the free surface, then the enclosed integral surface S reduces to a line integral along the measurement surface (M.S.). Then equation (7) becomes

$$-A(\omega)\mathbf{G}_0^D(\vec{r}_b,\vec{r}_s,\omega) = \iint_{MS} d\vec{s}' \left[\mathbf{P}(\vec{r}',\vec{r}_s,\omega)\frac{\partial}{\partial n}\mathbf{G}_0^D(\vec{r}_b,\vec{r}',\omega) - \mathbf{G}_0^D(\vec{r}_b,\vec{r}',\omega)\frac{\partial}{\partial n}\mathbf{P}(\vec{r}',\vec{r}_s,\omega)\right]. \qquad (8)$$

This is the wavelet estimation formula given by Weglein and Secrest (9). In order to use the formula, we need the pressure wavefield and its normal derivative along the cable. However in conventional marine seismic exploration, only the pressure wavefield is recorded, so we propose a method to compute the required normal derivative based on the pressure only.

One of the wavelet estimation methods is through direct measurement, but this measurement will be contaminated by the source ghost and the scattered wavefield when the water is not very deep, or the extent of the wavelet is not short in time. However, the algorithm we propose here will effectively remove the contribution of the source ghost and the scattered wavefield.

2.1 Extinguishing the scattered wavefield

Now we demonstrate that the scattered wavefield due to the sub-surface scatterers is extinguished in equation (8). Let's define

$$\mathbf{P}(\vec{r}',\vec{r}_s,\omega) = \mathbf{P}_0(\vec{r}',\vec{r}_s,\omega) + \mathbf{P}_s(\vec{r}',\vec{r}_s,\omega), \qquad (9)$$

which states that the total wavefield $\mathbf{P}(\vec{r}', \vec{r}_s, \omega)$ could be expressed as the summation of the reference wavefield $\mathbf{P}_0(\vec{r}', \vec{r}_s, \omega)$, the wavefield due to the actual source in a homogeneous velocity reference medium, and the scattered field $\mathbf{P}_s(\vec{r}', \vec{r}_s, \omega)$, the wavefield due to the scatterers (deviation from the reference medium) in a homogeneous velocity reference medium. Substituting equation (9) into equation (8), the formula for wavelet estimation gives

$$\begin{aligned} & -A(\omega)\mathbf{G}_0^D(\vec{r}_b, \vec{r}_s, \omega) \\ &= \iint\limits_{MS} d\vec{s}' \left[\mathbf{P}_0(\vec{r}', \vec{r}_s, \omega)\frac{\partial}{\partial n}\mathbf{G}_0^D(\vec{r}_b, \vec{r}', \omega) - \mathbf{G}_0^D(\vec{r}_b, \vec{r}', \omega)\frac{\partial}{\partial n}\mathbf{P}_0(\vec{r}', \vec{r}_s, \omega)\right] \\ &- \iint\limits_{MS} d\vec{s}' \left[\mathbf{P}_s(\vec{r}', \vec{r}_s, \omega)\frac{\partial}{\partial n}\mathbf{G}_0^D(\vec{r}_b, \vec{r}', \omega) - \mathbf{G}_0^D(\vec{r}_b, \vec{r}', \omega)\frac{\partial}{\partial n}\mathbf{P}_s(\vec{r}', \vec{r}_s, \omega)\right]. \end{aligned} \tag{10}$$

We will prove that the scattered portion in equation (10) is zero. This means that the contribution for the wavelet estimation due to the scattered wavefield $\mathbf{P}_s(\vec{r}', \vec{r}_s, \omega)$ will be zero.

In the homogeneous medium, the scattered (reflected) wavefield satisfies the following equation

$$\nabla^2\mathbf{P}_s(\vec{r}', \vec{r}_s, \omega) + \frac{\omega^2}{c_0^2}\mathbf{P}_s(\vec{r}', \vec{r}_s, \omega) = \frac{\omega^2}{c_0^2}\alpha(\vec{r}')\mathbf{P}(\vec{r}', \vec{r}_s, \omega). \tag{11}$$

Substituting the scattered wavefield $\mathbf{P}_s(\vec{r}', \vec{r}_s, \omega)$ and Green's function $\mathbf{G}_0^D(\vec{r}, \vec{r}', \omega)$ into Green's second identity, it is easy to prove that the surface integral of the scattered wavefield in equation (10) is zero. Hence equation (8) is simplified to be

$$-A(\omega)\mathbf{G}_0^D(\vec{r}_b, \vec{r}_s, \omega) = \iint\limits_{MS} d\vec{s}' \left[\mathbf{P}_0(\vec{r}', \vec{r}_s, \omega)\frac{\partial}{\partial n}\mathbf{G}_0^D(\vec{r}_b, \vec{r}', \omega) - \mathbf{G}_0^D(\vec{r}_b, \vec{r}', \omega)\frac{\partial}{\partial n}\mathbf{P}_0(\vec{r}', \vec{r}_s, \omega)\right]. \tag{12}$$

Therefore we have proven that the wavelet is only related to the reference wavefield $\mathbf{P}_0(\vec{r}, \vec{r}_s, \omega)$ in the half space, and the scattered field is filtered out.

2.2 Extinguishing the source ghost

After extinguish the effect of the scattered wavefield, we proceed by proving that the contribution of the source ghost to the wavelet estimation formula is also extinguished, and that only the direct wavefield due to the actual source is used to compute the wavelet. Let's define the reference wavefield $\mathbf{P}_0(\vec{r}', \vec{r}_s, \omega)$ as

$$\mathbf{P}_0(\vec{r}', \vec{r}_s, \omega) = \mathbf{P}_0^d(\vec{r}', \vec{r}_s, \omega) + \mathbf{P}_0^{FS}(\vec{r}', \vec{r}_s, \omega), \tag{13}$$

where $\mathbf{P}_0^d(\vec{r}', \vec{r}_s, \omega)$ is that portion of the reference wavefield that travels directly from the source to the receiver without reflecting off the free surface (in a homogeneous whole space) and $\mathbf{P}_0^{FS}(\vec{r}', \vec{r}_s, \omega)$ is that portion of the reference wavefield that only exists due to the presence of the free surface. That is the source ghost (see Figure 3). $\mathbf{P}_0^d(\vec{r}', \vec{r}_s, \omega)$ and $\mathbf{P}_0^{FS}(\vec{r}', \vec{r}_s, \omega)$ satisfy the following equations respectively

$$\nabla^2\mathbf{P}_0^d(\vec{r}', \vec{r}_s, \omega) + \frac{\omega^2}{c_0^2}\mathbf{P}_0^d(\vec{r}', \vec{r}_s, \omega) = A(\omega)\delta(\vec{r}' - \vec{r}_s), \tag{14}$$

$$\nabla^2 \mathbf{P}_0^{FS}(\vec{r}', \vec{r}_s, \omega) + \frac{\omega^2}{c_0^2}\mathbf{P}_0^{FS}(\vec{r}', \vec{r}_s, \omega) = -A(\omega)\delta(\vec{r}' + \vec{r}_s). \tag{15}$$

Note in equation (15), we assume the source ghost was created by an imaged source $A(\omega)$ across F.S. with opposite polarity. Substituting equation (13) into equation (12) yields

$$\begin{aligned} -A(\omega)\mathbf{G}_0^D(\vec{r}_b, \vec{r}_s, \omega) = &\iint\limits_{MS} d\vec{s}' \left[\mathbf{P}_0^d(\vec{r}', \vec{r}_s, \omega)\frac{\partial}{\partial n}\mathbf{G}_0^D(\vec{r}_b, \vec{r}', \omega) - \mathbf{G}_0^D(\vec{r}_b, \vec{r}', \omega)\frac{\partial}{\partial n}\mathbf{P}_0^d(\vec{r}', \vec{r}_s, \omega)\right] \\ &+ \iint\limits_{MS} d\vec{s}' \left[\mathbf{P}_0^{FS}(\vec{r}', \vec{r}_s, \omega)\frac{\partial}{\partial n}\mathbf{G}_0^D(\vec{r}_b, \vec{r}', \omega) - \mathbf{G}_0^D(\vec{r}_b, \vec{r}', \omega)\frac{\partial}{\partial n}\mathbf{P}_0^{FS}(\vec{r}', \vec{r}_s, \omega)\right]. \end{aligned} \tag{16}$$

Substituting $\mathbf{P}_0^{FS}(\vec{r}, \vec{r}_s, \omega)$ and the Green's function $\mathbf{G}_0^D(\vec{r}, \vec{r}', \omega)$ into Green's theorem. If we choose the same integral domain as before, i.e. the one bounded by the free surface and the measurement surface (Figure 3), and since $\vec{r} = \vec{r}_b$ is below M.S., and $-\vec{r}_s$ is above F.S., we have

$$\iint\limits_{S} d\vec{s}' \left[\mathbf{P}_0^{FS}(\vec{r}', \vec{r}_s, \omega)\frac{\partial}{\partial n}\mathbf{G}_0^D(\vec{r}, \vec{r}', \omega) - \mathbf{G}_0^D(\vec{r}, \vec{r}', \omega)\frac{\partial}{\partial n}\mathbf{P}_0^{FS}(\vec{r}', \vec{r}_s, \omega)\right] = 0.$$

Therefore equation (16) becomes

$$-A(\omega)\mathbf{G}_0^D(\vec{r}_b, \vec{r}_s, \omega) = \iint\limits_{MS} d\vec{s}' \left[\mathbf{P}_0^d(\vec{r}', \vec{r}_s, \omega)\frac{\partial}{\partial n}\mathbf{G}_0^D(\vec{r}_b, \vec{r}', \omega) - \mathbf{G}_0^D(\vec{r}_b, \vec{r}', \omega)\frac{\partial}{\partial n}\mathbf{P}_0^d(\vec{r}', \vec{r}_s, \omega)\right]. \tag{17}$$

Equation (17) verifies that the wavelet below M.S. is extracted only from the direct wavefield $\mathbf{P}_0^d(\vec{r}, \vec{r}_s, \omega)$ in the whole space, i.e. the source ghost is also filtered out.

We have proven that both the scattered wavefield and the source ghost wavefield are annihilated, so the wavelet obtained through equation (8), the formula for wavelet estimation, is determined only by the direct wavefield portion of the total field. If we can separate the reference wavefield from the total wavefield, then it is simpler to use equation (12) to estimate the wavelet.

3 Normal derivative of the wavefield

In this section, we derive the normal derivative of the wavefield based on the pressure wavefield itself only. That is required for the wavelet estimation equation (8). Let's first build the Green's function, $\mathbf{G}_0^{DD}(\vec{r}, \vec{r}', \omega)$, that satisfies the boundary condition (19) on both the free surface (F.S.) and the measurement surface (M.S.) in the homogeneous reference medium having velocity c_0, is the solution to the equation (18):

$$\nabla^2 \mathbf{G}_0^{DD}(\vec{r}, \vec{r}', \omega) + \frac{\omega^2}{c_0^2}\mathbf{G}_0^{DD}(\vec{r}, \vec{r}', \omega) = \delta(\vec{r} - \vec{r}'), \tag{18}$$

$$\mathbf{G}_0^{DD}(\vec{r}, \vec{r}', \omega)|_{\vec{r}=F.S.,M.S.} = 0. \tag{19}$$

where $\vec{r}$ is chosen to be inside the volume V enclosed by the free surface (F.S.), the measurement surface (M.S.), and two infinite semi-circles connecting F.S. and M.S. (see Figure 1).

Substituting $\mathbf{P}(\vec{r}', \vec{r}_s, \omega)$ in equation (1) and $\mathbf{G}_0^{DD}(\vec{r}, \vec{r}', \omega)$ in equation (18) into Green's theorem yields

$$\iiint_V d\vec{r}' \left[\mathbf{P}(\vec{r}', \vec{r}_s, \omega)\nabla^2\mathbf{G}_0^{DD}(\vec{r}, \vec{r}', \omega) - \mathbf{G}_0^{DD}(\vec{r}, \vec{r}', \omega)\nabla^2\mathbf{P}(\vec{r}', \vec{r}_s, \omega)\right] = \iint_S ds' \left[\mathbf{P}(\vec{r}', \vec{r}_s, \omega)\frac{\partial}{\partial n}\mathbf{G}_0^{DD}(\vec{r}, \vec{r}', \omega) - \mathbf{G}_0^{DD}(\vec{r}, \vec{r}', \omega)\frac{\partial}{\partial n}\mathbf{P}(\vec{r}', \vec{r}_s, \omega)\right], \tag{20}$$

where integral surface S is the enclosed surface of volume V.

Substituting equation (1) and (18) into the left-hand-side of equation (20), and using equation (2) yields

$$\begin{aligned}\iiint_V d\vec{r}' &\left[\mathbf{P}(\vec{r}', \vec{r}_s, \omega)\nabla^2\mathbf{G}_0^{DD}(\vec{r}, \vec{r}', \omega) - \mathbf{G}_0^{DD}(\vec{r}, \vec{r}', \omega)\nabla^2\mathbf{P}(\vec{r}', \vec{r}_s, \omega)\right] \\ &= \iiint_V d\vec{r}' \left[\mathbf{P}(\vec{r}', \vec{r}_s, \omega)\delta(\vec{r} - \vec{r}') - \frac{\omega^2}{c_0^2}\mathbf{G}_0^{DD}(\vec{r}, \vec{r}', \omega)\alpha(\vec{r}')\mathbf{P}(\vec{r}', \vec{r}_s, \omega)\right] \\ &\quad + \iiint_V d\vec{r}' \left[-A(\omega)\mathbf{G}_0^{DD}(\vec{r}, \vec{r}', \omega)\delta(\vec{r}' - \vec{r}_s)\right].\end{aligned} \tag{21}$$

As shown in Figure (1), since the scatterers $\alpha(\vec{r}')$ are outside the volume integral domain V, the second term on the right-hand-side of equation (21) will be zero. Applying the sifting property of the Dirac delta function, and combining equation (21) and (20), we obtain

$$\begin{aligned}&\mathbf{P}(\vec{r}, \vec{r}_s, \omega) - A(\omega)\mathbf{G}_0^{DD}(\vec{r}, \vec{r}_s, \omega) \\ &= \iint_S d\vec{s}' \left[\mathbf{P}(\vec{r}', \vec{r}_s, \omega)\frac{\partial}{\partial n}\mathbf{G}_0^{DD}(\vec{r}, \vec{r}', \omega) - \mathbf{G}_0^{DD}(\vec{r}, \vec{r}', \omega)\frac{\partial}{\partial n}\mathbf{P}(\vec{r}', \vec{r}_s, \omega)\right].\end{aligned} \tag{22}$$

Since the Green's function $\mathbf{G}_0^{DD}(\vec{r}, \vec{r}', \omega)$ satisfies Dirichlet conditions on both F.S. and M.S., and we are assuming that $\mathbf{P}(\vec{r}', \vec{r}_s, \omega) = 0$ on the free surface and that the contribution from the vertical sides of the volume V are negligible, then only the pressure term at the measurement surface remains. Hence,

$$\mathbf{P}(\vec{r}, \vec{r}_s, \omega) - A(\omega)\mathbf{G}_0^{DD}(\vec{r}, \vec{r}_s, \omega) = \iint_{MS} d\vec{s}' \left[\mathbf{P}(\vec{r}', \vec{r}_s, \omega)\frac{\partial}{\partial n}\mathbf{G}_0^{DD}(\vec{r}, \vec{r}', \omega)\right]. \tag{23}$$

As $\mathbf{G}_0^{DD}(\vec{r}, \vec{r}_s, \omega)$ is approximately zero when $\vec{r}$ approaches M.S., the second term on the left-hand-side of equation (23) can be ignored in comparison with the other terms. This results in the key observation, that is, the wavefield above the M.S. can be predicted based on only the wavefield on the cable, and it is almost compact for frequencies less than a cut-off frequency. For a cable depth of 6 m and water velocity 1500 m/s, the cut-off frequency is 125 Hz. For frequencies below the cut-off, the Green's function decays exponentially with horizontal distance by Tan (3).

However, just under the source, as $\frac{\partial}{\partial n}\mathbf{G}_0^{DD}(\vec{r}, \vec{r}_s, \omega)$ is not vanishingly small for a typical marine survey acquisition, we can not ignore its contribution, even if $\vec{r}$ is close to M.S. To predict the

normal derivative of the wavefield at M.S., we propose taking the normal derivative of equation (23) directly without dropping $A(\omega)\mathbf{G}_0^{DD}(\vec{r},\vec{r}_s,\omega)$ term. Hence

$$\frac{\partial}{\partial z}\mathbf{P}(\vec{r},\vec{r}_s,\omega) - A(\omega)\frac{\partial}{\partial z}\mathbf{G}_0^{DD}(\vec{r},\vec{r}_s,\omega) = \iint\limits_{MS} d\vec{s}' \left[\mathbf{P}(\vec{r}',\vec{r}_s,\omega)\frac{\partial^2\mathbf{G}_0^{DD}(\vec{r},\vec{r}',\omega)}{\partial z\partial z'}\right]. \tag{24}$$

4 New Wavelet estimation

In this section, we present a new method to estimate the wavelet. Rewriting the wavelet estimation equation (8) and prediction equation (23) as following, for wavelet estimation,

$$-A(\omega)\mathbf{G}_0^{D}(\vec{r}_b,\vec{r}_s,\omega) = \iint\limits_{MS} d\vec{s}' \left[\mathbf{P}(\vec{r}',\vec{r}_s,\omega)\frac{\partial}{\partial n}\mathbf{G}_0^{D}(\vec{r}_b,\vec{r}',\omega) - \mathbf{G}_0^{D}(\vec{r}_b,\vec{r}',\omega)\frac{\partial}{\partial n}\mathbf{P}(\vec{r}',\vec{r}_s,\omega)\right], \tag{25}$$

for prediction equation,

$$\mathbf{P}(\vec{r},\vec{r}_s,\omega) - A(\omega)\mathbf{G}_0^{DD}(\vec{r},\vec{r}_s,\omega) = \iint\limits_{MS} d\vec{s}' \left[\mathbf{P}(\vec{r}',\vec{r}_s,\omega)\frac{\partial}{\partial n}\mathbf{G}_0^{DD}(\vec{r},\vec{r}',\omega)\right]. \tag{26}$$

As the wavelet estimation formula given by equation (25) is the same as that provided by the wavefield prediction formula in equation (26) evaluated on the cable (as in (5)), they are linearly dependent, so we can not use equation (26) to predict the normal derivative on the cable, and substitute it into equation (25).

In order to use equation (8) to calculate the wavelet below the measurement surface, we require the normal derivatives of the wavefield under the source, so we modify the idea of calculating the normal derivatives above the cable by making an alteration to the equation by deliberately introducing some perturbation. In our case we choose the surface above the cable, and obtain the normal derivatives there without dropping the wavelet term $A(\omega)\mathbf{G}_0^{DD}(\vec{r},\vec{r}_s,\omega)$ in equation (24), regarding them as the derivatives on the cable, and then substitute them into the Weglein-Secrest equation (8).

Consider the equation,

$$\mathbf{A}\vec{x} = \vec{b}$$

If $|\mathbf{A}| = 0$, in order to solve it, we add some perturbation to the matrix

$$(\mathbf{A} + \varepsilon)\vec{x} = \vec{b},$$

then find the solution through a reverse operation

$$\vec{x} = (\mathbf{A} + \varepsilon)^{-1}\vec{b}.$$

In our situation, we choose

$$\frac{\partial}{\partial z}\mathbf{P}(\vec{r} = FS,\vec{r}_s,\omega) \approx \frac{\partial}{\partial z}\mathbf{P}(\vec{r} = PS,\vec{r}_s,\omega).$$

where P.S. is a pseudo measurement surface above M.S.. We also assume that the derivative of the wavefield is continuous, so that when P.S. approximates to M.S., we assume that the derivative at P.S. will approximate the one at M.S.

Hence we approximate the required derivative at P.S. by

$$\frac{\partial}{\partial z}\mathbf{P}(\vec{r},\vec{r}_s,\omega) = A(\omega)\frac{\partial}{\partial z}\mathbf{G}_0^{DD}(\vec{r},\vec{r}_s,\omega) + \frac{\partial}{\partial z}\mathbf{T}(\vec{r},\vec{r}_s,\omega) \tag{27}$$

where

$$\frac{\partial}{\partial z}\mathbf{T}(\vec{r},\vec{r}_s,\omega) = \frac{\partial}{\partial z}\iint\limits_{MS} d\vec{s}' \left[\mathbf{P}(\vec{r}',\vec{r}_s,\omega)\frac{\partial}{\partial n}\mathbf{G}_0^{DD}(\vec{r},\vec{r}',\omega)\right].$$

Substituting equation (27) into equation (8), and rearranging the terms, we achieve

$$\begin{aligned} -A(\omega)\left[\mathbf{G}_0^{D}(\vec{r}_b,\vec{r}_s,\omega) + \iint\limits_{MS} d\vec{s}'\mathbf{G}_0^{D}(\vec{r}_b,\vec{r}',\omega)\frac{\partial}{\partial z}\mathbf{G}_0^{DD}(\vec{r},\vec{r}_s,\omega)\right] \approx \\ \iint\limits_{MS} d\vec{s}'\left[\mathbf{P}(\vec{r}',\vec{r}_s,\omega)\frac{\partial}{\partial n}\mathbf{G}_0^{D}(\vec{r}_b,\vec{r}',\omega) - \mathbf{G}_0^{D}(\vec{r}_b,\vec{r}',\omega)\frac{\partial}{\partial z}\mathbf{T}(\vec{r},\vec{r}_s,\omega)\right]. \end{aligned} \tag{28}$$

Compared with equation (8), equation (28) has one extra term, that takes into account the contribution under the source for derivative. This is the equation we are going to use to estimate the wavelet below the cable.

The triangle relationship states that measured values of $\mathbf{P}(\vec{r},\vec{r}_s,\omega)$ and its normal derivative along a cable and $A(\omega)$ satisfy exactly equation (8). One might think that the wavefield prediction formula, equation (24), when evaluated on the cable, provides a second independent relationship that would allow the wavelet to be directly determined from along the cable. However, Weglein and Amundsen Weglein and Amundsen (5) demonstrate that these are the same relationship. If you temporarily ignore this fact, and substitute equation (24) into equation (8) to eliminate $\frac{\partial}{\partial n}\mathbf{P}(\vec{r},\vec{r}_s,\omega)$, then when $\vec{r}$ approaches the cable, the inverse of solving the wavelet in equation (28) is "unstable". To avoid this instability in the inversion, we suggest here that values above the cable for $\frac{\partial}{\partial n}\mathbf{P}(\vec{r},\vec{r}_s,\omega)$ and $\frac{\partial}{\partial n}G_0^{DD}(\vec{r},\vec{r}_s,\omega)$ are substituted for those at the cable in the integral to avoid the singularity. This has the effect of avoiding a singular division by solving a nearby perturbed problem in anticipation that this will lead to a stable approximate solution.

5 Synthetic examples

We build a model in the homogeneous medium with three scatterers. The source is 2 m below the free surface, the source wavelet is a Ricker wavelet with central frequency f=40 Hz, the cable is 6 m below the free surface, the receiver interval is 2 m, there are a total of 200 receivers, the time sample interval is 1 ms, and the predicted surface is changing from 0.3 m to 2.5 m above M.S.

Figure 4 shows all the estimated wavelet results with prediction surfaces changing from 0.3 m to 2.5 m above M.S. by equation (28), we see the estimated wavelet at 0.7 m matches the input. Figure 5 indicates the error with respect to the distance of the prediction surface from M.S., and

Figure 6 shows the error with respect to the ratio of the distance of the prediction surface to the wavelength. It is shown that the least error location is about 0.7 m above M.S in Figure 5, the ratio is about 0.02 in Figure 6. When you get closer to M.S., the error rapidly increases. This means the equation here approximates an unstable state. When it is farther from the M.S., because the normal derivative has a greater error, the error in the wavelet estimation also increases.

To test the stability (simulate the cable depth changes due to, e.g., sea tide, wind) of the wavelet estimation equation (28), we assume the cable depth has $\pm 15\%$ error, but still think the cable is at its original depth, then use equation (28) to estimate the wavelet. The results of the comparison between the correct cable depth, and two error depths, are shown in Figure 7. All of the three estimated wavelets are close to the actual input wavelet.

We test synthetic datasets with reflectors at 40 m, 60 m, and 80 m, the water layer of velocity 1500 m/s overlying a half space solid of velocity 2000 m/s. We add 10% random noise to the 40 m model. The models were provided without knowing the wavelet, and after estimating the wavelet, we compare it with the actual wavelet. The acquisition geometry is the same as before. Then equation (28) is used to estimate the wavelet, the results are shown in Figure 8. There are some differences at the peak and trough of the wavelet. The one estimated from the 80 m model has artifacts that starts at about 110 ms, the 40 m model has artifacts closer to the source, that is due to the reflection interference with the direct wavefield. The method is found to be stable with about 10% random noise.

We also test the multiple attenuation using the energy-minimum-method when the primary interferes with multiple (see Figure 9). As the current energy-minimum-method assumes that the total energy of the demultipled data is less than the total energy of the input, however in our specially designed example, the assumption is broken, because the total energy of the demultipled data is more than the total energy of the input. The results are shown in Figure 10 and 11. Figure 10 is the demultiple without the wavelet; Figure 11 is the demultiple with the estimated wavelet, the primary was preserved.

6 Conclusions

A method for estimating the wavelet directly from the data on a towed streamer was recently proposed by Weglein et al. (10). That method proposed using the wavefield prediction method of Tan (3) to approximate the needed normal derivative along the cable. However, the wavelet method requires an integral over all receivers for a given shot, and the prediction is not accurate under the source. In order to use equation (8) to calculate the wavelet below the measurement surface, we require the normal derivatives of the wavefield under the source, and we modify the idea of calculating the normal derivatives above the cable by making an alteration to the equation by introducing some perturbation.

In this paper, we addressed this problem by keeping the term that is small away from the source to achieve an algorithm that is valid for all offsets needed in the integral.

An intrinsic instability in this approach is addressed by seeking an approximate solution that replaces the unstable inversion by a "nearby" (i.e., perturbed) operation. Tests for different prediction depths and noise stability on synthetic data are encouraging.

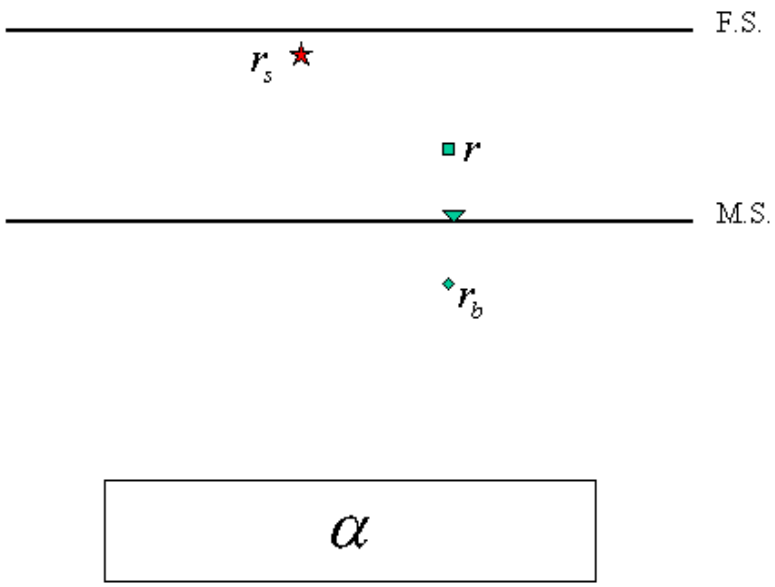

Figure 1: *Sketch of the marine survey: $\vec{r}_s$ is the source position, $\vec{r}$ is above M.S., $\vec{r}_b$ is below M.S., and the integral volume V is the region between F.S. and M.S. the scatter α is outside of V.*

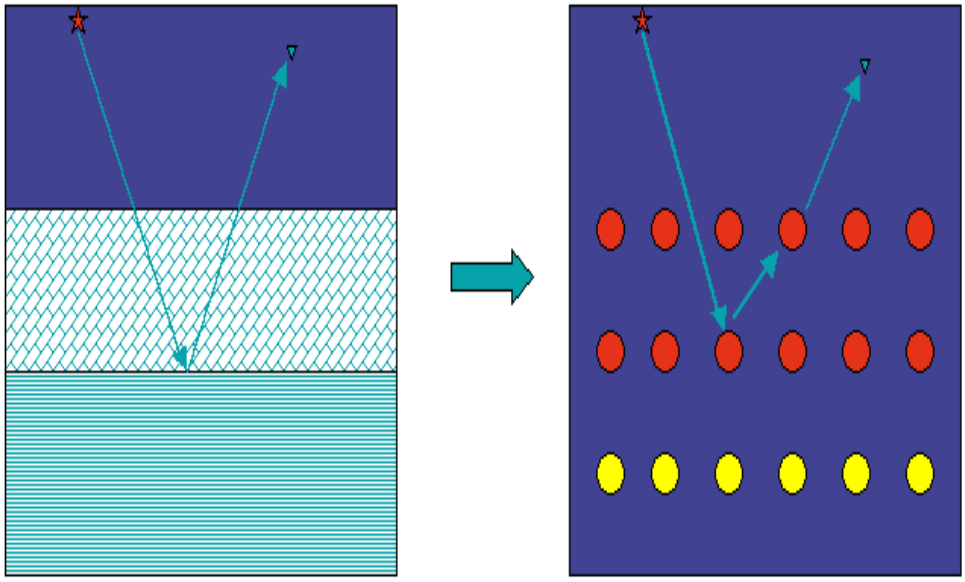

Figure 2: *The actual heterogeneous medium (left) can be parameterized as a homogeneous velocity reference medium (right) with embedded point scatterers.*

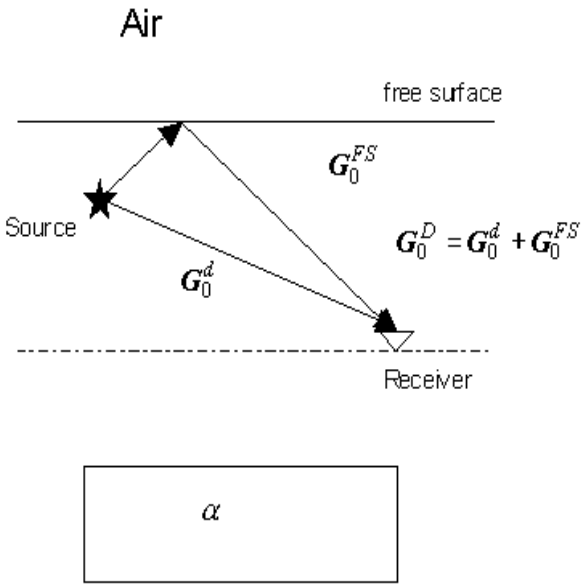

Figure 3: *The Green's function* $\mathbf{G}_0^D(\vec{r},\vec{r}_s,\omega)$ *is the summation of* $G_0^d(\vec{r},\vec{r}_s,\omega)$*, direct propagating part, and* $\mathbf{G}_0^{FS}(\vec{r},\vec{r}_s,\omega)$*, the source ghost part. The corresponding wavefield is* $\mathbf{P}_0(\vec{r},\vec{r}_s,\omega)$*,* $\mathbf{P}_0^d(\vec{r},\vec{r}_s,\omega)$ *and* $\mathbf{P}_0^{FS}(\vec{r},\vec{r}_s,\omega)$ *respectively.*

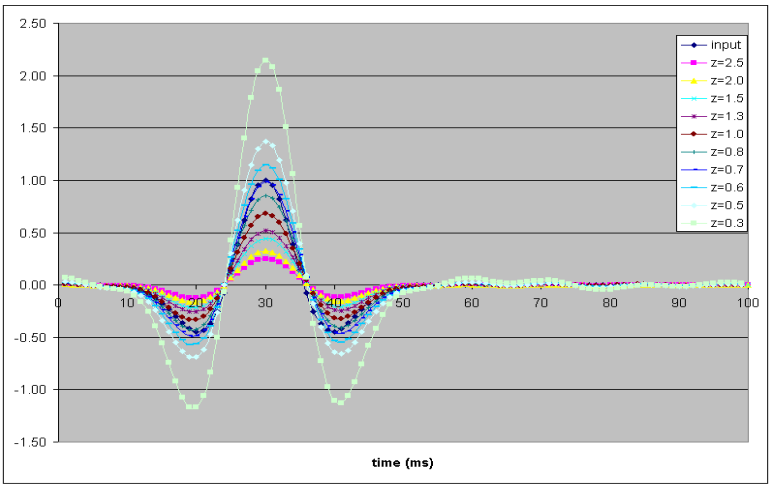

Figure 4: *Wavelet estimation for different prediction depths changing from z=0.3 m to 2.5 m above the measure surface, the estimated wavelet at* $z = 0.7$ *m matches the input wavelet very closely.*

References

[1] Carvalho, P. M. (1992). *Free-surface multiple reflection elimination method based on nonlinear inversion of seismic data.* Ph. D. thesis, Universidade Federal da Bahia.

[2] Osen, A., B. G. Secrest, L. Amundsen, and A. Reitan (1998). Wavelet estimation from marine pressure measurements. *Geophysics 63*(6), 2108–2119.

[3] Tan, T.-H. (1999). Wavelet spectrum estimation. *Geophysics 64*(6), 1836–1846.

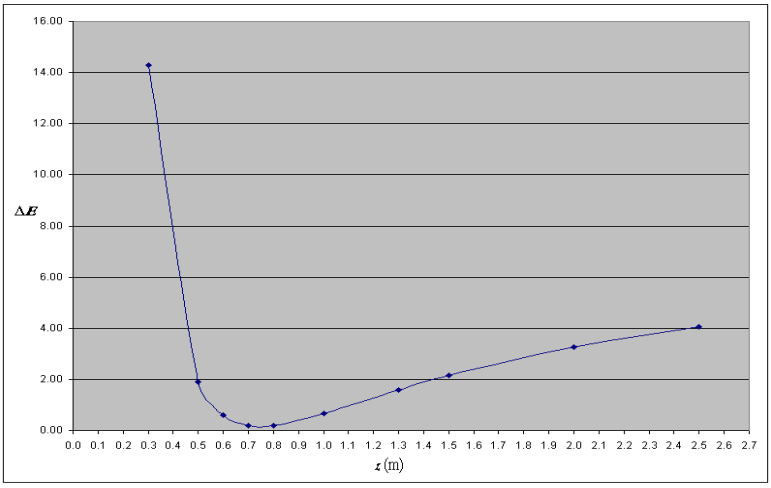

Figure 5: *Energy error analysis, the estimated wavelet at $z = 0.7$ m above M.S. has least error; the closer to M.S. (z=0), the bigger the error, because it is close to the unstable state. When the prediction surface is away from M.S., the normal derivative has a greater error, therefore, the error in the wavelet estimation also increases.*

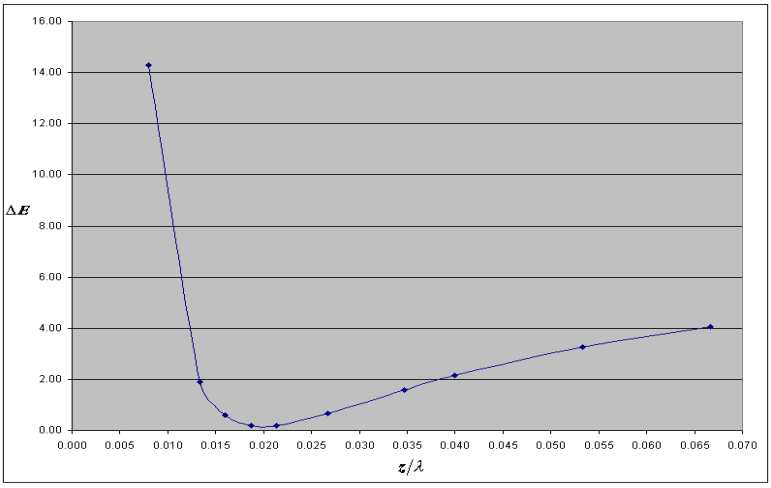

Figure 6: *Energy error vs. the ratio of the prediction depth to the wavelength, the ratio at 0.02 has least error, which corresponds to the prediction surface 0.7 m above M.S. in FIG 5.*

[4] Verschuur, D. J., A. J. Berkhout, and C. P. A. Wapenaar (1992). Adaptive surface-related multiple elimination. *Geophysics 57*, 1166–1177.

[5] Weglein, A. B. and L. Amundsen (2003). g_0^{DD} and g_0^D integral equations relationships; the triangle relation is intact. *M-OSRP Annual Report 2*.

[6] Weglein, A. B., F. V. Araújo, P. M. Carvalho, R. H. Stolt, K. H. Matson, R. T. Coates, D. Corrigan, D. J. Foster, S. A. Shaw, and H. Zhang (2003). Inverse scattering series and seismic exploration. *Inverse Problems 19*, R27–R83.

[7] Weglein, A. B., F. A. Gasparotto, P. M. Carvalho, and R. H. Stolt (1997). An inverse-scattering series method for attenuating multiples in seismic reflection data. *Geophysics 62*(6), 1975–1989.

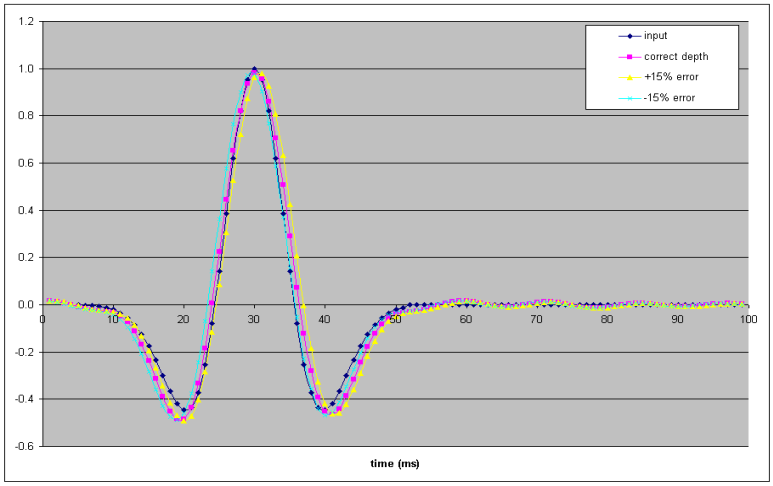

Figure 7: *Wavelet estimation with cable depth ±15% error, but still assume the cable depth is original in estimation. The estimated wavelet is close to the input even if the cable depth has ±15% error.*

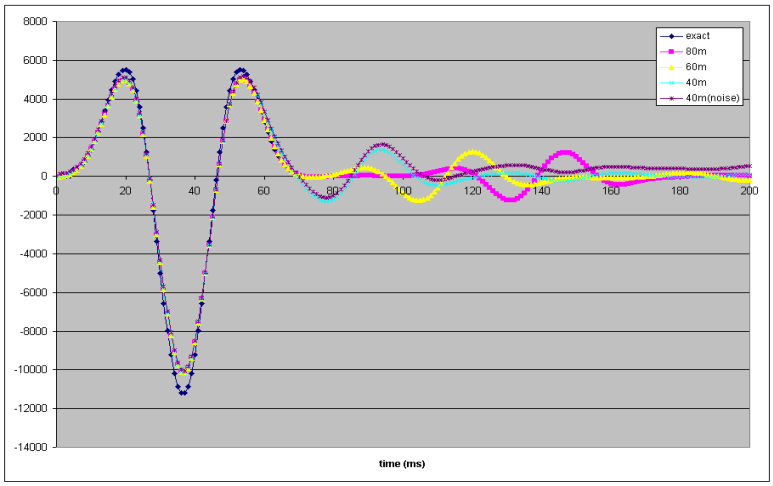

Figure 8: *Wavelet estimation from three models: 40 m, 60 m, and 80 m reflector, 10% random noise is added to the 40 m model. The estimated wavelets are close to the input, but show a tail. The tail in 40 m model is closer to the wavelet due to the interference of the direct wavefield and reflection wavefield.*

[8] Weglein, A. B., K. H. Matson, D. J. Foster, P. M. Carvalho, D. Corrigan, and S. A. Shaw (2000). imaging and inversion at depth without a velocity model: Theory, concepts and initial evaluation. In *70th Annual Internat. Mtg., Soc. Expl. Geophys., Expanded Abstracts*, pp. 1016–1019. Soc. Expl. Geophys.

[9] Weglein, A. B. and B. G. Secrest (1990). Wavelet estimation for a multidimensional acoustic or elastic earth. *Geophysics 55*(7), 902–913.

[10] Weglein, A. B., T. H. Tan, K. H. Matson, S. A. Shaw, and D. J. Foster (2000). prediction of the wavefield anywhere above an ordinary towed streamer: Applications to source wavelet esti-

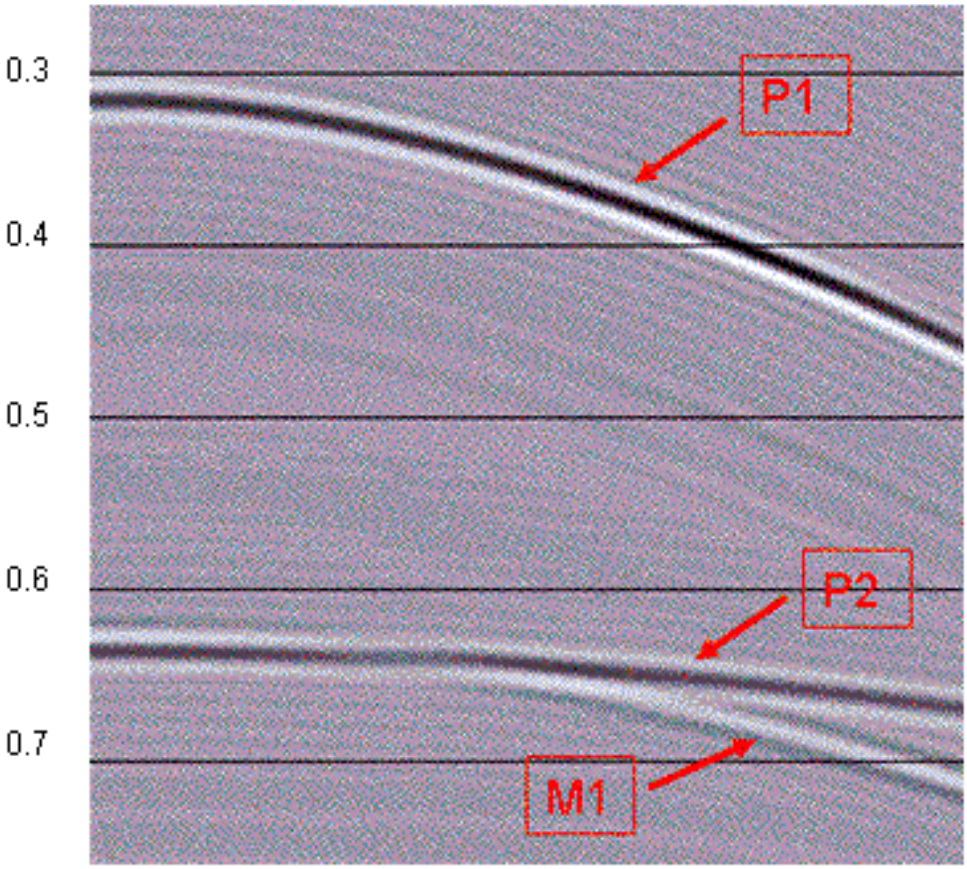

Figure 9: *Multiple interferes with primary, P1 represents first primary, P2 represents second primary, M1 represents first order free surface multiple. Vertical axis is time in seconds.*

mation, demultiple, and imaging. In *70th Annual Internat. Mtg., Soc. Expl. Geophys., Expanded Abstracts*, pp. 2413–2415. Soc. Expl. Geophys.

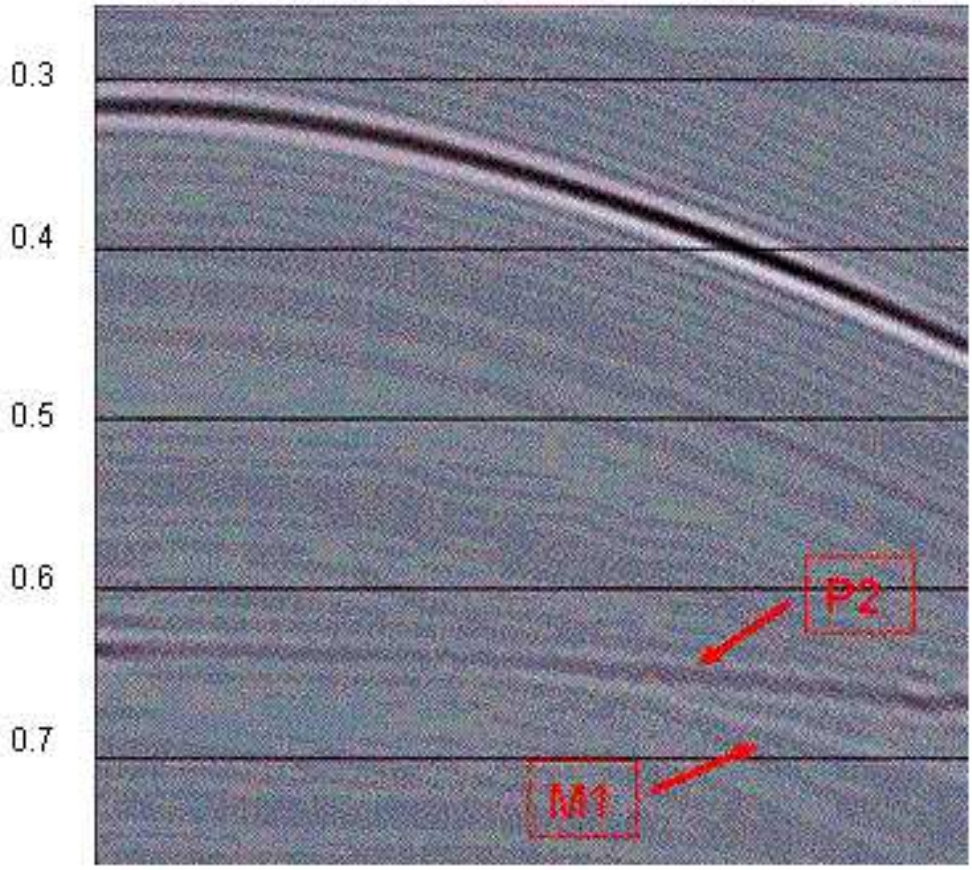

Figure 10: *Demultiple using energy-minimum-method without the wavelet, P2 is the primary, M1 is the multiple. When the multiple was attenuated, the energy of the primary increases, that's why the primary also is attenuated. Vertical axis is time in seconds.*

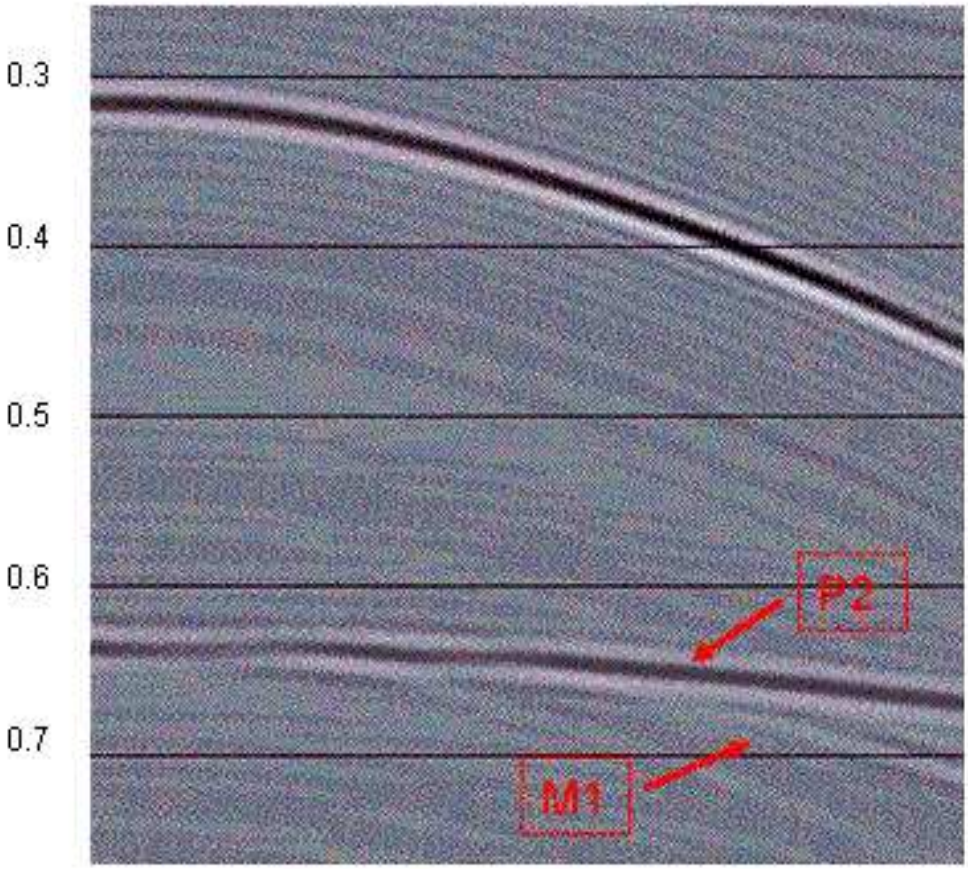

Figure 11: *Demultiple with the wavelet, P2 is the primary, M1 is the multiple. When the multiple was attenuated, the primary was preserved. Vertical axis is time in seconds.*

Extinction Theorem deghosting method using towed streamer pressure data: Analysis of the receiver array effect on deghosting and subsequent free surface multiple removal

Jingfeng Zhang and Arthur B. Weglein

Abstract

Deghosting is a prerequisite procedure for free surface multiple removal (FSMR), internal multiple attenuation/elimination, imaging and inversion (Weglein *et al.*, 2003). The effectiveness of deghosting directly affects the performance of these methods. Last year, we presented numerical tests of the deghosting algorithm given by Weglein *et al.*, (2002). Those numerical tests demonstrate the accuracy of the predicted up-going field at the receiver side. This year, numerical tests of the totally deghosted field (*i.e.* down-going at source side and up-going at receiver side) are presented.

First, we use point receiver data to perform deghosting since wave theory assumes point receiver data. Subsequently, receiver array data is supplied to the deghosting algorithm (Receiver arrays are widely used in practice and hence it is critical to characterize their effect). Finally the first order FSMR (Weglein *et al.*, 1997; 2003) procedure is applied to the point receiver and receiver array data respectively in order to further characterize the effect of the receiver array. The effectiveness of the deghosting and FSMR algorithm is demonstrated by the numerical tests. The algorithms give useful results for both data sets. It is shown that the deghosting results are accurate when supplied with point receiver data, in other words, the direct wave is removed and the deghosted scattered field is predicted accurately (both in phase and amplitude). Using receiver array data, we find that (1) the direct wave needs to be removed separately; (2) the phase of the deghosted scattered field is very close to the phase of the numerically determined exact field and (3) there is a slight error in the amplitude at non-zero offset. The first order FSMR method is applied to the two deghosted data sets. We find that the first order free surface multiple is removed completely from the point receiver data. In the case of the receiver array data, the first order free surface multiple is reduced effectively, although not eliminated.

1 Introduction

In marine seismic exploration, reflection data is obtained from the wavefield, generated with a source of energy (*e.g.*, an air gun), which propagates into the earth. When the wavefield reaches a reflector, a portion of it is reflected upward towards the receivers which are just below the air-water interface (free surface or FS). From a wave theory point of view, point receivers are supposed to be used. However, in order to improve the signal/noise ratio, receiver arrays are widely used in practice. A receiver array is a set of receivers whose records are summed together so that the signal can be enhanced and the random noise suppressed. This summation will inevitably damage the actual wavefield. So it is critical to characterize its effect on any wave theoretical approach.

¿From all the events recorded in the data, we can identify the following events as ghosts: (1) Direct arrival ghost: the wave that goes up from the source, reflects from the free surface and then goes to

the receiver. (2) Source ghosts: the waves that began their history as upgoing waves (3) Receiver ghosts: the waves that ended their propagation as downgoing waves.

A common sequence of data processing is source wavelet estimation/deconvolution, deghosting, free surface multiple removal (FSMR), internal multiple attenuation/elimination, depth imaging and inversion (characterization of medium properties). The order of these operations is important since the later tasks need the results of the earlier ones as their inputs and hence, the performance of the later operations are directly affected by the accomplishment of the earlier ones. Some recently developed processing techniques such as imaging without velocity (Shaw *et at.*, 2004, Liu *et al.*, 2004) and nonlinear inversion (Zhang *et al.*, 2004) put a very high bar on the data preprocessing (wavelet estimation, deghosting and multiple removal) since those techniques engage the data fully and non-linearly (Shaw *et al.*, 2004) which includes the source wavelet and a chosen reference medium's properties. For example, in imaging without velocity, the method is non-linear in the scattered field, using non-linearly the amplitude of certain events in the data as well as their arrival time; it requires effective data preprocessing.

In this paper, assuming the source wavelet is available (Weglein and Secrest, 1994, Guo *et al.*, 2005), we study the effect of the receiver array on our deghosting and free surface multiple removal algorithm. Only point sources are considered in this paper, although source arrays are generally applied in practice. The array effect on the source wavelet estimation procedure is studied by Guo *et al.*, (2005).

In the following chapters, we will briefly review our deghosting algorithm and FSMR procedures, then we will present the numerical test results, which are followed by the concluding remarks.

2 Theory

As an important data processing procedure, deghosting has been widely discussed (Schneider *et al.*, 1964, Sϕnneland and Berg, 1985, Robertsson and Kragh, 2002, Amundsen *et al.*, 2001; 2005). The deghosting method we use is:

$$P^{\text{deghosted}}(\mathbf{r}, \mathbf{r}_s, \omega) = \int\limits_{MS} \left(P(\mathbf{r}', \mathbf{r}_s, \omega) \frac{\partial G_0^+(\mathbf{r}, \mathbf{r}', \omega)}{\partial \mathbf{n}'} - G_0^+(\mathbf{r}, \mathbf{r}', \omega) \frac{\partial P(\mathbf{r}', \mathbf{r}_s, \omega)}{\partial \mathbf{n}'} \right) \cdot d\mathbf{S}', \qquad (1)$$

where MS denotes the measurement surface and $G_0^+(\mathbf{r}, \mathbf{r}', \omega)$ is the causal Green's function in the reference medium, satisfying

$$\nabla'^2 G_0(\mathbf{r}, \mathbf{r}', \omega) + \frac{\omega^2}{c_0^2} G_0(\mathbf{r}, \mathbf{r}', \omega) = \delta(\mathbf{r} - \mathbf{r}'). \qquad (2)$$

Eq.(1) computes the receiver side up-going field. The same integral on the source side will get rid of the source ghost. This deghosting procedure only requires the pressure field, P, and its vertical derivative $\frac{\partial P}{\partial \mathbf{n}'}$. However, $\frac{\partial P}{\partial \mathbf{n}'}$ is usually not measured in practice. $\frac{\partial P}{\partial \mathbf{n}'}$ can certainly be predicted if the source is below the measurement surface (MS) (Amundsen *et al.*, 1995). But for the case where the air gun is located between the free surface and measurement surface, the source wavelet ($A(\omega)$)

must be known in order to predict P and its derivative (Tan, 1992, Osen *et al.*, 1998, Weglein *et al.*, 2000):

$$P(\mathbf{r},\mathbf{r}_s,\omega) = A(\omega)G_0^{DD}(\mathbf{r},\mathbf{r}_s,\omega) + \int_{M.S.} P(\mathbf{r}',\mathbf{r}_s,\omega)\frac{\partial}{\partial z'}G_0^{DD}(\mathbf{r}',\mathbf{r},\omega)dS', \tag{3}$$

$$\frac{\partial P(\mathbf{r},\mathbf{r}_s,\omega)}{\partial z} = A(\omega)\frac{\partial G_0^{DD}(\mathbf{r},\mathbf{r}_s,\omega)}{\partial z} + \int_{M.S.} P(\mathbf{r}',\mathbf{r}_s,\omega)\frac{\partial^2 G_0^{DD}(\mathbf{r},\mathbf{r}',\omega)}{\partial z'\partial z}dS'. \tag{4}$$

where G_0^{DD} is the Green's function that satisfies Eq. (2) and vanishes both on the FS and on the MS.

There is a relationship called the triangle relationship among the pressure wavefield, P, its normal derivative $\frac{dP}{dz}$ on the MS and the wavelet $A(\omega)$ (Weglein and Secrest, 1994, Amundsen *et al.*, 1995). Knowing any two of the three variables, we can predict the third one. In principle, the triangle relationship says that the source wavelet can not be obtained exactly from the pressure measurements on the MS only. A very good approximation, however, can be obtained by the method proposed by Guo *et al.*, (2005). This perturbed technique implies that, essentially, the deghosting algorithm we use can be performed only from the pressure measurements on the MS.

After the deghosting procedure is completed, we can perform the FSMR. Various methods (Barr *et al.*, 1989, Amundsen 2001) have been proposed to this end. The FSMR procedure we use is derived from the inverse scattering series (Weglein *et al.*, 1997; 2003). It is a model type independent procedure so it works for acoustic/elastic/nonelastic, isotropic/anisotropic, absorptive/non-absorptive medium, and makes no assumptions regarding the structure of the earth. The model type independent characteristic is indicated by the use of $V_1(k_1,k_2,\omega)$ instead of $V_1(k,\omega)$ or any specific form of potential in the derivation. This algorithm removes free surface multiples through an order by order iteration. The first order FSMR exactly eliminates the first order free surface multiples and at the same time alters the higher order free surface multiples so that they can be removed by higher order operations. The formulas are given by:

$$D_n'(k_g,k_s,\omega) = \frac{2}{iA(\omega)}\int_{-\infty}^{\infty} dkqe^{iq(z_q+z_s)}D_1'(k_g,k,\omega)D_{n-1}'(k,k_s,\omega), \tag{5}$$
$$n = 2,3,4,.....,$$

and

$$D'(k_g,k_s,\omega) = \sum_{n=1}^{\infty} D_n'(k_g,k_s,\omega), \tag{6}$$

where $D_1'(k_g,k_s,\omega) \equiv D_1'(k_g,z_g,k_s,z_s)$ is the deghosted data containing primaries, free surface multiples and internal multiples. The variables k_g and k_s are Fourier conjugates of x_g and x_s respectively and z_g and z_s are the depths of the receivers and sources respectively. $D'(k_g,k_s,\omega)$ represents the data after FSMR. The mathematical details can be found in Weglein *et al.* (1997; 2003) and Carvalho (1992). For a 1D medium, the integral in Eq.(5) will reduce to a simple multiplication since $D(k_g,z_g,k_s,z_s,\omega) = 0$ unless $k_g = k_s$.

In Eq.(5), the coefficient is different from the one provided in the references due to different Fourier transform conventions. Eq.(5) is derived from the following convention:

$$D(k_g, z_g, k_s, z_s, \omega) = \frac{1}{2\pi} \int_{-\infty}^{\infty} e^{-ik_g x_g} D(x_g, z_g, x_s, z_s, \omega) e^{ik_s x_s} \, dx_g \, dx_s \tag{7}$$

$$D(x_g, z_g, x_s, z_s, \omega) = \frac{1}{2\pi} \int_{-\infty}^{\infty} e^{ik_g x_g} D(k_g, z_g, k_s, z_s, \omega) e^{-ik_s x_s} \, dk_g \, dk_s. \tag{8}$$

Note that different Fourier transform conventions are chosen on source and receiver sides.

3 Numerical tests for towed streamer data

The numerical tests presented in this report, are based on a simple 1D acoustic model. Using the Cagniard-de Hoop method (Aki and Richards, 2002), we generate synthetic data for the following model (Figure 1): a free surface (FS) overlies 300m of water (wave speed 1500m/s), below which is a homogeneous acoustic half space characterized by wave speed 2250m/s. The density is constant. The source is located at (0,2m) and the source wavelet is a Ricker wavelet (Figure 2). The advantage of the Cagniard-de Hoop method is that we can accurately calculate any specific event we are interested in so that we can compare it with the results predicted by our deghosting and FSMR algorithms.

3.1 Array effect on deghosting

The first test's objective is to determine the accuracy of the deghosting result obtained from point receiver data. For this test, the receiver interval is 1m. Since the medium is 1D, a single shot-record is sufficient to perform deghosting on both source and receiver sides. The input data contains the direct wave, the primary, multiples and their related ghosts. Here the direct wave (G_0) contains a component that travels directly from the source to the receiver (G_0^d) and a component that travels upward from the source to the free surface and is then reflected back to the receivers (G_0^{fs}). The data for the towed streamer cable (6m) is shown in Figure 3. The source and receiver deghosted results at several offsets are presented in Figure 4. Clearly, using point receiver data, the predicted deghosting results agree very well with the exact results.

For the array data test, the receiver array configuration we use is called Guardian; its parameters are shown in Figure 5. The records of the eight receivers are summed together with equal weights to produce one record at the center location of the array. The record/group interval is 12.5m. Figure 3 shows the generated array data. There is a visible difference between the point receiver data and the receiver array data. The deghosting results are compared with the exact results in Figure 6. We find that the direct wave can not be removed at all of the four offsets. For the scattered field:

(1) at zero offsets, both the amplitude and the phase of the primary and the first order free surface multiple are very accurate;

(2) at large offsets, the phase of the scattered field are roughly correct although there is a slight error in the amplitude.

For the scattered field, the above results are explainable by considering how the receiver array changes the data at different offsets. At zero offset, for example, the receiver array is tangential to the wavefront. So the summation of the field produces less damage to the actual field. While for large offset, the angle between the array and the wavefront is bigger and thus, the field is more severely damaged. Therefore the results at zero offsets are better. The higher order free surface multiples are very weak at zero offsets so they are easily swamped by numerical artifacts.

For the direct wave, although the wavefront is tangential to the array at zero offset, the wave field at zero offset varies rapidly in space. Hence the damage of the array to the wave field is non-trivial. While at large offsets, the wavefront is almost vertical to the array. Hence compared to the scattered field, the direct wave is more affected by the receiver array. Another reason that the receiver array affects the direct wave is that the large receiver interval (12.5m) is too big to sufficiently measure the quickly varying direct wave at small offsets.

Since the direct wave can not be effectively removed using array data, it would be advisable to remove it before deghosting. We can either mute it or predict the direct wave and subtract it from the original data, since we assume we have the source wavelet. Which method to choose depends on the situation. For shallow water case, for example, the prediction-subtraction method is preferred since the direct wave overlaps with the scattered field very early. When the water is deep, as is is in our model, we can simply mute off the direct wave. The deghosting results after the direct wave is eliminated are shown in Fig(7).

These numerical tests have demonstrated the effectiveness of the deghosting algorithm. When supplied with point receiver data, very accurate results are obtained. With receiver array data, the algorithm still produce useful results. Whether this usefulness is adequate or not depends on the objective. If the amplitude is not critical (structure mapping, for example), then the receiver array data is sufficient. For cases like inversion, where the amplitude is important, the angle/offset dependent small error in the amplitude could produce serious error in the results.

3.2 Array effect on free surface multiple removal (FSMR)

The above point receiver deghosting results are put into Eq. (5) and Eq. (6) to remove the free surface multiple. Only the first order free surface multiple removal is performed. After the FSMR operation on the deghosted data, we obtain the first order FSMR results (Figure 8). Obviously, the primary remains untouched and the first order free surface multiples have been eliminated.

For receiver array data, after the elimination of the direct wave and deghosting, the FSMR is performed. Results are shown in Figure 9. Just like the deghosting case, the FSMR result is very good at zero offset. At larger offsets, there is a small error in the amplitude of the primary, which occurs because the small error already exists in the deghosting results. We can also see that the first order free surface multiple has been effectively reduced, although it has not been eliminated. This effectiveness is adequate or not again depending on the objectives of the operations to follow it. For example, if the primary and the multiples are not overlapping and one just want to separate the primary and multiples for interpretation, then the receiver array data result is adequate. The same result will not be adequate, however, if the interested primary coincidentally overlaps with this particular free surface multiple. This result can also be regarded as an immediate example of how the deghosting results directly affect the subsequent processing steps.

4 Conclusions

Both point receiver and receiver array data for a simple 1D medium have been supplied to the deghosting and FSMR algorithm in order to characterize the effect of the receiver array. Useful results have been obtained for both data sets. It is shown that when point receiver data is used, both the deghosting and FSMR results agree very well with the exact ones.

When receiver array data is provided, the direct wave has to be removed separately before deghosting. Compared to the exact results, the phase of the deghosting results of the scattered field are very accurate while a small error in the amplitude is observed. The first order free surface multiple is significantly reduced after performing a FSMR procedure.

The effect of those small errors in the deghosting and FSMR results depends on the subsequent processing objectives. For the deghosting algorithm, if the results are just used to perform structure mapping, then those small error could be tolerable. Serious prediction errors could occur for cases like inversion where amplitude is critical. The result of FSMR faces the same situation.

Acknowledgements

We thank Kenneth Matson (BP) for his invaluable suggestions and his FSMR code. William Dragoset (WesternGeco) is thanked for his suggestions of the models of the receiver arrays. And we appreciate Kristopher A. Innanen, and Bogdan Nita for their help in the preparation of the paper and valuable discussions. We are grateful to the sponsors of M-OSRP for supporting this project.

References

1. Aki, K. and Richards, P., Quantitative Seismology, 2002
2. Amundsen, L., B.G. Secrest and B. Arntsen, 1995, Extraction of the normal component of the particle velocity from marine pressure data: Geophysics, **60**, 212-222.
3. Amundsen, L.2001, Elimination of free-sruface related multiples without need of the source wavelet: Geophysics, **66**, 327-341.
4. Amundsen, L., Sten, T.R., Robertsson, J.O.A., Kragh, E., 2005, Rough-sea deghosting of streamer seismic data using pressure gradient approximations: Geophysics, **50**, v1-v9.
5. Barr, F.F. and Sanders, J.I., 1989, Attenuation of water column reverberations using pressure and velocity detectors in a water-bottom cable, 59th Ann. Internat. Mtg: Soc. of Expl. Geophys., 653-656.
6. Carvalho P.M., 1992, Free surface multiple reflection elimination method based on nonlinear inversion of seismic data, PhD Thesis, Universidade Federal da Bahia, Brazil (in Portuguese).
7. Guo, Z., Weglein, A.B. and Tan H., 2005, The receiver array effect on wavelet estimation, M-OSRP annual report.

8. Guo, Z., Weglein, A.B., 2005, A new source wavelet estimation method, in preparation.

9. Osen, A., B.G. Secrest, L. Admundsen and A. Reitan, 1998, Wavelet estimation from marine pressure measurements: Geophysics, **63**, 2108-2119.

10. Schneider, W.A., Larner, K.L., Burg, J.P., and Backus, M.M., 1964, A new data processing technique for the elimination of ghost arrivals on reflection seismograms: Geophysics, **29**, 5, p. 783-805.

11. Shaw, S. and Weglein, A.B., 2004, A leading order imaging series for prestack data acquired over a laterally invariant acoustic medium, Part I: Derivation and preliminary analysis, 2003 M-OSRP annual report.

12. Tan, T.H., 1992, Source signature estimation: Presented at the Internat. Conf. And Expo. Of Expl. And Development Geophys., Moscow, Russia.

13. Weglein, A.B., Gasparotto F. A., Carvalho P.M. and Stolt R.H. 1997, An inverse scattering series method for attenuating multiples in seismic reflection data, Geophysics, **62**, 1975-1989.

14. Weglein, A.B., and Secrest, B.G., Wavelet estimation for a multidimensional acoustic or elastic earth, Geophysics, **55**, 902-913.

15. Weglein, A.B., S.A. Shaw, K.H. Matson, J.L. Sheiman, R.H. Stolt, T.H. Tan, A. Osen, G.P. Correa, K.A. Innanen, Z. Guo and J. Zhang, 2002, New approaches to deghosting towed-streamer and ocean-bottom pressure measurements, 72nd SEG Annual Meeting, Salt Lake City, Utah.

16. Weglein, A.B., Shaw, S.A., Matson, K.H., Sheiman, J.L., Tan, T.H., Osen, A., Correa, G., Innanen, K.A., Guo, Z., and Zhang, J., 2002, New approaches to deghosting towed-streamer and ocean-bottom pressure measurements, 72nd SEG abstract, 1016-1019.

17. Weglein, A.B., Araújo, F.V., Carvalho, P.M., Stolt, R.H., Matson, K.H., Coates, R.T., Corrigan, D., Foster, D.J., Shaw, S.A.and Zhang, H., 2003, Inverse scattering series and seismic exploration, Inverse Problems, **19**, R27-R83.

18. Zhang, J. and Weglein, A.B., 2003, Deghosting of towed streamer and ocean bottom cable data, M-OSRP annual report.

19. Zhang, H. and Weglein, A.B., 2004, Target identification using the inverse scattering series; data requirements for the direct inversion of large-contrast, inhomogeneous elastic media, 2003 M-OSRP annual report.

General References

20. Amundsen, L., 1993, Wavenumber-based filtering of marine point source data: Geophysics, **58**, 1335-1348.

21. Ball, V.L. and Corrigan, D., 1996, Dual sensor summation of noisy ocean-bottom data, 66th Ann. Internat. Mtg: Soc. of Expl. Geophys., 28-31.

22. Delima, G.R., Weglein, A.B., Porsani, M.J., and Ulrych, T.J., 1990, Robustness of a new source-signature estimation method under realistic data conditions: A deterministic-statistical approach: 60^{th} Ann. Internat. Mtg. SOc. Expl. Geophys. Expanded Abstracts, 1658-1660.

23. Dragoset, B., and Barr, F.J., 1994, Ocean-bottom cable dual-sensor scaling: 64^{th} Ann. Internat. Mtg. SOc. Expl. Geophys. Expanded Abstracts, 857-860.

24. Fokkema, J., and van den Berg, P.M., 1993, Seismic applications of acoustic reciprocity: Elsevier Science Publ..

25. Liu, F., Nita, B.G., Weglein, A.B. and Innanen, K.A., 2004, Inverse scattering series for laterally-varying media, 2003 M-OSRP annual report.

26. Robertsson, J.O.A. and E.Kragh, 2002, Rough sea deghosting using a single streamer and a pressure gradient approximation: Geophysics, **67**, 2005-2011

27. Sϕnneland, L. and Berg, L.E., 1985, A new method for separating wavefields into up- and downgoing componenets. Presented at the 47th Mtg., Eur.Assn.Geosci.Eng.

28. Tan, T.H., 1999, Wavelet spectrum estimation: Geophysics, **64**, 6, 1836-1846

29. Weglein, A.B., and Secrest, B.G., 1990, Wavelet estimation for a multidimensional acoustic or elastic earth: Geophysics, **55**, 902-913.

30. Ziolkowski, A., 1980, Source array scaling for wavelet deconvolution: Geophysical Prospecting, **28**, 902-918

Appendix: Numerical test procedures

In this appendix, we would like to briefly list the steps that we performed in deghosting and FSMR.

Deghosting:

1.$D(x_g, z_g, x_s, z_s, t) \rightarrow D(x_g, z_g, x_s, z_s, \omega)$;

2 f by f:

Predict $P(x_g, z_1, x_s, z_s, \omega)$ and $\frac{\partial P(x_g, z_1, x_s, z_s, \omega)}{\partial z}$, where $z_s < z_1 < z_g$;
Predict the up-going field at the receiver side $P(x_g, z_2, x_s, z_s, \omega)$, where $z_2 < z_1$;
Switch the source and receiver coordinates: $x_g \Leftrightarrow x_s$,$z_2 \Leftrightarrow z_s$: $P(x_g, z_2, x_s, z_s, \omega) \rightarrow P(x_s, z_s, x_g, z_2, \omega)$;
Predict $P(x_s, z_3, x_g, z_2, \omega)$ and $\frac{\partial P(x_s, z_3, x_g, z_2, \omega)}{\partial z}$, where $0 < z_3 < z_s < z_2$;
Predict the up-going field at the source side $P(x_s, z_4, x_g, z_2, \omega)$, where $0 < z_4 < z_3 < z_s < z_2$;
Switch the source and receiver coordinates: $x_g \Leftrightarrow x_s$,$z_4 \Leftrightarrow z_2$: $P(x_s, z_4, x_g, z_2, \omega) \rightarrow P(x_g, z_2, x_s, z_4, \omega)$;

3. Fourier transform back to time domain: $P(x_g, z_2, x_s, z_4, t)$

Free Surface Multiple Removal (FSMR):

The input of the FSMR is the deghosting result: $P(x_g, z_g, x_s, z_s, \omega)$

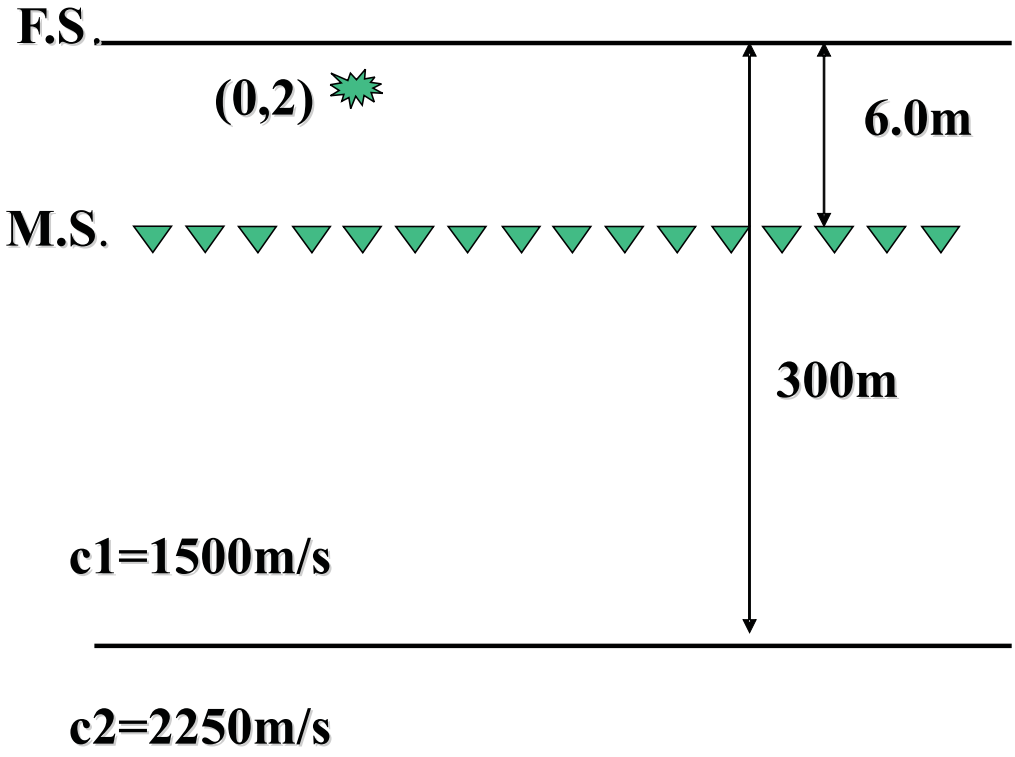

Figure 1: *One dimensional acoustic constant density medium.*

1.$P(x_g, z_g, x_s, z_s, \omega) \rightarrow P(k_g, z_g, k_s, z_s, \omega)$;

2.Calculate the integrand of Eq. (5) and do the summation in Eq. (6);

3.$P(k_g, z_g, k_s, z_s, \omega) \rightarrow P(x_g, z_g, x_s, z_s, \omega)$;

4.Fourier transform back to time domain: $P(x_g, z_g, x_s, z_s, t)$

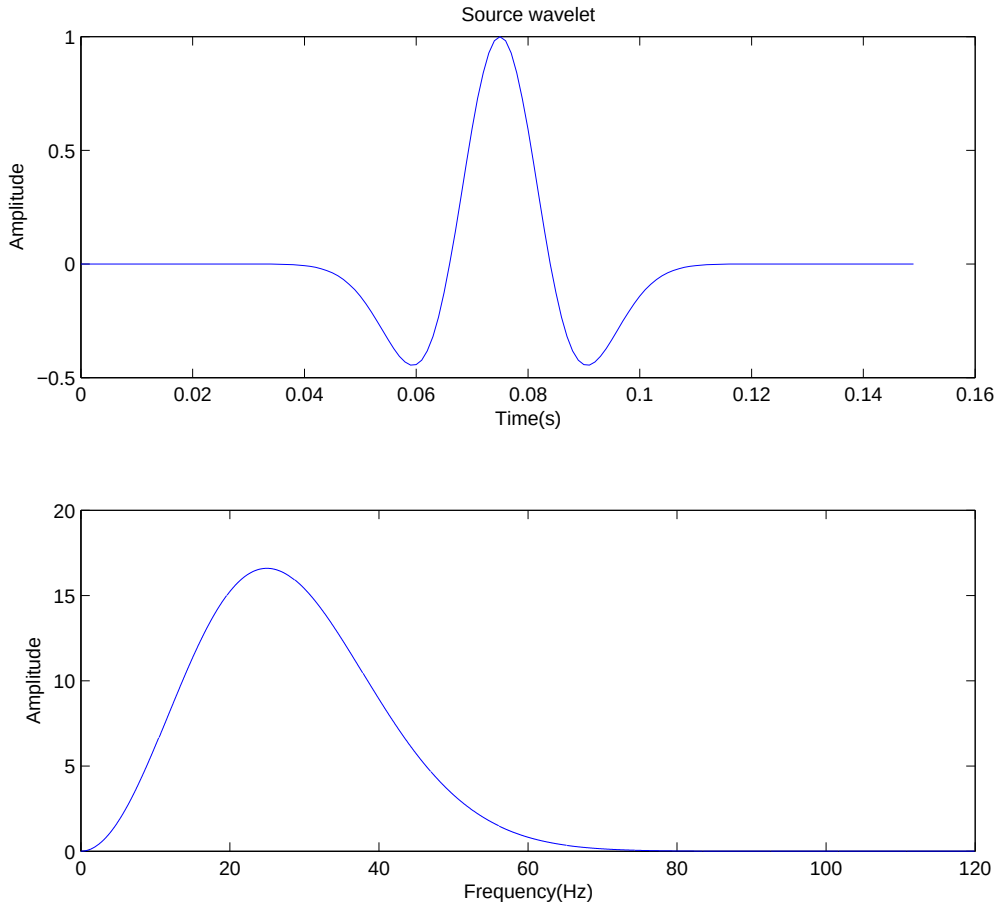

Figure 2: *The Ricker source wavelet.*

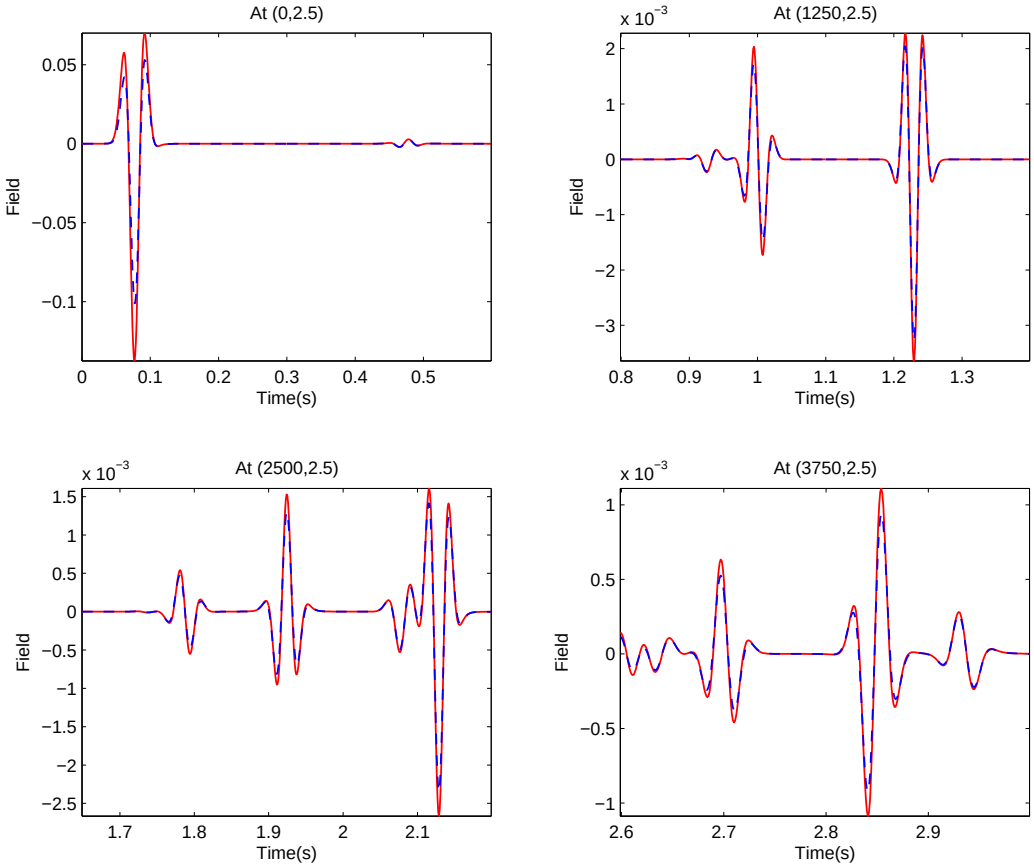

Figure 3: *Red solid: Point receiver data; Blue dash: Receiver array data.*

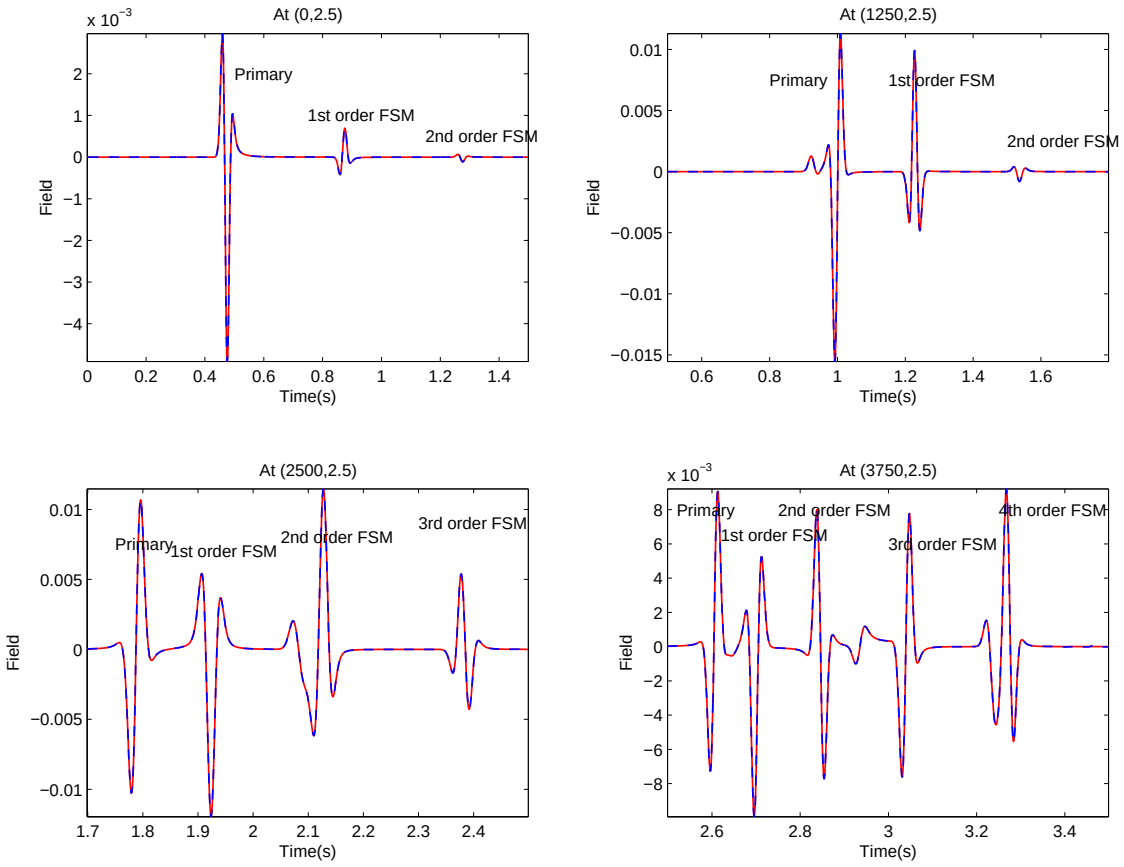

Figure 4: *Red solid: Exact source-receiver deghosted results; Blue dash: Calculated deghosting results (using point receiver data).*

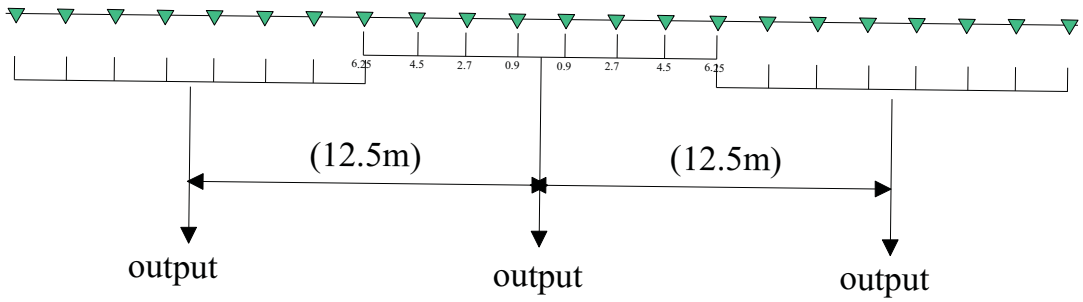

Figure 5: *Diagram of Guardian receiver array.*

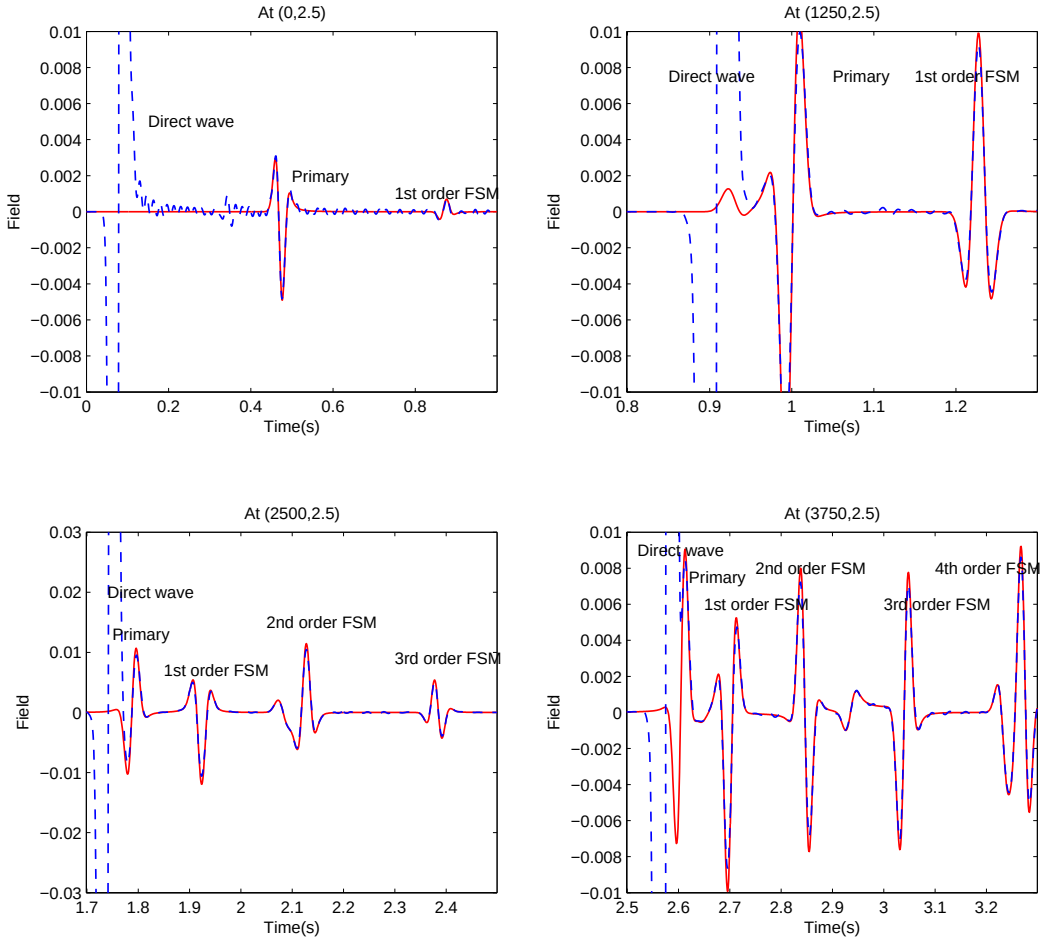

Figure 6: *Red solid: Exact source-receiver deghosted results; Blue dash: Calculated deghosting results (using receiver array data).*

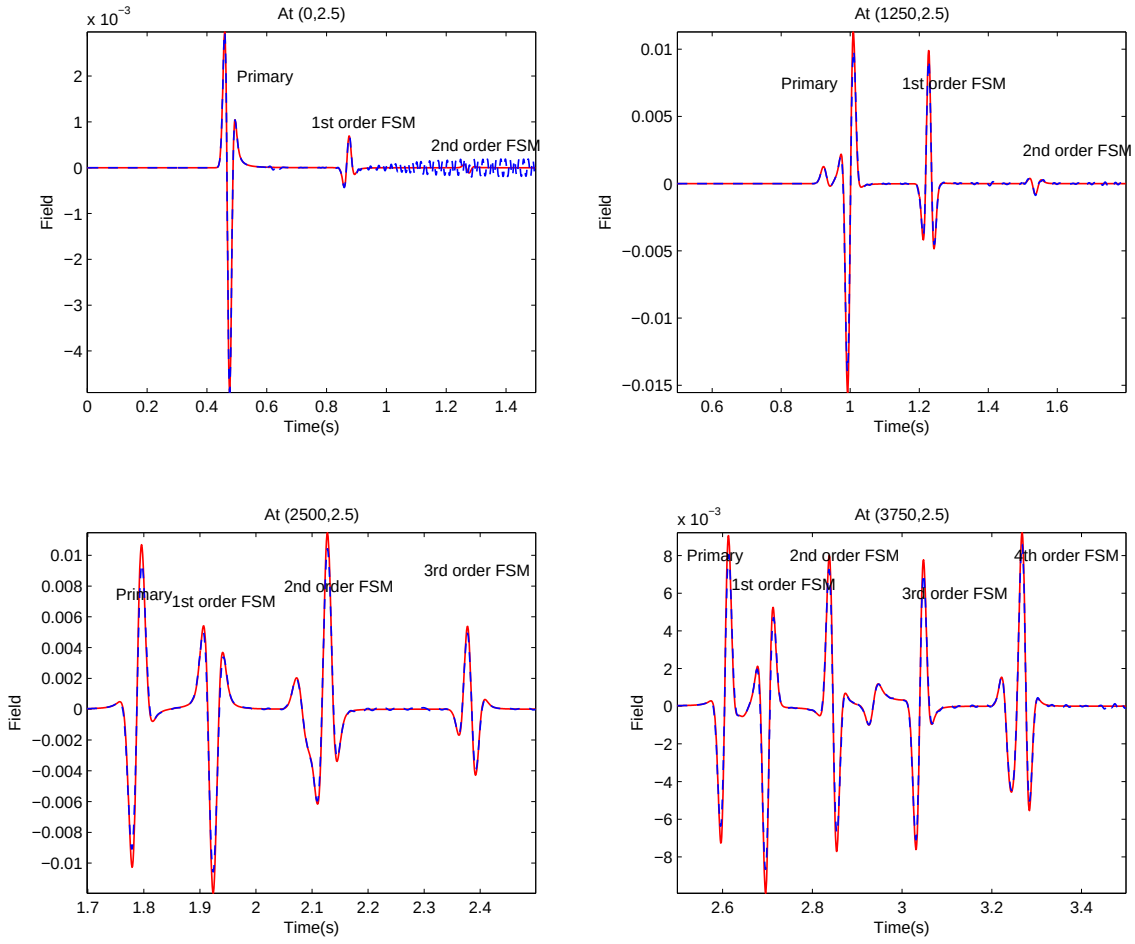

Figure 7: *Red solid: Exact source-receiver deghosted results; Blue dash: Calculated deghosting results (using receiver array data after the elimination of the direct wave).*

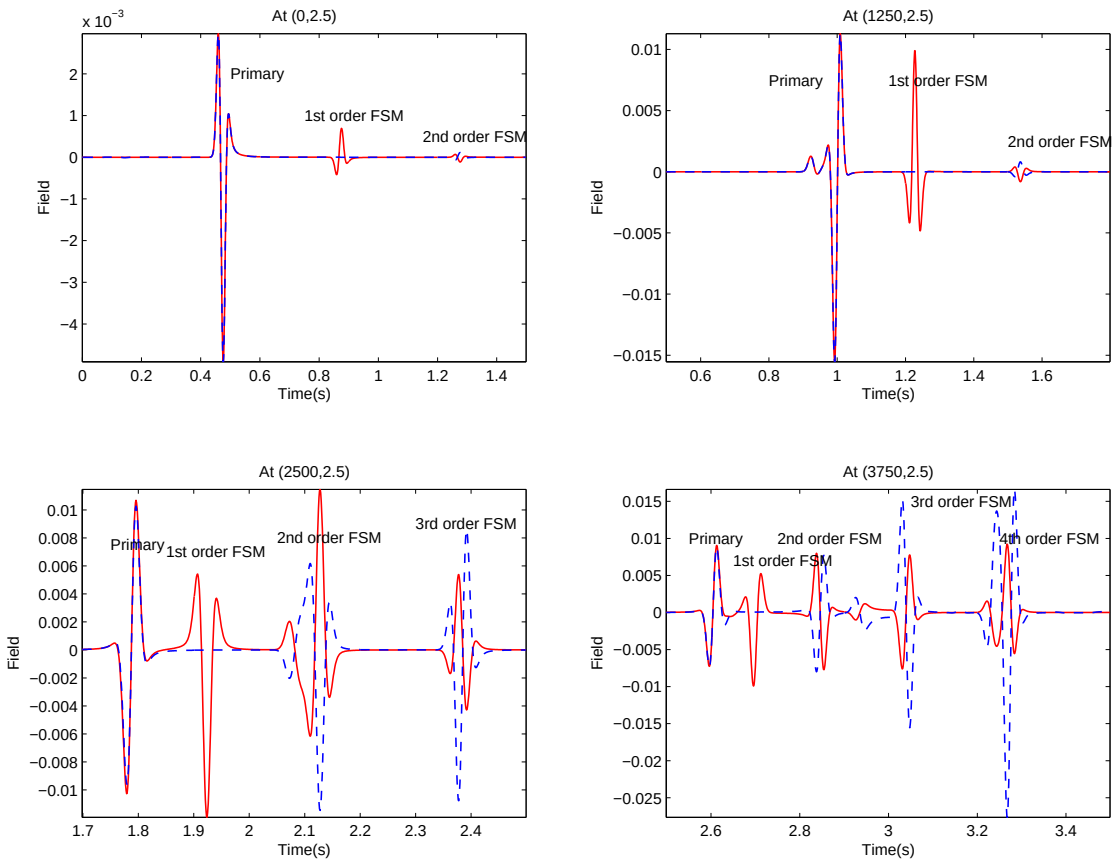

Figure 8: *Red solid: Exact source receiver deghosted data; Blue dash: After the first order FSMR (Using point receiver data).*

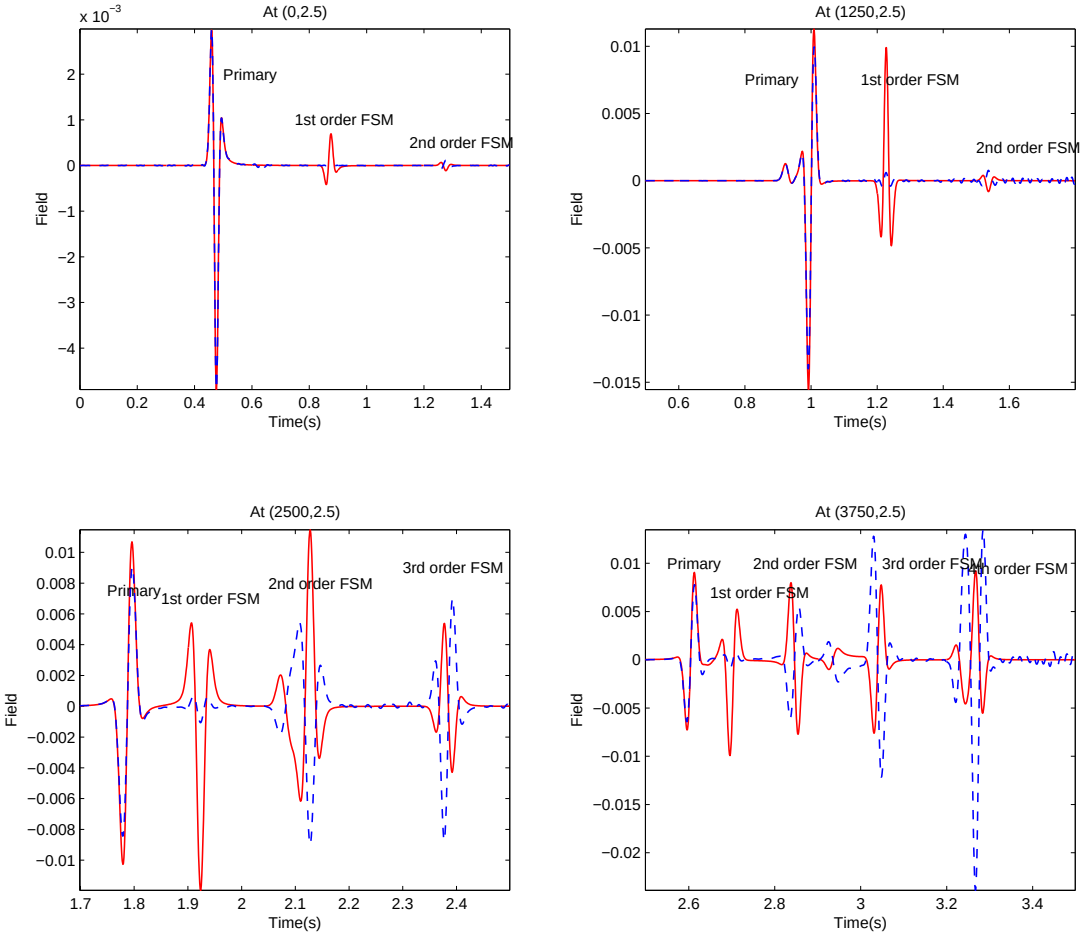

Figure 9: *Red solid: Exact source receiver deghosted data; Blue dash: After the first order FSMR (Using receiver array data).*

Society of
Exploration
Geophysicists

MULTIPLE ATTENUATION

Edited by
Arthur B. Weglein
William H. Dragoset, Series Editor

Daniel Ebrom *Geophysics Reprint Series*

Preface

Papers selected for this SEG reprint volume on multiple attenuation sample the geophysical literature from 1948 through 2003. For the past fifty-odd years the presence of multiply reflected energy in seismic data has been a serious issue and challenge for geophysicists. It remains so today. Nevertheless, the seismic exploration community has made dramatic progress in multiple attenuation. This volume chronicles and examines the amazing history and evolution of methods for attenuating multiples. The papers are organized into nine thematic chapters, and appear chronologically (sometimes within subtopics) within each.

The volume begins with a short introduction to some basic concepts of multiple attenuation. Next, Chapter 1 focuses on the era when multiple reflections in seismic data were first clearly seen and characterized. Interestingly, prior to the late 1940's many geophysicists thought that multiples were so weak that they would never be seen at all, much less be a significant problem. Chapter 2 describes some of the first efforts at attenuating multiples – signal processing algorithms that deconvolve or otherwise remove periodic events in seismic traces – as well as some more recent developments using such approaches. In contrast, the papers in Chapter 3 describe methods that attenuate multiples based on moveout discrimination or some other event characteristic that distinguishes them from primary reflections. Papers describing the popular Radon transform-based method of multiple attenuation appear in this chapter.

Chapters 4 and 5 describe two categories of multiple attenuation methods that are directed at accommodating a fully multi-dimensional subsurface: (1) linear methods of modeling and subtracting multiples that require an explicit or implicit model of the reflections that generate multiples; and (2) nonlinear methods that do not require such a model. The latter of these represents a major conceptual advance: the idea that, using nonlinear multi-dimensional wave equation-based methods, multiple reflections can be fully predicted from the information contained within a seismic data set independently of any assumptions or knowledge about the subsurface. Once so predicted, multiples can be subtracted from the original data, yielding a multiple-free result. Because practical applications based on this idea are relatively new, many geophysicists who read this volume may not have been exposed to it during their formal education. Hence, following our Chapter 4 introduction we have included a brief tutorial section that explains the basic concepts of this type of multiple prediction.

There are two complementary ways of thinking about nonlinear wave equation-based multiple prediction. Chapter 4 covers the free-surface and interface model, and Chapter 5 the free-surface and point scatterer model. Compared to earlier methods of multiple attenuation, these multiple prediction schemes place certain conditions on the seismic experiment rather than requiring assumptions about the nature of the subsurface. For example, the source signature must be known, and, as in migration, the data set aperture becomes important. The papers in Chapter 6 discuss some of the consequential difficulties and issues that must be dealt with to make nonlinear wave equation-based multiple prediction practical for field data sets. In particular, many of the Chapter 6 papers describe ways of coping with the 3-D nature of the primary and multiple wavefields when the acquisition experiment itself is not spatially sampled in a full 3-D sense.

The words "multiple attenuation" immediately make many geophysicists think of marine streamer data. Chapter 7 reminds us that multiples are also an important problem for land data sets and marine data recorded by methods other than horizontally towed streamers. Chapter 8 contains a collection of tutorial papers that emphasize recent multiple attenuation concepts and methodologies.

Finally, Chapter 9 presents an alternative approach to dealing with multiple reflections – using them as signal to enhance the subsurface image rather than considering them as noise that must be removed. The serious challenges facing such an endeavor are also described.

Editors of a reprint volume usually face two dilemmas: what criteria are used to select the papers and how many papers should be included. Paper selection was difficult – and necessary – because no reprint volume could contain all the worthy papers on a subject as broad as multiple attenuation. Except for Chapters 1 and 9, we decided to include only papers that directly address the attenuation of multiples. This basic criterion meant that papers about technology that could be used for multiple attenuation, but that contained little or no discussion of multiple attenuation itself, were not selected. Thus, for example, no papers on the fundamentals of the Radon transform appear in this volume. Having established the basic criterion, we then selected papers that we considered to be important and influential. We also polled some of our colleagues and acquaintances for suggestions, especially for early papers about multiple attenuation. Finally, we scanned through the references of selected papers, searching for additional papers that those authors had considered important.

Our objective in this volume is to collect, synthesize, and provide a perspective for the literature on multiple attenuation, an important cornerstone of seismic data processing. Not all of the papers in this volume received a traditional peer review prior to their original publication. In recent years papers in *The Leading Edge*, *First Break*, and the SEG and EAGE *Expanded Abstracts* have formed an increasingly important repository of technical literature. We feel – and we hope that the readers will agree – that including papers from those sources falls within our objective.

Acknowledgments

We thank the authors and the previous publishers for their permissions to reproduce the papers, and reprint series editor Dan Ebrom for his suggestions. Others who contributed suggestions and deserve our thanks include Sven Treitel, Tad Ulrych, Clement Kostov, and Ken Matson. We give special thanks to Simon Shaw for sharing his technical insights and helping with the manuscript preparation. We also are grateful to (insert SEG Publication Staff names here) for their support in publishing this volume.

Art Weglein and Bill Dragoset
May 2004

Volume Introduction

Most of the papers in this reprint volume address the problem of multiple reflections that appear in marine seismic data. In seeking to analyze such data, it helps to classify the recorded events according to the reflections and propagations they have experienced. For typical towed streamer exploration, both the seismic source and the receivers are deployed within the water layer. Figures 1, 2, and 3 show examples of various classes of events for streamer data. The first classification separates events that have experienced the earth's subsurface below the water layer from those that have not. The latter category (Figure 2a) consists of two events:

- the direct arrival, which is energy that travels in a straight-line path from source to receiver, and
- the direct arrival ghost, which is energy that propagates upwards from the source, reflects off the water surface, and then straight to the receiver.

All other recorded events either propagate within the earth or at least encounter the earth at the water bottom. (Seismic energy can reflect from sharp velocity or density contrasts within the water layer. This happens only rarely, so such events are not considered in the classification scheme described here.)

The category of events that experience the earth includes reflections, refractions, diffractions, mode conversions, and an infinite variety of combinations thereof. These events can be further subdivided into two main categories:

- events that propagate downwards from the source and are recorded as up-going waves at a receiver, and
- events that either propagate upwards from the source and/or are recorded as down-going waves at a receiver.

These latter events are called ghosts, of either source or receiver variety, respectively (Figure 2).

Excluding the ghosts, the remaining reflection events can be classified as either primary or multiple depending on the number of upward reflections experienced:

- primary events experience one upward reflection (Figure 1a), and
- multiple events experience two or more upward reflections (Figures 1b-1f).

Here, an upward reflection is defined as one where the incident wave moves away from the measurement surface (that is, the streamer) towards the reflector and the reflected wave moves away from the reflector towards the measurement surface. The incident wave in a downward reflection moves towards the measurement surface and then away from the measurement surface after reflection. Reflections are possible that are neither upward nor downward by these definitions. An example is shown at the right-hand side of Figure 3a. Nevertheless, traditionally, primaries and multiples are defined only in terms of the number and location of upward and downward reflections in their raypaths. The event in Figure 3a has one upward reflection, no downward reflections, and one reflection that is neither; hence, it is a primary.

The final classification defines particular types of multiply reflected events based on the location of their downward reflections:

- A multiple with one or more downward reflections at the free surface (that is, the water surface) is called a free-surface multiple, independent of the rest of its trajectory.
- An internal multiple has all of its downward reflections below the free surface.

Interbed multiple is a common alternative name for internal multiple. Note that although source and receiver ghosts are free surface-related events that experience a downward reflection at the free surface, they do not qualify as free-surface multiples because they were excluded at an earlier step in the classification scheme.

Interbed multiple is a common alternative name for internal multiple. Note that although source and receiver ghosts are free surface-related events that experience a downward reflection at the free surface, they do not qualify as free-surface multiples because they were excluded at an earlier step in the classification scheme.

Sound waves in the earth sometimes experience more complicated raypaths than alternating up and down reflections. For example, events that do not easily fit into the classes described above include those that experience refractions or diffractions within their history. The event in Figure 3b has only one upward reflection, but that event is clearly not a primary. The need to accommodate a broader range of events, coupled with advances in multiple attenuation theories and algorithms, suggests the need for more general definitions:

- A prime event (or primary) is a recorded event that cannot be decomposed into other events recorded within the same data set.
- A composite event (or multiple) is a recorded event that can be decomposed into a number of other events that appear within the same data set.

The phrases "can be decomposed" and "cannot be decomposed" refer to whether or not the travel time of the event in question can be expressed as sums and differences of the travel times of other events within the data set (see Figure 3). The concept of "data set" refers to a complete set of shot records that spans sufficient spatial aperture to record all of a multiple's composite events. Note that the decomposition of higher-order multiples can be accomplished in more than one way, and can include events that are themselves multiples. For example, the multiple in Figure 3f can be decomposed into primary events 1-3, 2-3, 2-4, and 4-5 or alternatively into a multiple event, 1-4, and a primary event, 4-5. This more general scheme of classifying primary and multiple events becomes important in Chapters 4 and 5, which include comprehensive methods that attenuate all events that are composites within the measurement set, including event types beyond the simple upward/downward reflection definition. Further details are presented in the Chapter 4 tutorial.

In the literature, one finds mention of multiple attenuation, elimination, and suppression. Generally, these terms are used interchangeably. In this volume, however, we assign specific definitions to these terms. Attenuation and suppression are synonyms that refer to a process in which the amplitudes of the multiple events in a seismic data set are reduced. Elimination refers to a process in which at least one class of multiples is completely removed from a seismic data set. Thus, elimination is a form of attenuation in which the amplitude reduction is complete. This distinction is important. Some multiple removal algorithms are, at least in principle, eliminators, while others are only attenuators. There is also an important and increasingly significant difference between an explicit prediction of amplitude and phase (time) of a multiple and the assumption that whatever falls on a given traveltime trajectory is a multiple to be eliminated. In practice even an elimination algorithm usually accomplishes only partial multiple removal because field data sets seldom meet all of the prerequisites for elimination. This is an important issue, but it is unrelated to the intrinsic capability of the algorithm. The distinction between the intrinsic capabilities of a method and limitations imposed on those capabilities by external factors (such as data collection, subsurface assumptions, etc.) is important for two reasons: an understanding of when application

of a procedure is appropriate, and clarity in attributing lack of effectiveness to the proper cause, thereby guiding those seeking better methods in the future.

In geophysics, as in all fields of science, progress sometimes appears to be somewhat chaotic. Over a period of many years, however, an evolutionary pattern often emerges from the chaos. Table 1 shows such a pattern for the discipline of multiple attenuation. The leftmost column lists advances in the evolution of multiple attenuation that are presented in Chapters 2 through 5 of this volume. The next column indicates the complexity and realism of the physical models that the attenuation methods can accommodate. More checks indicate higher complexity, realism, and completeness of the physics behind the method. For example, algorithms that attenuate multiples based on periodicity are based on a simple 1-D model of the subsurface, whereas moveout discrimination methods are based on a more complex 2-D ray-tracing model. Together, these two columns represent an overall trend: more complete, realistic physics allows significant advances, and hence improvements, in multiple attenuation. Such improvements reduce the risk of producing poor quality processed seismic data sets, and thus, ultimately, lower the overall risk of hydrocarbon exploration itself. The third column ranks the complexity of the ancillary subsurface information needed by each multiple attenuation method. For example, moveout discrimination requires a nominal velocity profile, and, if one wishes to attenuate selected interbed multiples, the free-surface and interface wavefield method requires specification of a multiple-generating horizon or region. The fourth column describes the need for description of the seismic experiment, such as information about the source signature and the receiver depths. Finally, the rightmost column indicates the data acquisition and computational burden of each method.

Table 1 shows that as the complexity of the physical model that a method can accommodate increases, the burden on data acquisition and processing likewise increases. Simply accommodating a higher dimension of variability in the subsurface requires more thorough surface data acquisition, regardless of the nature of the seismic processing algorithm. Consider the bottom row in the table. Applying a true 3-D version of the free-surface and point scatterer method to attenuate all multiples requires not only a massive computational effort, but also wide-aperture, full-azimuth recorded data. A skeptic, then, might be inclined to ask, "Why develop such an algorithm?" The short answer to this question can be found two rows up the table. When development of the 2-D free-surface and interface model began in earnest during the 1980's, the skeptic, justifiably, could have asked the same question. Yet today, many years later, that technology is being used routinely to process data from large marine streamer 3-D surveys. This example teaches an important lesson for everyone in the exploration geophysics business: *If a method is discovered that solves an important problem, eventually computational technology and data acquisition practices will evolve to a point that makes that method practical.* This is the nature of progress in the science of seismic exploration.

An interesting, and perhaps counterintuitive, aspect of recent advances in multiple attenuation is that the complexity of the required ancillary subsurface information and, more broadly, the necessary assumptions about the earth's subsurface do not increase as the attenuation algorithms reach their ultimate sophistication. Instead, these new algorithms shift the responsibility for providing detailed subsurface information upwards to the data acquisition at the surface. That shift has an important practical implication – success at removing multiples is no longer limited by uncertainty in subsurface assumptions and information, but instead by the effort one is willing to expend on data acquisition and processing. Prior to these new developments, success in removing multiples was not necessarily commensurate with money spent. With the new technology, however, an Ex-

ploration and Production company interested in paying more to achieve better multiple attenuation has that option.

Table 1 could have had many more columns and rows. For example, we could have listed the advantages and disadvantages of each method, their success or failure at attenuating different types of multiples, the years during which the methods were first proposed and then widely practiced, and so on. However, doing that would have spoiled some of the fun readers of this volume will have discovering or rediscovering the history of multiple attenuation.

Multiple attenuation method	Subsurface complexity and reality that method can accomodate	Requirement for ancillary subsurface information and interpretive intervention	Requirement for the description of seismic experiment (e.g., source signature)	Requirements on data acquisition, reconstruction, regularization and computation
Deconvolution based on periodicity of multiples	*	*	*	*
Moveout discrimination methods	**	**	*	**
Free-surface and interface model, 2-D and pseudo 3-D	***	*	***	***
Free-surface and point scatterer model, 2-D and pseudo 3D	****		***	****
Free-surface and interface *and* free-surface and point scatterer models, true 3-D	*****		***	******

Table 1: Major stages in the evolution of multiple attenuation.

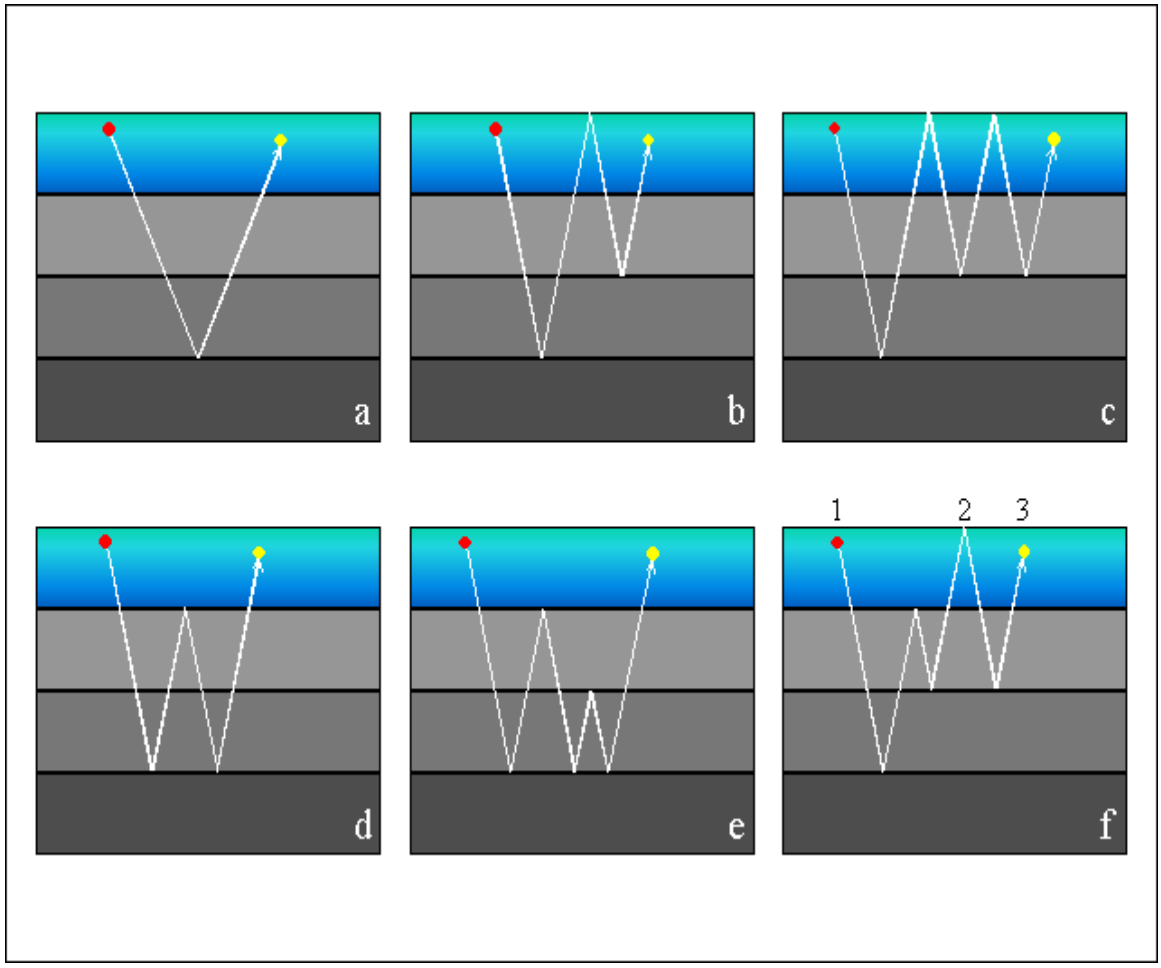

Figure 1: *Traditional definition of primary and multiple events. The blue-green area represents the water layer. The red and yellow dots indicate the positions of seismic sources and receivers, respectively. The white lines are raypaths of the events being defined. For the sake of simplicity in the figure, the rays do not refract as they cross reflecting horizons.*

a) A primary event has one upward reflection.

b) A multiple event has at least two upward reflections. This example is a 1^{st}-order free-surface multiple because it has a single downward reflection generated by the water surface.

c) A 2^{nd}-order surface multiple.

d) This event is a 1^{st}-order internal multiple because the generating horizon that produces the downward reflection is located in the subsurface.

e) A 2^{nd}-order internal multiple.

f) Hybrid event 1-3 is classified as a free-surface multiple. Even though one generating horizon is below the surface, an algorithm that attacks free-surface multiples will attenuate this event. However, event 1-2, an internal multiple, will remain in the data set after surface multiple attenuation.

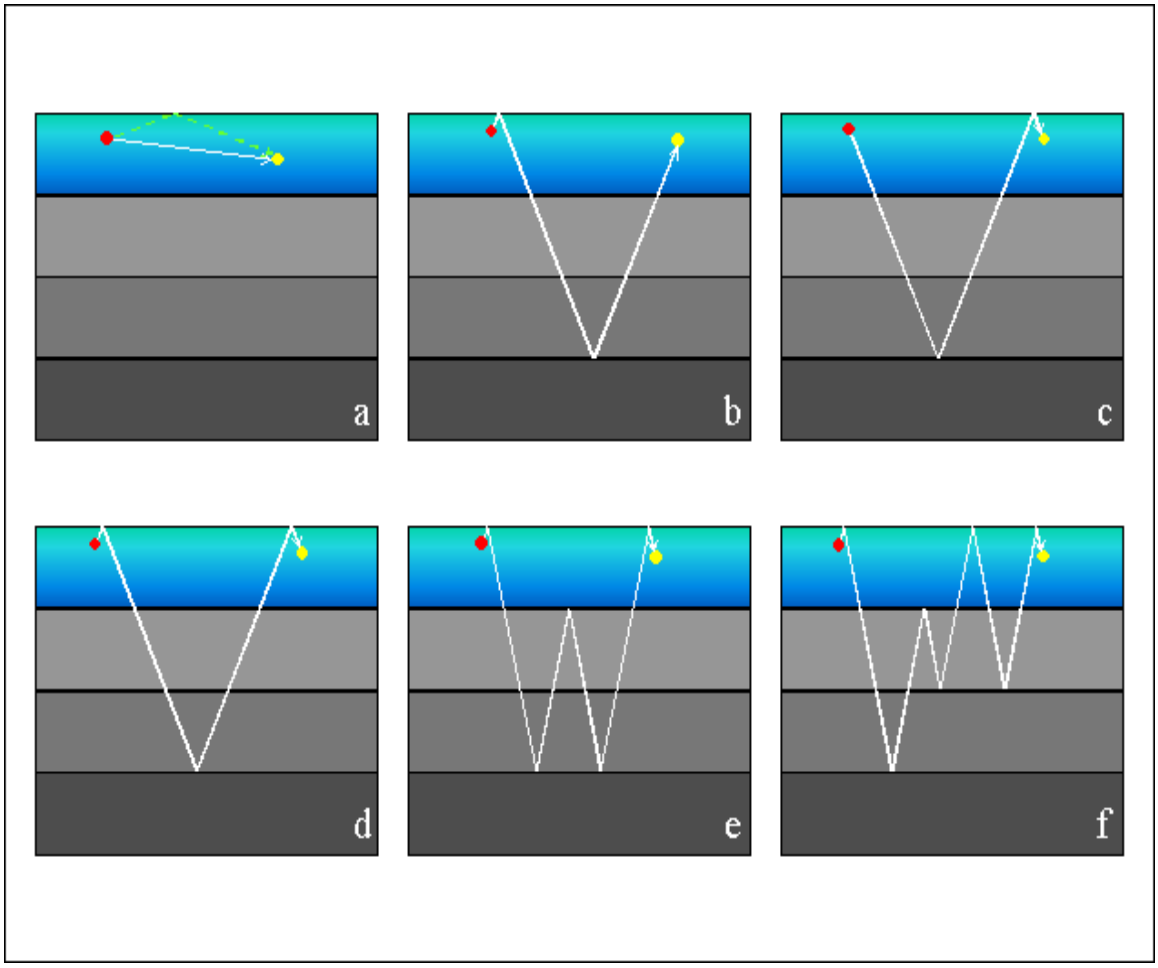

Figure 2: *Definition of direct arrivals and ghosts. The blue-green area represents the water layer. The red and yellow dots indicate the positions of seismic sources and receivers, respectively. The white and green lines are raypaths of the events being defined. For the sake of simplicity in the figure, the rays do not refract as they cross reflecting horizons.*
a) A direct arrival (white) and its ghost (green).
b) A source ghost.
c) A receiver ghost.
d) A primary reflection with both a source ghost and a receiver ghost.
e) 1^{st}-order surface multiple reflection with both ghosts.
f) 2^{nd}-order multiple reflection with both ghosts. Usually, removal of direct arrival and ghost events during seismic data processing is a separate issue from attenuating multiples.

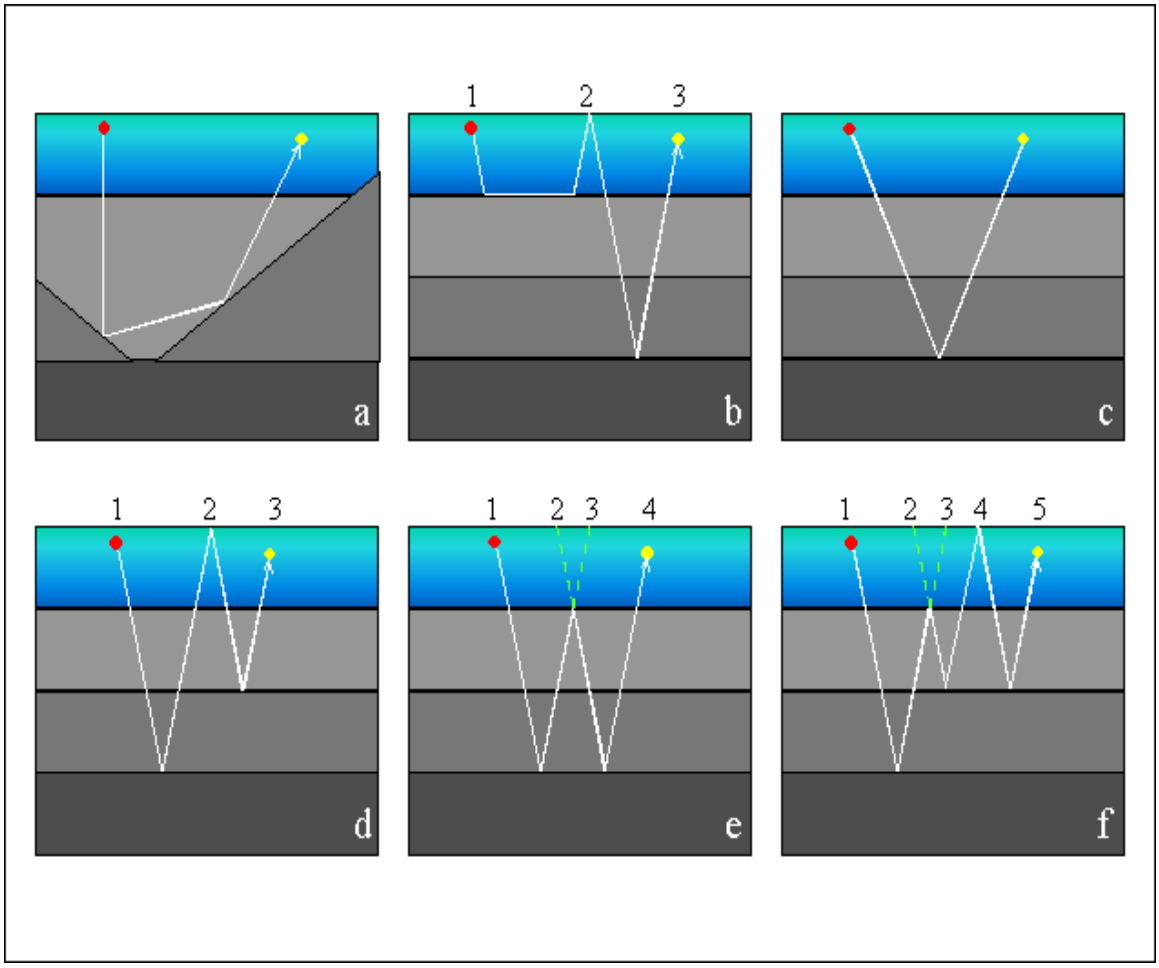

Figure 3: *A more general definition of a multiple is: a recorded event that can be decomposed into a number of other recorded events. The dashed green lines in e) and f) represent events whose travel times are subtracted to obtain the multiple's travel time (see below).*

a) This event is classified as a primary because it cannot be decomposed into other events.

b) In the traditional classification this event is a primary because it has only one upward reflection. The more general definition classifies it as a multiple since it can be divided into two other recorded events, event 1-2 and event 2-3.

c) This event is a primary reflection. It cannot be decomposed into other recorded events.

d) This event is a multiple because it can be divided into two other recorded events: the primary reflections 1-2 and 2-3. The travel time of the multiple is the sum of the travel times of the two primaries.

e) An internal multiple composed of events 1-3, 2-3, and 2-4. The multiple's travel time is the sum of the travel times of events 1-3 and 2-4, minus the travel time of event 2-3.

f) Another multiple. The sum of travel times 1-3, 2-4, and 4-5, minus travel time 2-3 gives the multiple's travel time.

Chapter 1

Historical papers: characteristics of multiples

From today's perspective the January 1948 issue of *Geophysics* makes for fascinating reading. The topic of that issue was multiple reflections – not so much about how to attenuate them, but rather about whether they even existed in seismograms recorded on land. Consider, for example, the very first sentence in the first paper of this volume: "On several occasions ... various geophysicists have expressed ... doubt regarding the existence of multiple reflections ..." *(Dix, 1948)*. Dix went on to argue in favor of the existence of multiples, but in the end he conceded "The evidence ... does not yet make their existence 'strictly certain' ..." *Hansen (1948)*, however, had no doubts about the existence of multiples. He reports identifying them by their low average velocities in reflection velocity profiles from Argentina. Interestingly, the translator of Hansen's paper from its original Spanish had to remove the paper's "slightly defensive tone," which he attributed to the fact that "... when Mr. Hansen's paper was originally published ... few geophysicists and fewer executives reacted favorably to the idea that multiple reflections could be of any practical importance in seismograph exploration ..."

Many of the papers in the January 1948 issue of *Geophysics* were presented orally two years earlier at a symposium during the SEG's 1946 meeting in Los Angeles. The lead paper of that symposium *(Ellsworth, 1948)* presents solid evidence of multiple reflections in seismic records from Sacramento Valley, California. Ellsworth also describes several kinds of multiples, naming them Type 1, Type 2, and Type 3. Today geophysicists call those types surface multiples, peg-leg multiples, and near-surface multiples. *Johnson (1948)* presents indisputable evidence from Butte County, California of multiple reflections between a basalt layer and the bottom of the weathering zone. Even those geophysicists of the 1948 era who believed that multiples were present apparently were not too concerned. For example, Ellsworth concluded his paper with the statement "... the multiple-reflection question as a whole does not seem to present a serious limitation to seismograph interpretation except in isolated cases." One exception to that widely held viewpoint was Johnson's, who perhaps had a glimmer of the future when he wrote in his paper's conclusion "Thus a highly suspicious attitude toward *every* reflection in areas known to return *some* multiple reflections seems to be justified."

In marine seismograms geophysicists often observed a mysterious phenomenon dubbed "sing-ing". As reported by *Burg et al. (1951)* and later by *Werth et al. (1959)* and *Levin (1962)*, singing marine seismograms were dominated by sinusoidal, nearly constant frequency energy. Singing was clearly a localized phenomenon, often appearing and then disappearing several times along the length of a single seismic line. Burg et al. analyzed some examples of singing and explained them theoretically by considering the water layer as a seismic wave guide within which normal modes of propagation were produced by constructive interference. Werth et al. describe the recording and analysis of an experiment designed to reveal the cause of singing. They concluded that, at least in their test area, singing was caused by short-period multiple reverberations in the water layer rather than by a wave guide-like excitation of the water layer by the seismic source. Levin's paper describes an experiment to understand the seismic properties of Lake Maracaibo, which even today has a reputation for producing seismic records that are difficult to process and interpret. Levin found that singing was associated with areas having a high water-bottom reflection coefficient caused by low velocity in gas-saturated bottom mud, a situation certainly conducive to multiple generation.

The papers in this chapter provide a history of significant pioneering and discovery. By their example, they serve to guide and encourage those striving for new scientific understanding.

Chapter 1 Papers

Dix, C.H., 1948, The existence of multiple reflections: Geophysics, **13**, 49-50.

Ellsworth, T.P., 1948, Multiple reflections: Geophysics, **13**, 1-18.

Hansen, R.F., 1948, Multiple reflections of seismic energy: Geophysics, **13**, 58-85.

Johnson, C.H., 1948, Remarks regarding multiple reflections: Geophysics, **13**, 19-26.

Burg, K.E., Ewing, M., Press, F. and Stulken, J., 1951, A seismic wave guide phenomenon: Geophysics, **16**, 594-612.

Werth, G.C., Liu, D.T. and Trorey, A.W., 1959, Offshore singing – field experiments and theoretical interpretation: Geophysics, **24**, 220-232.

Levin, F.K., 1962, Seismic properties of Lake Maracaibo: Geophysics, **27**, 35-47.

Chapter 2

Multiple attenuation based on a convolutional model

Multiple reflections have many properties that can distinguish them from primaries. The papers in this chapter discuss algorithms that, in essence, attenuate multiples by exploiting one of those properties, their periodicity. Multiply reflected energy is truly periodic only in a 1-D medium. Nevertheless, short-period multiples, such as those that occur in many shallow-water layer areas, are nearly periodic, making simple inverse filtering or deconvolution viable methods of eliminating such multiples. For example, in his classic paper about water reverberations *Backus (1959)* treats the effect of the water layer as an approximate linear filter, and subsequently removes the water-layer reverberations by convolving seismic traces with the inverse of that filter. *Goupillaud (1961)* presents a non-linear generalization of the inverse filter concept, which ideally removes the effect of reverberations in a shallow layer for either land or marine seismic data.

Watson (1965) proposes a simple 1-D scheme that models first-order surface multiples as the convolution of a reflectivity sequence with itself (with an adjustment for the surface reflection coefficient). This leads to an inverse equation for a multiple-free primary trace. Watson approximately solved that equation with a feedback loop procedure. *Anstey and Newman (1966)* discuss the auto-correlogram, which measures the periodicity of seismic traces, and the retro-correlogram (Watson's method under another name), which predicts multiples. They use the auto-correlogram to determine the presence of multiples and suggest, like Watson, the use of a feedback mechanism with the retro-correlogram to attenuate multiples. Many of the papers in Chapter 4 (e.g., *Berkhout and Verschuur, 1997*) discuss a multiple prediction method that is essentially a 2-D generalization of the idea in the Watson and Anstey and Newman papers. The differences are interesting. In Watson's equation (9), for example, the wavelet term $c_1(t)$ "approximates the additional filtering provided the multiples by their relatively longer paths in the more highly attenuating near-surface formations." In a 2-D prediction, such a term is not required because the prediction operator accounts for such effects automatically. Anstey and Newman recognized that their 1-D retro-correlogram did not produce accurate results for large offsets or dipping events. A 2-D prediction, on the other hand, does incorporate the effects of offset and dip. The paper by *Kunetz and Fourmann (1968)* offers two efficient schemes for computing 1-D-based multiple deconvolution operators.

The digital least-squares inverse filtering method known as predictive deconvolution is a widely used tool for attenuating periodic events in seismic traces. *Peacock and Treitel (1969)* explain the basic theory of predictive deconvolution and then discuss some practical issues. They also emphasize the key feature of predictive deconvolution: the ability to specify the prediction distance allows selective attenuation of repetitive waveforms that have some particular period. This makes the method ideal for eliminating periodic multiples from seismic traces.

The final three papers in this chapter extend the deconvolution approach to multiple attenuation to situations where the multiple reflections are not periodic. *Taner et al. (1995)* accomplish this by multichannel predictive deconvolution performed in the x-t domain. This paper is notable for its thorough introduction to the concept of multichannel deconvolution and how that approach is related to other multiple attenuation methods. *Lamont and Uren (1997)* introduce a "multiple moveout" procedure that makes multiples periodic, and follow that by "isostretch radial trace" to stabilize the wavelet in time. Together, the two transformations pre-condition multiple events to

make them suitable for a simple 1-D deconvolution. *Parrish (1998)* describes regularizing water-layer multiples spatially and temporarily by migrating the data using the water velocity. This makes single trace dereverberation more effective. After multiple attenuation residual migration relocates the remaining primary reflections to their final positions.

Overall, the papers in this chapter show that the convolutional model has provided tremendous practical value. Simultaneously, it planted the seeds that grew into multi-dimensional wave theoretic methods for dealing with multiple reflections (see, for example, *Riley and Claerbout (1976)* in Chapter 4).

Chapter 2 Papers

Backus, M.M., 1959, Water reverberations – their nature and elimination: Geophysics **24**, 233-261.

Goupillaud, P.l., 1961, An approach to inverse filtering of near-surface layer effects from seismic records, Geophysics, **26**, 754-760.

Watson, R.J., 1965, Decomposition and suppression of multiple reflections: Geophysics, **30**, 54-71.

Anstey, N.A. and Newman, P., 1966, The sectional auto-correlogram and the sectional retro-correlogram: Geophysical Prospecting, **14**, 389-426.

Kunetz, G. and Fourman, J.M., 1968, Efficient deconvolution of marine seismic records: Geophysics **33**, 412-423.

Peacock, K.L. and Treitel, S., 1969, Predictive deconvolution: theory and practice: Geophysics, **34**, 155-169.

Taner, M.T., O'Doherty, R.F. and Koehler, F., 1995, Long-period multiple suppression by predictive deconvolution in the x-t domain: Geophysical Prospecting, **43**, 433-468.

Lamont, M.G. and Uren, N.F., 1997, Multiple elimination using wavefield transformations off the coast of Western Australia: APPEA Journal, 777-785.

Parrish, J.F., 1998, Dereverberation after water migration: SEG Expanded Abstracts, 1325-1328.

Chapter 3

Multiple attenuation based on event characteristics

Aside from periodicity or near periodicity (see Chapter 2), multiple reflections can differ from primary reflections in other ways that can be exploited to attenuate them. Chief among these is differential moveout. For some seismic data sets simple CMP stacking is effective at reducing the amplitudes of multiples. In the words of Harry Mayne, inventor of the CMP method, "reflections which follow the assumed travel paths are greatly enhanced, and other events are reduced" (*Mayne, 1962*). When stacking alone is insufficient, better separation of primary and multiple events can be achieved by weighted stacking. *Schneider et al. (1965)* demonstrate a method of weighted stacking where the weights are determined by prestack application of optimal filters designed by a multichannel least-squares method. *Schoenberger (1996)* presents an excellent tutorial on the subject of weighted stacking. Although weighted stacking can be quite effective, as Schoenberger demonstrates, it does have a major disadvantage: only stacked traces are output. That limitation can be overcome by 2-D velocity filtering methods. For example, *Ryu (1982)* describes a filter applied to NMO-corrected CMP gathers in the space-time domain that separates multiples from primaries. The velocity function for the NMO lies between the velocity functions for primary events and multiple events. This, in effect, maps the events into different quadrants of the *f-k* domain, thereby making their separation possible by dip discrimination.

The next seven papers in this chapter describe multiple attenuation based on discrimination in a Radon transform domain. Currently this is the seismic exploration industry's most popular method of attenuating multiples. In a landmark paper, *Hampson (1986)* reports on multiple discrimination in the parabolic Radon transform domain. An NMO correction was applied to make the originally hyperbolic events in CMP gathers nearly parabolic in the x-t domain, thereby mapping them into approximately discrete points after the parabolic transform. Theoretically, then, multiple discrimination is simple. Provided that a sufficient moveout difference existed originally between the two classes of events, they should map into separate regions in the Radon domain. In practice, unfortunately, things are not so simple. Usually the hoped for discrete points in the parabolic Radon domain are smeared out into overlapping zones of energy, making primary-multiple discrimination difficult. Since Hampson's 1986 paper, many authors have described refinements to his algorithm. *Yilmaz (1989)* improves on Hampson's method by replacing the NMO correction prior to the transform with a t^2-stretching of the CMP data.

In spite of the advances by Yilmaz and Foster and Mosher, Radon transforms were still sometimes a less than satisfactory way of discriminating between primary and multiple events. There were two basic problems:

- The finite spatial sampling and limited aperture in field data records limited resolution in the Radon domain (Thorson and Claerbout, 1985; Sacchi and Ulrych, 1995; Trad et al., 2003).
- In situations with complex geology the apexes of the hyperbolic events might not be at zero offset (as is assumed by a standard Radon transform).

The solution to the first problem was a so-called "high resolution" Radon transform, in which a priori statistical requirements were imposed that forced a sparse distribution of events in the Radon domain. Early forms of this type of transform required an expensive, iteratively re-weighted

solution to a least-squares problem (see the references cited above). *Herrmann et al. (2000)* present a relatively inexpensive, non-iterative scheme to solve the problem. Their method is recursive; that is, the weights at each frequency depend on the Radon transform solution found at earlier frequencies. As an alternative, *Moore and Kostov (2002)* suggest a non-iterative, non-recursive scheme that derived the weights from semblance computations along the offset axis. *Hargreaves et al. (2003)* propose a solution to the second problem. Specifically, they address the attenuation of so-called diffracted multiples that arise from scatterers near the ocean bottom. Normal two-dimensional Radon transforms do a poor job of suppressing these multiples because their apexes do not occur at zero offset. Hargreaves et al. show that by adding a third Radon transform parameter, representing the apex location of hyperbolic events, superior separation of primaries and diffracted multiples is possible. *Trad (2003)* shows that a Stolt-type migration operator can be used to implement a very fast apex-shifted Radon transform that performs well in practice.

The design of the reject filter is a problem faced by all 2-D velocity filtering methods, regardless of the domain in which they operate. Ideally, the amplitudes of the transformed multiples and primaries would appear in well-localized and -separated regions so that the data processor could distinguish between these regions. In practice, the amplitudes are often not well-localized and the regions overlap, making selection of the reject filter difficult. *Zhou and Greenhalgh (1996)* solve this problem by using the 2-D transform of wave-equation-based multiple predictions (see Chapter 4) to design the optimal reject filters in the 2-D transform space. Zhou and Greenhalgh have published a series of papers showing that this method can be applied in any 2-D transform domain. Their paper included here discusses application to the parabolic Radon transform domain to attenuate water-layer multiples. *Landa et al. (1999)* extend Zhou and Greenhalgh's idea to attenuate both surface and interbed multiples.

Multiple reflections can be removed from seismic data by exploiting characteristics other than periodicity or moveout. For example, each multiple in a data set is kinematically and dynamically related to the primary events from the reflecting horizons involved in generating the multiple (see Chapter 4). The two papers by *Doicin and Spitz (1991)* and *Manin and Spitz (1995)* describe a multichannel pattern recognition technique that can target and eliminate a particular multiple based on its relationship with primary reflections. The 1991 and 1995 papers describe 2-D and 3-D applications of this idea, respectively. The method requires knowledge of the generating mechanism of a targeted multiple.

Various forms of stacking and 2-D velocity filtering generally have the most difficulty separating primaries from multiples at near offsets, where the instantaneous apparent velocity differences between the two kinds of events typically vanish. *Houston (1998)* proposes enhancing the event discrimination at near offsets by applying a localized multichannel coherency filter to gathers NMO corrected with the moveout appropriate for multiples. If multiples are flattened, then they become laterally predictable, whereas overcorrected primary events are not. Houston's coherency filter appears to be more effective than f-k filtering in suppressing multiples without distorting primary reflections. *Hu and White (1998)* describe separating multiples from primaries using another type of coherency-based multichannel filtering called data-adaptive beamforming. This algorithm starts with a beamforming filter based on an initial model of coherent noise (i.e., a multiple) in a data set and then adaptively refines that model to optimize the ability of the beamforming filter to isolate that event. Hu and White show a prestack data example in which the performance of their method was superior to Radon transform-based multiple attenuation.

Finally, *Zhang and Ulrych (2003)* describe a method of separating primaries and multiples based on migration focusing. They first migrate the data prestack, using a velocity function appropriate for multiples, to focus the multiples, but not the primaries. Next, they apply a standard statistical measure, called the median of absolute deviations, along hyperbolic trajectories at the residual velocity of the primaries to identify samples that are outliers. Because only the multiples are focused, such outliers are almost certainly multiples. After replacing these samples with the median and demigrating, the multiples are significantly attenuated.

The papers in this chapter illustrate that attenuation methods based on differences between primaries and multiples are often an effective and appropriate choice within the toolbox of multiple attenuation techniques.

Chapter 3 References

Thorson, J.R. and Claerbout, J.F., 1985, Velocity-stack and slant-stack stochastic inversion: Geophysics, 50, 2727-2741.

Sacchi, M.D. and Ulrych, T.J., 1995, High resolution velocity gathers and offset-space reconstruction: Geophysics, 60, 1169-1177.

Trad, D., Ulrych, T. and Sacchi, M., 2003, Latest views of the sparse Radon transform: Geophysics, **68**, 386-399.

Chapter 3 Papers

Mayne, W.H., 1962, Common reflection point horizontal data stacking techniques: Geophysics, **27**, 927-938.

Schneider, W.A., Prince, E.R., and Giles, B.F., 1965, A new data-processing technique for multiple attenuation exploiting differential normal moveout: Geophysics, **30**, 348-362.

Schoenberger, M., 1996, Optimum weighted stack for multiple suppression: Geophysics, **61**, 891-901.

Ryu, J.V., 1982, Decomposition (DECOM) approach applied to wave field analysis with seismic reflection records: Geophysics, **47**, 869-883.

Hampson, D., 1986, Inverse velocity stacking for multiple elimination: Journal of the CSEG, **22**, 44-55.

Yilmaz, O., 1989, Velocity-stack processing: Geophysical Prospecting, **37**, 357-382.

Foster, D.J. and Mosher, C.C., 1992, Suppression of multiple reflections using the Radon transform: Geophysics, **57**, 386-395.

Herrmann, P., Mojesky, T., Magesan, M. and Hugonnet, P., 2000, De-aliased, high-resolution Radon transform: SEG Expanded Abstracts, 1953-1956.

Moore, I. And Kostov, C., 2002, Stable, efficient, high-resolution Radon transforms: EAGE Expanded Abstracts, F34.

Hargreaves, N., ver West, B., Wombell, R. and Trad, D., 2003, Multiple attenuation using an apex-shifted Radon transform: SEG Expanded Abstracts, 1929-1932.

Trad, D., 2003, Interpolation and multiple attenuation with migration operators: Geophysics, **68**, 2043-2054.

Zhou, B. and Greenhalgh, S.A., 1996, Multiple suppression by 2D filtering in the parabolic τ-p domain: a wave-equation-based method: Geophysical Prospecting, **44**, 375-401.

Landa, E., Belfer, I. and Keydar, S., 1999, Multiple attenuation in the parabolic tau-p domain using wavefront characteristics of multiple generating primaries: Geophysics, **64**, 1805-1815.

Doicin, D. and Spitz, S., 1991, Multichannel extraction of water-bottom peg legs pertaining to high-amplitude reflection: SEG Expanded Abstracts, 1439-1442.

Manin, M. and Spitz, S., 1995, 3D extraction of a targeted multiple: SEG Expanded Abstracts, 1468-1469.

Houston, L.M., 1998, Multiple suppression using a local coherence filter: Geophysics, **63**, 652-659.

Hu, T. and White, R. E., 1998, Robust multiple suppression using adaptive beam-forming: Geophysical Prospecting, **46**, 227-248.

Zhang, R. and Ulrych, T., 2003, Multiple suppression based on the migration operator and a hyperbolic median filter: SEG Expanded Abstracts, 1949-1952.

Chapter 4

Multi-dimensional wavefield methods: Part I

In the volume introduction, we explained that every multiple event in a seismic data set, no matter how complicated, is a composite of two or more simpler events (hereafter called "subevents") that have their termination points at the free surface. This relationship suggests the possibility of manipulating a data set in a way that uses its subevents to predict its multiples. Indeed, Chapter 2 included several papers that discussed 1-D prediction of multiples from primaries. This chapter and the next include papers that carry this idea beyond 1-D to multi-dimensional wavefield manipulation methods that predict the multiple events in a data set. If such a prediction is sufficiently accurate, multiples can be eliminated simply by subtracting the predictions from the original data. This concept theoretically allows satisfactory multiple attenuation in situations where traditional methods, like those in Chapters 2 and 3, fail. In deep water, for example, simple periodicity-based methods fail because the multiples are not periodic. Furthermore, in recent years the search for petroleum targets has extended to geologic settings beneath complex heterogeneous overburdens such as salt, basalt, karsted sediments and volcanics. The lateral rapid heterogeneity and ill-defined boundaries in these settings are often too complex for any traditional methods of multiple attenuation to accommodate.

Three major methodologies for multiple prediction via multi-dimensional wavefield manipulation have evolved. The *wavefield propagation method* directly models multiples by propagating subevents through one or more cycles of reverberation (*e.g., Wiggins (1988)*). This approach requires a model of the medium, including velocities and reflection coefficients. Thus, it is useful mainly for water layer multiples since the required model information (water velocity and the water-bottom reflection coefficient) is relatively simple. For more complex reverberations, and especially for those in complex geologic settings, direct modeling is not usually considered a viable option because the required a-priori subsurface information is not known sufficiently well. Two alternative approaches, however, provide a capability of predicting multiples that avoid this problem. The *feedback free-surface and interface model* and the *inverse-scattering series free-surface and point scatterer model* are two distinct approaches for predicting both free-surface and internal multiples that reduce or eliminate the need for a-priori subsurface information. This is accomplished by using the data themselves to construct operators that predict the multiples contained within the data (*e.g., Verschuur et al., (1992)*). In particular, both methods can predict surface multiples without any need for a subsurface model. The two methods require knowledge of the acquisition wavelet in order to produce accurate multiple predictions. This chapter includes papers on the wavefield propagation and feedback methods; the inverse series procedures are found in Chapter 5. Because the basic concepts of these latter two methods are not widely known, we introduce them in a brief tutorial immediately following this chapter introduction.

In the first of the wavefield propagation papers, *Bernth and Sonneland (1983)* predict multiples by applying a water layer extrapolation operator in the frequency-wavenumber domain to prestack data. The predicted multiples are adaptively subtracted from the original data to accommodate timing and amplitude errors in the prediction. *Morley and Claerbout (1983)* use a "Split-Backus" model to predict water layer peg-leg multiples. The modeling assumes near-vertical travel in the water layer, but can handle situations where the source and receiver depths are unequal and the

water depth and water-bottom reflection coefficient vary along a line. The multiple modeling procedure suggested by *Berryhill and Kim (1986)* removes two important limitations present in the previous two papers. First, unlike the Bernth and Sonneland algorithm, the method can accommodate any sea-floor profile. Second, unlike the Morley and Claerbout procedure, the prediction is not limited to multiples that propagate nearly vertically in the water layer. The water-bottom reflection coefficient does not appear explicitly in Berryhill and Kim's multiple prediction procedure; instead, its effects are accounted for in an adaptive subtraction of the predicted multiples from the original data.

Wiggins (1988) derives a method of attenuating water-bottom multiples that allows for a locally varying water-bottom reflection coefficient. The wavefield propagation through the water layer is split into two pieces: a forward-in-time propagation from the surface to the water bottom and a backward-in-time propagation from the surface to the water bottom. The two wavefields at the water bottom then should be identical, trace-by-trace, except for the effects of the water-bottom and water-surface reflectivity. Minimizing the observed difference allows derivation of a filter representing the effects of the water-bottom reflectivity. That filter is then used to calculate the multiple-free wavefield. *Lokshtanov (2000)* describes a wave propagation method that is applied to CMP gathers in the τ-p domain. One advantage of this is that the method easily handles angular dependence of the water-bottom reflection coefficient. Finally, *Hill et al. (2002)* suggest predicting multiples using beam methods to extrapolate the wavefield. A predictive matched filtering to identify and remove multiples from the original data is applied to beam components. Using certain assumptions about the earth model, Hill et al. produce a form of their method that can be used with conventionally recorded 3-D marine data.

As explained in the Chapter 4 Tutorial, the feedback free-surface and interface model is a scheme for the forward modeling of seismic reflection data. When carried out in the seismic data processing, or inverse sense, it provides the opportunity to predict and attenuate multiples that are associated with the reflectors. Early versions of this concept can be found in the landmark works of *Riley and Claerbout (1976)*, and *Kennett (1979)*. Riley and Claerbout begin by using Z-transforms to derive an algorithm that removes surface multiples for a 1-D earth model by, in essence, convolving the data with themselves. Their algorithm includes the inverse of the acquisition wavelet, and they describe how, in some cases, that wavelet can be found using a least-squares minimization of the difference between the seafloor primary convolved with itself and the first-order multiple water-bottom multiple. The paper then addresses 2-D multiple reflections. The authors derive an approximate finite difference-based solution that is analogous to their 1-D solution. The paper concludes with a lengthy discussion of the practical problems expected when the method is applied to less-than-ideal field data sets. Kennett describes construction of a surface multiple suppression operator in the frequency-wavenumber domain for plane-layered elastic and acoustic media. The fundamental concept is the same as in the Riley and Claerbout paper, but Kennet's method is not restricted to wavefields that travel nearly vertically. Kennett also describes generalization of the method to land data. As is characteristic of the feedback free-surface methods, detailed knowledge of the acquisition wavelet is necessary.

In the early 1980's, Berkhout published a comprehensive treatment of the free-surface and interface model using a feedback formalism (*Berkhout, 1982*). In particular, Berkhout described an elegant, fully multi-dimensional ω-x formulation that could be described and implemented by simple matrix manipulations. Furthermore, the method placed no restrictions on the nature of the subsurface. This work launched a long-term effort, centered at Delft University, that addressed conceptual

and practical issues and eventually brought this method – which is now known as "surface-related multiple elimination" (SRME) – to widespread industry usage. From among the numerous contributions from the Delft group, this chapter includes: *Verschuur et al. (1992), Verschuur and Kabir (1992), Berkhout and Verschuur (1997),* and *Verschuur and Berkhout (1997).* Verschuur et al. present the derivation of an ω-x matrix equation for eliminating free-surface multiples. The equation requires no information about the subsurface, but it does require knowledge of the acquisition wavelet. Since that wavelet is typically not well known, the authors propose an adaptive procedure that estimates the wavelet by minimizing the energy in the data after multiples are removed. The matrix equation includes the inverse of a large matrix, which is computationally expensive and may have stability issues. To overcome these problems, Verschuur et al. do a series expansion of the matrix inverse and keep only a few lower-order terms. The authors also mention briefly a recursive scheme for attenuating internal multiples as well (see below). Verschuur and Kabir make a comparison between surface-related multiple elimination and Radon transform multiple elimination. They conclude that the two methods complement each other. This paper also includes a simplified version of the SRME theory, which makes it a good starting point for readers new to the concept. The Berkhout and Verschuur and Verschuur and Berkhout papers are companions: the first is concerned with theory, and the second with practical issues and examples. In these two papers, the authors explain and illustrate an iterative version of the SRME method.

A reciprocity formulation of this free-surface and interface model for multiple removal also had its historical roots and activity centered in Delft University, from the school of Professor A. deHoop. For example, *Fokkema and Van den Berg (1990)* developed these concepts within a wave-theoretical integral equation framework, thereby providing mathematical clarity and physical insight. This approach furthered the understanding of the relationship between the feedback and inverse-scattering methods (see Chapter 5) for free-surface multiple attenuation, and the role, for example, that the obliquity factor (*Born and Wolf, 1964*) plays in those theories. The wave theoretical angle-dependent obliquity factor is important, particularly for long offsets and shallow targets, as illustrated by three figures from an EAGE Convention paper by *Dragoset (1993).* The figures, which do not appear in the original published abstract, are included at the end of this chapter introduction.

In addition to those from the Delft group, this chapter includes a few other notable papers on the feedback free-surface and interface model. In the early 1980's Pann filed for a US Patent, *Pann (1989)*, for a multi-dimensional method of predicting and removing surface multiples that is based on Huygens' principle. Numerically, the steps in Pann's method for predicting multiples of a certain order for a specific trace are the same as those in the Delft scheme. Pann, however, did not reveal any method for easily selecting which combinations of traces need to be convolved. The matrix formulation of the Delft method accomplishes that task automatically. *Dragoset and Jericevic (1998)* derive the equations for SRME in an intuitive fashion by making an analogy between surface multiple prediction and the diffraction aperture problem of classical optics. The Kirchhoff integral solves both problems, and the authors show how the integration can be accomplished by matrix manipulations. They also present and discuss a list of survey design suggestions intended to provide data that are most suitable for the SRME process. Finally, *Al-Bannagi and Verschuur (2003)* propose a method of applying SRME to post-stack data. For a given post-stack trace, the data are demigrated to produce sufficient pre-stack traces for predicting the multiples in the (zero offset) post-stack trace. This approach has several advantages when applying SRME to land data:

- The multiple prediction is performed with traces that have good signal-to-noise ratio compared to that of pre-stack land traces.

- Problems with irregular and sparse spatial sampling of the surface wavefield are avoided.
- Detailed structural variations in the subsurface are accommodated.
- The method is computationally efficient.

As several of the papers in this chapter discuss, the feedback free-surface and interface model method can be applied to the prediction and attenuation of internal multiples. Starting with the free surface and proceeding to the next shallowest reflector, the water bottom, one sequentially predicts and removes first all multiples having downward reflections at the free surface and then all multiples having their shallowest downward reflection at the water bottom. Continuing in this manner, all free-surface and internal multiples are attenuated - one interface at a time. Carrying out this strategy requires accurate depth migration to each interface and good estimation of the reflectivity properties at that imaged reflector. However, extension of the composite event concept to internal multiples allows certain important characteristics of those multiples to be predicted in a simpler fashion. In particular, all internal multiples from a given interface can have their travel times predicted precisely without any knowledge of the subsurface except for the location in time of that reflector. Amplitudes, however, are predicted only approximately with an accuracy that depends on the type of internal multiple. For further discussion of various issues involving internal multiple prediction see the tutorial following this introduction as well as *Coates and Weglein (1996)* and *Weglein and Matson (1998)* in Chapter 5. Here, we include one paper, *Jakubowicz (1998)*, that describes the prediction of internal multiples based on the composite event concept and the free-surface and interface model.

The Delft University feedback formulation for multiple prediction has met with much success, and, in fact, has become an industry-wide standard method of removing multiples. Other related formulations have also led to viable wave equation-based methods of predicting and attenuating multiples. This chapter concludes with one such effort: *Liu et al. (2000)*. These authors derive multiple attenuation formulas using the invariant embedding approach. The results resemble those that appear in the Delft papers. However, the method is implemented in the τ-p domain. For media with only gentle dips, the resulting algorithm is quite efficient because the matrices involved in the multiple prediction are sparse.

Chapter 4 References

Born, M. and Wolf E., 1964, Principles of optics, 2^{nd} Ed.: MacMillan, Chapter 8.

Berkhout, A.J., 1982, Seismic migration: Imaging of acoustic energy by wavefield extrapolation. A. Theoretical aspects, 2^{nd} Ed.: Elsevier.

Chapter 4 Papers

Bernth, H. and Sonneland, L., 1983, Wavefield extrapolation techniques for prestack attenuation of water reverberations: SEG Expanded Abstracts, 264-265.

Morley, L. and Claerbout, J., 1983, Predictive deconvolution in shot-receiver space: Geophysics, **48**, 515-531.

Berryhill, J.R. and Kim, Y.C., 1986, Deepwater peg-legs and multiples: emulation and suppression: Geophysics, **51**, 2177-2184.

Wiggins, J.W., 1988, Attenuation of complex water bottom multiples by wave equation based prediction and subtraction: Geophysics, **53**, 1527-1539.

Lokshtanov, D., 2000, Suppression of water-layer multiples – from deconvolution to wave-equation approach: SEG Expanded Abstracts, 1981-1984.

Hill, N.R., Langan, R.T., Nemeth, T., Zhao, M. and Bube, K.P., 2002, Beam methods for predictive suppression of seismic multiples in deep water: SEG Expanded Abstracts, 2118-2121.

Riley, D.C. and Claerbout, J.F., 1976, 2-D multiple reflections: Geophysics, **41**, 592-620.

Kennett, B.L.N., 1979, The suppression of surface multiples on seismic records: Geophysical Prospecting., **27**, 584-600.

Pann, K., 1989, Removal of surface multiples, U.S. Patent No.4,887,243.

Fokkema, J.T. and Van den Berg, P.M., 1990, Removal of surface-related wave phenomena: the marine case: SEG Expanded Abstracts, 1689-1692.

Verschuur, D.J., Berkhout, A.J. and Wapenaar, C.P.A., 1992, Adaptive surface-related multiple elimination: Geophysics, **57**, 1166-1177.

Verschuur, D.J. and Kabir, M.M.N., 1992, Comparison of surface-related multiple elimination with Radon multiple elimination: Journal of Seismic Exploration, **1**, 363-377.

Dragoset, W. H., 1993, Surface multiple attenuation - theory, practical issues, examples: EAGE Expanded Abstracts, B027.

Berkhout, A. J. and Verschuur, D. J., 1997, Estimation of multiple scattering by iterative inversion, Part I: Theoretical considerations: Geophysics, **62**, 1586-1595.

Verschuur, D. J. and Berkhout, A. J., 1997, Estimation of multiple scattering by iterative inversion, Part II: Practical aspects and examples: Geophysics, **62**, 1596-1611.

Dragoset, W. H. and Jericevic, Z., 1998, Some remarks on surface multiple attenuation: Geophysics, **63**, 772-789.

Al-Bannagi, M.S. and Verschuur, D.J., 2003, Enhanced post-stack multiple prediction using demigration: EAGE Expanded Abstracts, B42.

Jakubowicz, H., 1998, Wave equation prediction and removal of interbed multiples: SEG Expanded Abstracts, 1527-1530.

Liu, F., Sen, M.K. and Stoffa, P.L., 2000, Dip selective 2-D multiple attenuation in the plane-wave domain: Geophysics, **65**, 264-274.

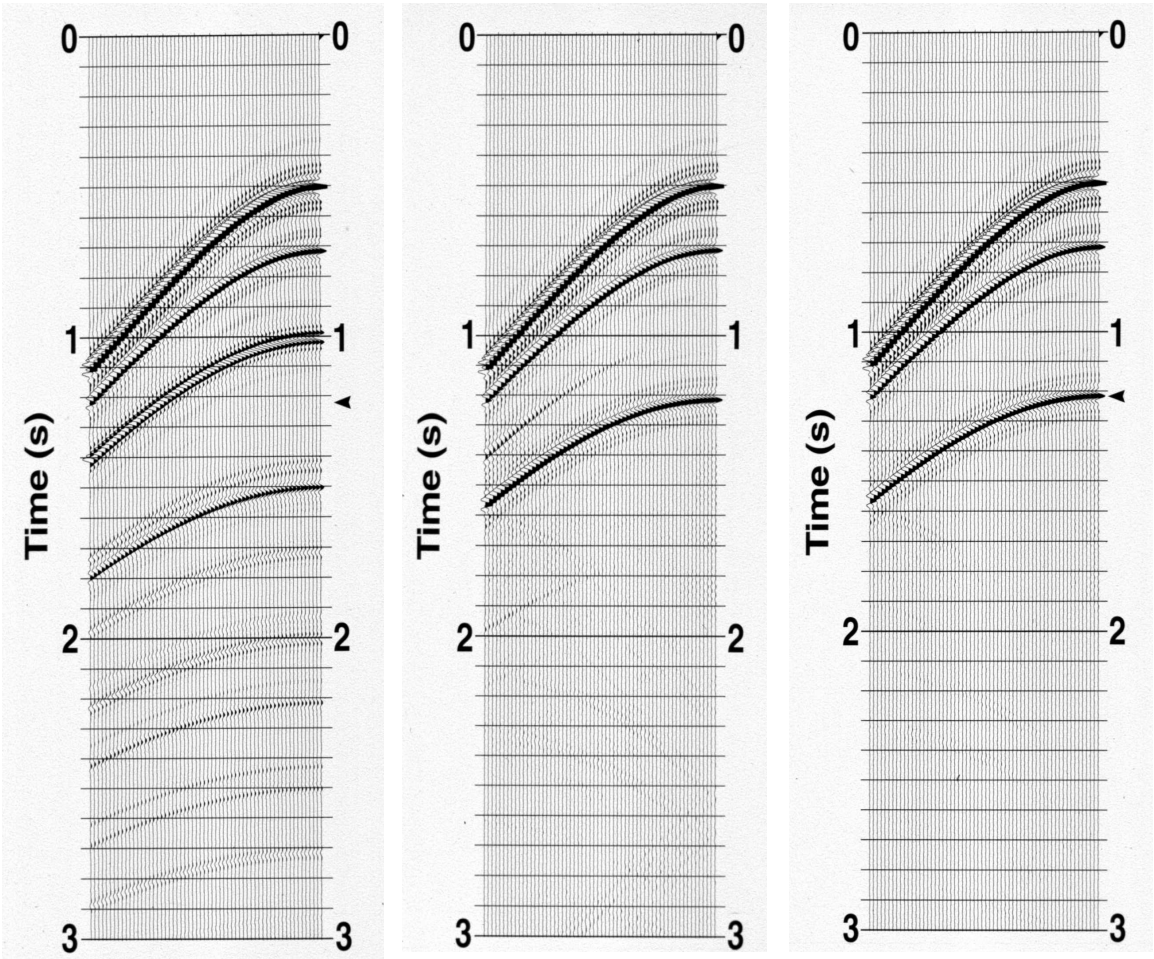

Figure 4: *Figure A: Synthetic marine shot record for testing SRME algorithms. The model has three flat reflecting horizons in a constant velocity medium. The zero-offset arrival times for the three primary events are about 0.5, 0.7, and 1.2 s. The reflection coefficients were chosen such that the third primary event (at the arrow) is exactly cancelled by one of the surface-related multiples. The strong event at 1.0 s and all of the events below 1.2 s are surface-related multiples. Figure B. Surface-related multiples eliminated – no obliquity factor. This result was obtained by directly inverting the matrix at each frequency that represents the SRME operator. That operator is derived from the Kirchhoff integral (Dragoset and Jericevic, 1998). Here, the obliquity factor part of the Kirchhoff integral was ignored by setting it equal to one for all wavefront angles of incidence at the surface. Figure C. Surface-related multiples eliminated – proper obliquity factor applied. Compare this result to that in Figure B. Using the proper obliquity factor improves multiple elimination at the large offsets. This is to be expected, because the raypaths are most oblique to the surface at large offsets.*

Chapter 5

Multi-dimensional wavefield methods: Part II

The free-surface and point scatterer model for the generation of seismic reflection data provides a free-surface model for free-surface multiple generation and a point scatterer model for generating primaries and internal multiples. When this model operates in an inverse sense, the free-surface model removes ghosts and free-surface multiples while the point-scatterer model allows for processing primaries to produce structure maps, earth property estimates, and the removal of internal multiples. The history of this approach derives from a form of perturbation theory called scattering theory and describes how altering (or perturbing) a medium will result in an altered or perturbed wave-field. The tremendous flexibility in scattering theory allows using either a surface, interface or point scatterer model to characterize the difference between a reference medium (typically a nominal velocity model) and a perturbed medium (the actual earth) depending on one's ability to provide or define that difference in an inverse or processing sense. For example, since the air-water boundary is fairly well defined, a free-surface description for that perturbation is chosen and that model is then used to generate and remove free-surface multiples. Since typical subsurface detail is much less well defined, a point scatterer description of the perturbation is chosen for generating and processing primaries and internal multiples.

The origin of the inverse scattering series is found in atomic and nuclear scattering (*Moses, 1956*) and was extended to acoustics, (*Prosser (1969), Razavy (1975)*), and then to seismic exploration by *Weglein, Boyse and Anderson (1981).* Convergence problems and other practical issues precluded the series, in that pristine form, from providing any practical value. To extract some practical usefulness from this most general and flexible formalism, Weglein, Carvalho, Araujo, and Stolt sought to separate the series into task-specific subseries resulting in distinct algorithms for attenuating free-surface and internal multiples, and to investigate their convergence and practical requirements. *Carvalho et al. (1991, 1992)* develop the free-surface inverse-scattering subseries and then apply it successfully to synthetic data (1991) and to field data (1992). *Araujo et al. (1994)* first identify the subseries that attenuates internal multiples, and then demonstrate it with tests that include free-surface and internal multiples. *Weglein et al. (1997)* present the first comprehensive theory for attenuating all multiples from a multi-dimensional heterogeneous earth with absolutely no information about the subsurface. The excellent convergence properties of these subseries and their ability to accommodate field data were in marked contrast to properties of the overall series.

Coates and Weglein (1996) examine and test the efficacy of prediction of the amplitude and phase of internal multiples for acoustic and elastic media. The phase of all internal multiples is correctly predicted, including that of converted-wave multiples, and the predicted amplitude well attenuates internal multiples of an entire p-wave history. *Weglein and Matson (1998)* use an analytic example to understand the precise nature of the amplitude predicted in the internal multiple algorithm and provide a sub-event interpretation for the time of the predicted internal multiple phase. *Matson (1996)* provides a map between the forward construction of seismic events in the scattering series and the primaries and multiples in seismic data.

A series describes primaries and internal multiples in terms of reference propagation and repeated point scatterer interactions where the scattering from any point depends on the difference between actual and reference medium properties at that point. The inverse processes on primaries and

multiples require only reference propagation and reflection data. The individual terms in the inverse series that remove internal multiples attenuate all internal multiples of a given order from all interfaces at once – without interpretive intervention or event picking of any kind – and automatically accommodate multiples due to specular, corrugated or diffractive origin. The leading term in the removal series predicts the time of internal multiples precisely; higher-order terms increase the accuracy of the amplitudes of the predicted multiples. As more terms are used, the internal multiple attenuation moves closer to multiple elimination. Although the feedback-interface method (see Chapter 4) is computationally efficient when the reflector causing the downward reflection can be isolated, the ability to automatically attenuate internal multiples under complex geologic conditions without requiring any subsurface information, isolation of reflectors, or interpretive intervention, remains the unique strength of the inverse scattering method of attenuating internal multiples.

Chapter 5 References

Moses, H.E., 1956, Calculation of scattering potential from reflection coefficients: Phys. Rev.**, 102**, 559-567.

Prosser, R.T., 1969, Formal solutions of inverse scattering problems: J. Math. Phys., **10**, 1819-1822.

Razavy, M., 1975, Determination of the wave velocity in an inhomogeneous medium from reflection data: J. Acoust. Soc. Am., **58**, 956-963.

Weglein, A.B., Boyse, W.E. and Anderson, J.E., 1981, Obtaining three-dimensional velocity information directly from reflection seismic data: An inverse scattering formalism: Geophysics, **46**, 1116-1120.

Chapter 5 Papers

Carvalho, P.M., Weglein, A.B. and Stolt, R.H., 1991, Examples of a nonlinear inversion method based on the T matrix of scattering theory: application to multiple suppression: SEG Expanded Abstracts, 1319-1322**.**

Carvalho, P.M., Weglein, A.B. and Stolt, R.H., 1992, Nonlinear inverse scattering for multiple suppression: application to real data. Part I: SEG Expanded Abstracts, 1093-1095.

Araújo, F.V., Weglein, A.B., Carvalho, P.M. and Stolt, R.H., 1994, Inverse scattering series for multiple attenuation: an example with surface and internal multiples: SEG Expanded Abstracts, 1039-1041.

Coates, R.T. and Weglein, A.B., 1996, Internal multiple attenuation using inverse scattering: results from prestack 1-D and 2-D acoustic and elastic synthetics: SEG Expanded Abstracts, 1522-1525.

Matson, K.H., 1996, The relationship between scattering theory and the primaries and multiples of reflection seismic data: Journal of Seismic Exploration, **5**, 63-78.

Weglein, A.B., Gasparotto, F.A., Carvalho, P.M. and Stolt, R.H., 1997, An inverse scattering series method for attenuating multiples in seismic reflection data: Geophysics, **62**, 1975-1989.

Weglein, A.B. and Matson, K., 1998, Inverse-scattering internal multiple attenuation: an analytic example and subevent interpretation: Proceedings of SPIE, **3453**, 1008-1017.

Chapter 6

Multiple prediction for field data sets

Both the multiple prediction method developed at Delft University and by others (Chapter 4) and the method based on scattering theory (Chapter 5) are complete and realistic algorithms from a multidimensional physics point of view. Theoretically, such completeness and realism allow accurate multiple prediction without requiring detailed a priori subsurface information. However, while these methods can accommodate complex wave propagation effects without knowledge of the subsurface, they do place stringent requirements on the definition and completeness of the seismic measurements at the surface. Typically, those requirements are not fully met by present day routine data acquisition practices. This chapter contains papers that describe efforts to overcome the problems that occur when multiples are predicted using less than ideal surface wavefield measurements.

There are two types of stringent requirements. (The Chapter 4 tutorial and *Dragoset and Jericevic (1998)*, also in Chapter 4, discuss the reasons for these requirements.) First, the acquisition wavelet must be either measured or estimated accurately for each shot in the recorded data set. The acquisition wavelet consists of the source signature, the source and receiver array radiation patterns including surface ghost effects, and the recording system filters. Note that the acquisition wavelet is angle dependent and that it does not include any earth filtering effects. Second, the wavefield measured at the surface must be fully sampled and non-aliased. Fully sampled means the following: Suppose a particular recorded trace is defined by its shot and receiver locations at the surface. To predict surface multiples for that trace requires that its shot also be recorded by a 2-D spread of receivers that spans all possible surface locations at which the various multiples in the trace may have their downward reflections. Furthermore, the trace's receiver must record data from a 2-D spread of shots that spans the same surface locations. The size of the aforementioned 2-D spreads - that is, the surface recording aperture - depends on the subsurface structure. For example, if the structure is predominantly 2-D and seismic lines are shot parallel to the dip direction, then 1-D spreads and 2-D multiple prediction suffice. If, however, the subsurface contains 3-D structures - such as ocean-bottom diffractors, reflecting horizons with crossline dip, and salt structures - then 2-D spreads and 3-D multiple prediction are required. Generally, the size of the required crossline aperture is a function of crossline dip.

The requirement for an accurate acquisition wavelet was an important obstacle to the early acceptance and application of wave equation-based multiple prediction technology. An early response to that challenge sought to exploit the wavelet requirement by using the multiple attenuation algorithm itself to find the required wavelet. The basic assumption was that seismic data without multiples had fewer events and hence less energy. Therefore, the desired wavelet could be found by searching for the wavelet that produced an energy minimum when multiples predicted using that wavelet were subtracted from the original data. Various incarnations of this concept were introduced. *Verschuur et al. (1992)* (see Chapter 4) propose a preprocessing deconvolution to remove the angle-dependent components of the acquisition wavelet from the data and follow that with a frequency-dependent energy-minimizing search to determine the residual wavelet amplitude and phase. *Carvalho and Weglein (1994)* describe a global and robust searching of the minimum-energy objective function surface designed to avoid local minima. *Ikelle et al. (1997)* truncate the scattering series formulation of multiple prediction after two terms, which results in a linear relationship

between the acquisition wavelet and the free-surface reflections. Ignoring truncation errors, the resulting energy-minimization problem for the wavelet has an analytic solution (that can be refined through an iterative scheme to account for truncation effects). *Dragoset and Jericevic (1998)* (see Chapter 4) formulate the surface multiple attenuation algorithm using a closed-form expression of the multiple prediction series. Unfortunately, that formulation results in the expression for the acquisition wavelet being inside of a rather large matrix that must be inverted, making an iterative wavelet search quite expensive. They show, however, that by applying eigenvalue decomposition to the matrix the acquisition wavelet factor can be isolated in a diagonal matrix, which, of course, is inverted easily and cheaply.

All of these methods for estimating the acquisition wavelet work at cross-purposes to the underlying physics of the multiple attenuation methods they are meant to serve. For example, destructively interfering events cause no problem for the physics of the algorithms but can cause problems with minimum-energy wavelet estimation approaches. There are other approaches to finding the acquisition wavelet, such as near-field source measurements (*Ziolkowski et al., 1982*), that are independent of the multiple attenuation process. *Ziolkowski, et al. (1999)* propose a wave-theoretical multiple attenuation algorithm that uses near-field source measurements to avoid three problems common to most methods of Chapters 4 and 5. They are: 1) the assumption that the source is a point, 2) the presence of the incident source field in the recorded data, and 3) the need to estimate the wavelet using a minimum-energy criterion. (Note: being a wavefield method, the *Ziolkowski, et al., 1999* paper could have been included in Chapter 4. However, its emphasis on dealing with problems in field data sets makes it at home in this chapter as well.) A variant of Green's theorem known as the extinction theorem provides another possibility for satisfying the need to know the acquisition wavelet (*Weglein et al., 2000*).

Prior to the year 2002, the attenuation methods of Chapters 4 and 5 were typically implemented as 2-D algorithms, and applied to data that were, at best, quasi 3-D. In the presence of 3-D subsurface structures, the resulting timing errors in predicted multiples can be quite large; see, for example, *Ross et al. (1999)*. Furthermore, such timing errors are complicated; they depend on crossline dip, offset, and the order of the multiples. The obvious solution to this problem was to apply 3-D prediction algorithms to 3-D data, but costs generally prohibited this. Therefore, a more pragmatic solution was sought for and developed: sophisticated adaptive subtraction. The general idea behind this approach is that because of imperfections in field data sets and use of prediction algorithms that ignore 3-D complications, effective multiple attenuation can seldom be accomplished in just one step. Instead, a two-step method is necessary: (1) the multiples are imperfectly predicted followed by (2) adaptive subtraction that compensates for the imperfections, thereby producing reasonably good attenuation in spite of them. Note that adaptive subtraction compensates for prediction errors that arise due to imperfect knowledge of the acquisition wavelet as well as the errors due to use of 2-D rather than 3-D multiple prediction.

Adaptive subtraction can be applied to different data domains (e.g., common shot, common offset, etc.) using many different algorithms, all of which have parameter settings that can affect the results. This flexibility is a mixed blessing: it allows for good results in a wide variety of situations, but the data processing practitioner can face an overwhelming smorgasbord of choices. Using synthetic data, *Abma et al. (2002)* compare the performance of least-squares 1-D matching filters, pattern-matching (*Spitz, 1999*), and shaped 2-D filters. They conclude that, of those three choices, 1-D matching filters (computed from and applied to a 2-D window of data) are the safest to use for adaptive subtraction. The other two methods, while theoretically more accommodating of errors

in the predicted multiples, tend to attenuate primary reflections along with the multiples. *van Borselen et al. (2003)* present a target-oriented adaptive subtraction approach. Their method uses the same 1-D matching algorithm as studied by Abma et al., but it is applied to subtract only multiples having some particular characteristic, such as a predominant dip or frequency range. Presumably, such a constraint minimizes the chance that the adaptive subtraction process will affect primary reflections. *Guo (2003)* describes a more advanced pattern-matching algorithm than that studied by Abma et al. It iteratively calculates the prediction error filter for the primaries and uses a projection signal filter to reduce the effects of random noise. Guo's results on the simple synthetic data sets analyzed by Abma et al. look superior to results of other methods applied to those data sets. In a somewhat different approach, *Ross et al. (1999)* suggest applying time-variant deterministic time corrections to the predicted multiples prior to the adaptive subtraction. The time corrections are derived from a 3-D model of the subsurface.

The need to accommodate errors in multiples produced by applying 2-D prediction to data from a 3-D subsurface was one main impetus behind the development of adaptive subtraction as part of the multiple attenuation process. Although the method of 2-D prediction followed by adaptive subtraction has had many successes, its limitations are also evident. Consider, for example, the offshore Norway data set results displayed by *Hadidi et al. (2002)*. A simple CMP stack (Figure 4) shows a semi-coherent noisy region that is produced by diffracted surface multiples. A 2.5-D application of surface multiple attenuation (see the paper for an explanation of 2.5-D) produced good results when the source-to-receiver crossline separation was small and noticeably poorer results when the source-to-receiver crossline separation was large (Figures 6 and 13, respectively). In neither case was the incoherent noise caused by the diffracted multiples completely attenuated. This result is not a surprise since diffracted multiples are an inherently 3-D phenomenon. The inability to attenuate them fully is due to limitations of current data acquisition practices.

Although possible remedies to the limitations of current data acquisition practices were envisioned at about the same time as when adaptive subtraction became widely used, practical applications of those ideas have appeared in the literature only recently. Two types of remedies are possible. Although full 3-D marine acquisition with towed streamers may never be practical, there are novel acquisition schemes that offer benefits. Alternatively, data acquired with standard survey designs may be extrapolated and interpolated in various ways and at various processing stages to simulate full 3-D data acquisition. *Keggin et al. (2003)* present a simple, but expensive, acquisition remedy for the problems created by 3-D diffracted multiples. Using an 8-cable streamer ship and a separate shooting ship, a single target swath was acquired nine times with different source-receiver configurations. Stacking the resulting multi-azimuth data sets produced a significant reduction in the noise due to diffracted multiples.

If a 3-D surface multiple prediction algorithm is applied to standard 3-D marine streamer data the sparse crossline sampling of the surface wavefield causes the predicted multiples to be a poor representation of the actual multiples. The next two papers, *van Dedem and Verschuur (2001)* and *Hokstad and Sollie (2003)*, attack this problem using sparse inversion (based on assumptions of hyperbolic and parabolic shaped events, respectively) applied to the crossline multiple contribution gathers. (These gathers consist of the collection of traces that are summed to produce a trace containing predicted multiples.) Specifically, the inversion produces a parametric representation of the information in a sparsely populated crossline multiple contribution gather from which accurate predicted multiples are calculated as if the gather were fully populated. *Nekut (1998)* offers a different solution to the sparse crossline sampling problem of streamer acquisition. He proposes

using least-squares migration-demigration as an interpolation and extrapolation process to create a fully populated 3-D data set from standard 3-D field measurements. Although computationally expensive, small-scale synthetic data set tests suggest that the method has promise. The final paper in this chapter, *Kleemeyer et al. (2003)*, is the first exploration industry publication to describe actual application of 3-D surface multiple attenuation to an entire 3-D marine streamer survey. Multiple prediction was accomplished by Shell's MAGIC3D algorithm (*Biersteker, 2001*), which includes a massive data regularization, extrapolation, and interpolation effort. Interestingly, in Kleemeyer et al. the predicted multiples are subtracted from the data after both were prestack depth migrated. The results show superior attenuation of diffracted multiples compared to earlier processing efforts.

As this reprint volume goes to press, we think that the seismic industry is just at the beginning of a major effort to develop practical, cost-effective ways of applying 3-D surface multiple prediction to 3-D marine streamer surveys. Although the theory and underlying physical basis of the method are well understood, many pragmatic compromises will likely be necessary and remain to be discovered. While deterministic prediction of multiples brings greater effectiveness, such predictions will never be perfect; hence, there will always be a role for statistical and adaptive procedures. These issues also motivate the drive for more effective data collection, such as single sensor data, and extrapolation and interpolation methods. The heightened demand on definition and completeness will be increasingly satisfied in the coming years, leading to a new level of effectiveness for the attenuation of free surface and internal multiples, and the subsequent imaging and inversion methods for primaries.

Chapter 6 Reference

Ziolkowski, A., Parkes, G., Hatton, L. and Haugland, T., 1982, The signature of an air gun array: Computation from near-field measurements including interactions: Geophysics, **47**, 1413-1421.

Spitz, S., 1999, Pattern recognition, spatial predictability, and subtraction of multiple events: The Leading Edge, **18**, 55-58.

Chapter 6 Papers

Carvalho, P.M. and Weglein, A.B., 1994, Wavelet estimation for surface-related multiple attenuation using a simulated annealing algorithm: SEG Expanded Abstracts, 1481-1484.

Ikelle, L.T., Roberts, G. and Weglein, A.B., 1997, Source signature estimation based on the removal of first-order multiples: Geophysics, 62, 1904-1920.

Ziolkowski, A., Taylor, D.B. and Johnston, R.G.K., 1999, Marine seismic wavefield measurement to remove sea-surface multiples: Geophysical Prospecting, **47**, 841-870.

Weglein, A.B., Tan, T.H., Shaw, S.A., Matson, K.H. and Foster, D.J., 2000, Prediction of the wavefield anywhere above an ordinary towed streamer: application to source waveform estimation, demultiple, deghosting, data reconstruction and imaging: SEG Expanded Abstracts, 2413-2415.

Ross, W.S., Yu, Y. and Gasparotto, F.A., 1999, Traveltime prediction and suppression of 3-D multiples: Geophysics, **64**, 261-277.

Abma, R., Kabir, N., Matson, K., Shaw, S.A., McLain, B. and Michell, S., 2002, Comparison of adaptive subtraction techniques for multiple suppression: SEG Expanded Abstracts, 2186-2189.

van Borselen, R., Fookes, G. and Brittan, J., 2003, Target-oriented adaptive subtraction in data-driven multiple removal: The Leading Edge, **22**, 340-343.

Guo, J., 2003, Adaptive multiple subtraction with a pattern-based technique: SEG Expanded Abstracts, 1953-1956.

Keggin, J., Widmaier, M., Hegna, S. and Kjos, E., 2002, Attenuation of multiple diffractions by multi-azimuth streamer acquisition: EAGE Expanded Abstracts, F39.

Hadidi, M.T., Baumstein, A.I. and Kim, Y.C., 2002, Surface-related multiple elimination on wide-tow marine data: The Leading Edge, **21**, 787-790.

van Dedem, E.J. and Verschuur, D.J., 2001, 3D surface multiple prediction using sparse inversion: SEG Expanded Abstracts, 1285-1288.

Hokstad, K. and Sollie, R., 2003, 3-D surface-related multiple elimination using parabolic sparse inversion: SEG Expanded Abstracts, 1961-1964.

Nekut, A.G., 1998, 3D surface-related multiple prediction: SEG Expanded Abstracts, 1511-1514.

Biersteker, J., 2001. MAGIC: Shell's surface multiple attenuation technique: SEG Expanded Abstracts, 1301-1304.

Kleemeyer, G., Pettersson, S.E., Eppenga, R., Haneveld, C.J., Biersteker, J. and den Ouden, R., 2003, It's magic – industry first 3D surface multiple elimination and pre-stack depth migration on Ormen Lange: EAGE Expanded Abstracts, B43.

Chapter 7

Multiple attenuation for land, ocean bottom, and vertically-deployed marine receiver data sets

Interestingly, most of the technical literature on multiple attenuation addresses the problem of multiple reflections in marine streamer data. Perhaps, arguing that the relatively high reflection coefficients of the water surface and the water bottom make multiples in marine data more of a problem than those in land data, we should laud geophysicists for tackling the tougher problem. On the other hand, one could counter that their very subtlety makes multiples in land data the tougher problem of the two. Regardless of the outcome of such an argument, it is certainly true that the non-uniformity and noise contamination of typical land data sets makes removing multiples a difficult, expensive problem indeed. Furthermore, because the source of multiples in a land data set is rarely obvious, data processors are often left with a nagging uncertainty: Were the events affected by that process really multiples, or were they perhaps primary reflections?

Kelamis et al. (1990) describe a practical methodology for applying the Radon transform (*Yilmaz (1989)*, Chapter 3) to attenuate multiples in high-density land data sets. By using a pre-processing step to reduce the multiplicity and regularize the geometry, they managed to obtain convincing results at a modest cost. Ten years later, *Kelamis and Verschuur (2000)* investigated the application of surface-related multiple elimination (SRME) (*Verschuur et al. (1992)*, Chapter 4) to land data sets. SRME was originally conceived as a method of eliminating surface multiples in marine data, where the surface has a nearly uniform reflection coefficient. To make this method applicable for land data, Kelamis and Verschuur balanced the data amplitudes in a pre-processing step so as to have smooth multiple prediction operators. They obtained good multiple suppression in land data sets for which other methods (moveout discrimination and predictive deconvolution) were unsatisfactory.

Technologies for recording exploration-quality seismic data on the sea floor have become viable only since about 1990. The main difficulty with sea-floor recording (other than hardware issues) is the impact of the receiver ghost reflection and subsequent water-column reverberations on the data bandwidth. Many years ago, *J. E. White (1965)* proposed a solution to that problem for pressure measurements. Currently, the seismic industry has many schemes based on White's idea to record both pressure and the vertical component of particle velocity and combine those measurements to cancel reverberations in the water column. *Barr (1997)* presents an overview of this method and *Barr et al. (1997)* compare several different variations of the method. *Amundsen et al. (1998)* describe a generalization of the concept: up/down splitting based on the elastodynamic representation theorem. Unlike earlier methods, their algorithm is valid for a dipping sea floor with medium parameters that vary laterally. *Osen et al. (1999)* extended White's concept to remove water-layer multiples from multicomponent sea-floor data, including the horizontal components of particle velocity. Finally, *Amundsen (2001)* describes an algorithm, based on up/down wavefield separation, that removes the effect of the free surface entirely as well as accomplishing signature deconvolution. Up/down wavefield separation requires two recordings: either pressure and the vertical component of particle velocity or pressure and its vertical derivative. The method also requires measurement of the direct arrival from the marine source.

Although marine data sets recorded by towed streamers and ocean-bottom sensors differ in many

ways, they do have one characteristic in common: the receivers are deployed in a horizontal or near-horizontal plane. *Sonneland et al. (1986)* describe using data recorded with two horizontal marine streamers, one above the other in the vertical plane, to accomplish receiver deghosting. Their algorithm is based on up/down wavefield separation, and thus, as in *Amundsen (2001)* allows both dereverberation and designature. An alternative vertical acquisition scheme is to deploy entire marine cables vertically, a method developed during the 1990's. As with the borehole VSP method, vertical marine cables allow separation of the recorded pressure wavefield into its up- and down-going components. That capability by itself does not, however, solve the multiple problem. *Wang et al. (2000)* describe attenuating multiples in vertical cable data using a three-step process: a common-shot τ-p filter (*Yilmaz, 2001*) to remove receiver ghost multiples, common-receiver deconvolution to remove source ghosts, and a Radon filter to remove other multiples.

Chapter 7 Reference

White, J.E., 1965, Seismic waves: Radiation, transmission and attenuation: McGraw-Hill Inc., pp.42-43

Yilmaz, O., 2001, Seismic data analysis: processing, inversion, and interpretation of seismic data: Society of Exploration Geophysics, Chapter 6.

Chapter 7 Papers

Kelamis, P.G., Chiburis, E.F. and Shahryar, S., 1990, Radon multiple elimination, a practical methodology for land data: SEG Expanded Abstracts, 1611-1614.

Kelamis, P.G. and Verschuur, D.J., 2000, Surface-related multiple elimination on land seismic data – Strategies via case studies: Geophysics, **65**, 719-734.

Barr, F.J., 1997, Dual-sensor OBC technology: The Leading Edge, **16**, 45-51.

Barr, F.J., Chambers, R.E., Dragoset, W. and Paffenholz, J., 1997, A comparison of methods for combining dual-sensor ocean-bottom cable traces: SEG Expanded Abstracts, 67-70.

Amundsen, L., Ikelle, L.T. and Martin, J., 1998, Multiple attenuation and P/S splitting of OBC data at a heterogeneous sea floor: EAGE Expanded Abstracts, P044.

Osen, A., Amundsen, L. and Reitan, A., 1999, Removal of water-layer multiples from multicomponent sea-bottom data: Geophysics, **64**, 838-851.

Amundsen, L., 2001, Elimination of free-surface related multiples without need of the source wavelet: Geophysics, **66**, 327-341.

Sonneland, L., Berg, L.E., Eidsvig, P., Haugen, A., Fotland, B. and Vestby, J., 1986, 2-D deghosting using vertical receiver arrays: SEG Expanded Abstracts, 516-519.

Wang, H., Druzhinin, A. and Li, X-Y., 2000, The impact of multiple suppression on vertical cable data imaging: SEG Expanded Abstracts, 2173-2176.

Chapter 8

Tutorials, reviews and case histories

The papers in this chapter were written specifically to educate the reader about various aspects of multiple attenuation technology. They are divided into two sets: 1) general reviews, overviews, and case histories, and 2) comparisons of different wave theoretic approaches to multiple attenuation. The first set emphasizes verbal, rather than mathematical, explanations, although some of the papers do contain simple equations. Because of its subject, the second set, although also tutorial, relies more heavily on mathematics. The papers in the second set refer liberally to many of the papers in Chapters 4 and 5. Readers who are not intimately familiar with the math may want to review those papers before perusing those included here.

Hardy and Hobbs (1991) present a tutorial that describes how to select a reasonably effective multiple suppression strategy for any particular data set. The words "reasonably effective" mean that multiples are adequately suppressed, without harming primary reflections, as efficiently as possible. Given the wide range of suppression methods discussed in this volume, such a selection process is by no means a trivial exercise. Hardy and Hobbs suggest that with a basic knowledge of multiple attenuation theory and a preliminary data analysis, selection of the likely best suppression method can be accomplished with very little actual data set testing. They provide a reasonable application strategy and perspective for multiple attenuation methods that were widely available in 1991.

The January 1999 issue of *The Leading Edge* contains a special section devoted to multiple attenuation. Based partly on a 1997 research workshop organized by the SEG Research Committee, the special section aimed to present the then current state-of-the-art in multiple attenuation technology. Several of the papers in the special section were the work of the inverse scattering researchers at Atlantic Richfield Company (ARCO). They were deliberately written in a tutorial style for *The Leading Edge* . They include: "Multiple attenuation: an overview of recent advances and the road ahead" (*Weglein, 1999*); "How can the inverse-scattering method really predict and subtract all multiples from a multidimensional earth with absolutely no subsurface information?" (*Weglein, 1999*); and "A comparison of three multiple-attenuation methods applied to a hard water-bottom data set" (*Matson et al., 1999*). A year later, a tutorial (*Matson, 2000*) on the requisite wavelet estimation method for free-surface multiples was published. It describes the use of free-surface multiple removal algorithms (see Chapters 4, 5, and 6) to estimate the acquisition wavelet.

Ellis and van Borselen (2003) present a case history involving wave equation-based surface multiple attenuation (see Chapter 4). Their conclusion is important for all practitioners of this technology: extensive analysis and quality control are required to gauge the performance of both multiple prediction and adaptive subtraction. *Reshef et al. (2003)* offer an alternative approach to dealing with the multiple problem. If multiple events can be reliably predicted, then those predictions can be used as an interpretation tool. That is, the predicted multiples can alert an interpreter to portions of a data set where he must be aware that multiples may cause interpretation difficulties. Reshef et al. describe a purely kinematic prediction scheme that does not require pre-stack data. This allows the method to be used in an interactive mode.

Chapters 4 and 5 describe two wave theoretical methods of multiple attenuation developed and promoted during the 1980's and 1990's. Around 1998, the two most prominent groups involved

in the development of those two methods - the inverse scattering developers at ARCO and the feedback researchers at Delft University - began a collaborative project to compare and contrast their approaches. One outcome of this collaboration was two pairs of jointly published papers that compare the two methods. All four papers are included here. The first pair (*Verschuur et al., 1998 and Matson et al., 1998*) are extended abstracts of two oral talks that were presented at the 1998 SEG Annual Convention. Two years later, the two groups again presented joint papers at the 2000 Offshore Technology Conference (*Berkhout et al., 2000 and Weglein, et al., 2000*). In summary: (1) The free-surface multiple removal method derived from the inverse scattering series is physically complete, whereas the feedback procedure has a compromise that includes the absence of the obliquity factor. It is argued that the effect of omitting the obliquity factor is partially mitigated by not deghosting the source prior to multiple prediction. Even so, as offset increases the error in predicted multiples becomes more significant and requires the angle-dependent nature of the obliquity factor to be incorporated into an angle-dependent or offset-dependent adaptive "wavelet." Since the resulting "wavelet" is no longer equivalent to simply the acquisition wavelet, it should not be used to deconvolve the seismic data. The obliquity-compromised form is computationally efficient and results in a simple f-x formalism. However, that compromise is being revisited in the current industry trend of seeking greater effectiveness in removing multiples. (2) For internal multiples, the two formalisms are quite different between the two methods. However, the recent recasting of the interface method as a selected "single interface" or "interval" procedure captures some of the inclusiveness and lack of interpretive intervention of the internal multiple prediction of the inverse scattering internal multiple procedure.

Ikelle et al. (2003), compare and contrast multiple attenuation methods derived from two different integral equations: the Lippmann-Schwinger equation and the representation theorem. The authors show that these two different starting points eventually lead to equivalent results. Finally, there are two recent papers of interest on the subject of inverse scattering methods for attenuating internal multiples. *ten Kroode (2002)* provides an important and rigorous analysis of the inverse scattering internal multiple algorithm. A central assumption in the paper is that the attenuating algorithm (that is, the leading term in a removal series) is designed to remove the leading order *approximation* to internal multiples. In contrast, *Weglein et al. (2003)* recently demonstrated that the internal multiple attenuation algorithm has greater efficacy on *actual* internal multiples than on a Born approximation to those multiples. At this time, these researchers are actively engaged in an ongoing collaborative communication about these matters. We are confident that this will soon produce a deeper understanding of the strengths and underlying assumptions of current algorithms, as well as generalizations that point the way toward improved algorithms for dealing with coherent noise and troublesome composite events.

Chapter 8 Reference

Weglein, A.B., Arajo, F.V., Carvalho, P.M., Stolt, R.H., Matson, K.H., Coates, R.T., Corrigan, D., Foster, D.J., Shaw, S.A. and Zhang, H., 2003, Inverse scattering series and seismic exploration: Inverse Problems, **19**, R27-R83.

ten Kroode, F., 2002, Prediction of internal multiples: Wave Motion, **35**, 315-338.

Chapter 8 Papers

Hardy, R.J.J. and Hobbs, R.W., 1991, A strategy for multiple suppression: First Break, **9**, 139-144.

Weglein, A.B., 1999, Multiple attenuation: an overview of recent advances and the road ahead (1999): The Leading Edge, **18**, 40-44.

Weglein, A.B., 1999, How can the inverse-scattering method really predict and subtract all multiples from a multidimensional earth with absolutely no subsurface information?: The Leading Edge, **18**, 132-136.

Matson, K.H., Paschal, D. and Weglein, A.B., 1999, A comparison of three multiple-attenuation methods applied to a hard water-bottom data set : The Leading Edge, **18**, 120-126.

Matson, K.H., 2000, An overview of wavelet estimation using free-surface multiple removal: The Leading Edge, **19**, 50-55.

Ellis, D, and van Borselen, R., 2003, Multiple prediction and subtraction – an SRME and IME case history: EAGE Expanded Abstracts, B44.

Reshef, M., Keydar, S. and Landa, E., 2003, Multiple prediction without prestack data: an efficient tool for interpretive processing: First Break, **21**, March, 29-37.

Verschuur, D.J., Berkhout, A.J., Matson, K.H., Weglein, A.B. and Young, C.Y., 1998, Comparing the interface and point-scatterer methods for attenuating internal multiple: a study with synthetic data – Part 1: SEG Expanded Abstracts, 1519-1522.

Matson, K.H., Weglein, A.B., Young, C.Y., Verschuur, D.J. and Berkhout, A.J., 1998, Comparing the interface and point-scatterer methods for attenuating internal multiple: a study with synthetic data – Part 2: SEG Expanded Abstracts, 1523-1526.

Berkhout, A.J., Weglein, A.B. and Verschuur, E., 2000, Wave theoretic approaches to multiple attenuation: Concepts, status, open issues, and plans: Part I, OTC 12010, Houston, TX.

Weglein, A.B., Matson, K.H. and Berkhout, A.J., 2000, Wave theoretic approaches to multiple attenuation: Concepts, status, open issues, and plans: Part II: OTC 12011, Houston, TX.

Ikelle, L.T., Amundsen, L., Gangi, A. and Wyatt, S.B., 2003, Kirchhoff scattering series: Insight into the multiple attenuation method: Geophysics, **68**, 16-28.

Chapter 9

Multiples as signal

There are two basic views of seismic reflection data. The inclusive view treats all reflection data as signal, since all events contain information about the subsurface. In contrast, the exclusive view treats only primary reflections as signal and considers multiples an undesirable noise. The latter view – that espoused by the first eight chapters of this volume – by far dominates, for a good reason. Extracting accurate depth images from just primary reflection information is, in general, a complex, difficult task. Conventional wisdom is that imaging with multiples must be significantly more challenging. As the papers in this chapter illustrate, however, challenging conventional wisdom can lead to surprising and promising ideas. Specifically, extracting useful information from multiple reflections may not be as difficult as traditionally thought.

Reiter et al. (1991) demonstrate the use of receiver-side, first-order surface multiples to enhance migrated primary reflection images in data recorded on the ocean bottom. This was accomplished by using moveout discrimination to isolate the multiples of interest and then migrating them using a ray-based Kirchhoff depth migration. The resulting composite image had improved signal-to-noise ratio and extended lateral subsurface coverage. In contrast to Reiter et al., *Berkhout and Verschuur (1994)* propose a general scheme for migrating all surface multiples in a data set rather than just those with a specific ray path. The method requires isolation of the surface multiple component of the seismic response and the formation of areal source wavefields using the total seismic response. The authors note that the method can be extended to internal multiples, although no details are given. *Sheng (2001)* suggests yet another method of using the information in surface multiples. First-order surface multiples are cross-correlated with primaries to remove the first leg of their raypath. The remaining second leg is migrated using the appropriate primary migration operator. *Youn and Zhou (2001)* describe a migration scheme that propagates a source wavelet in the forward direction and the recorded traces in a shot record in the backward direction, using - for both cases - a full two-way scalar wave equation. The two propagated wavefields are correlated and summed over all time indices to produce an image frame. The claim is that this scheme uses all types of events to produce a depth migrated image directly from raw field records. Because of the massive data storage and computational requirements, the authors applied the algorithm to only an extremely decimated version of the synthetic Marmousi model. Finally, *Berkhout and Verschuur (2003)* introduce the notion of a "focal transform," a variation on the feedback model method of multiple prediction (see Chapter 4) that involves correlation rather than convolution. The focal transform reduces the order of each surface multiple in a data set by one. This allows primary information to be extracted from multiples. One application is the extracting of short-offset primary reflections (that are not directly recorded) from longer-offset multiples (that are directly recorded).

The papers in this chapter clearly support the premise that the multiple wavefield in a seismic data set contains useful information about the earth's subsurface. Thus, arguably a better approach to the multiple problem is using that information rather than discarding it. Based on the papers included here, data correlation seems to be a key to making use of multiples. Other papers (among them, for example: *Tarantola, 1984; Clement, et al., 2001; and He and Schuster, 2003*) have suggested various seismic data inversion schemes that can accommodate the presence of multiply reflected energy. Although such inversion papers are beyond the scope of this volume, they are

recommended reading for anyone interested in all possible methods of dealing with the multiple problem. *Tarantola (1984)* formulated the geophysical inverse problem in a Baysian framework and described algorithms for estimating the minimum of an objective function based on local or gradient descent optimization. Although data inclusive in philosophy, the limitations of these specific indirect inversion approaches included their strong dependence on the choice of starting model, the computation of sensitivity matrices or Frechet derivatives, manipulating large matrices and inability to update the slowly varying part of the velocity field with field data. Indirect inversion has progressed to global optimization methods – such as simulated annealing and genetic algorithms – that avoid certain pitfalls with gradient methods. For example, *Sen and Stoffa (1995)* describe several global optimization methods for application to geophysical inversion and, despite significant computational needs, provide encouraging examples of effectiveness for 1-D inversion with primaries and multiples as input and for migration velocity analysis with primaries.

Use of multiply reflected energy is still a relatively unexplored terrain. Other means of exploiting, rather than attenuating, multiple energy may remain to be discovered. We expect further efforts in this area in the years ahead.

Chapter 9 Reference

Tarantola, A., 1984, Inversion of seismic reflection data in the acoustic approximation: Geophysics, **49**, 1259-1266.

Sen, M.K. and Stoffa, P.L., 1995, Global Optimization Methods in Geophysical Inversion: Elsevier Science Publishing Co.

Clement, F., Chavent, G. and Gomez, S., 2001, Migration-based traveltime waveform inversion of 2-D simple structures; A synthetic example: Geophysics, **66**, 845-860.

He, R. and Schuster, G., 2003, Least squares migration of both primaries and multiples: SEG Expanded Abstracts, 1035-1038.

Chapter 9 Papers

Reiter, E.C., Toksoz, M.N., Keho, T.H. and Purdy, G.M., 1991, Imaging with deep-water multiples: Geophysics, **56**, 1081-1086.

Berkhout, A.J. and Verschuur, D.J., 1994, Multiple technology part II: Migration of multiple reflections: SEG Expanded Abstracts, 1497-1500.

Sheng, J., 2001, Migrating multiples and primaries in CDP data by crosscorrelogram migration: SEG Expanded Abstracts, 1297-1300.

Youn, O.K. and Zhou, H.-W., 2001, Depth imaging with multiples: Geophysics, **66**, 246-255.

Berkhout, A.J. and Verschuur, D.J., 2003, Transformation of multiples into primary reflections: SEG Expanded Abstracts, 1925-1928.

Internal multiple attenuation code-development and implementation

Sam T. Kaplan, Kristopher A. Innanen, Einar Otnes and Arthur B. Weglein

Abstract

We report on the progress of the internal multiple attenuation code-development and implementation project at M-OSRP for the year 2004–2005. We develop a standard for M-OSRP code generation and delivery that will serve as a benchmark for future large-scale programming solutions created here; this serves primarily the research and educational interests of the consortium, but aligns strongly with the interests of the sponsors. In this paper we further detail the mathematical and physical underpinning for (a) the logic of the code structure and (b) a number of optimization strategies for increasing the efficiency of this computationally expensive procedure. Examples and illustrations of the code, the computation of its inputs from seismic data, and the creation of synthetic data to validate and test the algorithm are provided. We sketch out our plans for the coming year.

1 Introduction

In March of 2004 an implemenation and code-development of the internal multiple attenuation (IMA) algorithm was announced. It has arisen to fill our research needs, to wit: our objectives involve characterization of the scope and applicability of the algorithm and efforts to "move beyond" attenuation (all described within this report), and these are served by having an in-house version of the code for 1.5D, 2D, and potentially 3D applications. Furthermore, as we move our flagship projects (namely algorithms acting on primaries) towards multiple dimensions, in which finite-difference modelling will the necessary standard for input synthetic data creation, the need for an operational IMA to remove the coherent noise will be very strong. Personnel and objectives (the latter to be discussed below) were in place as of June 2004, and we are pleased to be able to report progress in keeping with, and beyond, plans.

This note will serve as a report on the status, a delivery time-line, and an outline of the objectives and standards for this code development. Moreover, it contains, with an appropriate level of detail, the physically- and mathematically-based insights that lie behind the algorithm as it has been implemented. This report, and the documentation that will accompany the delivery of the code, therefore constitute an explicit description of the logic-train of the implementation.

In the remainder of **section 1**, we discuss explicitly the project objectives, and standards we have set for implementing (and distributing) large-scale computer codes. We are entering a phase of research in which our ideas and algorithms are expanding from 1D to multi-D, and as a consequence matters of computation come to the fore. The IMA project should be considered not just on its own, but as the testing ground upon which a standard for code implementation is developed that all subsequent M-OSRP projects adhere to. We comment on our current vision of this standard of what we refer to as "research-grade code", and some of its features.

In **section 2**, we discuss practical issues of an implementation of the IMA algorithm. Important amongst these is the computation of the main input to the algorithm, which is akin to an un-collapsed Stolt migration of the data with water speed, and as such involves familiar issues of avoidance of evanescence, and interpolation, etc. Other issues range from the "look" of the code, as a set of transparently organized, and interchangeable processing tasks, to order-of-operations characterization of the computational burden of the algorithm and comparisons to free-surface de-multiple methods, to integral identities and representations that, although mathematically equivalent, lead to varying levels of computational efficiency.

In **section 3** we provide some numerical examples of the IMA code working on 1D and 2D pre-stack synthetic data sets, and in particular comment on the stringent requirements that the IMA algorithm places on forward modelling procedures as generators of synthetics for validation purposes. We discuss an appropriate finite-difference approach and an M-OSRP implementation of this code that will be made available at the time of the IMA code delivery.

Finally in **section 4** we summarize the project to date and comment on objectives for the 2005–2006 year.

1.1 Project objectives and code delivery time-line

2004–2005 is the first year in which the projects of M-OSRP are leading to the construction (and delivery) of large-scale codes. The IMA implementation has been carried out with an eye for developing a set of code-writing and delivery objectives that serves the research and educational needs of the group internally. Hence we will devote some space in this year's report to carefully outlining these objectives. The 1D and 2D pre-stack versions of the internal multiple attenuation code will be made available to the sponsors at the end of May 2005. At that time, an auxiliary forward modelling code for validation of the IMA algorithm will be distributed also.

1.2 "Research-grade code": a standard for M-OSRP software

Our objective is to develop theory and algorithms for the processing and inversion of seismic data that directly address actual concerns of the petroleum industry. The validation of these algorithms requires code development, and our internal standards for code-writing will result in implementations of all of our algorithms that will be shared and discussed with sponsors. The research interests of M-OSRP suggests a standard for our code generation that we refer to as "research-grade".

Our standard for writing large scale codes is borne out of the research requirements of the students and associates at M-OSRP. Every project is in general linked to every other project, a point that has been hit upon repeatedly: many projects involve the creation of processing algorithms, the output of which is the input to other projects. Moreover, many of the research projects underway span several "generations" of graduate students and researchers; new graduate students may by necessity inherit the codes and implementations of senior graduate students.

In either case, there is a need for a coding style and standard for documentation and design that makes *use* and *understanding* of the implementation straightforward for others. These internal research needs lead to a schema for code production that involves:

1. Documentation at the level of:
   a. descriptive report writing,
   b. pseudo-code,
   c. commenting within code; and
2. Code design that
   a. renders the logic of the algorithm transparent, and
   b. is straightforward to alter.

The remainder of this report is an initial model of algorithm description, logic, documentation and pseudo-code.

2 Implementing the IMA algorithm

We begin the discussion by quoting the form of the algorithm; readers are directed to any one of the references herein. We will consider two versions of the IMA algorithm in the analysis and discussions of this paper. The 1D normal incidence algorithm is (3)

$$b_{3IM}(\omega) = \int_{-\infty}^{\infty} b_1(z_1) e^{i2kz_1} \int_{-\infty}^{z_1-\epsilon} b_1(z_2) e^{-i2kz_2} \int_{z_2+\epsilon}^{\infty} b_1(z_3) e^{i2kz_3} dz_3 dz_2 dz_1 \tag{1}$$

where $b_1(z) = D(z)$ and $D(z)$ is the data trace, in pseudo-depth z, obtained from a normally incident experiment. In two dimension, the algorithm is written (5; 4),

$$b_{3IM}(k_{gx}, k_{sx}, \omega) = \frac{1}{(2\pi)^2} \int_{-\infty}^{\infty} \int_{-\infty}^{\infty} \int_{-\infty}^{\infty} e^{i(k_{gz}+k_{1z})z_1} b_1(k_{gx}, k_1, z_1) \int_{-\infty}^{z_1-\epsilon} e^{-i(k_{1z}+k_{2z})} b_1(k_1, k_2, z_2) \cdot \int_{z_2+\epsilon}^{\infty} e^{i(k_{2z}+k_{sz})z_3} b_1(k_2, k_{sx}, z_3) dz_3 dz_2 dz_1 dk_1 dk_2 \tag{2}$$

where

$$b_1(k_{gx}, k_{sx}, k_z) = -i2k_{sz} D(k_{gx}|k_{sx}; k_z) \tag{3}$$

and $D(k_{gx}|k_{sx}; k_z)$ is the downward continued scattered wave-field.

Broadly, the output of this code is $b_{3IM}(k_{gx}, k_{sx}, \omega)$, in one or other case of dimensionality. It is a quantity in data space that is an approximation to the negative of the internal multiples in the input data, ready for subtraction. The input, b_1, is closely related to the data, and includes no auxiliary information apart from water speed.

The task of this project is to compute the inputs and integrals of equations (2) and (3) efficiently and accurately. The first ingredient, then, is seismic data in the form of $b_1(z)$ (or $b_1(k_{gx}, k_{sx}, z)$), where z is pseudo-depth. The second ingredient is a chosen reference wave-speed c_0 (e.g. water speed) whose use is two-fold. First, it maps the data from two way travel time t to pseudo-depth z. In one dimension this relation is, simply, $z = c_0 t/2$, and in two dimensions, the mapping is

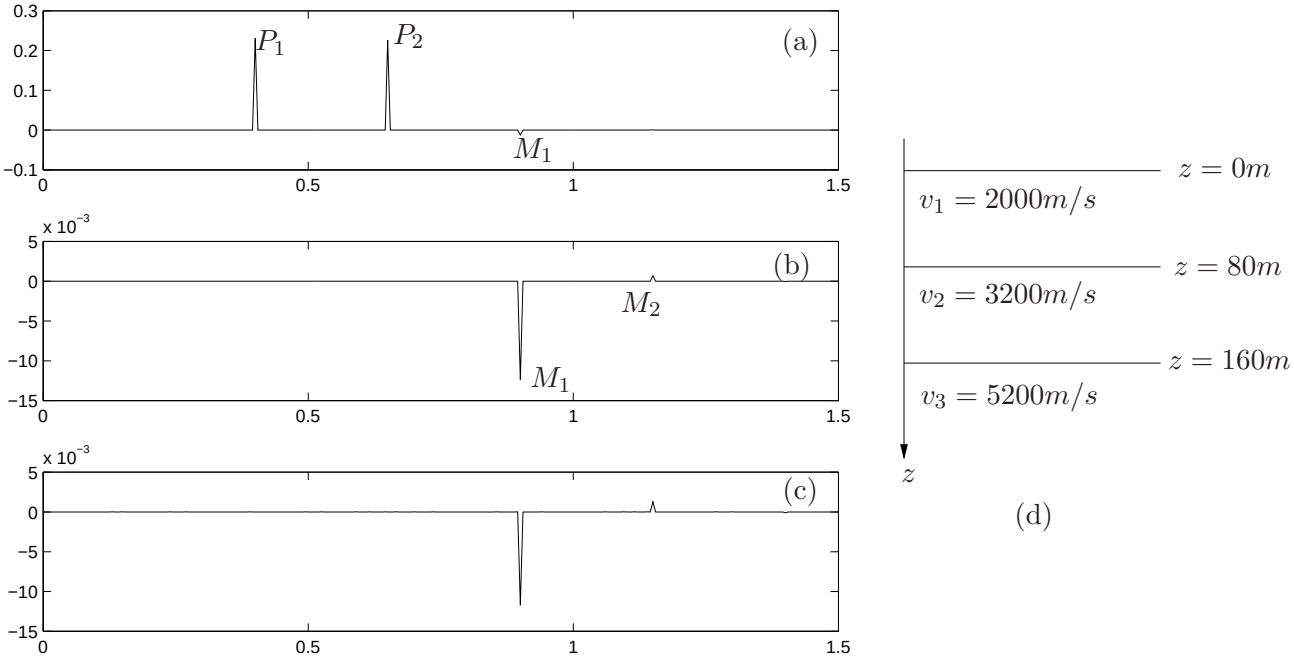

Figure 1: *1D attenuation internal multiple attenuation example. (a) Data with primary (P_1, P_2) and internal multiple (M_1) events. (b) Data with, only, internal multiple (M_1, M_2) events. (c) Internal multiples predicted by the algorithm. The data is generated from the model in (d).*

provided by fk migration. Second, c_0 is used in the computation of $k = \omega/c$ and $k_z = k_{gz} + k_{sz}$ where k_{gz} and k_{sz} are given by the dispersion relations,

$$k_{gz} = -\text{sgn}(\omega)\sqrt{\frac{\omega^2}{c_0^2} - k_{gx}^2} \qquad\qquad k_{sz} = -\text{sgn}(\omega)\sqrt{\frac{\omega^2}{c_0^2} - k_{sx}^2}. \tag{4}$$

The third and final ingredient is $\epsilon > 0$, whose value is chosen to ensure that the scattering interactions inherent in equations (1) and (2) are representative of only internal multiples, and do not, in addition, predict primary events.

Figure 1 illustrates the algorithm in one dimension. Figure 1b plots the data's internal multiples, where the data (Figure 1a) is synthesized from the one dimensional Earth model shown in Figure 1d. Figure 1c is the approximation to those internal multiples afforded by the multiple attenuation algorithm. The phase of the predicted multiples exactly matches that of the data, while their amplitudes differ (3).

2.1 A quick look at the code

Before we discuss this computation in a more detailed way, we briefly consider the form of the code, in other words we describe the look and feel of how these algorithm details appear in the code.

In the computation of b_{3IM}, we identify a variety of sub-tasks of the algorithm, many of which are standard to any processing shop: for instance, sorting, Fourier transforms, etc. Each of these tasks

have been implemented from the ground up in this project, but it is likely and expected that many of these functions will be dropped and replaced by in-house procedures.

A goal of this project has been to make that as simple as possible. Figure 2 contains an illustration of a particular portion of the code (in fact, the portion that computes b_1, the details of which are discussed in section 2.2). Each "paragraph" of the code corresponds to a task, and so the processing flow – modular as such – is easily altered.

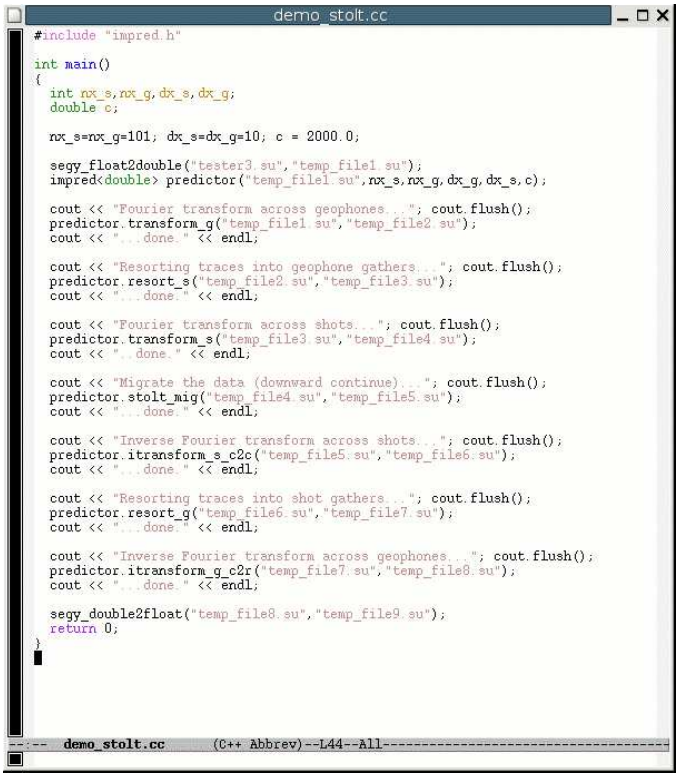

Figure 2: *Illustration of the code (in this case the computation of b_1). The organization is such that separable subtasks of the algorithm are easily removed and replaced by a user's preferred algorithm or subroutine.*

2.2 Computing the input to IMA: from data to b_1

In the previous section, we state that, for two spatial dimensions, the first ingredient required by the internal multiple attenuation algorithm is $b_1(k_{gx}, k_{sx}, z)$. This quantity is provided by equation (3) where $D(k_{gx}|k_{sx}; k_z)$ is the wave-field downward continued from the measurement surface, and $-i2k_{sz}$ is called the obliquity factor. We effect the downward continuation of the data by a change of variables from ω to k_z. This change of variables is determined by the dispersion relation (equation (4)).

The quantities b_1 and b_{3IM} are model-type independent, that is, their form does not change regardless of whether the medium of interest has been determined to behave acoustically, elastically, anelastically, etc. The input b_1 has been designed this way (Weglein et al., 1997), as an alteration to

the quantity that is normally found under desired component of the third-order inverse scattering series integral.

In practice, $D(k_{gx}|k_{sx};\omega)$, and thus $D(k_{gx}|k_{sx};k_z)$ are only known for a finite set of values. If $D(k_{gx}|k_{sx};\omega)$ is computed using fast Fourier transforms, then it will be evaluated on some regular grid in ω; but, given the nonlinearity of the dispersion relation, on some irregularly sampled grid in k_z. To facilitate the use of the fast Fourier transform in computing an integration over k_z, it is first necessary to interpolate such that the grid in ω becomes irregular, and the grid in k_z becomes regular. This mapping of D from a regular grid in ω to an irregular grid in ω is achieved using sinc interpolation.

We consider the interpolation for two spatial dimensions. The irregular grid for ω is chosen according to (2),

$$\omega(k_{gx},k_{sx},k_z)=\frac{c_0k_z}{2}\sqrt{\left(1+\frac{(k_{gx}+k_{sx})^2}{k_z^2}\right)\left(1+\frac{(k_{gx}+k_{sx})^2}{k_z^2}\right)} \tag{5}$$

and some regular grid in k_z. In detail, we (1) form regular grids in time t_r and temporal frequency ω_r,

$$\begin{aligned} t_r &= \left[\begin{array}{ccccc} 0 & \Delta t & 2\Delta t & \cdots & (n-1)\Delta t \end{array}\right] \\ \omega_r &= \left[\begin{array}{ccccccc} 0 & \Delta\omega & 2\Delta\omega & \cdots & (n/2)\Delta\omega & -(n/2-1)\Delta\omega & -(n/2-2)\Delta\omega & \cdots & -\Delta\omega \end{array}\right] \end{aligned}$$

where n is an even integer and $\Delta\omega=2\pi/(n\Delta t)$. (2) we find corresponding regular grids in pseudo-depth and vertical wave-number using the reference wave-speed c_0,

$$\begin{aligned} z_r &= \left[\begin{array}{ccccc} 0 & c_0\Delta t/2 & c_0\Delta t & \cdots & c_0(n-1)\Delta t/2 \end{array}\right] = \left[\begin{array}{ccccc} 0 & \Delta z & 2\Delta z & \cdots & (n-1)\Delta z \end{array}\right] \\ k_{zr} &= \left[\begin{array}{ccccccc} 0 & \Delta k_z & 2\Delta k_z & \cdots & (n/2)\Delta k_z/2 & -(n/2)\Delta k_z & -(n/2-2)\Delta k_z & \cdots & -\Delta k_z \end{array}\right] \end{aligned}$$

where $\Delta k_z=2\pi/(n\Delta z)$. (3) The irregular ω_i is computed according to equation (5) such that

$$\omega_i=\{\omega(k_{gx},k_{sx},k_z)|k_z\in k_{zr}\}\,.$$

Following steps (1)-(3), outlined above, we find ω_i corresponding, precisely, to the desired regular grid k_{zr}.

The mapping of $D(k_{gx},k_{gy}|k_{sx},k_{sy};\omega)$ from ω_r to ω_i, and thus k_{zr}, requires an interpolation from

$$D_r=\{D(k_x,k_y,\omega)|\omega\in\omega_r\}$$

to

$$D_i=\{D(k_x,k_y,\omega)|\omega\in\omega_i\}\,.$$

We utilize sinc interpolation to effect this mapping, which given adequate bandwidth in D provides a perfect result. We consider the real and imaginary parts of D_r, $\mathcal{R}[D_r]$ and $\mathcal{I}[D_r]$, separately. For the moment, we consider only the real component, and its convolution with a sinc filter (the exact same analysis holds true for the imaginary component),

$$h(\omega)=\mathrm{sinc}(\beta_n\omega)=\frac{\sin(\beta_n\omega)}{\beta_n\omega} \tag{6}$$

where β_n is the appropriate Nyquist frequency of D_r:

$$\beta_n = \frac{\pi}{\Delta\omega}$$

To avoid aliasing, β_n must exceed the bandwidth of D_r, but β_n is inversely proportional to $\Delta\omega$ which, in turn, is inversely proportional to the duration of $D_r(k_{gx}|k_{sx}, t)$ in time. This means that β_n is proportional to the duration of $D_r(k_{gx}|k_{sx}, t)$, and that we can avoid aliasing by padding in time such that

$$\beta_n > B$$

and B is the bandwidth of $D_r(k_{gx}|k_{sx}, \omega)$. In our algorithm, we pad $\mathcal{R}[D_r]$ out to at least $2n/0.6$ points, and convolve it with an 8-point sinc filter to effect the interpolation, providing

$$D_i = \{D(k_{gx}|k_{sx}, \omega)|\omega \in \omega_i\} = \{D(k_{gx}|k_{sx}, k_z)|k_z \in k_{zr}\}$$

which is the downward continued wave-field.

While the dispersion relation does provide a mapping between ω and k_z, it is evident from equation (4) that for certain values of (k_{gx}, k_{sx}, ω), k_z will be complex. The corresponding portion of the wave-field is called evanescent, and is not used in the computation of b_1. A trivial analysis of equation (4) shows that the non-evanescent portion of the wave-field, corresponding to real values of k_{gz} and k_{sz}, is found when

$$\{|k_{gx}|, |k_{sx}|\} \leq \frac{\omega}{c_0},$$

and only frequencies that obey this inequality are used to compute b_1.

Taking the above considerations into account, we present a pseudo-code for the computation $b_1(k_{gx}, k_{sx}, z)$ in Algorithm 1, and which is, therefore, a necessary prerequisite to the internal multiple attenuation algorithm.

Algorithm 1 Computation of $b_1(k_{gx}, k_{sx}, z)$

1: Fourier transform: $D(x_g|x_s; t) \rightarrow D(k_{gx}|k_{sx}; t)$.
2: **for** each (k_{gx}, k_{sx}) pair **do**
3: Zero pad $D(x_g|x_s; t)$ in time to avoid aliasing ($> 2n/0.6$ samples).
4: Fourier transform: $D(k_{gx}|k_{sx}; t) \rightarrow D(k_{gx}|k_{sx}; \omega)$
5: Isolate the non-evanescent portion of $D(k_{gx}|k_{sx}; \omega)$ by the dispersion relation.
6: Given a regular grid in k_z, compute an irregular grid in ω.
7: Do sinc interpolation: $D(k_{gx}|k_{sx}; \omega_r) \rightarrow D(k_{gx}|k_{sx}; \omega_i) \rightarrow D(k_{gx}|k_{sx}; k_{zr})$.
8: Apply the obliquity factor: $b_1(k_{gx}, k_{sx}, k_z) = -i2k_{sz}D(k_{gx}|k_{sx}; k_z)$.
9: Inverse Fourier transform: $b_1(k_{gx}, k_{sx}, k_z) \rightarrow b_1(k_{gx}, k_{sx}, z)$.
10: Truncate the data in z, thereby reversing the zero padding operation.
11: **end for**

2.3 The computational expense of IMA: a comparison to 3D FSMR

To get a handle on the computational expense of IMA, we compare the computation of $b_1(k_{gx}, k_{sx}, \omega)$ and equation (2) with an implementation of the expression for the free surface multiple elimination

algorithm (e.g. Weglein et al., 1997) in three spatial dimensions, given by

$$D'(k_{gx}, k_{gy}|k_{sx}, k_{sy}; \omega) = \int_{-\infty}^{\infty}\int_{-\infty}^{\infty} D(k_{gx}, k_{gy}|k_x, k_y; \omega) 2ik_{sz} D(k_x, k_y|k_{sx}, k_{sy}; \omega) dk_x dk_y. \quad (7)$$

Assuming that each of the dimensions contains the same number of samples, the 3D data have N^5 samples. Let us consider the calculation of equation (7) for a single realization of $D'(k_{gx}, k_{gy}|k_x, k_y; \omega)$. The integrals require N^2 summation operations. For a single temporal frequency, computing the left hand side for all wave numbers, therefore, requires N^4 summations. Hence, a very rough estimate of the 3D free surface multiple attenuation involves N^6 summations for each temporal frequency component.

Now consider the internal multiple attenuation algorithm for two spatial dimensions (equation (2)). Assuming each dimension contains N samples, the 2D data have N^3 samples. Let us now consider the case with single temporal frequency. For each combination of source/receiver coordinates (N^2) we need to calculate five nested integrals, involving on the order of N^5 summations. Hence, the 2D internal multiple attenuation is of order N^7 summations. Additionally, b_1 requires Stolt migration involving both fast Fourier transforms and sinc interpolations. Hence, we conclude that the computational complexity of the 2D internal multiple attenuation algorithm is greater than the 3D Free surface multiple attenuation algorithm.

2.4 Strategies for computational efficiency

The computational demand of the internal multiple attenuation algorithm is such that effort expended in developing reductions in its complexity are well-worthwhile. Here we discuss three categories of strategy for increasing the efficiency of IMA. The first is based on mathematical considerations of the algorithm itself, and more- vs. less-efficient, although fully equivalent, representations of IMA quantities. The second is based on the ability to limit the integration intervals of the method with a knowledge of the dip, or maximum dip, of structures in the medium. It is important to emphasize that prior knowledge of this kind is not a *requirement* of the method, but that it can be used to accelerate its computation.

ALGORITHMIC OPTIMIZATIONS

The one and two dimensional multiple attenuation algorithms presented in equations (1) and (2) respectively, both require the evaluation of a triple nested integral in pseudo-depth z. We consider two simplifications to the algorithms. First, by decoupling the two most inner integrals, and, second, by finding an efficient recursive formulation.

First, we consider the decoupling of the two most inner nested integrals. To aid in the analysis, we introduce the following lemma,

Lemma 1. *Let $f(z)$ and $g(z)$ be any integrable functions. Then,*

$$\int_{-\infty}^{\infty} f(z) \int_{-\infty}^{z-\epsilon} g(z')dz'dz = \int_{-\infty}^{\infty} g(z) \int_{z+\epsilon}^{\infty} f(z')dz'dz$$

Proof.

$$\begin{aligned}\int_{-\infty}^{\infty} f(z)\int_{-\infty}^{z-\epsilon} g(z')dz'dz &= \int_{-\infty}^{\infty} f(z)\int_{-\infty}^{\infty} H(z-\epsilon-z')g(z')dz'dz \\ &= \int_{-\infty}^{\infty} f(z')\int_{-\infty}^{\infty} H(z'-\epsilon-z)g(z)dzdz' \\ &= \int_{-\infty}^{\infty} g(z)\int_{-\infty}^{\infty} H(z'-(z+\epsilon))f(z')dz'dz \\ &= \int_{-\infty}^{\infty} g(z)\int_{z+\epsilon}^{\infty} f(z')dz'dz.\end{aligned}$$

□

The de-coupling of the nested integrals follows from Lemma 1. In particular, we let

$$\begin{aligned}f(z) &= b_1(z)e^{ik_z z} \\ g(z) &= b_1(z)e^{-ik_z z}\int_{z+\epsilon}^{\infty} b_1(z_1)e^{ik_z z_1}dz_1\end{aligned}$$

so that equation (1) becomes

$$\begin{aligned}b_{3IM}(k_z) &= \int_{-\infty}^{\infty} f(z_1)\int_{-\infty}^{z_1-\epsilon} g(z_2)dz_2dz_1 \\ &= \int_{-\infty}^{\infty} g(z_1)\int_{z_1+\epsilon}^{\infty} f(z_2)dz_2dz_1 \\ &= \int_{-\infty}^{\infty} b_1(z_1)e^{-ik_z z_1}\int_{z_1+\epsilon}^{\infty} b_1(z_2)e^{ik_z z_2}dz_2\int_{z_1+\epsilon}^{\infty} b_1(z_2)e^{ik_z z_2}dz_2dz_1 \\ &= \int_{-\infty}^{\infty} b_1(z_1)e^{-ik_z z_1}\left[\int_{z_1+\epsilon}^{\infty} b_1(z_2)e^{ik_z z_2}dz_2\right]^2 dz_1 \qquad (8)\end{aligned}$$

For the evaluation of the two inner integrals, this reduces the complexity of the algorithm–from $O(n^2)$ to $O(n)$. In two dimensions, we have a similar analysis. From equation (2), we consider the integrations over pseudo-depth by defining,

$$\begin{aligned}\rho(k_{gx},k_{sx},k_1,k_2,\omega) = \int_{-\infty}^{\infty} b_1(k_{gx},k_1,z_1)e^{i(k_{gz}+k_{1z})z_1}\int_{-\infty}^{z_1-\epsilon} b_1(k_1,k_2,z_2)e^{-i(k_{1z}+k_{2z})z_2} \\ \cdot\int_{z_2+\epsilon}^{\infty} b_1(k_2,k_{sx},z_3)e^{i(k_{2z}+k_{sz})z_3}dz_3dz_2dz_1, \qquad (9)\end{aligned}$$

where

$$b_{3IM}(k_{gx},k_{sx},\omega) = \int_{-\infty}^{\infty}\int_{-\infty}^{\infty}\rho(k_{gx},k_{sx},k_1,k_2,\omega)dk_1dk_2.$$

To enable the application of Lemma 1, we let

$$\begin{aligned}f(z) &= b_1(k_{gx},k_1,z)e^{i(k_{gz}+k_{1z})z} \\ g(z) &= b_1(k_1,k_2,z)e^{-i(k_{1z}+k_{2z})z}\int_{z+\epsilon}^{\infty} b_1(k_2,k_{sx},z_1)e^{i(k_{2z}+k_{sz})z_1}dz_1,\end{aligned}$$

so that equation (9) becomes

$$\rho(k_{gx}, k_{sx}, k_1, k_2, \omega) = \int_{-\infty}^{\infty} f(z_1) \int_{-\infty}^{z_1-\epsilon} g(z_2) dz_2 dz_1 = \int_{-\infty}^{\infty} g(z_1) \int_{z_1+\epsilon}^{\infty} f(z_2) dz_2 dz_1,$$

and substituting for our definitions of f and g gives,

$$\rho(k_{gx}, k_{sx}, k_1, k_2, \omega) = \int_{-\infty}^{\infty} b_1(k_1, k_2, z_1) e^{-i(k_{1z}+k_{2z})z_1} \left[\int_{z_1+\epsilon}^{\infty} b_1(k_2, k_{sx}, z_2) e^{-i(k_{1z}+k_{2z})z_2} dz_2 \right] \cdot \left[\int_{z_1+\epsilon}^{\infty} b_1(k_{gx}, k_1, z_2) e^{i(k_{gz}+k_{1z})z_2} dz_2 \right] dz_1 \quad (10)$$

Once again, we see the de-coupling of integrals, reducing the complexity of computing the inner most two integrals from $O(n^2)$ to $O(n)$.

We can apply a further simplification to the one and two dimensional algorithms in equations (8) and (10) by using a recursive formulation for evaluating the integrals. First, we consider the algorithm in one dimension. To facilitate the ensuing analysis, we let

$$\begin{aligned} f(k, z) &= b_1(z) e^{-i2kz} \\ g(k, z) &= b_1(z) e^{i2kz} \end{aligned}$$

so that equation (8) becomes

$$b_{3IM}(k) = \int_{-\infty}^{\infty} f(k, z_1) \left[\int_{z_1+\epsilon}^{\infty} g(k, z_2) dz_2 \right]^2 dz_1, \quad (11)$$

and approximating the integrals in equation (11) with Riemann sums gives

$$b_{3IM}(k) = f_1 \left[g_{1+\epsilon} + g_{2+\epsilon} + \cdots \right]^2 + f_2 \left[g_{2+\epsilon} + g_{3+\epsilon} + \cdots \right]^2 + \cdots$$

where $f_i = f(k, z_i)$, $g_{i+\epsilon} = g(k, z_i + \epsilon)$ and $z_i \in z$. Next, we write

$$b_{3IM}(k) = \sum_i f(k, z_i) G_i(g(k, z))^2$$

where

$$G_i(g(k, z)) = [g_{i+\epsilon} + g_{i+1+\epsilon} + \cdots] \quad (12)$$

It is evident, from equation (12), that G_i can be computed recursively:

$$\begin{aligned} G_1(g(k, z)) &= g_{1+\epsilon} + g_{2+\epsilon} + \cdots \\ G_2(g(k, z)) &= g_{2+\epsilon} + g_{3+\epsilon} + \cdots = G_1(g(k, z)) - g_{1+\epsilon} \\ G_3(g(k, z)) &= g_{3+\epsilon} + g_{4+\epsilon} + \cdots = G_2(g(k, z)) - g_{2+\epsilon} \\ &\cdots \end{aligned} \quad (13)$$

Thus, providing a further efficiency to the internal multiple attenuation algorithm.

In two spatial dimensions, we find a similar relation. Letting

$$\begin{aligned} f(k_1,k_2,\omega,z) &= b_1(k_1,k_2,z)e^{-i(k_{1z}+k_{2z})z} \\ g(k_1,k_{gx},\omega,z) &= b_1(k_{gx},k_1,z)e^{i(k_{gz}+k_{1z})z} \\ h(k_2,k_{sx},\omega,z) &= b_1(k_2,k_{sz},z)e^{i(k_{2z}+k_{sz})z}, \end{aligned}$$

equation (10) becomes

$$\rho(k_1,k_2,k_{gx},k_{sx},\omega) = \int_{-\infty}^{\infty} f(k_1,k_2,\omega,z_1)\left[\int_{z_1+\epsilon}^{\infty} g(k_1,k_{gx},\omega,z_2)dz_2\right]\left[\int_{z_1+\epsilon}^{\infty} h(k_2,k_{sx},\omega,z_2)dz_2\right]dz_1.$$

In analogy with the one dimensional case, we approximate the integrals with Riemann sums,

$$\begin{aligned} \rho(k_1,k_2,k_{gx},k_{sx},\omega) = f_1\left[g_{1+\epsilon}+g_{2+\epsilon}+\cdots\right]\left[h_{1+\epsilon}+h_{2+\epsilon}+\cdots\right] \\ + f_2\left[g_{2+\epsilon}+g_{3+\epsilon}+\cdots\right]\left[h_{2+\epsilon}+h_{3+\epsilon}+\cdots\right]+\cdots \end{aligned}$$

where $f_i = f(k_1,k_2,\omega,z_i)$, $g_{i+\epsilon} = g(k_1,k_{gx},\omega,z_i+\epsilon)$, $h_{i+\epsilon} = h(k_2,k_{sx},\omega,z_i+\epsilon)$ and $z_i \in z$. Next, we write

$$\rho(k_1,k_2,k_{gx},k_{sx},\omega) = \sum_i f(k_1,k_2,\omega,z_i)G_i(g(k_1,k_{gx},\omega,z))H_i(h(k_2,k_{sx},\omega,z))$$

and note the recursive formulation for G_i and H_i, such that

$$\begin{aligned} G_1(g(k_1,k_{gx},\omega,z)) &= g_{1+\epsilon}+g_{2+\epsilon}+\cdots \\ G_2(g(k_1,k_{gx},\omega,z)) &= g_{2+\epsilon}+g_{3+\epsilon}+\cdots = G_1(g(k_1,k_{gx},\omega,z)) - g_{1+\epsilon} \\ G_3(g(k_1,k_{gx},\omega,z)) &= g_{3+\epsilon}+g_{4+\epsilon}+\cdots = G_2(g(k_1,k_{gx},\omega,z)) - g_{2+\epsilon} \\ &\cdots \end{aligned}$$

and

$$\begin{aligned} H_1(h(k_2,k_{sx},\omega,z)) &= h_{1+\epsilon}+h_{2+\epsilon}+\cdots \\ H_2(h(k_2,k_{sx},\omega,z)) &= h_{2+\epsilon}+h_{3+\epsilon}+\cdots = H_1(h(k_2,k_{sx},\omega,z)) - h_{1+\epsilon} \\ H_3(h(k_2,k_{sx},\omega,z)) &= h_{3+\epsilon}+h_{4+\epsilon}+\cdots = H_2(h(k_2,k_{sx},\omega,z)) - h_{2+\epsilon} \\ &\cdots . \end{aligned}$$

The algorithmic optimizations to the one and two dimensional multiple attenuation algorithms, described above, are arrived at through mathematical analysis of the algorithms, and provides a first pass at a suitable algorithm, the pseudo-code for which is shown in Algorithm 2. See the examples section for numerical examples of the output of these optimizations.

LIMITING THE INTEGRATION INTERVAL GIVEN A MAXIMUM DIP

Here, we consider an additional optimization that can be applied to the internal multiple attenuation algorithm. In particular, we concern ourselves with simplifications afforded by some prior knowledge

Algorithm 2 Internal Multiple Attenuation

1: Using Algorithm 1, compute $b_1(k_{gx}, k_{sx}, z)$.
2: **for** each positive ω in $b_{3IM}(k_{gx}, k_{sx}, \omega)$ **do**
3: Determine the domain of non-evanescence using the dispersion relation $[k_{min}, k_{max}]$.
4: **for** each non-evanescent (k_{gx}, k_{sx}) pair **do**
5: Initialize $b_3(k_{gx}, k_{sx}, \omega(k_z)) = 0$.
6: **for** each non-evanescent (k_1, k_2) pair **do**
7: Compute $\rho(k_{gx}, k_{sx}, k_1, k_2, \omega)$.
8: Update: $b_{3IM}(k_{gx}, k_{sx}, \omega) \leftarrow b_{3IM}(k_{gx}, k_{sx}, \omega) + \rho(k_{gx}, k_{sx}, k_1, k_2, \omega)$.
9: **end for**
10: **end for**
11: **end for**
12: Inverse Fourier transform: $b_3(k_{gx}, k_{sx}; \omega) \rightarrow b_{3IM}(x_g, x_s; \omega)$.
13: Inverse Fourier transform (complex to real): $b_3(x_g, x_s, \omega) \rightarrow b_{3IM}(x_g, x_s, t)$.

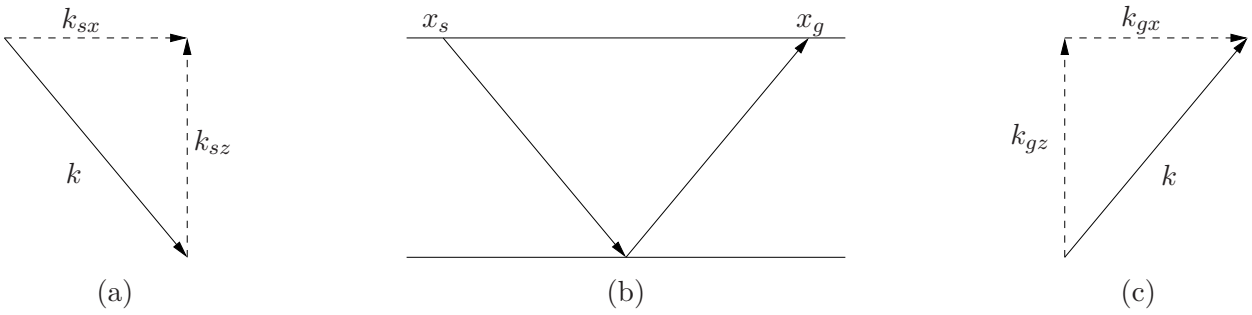

Figure 3: *The one dimensional model in (b) provides a simplification for the two dimensional multiple attenuation algorithm. In particular, (a) and (c) allow us to conclude that* $k_{sx} = k_{gx}$.

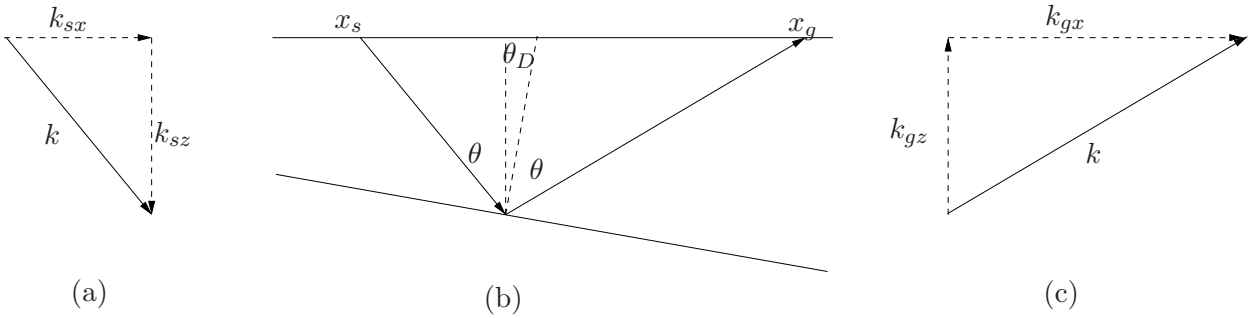

Figure 4: *If a two dimensional model can be characterized by the dip of its interface* θ_D*, as shown in (b), then we can find a simplification to the two dimensional algorithm. In particular, (a) and (c) allow for equation (14). The simplification utilizes both* θ_D *and the angle of incidence* θ.

of the model. We consider both one dimensional models, and two dimensional models which can be characterized by the dips of their interfaces.

For $1.5D$ data, we have, as is illustrated in the examples section in Figure 3, $k_{sx} = k_{gx}$. This, in turn, implies that $\rho(k_{gx}, k_{sx}, k_1, k_2, \omega)$ need only be evaluated when

$$k_{gx} = k_{sx} = k_1 = k_2,$$

thus providing a significant increase in efficiency when the internal multiple attenuation algorithm is applied to $1.5D$ data. In particular, it allows for the simplification of equation (2) so that it becomes,

$$b_{3IM}(k_{gx} = k_{sx}, \omega) = \frac{1}{(2\pi)^2} \int_{-\infty}^{\infty} b_1(k_1 = k_2 = k_{sx}, z_1) e^{-i(k_{1z}+k_{2z})z_1} \cdot \left[\int_{z_1+\epsilon}^{\infty} b_1(k_{gx} = k_1 = k_{sx}, z_2) e^{i(k_{gz}+k_{1z})z_2} dz_2 \right] \left[\int_{z_1+\epsilon}^{\infty} b_1(k_2 = k_{sx}, z_2) e^{i(k_{2z}+k_{sz})z_2} dz_2 \right] dz_1.$$

Hence, for $1.5D$ data, the computational complexity of evaluating b_{3IM} for a given value of k_{gx} is equivalent to the one dimensional, normally incident algorithm.

If a two dimensional model is restricted to a single dipping interface, with dip θ_D (see Figure 4), then it is readily shown that

$$k_{gx} = k_{sx} \frac{\sin(\theta + \theta_D)}{\sin(\theta - \theta_D)} = f(k_{sx}, \theta, \theta_D) = f(k_{sx}, \omega, \theta_D)$$

where θ is the angle of the plane wave incident on the dipping event, and can be expressed in terms of k_{gx} and θ_D,

$$\theta = \theta_D + \sin^{-1}\left(\frac{c_0 k_{gx}}{\omega}\right).$$

Letting $f_{sx} = f(k_{sx}, \omega, \theta_D)$, we have the following simplification to the internal multiple attenuation algorithm in two spatial dimensions:

$$b_{3IM}(k_{gx} = f_{sx}, \omega) = \frac{1}{(2\pi)^2} \int_{-\infty}^{\infty} b_1(k_1 = k_2 = f_{sx}, z_1) e^{-i(k_{1z}+k_{2z})z_1} \cdot \left[\int_{z_1+\epsilon}^{\infty} b_1(k_{gx} = k_1 = f_{sx}, z_2) e^{i(k_{gz}+k_{1z})z_2} dz_2 \right] \left[\int_{z_1+\epsilon}^{\infty} b_1(k_2 = f_{sx}, z_2) e^{i(k_{sz}+k_{gz})z_2} dz_2 \right] dz_1 \quad (14)$$

In practice, it may be more useful to specify the maximum expected dip in the model, and evaluate equation (14) for a range of f_{sx}. In addition to the simplifications described in this section, reciprocity can be used to avoid redundant calculations.

3 Internal multiple attenuation examples

In this section we illustrate the output of the code for 1D and 2D pre-stack inputs; the figures included are additionally designed to exemplify the dip arguments of the previous section. We begin with a discussion of the forward modelling code used and its importance.

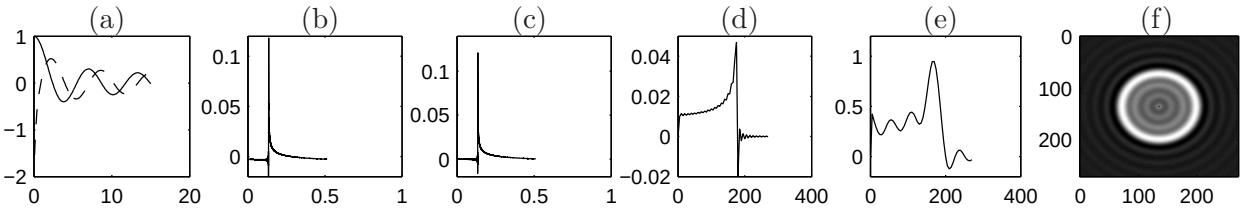

Figure 5: The analytic wave-field in pictures. (a) The real component of the Hankel function is a Bessel function of the first kind (solid line), and its imaginary component is a Bessel function of the second kind (dashed line). (b) $\hat{u}(\rho_0, \phi, t)$ plotted versus t when f is a delta function. (c) $u(\rho_0, \phi, t)$ plotted versus t with, again, f a delta function. $u(\rho, \phi, t_0)$ plotted versus ρ with (d) f a delta function and (e) f a sinc function. (f) A snapshot of the wave-field $u(\rho, \phi, t_0)$ where, again, f is a sinc function.

3.1 Creating synthetic data appropriate to the IMA algorithm

The internal multiple attenuation algorithm expects to process data constructed from a complete solution to the wave equation. In our tests, we found that data modeled using a high-frequency approximation to the wave equation (i.e. ray-tracing), results in phase errors in the predicted multiples; it is instructive to see that the multiple prediction algorithm, which is extracted from a series solution to the wave equation, does, in-fact, require input data constructed from a complete solution to the wave equation.

The finite difference method used in this paper follows the work of Alford et al. (1) in which initial time snapshots of the wave-field, used to bootstrap the finite difference equations, are derived analytically. Here, we present a brief analysis of these snapshots.

The finite difference algorithm propagates a solution to the acoustic wave equation

$$\left[\nabla^2 + \frac{1}{c^2}\frac{\partial^2}{\partial t^2}\right] u(\rho, \phi, t) = -4\pi \frac{\delta(\rho - \rho_s)\delta(\phi - \phi_s) f(t)}{\rho} \tag{15}$$

using a fourth order representation of the Laplacian. $f(t)$ is the time variation of the source distribution. As already mentioned, initial conditions for the finite difference algorithm are formed from an analytic solution to equation (15) (1):

$$u_s(\rho, \phi, t) = \frac{1}{2\pi} \int_{-\infty}^{\infty} \left[-i\pi H_0^{(2)}\left(k|\varrho - \varrho_s|\right)\right] F(\omega) e^{i\omega t} d\omega$$

where $|\varrho - \varrho_s|$ is the distance from the source, and $H_0^{(2)}$ is the second Hankel function of order 0,

$$H_0^{(2)}(z) = J_0(z) - iY_0(z).$$

J_0 and Y_0 are Bessel functions of the first and second kind respectively, and are plotted in Figure (5)a. Notice that $Y_0(z)$ (dashed line) has a vertical asymptote at $z = 0$. This means that $u_s(\rho, \phi, \omega)$ is undefined where either $\omega = 0$ or $\varrho = \varrho_s$.

We account for the vertical asymptote of Y in two steps. First, we simply let $u_s = 0$ when $\varrho = \varrho_s$. Second, we set the DC component of u_s to zero giving an approximate wave-field $\hat{u}_s(\rho_0, \phi_0, t)$

(Figure 5b). For a given value of $\rho = \rho_0$, we expect $u(t, \rho_0, \phi_0) = 0$ for $t < t_0 = \rho_0/c$. In other words, the displacement in the medium is null until the first arrival of energy. Hence, an appropriate scheme for computing the DC component u_{dc} of the wave-field is given by the mean,

$$u_{dc} = \frac{1}{\frac{3}{4}t_0} \int_0^{\frac{3}{4}t_0} u(t)dt. \tag{16}$$

The corrected signal,

$$u(\rho_0, \phi_0, t) = \hat{u}(\rho_0, \phi_0, t) + u_{dc},$$

is plotted in Figure 5c, and has the expected behavior for $t < t_0$. Figure 5d plots $u(\rho, \phi_0, t_0)$ for $t_0 = 0.09s$. Figures 5a-d are computed when f is a delta function. Figure 5e plots $u(\rho, \phi_0, t_0)$ when f is a zero-phase sinc function. Finally, Figure 5f plots $u(\rho, \phi, t_0)$ for $\phi \in [0, 2\pi)$ and $\rho \in [0, 255]$.

As an illustration of the algorithm's dependence on the type of input data, consider Figure 6 which plots data $D(x_g|x_s; t)$, $b_1(x_g, x_s, t)$ and $b_{3IM}(x_g, x_s, t)$ for a single trace ($x_s = x_g = 400m$) taken from $1.5D$ data similar to Figure 8. Figures 6a,c,e plot $D(x_g|x_s; t)$, $b_1(x_g, x_s, t)$ and $b_{3IM}(x_g, x_s, t)$ given ray-traced data, and Figures 6b,d,f plot the same for finite differenced data. A quick, visual inspection of the plots reveals the effects of the low-frequencies missing from the ray-traced data.

3.2 A 1D IMA example

Figures 7 and 8 illustrate the internal multiple attenuation algorithm for $1.5D$ data. Figure 8a plots data generated from the model in Figure 7. The predicted multiples are plotted in Figure 8.

3.3 A 2D IMA example

We consider the example presented in Figures 9 and 10. The data in Figure 10a is produced using a one parameter, acoustic finite difference code applied to the model in Figure 9 . The data $D(x_g|x_s; t)$, without the direct arrival and effects of the free-surface, is collected for

$$\{(x_s, x_g, t)|x_s = 0, 10, \ldots 800m, x_g = 0, 10 \ldots 800m, t = 0, .005, \ldots 1.5s\}.$$

Figure 10a plots a subset of this data, for $x_s = 400 \ldots 600m$ and $x_g = 400 \ldots 600m$. It is plotted in the pre-stack domain, and is organized into shot gathers. Visible in the data, are two primaries and an internal multiple. Figure 10b plots the predicted internal multiple provided by the internal multiple attenuation algorithm.

4 Summary and conclusions

This paper reports on the progress of the internal multiple attenuation algorithm code development project for the 2004–2005 year. We document progress on transparent code development in accordance with our standards for M-OSRP code design ("research-grade code"), often involving mathematical and physical alterations and improvements to the algorithm for efficiency.

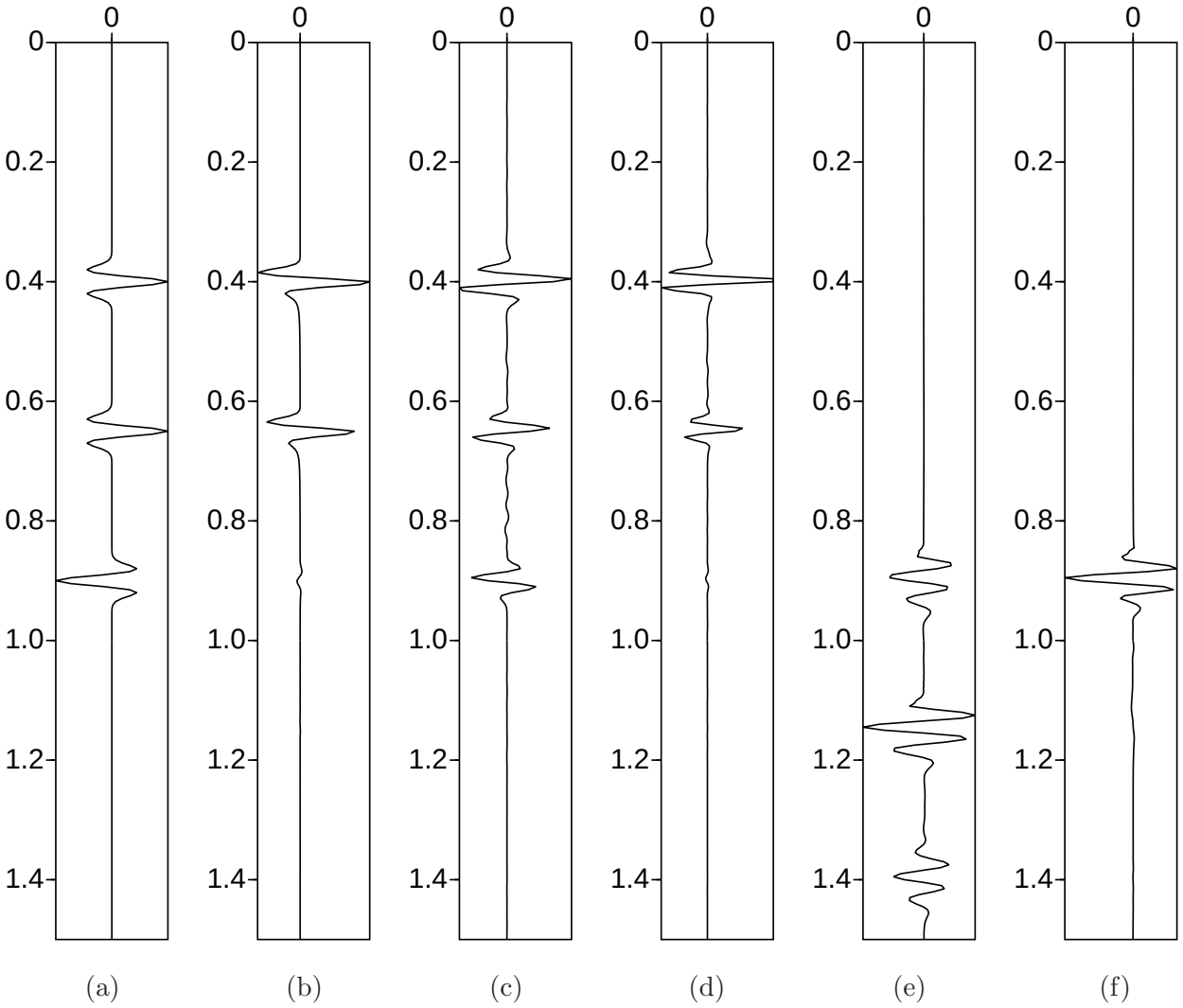

Figure 6: Here, we consider the internal multiple attenuation algorithm applied to data generated, first using ray-tracing, and second using finite differencing to produce $1.5D$ data sets. We generate $1.5D$ data sets, and plot, for $x_s = x_g = 400m$, (a) the ray-traced data, (b) the finite differenced data. (c) b_1 computed from the ray-traced data, and (d) b_1 computed from the finite differenced data. Finally, we plot the multiple prediction b_{3IM} for (e) the ray-traced data, and (f) the finite differenced data. Please note that the ray-traced data is modeled without amplitude information.

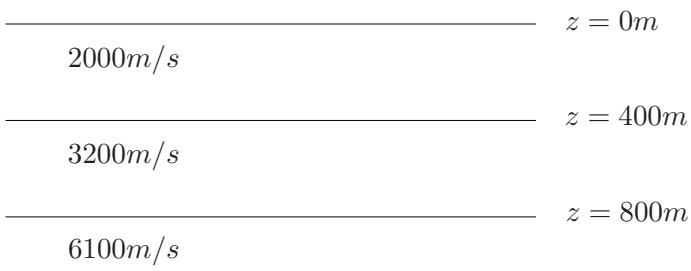

Figure 7: *A one dimensional model used to illustrate the internal multiple attenuation algorithm in two spatial dimensions with the simplification $k_{gx} = k_{sx}$. The corresponding seismic data, and multiple estimation are shown in Figure 8.*

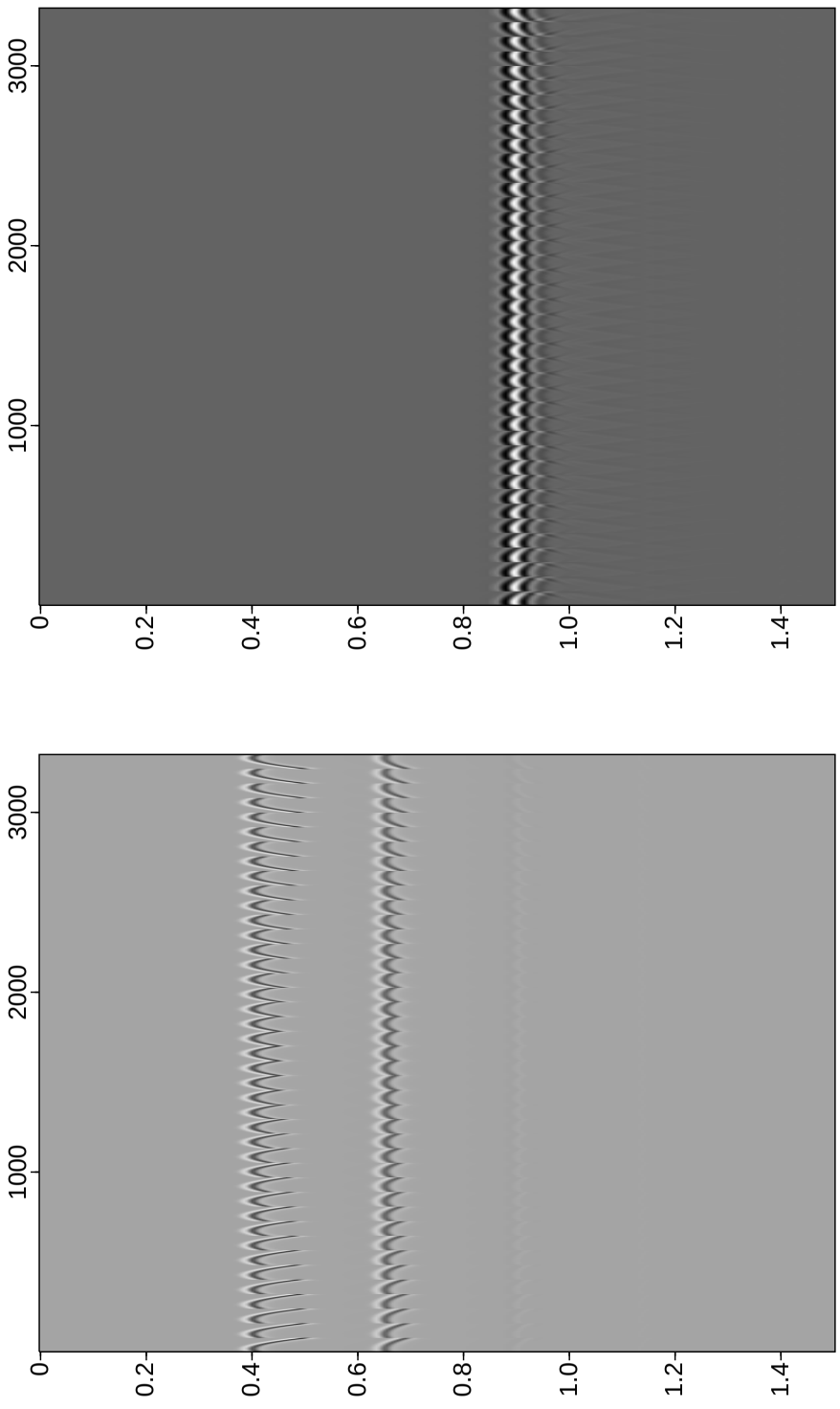

Figure 8: *(a) A subset of the data generated with finite differencing and the model in Figure 7, and (b) the corresponding internal multiple prediction. Visible in the data are two primary events and the first order internal multiple.*

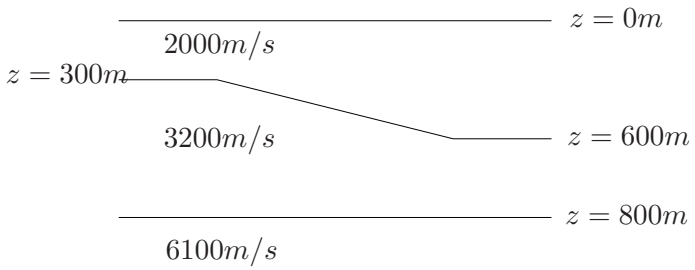

Figure 9: *A two dimensional model used to illustrate the internal multiple attenuation algorithm in two spatial dimensions. The corresponding seismic data, and multiple estimation are shown in Figure 10.*

We are preparing to make two related codes available for the end of May 2005, the IMA code and the finite difference forward modelling code that has been adapted to ideally test and validate the de-multiple method.

The coming year will see a greater degree of testing of the algorithm on 2D cases, including and especially instances that test the ability of the algorithm to handle pathological models set to challenge the "lower-higher-lower in pseudo-depth" requirement (e.g., Nita and Weglein, 2005).

Further, we will characterize the 3D IMA problem in terms of computational burden; un-questionably it is an enormous computing problem, by any definition of the word. We are investigating various routes of parallelization of the problem and various platforms for same; we are benefiting strongly from our contacts at IBM on this. For example, a working-team is sketching out the appropriateness of an IBM BlueGene architecture to this end.

5 Acknowledgments

The authors are grateful for the constructive comments and advice of Ken Matson and Andrew Fritz.

References

[1] Alford, R. M., K. R. Kelly, and D. M. Boore. "Accuracy of Finite-Difference Modeling of the Acoustic Wave Equation." *Geophysics* 39 (December 1974): 834–842.

[2] Etgen, John T. Elastic Prestack Migration of Two Component Data. Technical Report 57, SEP, 1988.

[3] Weglein, A. B. and K. H. Matson. "Inverse Scattering Internal Multiple Attenuation: An Analytic Example and Subevent interpretation." *SPIE Conference on Mathematical Methods in Geophysical Imaging*. 1998, 108–117.

[4] Weglein, Arthur B., Fernanda V. Araújo, Paulo M. Carvalho, Robert H. Stolt, Kenneth H. Matson, Richard T. Coats, Dennis Corrigan, Douglas J. Foster, Simon A. Shaw, and Haiyan Zhang. "Inverse Scattering Series and Seismic Exploration." *Inverse Problems* (2003): R27–R83.

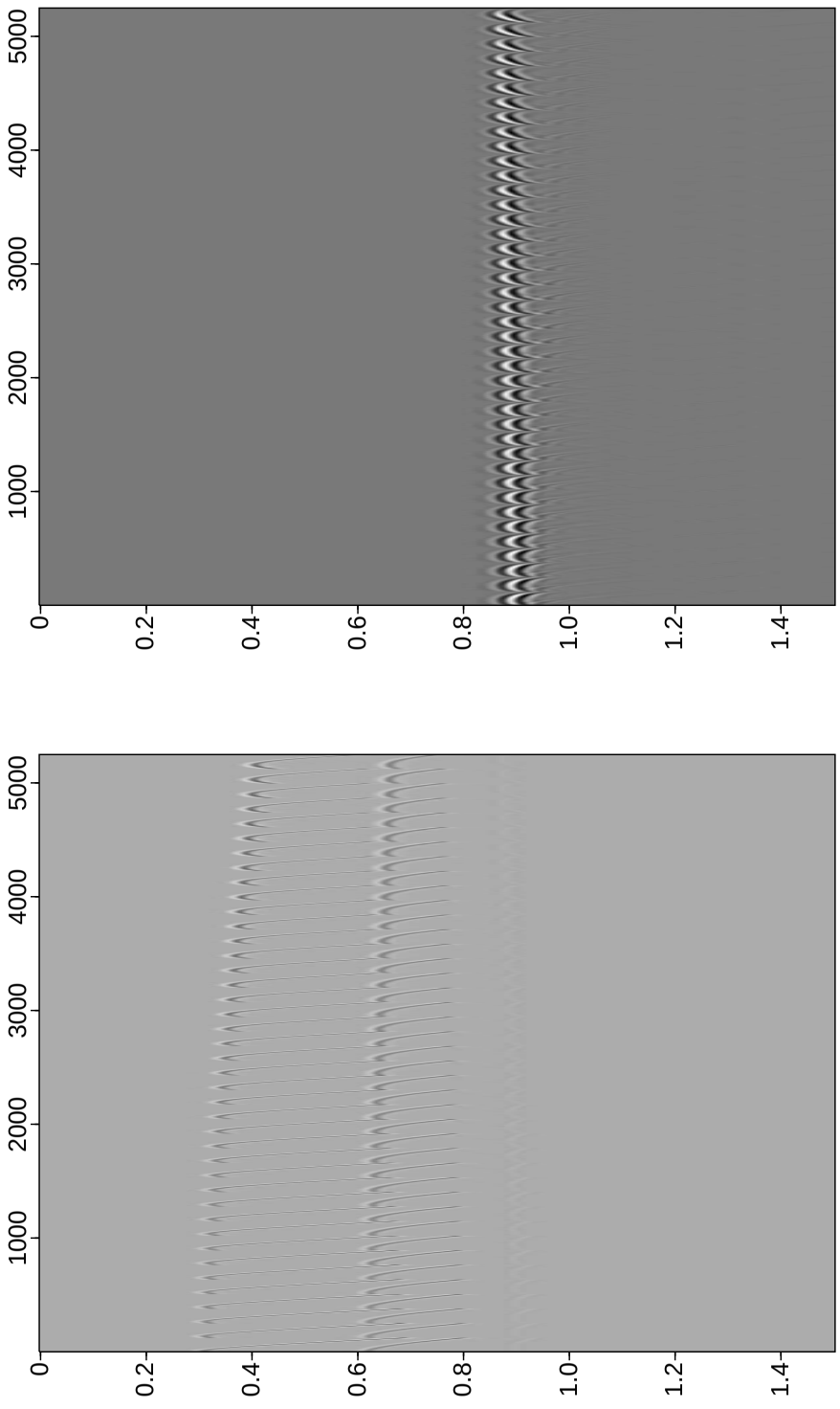

Figure 10: *(a) A subset of the data generated with finite differencing and the model in Figure 9, and (b) the corresponding internal multiple prediction. Visible in the data are two primary events and the first order internal multiple.*

[5] Weglein, Arthur B., Fernanda Araújo Gasparotto, Paulo M. Carvalho, and Robert H. Stolt. "An Inverse-Scattering Series Method for Attenuating Multiples in Seismic Reflection Data." *Geophysics* 62 (November-December 1997): 1975–1989.

Inverse scattering internal multiple attenuation algorithm in complex multi-D media: the pseudo-depth/vertical-time monotonicity condition and higher dimension analytic analysis

Bogdan G. Nita and Arthur B. Weglein

Abstract

In this paper we discuss the multi-D inverse scattering internal multiple attenuation algorithm focusing our attention on the prediction mechanisms. Roughly speaking, the algorithm combines amplitude and phase information of three different arrivals (sub-events) in the data set to predict one interbed multiple. The three events are conditioned by a certain relation which requires that their pseudo-depths, defined as the depths of their turning points relative to the constant background velocity, satisfy a lower-higher-lower relationship. This implicitly assumes a pseudo-depth monotonicity condition, i.e. the relation between the actual depths and the pseudo-depths of any two sub-events, is the same. We study the lower-higher-lower relation in pseudo-depth and show that it is directly connected with a similar longer-shorter-longer relationship between the vertical or intercept times of the sub-events and hence the pseudo-depth monotonicity is equivalent to a vertical time monotonicity condition. The paper also provides the first pre-stack analysis of the algorithm with analytical data showing how the sub-events are selected and combined to exactly predict the time and well approximate the amplitude of an interbed multiple. Among other results we show that the construction of internal multiples is performed in the plane waves domain and, as a consequence, the internal multiples with head-waves sub-events are also predicted by the algorithm. Furthermore we analyze the differences between the time monotonicity condition in vertical or intercept time and total travel time and show a 2D example which satisfies the former (and hence is predicted by the algorithm) but not the latter. Finally we discuss one case in which the monotonicity condition is not satisfied by the sub-events of an internal multiple which, as a consequence, will not be predicted. For these cases, the monotonicity condition turns out to be too restrictive and we discuss ways of lowering these restrictions and hence expanding the algorithm to address these types of multiples.

Introduction

The inverse scattering series is presently the only multidimensional method for inverting for the properties of an unknown medium without adequate information about that medium. When the series converges it achieves full inversion given the whole data set (including free surface and internal multiples) and information about a chosen reference medium. Carvalho (6) tested numerically the convergence properties of the full inverse scattering series and found that the series converges only when the reference medium of choice is within 11% from the actual medium, a non-realistic situation. In the '90's, Weglein and collaborators developed the "subseries method" (for a history and description see (20)) which consists in identifying task specific subseries in the full series, with targeted usefulness and better convergence properties than the whole series. These subseries were imagined to be a sequence of steps, similar to the processing steps undertaken in geophysical exploration, which would achieve 1. Free surface multiple elimination; 2. Internal multiple elimination;

3. Imaging in depth; and 4. Inversion for the medium properties. It is reasonable to assume, and the experience showed this assumption to be true, that since the full series only requires data and information about a reference medium to invert, the same holds for any of the four specific subseries.

The inverse scattering series, and the subsequent task specific subseries, assume that the input data satisfies several pre-requisites. First, it is assumed that the source signature or wavelet has been deconvolved from the data. Second, both the source and receiver ghosts have been eliminated from the collected data. Third, the collected data itself has an appropriate sampling or the data reconstruction algorithms are able to improve the acquisition sampling to an appropriate degree. When these prerequisites are not satisfied, the algorithms derived from this method will reach incorrect conclusions/results e.g. false or no prediction of free-surface and internal multiples, incorrect location of subsurface structures, and errors in parameter estimation. Last but not least we mention that the algorithms are derived from a point-source point-receiver wave theory approach and any deviations from that, e.g. source and receiver arrays, would have to be studied to understand how they affect the algorithms.

In 1994, Araujo (2) identified the first term in the subseries for internal multiple elimination (see also (19)). This first term by itself exactly predicts the time of arrival, or phase, and well approximates the amplitude of internal multiples, without being larger than the actual amplitude, and hence it represents an algorithm for *attenuation*. Weglein et al. (20) described the algorithm through an analytic 1D example and 2D synthetic numerics. Field data tests were also performed showing an extraordinary ability to predict difficult interbed multiples, e.g. superimposed primary and multiple etc., where other methods have failed.

The inverse scattering internal multiple attenuation algorithm was found through a combination of simple 1D models testing/evaluation and certain similarities between the way the data is constructed by the forward scattering series and the way arrivals in the data are processed by the inverse scattering series. This connection between the forward and the inverse series was analyzed and described by Matson (10), (11) and Weglein et al. (19), (20). Specifically, they showed that an internal multiple in the forward scattering series is constructed by summing certain types of scattering interactions which appear starting with the third order in the series. The piece of this term representing the first order approximation to an internal multiple is exactly the one for which the point scatterers satisfy a certain lower-higher-lower relationship in actual depth. Summing over all interactions of this type in the actual medium results in constructing the first order approximation to an internal multiple. By analogy, it was inferred that the first term in the subseries for eliminating the internal multiples would be one constructed from events satisfying the same lower-higher-lower relationship in pseudo-depth. The assumption that the ordering of the actual and the pseudo depths of two sub-events is preserved, i.e.

$$z_1^{actual} < z_2^{actual} \iff z_1^{pseudo} < z_2^{pseudo}, \tag{1}$$

has been subsequently called "the pseudo-depth monotonicity condition".

In this paper we further analyze this relation and show that it is equivalent to a vertical or intercept time (here denoted by τ) monotonicity condition

$$z_1^{actual} < z_2^{actual} \iff \tau_1 < \tau_2, \tag{2}$$

for any two sub-events. We also look at the differences between the time monotonicity condition in vertical or intercept time and total travel time. The latter was pointed out by a different algorithm derived from the inverse scattering series by ten Kroode (17) and further described by Malcolm and M.V. de Hoop (9). We show a 2D example which satisfies the former (and hence is predicted by the original algorithm) but not the latter. Finally we discuss one case in which the monotonicity condition is not satisfied by the sub-events of an internal multiple in either vertical or total travel time and consequently the multiple will not be predicted by either one of the two algorithms. For these cases, the monotonicity condition turns out to be too restrictive and we discuss ways of lowering these restrictions and hence expanding the algorithm to address these types of multiples.

In the context of the overall research efforts of M-OSRP, this paper represents a part of a project to characterize, implement, and build on the internal multiple attenuation algorithm that is reported on in this volume. Kaplan et al. (8) describe the development of a practical code to effect numerical examples of this de-multiple procedure in 1D prestack and 2D regimes; they further detail mathematically- and physically-based representations of the algorithm that lead to reduced computation time. Ramírez and Weglein (13) meanwhile work to progress towards a method for the elimination of interbed multiples through an analysis and incorporation of specific higher-order terms that yet mimic the pseudo-depth relationships we discuss herein. Ramírez and Weglein (14) concern themselves with the characterization of the attenuative nature of the algorithm. Here we provide a characterization of a different sort, as summarized above.

The paper is structured as follows. In Section 2 we will discuss the definition of a multiple and its evolution over time. In Section 3 we will describe the algorithm and show how a predicted multiple is constructed from events in the data. A 1.5D example is analyzed in Section 4 with analytical data and internal multiples with headwaves sub-events are shown to be predicted by the algorithm. We further look in Sections 5 and 6 at several 2D examples to better understand the relationship between the sub-events which are used by the algorithm to construct the phase and the amplitude of the internal multiple. Some comments and conclusions are presented in the last section.

Definition of an internal multiple

The definition of an internal multiple evolved over time keeping in step with our understanding of fundamental structure and processes that take place inside a medium. Once a certain definition is in place, one can then start the development of algorithms which address the so called (and defined) internal multiples to attenuate or even eliminate them. However, sometimes, after an algorithm is developed, its analysis leads to new definitions or generalizations of the notions/concepts themselves. This was the case of the inverse scattering internal multiple algorithm and the definitions resulted from it will be discussed in this section.

The early 1D models of a layered medium only allow up and down propagation and so it is easy to imagine a primary as having only one upward reflection and a multiple as having two or more upward reflection and one or more internal (i.e. not at the free surface) downward reflections. Notice that the directions up and down are defined by the positioning of the measurement surface: if an event is propagating towards the measurement surface it is said that it is moving upward. If the event is moving away from the measurement surface it is said that it is moving downward. In our discussion/pictures, we choose the x-axis to be along the measurement surface and hence the up-down direction to coincide with moving backward and forward along the z-axis.

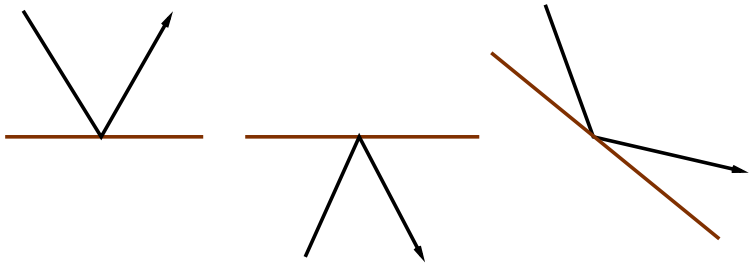

Figure 1: *An example of an upward, downward and a neutral reflection.*

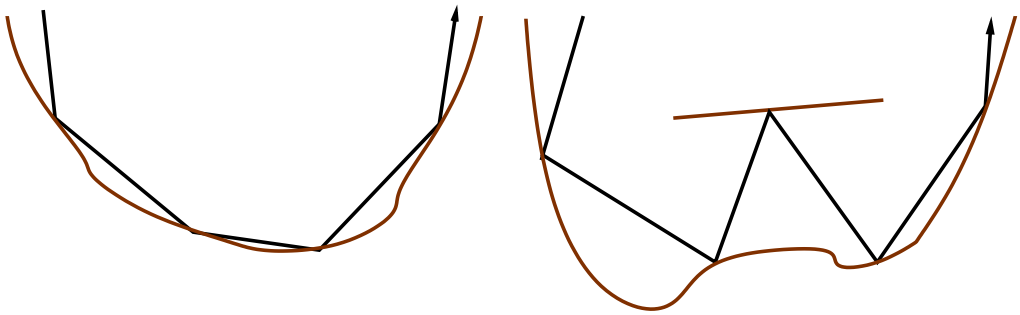

Figure 2: *A more general definition of a primary and a multiple. The primary has one upward reflection and any number of neutral reflections while the multiple has two or more upward reflections and any number of neutral reflections.*

When the medium is slightly more general, for example a 2D medium with only specular reflections, a new type of reflection occurs which is neither upward nor downward (see Figure 1). We will call this type of reflection a neutral reflection. For this situation we can easily generalize the definition of a primary as an event which contains one upward reflection and any number of neutral reflections and that of a multiple as an event which has two or more upward reflections, one or more downward reflections and any number of neutral reflections (an example is shown in Figure 2). However this definition does not cover the complexity of an arbitrary medium and there are events which do not fit the definition of a multiple as given so far. For example, the events pictured in Figure 3 (a)(b) do not have two upward reflections but a turning wave and a headwave respectively, while the event in Figure 3(c) is even of a more complex nature consisting in a diffraction on one leg of the full event. Recently, Weglein and Dragoset (21) have introduced more general definitions and designations for primary and multiply reflected events, namely prime and composite events. According to those definitions, a *prime event* is not decomposable into other recorded events such that those sub-event ingredients combine by adding and/or subtracting time of arrival to produce the prime. A *composite event* is composed of sub-events that combine in the above described manner to produce the event. With these definitions, the events pictured in Figure 3 can be categorized as composite events when their sub-events can be found in the recorded data. For example, the sub-events of the event pictured in Figure 3(a) are the turning wave and the reflections from the shallow and deep interfaces.

These definitions, which obviously generalize all the previous ones, and the notion of sub-events where suggested by the inverse scattering internal multiple attenuation algorithm which is going to be discussed in detail in the next sections.

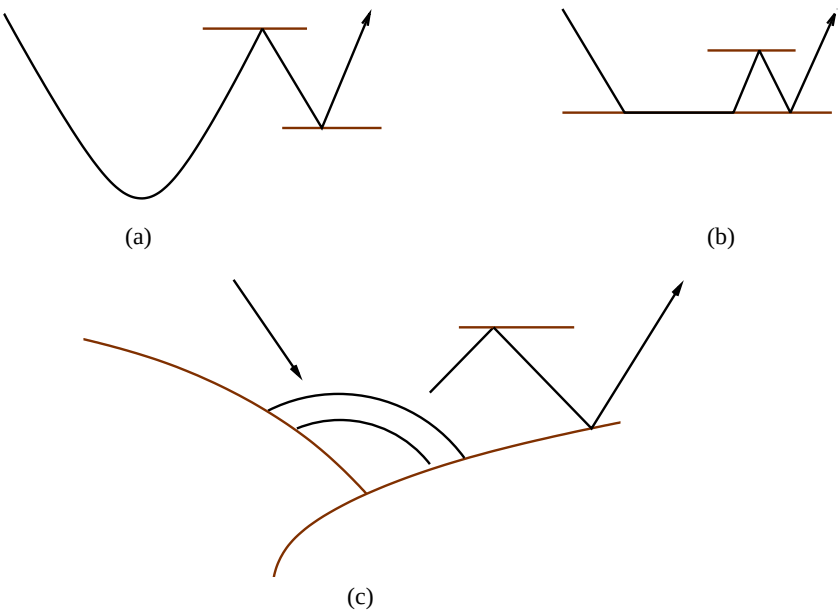

Figure 3: *Complex events difficult to include in a definition which only takes into account upward and downward reflections*

The inverse scattering series internal multiple attenuation algorithm

The first term in the inverse scattering subseries for internal multiple elimination is (see e.g. (20))

$$\begin{aligned} b_3(k_g,k_s,\omega) &= \frac{1}{(2\pi)^2}\int_{-\infty}^{\infty}\int_{-\infty}^{\infty} dk_1 e^{-iq_1(\epsilon_g-\epsilon_s)} dk_2 e^{iq_2(\epsilon_g-\epsilon_s)} \int_{-\infty}^{\infty} dz_1 e^{i(q_g+q_1)z_1} b_1(k_g,k_1,z_1) \\ &\times \int_{-\infty}^{z_1} dz_2 e^{i(-q_1-q_2)z_2} b_1(k_1,k_2,z_2) \int_{z_2}^{\infty} dz_3 e^{i(q_2+q_s)z_3} b_1(k_2,k_s,z_3) \end{aligned} \tag{3}$$

where $z_1 > z_2$ and $z_2 < z_3$ and b_1 is defined in terms of the original pre-stack data with free surface multiples eliminated, D', to be

$$D'(k_g,k_s,\omega) = (-2iq_s)^{-1} B(\omega) b_1(k_g,k_s,q_g+q_s) \tag{4}$$

with $B(\omega)$ being the source signature. Here k_s and k_g are horizontal wavenumbers, for source and receiver coordinates x_s and x_g, and q_g and q_s are the vertical wavenumbers associated with them. The b_3 on the left hand side represents the first order prediction of the internal multiples. An internal multiple in b_3 is constructed through the following procedure.

The deconvolved data without free-surface multiples in the space-time domain, $D(x_s,x_g,t)$ can be described as a sum of Dirac delta functions

$$D(x_s,x_g,t) = \sum_a R_a \delta(t-t_a) \tag{5}$$

representing different arrivals (primaries and internal multiples). Here R_a represents the amplitude of each arrival and it is a function of source and receiver position x_s and x_g and frequency ω. When transformed to the frequency domain the transformed function $D(x_s, x_g, \omega)$ is a sum

$$\tilde{D}(x_s, x_g, \omega) = \sum_a \tilde{R}_a e^{-i\omega t_a}. \tag{6}$$

Here t_a is the total traveltime for each arrival and it can be thought of as a sum of horizontal and vertical times $t_a = \tau_a + t_{xa}$ (see e.g. (7), (18)), where t_{xa} is a function of x_g and x_s. After Fourier transforming over x_s and x_g, the data is $\tilde{D}(k_s, k_g, \omega)$. The transforms act on the amplitude as well as on the phase of the data and transform the part of the phase which is described by the horizontal time t_{xa}. Hence $D(k_s, k_g, \omega)$ can now be thought of as a sum of terms containing $e^{i\omega\tau_a}$ with τ_a being the vertical or intercept time of each arrival

$$\tilde{D}(k_s, k_g, \omega) = \sum_a \tilde{R'}_a e^{-i\omega\tau_a} \tag{7}$$

and where $\tilde{R'}_a$ is the double Fourier transform over x_g and x_s of $\tilde{R}_a e^{-i\omega t_{xa}}$. The multiplication by the obliquity factor, $2iq_s$, changes the amplitude of the plane wave components without affecting the phase; hence $b_1(k_s, k_g, \omega)$ represents an effective plane wave decomposed data and is given by

$$b_1(k_s, k_g, \omega) = \sum_a \tilde{R''}_a e^{-i\omega\tau_a} \tag{8}$$

where $\tilde{R''}_a = 2iq_s\tilde{R'}_a$ and whose phase, $e^{i\omega\tau_a}$, contains information only about the recorded *actual* vertical or intercept time.

Notice that for each planewave component of fixed k_s, k_g and ω we have

$$\omega\tau_a = k_z^{actual} z_a^{actual} \tag{9}$$

where k_z^{actual} is the actual, velocity dependent, vertical wavenumber and z_a^{actual} is the actual depth of the turning point of the planewave. Since the velocity of the actual medium is assumed to be unkown, this relationship is written in terms of the reference velocity as

$$\omega\tau_a = k_z z_a \tag{10}$$

where k_z is the vertical wavenumber of the planewave in the reference medium, $k_z = \sqrt{\frac{\omega}{c_0} - k_s} + \sqrt{\frac{\omega}{c_0} - k_g}$, and z_a is the pseudo-depth of the turning point. This implicit operation in the algorithm is performed by denoting $b_1(k_s, k_g, \omega) = b_1(k_s, k_g, k_z)$ with the latter having the expression

$$b_1(k_s, k_g, k_z) = \sum_a \tilde{R''}_a e^{-ik_z z_a}. \tag{11}$$

The next step is to Inverse Fourier Transform over the reference k_z hence obtaining

$$b_1(k_s, k_g, z) = \int_{-\infty}^{\infty} e^{ik_z z} b_1(k_s, k_g, k_z) dk_z. \tag{12}$$

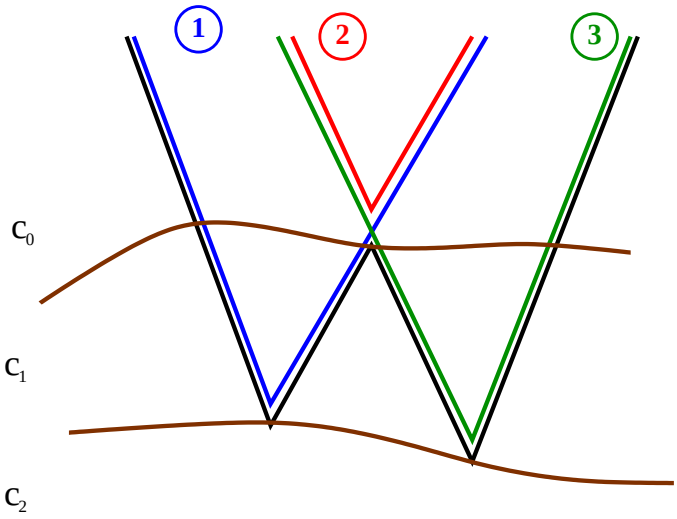

Figure 4: *The sub-events of an internal multiple: the green, blue and red are arrivals in the data which satisfy the lower-higher-lower relationship in pseudo-depths z. The algorithm will construct the phase of the internal multiple shown in black by adding the phases of the green and the blue primaries and subtract the one of the red primary.*

Putting together equations (11) and (12)) we find

$$b_1(k_s, k_g, z) = \sum_a \int_{-\infty}^{\infty} \tilde{R''}_a e^{ik_z(z-z_a)} dk_z \tag{13}$$

which represents a sum of delta-like events placed at pseudo-depths z_a and hence the b_1 from the last equation is actually $b_1(k_s, k_g, z_a)$. This last step can also be interpreted as a downward continuation on both source and receiver sides, with the reference velocity c_0, and an imaging with $\tau = 0$, or, in other words, an un-collapsed F-K migration (see e.g. (15) and (16)). A discussion of differences in imaging with τ and with t was given by Nita and Weglein (12).

Each internal multiple is constructed by considering three effective data sets b_1 and searching, in the horizontal-wavenumber–pseudo-depth domain, for three arrivals which satisfy the lower-higher-lower relationship in their pseudo-depths, i.e. $z_1 > z_2 < z_3$, (see Figure 4 for an example of three such primary events). Having found such three arrivals in the data, the algorithm combines their amplitudes and phases to construct a multiple by adding the phases of the two pseudo-deeper events and subtracting the one of the pseudo-shallower ones and by multiplying their amplitudes. One can then see (see e.g. (20)) that the time of arrival of an internal multiple is exactly predicted and its amplitude is well approximated by this procedure.

As pointed out in the first section, the lower-higher-lower restriction was inferred from the analogy with the forward scattering series description of internal multiples: the first order approximation to an internal multiple (which occurs in the third term of the series) is built up by summing over all scattering interactions which satisfy a lower-higher-lower relationship in actual depth. The assumption that this relationship is preserved in going from actual depth to pseudo-depth is called "the pseudo-depth monotonicity condition". (Recall that a monotonic function $f(x)$ satisfies $f(x_1) < f(x_2) \iff x_1 < x_2$, see also Figure 5; here, we regard the pseudo-depth as a function of actual depth). Notice that the lower-higher-lower relationship in pseudo-depth can be translated,

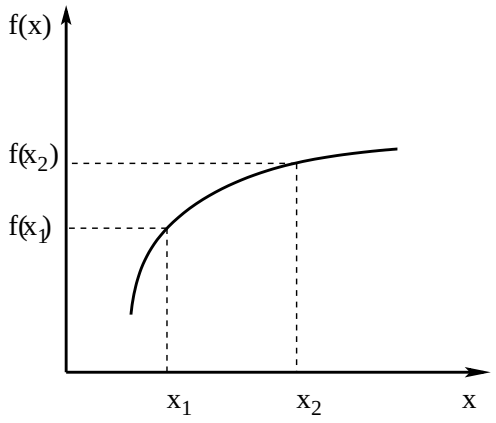

Figure 5: *A monotonic function.*

from equation (10), in a similar longer-shorter-longer relationship in the vertical or intercept time of the three events. Accordingly, the pseudo-depth monotonicity is also translated in a vertical time monotonicity condition. Notice that this is different from the total time monotonicity assumed by the algorithm introduced by ten Kroode (17). The latter is employing asymptotic evaluations of certain Fourier integrals which result in an algorithm in the space domain, having a ray theory assumption and the less inclusive total time monotonicity requirement. The justification for this approach was the attempt to attenuate a first order approximation to an internal multiple built by the forward scattering series. In contrast, the original algorithm is aimed at predicting and attenuating the actual multiples in the data and hence it takes into consideration the full wavefield, with no asymptotic compromises, and results in a more inclusive vertical time monotonicity condition. In Section 5 we discuss a 2D example in which the geometry of the subsurface leads to the existence of a multiple which satisfies the pseudo-depth/vertical-time but not the total time monotonicity condition.

In the next section we analyze a simple 1.5D example and show analytically how it predicts internal multiples by putting together amplitude and phase information from arrivals in the data satisfying the above condition. During this analysis we also show that the internal multiples with headwaves sub-events are attenuated by the algorithm.

Attenuation of internal multiples with headwaves sub-events: a 1.5D example

The model in this experiment is a 2D vertically varying medium. We consider one of the simplest cases which allow the existence of internal multiples, namely one layer between two semi-infinite half-spaces separated by horizontal interfaces (see Figure 6). The velocity only varies across the interfaces located at $z = z_a$ and $z = z_b$ and has the values c_0, c_1 and c_2 respectively. The sources and receivers are located at the same depth $z = 0$. The data for such a model is given in the

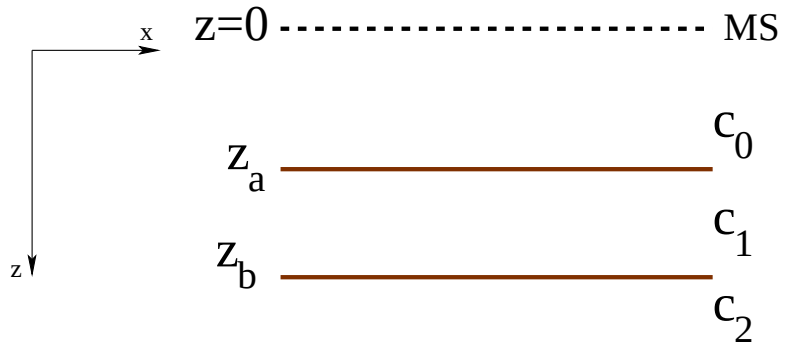

Figure 6: *The model for the 1.5D example.*

frequency ω domain by (see e.g. (1))

$$D(x_h,0;\omega)=\frac{1}{2\pi}\int_{-\infty}^{\infty}dk_h\frac{R_{01}+T_{01}R_{12}T_{10}e^{i\nu_1(z_b-z_a)}+\cdots}{iq_s}e^{ik_hx_h}e^{ik_zz_a} \tag{14}$$

where $k_z=q_g+q_s$, $k_h=k_g+k_s$, $x_h=\dfrac{x_g-x_s}{2}$ and $\nu_1=q_{1g}+q_{1s}$. The reflection and transmission coefficients at the corresponding interfaces R_{01}, T_{01}, R_{12} and T_{10} are all functions of k_h and ω. Only the primaries from the top and the bottom interfaces are written out explicitly in this equation; the dots "..." stand for other multiple arrivals. For simplicity we will drop the writing of the dots for the rest of this example; this will effect in the prediction of the first order internal multiple only.

Notice that the expression (14) represents both pre-critical and post-critical arrivals, as well as, for large offsets, headwaves along both interfaces. For a discussion of how to obtain the headwaves solutions from integrating Equation (14) see e.g. Aki and Richards (1) Chapter 6. The first order internal multiple that we seek to predict has the expression

$$IM^{1st}_{actual}(x_h,0;\omega)=\frac{1}{2\pi}\int_{-\infty}^{\infty}dk_h\frac{T_{01}R_{12}^2T_{10}R_{10}e^{2i\nu_1(z_b-z_a)}}{iq_s}e^{ik_hx_h}e^{ik_zz_a}. \tag{15}$$

This analytic formula contains both small and large offsets first order internal multiples arrivals including the multiples containing headwaves along the second interface as sub-events.

Fourier transforming the data given by equation (14) over x_h and x_m we find

$$D(k_h,0;\omega)=\frac{R_{01}+T_{01}R_{12}T_{10}e^{-i\nu_1(z_b-z_a)}}{iq_s}e^{-ik_zz_a}\delta(k_g-k_s). \tag{16}$$

Then $b_1(k_h,0;\omega)=iq_sD(k_h,0;\omega)$ is

$$b_1(k_h,0;\omega)=\left[R_{01}+T_{01}R_{12}T_{10}e^{-i\nu_1(z_b-z_a)}\right]e^{-ik_zz_a}\delta(k_g-k_s). \tag{17}$$

or

$$b_1(k_h,0;\omega)=\left[R_{01}e^{-ik_zz_a}+R'_{12}e^{-i\nu_1(z_b-z_a)e^{-ik_zz_a}}\right]\delta(k_g-k_s) \tag{18}$$

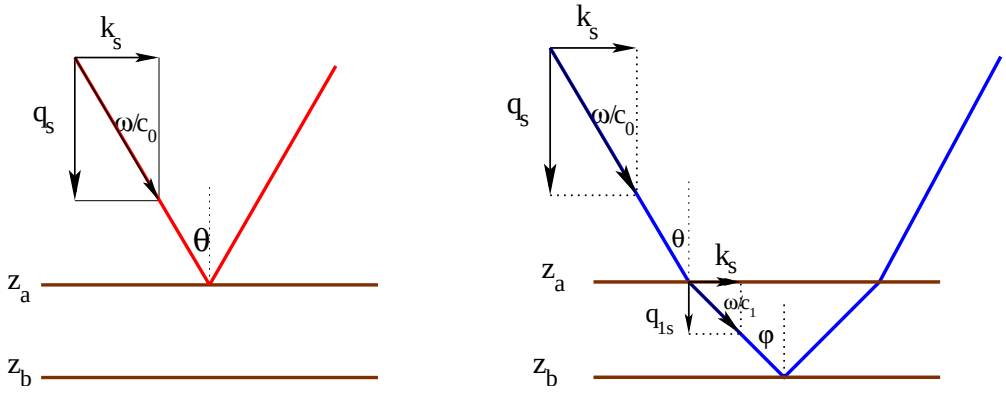

(a) *The geometry of the first primary in the data.*

(b) *The geometry of the second primary in the data.*

Figure 7: *Geometrical representation of the two primaries.*

where, for simplicity, we denoted $T_{01}R_{12}T_{10} = R'_{12}$.

For the first primary we can write (see Figure 7(a)) $\cos\theta = \dfrac{q_s}{\omega/c_0}$ which implies

$$q_s = \frac{\omega}{c_0}\cos\theta \tag{19}$$

or, noticing that $\dfrac{c_0}{\cos\theta} = c_v^1$, the vertical speed in the first medium,

$$q_s z_a = \frac{\omega}{c_0} z_a \cos\theta = \omega\frac{\tau^1}{2} \tag{20}$$

where τ^1 represents the intercept or vertical time of the first event. Similarly, on the receiver side we have

$$q_g z_a = \omega\frac{\tau^1}{2}. \tag{21}$$

Summing the last two equations we find for the first primary arrival (compare with equation 10)

$$k_z z_a = \omega\tau^1 \tag{22}$$

where we emphasize again that on the left hand side of the equation is the reference k_z and the pseudo-depth, which in this case coincides with the actual depth of of the reflector, z_a and on the right hand side we have the phase information contained in the recorded data. For the second event we can find, as before, that, for the portion propagating through the space in between the measurement surface and the depth z_a, we have

$$k_z z_a = \omega\tau_1, \tag{23}$$

where τ_1 is the vertical time through the first medium. For the part that is propagating through the second medium we can write $cos\varphi = \dfrac{q_{1s}}{\omega/c_1}$ which implies

$$q_{s1} = \frac{\omega}{c_1} cos\varphi, \tag{24}$$

or, noticing that $\frac{c_1}{cos\varphi} = c_v^2$, the vertical speed in the layer,

$$q_{1s}(z_b - z_a) = \frac{\omega}{c_1}(z_b - z_a)cos\varphi = \omega\frac{\tau_2}{2} \tag{25}$$

where τ_2 is the vertical time through the layer for this event. Similarly, on the receiver side we have

$$q_{1g}(z_b - z_a) = \omega\frac{\tau_2}{2}. \tag{26}$$

Summing the last two equations we find

$$\nu_1(z_b - z_a) = \omega\tau_2. \tag{27}$$

Summarizing, for the second primary we found from equations (23) and (27)

$$k_z z_a + \nu_1(z_b - z_a) = \omega\tau^2 \tag{28}$$

where τ^2 is the total vertical time for the second event.

Since the velocity of the second medium is not known, we can write $\omega\tau^2$ in terms of c_0 only as follows (see Equation (10)

$$\omega\tau^2 = k_z z_b' \tag{29}$$

where z_b' is a pseudo-depth which can be calculated in terms of the vertical time τ^2 and the vertical speed of the first medium. With these remarks, the expression (18) for b_1 becomes

$$b_1(k_h, 0; \omega) = \left[R_{01}e^{-ik_z z_a} + R'_{12}e^{-ik_z z_b'}\right]\delta(k_g - k_s) \tag{30}$$

To calculate $b_1(k_h, z)$ we first downward continue/extrapolate,

$$b_1(k_h, z; \omega) = \left[R_{01}e^{ik_z(z-z_a)} + R'_{12}e^{ik_z(z-z_b')}\right]\delta(k_g - k_s), \tag{31}$$

and then integrate over k_z (imaging) to obtain

$$b_1(k_h, z) = \int_{-\infty}^{\infty} dk_z b_1(k_h, k_z; \omega). \tag{32}$$

Notice that the reflection and transmission coefficients in the expression (31) are functions of ω and hence functions of k_z. Explicitly,

$$R_{01}(k_h, \omega) = \frac{\sqrt{\frac{4\omega^2}{c_0^2} - k_h^2} - \sqrt{\frac{4\omega^2}{c_1^2} - k_h^2}}{\sqrt{\frac{4\omega^2}{c_0^2} - k_h^2} + \sqrt{\frac{4\omega^2}{c_1^2} - k_h^2}}. \tag{33}$$

The integration over k_z in (32) hence amounts to an inverse Fourier transform of R_{01} and R'_{12} over k_z. This Fourier transform is difficult to write as an analytic result and hence the example can no longer continue in the (k_h, ω) domain.

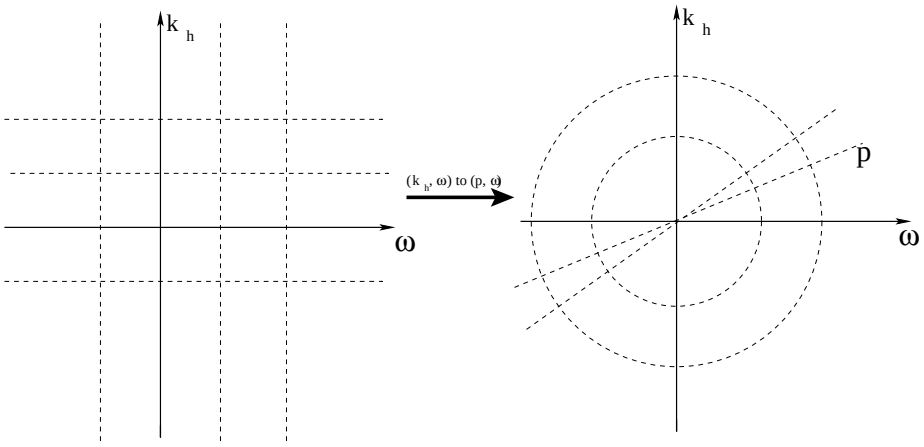

Figure 8: *The mapping* (k_h, ω) *to* (p, ω)

The imaging of the data can also be achieved in the (p, ω) domain with better analytical results and more meaningful amplitude analysis (see Bruin et al (1990)). To this end we map the data from the (k_h, ω) to (p, ω) domain. This mapping has been studied extensively by Bracewell (1956) and Bracewell and Riddle (1967). It mainly consists in reading the data along the lines going through the origin of the (k_h, ω) coordinate system instead of the original (k_h, ω) grid (see Figure 8). Notice that, if this mapping is performed, the reflection and the transmission coefficients are no longer dependent of the frequency ω or k_z. Explicitly, in the formula (33) for R_{01} we can factor ω and then divide by it and so the expression becomes

$$R_{01}(p) = \frac{\sqrt{\frac{4}{c_0^2} - p^2} - \sqrt{\frac{4}{c_1^2} - p^2}}{\sqrt{\frac{4}{c_0^2} - p^2} + \sqrt{\frac{4}{c_1^2} - p^2}}. \tag{34}$$

Similarly it can be shown that R'_{12} is mapped to a function of p only.

In this new coordinate system the imaging step reads

$$b_1(p, z) = \int_{-\infty}^{\infty} dk_z b_1(p, k_z; \omega) = \left[R_{01}(p)\delta(z - z_a) + R'_{12}(p)\delta(z - z'_b)\right] \delta(k_g - k_s). \tag{35}$$

Numerical results comparing imaging in (k_h, ω) and (p, ω) were shown and discussed in Bruin et al. (1990). The imaged data written in equation (35) is next taken through the internal multiple algorithm described in equation (3).

Given the data in the form (35), the algorithm performs similarly to the 1D normal incidence case. In the following, we are denoting by p_1, p_2 and p_3 the horizontal slownesses associated with $k_g + k_1$, $k_2 + k_s$ and $k_g + k_s$ respectively. The horizontal slowness associated with $k_s + k_g$ is also denoted by p. The four slownesses defined above are not independent, in fact we have that $p_3 = (p_1 + p_2) - p$.

The inner most integral towards calculating b_3 in the internal multiple algorithm is

$$\begin{aligned}
&\int_{z_2'+\varepsilon_1}^{\infty} dz_3' e^{ik_z z_3'} \left[R_{01}(p_2)\delta(z_3'-z_a) + R_{12}'(p_2)\delta(z_3'-z_b')\right]\delta(k_2-k_s) \qquad (36)\\
= &\int_{-\infty}^{\infty} dz_3' H(z_3'-(z_2'+\varepsilon_1)) e^{ik_z z_3'} \left[R_{01}(p_2)\delta(z_3'-z_a) + R_{12}'(p_2)\delta(z_3'-z_b')\right]\delta(k_2-k_s)\\
= &\left[H(z_a-(z_2'+\varepsilon_1))R_{01}(p_2)e^{ik_z z_a} + H(z_b'-(z_2'+\varepsilon_1))R_{12}'(p_2)e^{ik_z z_b'}\right]\delta(k_2-k_s).
\end{aligned}$$

The second integral in the algorithm is

$$\begin{aligned}
&\int_{-\infty}^{z_1'-\varepsilon_2} dz_3' e^{ik_z z_2'} \left[R_{01}(p_3)\delta(z_2'-z_a) + R_{12}'(p_3)\delta(z_2'-z_b')\right]\delta(k_1-k_2) \qquad (37)\\
\times\ &\left[H(z_a-(z_2'+\varepsilon_1))R_{01}(p_2)e^{ik_z z_a} + H(z_b'-(z_2'+\varepsilon_1))R_{12}'(p_2)e^{ik_z z_b'}\right]\delta(k_2-k_s)\\
=\ & R_{01}(p_2)R_{01}(p_3)H(z_a-(z_1'+\varepsilon_2))\underline{H(z_a-(z_a+\varepsilon_1))}e^{ik_z z_a}e^{-ik_z z_a}\delta(k_1-k_2)\delta(k_2-k_s)\\
+\ & R_{01}(p_2)R_{12}'(p_3)H((z_1'-\varepsilon_2)-z_a)H(z_b'-(z_a+\varepsilon_1))e^{ik_z z_b'}e^{-ik_z z_a}\delta(k_1-k_2)\delta(k_2-k_s)\\
+\ & R_{12}'(p_2)R_{01}(p_3)H((z_1'-\varepsilon_2)-z_b')\underline{H(z_a-(z_b'+\varepsilon_1))}e^{ik_z z_a}e^{-ik_z z_b'}\delta(k_1-k_2)\delta(k_2-k_s)\\
+\ & R_{12}'(p_2)R_{12}'(p_3)H((z_1'-\varepsilon_2)-z_b')\underline{H(z_b'-(z_b'+\varepsilon_1))}e^{ik_z z_b'}e^{-ik_z z_b'}\delta(k_1-k_2)\delta(k_2-k_s)
\end{aligned}$$

where all the underlined terms are zero.

The last integral over depth z in the calculation of b_3 is

$$\begin{aligned}
&\int_{-\infty}^{\infty} e^{ik_z z_1'} \left[R_{01}(p_1)\delta(z_1'-z_a) + R_{12}'(p_1)\delta(z_1'-z_b')\right]\delta(k_g-k_1) \qquad (38)\\
\times\ & R_{01}(p_2)R_{12}'(p_3)H((z_1'-\varepsilon_2)-z_a)H(z_b'-(z_a+\varepsilon_1))e^{ik_z z_b'}e^{-ik_z z_a}\delta(k_1-k_2)\delta(k_2-k_s)\\
=\ & R_{01}(p_1)R_{01}(p_2)R_{12}'(p_3)\underline{H(-\varepsilon_2)}H(z_b'-(z_a+\varepsilon_1))e^{ik_z z_a}\delta(k_g-k_1)\delta(k_1-k_2)\delta(k_2-k_s)\\
+\ & R_{12}'(p_1)R_{01}(p_2)R_{12}'(p_3)e^{ik_z(2z_b'-z_a)}H(z_b'-(z_a+\varepsilon_2))H(z_b'-(z_a+\varepsilon_1))\delta(k_g-k_1)\delta(k_1-k_2)\delta(k_2-k_s)\\
=\ & R_{12}'(p_1)R_{01}(p_2)R_{12}'(p_3)e^{2ik_z z_b'}e^{-ik_z z_a}\delta(k_g-k_1)\delta(k_1-k_2)\delta(k_2-k_s)
\end{aligned}$$

where we have used the fact that the underlined term is zero and that the last two Heaviside functions are identically equal to 1.

The result for the b_3, and hence the predicted first order internal multiple, is

$$b_3(p,\omega) = e^{2ik_z z_b'}e^{-ik_z z_a}\int_{-\infty}^{\infty} dk_1 \int_{-\infty}^{\infty} dk_2 R_{12}'(p_1)R_{01}(p_2)R_{12}'(p_3)\delta(k_g-k_1)\delta(k_1-k_2)\delta(k_2-k_s), \quad (39)$$

or, after evaluating the integrals and using the relationship between p_1, p_2, p_3 and p,

$$b_3(p,\omega) = R_{12}'^2(p)R_{01}(p)\delta(k_g-k_s)e^{2ik_z z_b'}e^{-ik_z z_a}. \quad (40)$$

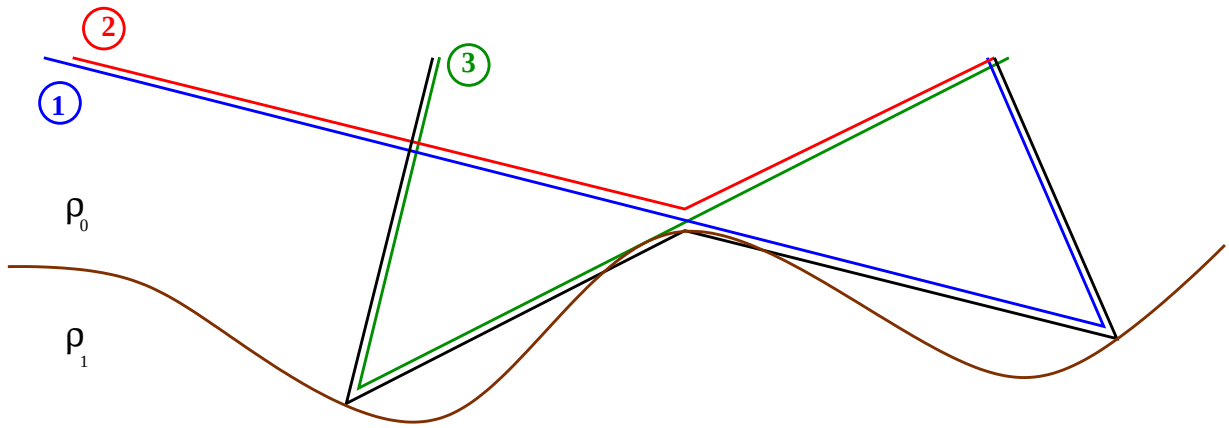

Figure 9: *A 2D earth model with an internal multiple satisfying the time monotonicity in the vertical time but not in the total travel time*

Recalling that $R'^2_{12}(p) = T_{01}(p)R_2(p)T_{10}(p)$ we find the final result to be

$$b_3(p,\omega) = T^2_{01}(p)R^2_2(p)T^2_{10}(p)R_{01}(p)\delta(k_g - k_s)e^{2ik_z z'_b}e^{-ik_z z_a} \tag{41}$$

consistent with the 1D normal incident result of (20). Integrating over k_h gives the prediction of the first order internal multiple in space frequency domain

$$IM^{1st}_{predicted}(x_h, 0; \omega) = \frac{1}{2\pi}\int_{-\infty}^{\infty} dk_h \frac{T^2_{01}R^2_{12}T^2_{10}R_{10}e^{2i\nu_1(z_b - z_a)}}{iq_s} e^{ik_h x_h}e^{ik_z z_a}. \tag{42}$$

Comparing this expression with Equation (15) for the actual multiple we see that the predicted multiple has the correct total time and a well approximated amplitude. The amplitude of the predicted multiple in the p-domain is within a $T_{01}(p)T_{10}(p)$ factor, a factor which is always close to, but always less than, 1. An integration over the horizontal wavenumber k_h will average these amplitudes and will result in the predicted amplitude in the space domain which again is going to be lower than, but close to, the actual amplitude of the internal multiple. In addition, since the phase and amplitude construction is performed in the plane waves domain, the internal multiples with headwaves sub-events are also predicted by the algorithm.

In the next section we will further discuss the lower-higher-lower relationship between the pseudo-depths of the sub-events and the similarities and differences of this relationship in total travel time and vertical or intercept time.

Vertical time and total travel time monotonicity: a 2D example

Consider the earth model shown in Figure 9. For simplicity we assume that only the density ρ varies at the interface and it has the value ρ_0 in the reference medium and ρ_1 in the actual medium. The velocity is constant c_0. The actual internal multiple is shown in black and the sub-events composing the multiple are shown in green, blue and red. First, notice that the total traveltime of the shallower reflection (the red event) is bigger than both deeper reflection (green and blue) due to the large

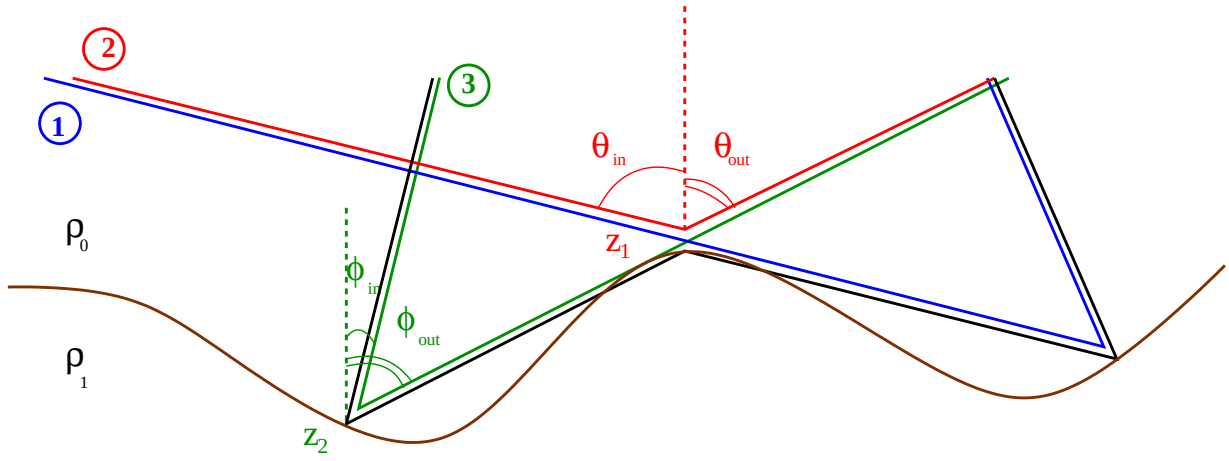

Figure 10: *A 2D earth model with an internal multiple satisfying the time monotonicity in the vertical time but not in the total travel time*

offsets needed to record such an event. This implies that the longer-shorter-longer relationship is not satisfied by these particular sub-events in the total traveltime.

Next we calculate the vertical times for individual sub-events. The vertical time for the red event along the left leg is (see Figure 10)

$$\tau_{red}^{1} = z_1 \frac{\cos\theta_{in}}{c_0} \tag{43}$$

and along the right leg is

$$\tau_{red}^{2} = z_1 \frac{\cos\theta_{out}}{c_0}. \tag{44}$$

Summing the two legs we find the total vertical time along the red event to be

$$\tau_{red} = \frac{z_1}{c_0}\left(\cos\theta_{in} + \cos\theta_{out}\right). \tag{45}$$

Similarly, for the green event we have

$$\tau_{green} = \frac{z_2}{c_0}\left(\cos\phi_{in} + \cos\phi_{out}\right). \tag{46}$$

Since the velocity is constant, $\theta_{out} = \phi_{out}$; we also have that $\phi_{in} < \theta_{in}$, and hence $\cos\phi_{in} > \cos\theta_{in}$, and $z_2 > z_1$ which results in

$$\tau_{green} > \tau_{red}. \tag{47}$$

It is not difficult to see that similarly, for this example, we have

$$\tau_{blue} > \tau_{red} \tag{48}$$

where τ_{blue} is the vertical time of the blue primary in Figure 10.

The conclusion is that for this model and particular internal multiple, the longer-shorter-longer relationship is satisfied by the vertical or intercept times of the three subevents but not by their total traveltimes. According to equation (10), this relation translates into the lower-higher-lower relationship between the pseudo-depths of the sub-events and hence the internal multiple depicted

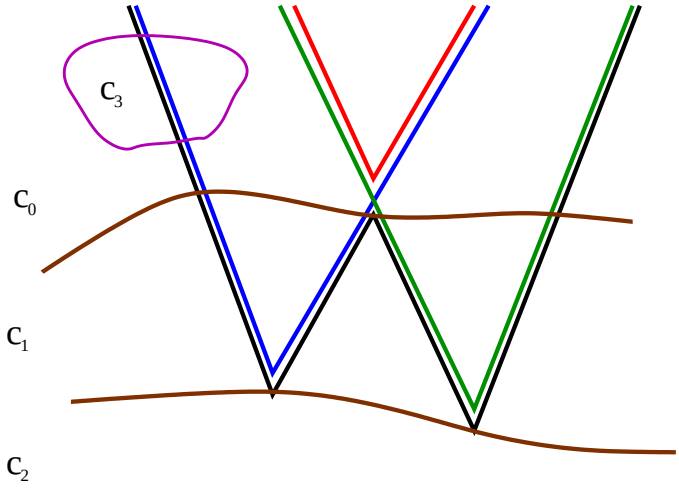

Figure 11: *A 2D earth model with an internal multiple containing sub-events which do not satisfy the time monotonicity in either total traveltime or vertical time.*

in Figure 9 will be predicted by the inverse scattering internal multiple attenuation algorithm in Equation (3).

In the next section we discuss an earth model and a particular internal multiple in which the longer-shorter-longer relationship in vertical and total travel time is not satisfied.

Breaking the time monotonicity: a 2D example

Consider the earth model shown in Figure 11 where $c_0 < c_1$. A high velocity zone, in which the propagation speed c_3 is much higher than c_0, intersects one leg of the internal multiple and hence one leg of one of the sub-events (the blue primary in Figure 11). Due to this high velocity zone and the fact that $c_0 < c_1$, one can easily imagine a situation in which both the total and the vertical time of the blue primary are shorter than the total and vertical times respectively of the red primary. In this case the lower-higher-lower relationship between the pseudo-depths of the sub-events is not satisfied and hence the internal multiple shown in the picture will not be predicted. The monotonicity is in consequence broken, since even though the actual depths still satisfy a lower-higher-lower relationship, the pseudo-depths, vertical times or total times of the sub-events do not.

To better understand the multiples which do not satisfy the pseudo-depth/vertical-time monotonicity condition and to expand the algorithm to address them, one has to study their creation in the forward scattering series. As indicated by Matson (10) (11) and Weglein et al. (20) the lower-higher-lower relationship in pseudo-depth z was pointed to by the forward scattering series: the first order approximation to an internal multiple is constructed in the forward scattering series from interactions with point scatterers which satisfy the lower-higher-lower relationship in actual depth. It would be interesting to analyze how a multiple that breaks the monotonicity assumption is constructed by the forward series and to determine if an analogy between the forward and the inverse process would be useful to expand the algorithm to address these kind of events. This particular issue and others will be the subject of future research.

Conclusions

In this paper we presented an analytic analysis of the inverse scattering internal multiple attenuation algorithm for multi dimensional media. We particularly focused on the mechanism of predicting amplitude and phase properties of an interbed multiple. We have presented the first prestack analysis with analytical data which shows the ability of the algorithm to exactly predict the time and well approximate the amplitude of internal multiples, including the ones with headwaves sub-events. We have discussed in detail the pseudo-depth/vertical-time monotonicity condition and compared it with a similar total traveltime relation. Furthermore, we showed that this restriction on the sub-events can be too strong and could prevent the prediction of some complex internal multiples.

This research is an important step forward in better understanding the inverse scattering series and the internal multiple attenuation algorithm derived from it. The analytic analysis presented, targets internal multiples which occur in complex multi-dimensional media. Having a better understanding of the structure and definition of such internal multiples opens up new possibilities of identifying, predicting and subtracting them from the collected data. The inverse scattering series is presently the only tool that can achieve these objectives without any knowledge about the actual medium.

Acknowledgments

This work was partially supported by NSF-CMG award number DMS-0327778. The support of M-OSRP sponsors is also gratefully acknowledged. Adriana C. Ramírez is thanked for providing the earth model in Figure 9. Jon Sheiman, Einar Otnes and Fons ten Kroode are acknowledged for their useful comments and insights on this work.

References

[1] K. Aki, P. G. Richards (1980), *Quantitative Seismology,* W. H. Freeman and Company, San Francisco.

[2] F. V. Araujo (1956), *Linear and Nonlinear Methods Derived from Scattering Theory: Backscattered Tomography and Internal Multiple Attenuation,* Ph.D. thesis, Department of Geophysics, Universidad Federal de Bahia, Salvador-Bahia, Brazil, 1994 (in Portuguese).

[3] R. N. Bracewell (1956), *Strip integration in radio astronomy*, Aust. J. Phys., Vol. 9, pp. 198-217.

[4] R. N. Bracewell, A. C. Riddle (1967), *Inversion of fan-beam scans in radio astronomy*, Astrophys. J., Vol. 150, pp. 427-434.

[5] C. G. M. Bruin, c. P. A. Wapenaar, A. J. Berkhout (1990), *Angle-dependent reflectivity by means of prestack migration*, Geophysics, Vol. 55, No. 9, pp. 1223-1234.

[6] P. M. Carvalho (1992), *Free Surface Multiple Reflection Elimination Method Based on Nonlinear Inversion of Seismic Data*, Ph.D. thesis, Department of Geophysics, Universidad Federal de Bahia, Salvador-Bahia, Brazil, (in Portuguese).

[7] J. B. Diebold and P. L. Stoffa (1981), *The traveltime equation, tau-p mapping, and inversion of common midpoint data*, Geophysics, Vol. 46, No. 3, pp. 238-254.

[8] S. T. Kaplan, K. A. Innanen, E. Otnes and A. B. Weglein (2005), *Internal multiple attenuation code-development and implementation project report*, M-OSRP Annual Report, 2005.

[9] A. Malcolm and M. V. de Hoop (2005), *A method for inverse scattering based on the generalized Bremmer coupling series*, Inverse Problems, submitted

[10] K. H. Matson (1996, *The relationship between scattering theory and the primaries and multiples of reflection seismic data*, J. Seismic Exploration, 5, pp. 63–78.

[11] K. H. Matson, *An Inverse Scattering Series Method for Attenuating Elastic Multiples from Multicomponent Land and Ocean Bottom Seismic Data*, Ph.D. thesis, Department of Earth and Ocean Sciences, University of British Columbia, Vancouver, BC, Canada, 1997.

[12] B. G. Nita and A. B. Weglein (2004), *Imaging with $\tau = 0$ versus $t = 0$: implications for the inverse scattering internal multiple attenuation algorithm*, SEG Expanded Abstracts, 74^{th} Annual Meeting of the Society for Exploration Geophysicists, Denver, Colorado.

[13] A. C. Ramírez and A. B. Weglein (2005), *Progressing the analysis of the phase and amplitude prediction properties of the inverse scattering internal multiple attenuation algorithm*, submitted to Journal of Seismic Exploration.

[14] A. C. Ramírez and A. B. Weglein (2005),

[15] R. Stolt (1978), *Migration by Fourier transform*, Geophysics, 43, pp. 23-48.

[16] R. Stolt and A. B. Weglein (1985), *Migration and inversion of seismic data*, Geophysics, 50, pp. 2458-2472.

[17] A. P. E. ten Kroode (2002), *Prediction of internal multiples*, Wave Motion, 35, pp. 315-338.

[18] S. Treitel, P. R. Gutowski and D. E. Wagner (1982), *Plane-wave decomposition of seismograms*, Geophysics, Vol. 47, No. 10, pp. 1374-1401.

[19] A. B. Weglein, F. A. Gasparotto, P. M. Carvalho, R. H. Stolt (1997), *An inverse scattering series method for attenuating multiples in seismic reflection data*, Geophysics, 62, pp. 1975-1989.

[20] A. B. Weglein, F. V. Araujo, P. M. Carvalho, R. H. Stolt, K. H. Matson, R. Coates, D. Corrigan, D. J. Foster, S. A. Shaw, H. Zhang (2003), *Inverse scattering series and seismic exploration*, Topical Review Inverse Problems, 19, pp. R27-R83.

[21] A. B. Weglein, W. Dragoset (2005), *Internal Multiples*, SEG Reprint Volume.

Progressing the analysis of the phase and amplitude prediction properties of the inverse scattering internal multiple attenuation algorithm

Adriana Citlali Ramírez and Arthur B. Weglein

Abstract

Predicting and removing internal multiples is an important and long-standing challenge in exploration seismology. The inverse scattering theory based internal multiple attenuation algorithm (14) (1) effectively reduces internal multiples with documented successful application to field datasets. Stated succinctly: the inverse scattering internal multiple attenuator predicts both time and amplitude. The amplitude prediction is approximately equal to and always less than the actual value. The internal multiple attenuator is the first term in an internal multiple removal series, which is, in turn, a subseries of the entire inverse scattering series. The inverse scattering series, and all of its task specific subseries, accomplish their objectives without knowing or determining the velocity or any properties beneath the measurement surface. This characteristic makes it ideal for addressing one of the current biggest challenges in exploration seismology: removing multiples and locating and identifying targets when the subsurface geology is complex and ill-defined.

Using an analytic data example, this paper extends an earlier analysis (17) to determine the efficacy of the attenuator towards its stated objective, *i.e.* precisely how effective is this temporal prediction and amplitude reduction process. The timing of the algorithm is perfect and (within the confines of the 1D layered earth normal incidence wave analysis presented here) we demonstrate that the difference between complete elimination and the attenuation, that the algorithm provides, resides in the attenuator having extra powers of transmission coefficients only for all the interfaces down to and including the depth of the shallowest downward reflection. The difference between the algorithm's amplitude prediction and the amplitude of the actual internal multiple is totally independent of the rest of the path, velocities and earth parameters beneath that shallowest reflector that the internal multiple has traveled. This property helps explain the high degree of effectiveness and impact observed in practical application of these algorithms on field data, especially under highly complex subsurface conditions (9) (17) (12).

The *forward* scattering series, starting with no a priori subsurface information, requires an infinite series to predict either the time and/or the amplitude of any internal multiple. In marked contrast, the *inverse* scattering subseries that removes internal multiples of a given order predicts the precise time and well approximates the amplitude of all internal multiples of that order with a single first term, called the attenuator. This remarkable difference is the reason the single term attenuator has such a practical and significant contribution. The most important aspect of predicting events is determining the arrival time. Having the precise amplitude but having the wrong arrival time is of little practical value. Having the perfect time and a well approximated amplitude is the hallmark of a useful event prediction method.

Introduction and background

In marine seismic exploration, towed streamer data is acquired with a seismic source and receivers located within the water column. For the purposes and objectives of exploration seismology, it

is convenient to catalog and separate the recorded data events into different categories (17). The first category consists of the direct arrival and the wave that goes from the source up to the free surface, reflects from that surface and then propagates directly to the receiver. Those latter two events have not experienced the subsurface. All of the other categories of events have experienced the earth.

Next, the events that experience the earth are further separated depending on whether they began as a wave moving upwards or downwards leaving the source or ended traveling upwards or downwards when they arrive at the receiver. Those moving upwards from the source are called source ghosts, those moving downwards when they arrive at the receiver are receiver ghosts, and those that have both properties are source receiver ghosts. All the ghost events are separated from the unghosted events, the latter originating as downgoing at the source and ending as upgoing at the receiver. Deghosted events are further catalogued by the number and location of their reflections. Deghosted events with one upward reflection are called primaries; events with more than one upward reflection are called multiples. Multiples are further divided into events that have experienced the free surface, and those that have not: The former are called free surface multiples and the latter are called internal multiples. For our purposes, the order of a free surface multiple is defined by the number of times it has experienced a downward reflection from the free surface, whereas, the order of an internal multiple is defined to be the number of downward reflections it experiences, without reference to the location of the downward reflection.

It is convenient, reasonable and standard practice to seek to remove all multiples from seismic reflection data and to then use the primaries to determine the location and properties of the single upward reflector they have experienced. Hence, the removal of multiples is an essential step in the seismic processing chain. Removing multiples is not a new idea, and there are many methods that have been developed that are often effective –an overview of multiple removal can be found in, *e.g.* Verschuur (1991)(13), Berkhout *et al* (1997)(2), Weglein (1999)(15) and Weglein and Dragoset (2005)(18). However, either deep water and/or a complex multidimensional earth can wreak havoc on many procedures that either assume the earth is 1D, or that a reasonable velocity estimate is obtainable. The inverse scattering series processing methods can accommodate a complex multidimensional earth (14), without requiring any subsurface information, including velocity; those distinct algorithms for free surface and internal multiples were the first comprehensive methods to address that challenge, and remain the high-water mark of effectiveness.

A review of the evolution and development of these inverse scattering series concepts and practical algorithms, with synthetic and field data examples can be found in Weglein *et al* (2003)(17). The objectives of this paper are to progress the study of amplitude prediction of the inverse scattering internal multiple attenuation algorithm, both to further clarify its properties and to suggest a path for future increased algorithmic capability towards addressing the challenge of removing multiples. The demand for added efficacy for multiple attenuation, and going beyond attenuation, is a pressing current need especially under complex geologic circumstances where adequate velocity information is unobtainable with our most effective velocity methods. We begin with a brief review of scattering theory, forward and inverse scattering series, and the steps required, e.g., to derive an internal multiple algorithm, or algorithms performing other seismic processing objectives, from the inverse scattering series.

Inverse Scattering Series

Scattering theory describes how a perturbation in a medium's properties relates to differences in the resulting wave field. The brief background presented here to scattering theory, forward scattering series, and inverse scattering series, and concepts for multiples and their attenuation, follows the development provided in Weglein *et al* (1997)(14), and (2003)(17), wherein further detail, contributors and references can be found.

For our purposes in exploration seismology, we choose the unperturbed medium to be a chosen reference medium and consider a perturbation that alters the reference into the actual medium, the earth. Let L_0 and L be the differential wave operators governing propagation in the reference and actual medium, and G_0 and G the corresponding Green's functions, respectively:

$$\begin{aligned} LG &= \delta, \\ L_0 G_0 &= \delta. \end{aligned} \tag{1}$$

We define the perturbation operator as $V = L_0 - L$ and the difference field, Ψ_s, as $G - G_0$. These quantities are related by the Lippmann Schwinger equation:

$$G = G_0 + G_0 V G. \tag{2}$$

The Lippmann Schwinger equation can be expressed as a forward series for $G - G_0$ in terms of G_0 and V and this is the forward scattering series. It is a series in orders of V:

$$G - G_0 \quad = G_0 V G_0 + G_0 V G_0 V G_0 + G_0 V G_0 V G_0 V G_0 + \cdots . \tag{3}$$

The inverse of this forward scattering series is the inverse scattering series, for V in orders of the measured values of the scattered field, $G - G_0$:

$$V = \Sigma_i V_i = V_1 + V_2 + V_3 + \cdots . \tag{4}$$

The equations for V_1, V_2, etc. are:

$$\begin{aligned} G_0 V_1 G_0 &= G - G_0 = D \\ G_0 V_2 G_0 &= -G_0 V_1 G_0 V_1 G_0 \\ G_0 V_3 G_0 &= -G_0 V_1 G_0 V_1 G_0 V_1 G_0 - G_0 V_1 G_0 V_2 - G_0 V_2 G_0 V_1 \\ &\vdots \end{aligned} \tag{5}$$

where D represents the measured scattered field, $D = (\Psi_s)_m$, and the subscript m indicates measured values. The forward series creates the perturbed wavefield from the reference propagator, G_0, and the medium perturbation, V. The inverse series constructs V from G_0 and measured values of $G - G_0$.

The inversion process –determination of the structural image of the subsurface including its physical properties- can be viewed as consisting of four intermediate steps and uncoupled tasks: (1) free-surface multiple removal, (2) internal multiple removal, (3) spatial location of reflectors and (4) identification of how medium properties change across reflectors. Subseries within the inverse scattering series performing these four tasks have been identified with two immediate advantages:

favorable convergence properties as well as the ability to benefit from completed earlier steps to improve the chances of subsequent tasks succeeding. The strategy is to accomplish one task at a time, and then restart the problem as if the just completed task never existed. The tasks associated with inversion are each carried out by the task specific subseries directly in terms of the measured scattered field, D, and the reference medium Green's function, G_0.

Internal Multiple Attenuation

Several steps of problem definition, forward concept and inverse analog were needed in coming to identify the part of the inverse scattering series that provides an activity, and subsequent algorithm, that attenuates all internal multiples of a given order. We will briefly discuss those defining issues further in this paper. Within the broad confines of what those definitions, constructs and concepts capture, an internal multiple algorithm is presented in Araújo (1994)(1), Weglein *et al* (1997)(14) and (2003)(17). That algorithm for a 2D earth is:

$$b_1(k_g,k_s,q_g+q_s) = -2iq_sD(k_g,k_s,\omega), \tag{6}$$

$$\begin{aligned} b_3(k_g,k_s,q_g+q_s) = \frac{1}{(2\pi)^2}\int_{-\infty}^{\infty} dk_1 e^{iq_1(x_s-x_g)} \int_{-\infty}^{\infty} dk_2 e^{iq_2(\epsilon_g-\epsilon_s)} \\ \times \int_{-\infty}^{\infty} dz_1 e^{i(q_g+q_s)z_1} b_1(k_g,-k_1,z_1) \\ \times \int_{-\infty}^{z_1-\epsilon_2} dz_2 e^{i(-q_1-q_2)z_2} b_1(k_1,-k_2,z_2) \\ \times \int_{z_2+\epsilon_1}^{\infty} dz_3 e^{i(q_2+q_s)z_3} b_1(k_2,-k_s,z_3), \end{aligned} \tag{7}$$

where ω represents the temporal frequency, c_0 is the acoustic velocity of water; k_g and k_s are the horizontal wavenumbers corresponding to receiver and source coordinates: x_g and x_s, respectively; the 2-D wavevectors: $\mathbf{k}_g = (k_g, -q_g)$ and $\mathbf{k}_s = (k_s, q_s)$ are constrained by $|\mathbf{k}_g| = |\mathbf{k}_s| = \frac{\omega}{c_0}$; the vertical wavenumbers are $q_g = sgn(\omega)\sqrt{(\frac{\omega}{c_0})^2 - {k_g}^2}$ and $q_s = sgn(\omega)\sqrt{(\frac{\omega}{c_0})^2 - {k_s}^2}$, and ϵ_i, $i = 1, 2$ is a small positive parameter chosen to insure that the relations $z_1 > z_2$ and $z_3 > z_2$ are satisfied.

In Eqs.(6) and (7), the quantity $b_1(k_g, k_s, q_g + q_s)$ is defined as a source obliquity factor times the 2D measured values of the scattered field, $(\Psi_s)_m = D$, and the variable z is the Fourier conjugate to the sum of the vertical wavenumbers, $k_z = -(q_g + q_s)$.

That single algorithm automatically accommodates all earth model types that satisfy the convolutional model(17), and neither requires nor determines any earth material properties (5)(9) (12). The 1D earth and normal incidence wave version of that multidimensional algorithm is

$$b_1(k) = D(\omega), \tag{8}$$

$$b_3(k) = \int_{-\infty}^{\infty} dz_1 e^{ikz_1} b_1(z_1) \int_{-\infty}^{z_1-\epsilon_2} dz_2 e^{-ikz_2} b_1(z_2) \int_{z_2+\epsilon_1}^{\infty} dz_3 e^{ikz_3} b_1(z_3), \tag{9}$$

where $k = 2\frac{\omega}{c_0}$. In the 1D normal incidence algorithm, Eq. (9), we will refer to k_z simply as k. This 1D version is convenient for analyzing the effectiveness of the algorithm where the data

is analytic and the algorithm's integrals can be analytically evaluated, hence completely avoiding any numerical error in either the data quality or the algorithm's degradation due to numerical integration errors. Furthermore, the analytic result precisely attributes the underlying strengths and limitations to the intrinsic character of the method, given exact data as input, and a flawless execution of the algorithm.

In the next section we first present the results of an earlier analysis in Weglein *et al* (2003)(17), in a 1D model with two interfaces, to determine the effectiveness of the attenuation algorithm. We then progress the insight and understanding of the internal multiple attenuator by extending the analysis to first three and then an arbitrary number of interfaces. These analytic examples further illustrate the ability of the inverse scattering algorithm to attenuate first order internal multiples without knowing or determining the velocity or any properties inside the medium.

Internal Multiple Amplitude Prediction

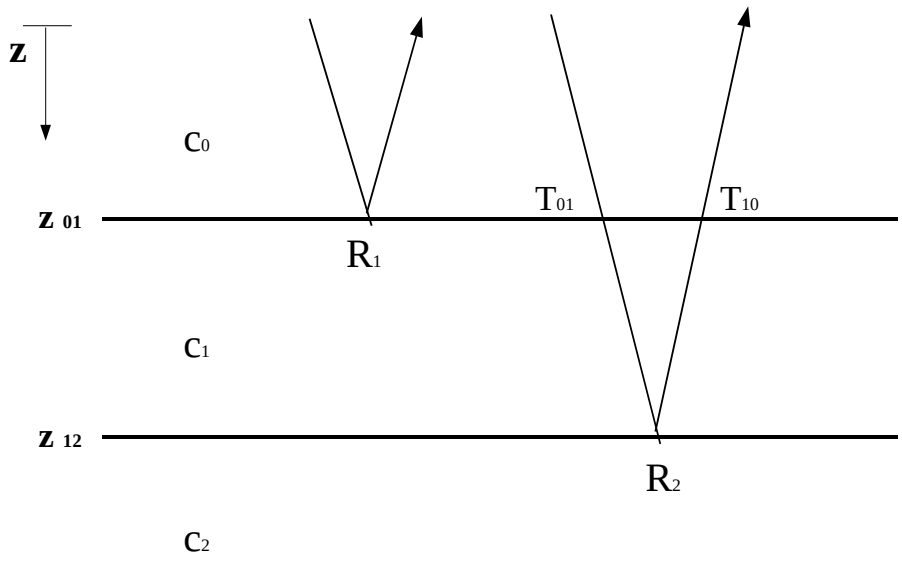

Figure 1: *One dimensional model with two interfaces.*

The multiple removal algorithm derived using the inverse series has the unique property that it expects the recorded seismic data, without both the effects of the free surface and the source wavelet, as input. To demonstrate the inner workings of the algorithm and further define its level of effectiveness, Weglein *et al* (2003)(17) considered the simplest model that produces data with internal multiples and could be taken analytically through Eq.(7). It is a 1D variable velocity,

constant density, acoustic model with two interfaces shown in Fig.(1): the data used in this example consists of two primaries created by a normal incident spike wave $\delta(t - \frac{z}{c})$:

$$D(t) = R_1\delta(t - t_1) + T_{01}R_2T_{10}\delta(t - t_2) + \cdots , \tag{10}$$

where t_1, t_2 are the two way travel times of the primaries from the two reflectors, R_1 and R_2 are the reflection coefficients from the interfaces at z_{01} and z_{12} respectively, and T_{01} and T_{10} are the transmission coefficients when going down and up through the interface at z_{01}. Performing a temporal Fourier transform of $D(t)$, and using $k = 2\frac{\omega}{c_0}$, gives:

$$D(\omega) = R_1e^{i(\frac{2\omega}{c_0})(\frac{c_0t_1}{2})} + T_{01}R_2T_{10}e^{i(\frac{2\omega}{c_0})(\frac{c_0t_2}{2})} + \cdots , \tag{11}$$

and

$$b_1(k) = R_1e^{ikz_1} + T_{01}R_2T_{10}e^{ikz_2} + \cdots . \tag{12}$$

The $-2iq_s$ factor in $b_1(k_g, k_s, q_g + q_s)$ –Eq.(6)- is a result of a point source experiment; when the incident wave is a spike wave that factor is not required. The pseudo-depths z_1 and z_2 are defined in the reference medium as:

$$\begin{aligned} z_1 &\equiv \frac{c_0t_1}{2}, \\ z_2 &\equiv \frac{c_0t_2}{2}. \end{aligned} \tag{13}$$

The substitution of $b_1(k)$ into Eq.(9) gives the following prediction of a first order internal multiple:

$$b_3(k) = R_1R_2^2T_{01}^2T_{10}^2e^{2ikz_2}e^{-ikz_1}, \tag{14}$$

which in the time domain is:

$$b_3(t) = R_1R_2^2T_{01}^2T_{10}^2\delta(t - (2t_2 - t_1)). \tag{15}$$

The result predicts a first order internal multiple with the exact time and whose amplitude is the precise amplitude $(-T_{01}R_2R_1R_2T_{10})$, with opposite sign, multiplied by the transmission coefficients $(T_{01}T_{10})$ of the first interface. The difference between elimination and attenuation is determined by $1 - T_{01}T_{10}$ which is a small number even when R_1 corresponds to a large but realistic reflection coefficient. That $T_{01}T_{10}$ is less than one reflects the fact that the method is an attenuator, delivering a reduction of the first order internal multiple amplitude.

We now extend this analysis to several reflectors to determine a clearer and deeper understanding of the algorithm, taking you step by step on the same journey that data would take. The earth model is illustrated in Fig.(2); it consists of a reference whole space with velocity c_0 and three layers with respective wavespeeds of c_1, c_2, c_3 and layer boundaries at z_{01}, z_{12} and z_{23}. The source and receiver are located at depth $z = 0$.

The first term in the algorithm is the data itself, D. In this example, the data is assumed to be generated by a normal incident spike wave $\delta(t - z/c)$ in the 1D medium of this three reflector model (Fig. (2)). The data, $D(t)$ is:

$$D(t) = R_1\delta(t - t_1) + T_{01}R_2T_{10}\delta(t - t_2) + T_{12}T_{01}R_3T_{10}T_{21}\delta(t - t_3) + \cdots , \tag{16}$$

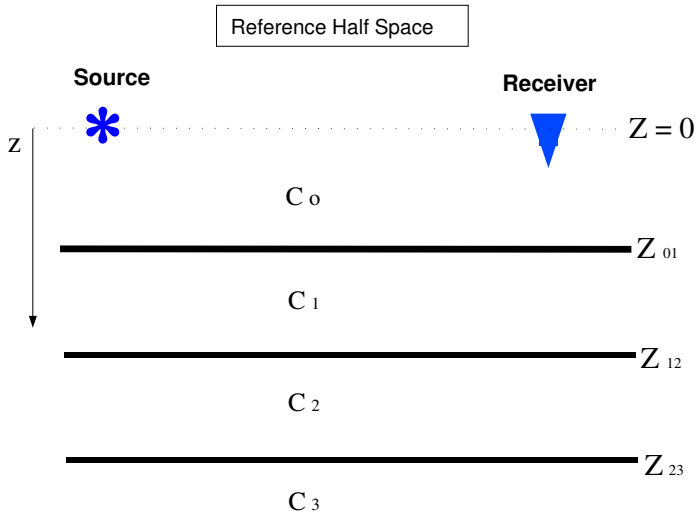

Figure 2: *1D layered medium.*

T_{12} and T_{21} are the transmission coefficients when going down and up, respectively, through the interface at z_{12}.

We use the definitions: $R'_2 = T_{01}R_2T_{10}$ and $R'_3 = T_{01}T_{12}R_3T_{21}T_{10}$, and apply a temporal Fourier transform to $D(t)$:

$$\begin{aligned} D(\omega) &= \int_{-\infty}^{\infty} dt D(t) e^{i\omega t} \\ &= R_1 e^{i\omega t_1} + R'_2 e^{i\omega t_2} + R'_3 e^{i\omega t_3}, \end{aligned} \tag{17}$$

We now introduce the wavenumber $k = 2\frac{\omega}{c_0}$ and the reference medium pseudodepths $z_i = \frac{c_0 t_i}{2}$:

$$\begin{aligned} b_1(k) &= D(\omega) = R_1 e^{ikz_1} + R'_2 e^{ikz_2} + R'_3 e^{ikz_3}, \\ b_1(z) &= \int_{-\infty}^{\infty} e^{-ikz} b_1(k)\, dk \\ &= \quad R_1\delta(z - z_1) + R'_2\delta(z - z_2) + R'_3\delta(z - z_3). \end{aligned} \tag{18}$$

We substitute the data from Eq.(18) into b_3, and evaluate the integrals analytically. The first integral in Eq.(9) towards computing b_3 is:

$$\begin{aligned} I_3(k) = \int_{z'+\epsilon_1}^{\infty} & dz'' e^{ikz''} (R_1\delta(z'' - z_1) + R'_2\delta(z'' - z_2) + R'_3\delta(z'' - z_3)) \\ &= R_1 e^{ikz_1} H(z_1 - (z' + \epsilon_1)) + R'_2 e^{ikz_2} H(z_2 - (z' + \epsilon_1)) \\ &\quad + R'_3 e^{ikz_3} H(z_3 - (z' + \epsilon_1)), \end{aligned} \tag{19}$$

where H is the Heaviside function. The second integral in Eq.(9) is:

$$\begin{aligned}
&\int_{-\infty}^{z-\epsilon_2} dz' e^{-ikz'}(R_1\delta(z'-z_1)+R_2'\delta(z'-z_2)+R_3'\delta(z'-z_3)+\cdots)(I_3(k)) \\
&= \quad R_1R_2'e^{ikz_2}H(z_2-(z_1+\epsilon_1))H((z-\epsilon_2)-z_1)e^{-ikz_1} \\
&\quad + R_1R_3'e^{ikz_3}H(z_3-(z_1+\epsilon_1))H((z-\epsilon_2)-z_1)e^{-ikz_1} \\
&\quad + R_2'R_3'e^{ikz_3}H(z3-(z_2+\epsilon_1))H((z-\epsilon_2)-z_3)e^{-ikz_3}, \qquad (20)
\end{aligned}$$

and the last integral gives:

$$\begin{aligned}
b_3(k) = \quad & R_1{R_2'}^2e^{2ikz_2}e^{-ikz_1}H(z_2-z_1-\epsilon_1)H(z_2-\epsilon_2-z_1) \\
& + R_1R_2'R_3'e^{ikz_2}e^{ikz_3}e^{-ikz_1}H(z_3-z_1-\epsilon_1)H(z_2-\epsilon_2-z_1) \\
& + R_1R_2'R_3'e^{ikz_2}e^{ikz_3}e^{-ikz_1}H(z_2-z_1-\epsilon_1)H(z_3-\epsilon_2-z_1) \\
& + R_1{R_3'}^2e^{2ikz_3}e^{-ikz_1}H(z_3-z_2-\epsilon_1)H(z_3-\epsilon_2-z_1) \\
& + R_2{R_3'}^2e^{2ikz_3}e^{-ikz_2}H(z_3-z_2-\epsilon_1)H(z_3-\epsilon_2-z_2). \qquad (21)
\end{aligned}$$

An inverse Fourier transform takes $b_3(k)$ back to the time domain, and we obtain:

$$\begin{aligned}
b_3(t) = & R_1R_2^2T_{01}^2T_{10}^2\delta(t-(2t_2-t_1)) + 2R_1R_2R_3T_{01}^2T_{10}^2T_{12}T_{21}\delta(t-(t_2+t_3-t_1)) \\
& + R_1R_3^2T_{01}^2T_{12}^2T_{21}^2T_{10}^2\delta(t-(2t_3-t_1)) + R_2R_3^2T_{01}^3T_{10}^3T_{12}^2T_{21}^2\delta(t-(2t_3-t_2)). \qquad (22)
\end{aligned}$$

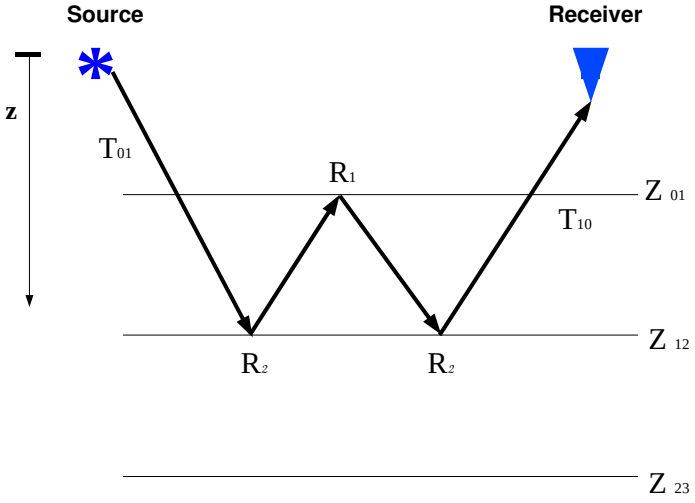

Figure 3: *First order internal multiple.*

The first term in Eq.(22), $R_1R_2^2T_{01}^2T_{10}^2\delta(t-(2t_2-t_1))$, agrees with the result of Eq.(15) for the internal multiple example illustrated in Fig.(3). The prediction has the correct time, and it is attenuated by the transmission coefficients $T_{01}T_{10}$. The same conclusion holds for the second and

third term in Eq.(22). These first three terms on the right hand side of Eq. (22) share the same overabundance of transmission coefficients in the prediction and they all correspond to first order internal multiples with their downward reflection at the same interface (z_{01}).

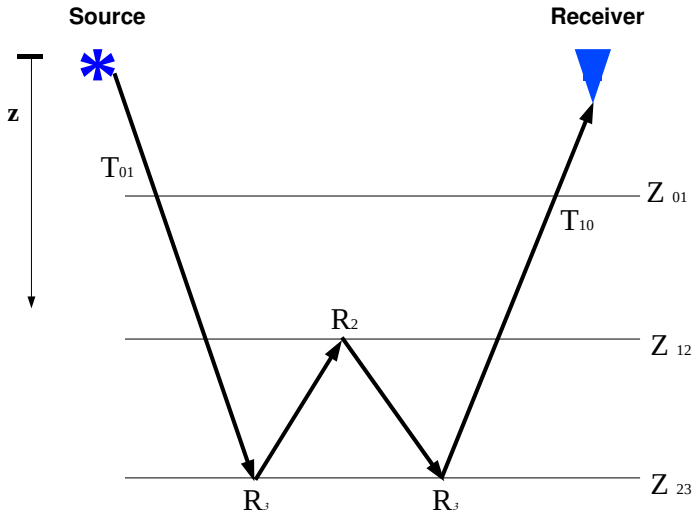

Figure 4: *A first order internal multiple with its downward reflection at* z_{12}.

The last term, $R_2R_3^2T_{01}^3T_{10}^3T_{12}^2T_{21}^2\delta(t-(2t_3-t_2))$, has the correct time of the first order internal multiple having, its downward reflection at z_{12} for the model used in the example. The actual internal multiple (see Fig.(4)) is precisely:

$$-T_{01}T_{12}R_3R_2R_3T_{21}T_{10}\delta(t-(2t_2-t_1). \tag{23}$$

Hence the time prediction is exact and the amplitude has an extra power of $T_{01}T_{10}$ $(T_{12}T_{21})^2$, which is always less than one. The conclusion is that, once again, the predictor has too much transmission (consistent with the method being an attenuator rather than an eliminator) down to and including the shallowest downward reflection point; the time prediction is precise, and the residual multiple after adding the data, $D=b_1$, to the attenuator, b_3, always has the same sign as the multiple.

To have a general formula for amplitude prediction of the algorithm, we need to generalize the example to a model with n layers with respective velocities of c_n; n being an integer. Using equations (9)-(22), the definitions $R_1=R_1'$ and $R_N'=R_N\Pi_{i=1}^{N-1}(T_{i-1,i}\ T_{i,i-1})$, Einstein's Summation Convention and the reflection data from a normal incident spike wave:

$$D(t)=R_n'\delta(t-t_n)+\cdots, \tag{24}$$

we obtain the result:

$$\begin{aligned} b_3(k) &= R_i'R_j'R_k'e^{ikz_i}H(z_i-(z_j+\epsilon_j))e^{-ikz_j}H(z_k-\epsilon_2-z_j)e^{ikz_k}, \\ b_3(t) &= R_i'R_j'R_k'\delta(t-(t_i+t_k-t_j). \end{aligned} \tag{25}$$

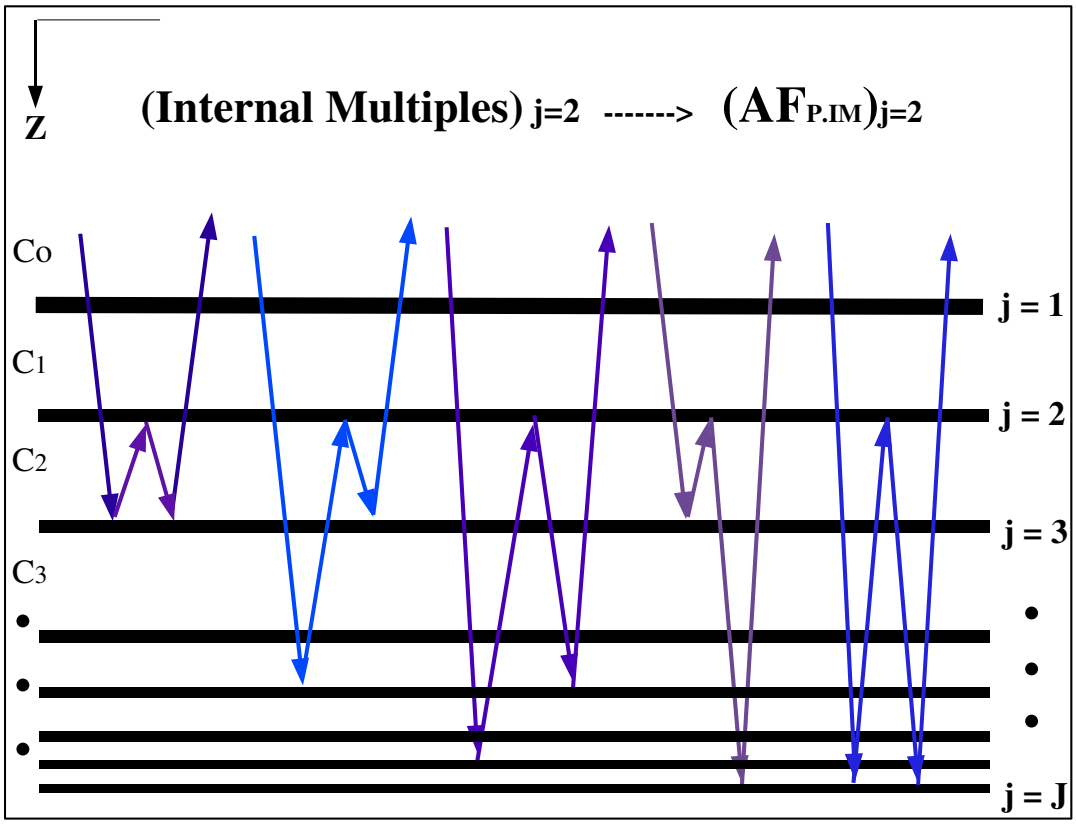

Figure 5: *Shows first order Internal Multiples with downward reflection at j=2. They all have the same attenuation factor* $AF_{P.IM} = T_{01}^2 T_{10}^2 T_{12} T_{21}$.

Evaluating Eq.(25) for different values of i, j and k we are able to generalize the amplitude prediction of first order internal multiples given by the leading term of the first order internal multiple removal subseries –Eq.(9). The generalization of the predicted internal multiple amplitude states that the overabundance of transmission coefficients depends on the position of the shallowest downward reflection. This attenuation factor of the predicted internal multiple, $(AF_{P.IM})$, is:

$$(AF_{P.IM})_j = \begin{cases} T_{0,1} T_{1,0} & \text{for } j = 1 \\ \Pi_{i=1}^{j-1} \left(T_{i,i-1}^2 T_{i-1,i}^2 \right) T_{j,j-1} T_{j-1,j} & \text{for } 1 < j < J \end{cases} \tag{26}$$

for each internal multiple; where j represents the interface where the downward reflection took place, and J is the total number of interfaces in the model. The interfaces are numbered with integers, starting with the shallowest location as shown in Fig.(5). Eq.(26) is valid for any number of layers, and it indicates that the actual algorithm predicts the precise arrival time and an attenuated amplitude using the recorded primary events.

The correct arrival time is not given by the reference medium, but by combinations of the data. b_3 predicts first order internal multiples using three events within the data (see Fig.(7)). The attenuation factor of the predicted internal multiple –Eq.(26)- is related directly with the trajectory

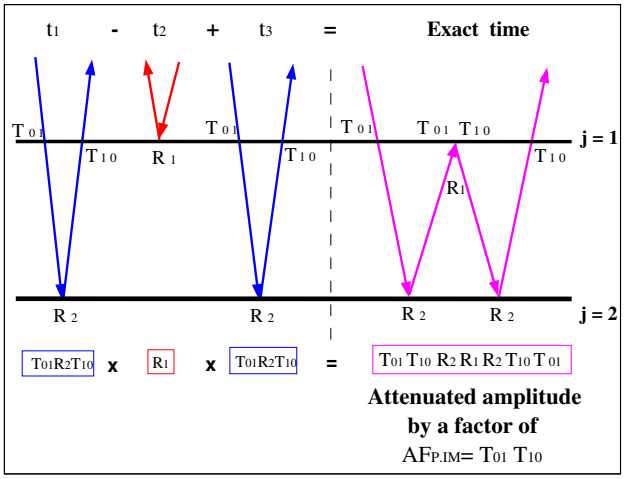

Figure 6: *Predicted Internal Multiple. From left to right, the third primary has a negative phase and corrects the time.*

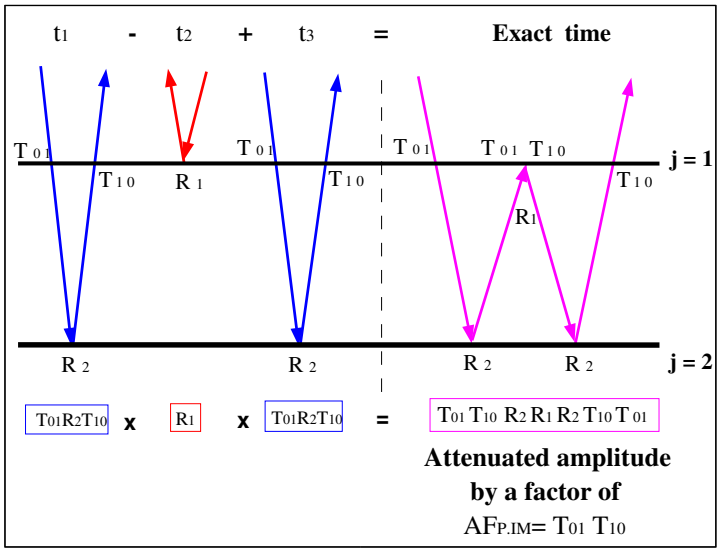

Figure 7: *Predicted Internal Multiple. From left to right, the third primary has a negative phase and corrects the time.*

of the event from b_1 computed with a negative sign in the phase for the second depth integral in Eq.(9); the detailed study of this approximate amplitude shows that it has an overabundance of two transmission coefficients at the interface where the downward reflection took place and four extra transmission coefficients at all the other interfaces above this one –see Fig.(8). The $AF_{P.IM}$ is completely independent of the place where the two upward reflections occurred; b_3 is always an amplitude attenuator that gives the precise time of all first order internal multiples.

In an important and significant paper, Ten Kroode (2002)(7) presents an analysis of the effectiveness of the inverse scattering internal multiple attenuator using the metric of how well the algorithm attenuates synthetic data corresponding to the first approximation of internal multiples in a forward

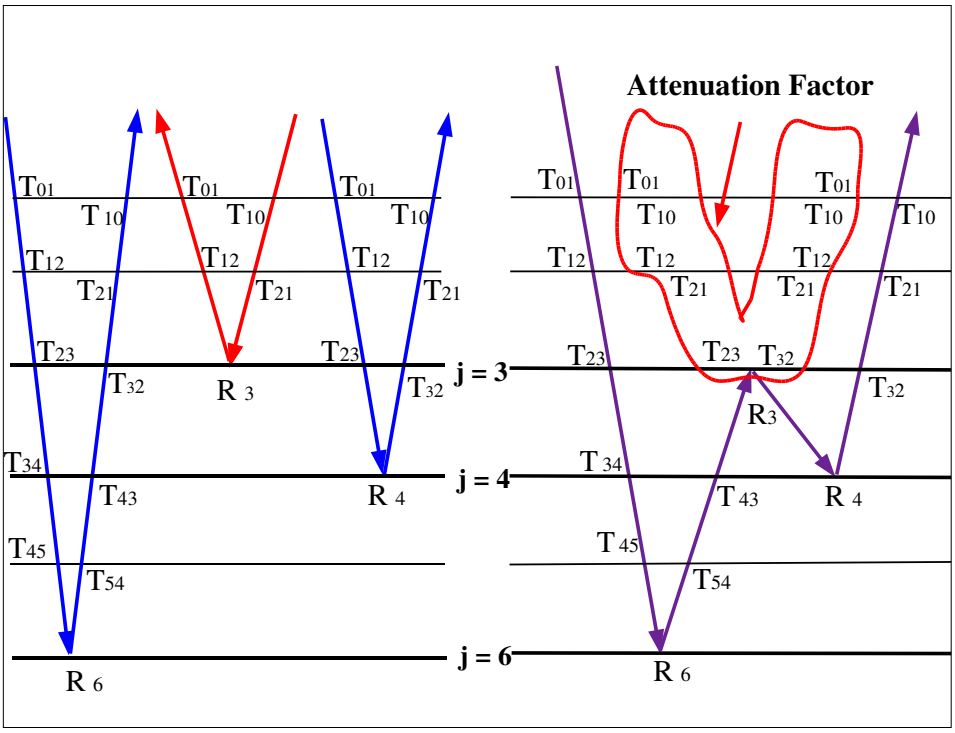

Figure 8: *The leftmost figure represents the amplitudes of the three primaries combined to predict the internal multiple showed on the right.*

series. The measure of effectiveness we adopt is how well the attenuator removes actual internal multiples, a measure that keeps us close to the field data problem (9). That paper, refers to the Weglein *et al* (1997)(14) internal multiple algorithm as predicting time but not the amplitude of internal multiples. Although in some pristine sense a true statement, it is hardly relevant since the algorithm is understood to be an attenuator, not an eliminator (14). More seriously, it does not convey the actual useful amplitude information predicted by the algorithm, as a very effective attenuator, and could lead to the erroneous conclusion that only time is predicted, and, subsequently, a significant discounting of the method's well understood intrinsic conceptual and practical value. In fact, as we have further demonstrated in this paper, the attenuator predicts the perfect time and an amplitude which is always a useful approximation to the actual.

As was mentioned earlier, there are several distinct conceptual steps taken in the development of the inverse scattering internal multiple attenuation algorithm, reviewed in Weglein *et al* (2003)(17) that are worth mentioning here for completeness and clarity.

First, there was a recognition that the inverse scattering series allows the inversion for V, directly from G_0, and recorded data, without updating the background or assuming the background is close to the actual. Second, there is a concept that inversion can be considered as a set of tasks, and that isolated tasks could be located and extracted to operate as task specific subseries. Third, if one of your tasks is the removal of internal multiples, the first step is to define the meaning of an internal multiple. Fourth, with a definition of what an internal multiple means, you seek to determine how and where those events appear in the forward scattering series, and then seek, by analog, where the

removal process might reside in the inverse series. Each of these steps is distinct and has different issues and assumptions, and will benefit from expanded concepts as well as the class and type of events you are able to accommodate in your classification. The conclusions of this paper are valid within the framework provided in (17) and seismic events accommodated therein, when applied to a 1D layered medium and a normal incident plane wave. Nita *et al* (2005) (11) have generalized the two reflector case of the attenuation compared to elimination issue for a 1D medium and prestack data and the corresponding prestack internal multiple attenuation algorithm. The conclusion is that each p component of the shot record data satisfies the $T_{01}(p)T_{10}(p)$ multiplicative difference between attenuation and elimination, the generalization of the $p = 0$ normal incidence case.

Issues around the definitions, and extensions of definitions, for multiples and primaries, and generalizations to what are now suggested as composite and prime events, are introduced and discussed in Weglein and Dragoset (2005)(18).

Discussion

There has been a rejuvenated interest in removing multiples, and internal multiples in particular, due to the industry trend to deep water and exploration beneath complex and ill-defined geologic overburdens, such as salt, basalt and karsted sediments. The inability to adequately determine material properties, and boundaries under these circumstances, is considered among the biggest impediments to current exploration seismology. The inverse scattering series has the potential of accomplishing all tasks associated with inversion, including the removal of internal multiples, with absolutely no knowledge or determination of the wave propagation properties in the earth. Hence, it is a direct response to the current significant challenge of producing effective methods for attenuating internal multiples under circumstances where the ability to determine the velocity is far from adequate. The order of an internal multiple is defined as the number of downward reflections it has experienced, independent of the location of the reflectors. All of the internal multiples of a given order are removed by a task specific subseries of the inverse scattering series.

The first term of that removal subseries is an attenuator; and, hence, as expected reduces the amplitude of all internal multiples of that order, by precisely predicting the time and approximately predicting the amplitude. The inverse scattering internal multiple attenuation algorithm, for a given order of multiples, is that first term in the removal series. The predicted amplitude differs from the actual in a precise and well understood manner, and the residual multiple after attenuation is always with the same sign as the original. Hence, the inverse scattering internal multiple algorithm predicts both the time and amplitude of internal multiples. The time is exact and the amplitude is approximate, which is faithful to its promise to be an attenuator. If you require more effectiveness in an attenuator, to *e.g.* move the algorithm closer to an eliminator, two paths suggest themselves:

1. provide a background medium closer to the actual, and once again choose the first term in the removal series, or
2. include higher terms in the removal series that operate without requiring any velocity information as input.

Examples of techniques that are in the former category are Berkhout *et al* (2000) (3) and Malcolm and De Hoop (2005) (8). In the former Berkhout and Verschuur feedback method a free surface and

interface model is used to successively remove free surface and then internal multiples having their shallowest downward reflection at a given reflector. That method requires precise information down to and including a given reflector to eliminate all the internal multiples having a shallowest reflector at that interface. The Malcolm and Dehoop method based on the Bremmer series assumes an accurate propagation velocity model everywhere and essentially models and subtracts the internal multiple. Each approach could provide value under different circumstances, and belongs in a tool box of techniques. However, the prime practical motivators of the rejuvenated interest in multiple removal, beginning about ten-fifteen years ago, (and the prime driver behind our efforts), was due to two factors: E&P moving to deep water and exploring beneath ever more complex and difficult to define overburdens. The inability to adequately model propagation in complex media is a very serious challenge for imaging and inverting primaries today, where both the wave or ray paths and reflections are fewer than the more complicated and elusive corresponding multiples. Hence, the second approach, pursuing the higher terms in the removal series, which do not require knowing or determining background velocity information, is the path we lean towards and generally advocate for achieving greater efficacy in addressing the current major prioritized real world challenges and concerns. That research program will be the subject of a future communication. When you are in a subsalt play and the primaries and multiples are all small and potentially interfering, a residual small multiple can be a serious problem.

Conclusions

In an earlier work, Weglein *et al* (2003)(17) examined a simple two reflector 1D model to determine the precise nature of the amplitude and phase prediction effectiveness of the internal multiple attenuation algorithm. This paper progresses that analysis and understanding by extending the evaluation to first three and then an arbitrary number of reflectors. The central conclusion of the current analysis is that the difference between removal and attenuation properties resides solely in too many factors of transmission coefficients down to and including the depth of the shallowest downward reflector. All of the differences between propagation in actual and propagation in reference below the shallowest downward reflection, play absolutely no role whatsoever in determining the amplitude efficacy of the inverse scattering attenuator. This positive and encouraging result helps explain the impact it has had with field data application, especially when applied in very complex geologic circumstances.

There are practical prerequisites for free and internal demultiple algorithms, including deghosting and wavelet estimation. The degree of effectiveness of the demultiple procedure can often depend upon the degree of satisfaction of its prerequisites. The energy minimizing adaptive subtraction method (*e.g.*, Verschuur (1991) (13), Carvalho and Weglein (1994) (4), Matson (2000) (10)) has demonstrated a reasonable record of positive impact but can tend to fail exactly when the underlying physics of the demultiple shines. The methods for satisfying and providing the prerequisites that serve the underlying demultiple deserve to be as strong and complete as the methods they are meant to serve. Efforts in that direction are exemplified by Weglein *et al*(2002) (16) and Guo (2005) (6). The overriding prerequisite is that data has been adequately collected and/or reconstructed consistent with the dimension of geological variation in the subsurface.

There are two ingredients in predicting a seismic event: the time and the amplitude. The former is critical since a correct amplitude at an incorrect time provides no value. Hence, the fact that the

very first term in an infinite series for removing all internal multiples of a given order predicts the correct time is fortuitous. The further understanding presented in this paper, that the first term in addition provides an amplitude approximation, whose error is independent of all properties below the shallowest reflector, only adds to its useful qualities. Finally, we remind ourselves that all of this benefit is provided with absolutely no subsurface information, whatsoever.

Acknowledgments

We acknowledge and thank the sponsors and members of M-OSRP and The NSF-CMG award number DMS-0327778 for the support of this research. Simon Shaw is thanked for useful comments and suggestions.

References

[1] Araújo, F. V., 1994, *Linear and nonlinear methods derived from scattering theory: Backscattered tomography and internal multiple attenuation*: Ph.D. thesis, Universidad Federal da Bahia, Brazil, (in Portuguese).

[2] Berkhout, A. J. and Verschuur, D. J., 1997, *Estimation of multiple scattering by iterative inversion, Part I: Theoretical considerations*: Geophysics, **62**, 1586-1595.

[3] Berkhout, A.J., Weglein, A.B. and Verschuur, E. (2000), *Wave theoretic multiple attenuation Part I* Invited paper to Offshore Technology Conference, Houston, Texas.

[4] Carvalho, P. M., and Weglein, A. B. (1994) *Wavelet estimation for surface multiple attenuation using a simulated annealing algorithm*, SEG Expanded Abstracts, Los Angeles, CA.

[5] Coates, R. T., and Weglein, A. B., 1996, *Internal multiple attenuation using inverse scattering: Results from prestack 1 and 2D acoustic and elastic synthetics*, 66th Ann. Internat. Mtg., Soc. Expl. Geophys., Expanded abstracts, 1522-1525.

[6] Guo, Z., (2005), *Wavelet estimation from only pressure data on the cable*: Ph.D. thesis, University of Houston, Texas.

[7] ten Kroode, F., 2002, *Prediction of internal multiples*, Wave Motion, **35**, p.315-338.

[8] Malcolm, A. E. and de Hoop, M. V. (2005). *A method for inverse scattering based on the generalized Bremmer coupling series*, Inverse Problems, (*sent for publication*).

[9] Matson, K., Carvalho, P., Corrigan, D., Weglein, A. and Young, C.Y., 1999. *Inverse scattering internal multiple attenuation: Results from complex synthetic and field data examples.* 69th Ann. Internat. Mtg: Soc. of Expl. Geophys., 1060-1063.

[10] Matson, K., 2000, *An overview of wavelet estimation using free-surface multiple removal*, The Leading Edge, **19**, no. 01, 50-55.

[11] Nita, B. G. and Weglein, A. B., 2005.*Inverse scattering internal multiple attenuation algorithm in complex multi-D media* Mission-Oriented Seismic Research Program (M-OSRP) Annual Report 2004-2005.

[12] Otnes, E., Hokstad, K. and Sollie, R., 2004. *Attenuation of internal multiples for multicomponent and towed streamer data* 74th Ann. Internat. Mtg., Soc. Expl. Geohys., Expanded Abstracts.

[13] Verschuur, D.J., 1991, *Surface-related multiple elimination, an inversion approach: Ph.D. thesis*, Delft Univ. of Techn.

[14] Weglein, A.B., Gasparotto, F. A., Carvalho, P. M., and Stolt, R. H., 1997, *An inverse scattering series method for attenuating multiples in seismic data*: Geophysics, **62**, 1975-1989.

[15] Weglein, A. B., 1999, *Multiple attenuation: An overview of recent advances and the road ahead (1999)*, The Leading Edge, p.40-44.

[16] Weglein, A.B., S.A. Shaw, K.H. Matson, J.L. Sheiman, R.H. Stolt, A. Osen, G.P. Correa, K.A. Innanen, Z. Guo, and J. Zhang (2002), *New approaches to deghosting towed-streamer and ocean-bottom pressure measurements*, 72nd International Meeting of the Society of Exploration Geophysicists, Salt Lake City, Utah.

[17] Weglein, A.B., Araújo, F. V., Carvalho, P. M., Stolt, R. H., Matson, K. H., Coates, R. T., Corrigan, D., Foster, D. J., Shaw, S. A. and Zhang, H., 2003. *Topical Review: Inverse scattering series and seismic exploration.* Inverse Problems, **19**: R27-R83.

[18] Weglein, A.B. and Dragoset, W.H., *Multiple Attenuation.* Daniel Ebrom, Editor, Geophysics reprint series, Soc. Expl. Geophys. (in print, 2005)

An inverse scattering internal multiple elimination method: Beyond attenuation, a new algorithm and initial tests

Adriana Citlali Ramírez and Arthur B. Weglein

Abstract

This paper presents our initial research efforts to address the complete removal of internal multiples from marine seismic data, without destroying primary reflections and with absolutely no knowledge of the subsurface. To address the problem of moving towards elimination we can either: introduce a variable background, or study higher order terms in the inverse scattering series with a constant background and find the subseries that is going to remove internal multiples. Although we encourage that both of these approaches be pursued, the concepts and methods of this paper belong to the second category. Avoiding the need for a velocity model has a practical impact especially in the cases when the adequate velocity is unobtainable. The inverse series can predict and remove internal multiples in terms of the collected data and a constant velocity model (usually waterspeed). This research aims to progress understanding the phase and amplitude properties of the inverse scattering internal multiple attenuator (F. Araújo, 1994 and Weglein *et al.*, 1997 and 2003) seeking to provide an improved amplitude prediction by studying higher order terms in the internal multiple elimination series. Analytical and numerical examples will be used to exemplify the concept of elimination of internal multiples based on inverse scattering series and to define the current state of understanding of this approach.

Introduction

A fundamental step in seismic processing is to seek to remove all multiples and to then use primaries to determine the depth location of reflectors and to identify where medium properties change in the subsurface. There are many methods, with different approaches and degrees of effectiveness, developed and implemented to deal with internal multiples (an overview can be found in Weglein, 1999, and in the introduction and chapter one of the reprint series by Weglein and Dragoset, 2005). These methods are defined as attenuators or eliminators, so it is convenient to distinguish between these two terms: attenuation refers to the amplitude reduction of an event in the seismic data and elimination refers to a complete subtraction of the amplitude of a specific event or set of events in the data.

There is a significant challenge of producing effective methods for dealing with internal multiples under circumstances where the ability to determine the velocity is far from adequate. In most circumstances the inverse scattering internal multiple attenuator offers a high degree of effectiveness (see *e.g.* Weglein *et al.*, 2003 and Nita and Weglein, 2005), nevertheless, the industry trend towards deep and ultra deep water, and exploration beneath complex and ill-defined geologic overburdens (*i.e.* salt, basalt and karsted sediments) represent circumstances when it is necessary and useful to go beyond reducing internal multiples. Furthermore, imaging techniques assume the data only contain primaries (the need for improved imaging-inversion is also driven by the overall industry

trend towards exploration and production in increasingly complex environments, Shaw and Weglein, 2004) and would definitely benefit from complete removal of internal multiples.

If multiples are not eliminated, they can be misinterpreted as primary reflections, or overlap with primaries. The internal multiple elimination series, presented in this work, can deal with internal multiple's energy masquerading a small primary, by giving the precise arrival time of the internal multiple and dealing with its amplitude without ever touching or affecting the primary; all that is required is the reference medium and recorded data.

In this report, we present an inverse scattering based algorithm that goes further in the removal of 1^{st} order internal multiples (the order of an internal multiple is defined by the number of downward reflections from subsurface reflector at any depth). First, we are going to give a brief summary of the phase and amplitude prediction properties of the inverse scattering internal multiple attenuator, $b_3^{IM_1}$. With this information, we are going to show how the attenuation factor of the amplitude predicted by $b_3^{IM_1}$ suggests where to look in the inverse series for higher order terms that are going to take the attenuator to an eliminator of 1^{st} order internal multiples in terms of a subseries that only requires the measured data and waterspeed. We then identify these terms and introduce their theory and diagrams. Finally, we present numerical examples where we aim at a small residual internal multiple after attenuation interfering with or masquerading a small target primary. Description of specific features in the movement from attenuation towards elimination will be presented in Appendix A. Open issues and future plans will be discussed.

Internal Multiple Attenuation

The material presented in this section is well known, but it is included for completeness; it follows the definitions and concepts introduced by Weglein *et al.* (1981) and F. Araújo (1994), and further developed in Weglein *et al.* (1997) and (2003).

The inverse scattering series is a multidimensional inversion method that determines subsurface physical properties using reflection measured data, D, and a reference medium Green's function, G_0. The wave propagation is characterized by differential wave operators, L and L_0, and its corresponding Green's functions, G and G_0, for actual and reference medium, respectively. For our purposes, we choose the reference medium to have homogeneous properties, *i.e.* constant velocity, and we define V, the perturbation operator, as the difference between the differential wave operators: $V = L_0 - L$. We also define the scattered field, Ψ_s, as: $\Psi_s = G - G_o$.

The forward scattering series constructs the seismic field, Ψ_s, in terms of reference medium propagation, and it is given by:

$$\Psi_s = G_0VG_0 + G_0VG_0VG_0 + G_0VG_0VG_0VG_0 + \cdots \tag{1}$$

The goal of inversion is to solve for V, which is done by writing V in orders of the measured data, $(\Psi_s)_m = G - G_0$ (the subscript m indicates measured values):

$$V = \sum_{i=1}^{\infty} V_i = V_1 + V_2 + V_3 + \cdots , \tag{2}$$

where V_1 is the first order approximation to V and is linear to the measured data, $D = (\Psi_s)_m$, the second term is quadratic, the third term is cubic and V_i is i^{th} order in the data. The expansion of V in terms of the measured data leads to the inverse scattering series:

$$\begin{aligned} D = & \; G_0 \left(\sum_{i=1}^{\infty} V_i \right) G_0 + G_0 \left(\sum_{i=1}^{\infty} V_i \right) G_0 \left(\sum_{i=1}^{\infty} V_i \right) G_0 + \cdots , \\ = & \; G_0 V_1 G_0 + G_0 V_2 G_0 + G_0 V_1 G_0 V_1 G_0 + G_0 V_3 G_0 + G_0 V_1 G_0 V_2 G_0 + \cdots \end{aligned} \tag{3}$$

The terms that are equal order in the data are equated to obtain:

$$G_0 V_1 G_0 = D \tag{4}$$
$$G_0 V_2 G_0 = -G_0 V_1 G_0 V_1 G_0 \tag{5}$$
$$G_0 V_3 G_0 = -G_0 V_1 G_0 V_1 G_0 V_1 G_0 - G_0 V_1 G_0 V_2 - G_0 V_2 G_0 V_1 \tag{6}$$
$$\vdots$$

These equations allow us to solve for V_1, V_2, V_3, etc. as a means to construct V from G_0 and measured data.

A part of the third term in the inverse scattering series: $(G_0 V_1 G_0 V_1 G_0 V_1 G_0)$ was identified to contain the leading order contribution for the removal series of 1^{st} order internal multiples, as described in Araújo (1994). The leading order term, known as the internal multiple attenuator, is an algorithm that attenuates internal multiples, operating without any knowledge or determination of the medium's velocity model.

To simplify the current analysis, we assume that the actual medium varies only in depth. The 2-D generalization of the $1st$ order internal multiple attenuator, $b_3^{IM_1}$, can be seen in *i.e.* Weglein *et al.* (2003). The 1D earth and normal incidence wave version is (Weglein *et al.*, 2003):

$$b_1(k) = D(\omega), \tag{7}$$
$$b_3^{IM_1}(k) = \int_{-\infty}^{\infty} dz_1 e^{ikz_1} b_1(z_1) \int_{-\infty}^{z_1-\epsilon_2} dz_2 e^{-ikz_2} b_1(z_2) \int_{z_2+\epsilon_1}^{\infty} dz_3 e^{ikz_3} b_1(z_3), \tag{8}$$

where $k = 2\frac{\omega}{c_0}$ is the vertical wavenumber and the superscript IM_1 refers to the $1st$ order internal multiple elimination series.

Let's follow a simple procedure to examine the inner workings of the attenuation algorithm:

1. Start with a 1D layered medium, a normal incident spike wave and its recorded data, D.
2. Take the 1D data, in time, and perform a temporal Fourier transform to take the data to ω space:
$$D(t) \longrightarrow D(\omega).$$
3. We now define the vertical wave number as $k_z = k = \frac{2\omega}{c_o}$, where c_o is the constant reference velocity, and introduce this definition into $D(\omega)$;
$$D(\omega) \longrightarrow D(k\frac{c_0}{2}).$$

4. Now, we can write the data in terms of k, which defines $b_1(k)$:

$$D(k) \longrightarrow b_1(k).$$

5. Then, we perform another Fourier transform that brings $b_1(k)$ to pseudodepth z (the pseudodepth is defined in the reference medium as $z = \frac{c_0 t}{2}$):

$$b_1(k) \longrightarrow b_1(z).$$

6. This is the effective data that is going to be taken through the ${b_3}^{IM_1}$ algorithm, Eq.(8), to obtain a first order internal multiple prediction.

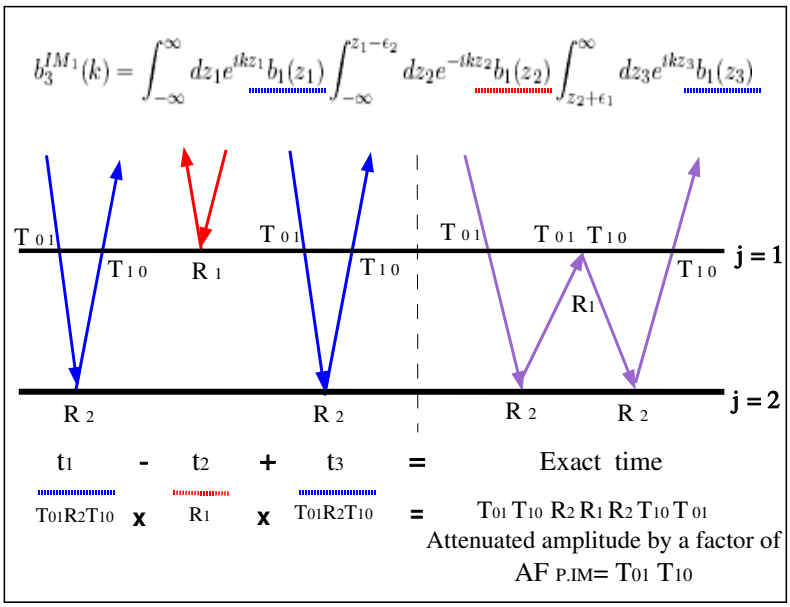

Figure 1: *Time and amplitude prediction of a 1^{st} order internal multiple.*

The attenuation algorithm constructs its prediction using three sets of data, refer to Fig.(1). For time prediction it takes the time of the first event, plus the time of a second event minus the time of a third event with a smaller pseudodepth. This subtraction can be seen in the negative phase of the second depth integral in Eq.(8); the process gives us the correct arrival time. In the case of the amplitude prediction the algorithm multiplies the amplitudes of the three events. The result is an estimate of the amplitude of the true internal multiple. This predicted amplitude is always less than the true amplitude and the error is a factor known as the attenuation factor of the predicted internal multiple, $AF_{P.IM}$,

$$(AF_{P.IM})_j = \begin{cases} T_{01}T_{10} & \text{for } j = 1 \\ \Pi_{i=1}^{j-1} \left(T^2_{i\ i-1} T^2_{i-1\ i}\right) T_{j\ j-1} T_{j-1\ j} & \text{for } 1 < j < J \end{cases} \tag{9}$$

where j represents the interface where the downward reflection took place, J is the total number of interfaces in the model and $T_{j-1\ j}$ and $T_{j\ j-1}$ are the transmission coefficients going down and

up through the interface j, respectively. The interfaces are numbered with integers, starting with the shallowest location. For the simplest first order internal multiple shown in Fig.(2), the true amplitude is $-T_{01}R_2R_1R_2T_{10}$ and the one predicted by $b_3^{IM_1}$ is $T_{01}T_{10}R_2R_1R_2T_{10}T_{01}$, therefore, the attenuation factor is $T_{01}T_{10}$, according to Eq.(9).

In a previous work, Ramírez and Weglein (2005) showed and concluded that the difference between complete elimination and the attenuation provided by $b_3^{IM_1}$, resides in the attenuator having extra powers of transmission coefficients down to and including only the depth of the downward reflection, completely independent of the rest of the path that the internal multiple has travelled.

Internal Multiple Elimination

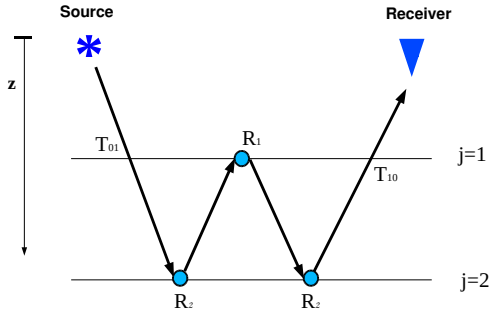

Figure 2: *First order internal multiple with downward reflection at* $j = 1$.

To build a first order internal multiple elimination series that starts with $b_3^{IM_1}$ we need to identify higher order terms which correct the 1^{st} order prediction towards the true amplitude while not affecting the primaries. The objective is to completely subtract the amplitude of multiples within the data, therefore, the inverse scattering subseries for internal multiples elimination should be able to predict the true amplitude for these events by correcting the attenuation factor –Eq.(9). The $AF_{P.IM}$ is always less than one, so after adding the next terms in the elimination series, the attenuation factor for the total series should be equal to one, thus, the internal multiple elimination series will completely remove the amplitude of the 1^{st} order internal multiples.

Using the two reflectors example shown in Fig.(2), we are going to seek how and where in the inverse series the removal process resides. The justification for using this simple analytic example to find and construct the elimination series, comes from the fact that the attenuation factor of the predicted internal multiple, Eq.(9), is affected by the history of the event down to and including only the depth of the shallowest reflection, independent of the place where the two upward reflections occurred. With one single example we are introducing the theory of the series for elimination of all $1st$ order internal multiples with downward reflection at the first interface.

For the multiple in Fig.(2), the predicted amplitude is attenuated by a factor of $(AF_{P.IM})_{j=1} = T_{01}T_{10}$. Since $b_3^{IM_1}$ has estimated the internal multiple amplitude, the purpose of the higher order

terms in the elimination series is to remove the effect of the attenuation factor. Hence those higher order terms need to build a series that sums up to $\frac{1}{T_{01}T_{10}}$. The quantity $\frac{1}{T_{01}T_{10}}$ can be described as an infinite geometric series:

$$\frac{1}{T_{01}T_{10}} = \frac{1}{(1-R_1^2)} = 1 + R_1^2 + R_1^4 + R_1^6 + \cdots \tag{10}$$

The right hand side is a Taylor expansion in terms of R_1 (the reflection coefficient for the shallowest interface). If we multiply Eq.(10) by the attenuation factor we find

$$T_{01}T_{10} * \left(\frac{1}{T_{01}T_{10}}\right) = T_{01}T_{10} * \left(1 + R_1^2 + R_1^4 + R_1^6 + \cdots\right). \tag{11}$$

This Taylor series is our initial key to searching for, and studying, the location of the first term beyond attenuation. On the left hand side of Eq.(11), the first term corresponds to the $(AF_{P.IM})_{j=1}$ given by ${b_3}^{IM_1}$ and our conjecture is that the second term should reside within higher order terms in the inverse series. On the right hand side of the equation, all higher order terms exhibit even powers of the reflection coefficient, R_1. This allows us to think that the second term in the removal series should be found within the fifth term in the inverse series:

$$\begin{aligned} V_5 = -(&V_1G_0V_1G_0V_1G_0V_1G_0V_1 + V_2G_0V_1G_0V_1G_0V_1 + V_1G_0V_2G_0V_1G_0V_1 \\ &+ V_1G_0V_1G_0V_2G_0V_1 + V_1G_0V_1G_0V_1G_0V_2 + V_3G_0V_1G_0V_1 \\ &+ V_1G_0V_3G_0V_1 + V_1G_0V_1G_0V_3 + V_4G_0V_1 + V_1G_0V_4). \end{aligned} \tag{12}$$

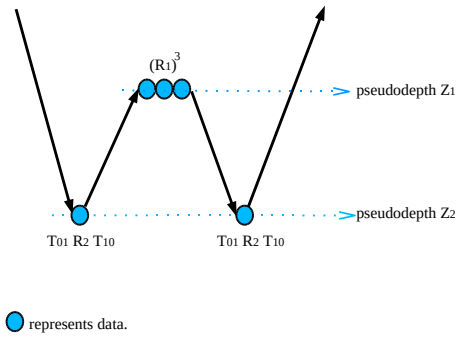

Figure 3: *Higher order diagram.*

The selected term should have the exact time of the true internal multiple, and three scattering interactions at the first interface to obtain the two extra reflection coefficients for the amplitude correction. A first diagram looks like the one in Fig.(3), and the algorithm is going to behave in the following way:

1. Start with a 1D medium, two reflectors and a normal incident spike wave. The data contain two primaries, one 1^{st} order internal multiple and higher order terms

$$D(t) = R_1\delta(t-t_1) + T_{01}R_2T_{10}\delta(t-t_2) - T_{01}R_2R_1R_2T_{10}\delta(t-(2t_2-t_1))\cdots$$

2. $b_1(k)$ is the effective data and it has the true amplitude for primaries and internal multiples within the data,

$$b_1(k) = D(\omega).$$

3. $b_3^{IM_1}$, the attenuator, is the leading order term in the elimination series. Its amplitude prediction for the internal multiple shown in Fig.(2) is

$$|b_3^{IM_1}| = T_{01}T_{10} * (T_{01}R_2R_1R_2T_{10}),$$

where the true internal multiple amplitude has been factored out.

4. $b_5^{IM_1}$ gives the next term in the elimination series,

$$|b_5^{IM_1}| = T_{01}T_{10} * R_1^2 * (T_{01}R_2R_1R_2T_{10}).$$

5. Adding the three terms, we obtain the second order estimate for the 1^{st} order internal multiple,

$$|b_1 + b_3^{IM_1} + b_5^{IM_1}| = primaries + \left[-1 + T_{01}T_{10} * (1 + R_1^2)\right] * (T_{01}R_2R_1R_2T_{10}).$$

In the factor $\left[-1 + T_{01}T_{10} * (1 + R_1^2)\right]$, the first term (-1) comes from the internal multiple term in the data. The second term, $T_{01}T_{10} * (1 + R_1^2)$, contains the first two terms in the geometric series in Eq.(10). Hence, $b_3^{IM_1} + b_5^{IM_1}$ gives us a better estimate of the internal multiple amplitude,

$$T_{01}T_{10} * (1 + R_1^2) \longrightarrow 1$$

and

$$\left[-1 + T_{01}T_{10} * (1 + R_1^2)\right] \longrightarrow 0.$$

This result shows the first attempt to move the attenuator closer to an eliminator; the amplitudes of primary reflections are preserved, and no knowledge of the subsurface is required. By induction, we can expect the internal multiple elimination series to reside only in odd terms of the inverse scattering series $(b_3^{IM_1} + b_5^{IM_1} + b_7^{IM_1} + \cdots)$.

The second term in the elimination series, ${b_5}^{IM_1}$, is the first step to move the algorithm towards an elimination of 1^{st} order internal multiples (a complete derivation of this term is given in appendix A); it comes from $V_1G_0V_3G_0V_1$, a part of the fifth term in the inverse scattering series –Eq.(12)- and it is given by

$$b_5^{IM_1}(k) = \int_{-\infty}^{\infty} dz e^{ikz} b_1(z) \times \int_{-\infty}^{z-\epsilon} dz' e^{-ikz'} \left[b_1(z')^3 + 2\, b_1(z') \int_{-\infty}^{z'-\epsilon} dz'''\, b_1(z''')^2 \right] \int_{z'+\epsilon}^{\infty} dz'' e^{ikz''} b_1(z''). \quad (13)$$

To provide a better understanding of the performance of $b_5^{IM_1}$ in the subtraction of multiples within the data, we are going to follow a simple example. The model is shown in Fig.(4).

The data contains:

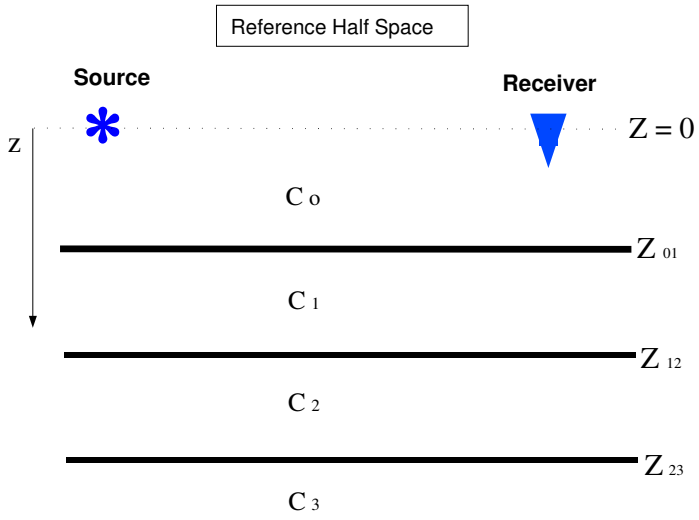

Figure 4: *1D layered medium.*

- Three primaries:

$$R_1\delta(t-t_1)+R_2'\delta(t-t_2)+R_3'\delta(t-t_3),$$

where $R_2'=T_{01}R_2T_{10}$ and $R_3'=T_{01}T_{12}R_3T_{21}T_{10}$.

- Four 1^{st} order internal multiples with downward reflection at the first interface:

$$\begin{aligned}(IM)_{j=1} =& -T_{01}R_2R_1R_2T_{10}\delta(t-(2t_2-t_1))-2T_{01}R_2R_1T_{21}R_3T_{12}T_{10}\delta(t-(t_2+t_3-t_1))\\ &-T_{01}T_{12}^2R_3R_1R_3T_{21}^2T_{10}\delta(t-(2t_3-t_1)).\end{aligned}$$

- One 1^{st} order internal multiple, generated at the second reflector:

$$(IM)_{j=2}=-T_{01}T_{12}R_3R_2R_3T_{10}T_{21}\delta(t-(2t_3-t_2)).$$

- Higher order internal multiples.

The effective data is:

$$\begin{aligned}b_1(z) &= \int_{-\infty}^{\infty} e^{-ikz}b_1(k)\,dk\\ &= R_1\delta(z-z_1)+R_2'\delta(z-z_2)+R_3'\delta(z-z_3)+\text{higher order terms.}\end{aligned}$$

And the output of the attenuator for 1^{st} order internal multiples is:

$$\begin{aligned}b_3(t) &= R_1R_2^2T_{01}^2T_{10}^2\delta(t-(2t_2-t_1))+2R_1R_2R_3T_{01}^2T_{10}^2T_{12}T_{21}\delta(t-(t_2+t_3-t_1))\\ &+R_1R_3^2T_{01}^2T_{12}^2T_{21}^2T_{10}^2\delta(t-(2t_3-t_1))+R_2R_3^2T_{01}^3T_{10}^3T_{12}^2T_{21}^2\delta(t-(2t_3-t_2)),\\ &= T_{01}T_{10}*(IM)_{j=1}+(T_{01}T_{10})^2*T_{12}T_{21}*(IM)_{j=2}.\end{aligned}\tag{14}$$

The second term in the multiple elimination series has two parts:

$$\begin{aligned} b_5^{IM_1}(k) = & \int_{-\infty}^{\infty} dz e^{ikz} b_1(z) \int_{-\infty}^{z-\epsilon} dz' e^{-ikz'} b_1(z')^3 \int_{z'+\epsilon}^{\infty} dz'' e^{ikz''} b_1(z'') \\ & + \int_{-\infty}^{\infty} dz e^{ikz} b_1(z) \int_{-\infty}^{z-\epsilon} dz' e^{-ikz'} \left[2\, b_1(z') \int_{-\infty}^{z'-\epsilon} d\chi b_1(\chi)^2 \right] \int_{z'+\epsilon}^{\infty} dz'' e^{ikz''} b_1(z'') \\ b_5^{IM_1}(k) = & \, b_{51}^{IM_1}(k) + b_{52}^{IM_1}(k). \end{aligned} \tag{15}$$

We substitute the effective data into $b_5^{IM_1}(k)$, and evaluate the integrals analytically. Then we perform an inverse Fourier transform to take $b_5^{IM_1}(k)$ back to the time domain, which gives:

$$\begin{aligned} b_{51}^{IM_1}(t) &= T_{01}T_{10} * R_1^2 * (IM)_{j=1} + (T_{01}T_{10})^2 * T_{12}T_{21} * (R_2')^2 (IM)_{j=2}, \\ b_{52}^{IM_1}(t) &= (T_{01}T_{10})^2 * T_{12}T_{21} * 2R_1^2 * (IM)_{j=2}. \end{aligned} \tag{16}$$

Thus,

$$b_5^{IM_1} = T_{01}T_{10} * R_1^2 * (IM)_{j=1} + (T_{01}T_{10})^2 * T_{12}T_{21} * \left[2R_1^2 + (R_2')^2\right] * (IM)_{j=2}. \tag{17}$$

Adding the effective data with the first two terms in the 1^{st} order internal multiple elimination series,

$$\begin{aligned} b_1 + b_3^{IM_1} + b_5^{IM_1} = & R_1\delta(t-t_1) + R_2'\delta(t-t_2) + R_3'\delta(t-t_3) \\ & + \left[-1 + T_{01}T_{10}(1+R_1^2)\right] * (IM)_{j=1} \\ & + \left[-1 + (T_{01}T_{10})^2 * T_{12}T_{21} * (1 + 2R_1^2 + (R_2')^2)\right] * (IM)_{j=1}. \end{aligned} \tag{18}$$

The factor that multiplies the internal multiples generated at the first reflector, $(IM)_{j=1}$, is the same as the one we found in the example of Fig.(2), and it can be compared with the geometric series in Eq.(11). The factor that multiplies the multiples generated at the second reflector, $(IM)_{j=1}$, corresponds to the first terms in the more complicated geometric series for:

$$\frac{1}{(T_{01}T_{10})^2 T_{12}T_{21}} = \frac{1}{(1-R_1^2)^2(1-R_2^2)} = 1 + 2R_1^2 + R_2^2 + 3R_1^4 + 2R_2^2R_1^2 + R_2^4 + 3R_2^2R_1^4 \cdots \tag{19}$$

The terms on the right hand side of this Taylor series, corresponds to the factors that we found in $b_5^{IM_1}$. Hence, adding these extra terms in the elimination series is building a sum of amplitude corrections that is going to improve the subtraction of internal multiples in the data. The second term in the 1^{st} order internal multiple elimination series can be separated in two parts, as we saw in the previous example, represented by the diagrams in Fig.(5). Both diagrams affect all 1^{st} order internal multiples:

- The upper diagram corresponds to the first term in Eq.(15) and it starts a series that eliminates all 1^{st} order internal multiples that were downward reflected at the shallowest reflector. It has three hits at the shallowest reflector indicating triple self interaction, which means that

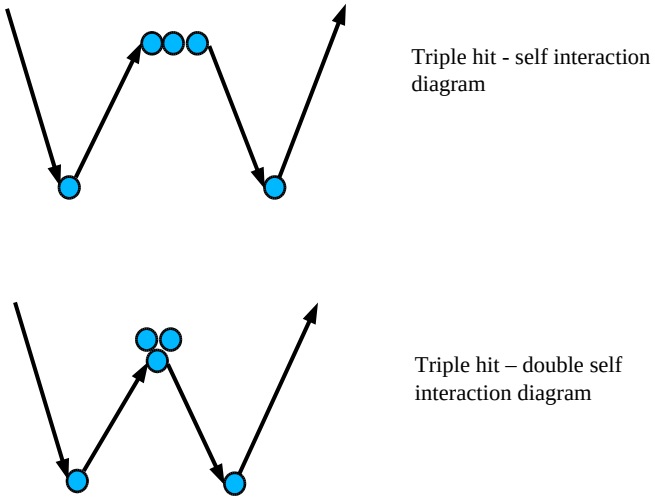

Figure 5: *Higher order diagrams for* $b_5^{IM_1}$.

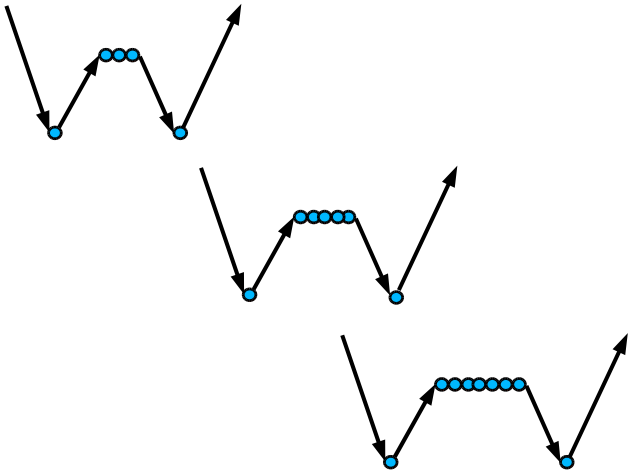

Figure 6: *Higher order diagrams.*

the data are combined with itself to give higher order amplitude information and the correct time. The self interacting data, contain amplitude information that corresponds to the reflection coefficient of the generating reflector (where the downward reflection took place). This diagram is the main contribution of $b_5^{IM_1}$ to the elimination of internal multiples. The subseries of the 1^{st} order internal multiple elimination series, that starts with this diagram, contains a contribution from each term in the elimination series, $b_3^{IM_1} + b_5^{IM_1} + b_7^{IM_1} + \cdots$. The first diagram for this subseries is the upper picture in Fig.(5) , which corresponds to $b_{51}^{IM_1}$, and the higher order terms are represented with the diagrams shown in Fig.(6). The

sum of these diagrams leads to the mathematical form:

$$\int_{-\infty}^{\infty} dz e^{ikz} b_1(z) \int_{-\infty}^{z-\epsilon} dz' e^{-ikz'} \left(|b_1(z')^2|/1 - |b_1(z')^2|\right) b_1(z') \int_{z'+\epsilon}^{\infty} dz'' e^{ikz''} b_1(z''). \quad (20)$$

- The diagram located at the bottom of Fig.(5) represents the second term in Eq.(15). Two self interacting data give second order corrections to the interfaces above the generating reflector, they give extra amplitude information of any interface above of the generating reflector. Since it corrects reflectors on the overburden of the generating reflector, it doesn't touch the 1^{st} order internal multiples that were downward reflected at the shallowest reflector, but it further attenuates all 1^{st} order internal multiples generated at deeper reflectors.

Although the multiple amplitude can be reduced substantially by the first term in the elimination series, $b_3^{IM_1}$, there is in some cases an observable residual that interferes with imaging, which can introduce interpretation uncertainties. The second term in the internal multiple elimination series, $b_5^{IM_1}$, always predicts the exact time of 1^{st} order internal multiples and improves their amplitude prediction by adding nonlinear contributions in terms of reflection coefficient's (corresponding to the reflectors at or above the generating reflector) to improve the prediction and help to move the attenuator closer to an eliminator of internal multiples, while leaving all primaries unaffected.

Numerical Example

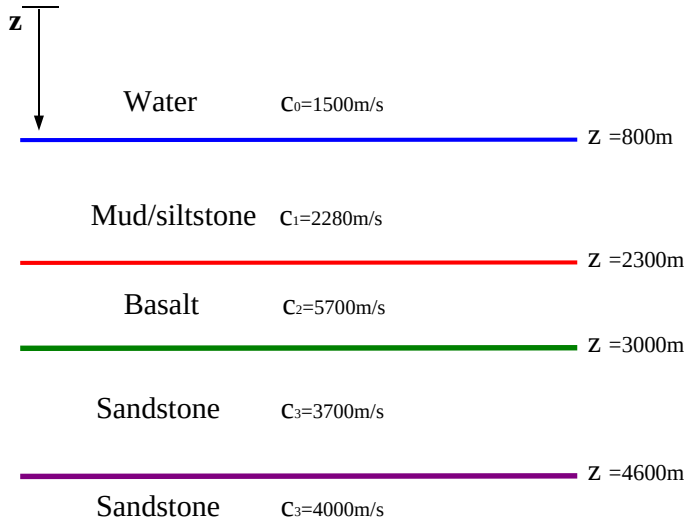

Figure 7: *1D model.*

An elimination series for internal multiples based on inverse scattering series has the potential and promise of attacking difficult multiples while preserving all primaries. The algorithm proposed here represents the second term, after the attenuator, that will help to move closer to a complete elimination of 1^{st} order internal multiples without the requirement of a velocity model or any

subsurface information. The objective of elimination using only recorded data and information about the reference medium is achievable through the inverse scattering subseries formalism, but it has some very important prerequisites: the source signature or wavelet should be deconvolved, source and receiver ghosts, and free surface multiples need to be eliminated from the measured data. If all the prerequisites are satisfied, the algorithms are able to predict and start the removal of 1^{st} order internal multiples within the data.

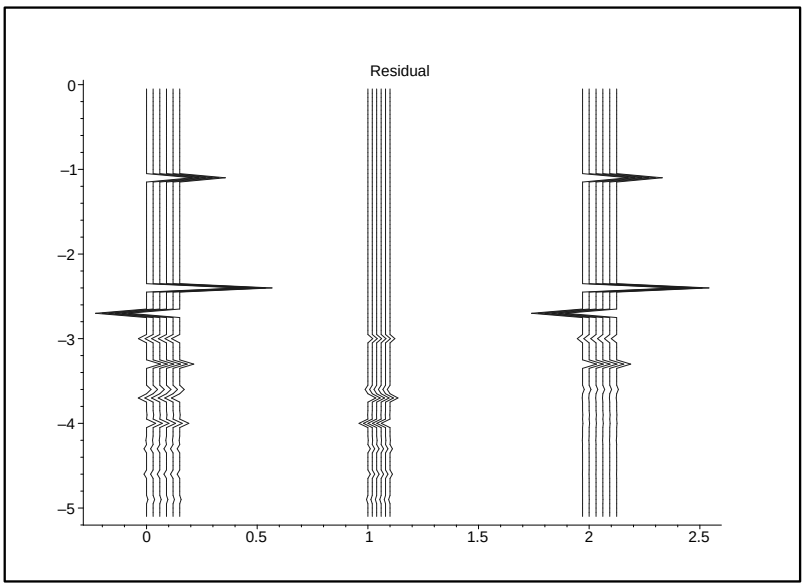

Figure 8: *The traces on the left are the data with primaries and 1^{st} order internal multiples. The traces in the middle are the prediction of $b_3^{IM_1}$. The traces on the right are the residual after adding $b_1 + b_3^{IM_1}$.*

To illustrate and test the performance of the demultiple algorithm given by $b_3^{IM_1} + b_5^{IM_1}$, we use a 1D model and a spike wave to generate synthetic data. The 1D layered medium is shown in Fig.(7). The algorithm for $b_5^{IM_1}$ is written in terms of b_1, the effective data, just as the attenuator. This gives a computational advantage, allowing to compute $b_3^{IM_1}$ together with $b_5^{IM_1}$. The interested reader can find details in the coding of the 1^{st} order internal multiple attenuator, $b_3^{IM_1}$ in Kaplan *et al.* (2005).

On the left side of Fig.(8) we observe the data with primaries and first order internal multiples. The inner traces are the output of the attenuator, $b_3^{IM_1}$, it leaves all primaries unaffected and gives the first estimate of the amplitude (with opposite sign) of 1^{st} order internal multiples with the correct time prediction. The traces on the right side of Fig.(8) are the primaries and the residual multiple after adding the data, $D = b_1$, to the attenuator, $b_3^{IM_1}$.

In Fig.(9) we observe the data (leftmost) with primaries and attenuated first order internal multiples $b_1 + b_3^{IM_1}$. The traces in the middle are the output of the second term in the elimination series, $b_5^{IM_1}$. The second term gives a second order approximation for the amplitude (with opposite sign) of 1^{st} order internal multiples and its time prediction is perfect. On the right side of Fig.(9), the traces are the primaries and a small residual multiple after adding the data, $D = b_1$, to the first two terms in the elimination series, $b_3^{IM_1} + b_5^{IM_1}$

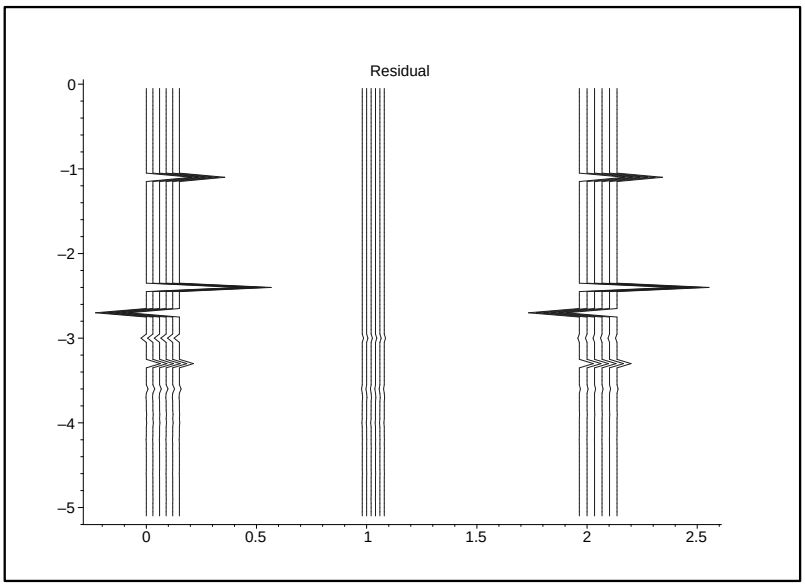

Figure 9: *The traces on the left are the residual after adding* $b_1 + b_3^{IM_1}$. *The traces in the middle are the prediction of* $b_5^{IM_1}$. *The traces on the right are the residual after adding* $b_1 + b_3^{IM_1} + b_5^{IM_1}$.

Conclusions

Many processing algorithms are based on the assumption that seismic data contain only primaries and the interpretation of seismic data is most straightforward when the multiples are completely removed from the traces. For this reason, effective demultiple techniques are required. We presented an algorithm and examples of a theory that doesn't assume any knowledge of the earth below the receivers and improves the attenuation of 1^{st} order internal multiples while leaving all primary reflections unaffected. The initial research reported here, showed that the prediction and removal of the true 1^{st} internal multiples amplitude can be achieved by the 1^{st} order internal multiple elimination series, based on inverse scattering, with a constant background or reference medium.

The first term in the elimination series is an attenuator, ${b_3}^{IM_1}$; it predicts the perfect time and always significantly reduces but doesn't eliminate the internal multiples from the data. To move beyond attenuation, we studied higher order terms in the inverse series and identified the elimination series for 1^{st} order internal multiples. Higher order terms towards elimination are determined by distinct non-linear mathematical expressions that only involve the measured data and the reference medium. The second term in the elimination series, ${b_5}^{IM_1}$, gives the precise arrival time of internal multiples, and it further attenuates the amplitude. The second term can be separated in two parts, the first one is the main contribution to improve the amplitude prediction and elimination of all 1^{st} order internal multiples and it begins an infinite subseries that further attenuates all multiples of this order and completely removes the ones generated at the first reflector. A closed form for this subseries has been identified, it shows a better estimate of the amplitudes and provides a significant improvement towards the elimination of 1^{st} order internal multiples.

In this theory, no assumptions about the earth below the receivers are made, this characteristic makes it ideal for addressing one of the current challenges in exploration seismology: removing multiples, locating and identifying targets in highly complex medium, when the velocity model is

unobtainable. The conclusions of this report are valid within the confines of the 1D layered earth wave analysis presented here and the framework provided in Weglein *et al.* (2003) and seismic events accommodated therein. The extension to a multidimensional earth as well as extensions of definitions of primaries and multiples are among our current research objectives.

The tests presented in this report, show value when going further in the inverse series for 1^{st} order internal multiple elimination with one term more than current attenuator.

Acknowledgments

Bogdan Nita (M-OSRP), Einar Otnes (STATOIL) and Mojdeh Niazmand (Univ. of Houston) are thanked for useful comments and suggestions. We acknowledge and thank the sponsors and members of M-OSRP and The NSF-CMG award number DMS-0327778 for the support of this research.

References

Araújo, F. V., 1994, "Linear and nonlinear methods derived from scattering theory: Backscattered tomography and internal multiple attenuation.": *Ph.D. thesis, Universidad Federal da Bahia, Brazil*, (1994): , (in Portuguese).

Kaplan, S.T., Innanen, K.A., Otnes, E. and Weglein, A.B., (2005) "Internal multiple attenuation code-development and implementation.":
M-OSRP annual meeting, (2004-2005)

Nita, B.G. and Weglein, A.B., (2005) "Inverse scattering internal multiple attenuation algorithm in complex multi-D media: the pseudo-depth/vertical-time monotonicity condition and higher dimension analytic analysis.":
M-OSRP annual meeting, (2004-2005)

Ramírez, A.C. and Weglein, A.B., (2005) "Progressing the analysis of the phase and amplitude prediction properties of the inverse scattering internal multiple attenuation algorithm.": *Journal of Seismic Exploration*, (*submittedd for publication*, April 2005).

Shaw, S.A., (2005) "Some remarks on the leading order imaging series algorithm for depth imaging when the velocity model is unknown.": *M-OSRP annual meeting*, (2004-2005).

Weglein, A.B., Gasparotto, F. A., Carvalho, P. M., and Stolt, R. H., 1997, "An inverse scattering series method for attenuating multiples in seismic data.": *Geophysics, 62*, (1997): , 1975-1989.

Weglein, A. B., 1999, "Multiple attenuation: An overview of recent advances and the road ahead (1999).": *The Leading Edge.*, (1999): , 40-44.

Weglein, A.B., Araújo, F. V., Carvalho, P. M., Stolt, R. H., Matson, K. H., Coates, R. T., Corrigan, D., Foster, D. J., Shaw, S. A. and Zhang, H., 2003. "Topical Review: Inverse scattering series and seismic exploration.": *Inverse Problems, 19*, (2003): , R27-R83.

Weglein, A.B. and Dragoset, W.H., "Multiple Attenuation.": *Daniel Ebrom, Editor, Geophysics reprint series, Soc. Expl. Geophys.*, (in print, 2005).

Appendix A

In this appendix we show the mathematical derivation that allows us to build a first order internal multiple elimination series that starts with $b_3^{IM_1}$. We examine higher order terms which contribute to the correction of the amplitude prediction of $b_3^{IM_1}$.

$b_3^{IM_1}$ predicts the precise arrival time and an attenuated amplitude using three primary events within the data. The attenuation factor of the predicted internal multiple –Eq.(9)- is associated with the trajectory of the event from b_1 computed with a negative sign in the phase at the second depth integral performed in $b_3^{IM_1}$ (the effective data, b_1, is the corresponding data representation of a model type independent V_1). This fact gives us an indication when moving the algorithm from attenuator towards an eliminator: the next term should not affect the outermost integrals but it should change the innermost one with a higher order term keeping the precise time prediction. Therefore, the first selection criteria is to look for higher order terms containing V_1 at the extremes.

Start with the fifth term in the inverse scattering series:

$$\begin{aligned} V_5 = -(&V_1G_0V_1G_0V_1G_0V_1G_0V_1 + V_2G_0V_1G_0V_1G_0V_1 + V_1G_0V_2G_0V_1G_0V_1 \\ &+ V_1G_0V_1G_0V_2G_0V_1 + V_1G_0V_1G_0V_1G_0V_2 + V_3G_0V_1G_0V_1 \\ &+ V_1G_0V_3G_0V_1 + V_1G_0V_1G_0V_3 + V_4G_0V_1 + V_1G_0V_4) \\ V_5 = &V_{51} + V_{52} + V_{53} + V_{54} + V_{55} + V_{56} + V_{57} + V_{58} + V_{59} + V_{5\ 10}. \end{aligned} \tag{21}$$

It contains four terms with V_1 at the extremes:

$$V_{51} = V_1G_0V_1G_0V_1G_0V_1G_0V_1 \tag{22}$$
$$V_{53} = V_1G_0V_2G_0V_1G_0V_1 \tag{23}$$
$$V_{54} = V_1G_0V_1G_0V_2G_0V_1 \tag{24}$$
$$V_{57} = V_1G_0V_3G_0V_1. \tag{25}$$

V_{51} can be separated in sixteen different terms but only one of them has the correct phase manipulation, corresponding to a similar behavior with the one that $b_3^{IM_1}$ shows at the outermost integrals; after manipulating the Green's functions, and converting $V_1 \longrightarrow b_1$:

$$\begin{aligned} B_{51}(k) = &\int_{-\infty}^{\infty} dz_1 e^{ikz_1} b_1(z_1) \int_{-\infty}^{\infty} dz_2 e^{-ikz_2} b_1(z_2) \int_{-\infty}^{\infty} dz_3 e^{ikz_3} b_1(z_3) \\ &\int_{-\infty}^{\infty} dz_4 e^{-ikz_4} b_1(z_4) \int_{-\infty}^{\infty} dz_5 e^{ikz_5} b_1(z_5). \end{aligned} \tag{26}$$

A part of this term has been studied by Araújo (1994), and identified as the leading order term of the second order internal multiple removal series. Some other parts of the term can predict

first order internal multiples nevertheless, they affect not only the amplitude but the time in the prediction.

We continue with V_{53}, where we can find eight terms; two of them may have value for our problem:

$$\int_{-\infty}^{\infty} dz_1 e^{ikz_1} b_1(z_1) \int_{-\infty}^{\infty} dz_2 e^{-ikz_2} b_2(z_2) \int_{-\infty}^{\infty} dz_3 b_1(z_3) \int_{-\infty}^{\infty} dz_4 e^{ikz_4} b_1(z_4), \tag{27}$$

and:

$$\int_{-\infty}^{\infty} dz_1 e^{ikz_1} b_1(z_1) \int_{-\infty}^{\infty} dz_2 b_2(z_2) \int_{-\infty}^{\infty} dz_3 e^{-ikz_3} b_1(z_3) \int_{-\infty}^{\infty} dz_4 e^{ikz_4} b_1(z_4). \tag{28}$$

Once more, the outermost integrals are the same as the ones found in $b_3^{IM_1}$. A part of these terms can be used to predict first order internal multiples, but due to the inner integrals, the time prediction is not correct. The same analysis holds for V_{54}.

It seems like the parts of V_{51}, V_{53} and V_{54} that can be related with 1^{st} order internal multiples are trying to invert these events, but not to remove them. Therefore we are not using any of these terms at this moment.

We are going to study $V_{57} = V_1 G_0 V_3 G_0 V_1$ in terms of data, b_1, and call the result: $B_{57}(k)$:

$$\begin{aligned} B_{57}(k) = & \int_{-\infty}^{\infty} dz b_1(z) \int_{-\infty}^{\infty} dz' b_3(z') \int_{-\infty}^{\infty} dz'' e^{ikz''} b_1(z'') \\ & + \int_{-\infty}^{\infty} dz b_1(z) \int_{-\infty}^{\infty} dz' e^{-ikz'} b_3(z') \int_{-\infty}^{\infty} dz'' b_1(z'') \\ & + \int_{-\infty}^{\infty} dz e^{ikz} b_1(z) \int_{-\infty}^{\infty} dz' e^{-ikz'} b_3(z') \int_{-\infty}^{\infty} dz'' e^{ikz''} b_1(z'') \\ & + \int_{-\infty}^{\infty} dz e^{ikz} b_1(z) \int_{-\infty}^{\infty} dz' b_3(z') \int_{-\infty}^{\infty} dz'' b_1(z'') \\ & + \Sigma residues \end{aligned} \tag{29}$$

$$B_{57}(k) = B_{571}(k) + B_{572}(k) + B_{573}(k) + B_{574}(k) + \Sigma residues \tag{30}$$

where the term b_3 will be understood as the data representation of a general model type independent $V_3 = -V_1 G_0 V_1 G_0 V_1 - V_1 G_0 V_2 - V_2 G_0 V_1$, just as b_1 is related with V_1; thus, the attenuator ${b_3}^{IM_1}$ is the part of b_3 that starts the elimination process of first order internal multiples.

$B_{573}(k)$ contains the correct $data-phase$ relation that is going to predict the true internal multiple's time. As an analogy to the term B_3 studied by Araújo, a part of $B_{573}(k)$ is associated with the removal series of first order internal multiples.

It can be separated in the following nine terms:

$$
\begin{aligned}
B_{573}(k) = & \int_{-\infty}^{\infty} dz e^{ikz} b_1(z) \int_{-\infty}^{z-\epsilon} dz' e^{-ikz'} b_3(z') \int_{z'+\epsilon}^{\infty} dz'' e^{ikz''} b_1(z'') \\
& + \int_{-\infty}^{\infty} dz e^{ikz} b_1(z) \int_{z+\epsilon}^{\infty} dz' e^{-ikz'} b_3(z') \int_{-\infty}^{z'-\epsilon} dz'' e^{ikz''} b_1(z'') \\
& + \int_{-\infty}^{\infty} dz e^{ikz} b_1(z) \int_{z+\epsilon}^{\infty} dz' e^{-ikz'} b_3(z') \int_{z'+\epsilon}^{\infty} dz'' e^{ikz''} b_1(z'') \\
& + \int_{-\infty}^{\infty} dz e^{ikz} b_1(z) \int_{-\infty}^{z-\epsilon} dz' e^{-ikz'} b_3(z') \int_{-\infty}^{z'-\epsilon} dz'' e^{ikz''} b_1(z'') \\
& + \int_{-\infty}^{\infty} dz e^{ikz} b_1(z) \int_{-\infty}^{\infty} dz' e^{-ikz'} b_3(z') \delta(z-z') \int_{-\infty}^{\infty} dz'' e^{ikz''} b_1(z'') \delta(z'-z'') \\
& + \int_{-\infty}^{\infty} dz e^{ikz} b_1(z) \int_{-\infty}^{\infty} dz' e^{-ikz'} b_3(z') \delta(z-z') \int_{z'+\epsilon}^{\infty} dz'' e^{ikz''} b_1(z'') \\
& + \int_{-\infty}^{\infty} dz e^{ikz} b_1(z) \int_{-\infty}^{\infty} dz' e^{-ikz'} b_3(z') \delta(z-z') \int_{-\infty}^{z'-\epsilon} dz'' e^{ikz''} b_1(z'') \\
& + \int_{-\infty}^{\infty} dz e^{ikz} b_1(z) \int_{z+\epsilon}^{\infty} dz' e^{-ikz'} b_3(z') \int_{-\infty}^{\infty} dz'' e^{ikz''} b_1(z'') \delta(z-z') \\
& + \int_{-\infty}^{\infty} dz e^{ikz} b_(z) \int_{-\infty}^{z-\epsilon} dz' e^{-ikz'} b_3(z') \int_{-\infty}^{\infty} dz'' e^{ikz''} b_1(z'') \delta(z-z'), \\
B_{573}(k) = & M_{51}(k) + M_{52}(k) + M_{53}(k) + M_{54}(k) + M_{55}(k) + M_{56}(k) \\
& + M_{57}(k) + M_{58}(k) + M_{59}(k). \qquad (31)
\end{aligned}
$$

$M_{51}(k)$ is the term satisfying the relations $z_1 > z_2$ and $z_3 > z_2$, which corresponds to the $lower - higher - lower$ representation of a first order internal multiple:

$$
M_{51}(k) = \int_{-\infty}^{\infty} dz e^{ikz} b_1(z) \int_{-\infty}^{z-\epsilon} dz' e^{-ikz'} b_3(z') \int_{z'+\epsilon}^{\infty} dz'' e^{ikz''} b_1(z''), \qquad (32)
$$

it contains the next term in the first order internal multiple elimination series: $b_5^{IM_1}$. To find an explicit form of $b_5^{IM_1}$, we need to select the part of b_3 that should be used in Eqn.(32) to predict 1^{st} order internal multiples with the precise arrival time and an amplitude similar to the prediction of the attenuator but with extra reflection coefficient factors. These extra reflection coefficients should correspond to the ones of the reflectors down to and including only the depth of the shallowest multiple reflection.

We now examine the term b_3 required in the second integral of M_{51}. From the third term in the inverse scattering series:

$$
V_3 = -V_1 G_0 V_1 G_0 V_1 - V_1 G_0 V_2 - V_2 G_0 V_1. \qquad (33)
$$

We select $V_1 G_0 V_1 G_0 V_1$ because it is going to give us self interacting hits (data) corresponding to the extra reflection coefficients that we need in order to move the attenuator towards an eliminator of 1^{st} order internal multiples, and when we introduce this term in M_{51} we find the correct phase relation that is going to give the precise time of these events.

The self interacting terms come from a part of $V_1G_0V_1G_0V_1$ that is different from $b_3^{IM_1}$. From Fernanda Araújo's thesis, we write $V_1G_0V_1G_0V_1$ in its data representation:

$$B_3(k) = \int_{-\infty}^{\infty} dz e^{ikz} b_1(z) \int_{-\infty}^{\infty} dz' e^{-ikz'} b_1(z') \int_{-\infty}^{\infty} dz'' e^{ikz''} b_1(z''). \tag{34}$$

$B_3(k)$ was originally separated in four terms by Araújo (1994) when she was looking to find an explicit form for the attenuator, $b_3^{IM_1}$. These four terms are:

$$\begin{aligned} B_3(k) = & \int_{-\infty}^{\infty} dz e^{ikz} b_1(z) \int_{-\infty}^{z} dz' e^{-ikz'} b_1(z') \int_{z'}^{\infty} dz'' e^{ikz''} b_1(z'') \\ & + \int_{-\infty}^{\infty} dz e^{ikz} b_1(z) \int_{z}^{\infty} dz' e^{-ikz'} b_1(z') \int_{-\infty}^{z'} dz'' e^{ikz''} b_1(z'') \\ & + \int_{-\infty}^{\infty} dz e^{ikz} b_1(z) \int_{z}^{\infty} dz' e^{-ikz'} b_1(z') \int_{z'}^{\infty} dz'' e^{ikz''} b_1(z'') \\ & + \int_{-\infty}^{\infty} dz e^{ikz} b_1(z) \int_{-\infty}^{z} dz' e^{-ikz'} b_1(z') \int_{-\infty}^{z'} dz'' e^{ikz''} b_1(z''). \end{aligned} \tag{35}$$

In this separation, we can recognize the first term in the right hand side to be equal to $b_3^{IM_1}$, except for the fact that $b_3^{IM_1}$ doesn't admit self interaction of the effective data, b_1, for this reason, an $\epsilon \ll 1$ was introduced in the limits of the integrals:

$$b_3^{IM_1}(k) = \int_{-\infty}^{\infty} dz_1 e^{ikz_1} b_1(z_1) \int_{-\infty}^{z_1-\epsilon} dz_2 e^{-ikz_2} b_1(z_2) \int_{z_2+\epsilon}^{\infty} dz_3 e^{ikz_3} b_1(z_3), \tag{36}$$

The ϵ ensures that the relations $z_1 > z_2$ and $z_3 > z_2$ are satisfied and avoids the possibility of $z_2 = z_1$ and/or $z_2 = z_3$ and/or $z_1 = z_3$, which are the data self interactions we are looking for.

The data self interactions can be found in the four terms of Eq.(35); therefore, we need to give a definition for these self interaction cases ($z_2 = z_1$, $z_2 = z_3$, $z_1 = z_3$ and $z_1 = z_2 = z_3$), and we will do it with the use of small parameters ($\epsilon \ll 1$) added or subtracted to the limits of the integrals.

We then expand Eq.(35) in nine terms as:

$$\begin{aligned}
B_3(k) = &\int_{-\infty}^{\infty} dz e^{ikz} b_1(z) \int_{-\infty}^{z-\epsilon} dz' e^{-ikz'} b_1(z') \int_{z'+\epsilon}^{\infty} dz'' e^{ikz''} b_1(z'') \\
&+ \int_{-\infty}^{\infty} dz e^{ikz} b_1(z) \int_{z+\epsilon}^{\infty} dz' e^{-ikz'} b_1(z') \int_{-\infty}^{z'-\epsilon} dz'' e^{ikz''} b_1(z'') \\
&+ \int_{-\infty}^{\infty} dz e^{ikz} b_1(z) \int_{z+\epsilon}^{\infty} dz' e^{-ikz'} b_1(z') \int_{z'+\epsilon}^{\infty} dz'' e^{ikz''} b_1(z'') \\
&+ \int_{-\infty}^{\infty} dz e^{ikz} b_1(z) \int_{-\infty}^{z-\epsilon} dz' e^{-ikz'} b_1(z') \int_{-\infty}^{z'-\epsilon} dz'' e^{ikz''} b_1(z'') \\
&+ \int_{-\infty}^{\infty} dz e^{ikz} b_1(z) \int_{-\infty}^{\infty} dz' e^{-ikz'} b_1(z') \delta(z-z') \int_{-\infty}^{\infty} dz'' e^{ikz''} b_1(z'') \delta(z'-z'') \\
&+ \int_{-\infty}^{\infty} dz e^{ikz} b_1(z) \int_{-\infty}^{\infty} dz' e^{-ikz'} b_1(z') \delta(z-z') \int_{z'+\epsilon}^{\infty} dz'' e^{ikz''} b_1(z'') \\
&+ \int_{-\infty}^{\infty} dz e^{ikz} b_1(z) \int_{-\infty}^{\infty} dz' e^{-ikz'} b_1(z') \delta(z-z') \int_{-\infty}^{z'-\epsilon} dz'' e^{ikz''} b_1(z'') \\
&+ \int_{-\infty}^{\infty} dz e^{ikz} b_1(z) \int_{z+\epsilon}^{\infty} dz' e^{-ikz'} b_1(z') \int_{-\infty}^{\infty} dz'' e^{ikz''} b_1(z'') \delta(z'-z'') \\
&+ \int_{-\infty}^{\infty} dz e^{ikz} b_1(z) \int_{-\infty}^{z-\epsilon} dz' e^{-ikz'} b_1(z') \int_{-\infty}^{\infty} dz'' e^{ikz''} b_1(z'') \delta(z'-z''), \\
B_3(k) = &\, B_{31}(k) + B_{32}(k) + B_{33}(k) + B_{34}(k) + B_{35}(k) + B_{36}(k) + B_{37}(k) + B_{38}(k) + B_{39}(k).
\end{aligned} \tag{37}$$

All of the terms in which $B_3(k)$ can be separated contain a negative phase factor in the innermost integral that is going to help to modify the time prediction. The first four terms on the right hand side of Eq.(37) do not allow data self interactions; the rest of the terms contain at least one data self interaction. We can observe that in the terms $B_{35}(k), B_{36}(k), B_{37}(k), B_{38}(k)$ and $B_{39}(k)$ the integration includes the functions $\delta(z'-z'')$ and/or $\delta(z-z')$. Thus, after performing the three integrations we end up with only one phase factor and the multiplication of the amplitudes of three sets of data.

We are interested in the terms that have only one phase factor, and which phase factor correspond to the deeper depth. So we drop:

$$B_{37}(k) = \int_{-\infty}^{\infty} dz e^{ikz} b_1(z) \int_{-\infty}^{\infty} dz' e^{-ikz'} b_1(z') \delta(z-z') \int_{-\infty}^{z'-\epsilon} dz'' e^{ikz''} b_1(z''), \tag{38}$$

and

$$B_{38}(k) = \int_{-\infty}^{\infty} dz e^{ikz} b_1(z) \int_{z+\epsilon}^{\infty} dz' e^{-ikz'} b_1(z') \int_{-\infty}^{\infty} dz'' e^{ikz''} b_1(z'') \delta(z'-z''), \tag{39}$$

because the result will give phase information that doesn't correspond to the deeper depth. In $b_{37}(k)$ a data self interaction exists at $z = z'$ with no phase factor and $z > z''$ with phase information corresponding to the shallowest point: $e^{ikz''}$. For $b_{38}(k)$ a data self interaction exists at $z' = z''$

with no phase factor and $z'' > z$ with phase information corresponding to the shallowest point: e^{ikz}.

This leaves us with only three terms:

$$\begin{aligned}
B_{35}(k) &= \int_{-\infty}^{\infty} dz e^{ikz} b_1(z) \int_{-\infty}^{\infty} dz' e^{-ikz'} b_1(z') \delta(z - z') \int_{-\infty}^{\infty} dz'' e^{ikz''} b_1(z'') \delta(z' - z'') \\
B_{36}(k) &= \int_{-\infty}^{\infty} dz e^{ikz} b_1(z) \int_{-\infty}^{\infty} dz' e^{-ikz'} b_1(z') \delta(z - z') \int_{z'+\epsilon}^{\infty} dz'' e^{ikz''} b_1(z'') \\
B_{39}(k) &= \int_{-\infty}^{\infty} dz e^{ikz} b_1(z) \int_{-\infty}^{z-\epsilon} dz' e^{-ikz'} b_1(z') \int_{-\infty}^{\infty} dz'' e^{ikz''} b_1(z'') \delta(z' - z'')
\end{aligned} \tag{40}$$

The first term, $B_{35}(k)$, is a primary with triple self interaction at the reflection depth. The second, $B_{36}(k)$ and third, $B_{39}(k)$, terms are symmetric terms, they represent primaries with a double self interaction on one of its legs and a single hit at the reflection point.

These are the terms that we are going to use to compute $b_5^{IM_1}$:

$$\begin{aligned}
b_5^{IM_1}(k) &= \int_{-\infty}^{\infty} dz e^{ikz} b_1(z) \int_{-\infty}^{z-\epsilon} dz' e^{-ikz'} \left[B_{35}(z') + B_{36}(z') + B_{39}(z') \right] \int_{z'+\epsilon}^{\infty} dz'' e^{ikz''} b_1(z'') \\
&= \int_{-\infty}^{\infty} dz e^{ikz} b_1(z) \int_{-\infty}^{z-\epsilon} dz' e^{-ikz'} b_1(z')^3 \int_{z'+\epsilon}^{\infty} dz'' e^{ikz''} b_1(z'') \\
&\quad + \int_{-\infty}^{\infty} dz e^{ikz} b_1(z) \int_{-\infty}^{z-\epsilon} dz' e^{-ikz'} \left[2\, b_1(z') \int_{-\infty}^{z'-\epsilon} d\chi\, b_1(\chi)^2 \right] \int_{z'+\epsilon}^{\infty} dz'' e^{ikz''} b_1(z'') \\
&= \int_{-\infty}^{\infty} dz e^{ikz} b_1(z) \\
&\quad \times \int_{-\infty}^{z-\epsilon} dz' e^{-ikz'} \left[(b_1(z'))^3 + 2\, b_1(z') \int_{-\infty}^{z'-\epsilon} d\chi\, b_1(\chi)^2 \right] \int_{z'+\epsilon}^{\infty} dz'' e^{ikz''} b_1(z'').
\end{aligned} \tag{41}$$

$b_5^{IM_1}$ needs five sets of data to produce a prediction of an internal multiple. This prediction will be added to b_1 and $b_3^{IM_1}$ in order to perform a better reduction of the amplitude of 1^{st} order internal multiples. From these five sets of data, used by $b_5^{IM_1}$, three of them are combined in the middle term: $B_{35}(z') + B_{36}(z') + B_{39}(z')$, which have data self interactions. This combination of five sets of data gives the precise internal multiple arrival time and an attenuated amplitude. Adding $b_3^{IM_1} + b_5^{IM_1}$ gives a better estimate of the amplitude of 1^{st} order internal multiples.

Some remarks on the leading order imaging series algorithm for depth imaging when the velocity model is unknown

Simon A. Shaw

Abstract

The inverse scattering series, a multidimensional direct inversion procedure, may be applied to the seismic inverse problem to derive processing algorithms for the most general cases where accurate *a priori* information about the subsurface is not available. Recently, some progress has been reported in using the inverse series to address the problem of depth imaging in areas of complex geology where the velocity model can be difficult to estimate accurately enough for current algorithms. This research is meant to address the problem of depth imaging when the velocity model is unknown or can not be accurately determined. A leading order imaging series, a task-specific subseries of the inverse series, has been isolated for a 1D constant-density acoustic medium and has been shown analytically to converge for any finite contrast between the chosen reference velocity function and the actual velocity model. This imaging series is a Taylor series expanded about each mislocated reflector whose approximate coefficients are leading order in the scattered field. In this paper, a condition is derived which, when satisfied, shows that the leading order imaging series improves the depths of reflectors over a linear imaging algorithm using the reference velocity. This condition is satisfied by the downgoing wave's transmission coefficient in the precritical regime. The impact of residual internal multiples on the imaging series is also studied. As expected, the effect of input data being contaminated by random noise is shown to have only a minor impact on the depths predicted by the leading order imaging series closed form.

1 Introduction

The inverse scattering series, a multidimensional direct inversion procedure, has been applied to the seismic inverse problem to derive multiple attenuation algorithms that require no *a priori* knowledge of the Earth's material properties. The inverse series also has the potential to image reflectors in depth without requiring the actual propagation velocity (7). Inverse series algorithms are non-linear in the scattered field, which includes the source wavelet and a chosen reference medium's properties.

The primary goal of depth imaging is to produce a spatially accurate map of reflectors below the Earth's surface. Current depth imaging algorithms can be formulated from a linear inverse scattering model in which the reference velocity is assumed to be close enough to the actual velocity that reflectors are placed at their correct spatial locations. In practice, especially in complex geological environments, the most accurate methods for deriving the reference velocity model may be inadequate for linear imaging algorithms inasmuch as they fail to focus the reflected wavefield at the correct location. This motivates the search for new imaging algorithms that have the ability to accurately locate reflectors, even when the precise velocity model is not known.

(11) proposed using the inverse scattering series to derive a velocity-independent imaging algorithm. The separation of inverse series terms that acted to correct the location of reflectors in a 1-D acoustic

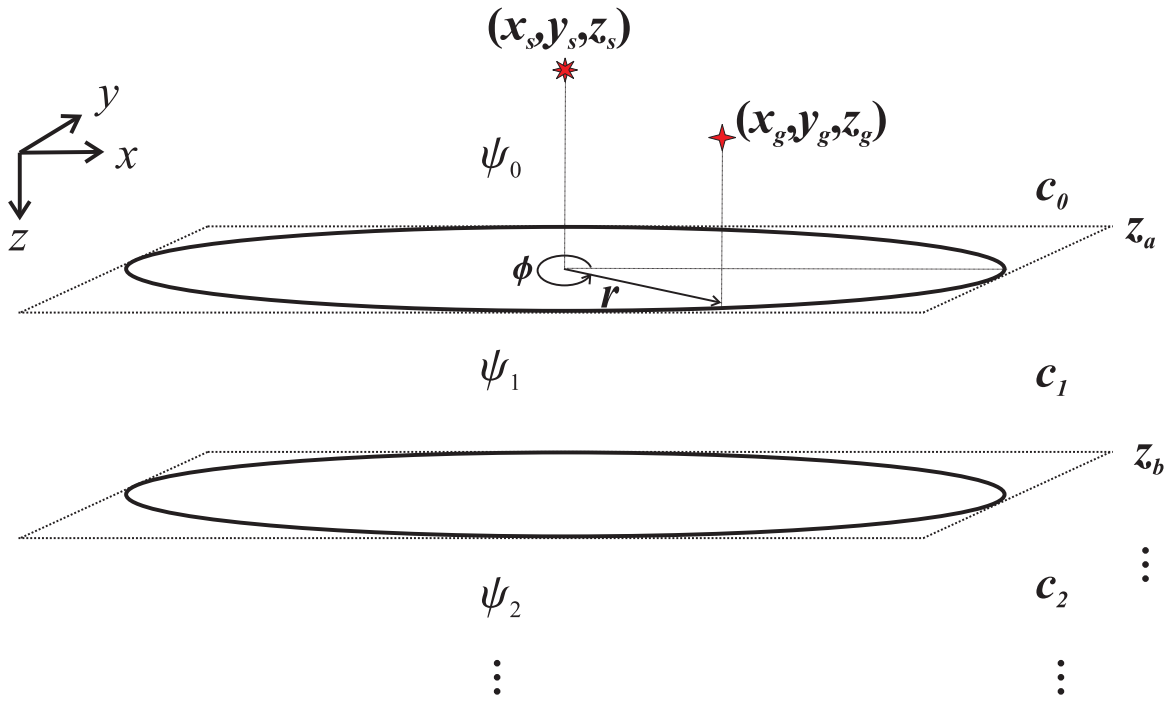

Figure 1: *A multi-layer 1-D constant density acoustic model and no free surface.*

medium was presented by (8). The authors demonstrated that these terms were consistent with the terms of a Taylor series expanded about the mislocated reflector. (6) isolated a leading order imaging series and analyzed its convergence properties. For a suite of interval velocity models, this leading order imaging series has been found numerically to improve the depths of reflectors compared with a linear imaging algorithm using the same reference velocity. While the algorithm benefits from having low frequency information, it was shown to retain effectiveness even when zero and some low frequencies are absent.

(4) have made progress extending the 1-D leading order imaging series to 2-D and (12) have generalized the task separation concepts (i.e., separating imaging from parameter estimation) in the inverse series to two-parameter acoustic and three-parameter elastic wave propagation. At the same time, (3) have isolated and analyzed another subseries that simultaneously images and inverts primaries to a high degree of accuracy for moderate contrasts between the actual and reference media.

2 A leading order imaging series for a 1-D constant density acoustic medium

We consider a constant density acoustic medium with point sources and receivers located at $\vec{x}_s = (x_s, y_s, z_s)$ and $\vec{x}_g = (x_g, y_g, z_g)$, respectively (see Fig. 1). Wave propagation in an acoustic medium

can be characterized by the wave equation

$$\left(\nabla^2 + \frac{\omega^2}{c^2(z)}\right)\psi(\vec{x}\,|\vec{x}_s;\omega) = -A(\omega)\delta(\vec{x} - \vec{x}_s), \tag{1}$$

where ψ is the pressure field, A is the source wavelet, c is the propagation velocity and ω is the angular temporal frequency. The pressure wavefield due to the same source in the reference medium which is chosen to be a wholespace with velocity, c_0, is denoted by ψ_0 and satisfies the equation

$$\left(\nabla^2 + \frac{\omega^2}{c_0^2}\right)\psi_0(\vec{x}\,|\vec{x}_s;\omega) = -A(\omega)\delta(\vec{x} - \vec{x}_s). \tag{2}$$

The scattering potential, defined as the difference between the wave equation operators in Eqs. (1) and (2), is

$$V = k_0^2\alpha, \tag{3}$$

where $k_0 = \omega/c_0$ and α is the velocity perturbation, a dimensionless parameter that relates the actual velocity, c, to the constant reference velocity, c_0, such that

$$\frac{1}{c^2(z)} = \frac{1}{c_0^2}\left[1 - \alpha\,(z)\right]. \tag{4}$$

For this acoustic problem, the goal of inversion is to solve for α which can be written as an infinite series:

$$\alpha = \alpha_1 + \alpha_2 + \alpha_3 + \ldots = \sum_{n=1}^{\infty}\alpha_n, \tag{5}$$

where α_1, the first term in the series for α, is linearly related to the scattered field on the measurement surface, $\psi_s(\vec{x}_g\,|\vec{x}_s\,;\omega)$. The second term, α_2, is quadratic in ψ_s, the third term, α_3, is cubic and so on.

After using the inverse scattering series (see, e.g., 7) to solve for α, we could then use Eq. (4) to solve for the unknown velocity, $c(z)$. However, the objective here is in fact not to solve for the medium parameters (in this case just c), but to solve directly for the *location* at which the perturbation, α, changes. This is the problem of imaging a medium whose velocity is not known before or after the imaging procedure.

(6) isolated a subseries of the inverse series that locates reflectors in depth but does not go beyond a linear inversion for medium properties at these reflectors. As such, this leading order imaging series is an example of a task-specific subseries that has the sole objective of imaging in depth. For prestack data, the leading order imaging series is

$$\alpha^{\mathrm{LOIS}}(z,p) = \sum_{n=0}^{\infty}\frac{(-1/2)^n}{n!\cos^{2n}\theta_0}\left[\int_0^z \alpha_1(z',p)dz'\right]^n\frac{\partial^n\alpha_1(z,p)}{\partial z^n}, \tag{6}$$

where the first term, $\alpha_1(z,p)$, is given by

$$\alpha_1(z,p) = -\,8\zeta_0\cos^2\theta_0\int_{-\infty}^{\infty}e^{-i\omega\zeta_0(2z-(z_g+z_s))}\int_0^{\infty}D(r;\omega)J_0(\omega pr)rdrd\omega. \tag{7}$$

The horizontal and vertical slownesses, p and ζ_0, respectively, are related to θ_0 by

$$p \doteq \frac{\sin\theta_0}{c_0} \text{ and } \zeta_0 \doteq \frac{\cos\theta_0}{c_0}.$$

The data, D, are the scattered field with the source wavelet deconvolved ($D = \psi_s/A$) and J_0 is the zeroth order Bessel function of the first kind that arises due to the azimuthal symmetry:

$$J_0(\omega pr) = \frac{1}{2\pi}\int_0^{2\pi} e^{i\omega pr\cos\phi} d\phi. \tag{8}$$

The leading order imaging series has been shown to have a closed form, which efficiently encapsulates an infinite number of terms in a single operation:

$$\alpha^{\text{LOIS}}(z,p) = \alpha_1\left(z-\Delta, p\right), \tag{9}$$

where

$$\Delta(z,p) = \frac{1}{2\cos^2\theta_0}\int_0^z \alpha_1(z',p)dz'. \tag{10}$$

In this paper, we will use this pre-stack closed form to analyze and evaluate the leading order imaging series.

3 Evaluation of the leading order imaging series shift

For a suite of interval velocity models, the leading order imaging series has been found to improve the depths of reflectors compared with a linear imaging algorithm using the reference velocity (see, e.g., 5). Here, we investigate analytically under what conditions the algorithm improves the depths of reflectors that have been imaged using current linear imaging algorithms supplied with the reference velocity.

Consider a reflector that is located at depth z_R. It is imaged at depth $\hat{z}_R$ by the constant reference velocity and at depth $\hat{z}_R^{\text{LOIS}}$ by the leading order imaging series (see Fig. 2). We would like to know how good an approximation $\hat{z}_R^{\text{LOIS}}$ is to z_R and, more importantly, whether $\hat{z}_R^{\text{LOIS}}$ is an improvement over $\hat{z}_R$. ¿From the travel time equation, the two-way vertical time to this reflector is

$$\tau(z_R) = 2\int_0^{z_R}\zeta(z')dz', \tag{11}$$

where, for simplicity, we assume that the sources and receivers are located at $z_s = z_g = 0$. Linear imaging with the constant reference velocity will predict its depth at

$$\begin{aligned}\hat{z}_R =& \frac{\tau(z_R)}{2\zeta_0}\\ =& \frac{1}{\zeta_0}\int_0^{z_R}\zeta(z')dz'.\end{aligned} \tag{12}$$

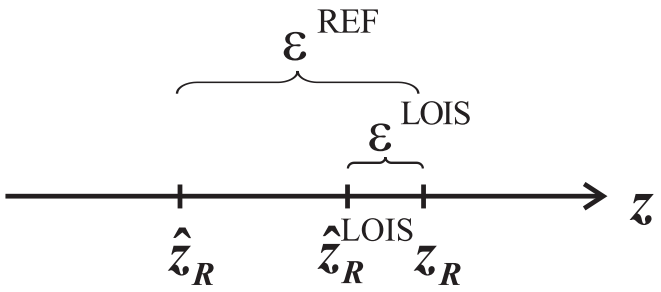

Figure 2: *Errors in the predicted depths. z_R is a reflector's true depth, $\hat{z}_R$ is the depth predicted by the reference velocity in the first term, and $\hat{z}_R^{LOIS}$ is the depth predicted by the leading order imaging series.*

This is its position in α_1. Only if the actual slowness happens to be ζ_0, will $\hat{z}_R = z_R$. Given the information contained in α_1 (a combination of the information in the recorded data and the chosen reference medium), the leading order imaging series will reposition the reflector at

$$\hat{z}_R^{\text{LOIS}} = \hat{z}_R + \frac{1}{2\cos^2\theta_0}\int_0^{\hat{z}_R} \alpha_1(z')dz'. \tag{13}$$

Our objective is to determine whether $\hat{z}_R^{\text{LOIS}}$ is, in general, closer to z_R than $\hat{z}_R$ is, i.e., under what conditions the leading order imaging series is an improvement upon current imaging methods that use an inadequate reference velocity. From Eq. (12), the error in the depth predicted by the first term is

$$\varepsilon^{\text{REF}} = \hat{z}_R - z_R = \int_0^{z_R} \frac{\zeta(z') - \zeta_0}{\zeta_0} dz' \tag{14}$$

which, when added to Eq. (13), gives the error in the depth predicted by α^{LOIS} :

$$\varepsilon^{\text{LOIS}} = \int_0^{z_R} \frac{\zeta(z') - \zeta_0}{\zeta_0} dz' + \frac{1}{2\cos^2\theta_0}\int_0^{\hat{z}_R} \alpha_1(z')dz'.$$

Both ε^{REF} and $\varepsilon^{\text{LOIS}}$ will be smaller when the integral of α is smaller, which will be the case when the actual velocity model is closer to the chosen reference velocity. The leading order imaging series is an improvement over a linear imaging algorithm when

$$|\varepsilon^{\text{LOIS}}| < |\varepsilon^{\text{REF}}|, \tag{15}$$

i.e., when

$$\left|\int_0^{z_R} \frac{\zeta(z') - \zeta_0}{\zeta_0} dz' + \frac{1}{2\cos^2\theta_0}\int_0^{\hat{z}_R} \alpha_1(z')dz'\right| < \left|\int_0^{z_R} \frac{\zeta(z') - \zeta_0}{\zeta_0} dz'\right|.$$

We can rearrange this inequality to arrive at

$$0 < \left(\frac{B}{A}\right) < 2 \tag{16}$$

where

$$A = \hat{z}_R - z_R = \varepsilon^{\mathrm{REF}} = \int_0^{z_R} \frac{\zeta(z') - \zeta_0}{\zeta_0} dz'$$
$$\text{and } B = \hat{z}_R - \hat{z}_R^{\mathrm{LOIS}} = \frac{-1}{2\cos^2\theta_0} \int_0^{\hat{z}_R} \alpha_1(z') dz'.$$

If the condition in Eq. (16) can be satisfied, then the leading order imaging series will predict a depth that is more accurate than current imaging with the reference velocity. For the simple example of two reflectors, we can show that the condition will be satisfied. We consider a two-reflector model where the vertical slowness profile is (see Fig. 1)

$$\zeta(z) = \zeta_0(z) + (\zeta_1 - \zeta_0)H(z - z_a) + [\zeta_2 - (\zeta_1 - \zeta_0)]\, H(z - z_b).$$

Then, for this example,

$$A = \int_0^{z_b} \left(\frac{\zeta(z') - \zeta_0}{\zeta_0} \right) dz' = \frac{\zeta_1 - \zeta_0}{\zeta_0}(z_b - z_a)$$
$$B = \frac{-1}{2\cos^2\theta_0} \int_0^{\hat{z}_b} \alpha_1(z') dz' = \frac{-1}{2\cos^2\theta_0} \left(-4\cos^2\theta_0 \frac{\zeta_0 - \zeta_1}{\zeta_0 + \zeta_1}(\hat{z}_b - z_a) \right)$$
$$= 2\left(\frac{\zeta_1}{\zeta_0} \frac{(\zeta_0 - \zeta_1)}{(\zeta_0 + \zeta_1)}(z_b - z_a) \right)$$

which, upon substitution into Eq. (16), gives

$$0 < \frac{2\zeta_1}{\zeta_0 + \zeta_1} < 2.$$

This result tells us that the downgoing transmission coefficient at the upper interface satisfies the condition necessary to show that the leading order imaging series improves the predicted depth of the second interface *independent* of (a) the depths of the two interfaces, or (b) the actual velocity below the first interface.

4 Numerical examples with three interfaces – more about the meaning of "leading order"

Analysis of the imaging subseries becomes more interesting for three or more reflectors because of the effect of transmission loss in the overburden. Consider a model that consists of three horizontal interfaces at depths z_a, z_b and z_c and a discontinuous velocity profile $c(z)$ as depicted in Fig. 1. The wavefield in the upper halfspace, ψ_0, consists of an incident field, ψ_i, and a reflected field, ψ_r. The measured reflected wavefield can be derived by decomposing the incident field into a sum of plane waves (the Sommerfeld integral) and then matching boundary conditions at each interface (see, e.g., 1). The result is

$$\psi_r(r;\omega) = \frac{i\omega}{4\pi} \int_0^\infty \frac{\left(R_{01} + \hat{R}_{12} e^{2i\omega\zeta_1(z_b - z_a)} + \hat{R}_{23} e^{2i\omega[\zeta_1(z_b - z_a) + \zeta_2(z_c - z_b)]} + \ldots \right)}{\zeta_0}$$
$$\times\, e^{i\omega\zeta_0(2z_a - z_s - z_g)} J_0(\omega p r) p dp \qquad (17)$$

where the reflection and transmission coefficients are functions of angle and are given by

$$R_{jk} = \frac{\zeta_j - \zeta_k}{\zeta_j + \zeta_k} \qquad j = 0, 1, 2, 3; k = j + 1 \tag{18}$$

$$T_{jk} = 1 - \frac{\zeta_j - \zeta_k}{\zeta_j + \zeta_k} = 1 - R_{jk} \qquad j = 0, 1, 2, 3; k = j + 1. \tag{19}$$

We have further defined the amplitudes $\hat{R}_{12} = T_{01}R_{12}T_{10}$ and $\hat{R}_{23} = T_{01}T_{12}R_{23}T_{21}T_{10}$. The vertical slownesses are functions of the incident angles in each layer:

$$\zeta_j = \frac{\cos\theta_j}{c_j} \ , \ \ j = 0, 1, 2, \ldots \tag{20}$$

The "+..." in Eq. (17) are the internal multiple reflections in the data. For now, an internal multiple removal algorithm, a subseries that begins in the third term of the inverse series, is assumed to have been applied before the imaging subseries. This results in a new effective data and a new effective α_1 that contain only primary reflection events. This step is part of the strategy of inverse series task separation described by Weglein et al. (7). For the two reflector examples studied earlier, the internal multiples were of no consequence since the imaging series only uses information recorded earlier than the primary event being imaged, which excluded the multiples. In the next section, we will study the effect of a residual first order internal multiple that arrives before the deepest primary being imaged.

Reverting to the symbol D for data that contain only primary reflections, and then performing a linear inversion of the data (Eq. 7), the first term in the series for $\alpha(z)$ for this three-reflector example is

$$\begin{aligned}\alpha_1(z,p) =& 8\cos^2\theta_0 \int_{-\infty}^{\infty} \frac{R_{01} + \hat{R}_{12}e^{2i\omega\zeta_1(z_b - z_a)} + \hat{R}_{23}e^{2i\omega[\zeta_1(z_b-z_a)+\zeta_2(z_c-z_b)]}}{4\pi i\omega\zeta_0} e^{-2i\omega\zeta_0(z-z_a)}d\omega \\ =& -4\cos^2\theta_0 \Big[R_{01}H\left(z - z_a\right) + \left(R_{01} + \hat{R}_{12}\right)H\left(z - \hat{z}_b\right) \\ & + \left(R_{01} + \hat{R}_{12} + \hat{R}_{23}\right)H\left(z - \hat{z}_c\right)\Big]\end{aligned} \tag{21}$$

where the dependence of both the amplitudes *and* the predicted depths on p is implied. The shallowest reflector is correctly located at z_a (since the velocity down to z_a was correct) but the deeper reflectors are mislocated at depths

$$\hat{z}_b = z_a + (z_b - z_a)\frac{\zeta_1}{\zeta_0} \tag{22}$$

$$\text{and} \hat{z}_c = \hat{z}_b + (z_c - z_b)\frac{\zeta_2}{\zeta_0}. \tag{23}$$

Inserting Eq. (21) into the leading order imaging series will result in a shift of the two mislocated interfaces to depths

$$\hat{z}_b^{\text{LOIS}} = \hat{z}_b + 2(\hat{z}_b - z_a)R_{01} \tag{24}$$

$$\hat{z}_c^{\text{LOIS}} = \hat{z}_c + 2(\hat{z}_b - z_a)R_{01} + 2(\hat{z}_c - \hat{z}_b)(R_{01} + \hat{R}_{12}). \tag{25}$$

Eq. (24) is the approximation to z_b that is leading order in R_{01}. We can show that Eq. (25) is the approximation to z_c that is leading order in the amplitudes of the scattered field. Equations (22) and (23) can be combined to give

$$z_c = z_a + (\hat{z}_b - z_a)\frac{\zeta_0}{\zeta_1} + (\hat{z}_c - \hat{z}_b)\frac{\zeta_0}{\zeta_2} \tag{26}$$

and then the slowness ratios can be expanded as series in the reflection coefficients where

$$\begin{aligned}
\frac{\zeta_0}{\zeta_1} &= \frac{1+R_{01}}{1-R_{01}} = 1 + 2R_{01} + 2R_{01}^2 + 2R_{01}^3 + \dots \ , |R_{01}| < 1 \\
\frac{\zeta_0}{\zeta_2} &= \left(\frac{1+R_{01}}{1-R_{01}}\right)\left(\frac{1+R_{12}}{1-R_{12}}\right) \\
&= 1 + 2R_{01} + 2R_{12} + 2R_{01}^2 + 2R_{12}^2 + 4R_{01}R_{12} + \dots \ , |R_{01}| < 1, |R_{12}| < 1.
\end{aligned} \tag{27}$$

Substituting these expressions into Eq. (26) gives

$$\begin{aligned}
z_c = \hat{z}_c &+ 2\,(\hat{z}_b - z_a)\left[R_{01} + R_{01}^2 + R_{01}^3 + \dots\right] \\
&+ 2\,(\hat{z}_c - \hat{z}_b)\left[R_{01} + R_{12} + R_{01}^2 + R_{12}^2 + 2R_{01}R_{12}\right. \\
&\qquad \left. + R_{01}^3 + R_{12}^3 + 2R_{01}R_{12}^2 + 2R_{01}^2R_{12} + \dots\right]
\end{aligned} \tag{28}$$

The shift calculated by the leading order imaging series (Eq. 25) is an approximation to the series in Eq. 28 to leading order in the data's amplitudes. The approximation reduces to

$$\begin{aligned}
(\hat{z}_b - z_a)R_{01} + (\hat{z}_c - \hat{z}_b)(R_{01} + \hat{R}_{12}) \approx\ & (\hat{z}_b - z_a)\left[R_{01} + R_{01}^2 + R_{01}^3 + \dots\right] \\
& + (\hat{z}_c - \hat{z}_b)\left[R_{01} + R_{12} + R_{01}^2 + R_{12}^2 + 2R_{01}R_{12} + \dots\right]
\end{aligned} \tag{29}$$

where we observe that leading order in the amplitudes of the scattered field, in general, implies non-linearity in the reflection coefficients:

$$\hat{R}_{12} = T_{01}R_{12}T_{10} = R_{12} + R_{01}^2R_{12}. \tag{30}$$

The leading order approximation to the shift of the reflector at $\hat{z}_c$ contains contributions that are linear and cubic in the reflection coefficients. For deeper reflectors, these contributions will be of increasingly higher order due to the transmission coefficients in the measured scattered field. It is to be expected that the leading order approximation will deteriorate for deeper reflectors due to the fact that the shift is a function of approximations (truncated geometric series) at all shallower reflectors. Higher order imaging terms are expected to improve the approximation.

Figures 3 and 4 illustrate the results for two choices of model parameters given in Table 1. In the first example, the layer velocity $c_1 > c_0$ and in the second example, $c_1 < c_0$ by the same amount (roughly 13%). As a result, the first term in the series "under-corrects" the deeper reflectors in Fig. 3 and "over-corrects" them in Fig. 4. In both cases, the leading order imaging series (computed analytically) shifts the mislocated interfaces closer to their true depths. It is interesting to note that, in the second example, α^{LOIS} positions the reflectors a small distance *shallower* than their actual depths, whereas the first term placed them a much greater distance *deeper*. Therefore, the sign of the depth error can change. The leading order imaging series has the effect of flattening image gathers closer to their true depths than a current linear imaging algorithm using the reference velocity.

In the next section we will study the impact of violating the assumption that internal multiples have been removed.

	Layer velocities (m/sec)			Interface depths (m)		
	c_0	c_1	c_2	z_a	z_b	z_c
Fig. 3	1500	1700	1800	100	140	170
Fig. 4	1500	1300	1600	100	140	170

Table 1: Model parameters corresponding to the results in Figs. 3 and 4.

5 The impact of internal multiples on the leading order imaging series

The strategy of isolating task-specific subseries of the inverse series that achieve important seismic processing objectives has proven to be a successful one (7). As part of this strategy, subseries algorithms are applied in sequence using the output from a preceding algorithm as input to the current one. While progress is being made in extending the inverse scattering internal multiple attenuation algorithm (9) towards an internal multiple removal algorithm (as described in this report), the current high-water mark in multiple attenuation when the Earth model is unknown is free-surface multiple removal and internal multiple attenuation.

The scattered field that includes three primary reflectors and a first order internal multiple that has reverberated in the first layer can be written analytically as

$$D(r;\omega) = \frac{i\omega}{4\pi}\int_0^\infty \left(\frac{R_{01} + \hat{R}_{12}e^{2i\omega\zeta_1(z_b-z_a)} + \hat{R}_{\rm IM}e^{4i\omega\zeta_1(z_b-z_a)}}{\zeta_0} + \frac{\hat{R}_{23}e^{2i\omega[\zeta_1(z_b-z_a)+\zeta_2(z_c-z_b)]}}{\zeta_0} \right) e^{i\omega\zeta_0(2z_a-z_s-z_g)}J_0(\omega pr)pdp. \quad (31)$$

The amplitude of the internal multiple is

$$\hat{R}_{\rm IM}(p) = T_{01}R_{12}R_{10}R_{12}T_{10} = -T_{01}R_{12}^2R_{01}T_{10} \quad (32)$$

which, after application of the inverse scattering internal multiple attenuation algorithm is reduced to (10)

$$\hat{R}_{\rm IM}(p) = -T_{01}R_{12}^2R_{01}T_{10}(1 - T_{01}T_{10}) \quad (33)$$

For this example, the first term in the series is

$$\alpha_1(z,p) = -4\cos^2\theta_0 \left[R_{01}H(z-z_a) + \left(R_{01}+\hat{R}_{12}\right)H(z-\hat{z}_b) + \left(R_{01}+\hat{R}_{12}+\hat{R}_{\rm IM}\right)H(z-\hat{z}_{\rm IM}) + \left(R_{01}+\hat{R}_{12}+\hat{R}_{\rm IM}+\hat{R}_{23}\right)H(z-\hat{z}_c)\right] \quad (34)$$

where $\hat{z}_{\rm IM}$ is the depth that the internal multiple is imaged at in the first term. The impact of residual multiples on the imaging series is two-fold. First, the multiples themselves will be imaged by the series and, second, they will impact the distance that events below them (or that arrive later in time) are shifted by the imaging series. In the following examples, we illustrate the latter effect only.

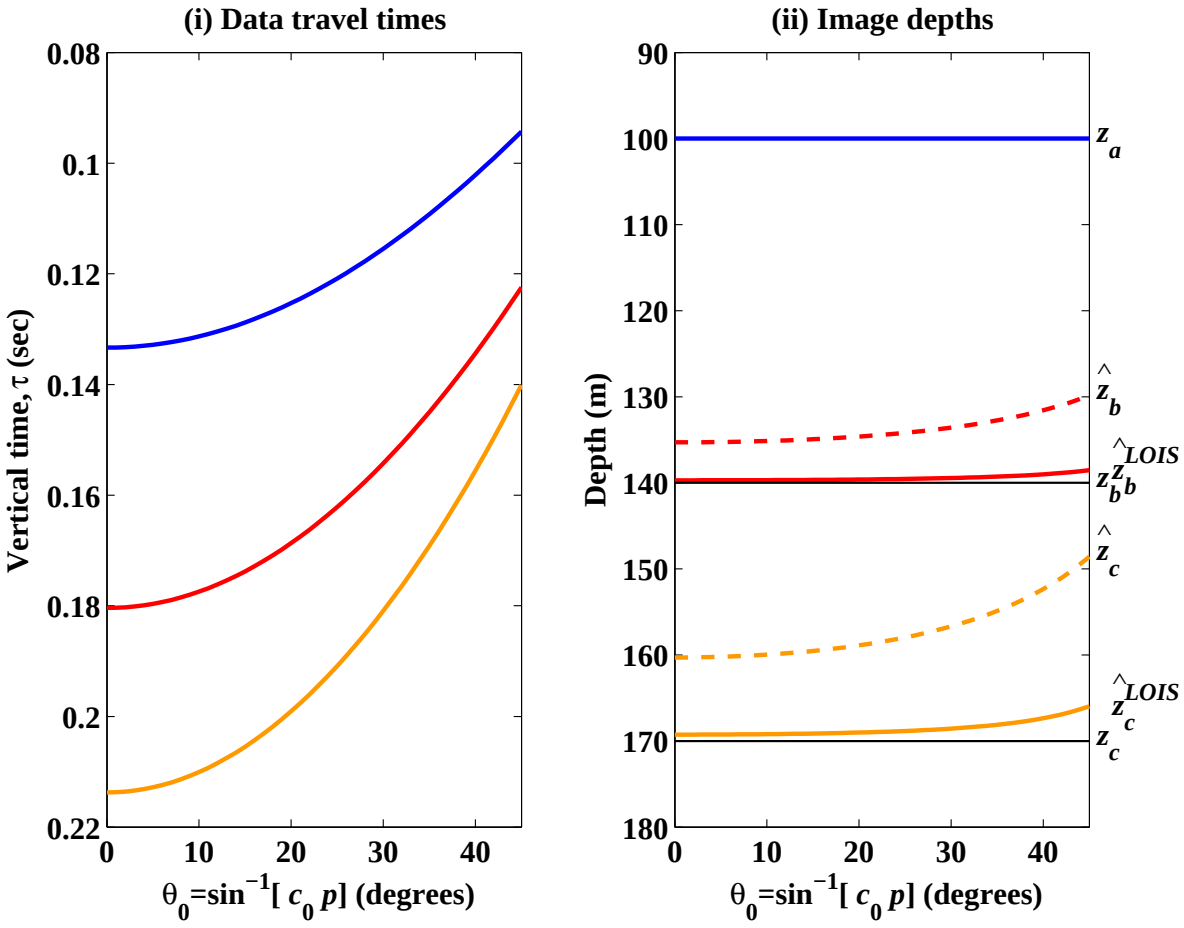

Figure 3: *(i) Travel time curves for three primaries. (ii) Depths predicted by the first term, z_a, $\hat{z}_b$ and $\hat{z}_c$, and the leading order imaging series, z_a, $\hat{z}_b^{LOIS}$ and $\hat{z}_c^{LOIS}$. Model parameters are given in Table 1.*

Figures 5 and 6 show the results of the leading order imaging series for the two specific models described in Table 2 and in the presence of a residual first order multiple that has reverberated between the interfaces at z_a and z_b. It is interesting to note that in both these examples, the impact of the residual internal multiple is to slightly improve the predicted depth of the reflector. The fact that non-linear terms simultaneously act to remove internal multiples does not preclude the possibility that internal multiples may, under some limited circumstances, improve the accuracy of the imaging series terms. However, in a two-reflector case, internal multiples can not impact the leading order imaging series because they arrive later in time (and deeper in reference depth) than the mislocated reflector. This implies that internal multiples are not needed by the inverse series' imaging terms. Clearly, a more careful analytical analysis is warranted here.

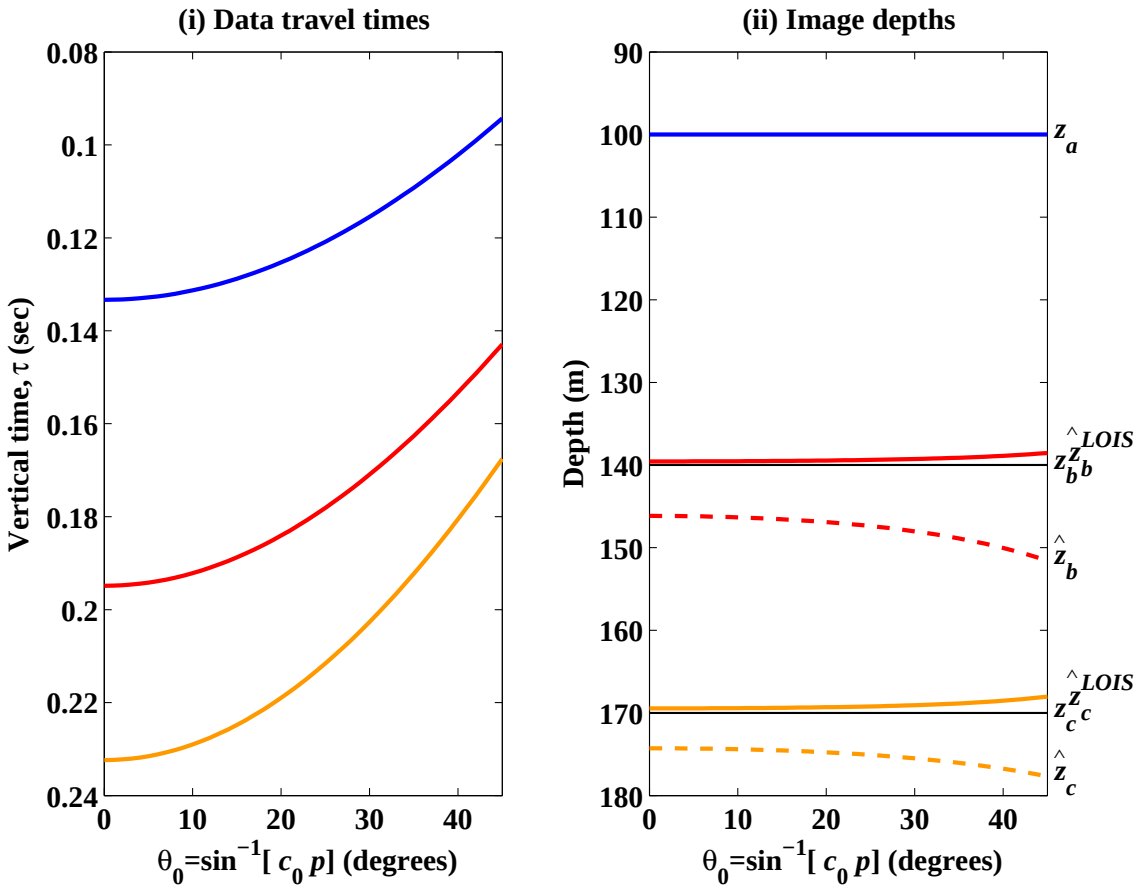

Figure 4: *(i) Travel time curves for three primaries. (ii) Depths predicted by the first term, z_a, $\hat{z}_b$ and $\hat{z}_c$, and the leading order imaging series, z_a, $\hat{z}_b^{LOIS}$ and $\hat{z}_c^{LOIS}$. Model parameters are given in Table 1.*

6 Band-limited numerical examples with random noise

A common question that arises when testing a new algorithm is: "What about noise?". Generally, noise in our input data is considered to be anything that is not explained by the underlying model. For the algorithm currently under investigation, examples of noise are a residual source wavelet, residual free-surface and internal multiples and anything that does not satisfy a 1-D constant density acoustic wave equation. Rarely does noise improve the effectiveness of an algorithm although sometimes white noise serves to stabilize a result.

Figures 7–9 illustrate the effect of different amounts of broadband *random noise* on the closed form of the leading order imaging series (Eq. 9). As might be expected, random noise does not have a significantly deleterious effect on the depths predicted by the leading order imaging series because the accuracy of the result depends on integrals of the data in the overburden. An integral of a random noise sequence will tend to be small.

It is anticipated that the series form of the algorithm (Eq. 6) would be more sensitive to random noise than the closed form because the series form requires high-order derivatives which can tend

	Layer velocities (m/sec)			Interface depths (m)		
	c_0	c_1	c_2	z_a	z_b	z_c
Fig. 5	1500	2000	1900	100	125	170
Fig. 6	1500	1350	1900	100	125	170

Table 2: *Model parameters corresponding to the results in Figs. 5 and 6 in which the impact on the leading order imaging series of a first order internal multiple is analyzed.*

to emphasize high frequency noise. (2) showed some robustness to random noise of a subseries that simultaneously images and inverts primaries. Probably the most serious form of noise is a coherent low frequency trend or DC shift. This noise will be accentuated by the integral of α_1 in the algorithm and will result in inaccurately predicted depths.

7 Conclusions

A condition has been derived which, when satisfied, demonstrates that the leading order imaging series will improve the depths of reflectors over a linear imaging algorithm using the reference velocity. For a two-reflector example, this condition is satisfied by the downgoing wave's transmission coefficient in the precritical regime. The impact of residual internal multiples on the imaging series has been studied using three-layer numerical examples. More analysis is needed in this area. Finally, the effect of input data being contaminated by random noise has been shown to have only a minor impact on the depths predicted by the leading order imaging series closed form. A closer look at the effect of coherent noise, especially at low frequencies, is probably worthwhile.

8 Acknowledgements

I would like to thank ConocoPhillips for their financial support during the last year. I am especially grateful to Hugh Rowlett and Rob Habiger. All the M-OSRP sponsors are thanked for their support of this research.

References

[1] Aki, K. and P. G. Richards (2002). *Quantitative Seismology* (2nd ed.). University Science Books.

[2] Innanen, K. A. (2003). *Methods for the treatment of acoustic and absorptive/dispersive wave field measurements.* Ph. D. thesis, University of British Columbia.

[3] Innanen, K. A., A. B. Weglein, and T. J. Ulrych (2004). Basic numerics in the non-linear inversion of primaries: simultaneous imaging and inversion II. *M-OSRP Annual Report 3.*

[4] Liu, F., B. G. Nita, A. B. Weglein, and K. A. Innanen (2004). Inverse scattering series in the presence of lateral variations. *M-OSRP Annual Report 3.*

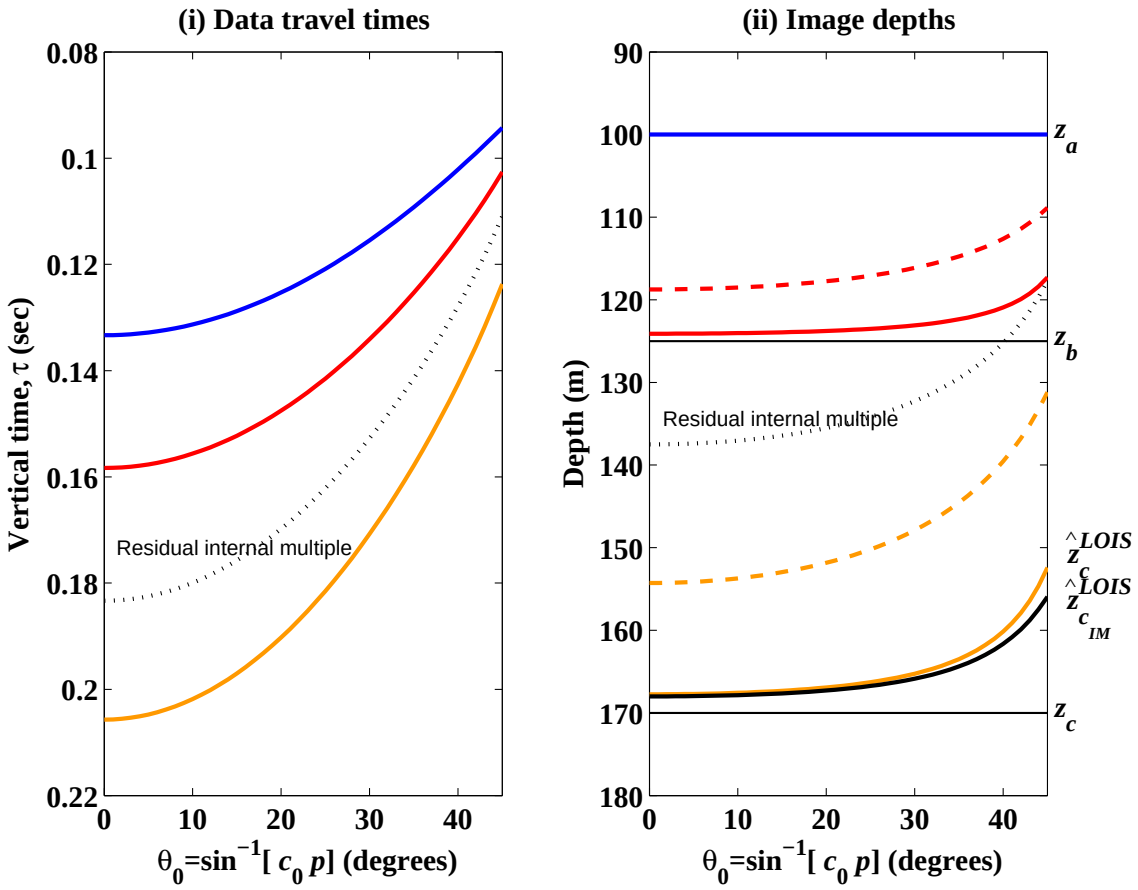

Figure 5: *(i) Travel time curves for three primaries and a first order internal multiple. (ii) Depths predicted by the first term, z_a, $\hat{z}_b$ and $\hat{z}_c$, and the leading order imaging series, z_a, $\hat{z}_b^{LOIS}$ and $\hat{z}_c^{LOIS}$ (all with the same colors and line styles as in Figs. 3 and 4). The depth $\hat{z}_{c_{IM}}^{LOIS}$ is the depth of the interface at z_c predicted by the leading order imaging series in the presence of the internal multiple. Model parameters are given in Table 2. In this case, $\hat{z}_{c_{IM}}^{LOIS}$ is an improvement over $\hat{z}_c^{LOIS}$.*

[5] Shaw, S. A. and A. B. Weglein (2004). A leading order imaging series for prestack data acquired over a laterally invariant acoustic medium. Part I: Derivation and preliminary analysis. *M-OSRP Annual Report 3*.

[6] Shaw, S. A., A. B. Weglein, D. J. Foster, K. H. Matson, and R. G. Keys (2003). Convergence properties of a leading order depth imaging series. In *73rd Annual Internat. Mtg., Soc. Expl. Geophys., Expanded Abstracts*, pp. 937–940. Soc. Expl. Geophys.

[7] Weglein, A. B., F. V. Araújo, P. M. Carvalho, R. H. Stolt, K. H. Matson, R. T. Coates, D. Corrigan, D. J. Foster, S. A. Shaw, and H. Zhang (2003). Inverse scattering series and seismic exploration. *Inverse Problems 19*, R27–R83.

[8] Weglein, A. B., D. J. Foster, K. H. Matson, S. A. Shaw, P. M. Carvalho, and D. Corrigan (2002). Predicting the correct spatial location of reflectors without knowing or determining

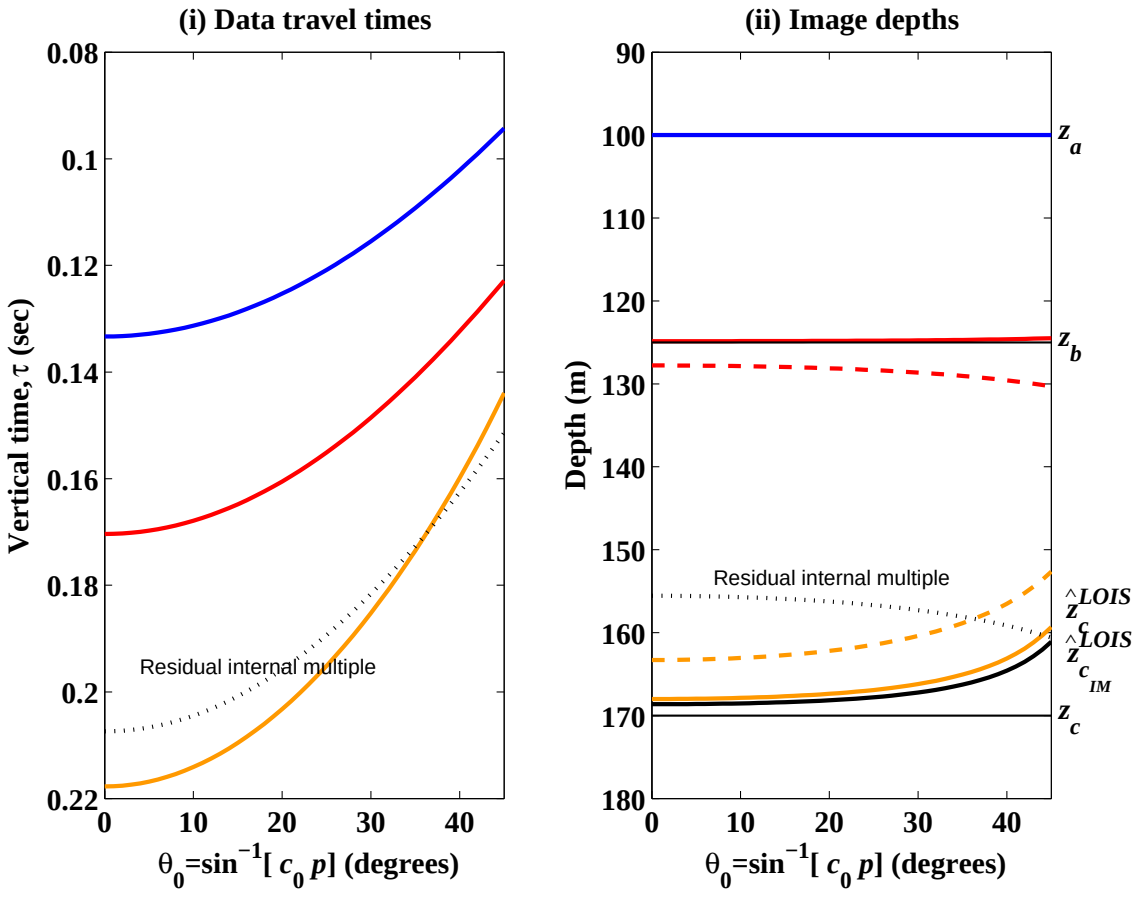

Figure 6: *(i) Travel time curves for three primaries and a first order internal multiple. (ii) Depths predicted by the first term, z_a, $\hat{z}_b$ and $\hat{z}_c$, and the leading order imaging series, z_a, $\hat{z}_b^{LOIS}$ and $\hat{z}_c^{LOIS}$. The depth $\hat{z}_{c_{IM}}^{LOIS}$ is the depth of the interface at z_c predicted by the leading order imaging series in the presence of the internal multiple. Model parameters are given in Table 2. In this case, $\hat{z}_{c_{IM}}^{LOIS}$ is* not *an improvement over $\hat{z}_c^{LOIS}$, which is predicted in the absence of internal multiples.*

the precise medium and wave velocity: initial concept, algorithm and analytic and numerical example. *Journal of Seismic Exploration 10*(4), 367–382.

[9] Weglein, A. B., F. A. Gasparotto, P. M. Carvalho, and R. H. Stolt (1997). An inverse-scattering series method for attenuating multiples in seismic reflection data. *Geophysics 62*(6), 1975–1989.

[10] Weglein, A. B. and K. H. Matson (1998). Inverse scattering internal multiple attenuation: an analytic example and subevent interpretation. In *Proc. SPIE*. SPIE.

[11] Weglein, A. B., K. H. Matson, D. J. Foster, P. M. Carvalho, D. Corrigan, and S. A. Shaw (2000). imaging and inversion at depth without a velocity model: Theory, concepts and initial evaluation. In *70th Annual Internat. Mtg., Soc. Expl. Geophys., Expanded Abstracts*, pp. 1016–1019. Soc. Expl. Geophys.

[12] Zhang, H. and A. B. Weglein (2004). Target identification using the inverse scattering series:

data requirements for the direct inversion of large-contrast, inhomogeneous elastic media. *MOSRP Annual Report 3*.

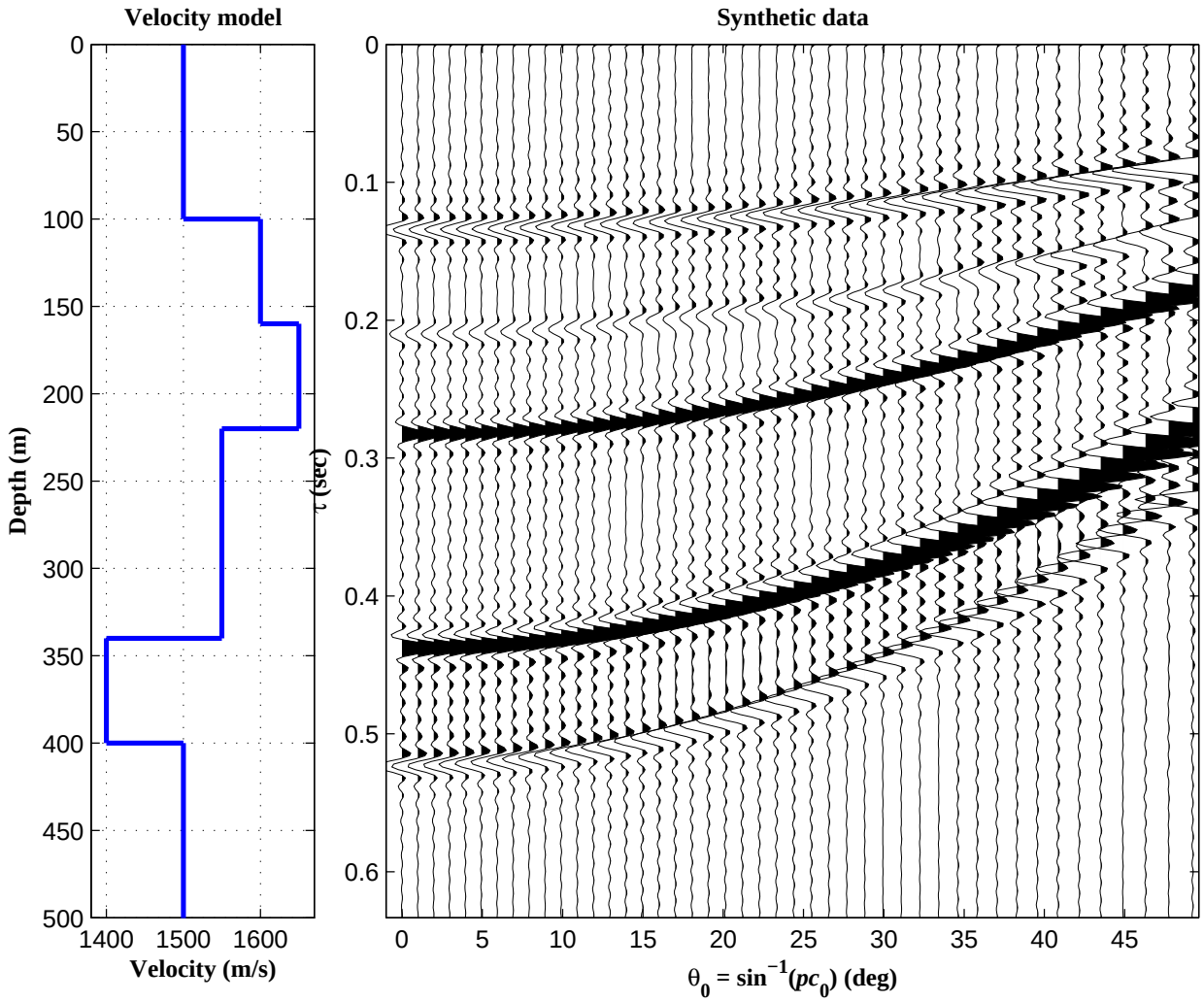

Figure 7: *Velocity model (left) and input data (right) generated through reflectivity modelling. The time derivatives of the slant stack data are displayed. The minimum and maximum frequencies are 0.125 Hz and 80 Hz, respectively.*

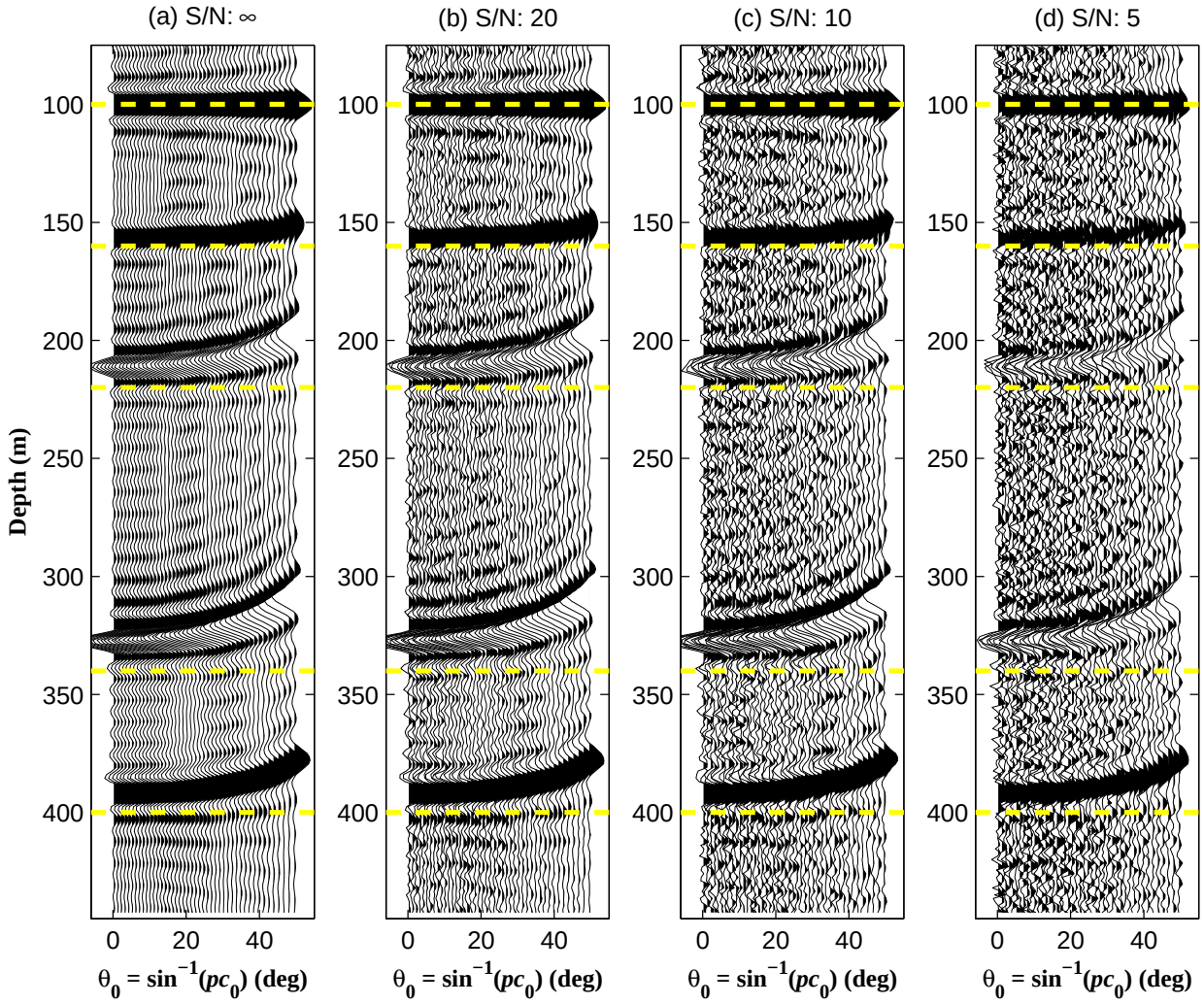

Figure 8: *Data in Fig. 7 imaged using the reference velocity, c_0, after being contaminated with various amounts of random noise. Signal-to-noise ratios are displayed at the top of each panel. The depth derivatives of α_1 are displayed. The dashed yellow lines indicate the actual depths of the reflectors.*

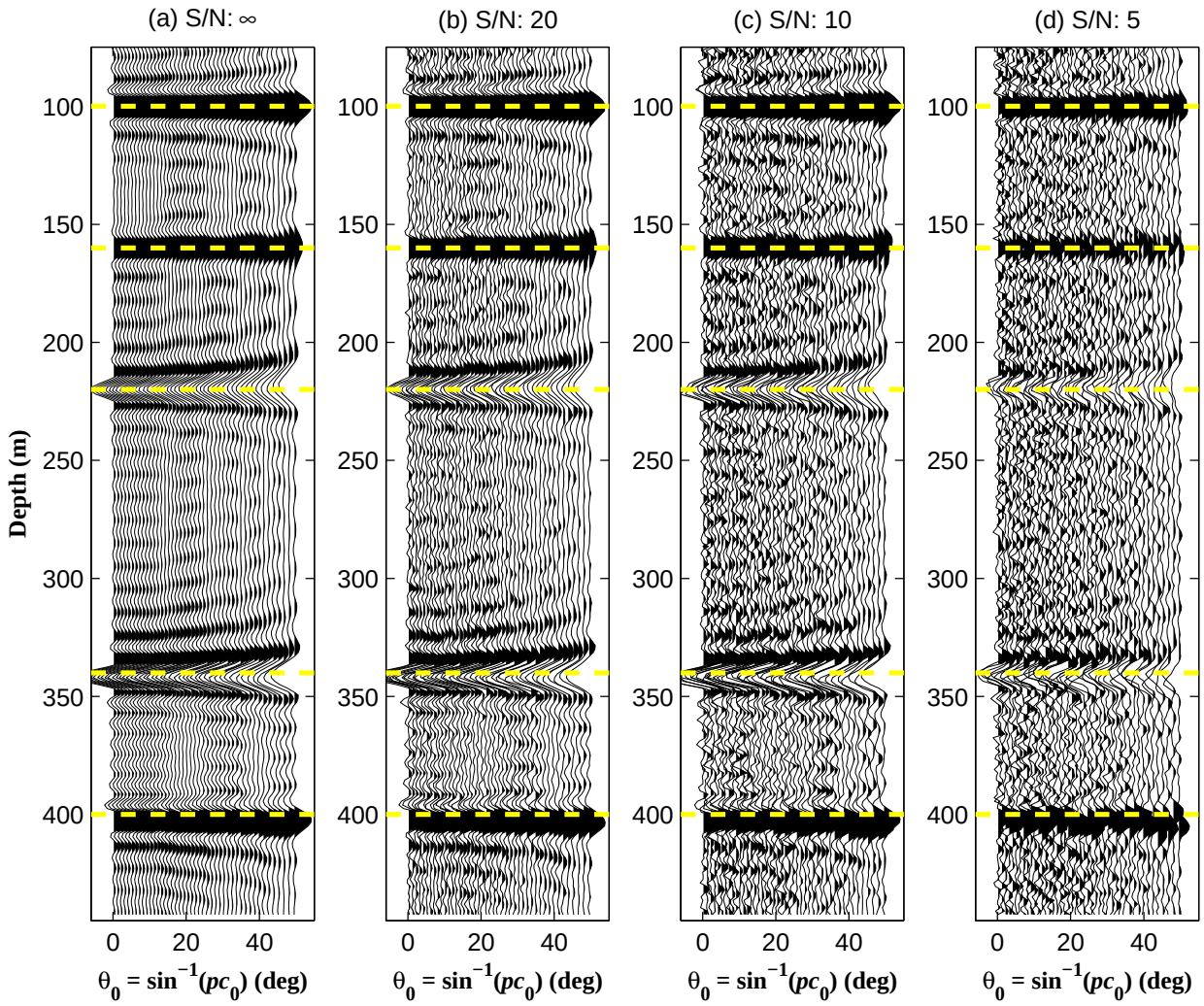

Figure 9: *Data in Fig. 7 imaged using the leading order imaging series after being contaminated with various amounts of random noise. Signal-to-noise ratios are displayed at the top of each panel. The depth derivatives of* α^{LOIS} *are displayed. The dashed yellow lines indicate the actual depths of the reflectors.*

Inverse scattering series for vertically and laterally varying media: application to velocity independent depth imaging

Fang Liu, Arthur B. Weglein, Kristopher A. Innanen and Bogdan G. Nita

Abstract

In this paper we consider the portion of the inverse scattering series, as applied to seismic reflection data, that is responsible for imaging, with emphasis on the structures of the imaging algorithms associated with a laterally varying earth. We approach the problem by analyzing the simplest possible multidimensional case: a single-parameter acoustic medium that varies both laterally and in depth. Manipulation and solution of inverse scattering series terms, for the above actual medium and using a homogeneous acoustic reference medium, leads to expressions for imaging in 2D media independent of the actual velocity model. Portions of the subseries are expressed as interpretable closed-form subsets of the full non-linear multidimensional reflector location machine. These portions are describable as being: (1) leading- and/or high-order in terms of response to medium contrast, (2) high-order in terms of correction in the depth coordinate, and (3) low-order in terms of correction of the lateral coordinate. Numerical tests on models that vary smoothly in the lateral coordinate are illustrated and discussed as providing growing evidence of the efficacy of multidimensional imaging capability of the inverse scattering series.

1 Introduction

The inverse scattering series is a comprehensive theory for the estimation of Earth medium parameters from reflected wave field measurements, with the capability for individual achievement of many externally-defined processing objectives, each without the traditional need for subsurface information. Velocity-independent algorithms have been derived from the inverse scattering series for free-surface multiple removal, internal multiple attenuation, imaging or reflector location, and parameter inversion or target identification (Weglein et al., 2003). Freedom from the requirement for an adequate velocity model is attractive especially for cases involving complex media, or, alternatively, media underlying complex boundaries. In this paper, we focus on aspects of this theory as it pertains to imaging in a laterally- and vertically-varying medium.

We begin with a word on the context of the research. Tasks and issues associated with structural determination, without knowing the medium, differ vastly depending on, for instance, the dimension-of-variation and number of velocities that are required for imaging. Hence, a staged approach and isolation-of-tasks philosophy is essential. We begin by, first, acquiring insight into the mechanisms of an algorithm, and then developing practical algorithms that incorporate more complete models.

Our non-linear methods engage the data in what we often refer to as inter-event communication – conversations, as it were, that work to locate and invert for material property contrasts without prior medium information. The nature of these conversations as we currently cast them is variable

(see, for instance, Zhang and Weglein, 2005) depending on the model type. The conversations ascribed to, and utilized for, a single-parameter acoustic medium will therefore in principle differ from those expected by elastic data. Many similarities and repetitions of mathematical patterns have been found to occur, however.

This means we benefit from a staged, isolationist means of developing these non-linear methods for processing primaries, that individually reveals elements of the complexity of the full problem. The stages for primaries include (1) a 1D earth with one parameter (typically velocity) as a function of depth, and a normal incidence wave; (2) a 1D earth with one parameter subsurface and multi-offset data, i.e., one shot record; (3) a 2D earth with one parameter, velocity, varying in x and z, and a suite of shot records; (4) a 1D acoustic earth with two parameters varying, velocity and density, one propagation velocity, and one shot record of PP data, and (5) a 1D elastic earth, two elastic isotropic parameters and density, and two wave speeds, for p and s waves, and multi-component acquisition corresponding to PP, PS, SP, and SS shot record data collected. Some of these tasks will be recognizable as being in our history; some of them are discussed in the present report. Within this framework the current paper of course is involved with (3). The lessons gleaned will lead to increased numeric tests and carefully-chosen field data tests; it is worth emphasizing beyond this, however, that a future synthesis of these individual lessons is a major goal.

To work towards understanding this aspect of non-linear imaging, i.e., the mechanisms of 2D reflector correction, we build on the work of Shaw et al. (2004) and Shaw (2005). They have brought the analysis and development of the leading order imaging subseries for vertically-varying media through a set of steps culminating in an algorithm that has a startling mixture of power and simplicity. These steps are, loosely:

1. The explicit derivation (up to third-order), through integration-by-parts, of inverse scattering series terms specifically geared to reflector location.
2. The identification of patterns within these terms that leads to the postulate of the form of the n'th term in the leading order imaging subseries.
3. The summation of this infinite series to closed-form.

The terms responsible for imaging are also visible and available in the inverse scattering series for laterally- and vertically-varying perturbations (Liu et al., 2004); however, the mathematics is considerably more involved. We are currently at an intermediate stage in the process of developing the above steps. This paper reports on a way-point in that development, and details some of the similarities and differences from the purely vertically-varying case, and other complexities and opportunities that arise for a multi-D Earth. We derive, explicitly, portions of the second, third, and fourth order terms, and combine them via an interpretation of their behavior that arises from the lessons gleaned from the 1D case. Portions of these terms are demonstrated to sum to closed form.

Full (infinite) order syntheses of terms acting in the depth direction are combined and seen to form low-order terms acting in the lateral direction. We thus expect efficacy of these chosen terms on models that vary smoothly in the lateral direction; we demonstrate this numerically and comment on plans for expanding to rapidly-varying Earth models.

The body of this paper is short and straightforwardly organized. Sections 2–4 contain sequential presentations of the derived forms (full and/or partial) for the 2nd–3rd 1st–3rd order terms, of a wavespeed perturbation that is permitted variation in lateral and vertical coordinates. Section 5 describes the organization and summation of subsets of the previously derived terms; section 6 describes the processing flow from data to our illustrated and interpreted output. Although presented concisely in this paper, these derivations contain relatively involved mathematics; much of the detail is included (along with several useful notations and conventions) in an extensive set of appendices. Relevant appendices are referred to within the body of the paper.

2 Inversion results for α_1

The inverse scattering series as we intend to analyze it in this paper is an order-by-order prescription for the solution for the wavespeed perturbation in terms of a homogeneous acoustic reference medium and measurements of the scattered wave field on a measurement surface. Omitting derivation (see, for instance, Weglein et al., 2003), the requisite form of the series equations is

$$D(x_g,z_g,x_s,z_s,\omega)=\int_{-\infty}^{\infty}dz'\int_{-\infty}^{\infty}dx'G_0(x_g,z_g,x',z',\omega)V_1(x',z')G_0(x',z',x_s,z_s,\omega), \tag{1}$$

at first order,

$$\begin{aligned}0=&\int_{-\infty}^{\infty}dz'\int_{-\infty}^{\infty}dx'G_0(x_g,z_g,x',z',\omega)V_2(x',z')G_0(x',z',x_s,z_s,\omega)\\&+\int_{-\infty}^{\infty}dz'\int_{-\infty}^{\infty}dx'G_0(x_g,z_g,x',z',\omega)V_1(x',z')\\&\times\int_{-\infty}^{\infty}dz''\int_{-\infty}^{\infty}dx''G_0(x',z',x'',z'',\omega)V_1(x'',z'')G_0(x'',z'',x_s,z_s,\omega),\end{aligned} \tag{2}$$

at second order,

$$\begin{aligned}0=&\int_{-\infty}^{\infty}dz'\int_{-\infty}^{\infty}dx'G_0(x_g,z_g,x',z',\omega)V_3(x',z')G_0(x',z',x_s,z_s,\omega)\\&+\int_{-\infty}^{\infty}dz'\int_{-\infty}^{\infty}dx'G_0(x_g,z_g,x',z',\omega)V_1(x',z')\\&\times\int_{-\infty}^{\infty}dz''\int_{-\infty}^{\infty}dx''G_0(x',z',x'',z'',\omega)V_2(x'',z'')G_0(x'',z'',x_s,z_s,\omega)\\&+\int_{-\infty}^{\infty}dz'\int_{-\infty}^{\infty}dx'G_0(x_g,z_g,x',z',\omega)V_2(x',z')\\&\times\int_{-\infty}^{\infty}dz''\int_{-\infty}^{\infty}dx''G_0(x',z',x'',z'',\omega)V_1(x'',z'')G_0(x'',z'',x_s,z_s,\omega)\\&+\int_{-\infty}^{\infty}dz'\int_{-\infty}^{\infty}dx'G_0(x_g,z_g,x',z',\omega)V_1(x',z')\\&\times\int_{-\infty}^{\infty}dz''\int_{-\infty}^{\infty}dx''G_0(x',z',x'',z'',\omega)V_1(x'',z'')\\&\times\int_{-\infty}^{\infty}dz'''\int_{-\infty}^{\infty}dx'''G_0(x'',z'',x''',z''',\omega)V_1(x''',z''')G_0(x''',z''',x_s,z_s,\omega),\end{aligned} \tag{3}$$

at third order, etc., in which

$$V_n(x,z) = \frac{\omega^2}{c_0^2}\alpha_n(x,z), \tag{4}$$

and $\alpha_n(x,z)$ is the n'th order component of the wavespeed perturbation $\alpha(x,z) = \sum_n \alpha_n(x,z)$, whose reconstruction is the aim of the inverse scattering series. This definition of the perturbation V corresponds to the single-parameter acoustic framework involving wavespeed variations only.

The linear term α_1 may be solved from data:

$$\widetilde{\widetilde{\alpha}}_1(k_m,k_z) = -\frac{4k_z^2}{k_z^2+k_m^2}\widetilde{\widetilde{D}}\left(\frac{k_m}{2},z_g,-\frac{k_m}{2},z_s,\omega\right). \tag{5}$$

where $\widetilde{\widetilde{D}}$ is the data in the frequency wave number domain. See Appendix C for a brief derivation, and a description of various ways of expressing the data D.

3 Inversion results for α_2

In the derivation of α_2 (see, for instance, Liu et al., 2004), begins to arise some of the complexity characteristic of this multidimensional Earth problem. As in the case of the linear term, in this section we merely present the result, referring those interested to Appendix D for a complete analysis. (See also Appendix B for an introduction to the derivation and analytical strategy used.) The second-order term α_2 is computed using α_1 via equation (69). In the final result, α_2 is split into 3 parts: $\alpha_2 = \alpha_{2,1} + \alpha_{2,2} + \alpha_{2,3}$. The first two terms are expressed in the (x,z) domain as

$$\alpha_{2,1}(x,z) = -\frac{1}{2}\alpha_1^2(x,z) - \frac{1}{2}\frac{\partial\alpha_1(x,z)}{\partial z}\int_{-\infty}^{z}\alpha_1(x,u)du, \tag{6}$$

and

$$\alpha_{2,2}(x,z) = \frac{1}{2}\frac{\partial\alpha_1(x,z)}{\partial x}\int_{-\infty}^{z}du\int_{-\infty}^{u}dv\frac{\partial\alpha_1(x,v)}{\partial x}. \tag{7}$$

Equation (6) is identical to the α_2 equation obtained by Shaw et al. (2004). From a mechanical point of view, we recall from Shaw's interpretation that the presence in the inverse scattering series of the weighted n'th partial derivative of α_1 with respect to z was indicative of the n'th term in a series to correct the location of a reflector in depth. In equation (6) we clearly see this z-corrective behavior in the multidimensional case also. What appears in this analysis for the first time is a weighted first partial derivative with respect to x, in equation (7). We regard this term, being a low order derivative with respect to the lateral coordinate of α_1, as a low order term in the construction of laterally corrective function. It is intriguing to note that the coefficient of this lateral corrector involves *depth* integrals, over z.

The last term is expressed in the (k_m, z) domain:

$$\widetilde{\alpha}_{2,3}(k_m,z) = \frac{1}{8\pi^2}\int_{-\infty}^{\infty} dk_1 \int_{-\infty}^{\infty} dz_1 \widetilde{\alpha}_1\left(0.5k_m - k_1, z_1\right) \int_{-\infty}^{z_1} dz_2 \widetilde{\alpha}_1\left(k_1 + 0,5k_m, z_2\right) \times \widetilde{\xi}_2\left(k_m, k_1, \frac{z_1+z_2}{2} - z, \frac{z_1 - z_2}{2}\right), \tag{8}$$

where $\widetilde{\xi}_2$ is defined as follows:

$$\widetilde{\xi}_2\left(k_m, k_1, \varepsilon_0, \varepsilon_1\right) = \int_{-\infty}^{\infty} e^{i(\varepsilon_0+\varepsilon_1)k_z} dk_z \left(i\frac{k_z^2 + k_m^2}{u_1} e^{i\triangle\psi} - ik_z + \frac{\varepsilon_1 a_1}{2}\right)$$
$$a_1 = k_m^2 - 4k_1^2 \qquad u_1 = \mathtt{sgn}(k_z)\sqrt{k_z^2 + a_1} \qquad \triangle\psi = \varepsilon_1(u_1 - k_z), \tag{9}$$

and is considered to be involved in coupled tasks (c.f. Innanen, 2003). We focus on separated imaging tasks in this paper.

4 Inversion results for α_3

Considerably more terms are present in α_3 (the third order term in the inverse scattering series). Merging and regrouping the terms derived in in equation (117) and (119), we may write the third order single-parameter inverse as $\alpha_3 = \alpha_{3,1} + \alpha_{3,2} + \alpha_{3,3} + \alpha_{3,4}$. The first three terms are expressible in the (x, z) domain as:

$$\alpha_{3,1}(x,z) = \frac{3}{16}\alpha_1^3 + \frac{1}{8}\frac{\partial^2\alpha_1}{\partial z^2}\left(\int_{-\infty}^{z}\alpha_1(x,u)du\right)^2 + \frac{3}{4}\frac{\partial\alpha_1}{\partial z}\alpha_1\int_{-\infty}^{z}\alpha_1(x,u)du$$
$$-\frac{1}{8}\frac{\partial\alpha_1}{\partial z}\int_{-\infty}^{z}\alpha_1^2(x,u)du - \frac{1}{16}\int_{-\infty}^{z}du\int_{-\infty}^{z}dv\frac{\partial\alpha_1(x,u)}{\partial u}\frac{\partial\alpha_1(x,v)}{\partial v}\alpha_1(u+v-z), \tag{10}$$

$$\alpha_{3,2}(x,z) = -\frac{1}{4}\frac{\partial}{\partial x}\left(\alpha_1^2 + \frac{\partial \alpha_1}{\partial z}\int_{-\infty}^{z}\alpha_1(x,u)du\right)F(x,z)$$
$$+\frac{1}{8}\frac{\partial \alpha_1}{\partial x}\frac{\partial}{\partial x}\int_{-\infty}^{z}du\int_{-\infty}^{u}dv\alpha_1^2(x,v) + \frac{1}{8}\frac{\partial \alpha_1}{\partial z}\int_{-\infty}^{z}du\left(\int_{-\infty}^{u}dv\frac{\partial \alpha_1(x,v)}{\partial x}\right)^2$$
$$+\frac{1}{4}\alpha_1(x,z)\left(\int_{-\infty}^{z}du\frac{\partial \alpha_1(x,u)}{\partial x}\right)^2 + \frac{1}{4}\frac{\partial \alpha_1}{\partial x}\int_{-\infty}^{z}du\left(\frac{\partial \alpha_1(x,u)}{\partial x}\int_{-\infty}^{u}dv\alpha_1(x,v)\right)$$
$$+\frac{1}{4}\frac{\partial^2 \alpha_1(x,z)}{\partial x^2}\left(\int_{-\infty}^{z}\alpha_1(x,u)du\right)^2 + \frac{1}{2}\alpha_1(x,z)\left(\int_{-\infty}^{z}du\alpha_1(x,u)\right)\frac{\partial^2}{\partial x^2}\left(\int_{-\infty}^{z}du\alpha_1(x,u)\right)$$
$$+\frac{1}{16}\int_{-\infty}^{z}du\frac{\partial \alpha_1(x,u)}{\partial x}\frac{\partial}{\partial x}\int_{-\infty}^{z}dv(z-v)\alpha_1(x,v)\alpha_1(u+v-z)$$
$$+\frac{1}{4}\int_{-\infty}^{z}du\frac{\partial \alpha_1(x,u)}{\partial x}\frac{\partial^2}{\partial x^2}\int_{-\infty}^{z}dv\alpha_1(x,v)\alpha_1(x,u+v-z)$$

and

$$
\begin{aligned}
\alpha_{3,3}(x,z) = &-\frac{1}{32}\frac{\partial^2\alpha_1(x,z)}{\partial x^2}\int_{-\infty}^{z} du \int_{-\infty}^{u} dv \frac{\partial^2}{\partial x^2}\left(\int_{-\infty}^{v} dw \alpha_1(x,w)\right)^2 + \frac{1}{32}\alpha_1(x,z)\left(\frac{\partial F(x,z)}{\partial x}\right)^2 \\
&- \frac{1}{8}\left(\int_{-\infty}^{z} du \frac{\partial F(x,u)}{\partial x}\right)\frac{\partial^2}{\partial x^2}\left(\alpha_1(x,z)\int_{-\infty}^{z} du \alpha_1(x,u)\right) \\
&+ \frac{1}{8}\frac{\partial\alpha_1(x,z)}{\partial x}\int_{-\infty}^{z} du\left[\frac{\partial F(x,u)}{\partial x}\int_{-\infty}^{z} dv \frac{\partial\alpha_1(x,v)}{\partial x}\right] \\
&+ \frac{1}{16}\frac{\partial^2\alpha_1(x,z)}{\partial x^2}\int_{-\infty}^{z} du\left(\left(\int_{-\infty}^{u} dv \alpha_1(x,v)\right)\frac{\partial F(x,z)}{\partial x}\right) \\
&+ \frac{1}{8}\frac{\partial}{\partial x}\left(\frac{\partial\alpha_1}{\partial x}F^2(x,z)\right) - \frac{1}{8}\frac{\partial\alpha_1}{\partial x}\frac{\partial}{\partial x}\int_{-\infty}^{z} du \int_{-\infty}^{u} dv\left\{\int_{-\infty}^{v} dw \frac{\partial\alpha_1(x,w)}{\partial x}\right\}^2 \\
&- \frac{1}{16}\alpha_1(x,z)\left\{\frac{\partial F(x,z)}{\partial x}\right\}^2 - \frac{1}{8}\frac{\partial^2\alpha_1(x,z)}{\partial x^2}\int_{-\infty}^{z} du\left\{\int_{-\infty}^{u} dv \alpha_1(x,v)\right\}\frac{\partial F(x,u)}{\partial x} \\
&+ \frac{1}{16}\frac{\partial^2\alpha_1(x,z)}{\partial x^2}\frac{\partial^2}{\partial x^2}\int_{-\infty}^{z} du \int_{-\infty}^{u} dv\left(\int_{-\infty}^{v} dw \alpha_1(x,w)\right)^2 \\
&- \frac{1}{16}\int_{-\infty}^{z} du \frac{\partial^2\alpha_1(x,u)}{\partial x^2}\frac{\partial^2}{\partial x^2}\int_{-\infty}^{z} dv (z-v)\alpha_1(x,v)\alpha_1(x,u+v-z) \\
&+ \frac{1}{16}\int_{-\infty}^{z} du (z-u)\frac{\partial\alpha_1^2(x,u)}{\partial x^2}\frac{\partial}{\partial x}\int_{-\infty}^{z} dv (z-v)\frac{\partial\alpha_1(x,v)}{\partial x}\alpha_1(x,u+v-z) \\
&+ \frac{1}{16}\int_{-\infty}^{z} du (z-u)\frac{\partial\alpha_1(u)}{\partial x}\frac{\partial}{\partial x}\int_{-\infty}^{z} dv (z-v)C(v)\frac{\partial\alpha_1(x,u+v-z)}{\partial x}
\end{aligned}
$$

where

$$
F(x,z) = \int_{-\infty}^{z} du \int_{-\infty}^{u} dv \frac{\partial\alpha_1(x,v)}{dx} dv. \tag{11}
$$

The complexity of the third order terms has clearly and not unexpectedly been enhanced with the addition of a lateral dimension to the variability of the perturbation. Nevertheless, the lessons of the 1D case lend an interpretability to them in particular with respect to reflector location. First, as with the second order case, an exact reproduction of all the 1D terms (i.e. alterations with respect to depth z) has occurred in $\alpha_{3,1}$. This suggests, as we further develop in the following

section, that the 1D inverse scattering series terms carry over to the 2D case; the depth-direction imaging and inversion terms behave, in other words, as the zero'th order part of an infinite series for the lateral correction of the linear model.

The third-order terms appear as first- and second-derivatives of α_1 and more complex quantities with respect to both x and z. The operations (e.g. "n'th derivative of α_1 times n'th power of the integral of α_1") that have led to imaging (or reflector location) behavior in 1D recur, but the quantities being operated on are of greater complexity. In Appendix A of Innanen (2005), it is noted that *locator-like operations acting on locator-like inputs* is characteristic of non leading-order imaging terms (whereas at leading-order terms are locator-like operations acting on the linear inverse). Here we see that they are also characteristic of higher dimensionality. In general, experience has shown that this is endemic of any subseries which we expect to involve cascaded infinite series (Shaw and Weglein, 2004).

Finally, in addition to imaging/inversion operations acting on subseries that involve α_1, rather than α_1 alone, we notice the appearance of cross-terms between derivatives in z and in x. Such terms will naturally be sensitive to coupling between the lateral and vertical rates of change in α_1, and work to alter locations as such.

The last third-order term is, as in the second order case, most conveniently expressed in the (k_m, z) domain:

$$\begin{aligned}\widetilde{\alpha}_{3,4}(k_m,z) =& \frac{1}{128\pi^3}\int_{-\infty}^{\infty}dk_1\int_{-\infty}^{\infty}dk_2\int_{-\infty}^{\infty}dz_1\int_{-\infty}^{\infty}dz_2\int_{-\infty}^{\infty}dz_3\widetilde{\alpha}_1(0.5k_m-k_1,z_1)\widetilde{\alpha}_1(k_1-k_2,z_2)\\ &\times\widetilde{\alpha}_1(k_2+0.5k_m,z_2)\widetilde{\xi}_3\left(k_m,k_1,k_2,\frac{z_1+z_3}{2}-z,\frac{|z_1-z_2|}{2},\frac{|z_2-z_3|}{2}\right)\\ &+\frac{1}{8\pi^2}\int_{-\infty}^{\infty}dk_1\int_{-\infty}^{\infty}dz_1\widetilde{\alpha}_2\left(0.5k_m-k_1,z_1\right)\int_{-\infty}^{\infty}dz_2\widetilde{\alpha}_1\left(k_1+0,5k_m,z_2\right)\\ &\times\widetilde{\xi}_2\left(k_m,k_1,\frac{z_1+z_2}{2}-z,\frac{|z_1-z_2|}{2}\right),\end{aligned} \tag{12}$$

where $\widetilde{\xi}_3$ is defined as:

$$\begin{aligned}&\widetilde{\xi}_3\left(k_m,k_1,k_2,\varepsilon_0,\varepsilon_1,\varepsilon_2\right)=\int_{-\infty}^{\infty}dk_z e^{ik_z(\varepsilon_0+\varepsilon_1+\varepsilon_2)}\times\\ &\left(\frac{\left(k_z^2+k_m^2\right)e^{i\triangle\psi}}{u_1u_2}-k_z^2-i\frac{\varepsilon_1a_1+\varepsilon_2a_2}{2}k_z-\left(k_m^2+2\left(k_1^2+k_2^2\right)^2-\frac{\left(\varepsilon_1a_1+\varepsilon_2a_2\right)^2}{8}\right)\right)\\ &a_1=k_m^2-4k_1^2\qquad a_2=k_m^2-4k_2^2\\ &u_1=\mathtt{sgn}(k_z)\sqrt{k_z^2+a_1}\qquad u_2=\mathtt{sgn}(k_z)\sqrt{k_z^2+a_2}\\ &\triangle\psi=\varepsilon_1(u_1-k_z)+\varepsilon_2(u_2-k_z)\end{aligned} \tag{13}$$

and $\widetilde{\xi}_2$ had already been defined in equation (9). We again tentatively ascribe mixed imaging/inversion tasks to this term and focus instead on its brethren.

5 Patterns and closed-forms

In this section we accumulate sets of terms that have aggregate meaning in light of our understanding of the 1D imaging subseries. We have stated above that, for instance, there is a complete recurrence of the depth-sensitive terms found in the 1D/1.5D analysis (discussed by Shaw et al., 2004).

Generally our approach has been to explicitly manipulate and compute terms in the inverse scattering series until patterns emerge that permit the prediction of certain subclasses of subsequent series terms. In Appendix G we present a component of the fourth order terms of the series; at present however, with second and third order components of α computed, there is sufficient information to identify and move forward with a set of patterns. Here we itemize these patterns and the closed-forms that result:

A closed form for the 0'th order lateral corrector

In both α_2 and α_3 inversion results appear terms (see equation (6) and (10)) that are in essence identical to expressions obtained under the 1D earth assumption (the only difference is an extra lateral variable x). As a result, not only may we write down the n'th term of what we refer to as the "most significant" part of the multidimensional imaging subseries, we may also write down a closed-form version of it:

$$\alpha^{LOIS}(x,z) = \alpha_1 \left(x, z - \frac{1}{2} \int_{-\infty}^{z} \alpha_1(x,u) du \right) \tag{14}$$

The first- and higher-order lateral corrector terms (involving lateral derivatives as discussed above), when collapsed in the correct way may be added to this term.

A closed form for part of the 1st order lateral corrector

We demonstrate the basic form of these to-be-added lateral correction terms with a look at the first order, i.e. those terms that involve first derivatives of α_1 with respect to x. Notice that $\alpha_{2,2}$ in equation (7) and the first term in $\alpha_{3,2}$ involve a depth integral of the lateral rate of change of α_1, multiplied by the first derivative (w.r.t. x) of a growing set of terms akin to the 1D depth imaging series. Using our experience with the 1D imaging mechanisms, we consider that such a weighted first derivative of α_1 with respect to x constitutes a first-order lateral correction. Calling the (growing) set of depth terms under the derivative $A(x,z)$, a lateral corrector of the form

$$\frac{1}{2} \frac{\partial A(x,z)}{\partial x} \int_{-\infty}^{z} du \int_{-\infty}^{v} dv \frac{\partial \alpha_1(x,v)}{\partial x}$$

is produced. We continue to analyze and incorporate terms involving higher-derivatives in the lateral coordinate.

Incorporating non-LOIS imaging components

The leading order imaging subseries is (as its name implies) not the full imaging subseries. There are higher order terms left out, whose absence will be marked at large contrasts. Innanen (2005) works to accommodate higher order imaging and inversion terms by designing generating functions that cast a wider net for terms that operate on primaries. Consider the 1D leading order imaging subseries:

$$\sum_{n=0}^{\infty} \frac{(-1/2)^n}{n!} \frac{d^n \alpha_1(z)}{dz^n} \left(\int_{-\infty}^{z} du \alpha_1(u) \right)^n .$$

The first step to higher-order imaging as such is to incorporate terms like $-\frac{1}{8}\frac{d\alpha_1(z)}{dz}\int_{-\infty}^{z} du\alpha_1^2(u)$ (in α_3). The higher-order imaging subseries including these kinds of terms is:

$$\alpha_1 \left(z - \frac{1}{2} \int_{-\infty}^{z} du \frac{\alpha_1(u)}{1 - \frac{1}{4}\alpha_1(u)} \right). \tag{15}$$

This arises from a summation of terms that involve increasing powers of α_1 under the integrals for the series coefficients.

Avoiding amplitude-related components at high-order

The work of Innanen (2005) incorporates higher order imaging terms, inversion (amplitude) terms, and mixed-task elements. It is, in general, less straightforward to uncouple imaging (reflector location) tasks from inversion (amplitude) tasks at high order, however. We present a means to separate tasks under these conditions; the numerical examples shown below utilize these forms. To achieve high-order imaging only (not both imaging and inversion), it turns out that the integral in equation (15) should be computed up to the location of the incorrect reflector, not the correct reflector. In other words (and somewhat glibly), we must operate in the domain of the input variable and not the output variable. We implement the formula

$$\alpha^{HOIS} \left(z + \frac{1}{2} \int_{-\infty}^{z} du \frac{\alpha_1(u)}{1 - \frac{1}{4}\alpha_1(u)} \right) = \alpha_1(z),$$

to this end.

6 Processing flow and numerical examples

In this section we present numerical tests on progressively complicated geological models. The major input to our algorithms are shot gathers with direct arrivals being removed, just like the input data in current exploration. In our current implementation, we use the portion of data corresponding to $k_h = 0$ so, in the computation of the linear inverse directly from the data (with a homogeneous reference medium), the Fourier transform over x_h is actually summing all the traces

with the same mid-point together. This step is described in equation (41) in Appendix A, but other choices (other than $k_h = 0$) are, of course, possible. The linear inverse, computed as above from the data and some specified removal of the data-redundancy, is then the input to all further second-order operations, third-order operations, and beyond.

A fourth-order finite difference scheme is used to generate all the synthetic data for these examples. First we generate the direct arrival using a homogeneous medium characterized by water speed, to be used later to remove the direct arrivals for all shot gathers.

In our numerical examples, the source wavelet is the first derivative of Gaussian with peak frequency about 28 Hz, the sampling interval in x is $\triangle x = 5$m, and the temporal sampling rate is $\triangle t = 2$ms. Although the theory requires removal of the source wavelet, experience (as described in M-OSRP03) has shown that the imaging algorithm is relatively insensitive to the presence of a wavelet of this particular form. We therefore continue to use it for the sake of convenience. In using the closed forms derived herein, data values away from the regular data grid are required. Our current implementation uses Fourier methods for off-grid interpolation.

Figures 1–2 illustrate the geological models under numeric study, in order of increasing 2D complexity and contrast. The models are designed to be horizontal at their lateral extremities, and to undergo smooth variation within. We have designed the models to include horizontal interfaces below the dipping interfaces so that the goal (correctly locating the horizontal reflectors) and erroneous deviations from this goal are easy to see. Figures 3–4 illustrate two typical shot gathers created synthetically from the given models, and used as inputs to create $\alpha_1(x, z)$, as described above.

Figures 5–6 illustrate the various imaging results for model 1. On the left of figure 5 is the linear inverse given a homogeneous reference medium. The first reflector is at its correct location (correct locations are indicated in red); the second and third reflectors are mis-located, as the primary has propagated in a perturbed regime in the medium. Furthermore, the right extremity of these reflectors are "pulled up", because they experience the high velocity zone to a greater extent. The errors are not large, since the perturbations (deviations of the actual medium from the reference) are kept relatively small. On the right is the 2D leading-order imaging subseries (LOIS), which is equivalent to Shaw et al. (2004) in the depth-coordinate, and utilizes low-order corrective mechanisms in the lateral-coordinate. The left and right sides of figure 6 compare the leading order (LOIS) and higher-order/large contrast (HOIS) imaging algorithms; little difference is noted at these levels of contrast. Both effectively correct the errors of the locations of the reflectors that are due to smooth lateral-variability of the model.

Figures 7–8 illustrate similarly the various imaging results for model 2. Here, because of the large contrasts involved, the linear inverse α_1 assuming a homogeneous reference medium contains marked location errors (correct locations are again overlain in red). Although it is an improvement over linear imaging, the leading-order imaging series (LOIS) cannot accommodate these levels of contrast and also can be seen to contain location errors. The high-order/large contrast version of the algorithm handles the contrasts well, and a result close to the actual depths is generated.

Imaging algorithms that accommodate different levels of contrast in discontinuities in depth of the Earth model, but are low-order approximations in their capacity as correctors of lateral location, are here clearly demonstrated to operate with efficacy when the lateral variability of the model is smooth. We expect these low-lateral-order approximations to require extension as the models we implement them with vary more rapidly in x.

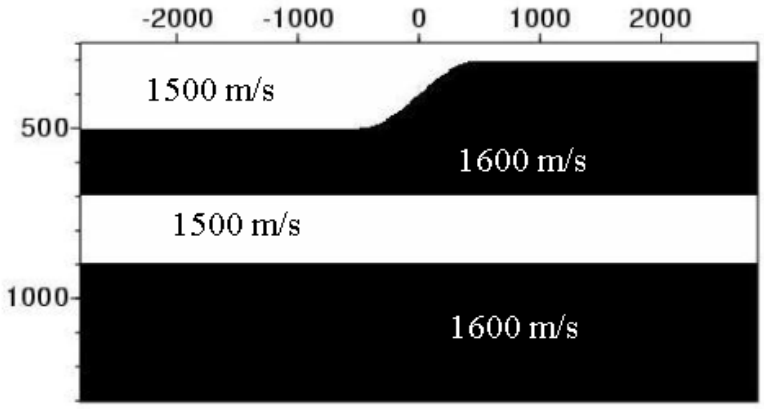

Figure 1: *Velocity model 1.*

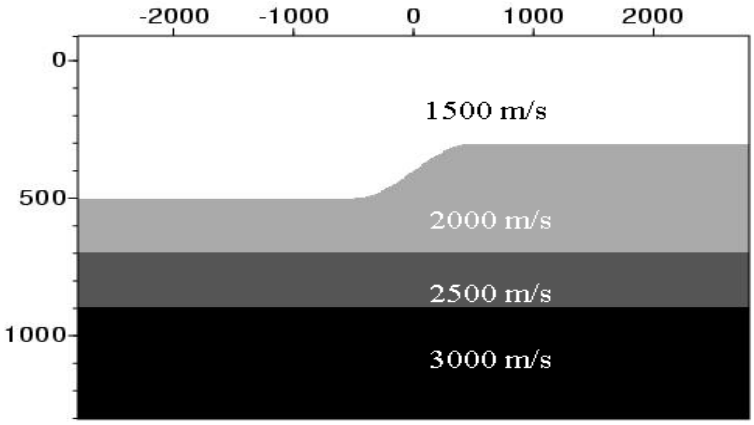

Figure 2: *Velocity model 2.*

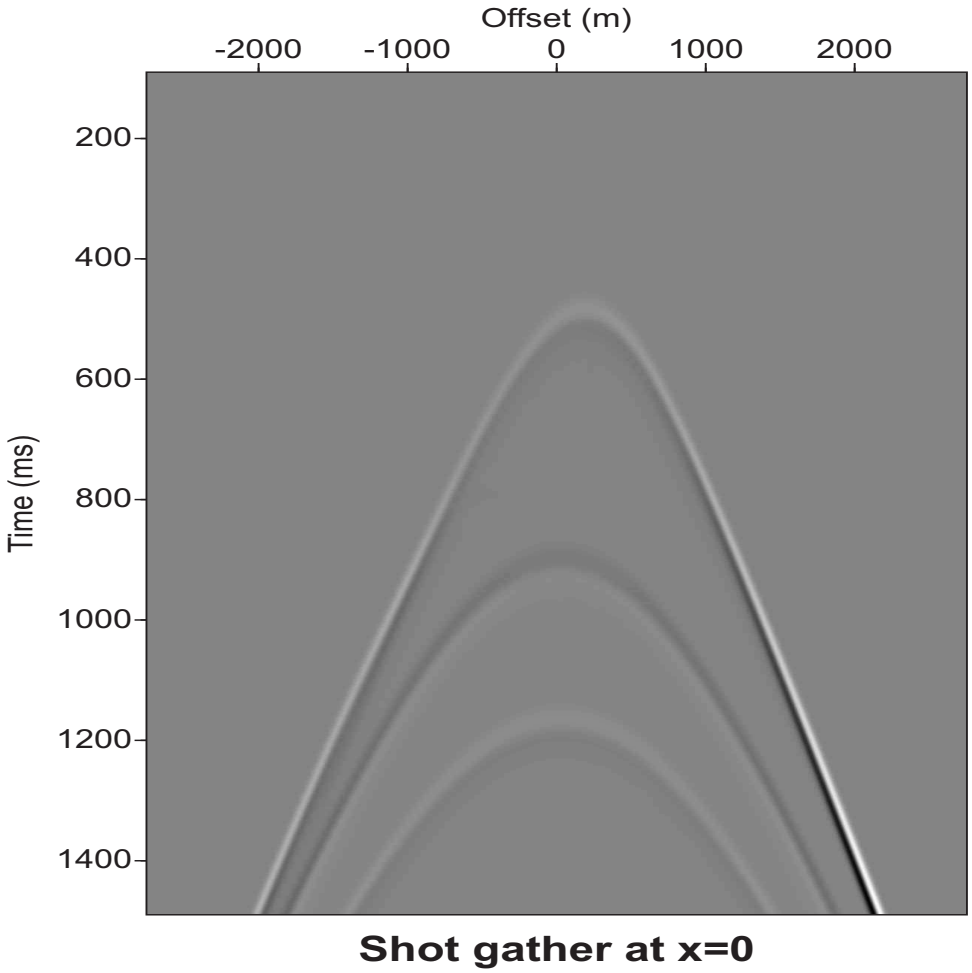

Figure 3: *A typical shot gather collected for Model 1 (the direct arrival has been removed).*

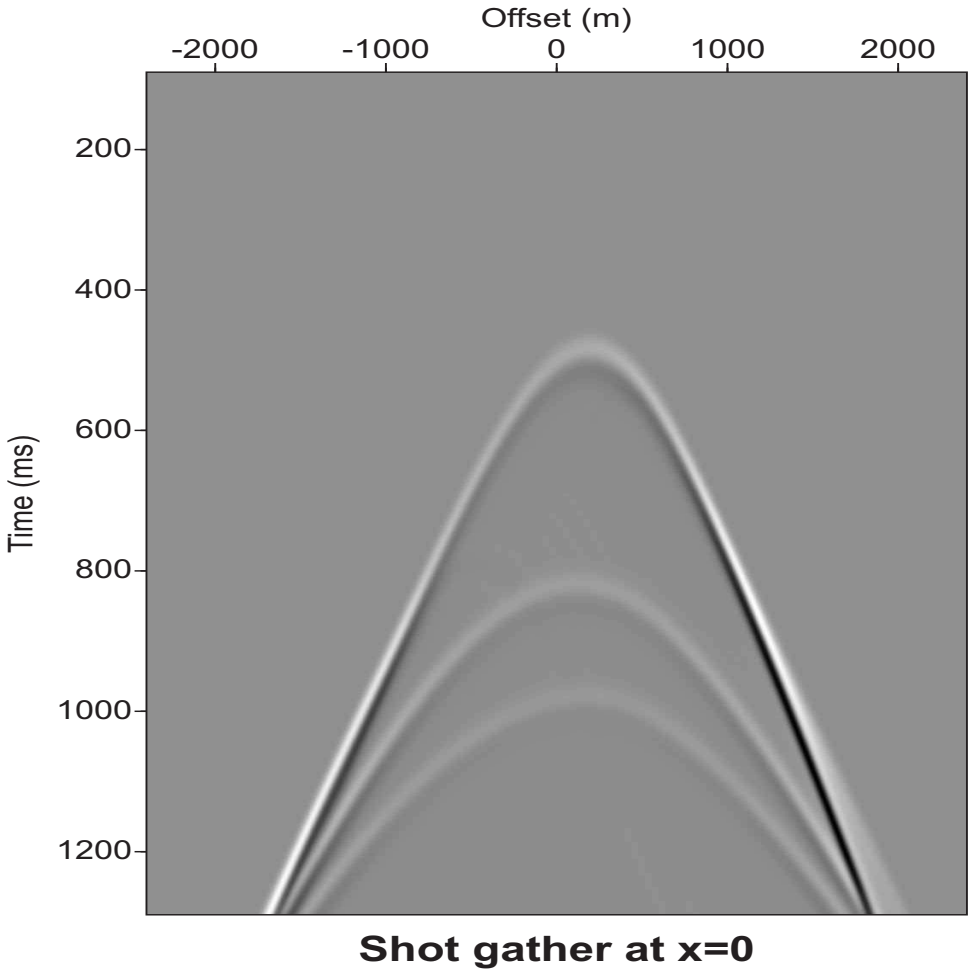

Figure 4: *A typical shot gather collected for the Model 2 (the direct arrival has been removed).*

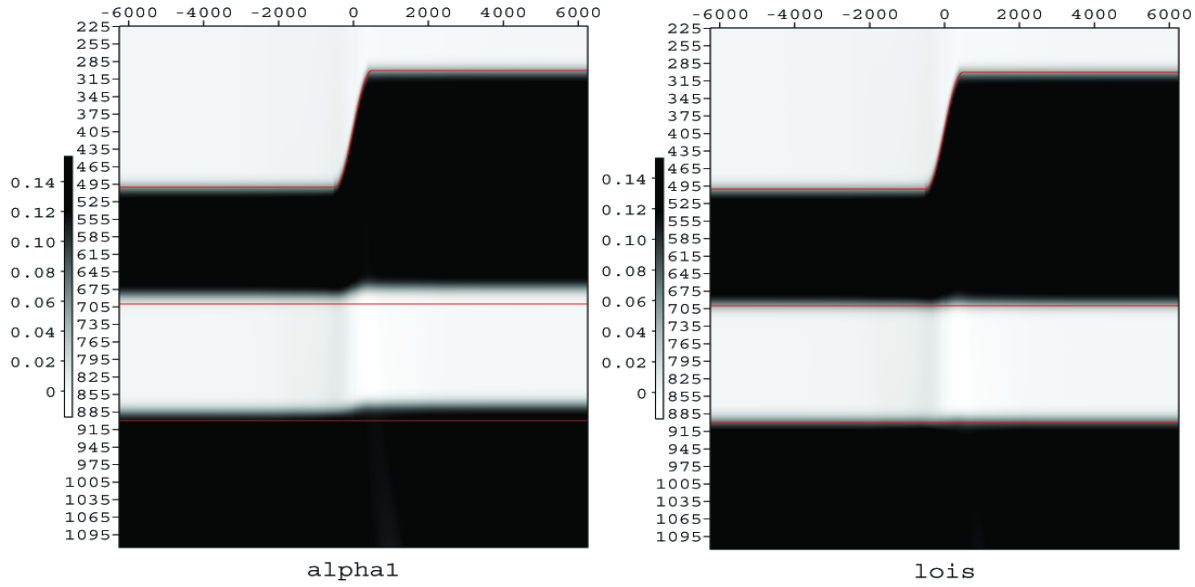

Figure 5: *Model 1 leading-order imaging results: (left) the linear inverse; (right) leading-order imaging subseries with low-order lateral correction.*

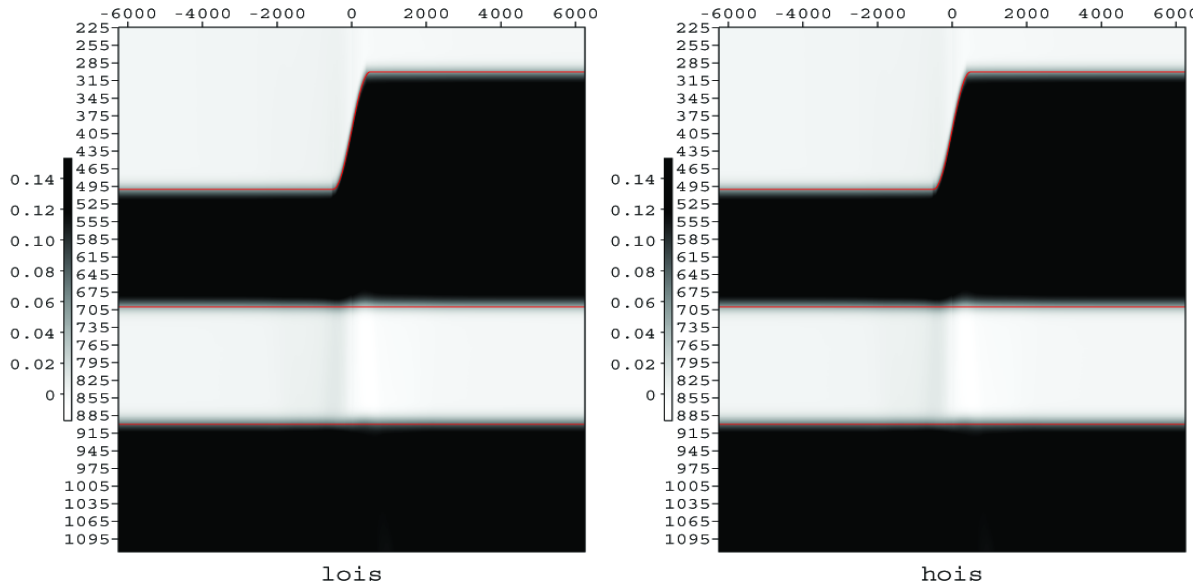

Figure 6: *Model 1 high-order imaging results: (left) the leading-order correction; (right) the high-order correction.*

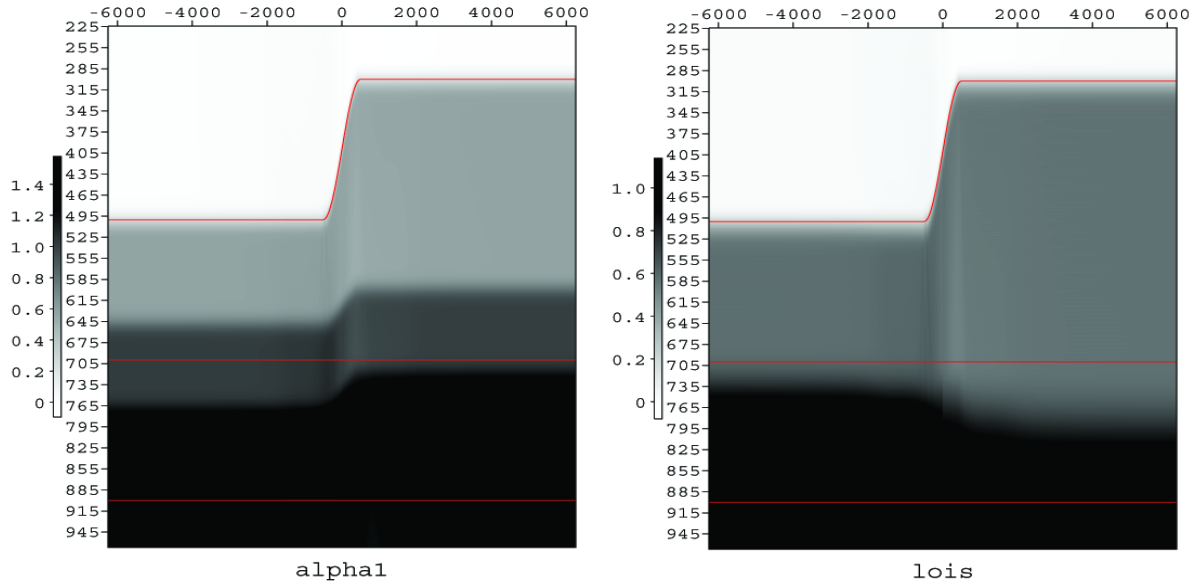

Figure 7: *Model 2 leading-order imaging results: (left) the linear inverse; (right) leading-order imaging subseries with low-order lateral correction.*

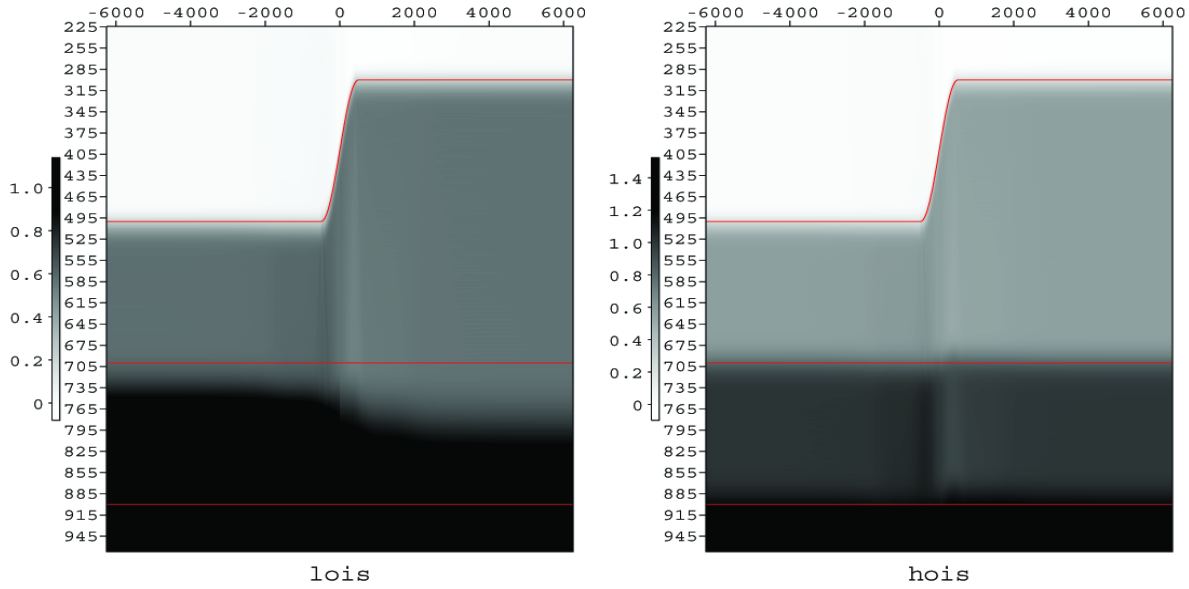

Figure 8: *Model 2 high-order imaging results: (left) the leading-order correction; (right) the high-order correction.*

7 Conclusions

We present a formalism for the nonlinear imaging and inversion of 2D wave field data over a medium with vertically and laterally varying parameters. The development is motivated by, and follows closely, the co-development of 1D (depth-varying) methods. We further present a form of this second order algorithm that directly mirrors the purposeful casting of the terms as those which

correspond separately and exclusively to tasks of imaging and inversion. These can be seen to compare closely to their 1D brethren. Numerically we see encouraging results given an unknown overburden with lateral variation.

Acknowledgments

We thank the sponsors and members of M-OSRP, especially Simon Shaw and Einar Otnes for their discussion and commentary.

References

Clayton, R. W. and Stolt, R. H. "A Born-WKBJ Inversion Method for Acoustic Reflection Data." *Geophysics 46*, (1981):1559.

Innanen, K. A. "Methods for the Treatment of Acoustic and Absorptive/Dispersive Wave Field Measurements." *Ph.D. Thesis, University of British Columbia*, (2003).

Innanen, K. A. "Reflector location using high-order inverse scattering series terms." *M-OSRP 04 Annual Report*, (2005).

Liu, F., Nita, B. G., Weglein, A. B. and Innanen, K. A., "Inverse scattering series for laterally-varying media" *M-OSRP 03 Annual Report*, (2004).

Morse, P. M., Feshbach, H. (1953). "Methods of Theoretical Physics": *New York, McGraw-Hill Book Co., Inc*

Shaw, S. A., and Weglein, A. B., "A Leading Order Imaging Series for Prestack Data Acquired Over a Laterally Invariant Acoustic Medium." *M-OSRP 03 Annual Report*, (2004).

Shaw, S. A., "Some remarks on the leading order imaging series algorithm for depth imaging when the velocity model is unknown." *M-OSRP 04 Annual Report*, (2005).

Weglein, A. B., Foster, D. J., Matson, K. H., Shaw, S. A., Carvalho, P. M., and Corrigan, D. "Predicting the Correct Spatial Location of the Reflectors without Knowing or Determining the Precise Medium and Wave Velocity: Initial Concept, and Analytic and Numerical Example." *Journal of Seismic Exploration 10*, (2002):367–382.

Weglein, A. B., Araujo, F. A., Carvalho, P. M., Stolt, R. H., Matson, K. H., Coates, R., Foster, D. J., Shaw, S. A., and Zhang, H. "Topical Review: Inverse-scattering Series and Seismic Exploration." *Inverse Problems 19*, (2003):R27–R83.

Zhang, H., and Weglein, A. B. "Velocity independent depth imaging and non-linear direct target identification for 1D elastic media: testing and evaluation for application to non-linear AVO, using only PP data." *M-OSRP04 Annual Report*, (2005).

Appendix A: Notations and conventions

We use x and z to denote the lateral and vertical coordinates in space, respectively. t is used to denote the time. The Fourier conjugate of t is ω. The Fourier transform between x and its Fourier conjugate k_m is defined as:

$$\widetilde{f}(k_m) = \int_{-\infty}^{\infty} dx e^{-ik_m x} f(x) \qquad f(x) = \frac{1}{2\pi} \int_{-\infty}^{\infty} dk_m e^{ik_m x} \widetilde{f}(k_m) \tag{16}$$

The Fourier transform between z and its Fourier conjugate k_z is defined as:

$$\widetilde{f}(k_z) = \int_{-\infty}^{\infty} dz e^{ik_z z} f(z) \qquad f(z) = \frac{1}{2\pi} \int_{-\infty}^{\infty} dk_z e^{-ik_z z} \widetilde{f}(k_z) \tag{17}$$

We use the tilde sign on top of a function to denote its Fourier transform throughout this note. A single tilde sign means that this expression is in (k_m, z) domain, double tilde sign means that this expression is in (k_m, k_z). Because α_1 is a function of (x, z), time is not explicitly present in α_1 and higher order terms $\alpha_2, \alpha_3, \ldots$. The only place where time is involved is when α_1 is calculated from measured data, which is a function of time.

A very useful concept to simplify inverse scattering terms is the permutation sum. It will be defined as follows: For a function of 2 variables, like $f(A, B)$, we define the permutation sum $\sum^{\odot}$ as:

$$\begin{aligned} \sum^{\odot} f(A, A) &= f(A, A) \\ \sum^{\odot} f(A, B) &= f(A, B) \qquad A \neq B \end{aligned} \tag{18}$$

For a function of 3 variables, like $f(A, B, C)$, we define the permutation sum $\sum^{\odot}$ as (assuming A, B, C are mutually distinct):

$$\begin{aligned} \sum^{\odot} f(A, A, A) &= f(A, A, A) \\ \sum^{\odot} f(A, A, B) &= f(A, A, B) + f(A, B, A) + f(B, A, A) \\ \sum^{\odot} f(A, B, C) &= f(A, B, C) + f(B, C, A) + f(C, A, B) \\ &\quad + f(A, C, B) + f(B, A, C) + f(C, B, A) \end{aligned} \tag{19}$$

Lots of derivatives and integrals over x and z will be used in our manipulation of the inverse scattering series terms. The following notations are suggested for conciseness: $\alpha^{x} \overset{\text{def}}{=} \frac{\partial \alpha}{\partial x}$, $\alpha^{z} \overset{\text{def}}{=} \frac{\partial \alpha}{\partial z}$, $\alpha^{x+z} \overset{\text{def}}{=} \frac{\partial^2 \alpha}{\partial x \partial z}$, $\alpha^{-z} = \int_{-\infty}^{z} du \alpha(x, u)$, $\alpha^{-2z} = \int_{-\infty}^{z} du \int_{-\infty}^{u} dv \alpha(x, v)$. These notations allow us to simply express most of the integrals in the derivation while retaining our ability to make physical interpretations of the terms.

Using superscripts to denote derivatives will cause confusion with powers. That's why in many places in the derivation procedure, the square of A is often written as AA rather than A^2. If we

assume both A B, and C are functions of x and z, then $\frac{\partial(AB)}{\partial z} = \frac{\partial A}{\partial z}B + A\frac{\partial B}{\partial z}$ can be expressed in the short hand notation as:

$$[AB]^z = A^z B + AB^z. \tag{20}$$

Likewise $\frac{\partial(AB)}{\partial x} = \frac{\partial A}{\partial x}B + A\frac{\partial B}{\partial x}$ can be expressed as:

$$[AB]^x = A^x B + AB^x. \tag{21}$$

With integration by parts, we have the following identity:

$$\int_{-\infty}^{z} A(u)B(u)du = \left(\int_{-\infty}^{z} A(u)du\right) B(z) - \int_{-\infty}^{z} \left(\int_{-\infty}^{z} A(v)dv\right) B'(u)du,$$

which can be very conveniently expressed in the following short-hand notation:

$$[AB]^{-z} = A^{-z}B - \left[A^{-z}B^z\right]^{-z}. \tag{22}$$

Of course, there is another way to do the integration by parts: $\int_{-\infty}^{z} A(u)B(u)du = A(z)\left(\int_{-\infty}^{z} B(u)du\right) - \int_{-\infty}^{z} A'(u)\left(\int_{-\infty}^{z} B(v)dv\right)du$. This may be expressed as

$$[AB]^{-z} = AB^{-z} - \left[A^z B^{-z}\right]^{-z}. \tag{23}$$

A very useful equation is:

$$\left[A\left[A^{-z}\right]^m\right]^{-z} = \frac{1}{m+1}\left[A^{-z}\right]^{m+1}. \tag{24}$$

This means: $\int_{-\infty}^{z} A(u)\left(\int_{-\infty}^{u} A(v)dv\right)^m du = \frac{1}{m+1}\left(\int_{-\infty}^{z} A(u)du\right)^{m+1}$. It can be proved by carrying out the $\frac{\partial}{\partial z}$ operation on both sides, both the left- and right-hand-side will end up with: $A(z)\left(\int_{-\infty}^{z} A(u)du\right)^m$.

Another useful simplification of integrals is the following:

$$\left[AB^{-z}\right]^{-z} + \left[A^{-z}B\right]^{-z} = A^{-z}B^{-z} \tag{25}$$

which can be easily proved by taking the partial derivative over z on both sides.

Several popular rules for integration over δ-functions are summarized below:

$$\int_{-\infty}^{\infty} f(z)\delta(z - z_0) = f(z_0) \tag{26}$$

$$\int_{-\infty}^{\infty} f(z)\delta'(z - z_0) = -f'(z_0) \tag{27}$$

$$\int_{-\infty}^{\infty} f(z)\delta''(z-z_0) = f''(z_0) \tag{28}$$

Rules mentioned above will be used over and over again in the derivation process. In order to make clear which rule is used, we use the following notation:

$$\cdots = \overrightarrow{(28)} = \cdots$$

to denote that the simplification rule specified in equation (28) is being used to justify the equivalence between the left and right-hand sides.

Inevitably, some integrals cannot be expressed in the form above. For example, the integral in the third term that is responsible for internal multiple removal, we define some integral involved in the higher-lower-higher relation (W-diagram), which is instrumental in the internal multiple algorithm in the inverse scattering series:

$$\mathbb{IM}_1(A,B,C) = \int_{-\infty}^{z} duA(u) \int_{-\infty}^{z} dvC(v)B(u+v-z) \tag{29}$$

$$\mathbb{IM}_2(A,B,C) = \int_{-\infty}^{z} duA(u) \int_{-\infty}^{z} dv(z-v)C(v)B(u+v-z) \tag{30}$$

$$\mathbb{IM}_3(A,B,C) = \int_{-\infty}^{z} duA(u) \int_{-\infty}^{z} dv(z-v)^2C(v)B(u+v-z) \tag{31}$$

$$\mathbb{IM}_{3X}(A,B,C) = \int_{-\infty}^{z} du\frac{\partial^2 A(x,u)}{\partial x^2}\frac{\partial^2}{\partial x^2} \int_{-\infty}^{z} dv(z-v)^2C(x,v)B(x,u+v-z) \tag{32}$$

$$\mathbb{IM}_4(A,B,C) = \int_{-\infty}^{z} du(z-u)A(u) \int_{-\infty}^{z} dv(z-v)C(v)B(u+v-z) \tag{33}$$

$$\mathbb{IM}_{4X}(A,B,C) = \int_{-\infty}^{z} du(z-u)\frac{\partial A(u)}{\partial x}\frac{\partial}{\partial x} \int_{-\infty}^{z} dv(z-v)C(v)B(u+v-z) \tag{34}$$

Appendix B: Derivation strategies

The mathematics involved in computation of the multidimensional inverse scattering series is complicated but can be made more straightforward with some simple conventions. This appendix provides an overview and intuitive introduction to a particular and useful derivation convention.

We begin by reviewing the first order portions of the inverse scattering series, closely following the development of, e.g., Weglein et al. (2003). The desired scattering potential V, which for our purposes describes perturbations of wavespeed away from a constant background wavespeed c_0:

$$V(x,z,\omega) = \frac{\omega^2}{c_0^2}\alpha(x,z),$$

(in which $\alpha(x,z) = 1 - c_0^2/c^2(x,z)$ for a true wavespeed distribution $c(x,z)$), can be expressed in terms which are first, second, third, ... order in data : $\alpha(x,z) = \sum_{n=1}^{\infty}\alpha_n(x,z)$. The relationship between various part of V, and corresponding part of α, can be summarized as:

$$V_n(x,z,\omega) = \frac{\omega^2}{c_0^2}\alpha_n(x,z), \qquad (n = 1,2,3,\ldots)$$

The first order (linear) portion of the inverse scattering series is an exact relationship between V_1 and the scattered field evaluated on the measurement surface (i.e. the data D). In the operator form, this relationship is

$$\mathbf{G_0 V_1 G_0 = D = G - G_0}. \tag{35}$$

Next, consider the well-known α_2 equation:

$$\mathbf{G_0 V_2 G_0 = -G_0 V_1 G_0 V_1 G_0}$$

With $n \geq 3$, the portion of α which is n-th order in data will contain considerably more terms. For example, α_3 contains three pieces:

$$\mathbf{G_0 V_3 G_0 = -G_0 V_1 G_0 V_1 G_0 V_1 G_0 - G_0 V_2 G_0 V_1 G_0 - G_0 V_1 G_0 V_2 G_0}.$$

Generally speaking, for an arbitrary positive integer m, the number of corresponding m'th order terms in the inverse series will depend on how many ways m can be expressed in terms of the sum of smaller positive integers. For example, if $m = 4$, we can express 4 in 7 different ways: $4 = 1+1+1+1 = 1+1+2 = 1+2+1 = 2+1+1 = 2+2 = 1+3 = 3+1$. That means α_4 will have seven pieces:

$$\begin{aligned}\mathbf{G_0 V_4 G_0 = -\ G_0 V_1 G_0 V_1 G_0 V_1 G_0 V_1 G_0 - G_0 V_1 G_0 V_1 G_0 V_2 G_0 - G_0 V_1 G_0 V_2 G_0 V_1 G_0}\\ \mathbf{- G_0 V_2 G_0 V_1 G_0 V_1 G_0 - G_0 V_2 G_0 V_2 G_0 - G_0 V_1 G_0 V_3 G_0 - G_0 V_3 G_0 V_1 G_0}.\end{aligned}$$

In order to make clear where each piece comes from, we denote each piece differently. One approach is to use newly defined functions. For example, we define $k = \omega/c_0$, and define the solution of the following problem:

$$G_0 k^2 F G_0 = -G_0 k^2 A_1 G_0 k^2 A_2 G_0$$

as

$$F = \mathcal{SC}_2 (A_1, A_2)$$

In this general formulism, both A_1 and A_2 can be α_1, α_2, α_3, ... For example, in the simplest case: $A_1 = A_2 = \alpha_1$, we obtain: $\alpha_2 = \mathcal{SC}_2 (\alpha_1, \alpha_1)$. Likewise, we define the solution of the following equation:

$$G_0 k^2 F G_0 = -G_0 k^2 A_1 G_0 k^2 A_2 G_0 k^2 A_3 G_0$$

as

$$F = \mathcal{SC}_3 (A_1, A_2, A_3)$$

Generally speaking, for an integer $n \geq 2$, we define the solution of the following equation:

$$G_0 k^2 F G_0 = -G_0 k^2 A_1 G_0 k^2 A_2 \cdots k^2 A_n G_0$$

as

$$F = \mathcal{SC}_n (A_1, A_2, \cdots, A_n)$$

With the definitions above, we have:

$$\begin{aligned}
\alpha_2 =& \mathcal{SC}_2 (\alpha_1, \alpha_1) \\
\alpha_3 =& \mathcal{SC}_3 (\alpha_1, \alpha_1, \alpha_1) + \mathcal{SC}_2 (\alpha_1, \alpha_2) + \mathcal{SC}_2 (\alpha_2, \alpha_1) \\
\alpha_4 =& \mathcal{SC}_4 (\alpha_1, \alpha_1, \alpha_1, \alpha_1) + \mathcal{SC}_3 (\alpha_1, \alpha_1, \alpha_2) + \mathcal{SC}_3 (\alpha_1, \alpha_2, \alpha_1) + \mathcal{SC}_3 (\alpha_2, \alpha_1, \alpha_1) \\
&+ \mathcal{SC}_2 (\alpha_2, \alpha_2) + \mathcal{SC}_2 (\alpha_1, \alpha_3) + \mathcal{SC}_2 (\alpha_3, \alpha_1)
\end{aligned}$$

These functions not only differentiate terms, they also shorten the derivation process. For example, $\mathcal{SC}_2$ can be derived once, and used repeatedly later.

One might notice that, for example, in the α_4 term, all different permutations of $(\alpha_1, \alpha_1, \alpha_2)$ are involved. It is natural to ask if the sum of these similar looking terms possess some symmetry not manifested in each individual term? The answer is yes, especially for the more significant portion which is the only surviving term if the earth is indeed horizontal.

We define the permutation sum of $\mathcal{SC}$ as $\mathbb{SC}$, for example, in the case of $\mathcal{SC}_2$, we define:

$$\mathbb{SC}_2 (A_1, A_2) = \sum\nolimits^{\odot} \mathbb{SC}_2 (A_1, A_2)$$

where $\sum^{\odot}$ acting on a function of 2 variables is defined in equation (18).

In the case of $\mathcal{SC}_3$, if we assume: A_1 A_2 , and A_3 are different from each other, we define:

$$\mathbb{SC}_3 (A_1, A_2, A_3) = \sum\nolimits^{\odot} \mathcal{SC}_3 (A_1, A_2, A_3)$$

where $\sum^{\odot}$ acting on a function of 3 variables is defined in equation (19).

Strictly speaking, $\mathcal{SC}_2$ is a function of (A_1, A_2), and can be expressed in (x, z), (k_m, z), or (k_m, k_z) domain. In this note, $\mathcal{SC}_3$ (without tilde above) means the representation in the (x, z) domain. $\widetilde{\mathcal{SC}}_2$ (with single tilde above) means the representation in the (k_m, z) domain. $\widetilde{\widetilde{\mathcal{SC}}}_2$ (with double tilde above) means the representation in the (k_m, k_z) domain. If not specified, $\mathcal{SC}_2$ is assumed as the function of (A_1, A_2).

For $\mathcal{SC}_3$, we use tilde sign to explicitly denote its domain, just like the case for $\mathcal{SC}_2$. If not specified, $\mathcal{SC}_3$ is assumed as a function of (A_1, A_2, A_3). Very similar logic applied to later functions.

With definitions above, α_4 can written as:

$$\alpha_4 = \mathbb{SC}_4(\alpha_1, \alpha_1, \alpha_1, \alpha_1) + \mathbb{SC}_3(\alpha_1, \alpha_1, \alpha_2) + \mathbb{SC}_2(\alpha_1, \alpha_3) + \mathbb{SC}(\alpha_2, \alpha_2) \tag{36}$$

Within one index n, especially when n is large, there remain many very different terms. We should differentiate those terms further. Here we introduce another index m, with $n \geq m \geq 1$, to denote how significant each term is. The reason behind this is that, in the equation to invert for $\mathcal{SC}_n$, we will obtain a distribution behave like k_z^{n-1} asymptotically in the k_z domain. If the earth is 1D, only the portion of the distribution which is of the order of k_z^{n-1} is needed, the other portions will be discarded by the sifting property of the δ-function (see Liu et. al. 2004). If the earth is not 1D, the other portions, which will be separated into lower powers of k_z as: $k_z^{n-2}, k_z^{n-3}, \cdots, k_z^0$. We can use $1 \leq m \leq n$ to denote the piece associated with k_z^{n-m}. We use $m = n + 1$ to denote the remaining parts.

Inside each (n, m), there are still very different looking terms. For example, in the internal multiple removal, only the part of the third term in which the 3 scatters satisfy the higher-lower-higher relation is necessary: $z_1 \geq z_2 \leq z_3$. How many high-low relations exist between n scatters: $z_1, z_2, \cdots, z_n$? There are 2^{n-1} of them because there 2 possible relations between 2 adjacent scatters z_j and z_{j+1}, we can either have: $z_j \geq z_{j+1}$ or $z_j \leq z_{j+1}$. That's why we introduce a third index l, $1 \leq l \leq 2^{n-1}$ to further differential each terms. In the current classification scheme, the equation to calculate the index l is:

$$l = (d_1 d_2 \cdots d_{n-1})_b + 1 \tag{37}$$

where $(d_1 d_2 \cdots d_{n-1})_b$ is an integer in binary representation, it's j-th digit, d_j is either 0 or 1 depending whether or not $z_j \geq z_{j+1}$.

In summary, we systematically classify the function $\mathcal{SC}_n$ into $\mathcal{SC}_{n,m,l}$, where $1 \leq m \leq n+1$ denotes the significance, with $m = 1$ defined as the more significant. The last index $1 \leq l \leq 2^{n-1}$ denotes where he high-low relationship between adjacent scatters.

Appendix C: Derivation of α_1

In order to solve α_1 (or equivalently V_1) in equation (35), we apply the causal Green's functions for homogeneous media (following Morse and Feshbach, 1953, Chapter 7 Vol. 1) :

$$G_0(x_g, z_g, x_s, z_s, \omega) = \frac{1}{2\pi} \int_{-\infty}^{\infty} dk_g \frac{e^{ik_g(x_g - x_s)} e^{iq_g|z_g - z_s|}}{2iq_g}, \tag{38}$$

where k_g is the Fourier conjugate to x_g, and $q_g = \mathrm{sgn}(\omega)\sqrt{(\omega/c_0)^2 - k_g^2}$.

Equation (35) can be solved by applying a Fourier transform: $\int_{-\infty}^{\infty} dx_g \int_{-\infty}^{\infty} dx_s e^{ik_s x_s - ik_g x_g}$, over the lateral source and receiver coordinates to obtain α_1. (Note that the "sign convention" of the Fourier transform is different for the source and geophone coordinates. See Clayton & Stolt 1981 for detail of this choice of Fourier transform) The solution of equation (35) with the constraint $k_h = k_g + k_s = 0$ is:

$$\widetilde{\widetilde{\alpha}}_1(k_m, k_z) = -\frac{4k_z^2}{k_z^2 + k_m^2} \widetilde{\widetilde{D}}\left(\frac{k_m}{2}, z_g, -\frac{k_m}{2}, z_s, \omega\right), \tag{39}$$

where, following the conventions discussed in Appendix A, k_s is the Fourier conjugate to x_s, and

$$q_s = \mathrm{sgn}(\omega)\sqrt{(\omega/c_0)^2 - k_s^2},$$

with

$$\omega = \mathrm{sgn}(k_z)\frac{c_0}{2}\sqrt{k_z^2 + k_m^2},$$

and $k_z = q_g + q_s$. The quantity $\widetilde{\widetilde{\alpha}}_1(k_m, k_z)$ is the double Fourier transform of $\alpha_1(x, z)$ over both x and z coordinates, and $\widetilde{\widetilde{D}}$ is the double Fourier transform of $D(x_g, z_g, x_s, z_s, \omega)$ over x_g and x_s coordinates. If we choose $k_h = 0$, we have:

$$\widetilde{\widetilde{D}}(\frac{k_m}{2}, z_g, -\frac{k_m}{2}, z_s, \omega) = \int_{-\infty}^{\infty} dx_m e^{-ik_m x_m} \int_{-\infty}^{\infty} dt e^{i\omega t} \mathcal{D}\left(x_m, t\right). \tag{40}$$

where $\mathcal{D}$ is simply summing of all traces within a CMP gather:

$$\mathcal{D}\left(x_m, t\right) = \int_{-\infty}^{\infty} dx_h D(x_m + \frac{x_h}{2}, z_g, x_m - \frac{x_h}{2}, z_s, t). \tag{41}$$

Appendix D: Derivation of $\mathcal{SC}_2$

In this appendix, we solve for: $F = \mathcal{SC}_2\left(A_1, A_2\right)$, or equivalently:

$$\mathbf{G_0}k^2 F\mathbf{G_0} = -\mathbf{G_0}k^2 A_1\mathbf{G_0}A_2\mathbf{G_0}. \tag{42}$$

Expressing equation (42) explicitly in the actual integral form, we have

$$\begin{aligned}
&\int_{-\infty}^{\infty} dx_1 \int_{-\infty}^{\infty} dz_1 G_0(x_g, z_g, x_1, z_1, \omega)\left(\frac{\omega}{c_0}\right)^2 F(x_1, z_1) G_0(x_1, z_1, x_s, z_s, \omega) \\
&= -\int_{-\infty}^{\infty} dx_1 \int_{-\infty}^{\infty} dz_1 G_0(x_g, z_g, x_1, z_1, \omega)\left(\frac{\omega}{c_0}\right)^2 A_1(x_1, z_1) \\
&\times \int_{-\infty}^{\infty} dx_2 \int_{-\infty}^{\infty} dz_2 G_0(x_1, z_1, x_2, z_2, \omega)\left(\frac{\omega}{c_0}\right)^2 A_2(x_2, z_2) G_0(x_2, z_2, k_s, z_s, \omega).
\end{aligned} \tag{43}$$

We next Fourier transform over lateral geophone and shot coordinates: $\int_{-\infty}^{\infty} dx_g \int_{-\infty}^{\infty} dx_s e^{ik_s x_s - ik_g x_g}$, and express the Green's function in the middle of the right-hand-side of equation (43) as

$$G_0(x_1, z_1, x_2, z_2, \omega) = \frac{1}{2\pi}\int_{-\infty}^{\infty} dk_1 \frac{e^{ik_1(x_1 - x_2)} e^{iq_1|z_1 - z_2|}}{2iq_1},$$

in which k_1 is conjugate to x_1, and $q_1 = \mathrm{sgn}(\omega)\sqrt{(\omega/c_0)^2 - k_1^2}$. This results in

$$\begin{aligned}
&-\frac{1}{4c_0^2}\frac{\omega^2}{q_g q_s}\widetilde{\widetilde{F}}(k_g - k_s, k_z) e^{-i(q_g z_g + g_s z_s)} = -\frac{i}{16\pi c_0^4}\int_{-\infty}^{\infty} dk_1 \frac{\omega^4}{q_g q_1 q_s}\int_{-\infty}^{\infty} dz_1 \widetilde{A_1}(k_g - k_1, z_1) \\
&\times \int_{-\infty}^{\infty} dz_2 \widetilde{A_2}(k_1 - k_s, z_2) e^{i[q_g(z_1 - z_g) + q_1|z_2 - z_1| + q_s(z_2 - z_s)]}.
\end{aligned} \tag{44}$$

The quantity

$$\widetilde{A_1}(k_m, z) = \frac{1}{2\pi}\int_{-\infty}^{\infty} dk_z e^{-ik_z z}\widetilde{\widetilde{A_1}}(k_m, k_z)$$

is the Fourier transform of $A_1(x_m, z)$, and $\widetilde{\widetilde{F}}(k_m, k_z)$ is the Fourier transform of $F(x_m, z)$ over both x_m and z.

We next compute F in the (k_m, z) domain: we apply the inverse Fourier transform $(1/2\pi)\int_{-\infty}^{\infty} e^{-ik_z z} dk_z$ to equation (44), resulting in:

$$\begin{aligned}
\widetilde{F}(k_g - k_s, z) =& \frac{1}{8\pi^2 c_0^2}\int_{-\infty}^{\infty} dk_1 \int_{-\infty}^{\infty} dz_1 \int_{-\infty}^{\infty} dz_2 \int_{-\infty}^{\infty} dk_z \\
& \frac{i\omega^2}{q_1}\widetilde{A_1}(k_g - k_1, z_1)\widetilde{A_2}(k_1 - k_s, z_2) e^{i[q_g(z_1 - z) + q_1|z_2 - z_1| + q_s(z_2 - z)]}.
\end{aligned} \tag{45}$$

The innermost integral of equation (45) contains $\widetilde{A_1}$ and $\widetilde{A_2}$, which depends on the measurement of the wave field; it can be taken out of this integral (with respect to k_z) if we parameterize the data such that the Fourier conjugate k_h of the lateral offset coordinate to be 0. See Clayton and Stolt (1981) for a more detailed discussion. Making this choice, we have:

$$\begin{aligned} k_h &= k_g + k_s = 0, \\ \frac{\omega}{c_0} &= \frac{1}{2}\mathrm{sgn}(k_z)\sqrt{k_z^2 + k_m^2}, \\ k_g &= -k_s = 0.5k_m, \end{aligned} \tag{46}$$

which results in a simplified expression for $\widetilde{F}(k_m, z)$:

$$\widetilde{F}(k_m, z) = \frac{1}{16\pi^2} \int_{-\infty}^{\infty} dk_1 \int_{-\infty}^{\infty} dz_1 \widetilde{A_1}(\frac{k_m}{2} - k_1, z_1) \int_{-\infty}^{\infty} dz_2 \widetilde{A_2}(k_1 + \frac{k_m}{2}, z_2) \widetilde{\gamma}_2(k_m, k_1; \varepsilon_0, \varepsilon_1), \tag{47}$$

where

$$\widetilde{\gamma}_2(k_m, k_1; \varepsilon_0, \varepsilon_1) = \int_{-\infty}^{\infty} dk_z i \frac{k_z^2 + k_m^2}{u_1} e^{i[\varepsilon_0 k_z + \varepsilon_1 u_1]} = \int_{-\infty}^{\infty} dk_z i \frac{k_z^2 + k_m^2}{u_1} e^{i\triangle\psi} e^{i[\varepsilon_0 + \varepsilon_1]k_z}, \tag{48}$$

and where we have defined:

$$\begin{aligned} \varepsilon_0 &= 0.5(z_1 + z_2) - z \\ \varepsilon_1 &= 0.5|z_1 - z_2| \\ u_1 &= 2q_1 = \mathrm{sgn}(k_z)\sqrt{k_z^2 + a_1} \\ a_1 &= k_m^2 - 4k_1^2 \\ \triangle\psi &= \varepsilon_1 \times (u_1 - k_z). \end{aligned} \tag{49}$$

Notice that the expression $\widetilde{\gamma}_2(k_m, k_1; \varepsilon_0, \varepsilon_1)$ does not depend on the measured data; we may compute it once and use it repeatedly, saving on computation.

Evaluation of $F = \mathcal{SC}_2(A_1, A_2)$ in the (k_m, z) domain

¿From equation (48), it's easy to tell that $\widetilde{\gamma}_2$ is not an ordinary function because $\lim_{k_z \to \infty} \frac{u_1}{k_z} = 1$, so the integrand $(k_z^2 + k_m^2)/(u_1)$ approaches k_z as $k_z \to \infty$. We can decompose $i \times e^{i\triangle\psi}(k_z^2 + k_m^2)/(u_1)$ as follows:

$$\begin{aligned} i \times \frac{k_z^2 + k_m^2}{u_1} e^{i\triangle\psi} &= i \times k_z - \frac{\varepsilon_1 a_1}{2} + \widetilde{\widetilde{\xi}}_2 \\ \widetilde{\widetilde{\xi}}_2 &= i \times \frac{k_z^2 + k_m^2}{u_1} e^{i\triangle\psi} - i \times k_z + \frac{\varepsilon_1 a_1}{2} \end{aligned} \tag{50}$$

Decomposition above is based on the fact that, after put into the integral of inverse Fourier transform $\int_{-\infty}^{\infty} dk_z e^{i(\varepsilon_0+\varepsilon_1)k_z}$, the first term k_z will result in a singular distribution:

$$\int_{-\infty}^{\infty} ik_z e^{i(\varepsilon_0+\varepsilon_1)k_z} dk_z = \frac{\partial \int_{-\infty}^{\infty} e^{i(\varepsilon_0+\varepsilon_1)k_z} dk_z}{\partial(\varepsilon_0+\varepsilon_1)} = (2\pi) \times \delta'(\varepsilon_0+\varepsilon_1)$$

Likewise another singular distribution is produced by the second term:

$$\int_{-\infty}^{\infty} -\frac{\varepsilon_1 a_1}{2} e^{i(\varepsilon_0+\varepsilon_1)k_z} dk_z = -\pi\varepsilon_1 a_1 \times \delta(\varepsilon_0+\varepsilon_1)$$

But the distribution produced by the third term:

$$\int_{-\infty}^{\infty} \widetilde{\widetilde{\xi}}_2 e^{i(\varepsilon_0+\varepsilon_1)k_z} dk_z$$

is regular because $\lim_{k_z \mapsto \infty} \widetilde{\widetilde{\xi}}_2 \times k_z = \frac{ik_m^2}{2} + 2k_1^2 - \frac{\varepsilon_1^2 a_1^2}{8}$, which is a finite constant. For the purpose of short notation, let's denote the numerically expressible function as $\widetilde{\xi}_2$:

$$\widetilde{\xi}_2(k_m, k_1; \varepsilon_0, \varepsilon_1) = \int_{-\infty}^{\infty} \widetilde{\widetilde{\xi}}_2 e^{i(\varepsilon_0+\varepsilon_1)k_z} dk_z \tag{51}$$

So we decompose $\widetilde{\gamma}_2(k_m, k_1; \varepsilon_0, \varepsilon_1)$ into 2 singular distributions and 1 regular distribution:

$$\widetilde{\gamma}_2(k_m, k_1; \varepsilon_0, \varepsilon_1) = (2\pi)\delta'(\varepsilon_0+\varepsilon_1) - \pi\varepsilon_1 a_1 \delta(\varepsilon_0+\varepsilon_1) + \widetilde{\xi}_2(k_m, k_1; \varepsilon_0, \varepsilon_1). \tag{52}$$

From equation (47) and equation (48), the explicit expression of the phase term $\varepsilon_0 + \varepsilon_1$ depends on $z_1 \geq z_2$ or $z_1 \leq z_2$. And in the first case $\varepsilon_0 + \varepsilon_1 = z_1 - z$. So equation (52) can be further expressed as:

$$\widetilde{\gamma}_2(k_m, k_1; \varepsilon_0, \varepsilon_1) = (2\pi)\delta'(z_1 - z) - \pi\varepsilon_1 a_1 \delta(z_1 - z) + \widetilde{\xi}_2\left(k_m, k_1; \frac{z_1+z_2}{2} - z, \frac{z_1 - z_2}{2}\right) \tag{53}$$

In the second case $\varepsilon_0 + \varepsilon_1 = z_2 - z$. So equation (52) can be further expressed as:

$$\widetilde{\gamma}_2(k_m, k_1; \varepsilon_0, \varepsilon_1) = (2\pi)\delta'(z_2 - z) - \pi\varepsilon_1 a_1 \delta(z_2 - z) + \widetilde{\xi}_2\left(k_m, k_1; \frac{z_1+z_2}{2} - z, \frac{z_2 - z_1}{2}\right) \tag{54}$$

Substituting equation (53) or equation (54) into equation (47), depending on $z_1 \geq z_2$ or $z_1 \leq z_2$, we can decompose F into 3 terms:

$$\begin{aligned}
&\widetilde{F}(k_m,z)=\frac{1}{16\pi^2}\int\limits_{-\infty}^{\infty}dk_1\times\\
&\left(\begin{array}{c}\int\limits_{-\infty}^{\infty}dz_1\widetilde{A_1}\left(\frac{k_m}{2}-k_1,z_1\right)\int\limits_{-\infty}^{z_1}dz_2\widetilde{A_2}\left(k_1+\frac{k_m}{2},z_2\right)\widetilde{\gamma}_2\left(k_m,k_1;\frac{z_1+z_2}{2}-z,\frac{z_1-z_2}{2}\right)\\ +\\ \int\limits_{-\infty}^{\infty}dz_2\widetilde{A_1}\left(k_1+\frac{k_m}{2},z_2\right)\int\limits_{-\infty}^{z_2}dz_1\widetilde{A_2}\left(k_1+\frac{k_m}{2},z_1\right)\widetilde{\gamma}_2\left(k_m,k_1;\frac{z_1+z_2}{2}-z,\frac{z_2-z_1}{2}\right)\end{array}\right)\\
&=\widetilde{\mathcal{SC}}_{2,1}+\widetilde{\mathcal{SC}}_{2,2}+\widetilde{\mathcal{SC}}_{2,3},
\end{aligned}\tag{55}$$

The split above is base on the classification idea talked in the equation (37). For the first case: $z_1 \geq z_2$, the binary expression for this relation is 0, it's corresponding index is $l = 0 + 1 = 1$. For the second case: $z_1 \leq z_2$, the binary expression for this relation is 1, it's corresponding index is $l = 1 + 1 = 2$.

The first term $\widetilde{\mathcal{SC}}_{2,1}$ is further decomposed as:

$$\widetilde{\mathcal{SC}}_{2,1}=\widetilde{\mathcal{SC}}_{2,1,1}+\widetilde{\mathcal{SC}}_{2,1,2}\tag{56}$$

$$\begin{aligned}
&\widetilde{\mathcal{SC}}_{2,1,1}=\frac{1}{16\pi^2}\int\limits_{-\infty}^{\infty}dk_1\int\limits_{-\infty}^{\infty}dz_1\delta'(z_1-z)\widetilde{A_1}(0.5k_m-k_1,z_1)\int\limits_{-\infty}^{z_1}dz_2\widetilde{A_2}(k_1+0.5k_m,z_2)(2\pi)\\
&\texttt{Using equation (27) we have}\\
&=-\frac{1}{8\pi}\int\limits_{-\infty}^{\infty}dk_1\frac{\partial\widetilde{A_1}(0.5k_m-k_1,z)}{\partial z}\int\limits_{-\infty}^{z}dz_2\widetilde{A_2}(k_1+0.5k_m,z_2)\\
&\quad-\frac{1}{8\pi}\int\limits_{-\infty}^{\infty}dk_1\widetilde{A_1}(0.5k_m-k_1,z)\widetilde{A_2}(k_1+0.5k_m,z)\\
&\widetilde{\mathcal{SC}}_{2,1,2}=\frac{1}{16\pi^2}\int\limits_{-\infty}^{\infty}dk_1\int\limits_{-\infty}^{\infty}dz_2\delta'(z_2-z)\widetilde{A_2}(k_1+0.5k_m,z_2)\int\limits_{-\infty}^{z_2}dz_1\widetilde{A_1}(0.5k_m-k_1,z_1)(2\pi)\\
&\texttt{Using equation (27) we have}\\
&=-\frac{1}{8\pi}\int\limits_{-\infty}^{\infty}dk_1\frac{\partial\widetilde{A_2}(k_1+0.5k_m,z)}{\partial z}\int\limits_{-\infty}^{z}dz_2\widetilde{A_1}(0.5k_m-k_1,z_2)\\
&\quad-\frac{1}{8\pi}\int\limits_{-\infty}^{\infty}dk_1\widetilde{A_1}(0.5k_m-k_1,z)\widetilde{A_2}(k_1+0.5k_m,z)
\end{aligned}\tag{57}$$

So we split $\widetilde{\mathcal{SC}}_{2,1,1}$ and $\widetilde{\mathcal{SC}}_{2,1,2}$ into 2 parts by integration by parts (which is used to get the last step in the derivation above). In each case, the first part contains the first 2 terms in the right-hand-side of the last equal sign above, they are purely responsible for imaging in the special case of $A_1 = A_2 = \alpha_1$. The last term is responsible for parameter inversion in the special case mentioned above. Only $\mathcal{SC}_{2,1}$ will not vanish if we indeed have a 1D earth.

$$\begin{aligned}
&\widetilde{\mathcal{SC}}_{2,2} = \frac{1}{16\pi^2} \int_{-\infty}^{\infty} dk_1 \times \\
&\left(\begin{array}{l} \int_{-\infty}^{\infty} dz_1 \widetilde{A_1}(0.5k_m - k_1, z_1) \int_{-\infty}^{z_1} dz_2 \widetilde{A_2}(k_1 + 0.5k_m, z_2)(-\pi\varepsilon_1 a_1)\delta(z_1 - z) \\ \int_{-\infty}^{\infty} dz_2 \widetilde{A_2}(k_1 + 0.5k_m, z_2) \int_{-\infty}^{z_2} dz_1 \widetilde{A_1}(0.5k_m - k_1, z_1)(-\pi\varepsilon_1 a_1)\delta(z_2 - z) \end{array} \right) \\
&= \widetilde{\mathcal{SC}}_{2,2,1} + \widetilde{\mathcal{SC}}_{2,2,2}
\end{aligned}$$

The split above is base on the high-low relation between z_1 and z_2. For the first case: $z_1 \geq z_2$, the binary expression for this relation is 0, it's corresponding index is $l = 0 + 1 = 1$. For the second case: $z_1 \leq z_2$, the binary expression for this relation is 1, it's corresponding index is $l = 1 + 1 = 2$.

$$\begin{aligned}
\widetilde{\mathcal{SC}}_{2,2} &= \widetilde{\mathcal{SC}}_{2,2,1} + \widetilde{\mathcal{SC}}_{2,2,2} \\
\widetilde{\mathcal{SC}}_{2,2,1} &= -\frac{1}{16\pi} \int_{-\infty}^{\infty} dk_1 \, (k_m^2 - 4k_1^2) \widetilde{A_1}(0.5k_m - k_1, z) \int_{-\infty}^{z} du (z - u) \widetilde{A_2}(k_1 + 0.5k_m, u) \\
\widetilde{\mathcal{SC}}_{2,2,2} &= -\frac{1}{16\pi} \int_{-\infty}^{\infty} dk_1 \, (k_m^2 - 4k_1^2) \widetilde{A_2}(0.5k_m + k_1, z) \int_{-\infty}^{z} du (z - u) \widetilde{A_1}(0.5k_m - k_1, u).
\end{aligned} \tag{58}$$

$\widetilde{\mathcal{SC}}_{2,2}$ will vanish if we have a 1D earth. Even for geological model with lateral variations, $\widetilde{\mathcal{SC}}_{2,2}$ is very clean for the portion where the earth is horizontal. $\widetilde{F}_2$ is strong where the model is laterally varying.

The third term is regular, and can be literally implemented as the form in equation (47). Because $\widetilde{\xi}_2(k_m, k_1; \varepsilon_0, \varepsilon_1)$ is regular, no integration by parts is needed.

$$\widetilde{\mathcal{SC}}_{2,3} = \widetilde{\mathcal{SC}}_{2,3,1} + \widetilde{\mathcal{SC}}_{2,3,2}$$

where:

$$\widetilde{\mathcal{SC}}_{2,3,1} = \frac{1}{16\pi^2}\int_{-\infty}^{\infty} dk_1 \int_{-\infty}^{\infty} dz_1 \widetilde{A_1}(0.5k_m - k_1, z_1) \int_{-\infty}^{z_1} dz_2 \times \widetilde{A_2}(k_1 + 0.5k_m, z_2)\widetilde{\xi_2}\left(k_m, k_1; \frac{z_1+z_2}{2} - z, \frac{z_1 - z_2}{2}\right)$$

$$\widetilde{\mathcal{SC}}_{2,3,2} = \frac{1}{16\pi^2}\int_{-\infty}^{\infty} dk_1 \int_{-\infty}^{\infty} dz_2 \widetilde{A_2}(0.5k_m + k_1, z_2) \int_{-\infty}^{z_2} dz_1 \times \widetilde{A_2}(0.5k_m - k_1, z_1)\widetilde{\xi_2}\left(k_m, k_1; \frac{z_1+z_2}{2} - z, \frac{z_2 - z_1}{2}\right), \tag{59}$$

where $\widetilde{\xi_2}$ is defined in equation (51)

The further classification is based on the relative high-low relation between z_1 and z_2.

Evaluation of $F = \mathcal{SC}_2(A_1, A_2)$ in the (x, z) domain

We can go a step further by applying the inverse Fourier transform $(1/2\pi)\int_{-\infty}^{\infty} dk_m e^{ik_m x}$ to the results above to have:

$$\begin{aligned}
\mathcal{SC}_{2,1,1}(x,z) &= \frac{1}{2\pi}\int_{-\infty}^{\infty} dk_m e^{ik_m x}\widetilde{\mathcal{SC}}_{2,1,1}(k_m, z) \\
&= -\frac{1}{16\pi^2}\int_{-\infty}^{\infty} dk_1 \int_{-\infty}^{\infty} e^{ik_m x} dk_m \frac{\partial \widetilde{A_1}(0.5k_m - k_1, z)}{\partial z} \int_{-\infty}^{z} dz_2 \widetilde{A_2}(k_1 + 0.5k_m, z_2) \\
&\quad - \frac{1}{16\pi^2}\int_{-\infty}^{\infty} dk_1 \int_{-\infty}^{\infty} e^{ik_m x} dk_m \widetilde{A_1}(0.5k_m - k_1, z)\widetilde{A_2}(k_1 + 0.5k_m, z) \\
&\texttt{Using equation (124) we have} \\
&= -\frac{1}{4}\left(\frac{\partial A_1(x,z)}{\partial z}\int_{-\infty}^{z} du A_2(x,u) \; + \; A_1(x,z)A_2(x,z)\right)
\end{aligned} \tag{60}$$

$$
\begin{aligned}
&\mathcal{SC}_{2,1,2}(x,z) = \frac{1}{2\pi}\int_{-\infty}^{\infty} dk_m e^{ik_m x}\widetilde{\mathcal{SC}}_{2,1,2}(k_m,z)\\
&= -\frac{1}{16\pi^2}\int_{-\infty}^{\infty} dk_1 \int_{-\infty}^{\infty} e^{ik_m x} dk_m \frac{\partial \widetilde{A_2}(k_1+0.5k_m,z)}{\partial z}\int_{-\infty}^{z} dz_1 \widetilde{A_1}(0.5k_m-k_1,z_1)\\
&\quad -\frac{1}{16\pi^2}\int_{-\infty}^{\infty} dk_1 \int_{-\infty}^{\infty} e^{ik_m x} dk_m \widetilde{A_1}(0.5k_m-k_1,z)\widetilde{A_2}(k_1+0.5k_m,z)\\
&\texttt{Using equation (124) we have}\\
&= -\frac{1}{4}\left(\frac{\partial A_2(x,z)}{\partial z}\int_{-\infty}^{z} du A_1(x,u) \;+\; A_1(x,z)A_2(x,z)\right)
\end{aligned}
\tag{61}
$$

We can sum the 2 equations above to have:

$$
\begin{aligned}
&\mathcal{SC}_{2,1}(x,z) = \mathcal{SC}_{2,1,1}(x,z) + \mathcal{SC}_{2,1,2}(x,z)\\
&= -\frac{1}{4}\left(\frac{\partial A_1(x,z)}{\partial z}\int_{-\infty}^{z} du A_2(x,u) \;+\; \frac{\partial A_2(x,z)}{\partial z}\int_{-\infty}^{z} du A_1(x,u) \;+\; 2A_1(x,z)A_2(x,z)\right)
\end{aligned}
\tag{62}
$$

$$
\begin{aligned}
&\mathcal{SC}_{2,2,1}(x,z) = \frac{1}{2\pi}\int_{-\infty}^{\infty} dk_m e^{ik_m x}\widetilde{\mathcal{SC}}_{2,2,1}(k_m,z)\\
&= -\frac{1}{64\pi^2}\int_{-\infty}^{\infty} dk_1 \int_{-\infty}^{\infty} dk_m e^{ik_m x}\,(k_m^2-4k_1^2)\widetilde{A_1}(0.5k_m-k_1,z)\times\\
&\qquad\qquad \int_{-\infty}^{z} dz_2 (z-z_2)\widetilde{A_2}(k_1+0.5k_m,z_2)\\
&\texttt{Using equation (125) we have} \quad = \frac{1}{4}\frac{\partial A_1(x,z)}{\partial x}\int_{-\infty}^{z} du \frac{\partial A_2(x,u)}{\partial x}(z-u)\\
&\texttt{Using equation (66) we have} \quad = \frac{1}{4}\frac{\partial A_1(x,z)}{\partial x}\int_{-\infty}^{z} du \int_{-\infty}^{u} dv \frac{\partial A_2(x,v)}{\partial x}
\end{aligned}
\tag{63}
$$

$$\mathcal{SC}_{2,2,2}(x,z) = \frac{1}{2\pi}\int_{-\infty}^{\infty} dk_m e^{ik_m x}\widetilde{\mathcal{SC}}_{2,2,2}(k_m,z)$$
$$= -\frac{1}{64\pi^2}\int_{-\infty}^{\infty} dk_1 \int_{-\infty}^{\infty} dk_m e^{ik_m x}\,(k_m^2 - 4k_1^2)\widetilde{A_2}(0.5k_m - k_1, z)$$
$$\times \int_{-\infty}^{z} dz_1 (z - z_2)\widetilde{A_1}(k_1 + 0.5k_m, z_2) \tag{64}$$
$$\texttt{Using equation (125) we have} = \frac{1}{4}\frac{\partial A_2(x,z)}{\partial x}\int_{-\infty}^{z} du \frac{\partial A_1(x,u)}{\partial x}(z-u)$$
$$\texttt{Using equation (66) we have} = \frac{1}{4}\frac{\partial A_2(x,z)}{\partial x}\int_{-\infty}^{z} du \int_{-\infty}^{u} dv \frac{\partial A_1(x,v)}{\partial x}$$

We can sum the 2 equations above to have:

$$\mathcal{SC}_{2,2}(x,z) = \mathcal{SC}_{2,2,1}(x,z) + \mathcal{SC}_{2,2,2}(x,z)$$
$$= \frac{1}{4}\frac{\partial A_1(x,z)}{\partial x}\int_{-\infty}^{z} du \int_{-\infty}^{u} dv \frac{\partial A_2(x,v)}{\partial x} \quad + \quad \frac{1}{4}\frac{\partial A_2(x,z)}{\partial x}\int_{-\infty}^{z} du \int_{-\infty}^{u} dv \frac{\partial A_1(x,v)}{\partial x} \tag{65}$$

In the derivation process above, the relation below was used to make the expression more symmetrical. For convenience, let's define: $B(x,z) = \int_{-\infty}^{z} du A(x,u)$, $dB(x,z) = A(x,z)dz$, we have:

$$\int_{-\infty}^{z} du A(x,u)(z-u) = \int_{-\infty}^{z} (z-u) dB(x,u)$$
$$= [(z-u)B(x,u)]_{u=-\infty}^{u=z} - \int_{-\infty}^{z} B(x,u) d(z-u) \tag{66}$$
$$= \int_{-\infty}^{z} B(x,u) du = \int_{-\infty}^{z} du \int_{-\infty}^{u} A(x,v) dv$$

Simplification and clarification in physical interpretations have occured after Fourier transformation of the singular terms $\mathcal{SC}_{2,1}$ and $\mathcal{SC}_{2,2}$. However, in the regular term $\mathcal{SC}_{2,3}$, no simplification and clarification have been found in this manner.

We can summarize various parts of $\mathcal{SC}_2(A_1, A_2)$ in the short-hand notation as:

	$\mathcal{SC}_2(A_1,A_2)$	$\mathcal{SC}_2(A_2,A_1)$
$\mathcal{SC}_{2,1,1}$	$-\frac{1}{4}\left(A_1^z A_2^{-z}+A_1A_2\right)$	$-\frac{1}{4}\left(A_2^z A_1^{-z}+A_1A_2\right)$
$\mathcal{SC}_{2,1,2}$	$-\frac{1}{4}\left(A_2^z A_1^{-z}+A_1A_2\right)$	$-\frac{1}{4}\left(A_1^z A_2^{-z}+A_1A_2\right)$
$\mathcal{SC}_{2,2,1}$	$-\frac{1}{4}A_1^x A_2^{x-2z}$	$-\frac{1}{4}A_2^x A_1^{x-2z}$
$\mathcal{SC}_{2,2,2}$	$-\frac{1}{4}A_2^x A_1^{x-2z}$	$-\frac{1}{4}A_1^x A_2^{x-2z}$
$\mathcal{SC}_{2,3,1}$	$\mathcal{SC}_{2,3,1}(A_1,A_2)$	$\mathcal{SC}_{2,3,2}(A_1,A_2)$
$\mathcal{SC}_{2,3,2}$	$\mathcal{SC}_{2,3,2}(A_1,A_2)$	$\mathcal{SC}_{2,3,1}(A_1,A_2)$

In the general case of $A_1 \neq A_2$, we have:

$$\begin{aligned}&\mathbb{SC}_2(A_1,A_2)=\mathcal{SC}_2(A_1,A_2)+\mathcal{SC}_2(A_2,A_1)\\&=-\frac{1}{2}\left(2A_1A_2+A_1^zA_2^{-z}+A_2^zA_1^{-z}\right)+\frac{1}{2}A_1^xA_2^{x-2z}+\frac{1}{2}A_2^xA_1^{x-2z}\\&+2\mathcal{SC}_{2,3,1}(A_1,A_2)+2\mathcal{SC}_{2,3,1}(A_2,A_1)\end{aligned}\tag{67}$$

In the special case of $A_1=A_2=A$, we have:

$$\mathbb{SC}_2(A,A)=\mathcal{SC}_2(A,A)=-\frac{1}{2}\left(A^2+A^zA^{-z}\right)+\frac{1}{2}A^xA^{x-2z}+2\mathcal{SC}_{2,3,1}(A,A)\tag{68}$$

Or in the simplest case: $A_1=A_2=\alpha_1$, we have α_2:

$$\alpha_2=\mathbb{SC}_2(\alpha_1,\alpha_1)=\mathcal{SC}_2(\alpha_1,\alpha_1)=-\frac{1}{2}\left(\alpha_1^2+\alpha_1^z\alpha_1^{-z}\right)+\frac{1}{2}\alpha_1^x\alpha_1^{x-2z}+2\mathcal{SC}_{2,3,1}(\alpha_1,\alpha_1)\tag{69}$$

where $Sc_{2,3,1}$ is implemented in the (k_m,z) domain as defined in equation (59)

Appendix E: Derivations of $\mathcal{SC}_3$

Next we consider the solution of the general third-order inverse scattering series equations. We have

$$G_0k^2FG_0 = -G_0k^2A_1G_0k^2A_2G_0k^2A_3G_0 \tag{70}$$

whose solution is written as:

$$F = \mathcal{SC}_3(A_1, A_2, A_3)$$

$$\begin{aligned}
&\int_{-\infty}^{\infty} dx_1 \int_{-\infty}^{\infty} dz_1 G_0(x_g, z_g, x_1, z_1, \omega) k^2 F(x_1, z_1) G_0(x_1, z_1, x_s, z_s, \omega) \\
&= -\int_{-\infty}^{\infty} dx_1 \int_{-\infty}^{\infty} dz_1 G_0(x_g, z_g, x_1, z_1, \omega) k^2 A_1(x_1, z_1) \\
&\quad \times \int_{-\infty}^{\infty} dx_2 \int_{-\infty}^{\infty} dz_2 G_0(x_1, z_1, x_2, z_2, \omega) A_2(x_2, z_2) \\
&\quad \times \int_{-\infty}^{\infty} dx_3 \int_{-\infty}^{\infty} dz_3 G_0(x_2, z_2, x_3, z_3, \omega) A_3(x_3, z_3) G_0(x_3, z_3, x_s, z_s, \omega).
\end{aligned} \tag{71}$$

Just like before, we Fourier transform over lateral geophone and shot coordinates:

$$\int_{-\infty}^{\infty} dx_g \int_{-\infty}^{\infty} dx_s e^{ik_s x_s - ik_g x_g},$$

and express the two Green's functions in the middle of the right-hand-side of equation (71) as

$$\begin{aligned}
G_0(x_1, z_1, x_2, z_2, \omega) &= \frac{1}{2\pi} \int_{-\infty}^{\infty} dk_1 \frac{e^{ik_1(x_1 - x_2)} e^{iq_1|z_1 - z_2|}}{2iq_1} \\
G_0(x_2, z_2, x_3, z_3, \omega) &= \frac{1}{2\pi} \int_{-\infty}^{\infty} dk_2 \frac{e^{ik_2(x_2 - x_3)} e^{iq_2|z_2 - z_3|}}{2iq_2} \\
q_1 = \mathrm{sgn}(\omega)\sqrt{(\omega/c_0)^2 - k_1^2} \quad & q_2 = \mathrm{sgn}(\omega)\sqrt{(\omega/c_0)^2 - k_2^2}
\end{aligned}$$

in which k_1 and k_2 are Fourier conjugate to x_1, x_2, respectively. This results in

$$\begin{aligned}
&-\frac{1}{4c_0^2} \frac{\omega^2}{q_g q_s} \widetilde{\widetilde{F}}(k_g - k_s, k_z) e^{-i(q_g z_g + g_s z_s)} = -\frac{1}{64\pi^2 c_0^6} \int_{-\infty}^{\infty} dk_1 \frac{\omega^6}{q_g q_1 q_2 q_s} \int_{-\infty}^{\infty} dz_1 \widetilde{A_1}(k_g - k_1, z_1) \\
&\times \int_{-\infty}^{\infty} dz_2 \widetilde{A_2}(k_1 - k_2, z_2) \int_{-\infty}^{\infty} dz_3 \widetilde{A_3}(k_2 - k_s, z_3) e^{i[q_g(z_1 - z_g) + q_1|z_2 - z_1| + q_2|z_3 - z_2| + q_s(z_2 - z_s)]}.
\end{aligned} \tag{72}$$

The quantity $\widetilde{\widetilde{F}}(k_m, k_z)$ is the Fourier transform of $F(x_m, z)$ over both x_m and z. We next compute F in the (k_m, z) domain: we apply the inverse Fourier transform $(1/2\pi)\int_{-\infty}^{\infty} e^{ik_z z} dk_z$ to equation (72), resulting in:

$$\begin{aligned}\widetilde{F}(k_g - k_s, z) = \frac{1}{32\pi^3}\int_{-\infty}^{\infty} dk_1 \int_{-\infty}^{\infty} dz_1 \int_{-\infty}^{\infty} dz_2 \int_{-\infty}^{\infty} dz_3 \int_{-\infty}^{\infty} dk_z \frac{(\omega/c_0)^4}{q_1 q_2} \\ \widetilde{A_1}(k_g - k_1, z_1)\widetilde{A_2}(k_1 - k_2, z_2)\widetilde{A_3}(k_2 - k_s, z_3) e^{i[q_g(z_1 - z) + q_1|z_2 - z_1| + q_2|z_3 - z_2| + q_s(z_2 - z)]}.\end{aligned} \tag{73}$$

The innermost integral of equation (73) contains $\widetilde{A_1}$, $\widetilde{A_2}$, and $\widetilde{A_3}$, which depends on the measurement of the wave field; just like the discussion in the $\mathcal{SC}_2$ derivation, it can be taken out of this integral by fixing the Fourier conjugate k_h of the lateral offset coordinate to be zero. With the choice of $k_h = 0$, we can simplify (73) using the relations in equation (46).

$$\begin{aligned}\widetilde{F}(k_m, z) =& \frac{1}{128\pi^3}\int_{-\infty}^{\infty} dk_1 \int_{-\infty}^{\infty} dk_2 \int_{-\infty}^{\infty} dz_1 \widetilde{A_1}(0.5k_m - k_1, z_1) \int_{-\infty}^{\infty} dz_2 \widetilde{A_2}(k_1 - k_2, z_2) \\ &\times \int_{-\infty}^{\infty} dz_3 \widetilde{A_3}(k_2 + 0.5k_m, z_3)\widetilde{\gamma}_3(k_m, k_1, k_2; \varepsilon_0, \varepsilon_1, \varepsilon_2),\end{aligned} \tag{74}$$

where

$$\begin{aligned}\widetilde{\gamma}_3(k_m, k_1, k_2; \varepsilon_0, \varepsilon_1, \varepsilon_2) &= \int_{-\infty}^{\infty} dk_z \frac{(k_z^2 + k_m^2)^2}{u_1 u_2} e^{i[\varepsilon_0 k_z + \varepsilon_1 u_1 + \varepsilon_2 u_2]} \\ &= \int_{-\infty}^{\infty} dk_z \frac{(k_z^2 + k_m^2)^2}{u_1 u_2} e^{i\triangle\psi} e^{i[\varepsilon_0 + \varepsilon_1 + \varepsilon_2]k_z}.\end{aligned} \tag{75}$$

$$\begin{aligned}&\varepsilon_0 = 0.5(z_1 + z_3) - z \qquad \varepsilon_1 = 0.5|z_1 - z_2| \qquad \varepsilon_2 = 0.5|z_2 - z_3| \\ &u_1 = 2q_1 = \mathrm{sgn}(k_z)\sqrt{k_z^2 + a_1} \qquad u_2 = 2q_2 = \mathrm{sgn}(k_z)\sqrt{k_z^2 + a_2} \\ &a_1 = k_m^2 - 4k_1^2 \qquad a_2 = k_m^2 - 4k_2^2 \\ &\triangle\psi = \varepsilon_1 \times (u_1 - k_z) + \varepsilon_2 \times (u_2 - k_z).\end{aligned} \tag{76}$$

Evaluation of $F = \mathcal{SC}_3(A_1, A_2, A_3)$ in the (k_m, z) domain

¿From equation (75) and (76), it's easy to tell that $\widetilde{\gamma}_3$ is not an ordinary function because $\lim_{k_z \to \infty} \frac{u_1}{k_z} = \frac{u_2}{k_z} = 1$, so the integrand $(k_z^2 + k_m^2)^2/(u_1 u_2)$ approaches k_z^2 as $k_z \to \infty$. We can decompose $(k_z^2 + k_m^2)^2 e^{i\triangle\psi}/(u_1 u_2)$ as follows:

$$\begin{aligned}\frac{(k_z^2 + k_m^2)^2 e^{i\triangle\psi}}{u_1 u_2} &= k_z^2 + i\frac{\varepsilon_1 a_1 + \varepsilon_2 a_2}{2} k_z + \left(k_m^2 + 2(k_1^2 + k_2^2) - \frac{(\varepsilon_1 a_1 + \varepsilon_2 a_2)^2}{8}\right) + \widetilde{\widetilde{\xi}}_3 \\ \widetilde{\widetilde{\xi}}_3 &= \frac{(k_z^2 + k_m^2)^2 e^{i\triangle\psi}}{u_1 u_2} - k_z^2 - i\frac{\varepsilon_1 a_1 + \varepsilon_2 a_2}{2} k_z - \left(k_m^2 + 2(k_1^2 + k_2^2) - \frac{(\varepsilon_1 a_1 + \varepsilon_2 a_2)^2}{8}\right)\end{aligned}$$

Decomposition above is based on the fact that, after put into the integral of inverse Fourier transform $\int_{-\infty}^{\infty} dk_z e^{i(\varepsilon_0+\varepsilon_1+\varepsilon_1)k_z}$, the first term k_z^2 will result in a singular distribution:

$$\int_{-\infty}^{\infty} k_z^2 e^{i(\varepsilon_0+\varepsilon_1+\varepsilon_2)k_z} dk_z = -\frac{\partial^2 \int_{-\infty}^{\infty} e^{i(\varepsilon_0+\varepsilon_1+\varepsilon_2)k_z} dk_z}{\partial(\varepsilon_0+\varepsilon_1+\varepsilon_1)^2} = -(2\pi) \times \delta''(\varepsilon_0+\varepsilon_1+\varepsilon_2)$$

Likewise another singular distribution is produced by the second term:

$$\int_{-\infty}^{\infty} ik_z \frac{\varepsilon_1 a_1 + \varepsilon_2 a_2}{2} e^{i(\varepsilon_0+\varepsilon_1+\varepsilon_2)k_z} dk_z = \pi(\varepsilon_1 a_1 + \varepsilon_2 a_2) \times \delta'(\varepsilon_0+\varepsilon_1+\varepsilon_2),$$

and the last singular distribution is produced by the third term:

$$\begin{aligned}&\int_{-\infty}^{\infty} \left(k_m^2 + 2(k_1^2+k_2^2) - \frac{(\varepsilon_1 a_1 + \varepsilon_2 a_2)^2}{8}\right) e^{i(\varepsilon_0+\varepsilon_1+\varepsilon_2)k_z} dk_z \\ &= 2\pi \left(k_m^2 + 2(k_1^2+k_2^2) - \frac{(\varepsilon_1 a_1 + \varepsilon_2 a_2)^2}{8}\right) \times \delta(\varepsilon_0+\varepsilon_1+\varepsilon_2)\end{aligned}$$

But the distribution produced by the fourth term:

$$\int_{-\infty}^{\infty} \widetilde{\widetilde{\xi}}_3 e^{i(\varepsilon_0+\varepsilon_1)k_z} dk_z$$

is regular because the the following limit is finite,

$$\lim_{k_z \mapsto \infty} \widetilde{\widetilde{\xi}}_3 \times k_z = \frac{k_m^2 + 2(k_1^2+k_2^2)}{2} (\varepsilon_1 a_1 + \varepsilon_2 a_2) - \frac{\varepsilon_1 a_1^2 + \varepsilon_2 a_2^2}{8} - \frac{(\varepsilon_1 a_1 + \varepsilon_2 a_2)^3}{48}$$

For the purpose of short notation, let's denote the numerically expressible function as $\widetilde{\xi}_3$:

$$\widetilde{\xi}_3(k_m, k_1, k_2; \varepsilon_0, \varepsilon_1, \varepsilon_2) = \int_{-\infty}^{\infty} \widetilde{\widetilde{\xi}}_3 e^{i(\varepsilon_0+\varepsilon_1+\varepsilon_2)k_z} dk_z$$

So we decompose $\widetilde{\gamma}_3(k_m, k_1, k_2; \varepsilon_0, \varepsilon_1, \varepsilon_2)$ into 3 singular distributions and 1 regular distribution:

$$\begin{aligned}&\widetilde{\gamma}_3(k_m, k_1, k_2; \varepsilon_0, \varepsilon_1, \varepsilon_2) = -(2\pi)\delta''(\varepsilon_0+\varepsilon_1+\varepsilon_2) + \pi(\varepsilon_1 a_1 + \varepsilon_2 a_2)\delta'(\varepsilon_0+\varepsilon_1+\varepsilon_2) \\ &+ 2\pi \left(k_m^2 + 2(k_1^2+k_2^2) - \frac{(\varepsilon_1 a_1 + \varepsilon_2 a_2)^2}{8}\right) \delta(\varepsilon_0+\varepsilon_1+\varepsilon_2) + \widetilde{\xi}_3(k_m, k_1, k_2; \varepsilon_0, \varepsilon_1, \varepsilon_2)\end{aligned} \tag{77}$$

Substituting equation (77) into equation (74), we can separate F as follows:

$$\begin{aligned}\widetilde{F}(k_m, z) = \frac{1}{128\pi^3} &\int_{-\infty}^{\infty} dk_1 \int_{-\infty}^{\infty} dk_2 \int_{-\infty}^{\infty} dz_1 \widetilde{A_1}(0.5k_m - k_1, z_1) \int_{-\infty}^{\infty} dz_2 \widetilde{A_2}(k_1 - k_2, z_2) \\ &\times \int_{-\infty}^{\infty} dz_3 \widetilde{A_3}(k_2 + 0.5k_m, z_3) \widetilde{\gamma}_3(k_m, k_1, k_2; \varepsilon_0, \varepsilon_1, \varepsilon_2) \\ = \widetilde{\mathcal{SC}}_{3,1} &+ \widetilde{\mathcal{SC}}_{3,2} + \widetilde{\mathcal{SC}}_{3,3} + \widetilde{\mathcal{SC}}_{3,4},\end{aligned}$$

where

$$\widetilde{\mathcal{SC}}_{3,1} = \frac{-1}{64\pi^2} \int_{-\infty}^{\infty} dk_1 \int_{-\infty}^{\infty} dk_2 \int_{-\infty}^{\infty} dz_1 \widetilde{A_1}(0.5k_m - k_1, z_1) \int_{-\infty}^{\infty} dz_2 \widetilde{A_2}(k_1 - k_2, z_2) \times \int_{-\infty}^{\infty} dz_3 \widetilde{A_3}(k_2 + 0.5k_m, z_3) \delta''(\varepsilon_0 + \varepsilon_1 + \varepsilon_2) \tag{78}$$

$$\widetilde{\mathcal{SC}}_{3,2} = \frac{1}{128\pi^2} \int_{-\infty}^{\infty} dk_1 \int_{-\infty}^{\infty} dk_2 \int_{-\infty}^{\infty} dz_1 \widetilde{A_1}(0.5k_m - k_1, z_1) \int_{-\infty}^{\infty} dz_2 \widetilde{A_2}(k_1 - k_2, z_2) \times \int_{-\infty}^{\infty} dz_3 \widetilde{A_3}(k_2 + 0.5k_m, z_3) \left[\varepsilon_1 a_1 + \varepsilon_2 a_2\right] \delta'(\varepsilon_0 + \varepsilon_1 + \varepsilon_2) \tag{79}$$

$$\widetilde{\mathcal{SC}}_{3,3} = \frac{-1}{64\pi^2} \int_{-\infty}^{\infty} dk_1 \int_{-\infty}^{\infty} dk_2 \int_{-\infty}^{\infty} dz_1 \widetilde{A_1}(0.5k_m - k_1, z_1) \int_{-\infty}^{\infty} dz_2 \widetilde{A_2}(k_1 - k_2, z_2) \int_{-\infty}^{\infty} dz_3 \times \widetilde{A_3}(k_2 + 0.5k_m, z_3) \left[k_m^2 + 2(k_1^2 + k_2^2) - \frac{(\varepsilon_1 a_1 + \varepsilon_2 a_2)}{8}\right] \delta(\varepsilon_0 + \varepsilon_1 + \varepsilon_2) \tag{80}$$

$$\widetilde{\mathcal{SC}}_{3,4} = \frac{-1}{64\pi^2} \int_{-\infty}^{\infty} dk_1 \int_{-\infty}^{\infty} dk_2 \int_{-\infty}^{\infty} dz_1 \widetilde{A_1}(0.5k_m - k_1, z_1) \int_{-\infty}^{\infty} dz_2 \widetilde{A_2}(k_1 - k_2, z_2) \int_{-\infty}^{\infty} dz_3 \times \widetilde{A_3}(k_2 + 0.5k_m, z_3) \widetilde{\xi}_3 \left(k_m, k_1, k_2, \frac{z_1 + z_3}{2} - z, \frac{|z_1 - z_2|}{2}, \frac{|z_2 - z_3|}{2}\right) \tag{81}$$

Except for the last term $\widetilde{\mathcal{SC}}_{3,4}$, all terms will be Fourier transformed from k_m to x in the following subsections. Only the first term $\mathcal{SC}_{3,1}$ is non-vanishing if the earth is 1D, it is called the more significant term.

Evaluation of $\widetilde{\mathcal{SC}}_{3,1}$ and $\mathcal{SC}_{3,1}$

First we Fourier transform equation (78) into (x, z) domain:

$$\mathcal{SC}_{3,1}(x,z) = \frac{1}{2\pi}\int_{-\infty}^{\infty} dk_m e^{ik_m x}\widetilde{\mathcal{SC}}_{3,1}$$

$$= \frac{-1}{128\pi^3}\int_{-\infty}^{\infty} dk_m e^{ik_m x}\int_{-\infty}^{\infty} dk_1\int_{-\infty}^{\infty} dk_2\int_{-\infty}^{\infty} dz_1\widetilde{A_1}(0.5k_m-k_1,z_1)$$

$$\times\int_{-\infty}^{\infty} dz_2\widetilde{A_2}(k_1-k_2,z_2)\int_{-\infty}^{\infty} dz_3\widetilde{A_3}(k_2+0.5k_m,z_3)\delta''(\varepsilon_0+\varepsilon_1+\varepsilon_2)$$

$$= \frac{-1}{128\pi^3}\int_{-\infty}^{\infty} dk_m e^{ik_m x}\int_{-\infty}^{\infty} dk_1\int_{-\infty}^{\infty} dk_2\int_{-\infty}^{\infty} dz_1\int_{-\infty}^{\infty} dx_1 A_1(x_1,z_1)e^{-i(0.5k_m-k_1)x_1}\int_{-\infty}^{\infty} dz_2$$

$$\times\int_{-\infty}^{\infty} dx_2 A_2(x_2,z_2)e^{-i(k_1-k_2)x_2}\int_{-\infty}^{\infty} dz_3\int_{-\infty}^{\infty} dx_3 A_3(x_3,z_3)e^{-i(k_2+0.5k_m)x_3}\delta''(\varepsilon_0+\varepsilon_1+\varepsilon_2)$$

$$= \frac{-1}{128\pi^3}\int_{-\infty}^{\infty} dz_1\int_{-\infty}^{\infty} dx_1 A_1(x_1,z_1)\int_{-\infty}^{\infty} dz_2\int_{-\infty}^{\infty} dx_2 A_2(x_2,z_2)\int_{-\infty}^{\infty} dz_3\int_{-\infty}^{\infty} dx_3 A_3(x_3,z_3)$$

$$\times\delta''(\varepsilon_0+\varepsilon_1+\varepsilon_2)\int_{-\infty}^{\infty} dk_m e^{ik_m(x-0.5x_1-0.5x_3)}\int_{-\infty}^{\infty} dk_1 e^{ik_1(x_1-x_2)}\int_{-\infty}^{\infty} dk_2 e^{ik_2(x_2-x_3)}$$

¿From this point, it should be very clear that the integral above can be greatly simplified because the inner 3 integrals are δ-functions:

$$\mathcal{SC}_{3,1}(x,z) = \frac{-8\pi^3}{128\pi^3}\int_{-\infty}^{\infty} dz_1\int_{-\infty}^{\infty} dx_1 A_1(x_1,z_1)\int_{-\infty}^{\infty} dz_2\int_{-\infty}^{\infty} dx_2 A_2(x_2,z_2)\int_{-\infty}^{\infty} dz_3\int_{-\infty}^{\infty} dx_3 A_3(x_3,z_3)$$

$$\times\delta''(\varepsilon_0+\varepsilon_1+\varepsilon_2)\delta(x-0.5x_1-0.5x_3)\delta(x_1-x_2)\delta(x_2-x_3)$$

$$= \frac{-1}{16}\int_{-\infty}^{\infty} dz_1\int_{-\infty}^{\infty} dz_2\int_{-\infty}^{\infty} dz_3\delta''(\varepsilon_0+\varepsilon_1+\varepsilon_2)\int_{-\infty}^{\infty} dx_1 A_1(x_1,z_1)$$

$$\times\int_{-\infty}^{\infty} dx_2 A_2(x_2,z_2)\delta(x_2-x_1)\int_{-\infty}^{\infty} dx_3 A_3(x_3,z_3)\delta(0.5x_1+0.5x_3-x)\delta(x_3-x_2)$$

$$= \frac{-1}{16}\int_{-\infty}^{\infty} dz_1 \int_{-\infty}^{\infty} dz_2 \int_{-\infty}^{\infty} dz_3 \delta''(\varepsilon_0+\varepsilon_1+\varepsilon_2) \int_{-\infty}^{\infty} dx_1 A_1(x_1,z_1)$$
$$\times \int_{-\infty}^{\infty} dx_2 A_2(x_2,z_2) A_3(x_2,z_3)\delta(0.5x_1+0.5x_2-x)\delta(x_2-x_1)$$
$$= \frac{-1}{16}\int_{-\infty}^{\infty} dz_1 \int_{-\infty}^{\infty} dz_2 \int_{-\infty}^{\infty} dz_3 \delta''(\varepsilon_0+\varepsilon_1+\varepsilon_2) \int_{-\infty}^{\infty} dx_1 A_1(x_1,z_1)A_2(x_1,z_2)A_3(x_1,z_3)\delta(x_1-x)$$

$$= \frac{-1}{16}\int_{-\infty}^{\infty} dz_1 \int_{-\infty}^{\infty} dz_2 \int_{-\infty}^{\infty} dz_3 \delta''(\varepsilon_0+\varepsilon_1+\varepsilon_2) A_1(x,z_1)A_2(x,z_2)A_3(x,z_3)$$
$$= \frac{-1}{16}\int_{-\infty}^{\infty} dz_1 A_1(x,z_1) \int_{-\infty}^{\infty} dz_2 A_2(x,z_2) \int_{-\infty}^{\infty} dz_3 A_3(x,z_3)\delta''(\varepsilon_0+\varepsilon_1+\varepsilon_2)$$
$$= \mathcal{SC}_{3,1,1}(x,z)+\mathcal{SC}_{3,1,2}(x,z)+\mathcal{SC}_{3,1,3}(x,z)+\mathcal{SC}_{3,1,4}(x,z)$$

According to equation (75), $\varepsilon_0+\varepsilon_1+\varepsilon_2$ has very different expressions depending on the relative relation between z_1, z_2, and z_3, that is, the higher-lower-higher relation which is crucial in the internal multiple attenuation.

Among different relative high-low relations between adjacent scatters. First let's consider $z_1 \geq z_2 \geq z_3$. Expressed in our classification scheme defined in equation (37), it's binary expression is $(00)_b = 0$, so we have: $l = 0+1 = 1$. So it should be written as $\mathcal{SC}_{3,1,1}(x,z)$. In this case $\varepsilon_0+\varepsilon_1+\varepsilon_2 = z_1 - z$.

$$\mathcal{SC}_{3,1,1}(x,z) = \frac{-1}{16}\int_{-\infty}^{\infty} dz_1 \delta''(z_1-z)\, A_1(x,z_1) \int_{-\infty}^{z_1} dz_2 A_2(x,z_2) \int_{-\infty}^{z_2} dz_3 A_3(x,z_3)$$

`Using equation (28) we have`

$$= \frac{-1}{16}\frac{\partial^2}{\partial z^2}\left(A_1(x,z)\int_{-\infty}^{z} dz_2 A_2(x,z_2)\int_{-\infty}^{z_2} dz_3 A_3(x,z_3)\right)$$
$$= -\frac{1}{16}\left[A_1\left[A_2A_3^{-z}\right]^{-z}\right]^{2z}$$
$$= -\frac{1}{16}\left(A_1^{2z}\left[A_2A_3^{-z}\right]^{-z} + 2A_1^{z}A_2A_3^{-z} + A_2^{z}A_1A_3^{-z} + A_1A_2A_3\right)$$

Next let's consider the relation $z_1 \leq z_2 \leq z_3$, in binary expression, it is $(11)_b = 3$. So we have $l = 3+1 = 4$. So the resulting integral is named $\mathcal{SC}_{3,1,4}(x,z)$. In this case $\varepsilon_0+\varepsilon_1+\varepsilon_2 = z_3 - z$.

$$\mathcal{SC}_{3,1,4}(x,z) = \frac{-1}{16}\int_{-\infty}^{\infty} dz_3\delta''(z_3-z)\,A_3(x,z_3)\int_{-\infty}^{z_3} dz_2 A_2(x,z_2)\int_{-\infty}^{z_2} dz_1 A_1(x,z_1)$$

`Using equation (28) we have`

$$= \frac{-1}{16}\frac{\partial^2}{\partial z^2}\left(A_3(x,z)\int_{-\infty}^{z} dz_2 A_2(x,z_2)\int_{-\infty}^{z_2} dz_1 A_1(x,z_1)\right)$$

$$= -\frac{1}{16}\left[A_3\left[A_2A_1^{-z}\right]^{-z}\right]^{2z}$$

$$= -\frac{1}{16}\left(A_3^{2z}\left[A_2A_1^{-z}\right]^{-z} + 2A_3^{z}A_2A_1^{-z} + A_2^{z}A_3A_1^{-z} + A_1A_2A_3\right)$$

Next let's study the case: $z1 \le z_2 \ge z3$, it's corresponding binary representation is $(10)_b = 2$, and $l = 2+1 = 3$. So correspondingly we have the name $\mathcal{SC}_{3,1,3}(x,z)$. In this case $\varepsilon_0+\varepsilon_1+\varepsilon_2 = z_2 - z$.

$$\mathcal{SC}_{3,1,3}(x,z) = \frac{-1}{16}\int_{-\infty}^{\infty} dz_2\delta''(z_2-z)\,A_2(x,z_2)\int_{-\infty}^{z_2} dz_1 A_1(x,z_1)\int_{-\infty}^{z_2} dz_3 A_3(x,z_3)$$

`Using equation (28) we have`

$$= \frac{-1}{16}\frac{\partial^2}{\partial z^2}\left(A_2(x,z)\int_{-\infty}^{z} dz_1 A_1(x,z_1)\int_{-\infty}^{z} dz_3 A_3(x,z_3)\right) = -\frac{1}{16}\left[A_2A_1^{-z}A_3^{-z}\right]^{2z}$$

$$= -\frac{1}{16}\left(A_2^{2z}A_1^{-z}A_3^{-z} + 2A_2^{z}A_1A_3^{-z} + 2A_2^{z}A_3A_1^{-z} + A_1^{z}A_2A_3^{-z} + A_3^{z}A_2A_1^{-z} + 2A_1A_2A_3\right)$$

We then consider the case $z_1 \ge z_2 \le z_3$, it's binary representation is $(01)_b = 1$, we have $l = 1+1 = 2$. So it's name is $\mathcal{SC}_{3,1,2}(x,z)$. In this case $\varepsilon_0+\varepsilon_1+\varepsilon_2 = z_1 - z_2 + z_3 - z$.

$$\mathcal{SC}_{3,1,2}(x,z) = \frac{-1}{16}\int_{-\infty}^{\infty} dz_3 A_3(x,z_3)\int_{-\infty}^{z_3} dz_2 A_2(x,z_2)\int_{z_2}^{\infty} dz_1 A_1(x,z_1)\delta''(z_1-z_2+z_3-z)$$

Following the derivation of Shaw et. al. (2003), we define a new variable $u = z_1 + z_3 - z_2$, and change the integration variable from z_2 to u, the last integral in the equation above become:

$$\int_{-\infty}^{\infty} du\delta''(u-z)\int_{-\infty}^{u} dz_3 A_3(z_3)\int_{-\infty}^{u} dz_1 A_1(z_1)A_2(z_1+z_3-u)$$

`Using equation (28) we have`

$$= \frac{\partial^2}{\partial z^2}\int_{-\infty}^{z} dz_3 A_3(z_3)\int_{-\infty}^{z} dz_1 A_1(z_1)A_2(z_1+z_3-z)$$

$$= \frac{\partial}{\partial z}\left(A_1[A_2A_3]^{-z} + A_3[A_2A_1]^{-z} - \int_{-\infty}^{z} dz_3 A_3(z_3) \int_{-\infty}^{z} dz_1 A_1(z_1) A_2'(z_1+z_3-z) \right)$$
$$= \left[A_1[A_2A_3]^{-z}\right]^{z} + \left[A_3[A_2A_1]^{-z}\right]^{z} - A_1[A_3A_2^{z}]^{-z} - A_3[A_1A_2^{z}]^{-z}$$
$$+ \int_{-\infty}^{z} dz_3 A_3(z_3) \int_{-\infty}^{z} dz_1 A_1(z_1) A_2''(z_1+z_3-z)$$

Following Shaw et. al. 2003, the derivatives in A_2 are evenly distributed to A_1 and A_3 using integration by parts as follows:

$$\int_{-\infty}^{z} dz_3 A_3(z_3) \int_{-\infty}^{z} dz_1 A_1(z_1) A_2''(z_1+z_3-z) = \int_{-\infty}^{z} dz_3 A_3(z_3) \int_{-\infty}^{z} A_1(z_1) dA_2'(z_1+z_3-z)$$
$$= A_1[A_2^{z}A_3]^{-z} - \int_{-\infty}^{z} dz_3 A_3(z_3) \int_{-\infty}^{z} dz_1 A_1'(z_1) A_2'(z_1+z_3-z)$$
$$= A_1[A_2^{z}A_3]^{-z} - \int_{-\infty}^{z} dz_1 A_1'(z_1) \int_{-\infty}^{z} dz_3 A_3(z_3) A_2'(z_1+z_3-z)$$

The last integral above can be rewritten using integration by parts once more to make it more symmetrical:

$$\int_{-\infty}^{z} dz_1 A_1'(z_1) \int_{-\infty}^{z} dz_3 A_3(z_3) A_2'(z_1+z_3-z)$$
$$= A_1[A_2^{z}A_3]^{-z} - A_3[A_1^{z}A_2]^{-z} + \int_{-\infty}^{z} dz_1 A_1'(z_1) \int_{-\infty}^{z} dz_3 A_3'(z_3) A_2(z_1+z_3-z)$$

In summary, we have:

$$\int_{-\infty}^{\infty} du \delta''(u-z) \int_{-\infty}^{u} dz_3 A_3(z_3) \int_{-\infty}^{u} dz_1 A_1(z_1) A_2(z_1+z_3-u)$$
$$= \left[A_1[A_2A_3]^{-z}\right]^{z} + \left[A_3[A_2A_1]^{-z}\right]^{z} - A_1[A_3A_2^{z}]^{-z} - A_3[A_1A_2^{z}]^{-z}$$
$$+ A_1[A_2^{z}A_3]^{-z} - A_3[A_1^{z}A_2]^{-z} + \int_{-\infty}^{z} dz_1 A_1'(z_1) \int_{-\infty}^{z} dz_3 A_3'(z_3) A_2(z_1+z_3-z)$$

$$
\begin{aligned}
&= \left[A_1[A_2A_3]^{-z}\right]^{z} + \left[A_3[A_2A_1]^{-z}\right]^{z} - A_3[A_1A_2^z + A_1^zA_2]^{-z} \\
&+ \int_{-\infty}^{z} dz_1 A_1'(z_1) \int_{-\infty}^{z} dz_3 A_3'(z_3) A_2(z_1+z_3-z) \\
&= \left[A_1[A_2A_3]^{-z}\right]^{z} + \left[A_3[A_2A_1]^{-z}\right]^{z} - A_1A_2A_3 + \int_{-\infty}^{z} dz_1 A_1'(z_1) \int_{-\infty}^{z} dz_3 A_3'(z_3) A_2(z_1+z_3-z) \\
&= \left[A_1[A_2A_3]^{-z}\right]^{z} + \left[A_3[A_2A_1]^{-z}\right]^{z} - A_1A_2A_3 + \mathbb{IM}_1(A_1^z, A_2, A_3^z) \\
&= A_1^z[A_2A_3]^{-z} + A_3^z[A_2A_1]^{-z} + A_1A_2A_3 + \mathbb{IM}_1(A_1^z, A_2, A_3^z)
\end{aligned}
$$

According to the results of Shaw et al, in the special case of $A_1 = A_2 = A_3 = \alpha_1$. This last integral in the equation above: $\mathbb{IM}_1(A_1, A_2, A_3)$, will give a box at the correct time for first order internal multiples, with a very small factor difference.

$$
\begin{aligned}
-16\mathcal{SC}_{3,1,1}(A_1,A_2,A_3) &= \left[A_1\left[A_2A_3^{-z}\right]^{-z}\right]^{2z} \\
-16\mathcal{SC}_{3,1,4}(A_1,A_2,A_3) &= \left[A_3\left[A_2A_1^{-z}\right]^{-z}\right]^{2z} \\
-16\mathcal{SC}_{3,1,3}(A_1,A_2,A_3) &= \left[A_2A_1^{-z}A_3^{-z}\right]^{2z} \\
-16\mathcal{SC}_{3,1,2}(A_1,A_2,A_3) &= A_1^z[A_2A_3]^{-z} + A_3^z[A_2A_1]^{-z} + A_1A_2A_3 + \mathbb{IM}_1(A_1^z, A_2, A_3^z)
\end{aligned}
$$

Because the relation between A_1, A_2, and A_3 is not fixed, we cannot simplify the expression above further. But in the inverse scattering theory, all the 6 permutation of (A_1, A_2, A_3) will also be present. (If there is any equality between A_1, A_2, A_3, the degeneracy can be easily handled by multiplying a factor.)

First, consider the permutation sum of $\mathcal{SC}_{3,1,1}$, we have:

$$
\begin{aligned}
&\mathbb{SC}_{3,1,1}(A_1,A_2,A_3) = \mathtt{sum}_1 + \mathtt{sum}_2 + \mathtt{sum}_3 \qquad \mathtt{where} \\
&\mathtt{sum}_1 = \mathcal{SC}_{3,1,1}(A_1,A_2,A_3) + \mathcal{SC}_{3,1,1}(A_1,A_3,A_2) \\
&= \frac{-1}{16}\left(\left[A_1\left[A_2A_3^{-z}\right]^{-z}\right]^{2z} + \left[A_1\left[A_3A_2^{-z}\right]^{-z}\right]^{2z}\right) = \overrightarrow{(25)} = \frac{-1}{16}\left[A_1A_2^{-z}A_3^{-z}\right]^{2z} \\
&\mathtt{sum}_2 = \mathbb{SC}_{3,1,1}(A_2,A_3,A_1) + \mathbb{SC}_{3,1,1}(A_2,A_1,A_3) = \overrightarrow{(25)} = \frac{-1}{16}\left[A_2A_3^{-z}A_1^{-z}\right]^{2z} \\
&\mathtt{sum}_3 = \mathbb{SC}_{3,1,1}(A_3,A_1,A_2) + \mathbb{SC}_{3,1,1}(A_3,A_2,A_1) = \overrightarrow{(25)} = \frac{-1}{16}\left[A_3A_1^{-z}A_2^{-z}\right]^{2z} \\
&\mathbb{SC}_{3,1,1}(A_1,A_2,A_3) = \frac{-1}{16}\left[A_1A_2^{-z}A_3^{-z} + A_1^{-z}A_2A_3^{-z} + A_1^{-z}A_2^{-z}A_3\right]^{2z}
\end{aligned}
$$

We then consider the permutation sum of $\mathcal{SC}_{3,1,4}$, because of the following equality:

$$
\mathcal{SC}_{3,1,4}(A_1,A_2,A_3) = \frac{-1}{16}\left[A_3\left[A_2A_1^{-z}\right]^{-z}\right]^{2z} = \mathcal{SC}_{3,1,1}(A_3,A_2,A_1)
$$

That is, every term in the permutation sum of $\mathbb{SC}_{3,1,4}$ is equivalent to one term in the permutation of $\mathbb{SC}_{3,1,1}$. It's easy to see that these 2 permutation sums are equivalent:

$$\mathbb{SC}_{3,1,4} = \mathbb{SC}_{3,1,1}$$

We then consider the permutation sum of $\mathcal{SC}_{3,1,3}$, because of the following equality:

$$\begin{aligned}&\mathcal{SC}_{3,1,1}(A_1, A_2, A_3) + \mathcal{SC}_{3,1,1}(A_1, A_3, A_2) = \frac{-1}{16}\left[A_1 A_2^{-z} A_3^{-z}\right]^{2z} \\ &= \mathcal{SC}_{3,1,3}(A_1, A_2, A_3) = \mathcal{SC}_{3,1,3}(A_1, A_3, A_2)\end{aligned}$$

That is, the sum of 2 terms of in the permutation sum of $\mathbb{SC}_{3,1,1}$ equals to one of the 2 identical terms in the permutation sum of $\mathbb{SC}_{3,1,3}$. We have:

$$\mathbb{SC}_{3,1,1} = \frac{1}{2}\mathbb{SC}_{3,1,3}$$

In summary, we have:

$$\begin{aligned}-16\mathbb{SC}_{3,1,1}(A_1, A_2, A_3) &= \left[A_1 A_2^{-z} A_3^{-z} + A_1^{-z} A_2 A_3^{-z} + A_1^{-z} A_2^{-z} A_3\right]^{2z} \\ &= \left\{\begin{array}{c} A_1^{2z} A_2^{-z} A_3^{-z} \\ A_1^{-z} A_2^{2z} A_3^{-z} \\ A_1^{-z} A_2^{-z} A_3^{2z} \end{array}\right\} + 3 \cdot \left\{\begin{array}{c} A_1^{z} A_2 A_3^{-z} \\ A_1^{z} A_2^{-z} A_3 \\ A_1 A_2^{z} A_3^{-z} \\ A_1 A_2^{-z} A_3^{z} \\ A_1^{-z} A_2 A_3^{z} \\ A_1^{-z} A_2^{z} A_3 \end{array}\right\} + 6 \cdot A_1 A_2 A_3 \\ \mathbb{SC}_{3,1,4}(A_1, A_2, A_3) &= \mathbb{SC}_{3,1,1}(A_1, A_2, A_3) \\ \mathbb{SC}_{3,1,3}(A_1, A_2, A_3) &= 2 \times \mathbb{SC}_{3,1,1}(A_1, A_2, A_3) \\ -16\mathbb{SC}_{3,1,2}(A_1, A_2, A_3) &= 4 \cdot \left\{\begin{array}{c} A_1^{z}[A_2 A_3]^{-z} \\ A_2^{z}[A_1 A_3]^{-z} \\ A_3^{z}[A_1 A_2]^{-z} \end{array}\right\} + 6 \cdot A_1 A_2 A_3 + 2 \cdot \left\{\begin{array}{c} \mathbb{IM}_1(A_1^{z}, A_2, A_3^{z}) \\ \mathbb{IM}_1(A_2^{z}, A_1, A_3^{z}) \\ \mathbb{IM}_1(A_1^{z}, A_3, A_2^{z}) \end{array}\right\}\end{aligned}$$

¿From the study above, even in the general case, after the permutation sum, symmetry was preserved between different high-low relations: all the non-w diagrams are essentially the same, they differ at most by a constant factor.

In α_3, the same symmetry between different high-low relation had already been extensively studied by Shaw et. al. and Innanen et. al.

The fact that the same symmetry shown in the simplest case in the permutation sum of more complicated terms, suggest in the derivation process, permutation sum can simplify the relations.

Let's summarize $\mathbb{SC}_3(A_1, A_2, A_3)$ in the most general case that these 3 scatters are distinct with each other:

$$\begin{aligned}\mathbb{SC}_{3,1}(A_1, A_2, A_3) = &-\frac{1}{4}\left\{\begin{array}{c} A_1^{2z}A_2^{-z}A_3^{-z} \\ A_1^{-z}A_2^{2z}A_3^{-z} \\ A_1^{-z}A_2^{-z}A_3^{2z}\end{array}\right\} - \frac{3}{4}\cdot\left\{\begin{array}{c} A_1^{z}A_2A_3^{-z} \\ A_1^{z}A_2^{-z}A_3 \\ A_1A_2^{z}A_3^{-z} \\ A_1A_2^{-z}A_3^{z} \\ A_1^{-z}A_2A_3^{z} \\ A_1^{-z}A_2^{z}A_3\end{array}\right\} - \frac{15}{8}\cdot A_1A_2A_3 \\ &-\frac{1}{4}\cdot\left\{\begin{array}{c} A_1^{z}[A_2A_3]^{-z} \\ A_2^{z}[A_1A_3]^{-z} \\ A_3^{z}[A_1A_2]^{-z}\end{array}\right\} - \frac{1}{8}\cdot\left\{\begin{array}{c} \mathbb{IM}_1(A_1^{z}, A_2, A_3^{z}) \\ \mathbb{IM}_1(A_2^{z}, A_1, A_3^{z}) \\ \mathbb{IM}_1(A_1^{z}, A_3, A_2^{z})\end{array}\right\}\end{aligned} \tag{82}$$

If among these 3 scatters: A_1, A_2, A_3, 2 of them are equal. We have:

$$\begin{aligned}\mathbb{SC}_{3,1}(A_1, A_1, A_2) = &-\frac{1}{8}\left\{\begin{array}{c} 2A_1^{2z}A_1^{-z}A_2^{-z} \\ A_1^{-z}A_1^{-z}A_2^{2z}\end{array}\right\} - \frac{3}{4}\cdot\left\{\begin{array}{c} A_1^{z}A_1A_2^{-z} \\ A_1^{z}A_1^{-z}A_2 \\ A_1A_1^{-z}A_2^{z}\end{array}\right\} - \frac{15}{16}\cdot A_1A_1A_2 \\ &-\frac{1}{8}\cdot\left\{\begin{array}{c} 2A_1^{z}[A_1A_2]^{-z} \\ A_2^{z}[A_1A_1]^{-z}\end{array}\right\} - \frac{1}{16}\cdot\left\{\begin{array}{c} 2\mathbb{IM}_1(A_1^{z}, A_1, A_2^{z}) \\ \mathbb{IM}_1(A_1^{z}, A_2, A_1^{z})\end{array}\right\}\end{aligned} \tag{83}$$

If all these 3 scatters are equal: $A_1 = A_2 = A_3 = A$. We have:

$$\mathbb{SC}_{3,1}(A, A, A) = -\frac{1}{8}A^{2z}A^{-z}A^{-z} - \frac{3}{4}A^{z}AA^{-z} - \frac{5}{16}A^3 - \frac{1}{8}A^{z}\left[A^2\right]^{-z} - \frac{1}{16}\mathbb{IM}_1(A^{z}, A, A^{z}) \tag{84}$$

The more significant term is the only non-vanishing term if the earth is 1D. Otherwise, less significant terms described below will be activated:

Evaluation of $\mathcal{SC}_{3,2}$ and $\mathbb{SC}_{3,2}$

We then Fourier transform equation (79) into (x, z) domain:

$$\begin{aligned}\widetilde{\mathcal{SC}}_{3,2}(k_m, z) = &\frac{1}{128\pi^2}\int_{-\infty}^{\infty}dk_1\int_{-\infty}^{\infty}dk_2\int_{-\infty}^{\infty}dz_1\widetilde{A_1}(0.5k_m - k_1, z_1) \\ &\times\int_{-\infty}^{\infty}dz_2\widetilde{A_2}(k_1 - k_2, z_2)\int_{-\infty}^{\infty}dz_3\widetilde{A_3}(k_2 + 0.5k_m, z_3)(\varepsilon_1a_1 + \varepsilon_2a_2)\delta'(\varepsilon_0 + \varepsilon_1 + \varepsilon_2) \\ = &\frac{I_1(A_1, A_2, A_3) + I_2(A_1, A_2, A_3)}{128\pi^2}\end{aligned}$$

where:

$$I_1(A_1,A_2,A_3)=\int_{-\infty}^{\infty}dk_1\int_{-\infty}^{\infty}dk_2\int_{-\infty}^{\infty}dz_1\widetilde{A_1}(0.5k_m-k_1,z_1)\int_{-\infty}^{\infty}dz_2\widetilde{A_2}(k_1-k_2,z_2)$$
$$\times\int_{-\infty}^{\infty}dz_3\widetilde{A_3}(k_2+0.5k_m,z_3)\frac{|z_1-z_2|}{2}\left(k_m^2-4k_1^2\right)\delta'\left(\frac{z_1+z_3}{2}-z+\frac{|z_1-z_2|}{2}+\frac{|z_2-z_3|}{2}\right)$$
$$I_2(A_1,A_2,A_3)=\int_{-\infty}^{\infty}dk_1\int_{-\infty}^{\infty}dk_2\int_{-\infty}^{\infty}dz_1\widetilde{A_1}(0.5k_m-k_1,z_1)\int_{-\infty}^{\infty}dz_2\widetilde{A_2}(k_1-k_2,z_2)$$
$$\times\int_{-\infty}^{\infty}dz_3\widetilde{A_3}(k_2+0.5k_m,z_3)\frac{|z_2-z_3|}{2}\left(k_m^2-4k_2^2\right)\delta'\left(\frac{z_1+z_3}{2}-z+\frac{|z_1-z_2|}{2}+\frac{|z_2-z_3|}{2}\right)$$

Let's consider $I_2(A_1,A_2,A_3)$, we will prove its equivalence with $I_1(A_3,A_2,A_1)$. So we only need to calculate half of the integral. The other half can be obtained by switching the first and third scatters: $A_1\longleftrightarrow A_3$. Because the switch mentioned above happens among different terms in the permutation sum, it will not change the permutation sum. The permutation sum of I_1 and I_4 are actually the same.

$$\sum^{\odot}I_1\left(A_1,A_2,A_3\right)=\sum^{\odot}I_2\left(A_1,A_2,A_3\right)$$

$$I_2(A_1,A_2,A_3)=\int_{-\infty}^{\infty}dk_1\int_{-\infty}^{\infty}dk_2\int_{-\infty}^{\infty}dz_1\widetilde{A_1}(0.5k_m-k_1,z_1)\int_{-\infty}^{\infty}dz_2\widetilde{A_2}(k_1-k_2,z_2)$$
$$\times\int_{-\infty}^{\infty}dz_3\widetilde{A_3}(k_2+0.5k_m,z_3)\frac{|z_2-z_3|}{2}\left(k_m^2-4k_2^2\right)\delta'\left(\frac{z_1+z_3}{2}-z+\frac{|z_1-z_2|}{2}+\frac{|z_2-z_3|}{2}\right)$$
$$\texttt{define}:\quad k_1'=-k_2\quad k_2'=-k_1\quad z_2'=z_2\quad z_1'=z_3\quad z_3'=z_1\quad \texttt{we have}$$
$$=\int_{-\infty}^{\infty}dk_1'\int_{-\infty}^{\infty}dk_2'\int_{-\infty}^{\infty}dz_1\widetilde{A_1}(0.5k_m+k_2',z_3')\int_{-\infty}^{\infty}dz_2'\widetilde{A_2}(k_1'-k_2',z_2')$$
$$\times\int_{-\infty}^{\infty}dz_3'\widetilde{A_3}(0.5k_m-k_1',z_3)\frac{|z_1'-z_2'|}{2}\left(k_m^2-4k_1'^2\right)\delta'\left(\frac{z_1'+z_3'}{2}-z+\frac{|z_1'-z_2'|}{2}+\frac{|z_2'-z_3'|}{2}\right)$$
$$=I_1(A_3,A_2,A_1)$$

Let's Fourier transform the left half of the integral expression for $\widetilde{\mathcal{SC}}_{3,2}$ (it will be denoted as $\widetilde{\mathcal{SC}}_{3,2}^{\texttt{left}}$ hereafter) into (x,z) domain.

$$\mathcal{SC}_{3,2}^{\texttt{left}}(x,z) = \frac{1}{2\pi}\int_{-\infty}^{\infty} dk_m e^{ik_m x} I_1(A_1,A_2,A_3)$$
$$= \frac{1}{256\pi^3}\int_{-\infty}^{\infty} dz_1 \int_{-\infty}^{\infty} dz_2 \int_{-\infty}^{\infty} dz_3 \delta'(\varepsilon_0+\varepsilon_1+\varepsilon_2)\varepsilon_1 \int_{-\infty}^{\infty} dk_m e^{ik_m x}$$
$$\times \int_{-\infty}^{\infty} dk_1 \int_{-\infty}^{\infty} dk_2 a_1 \widetilde{A_1}(0.5k_m-k_1,z_1)\widetilde{A_2}(k_1-k_2,z_2)\widetilde{A_3}(k_2+0.5k_m,z_3)$$

and further express $\widetilde{A_1}$, $\widetilde{A_2}$, and $\widetilde{A_3}$ in the (x,z) domain. The Fourier transform over x is defined in equation (16).

$$\widetilde{A_1}(0.5k_m-k_1,z_1) = \int_{-\infty}^{\infty} dx_1 e^{-i(0.5k_m-k_1)x_1} A_1(x_1,z_1)$$
$$\widetilde{A_2}(k_1-k_2,z_2) = \int_{-\infty}^{\infty} dx_2 e^{-i(k_1-k_2)x_2} A_1(x_2,z_2)$$
$$\widetilde{A_3}(k_2+0.5k_m,z_3) = \int_{-\infty}^{\infty} dx_3 e^{-i(k_2+0.5k_m)x_3} A_1(x_3,z_3)$$

we have:

$$\mathcal{SC}_{3,2}^{\texttt{left}}(x,z) = \frac{1}{256\pi^3}\int_{-\infty}^{\infty} dz_1 \int_{-\infty}^{\infty} dz_2 \int_{-\infty}^{\infty} dz_3 \delta'(\varepsilon_0+\varepsilon_1+\varepsilon_2)\varepsilon_1$$
$$\times \int_{-\infty}^{\infty} dx_1 A_1(x_1,z_1) \int_{-\infty}^{\infty} dx_2 A_2(x_2,z_2) \int_{-\infty}^{\infty} dx_3 A_3(x_3,z_3)$$
$$\times \int_{-\infty}^{\infty} dk_1 e^{ik_1(x_1-x_2)} \int_{-\infty}^{\infty} dk_2 e^{ik_2(x_2-x_3)} \left(k_m^2-4k_1^2\right) \int_{-\infty}^{\infty} dk_m e^{ik_m(x-0.5x_1-0.5x_2)}$$

`Using equation` (126) `we have`

$$= -\frac{1}{8}\int_{-\infty}^{\infty} dz_1 \int_{-\infty}^{\infty} dz_2 \int_{-\infty}^{\infty} dz_3 \delta'(\varepsilon_0+\varepsilon_1+\varepsilon_2)\varepsilon_1 \frac{\partial A_1(x,z_1)}{\partial x}\frac{\partial}{\partial x}\left[A_2(x,z_2)A_3(x,z_3)\right]$$
$$= -\frac{1}{16}\int_{-\infty}^{\infty} dz_1 \int_{-\infty}^{\infty} dz_2 \int_{-\infty}^{\infty} dz_3 \delta'(\varepsilon_0+\varepsilon_1+\varepsilon_2)\left|z_1-z_2\right| \frac{\partial A_1(x,z_1)}{\partial x}\frac{\partial}{\partial x}\left[A_2(x,z_2)A_3(x,z_3)\right]$$

The integrand can be naturally separated into 2 terms:

$$\begin{aligned}&\frac{\partial A_1(x,z_1)}{\partial x}\frac{\partial}{\partial x}\left[A_2(x,z_2)A_3(x,z_3)\right]\\=&\frac{\partial A_1(x,z_1)}{\partial x}\frac{\partial A_2(x,z_2)}{\partial x}A_3(x,z_3)+\frac{\partial A_1(x,z_1)}{\partial x}A_2(x,z_3)\frac{\partial A_3(x,z_3)}{\partial x}\end{aligned}$$

Similarly, the $\mathcal{SC}_{3,2}^{\texttt{left}}$ can be decomposed as follows:

$$\begin{aligned}16\mathcal{SC}_{3,2}^{\texttt{left}}(x,z)=&-\int_{-\infty}^{\infty}dz_1\int_{-\infty}^{\infty}dz_2\int_{-\infty}^{\infty}dz_3\delta'(\varepsilon_0+\varepsilon_1+\varepsilon_2)\left|z_1-z_2\right|\frac{\partial A_1(x,z_1)}{\partial x}\frac{\partial A_2(x,z_2)}{\partial x}A_3(x,z_3)\\&-\int_{-\infty}^{\infty}dz_1\int_{-\infty}^{\infty}dz_2\int_{-\infty}^{\infty}dz_3\delta'(\varepsilon_0+\varepsilon_1+\varepsilon_2)\left|z_1-z_2\right|\frac{\partial A_1(x,z_1)}{\partial x}A_2(x,z_3)\frac{\partial A_3(x,z_3)}{\partial x}\end{aligned}$$

Without considering the different x-wise operations on each factor, each of them is expressible in the product of 3 function of z: $B_1(z_1)B_2(z_2)B_3(z_3)$. So the z-wise integral is of the form:

$$\begin{aligned}&\Pi_z(B_1,B_2,B_3)=\\&-\int_{-\infty}^{\infty}dz_1\delta'(z_1-z)B_1(z_1)\int_{-\infty}^{z_1}dz_2\left(z_1-z_2\right)B_2(z_2)\int_{-\infty}^{z_2}dz_3B_3(z_3)\\&-\int_{-\infty}^{\infty}dz_3\delta'(z_3-z)B_3(z_3)\int_{-\infty}^{z_3}dz_2B_2(z_2)\int_{-\infty}^{z_2}dz_1\left(z_2-z_1\right)B_1(x_1,z_1)\\&-\int_{-\infty}^{\infty}dz_2\delta'(z_2-z)B_2(z_2)\int_{-\infty}^{z_2}dz_1\left(z_2-z_1\right)B_1(z_1)\int_{-\infty}^{z_2}dz_3B_3(z_3)\\&-\int_{-\infty}^{\infty}du\delta'(u-z)\int_{-\infty}^{u}dz_1B_1(z_1)\int_{-\infty}^{u}dz_3\left(u-z_3\right)B_2(z_1+z_3-u)B_3(z_3)\\=&\Pi_z^{(1)}+\Pi_z^{(2)}+\Pi_z^{(3)}+\Pi_z^{(4)}\end{aligned}\tag{85}$$

Integrals above can be simplified by the rule of integrating over δ-functions. See equation (27) for detail. In short, we have:

$$
\begin{aligned}
\Pi_z^{(1)} &= -\int_{-\infty}^{\infty} dz_1 \delta'(z_1 - z) B_1(z_1) \int_{-\infty}^{z_1} dz_2 \, (z_1 - z_2) \, B_2(z_2) \int_{-\infty}^{z_2} dz_3 B_3(z_3) \\
&= B_1^z \left[B_2 B_3^{-z}\right]^{-2z} + B_1 \left[B_2 B_3^{-z}\right]^{-z} \\
\Pi_z^{(4)} &= -\int_{-\infty}^{\infty} dz_3 \delta'(z_3 - z) B_3(z_3) \int_{-\infty}^{z_3} dz_2 B_2(z_2) \int_{-\infty}^{z_2} dz_1 \, (z_2 - z_1) \, B_1(x_1, z_1) \\
&= B_3^z \left[B_2 B_1^{-2z}\right]^{-z} + B_2 B_3 B_1^{-2z} \\
\Pi_z^{(3)} &= -\int_{-\infty}^{\infty} dz_2 \delta'(z_2 - z) B_2(z_2) \int_{-\infty}^{z_2} dz_1 \, (z_2 - z_1) \, B_1(z_1) \int_{-\infty}^{z_2} dz_3 B_3(z_3) \\
&= B_2^z B_3^{-z} B_1^{-2z} + B_2 B_1^{-z} B_3^{-z} + B_2 B_3 B_1^{-2z} \\
\Pi_z^{(2)} &= -\int_{-\infty}^{\infty} du \delta'(u - z) \int_{-\infty}^{u} dz_1 B_1(z_1) \int_{-\infty}^{u} dz_3 \, (u - z_3) \, B_2(z_1 + z_3 - u) B_3(z_3) \\
&= \mathbb{IM}_1(B_1, B_2, B_3) + B_1[B_2 B_3]^{-2z} - \mathbb{IM}_2(B_1, B_2^z, B_3) \\
&= B_1[B_2 B_3]^{-2z} + \mathbb{IM}_2(B_1, B_2, B_3^z)
\end{aligned}
$$

Summing the terms together, we have:

$$
\begin{aligned}
\Pi_z \left(B_1, B_2, B_3\right) &= \left\{B_1^z \left[B_2 B_3^{-z}\right]^{-2z} + B_1 \left[B_2 B_3^{-z}\right]^{-z}\right\} + \left\{B_3^z \left[B_2 B_1^{-2z}\right]^{-z} + B_2 B_3 B_1^{-2z}\right\} \\
&+ \left\{B_2^z B_3^{-z} B_1^{-2z} + B_2 B_1^{-z} B_3^{-z} + B_2 B_3 B_1^{-2z}\right\} \\
&+ \left\{\mathbb{IM}_1(B_1, B_2, B_3) + B_1[B_2 B_3]^{-2z} - \mathbb{IM}_2(B_1, B_2^z, B_3)\right\} \\
&= \left\{B_1^z \left[B_2 B_3^{-z}\right]^{-2z} + B_1 \left[B_2 B_3^{-z}\right]^{-z}\right\} + \left\{B_3^z \left[B_2 B_1^{-2z}\right]^{-z} + B_2 B_3 B_1^{-2z}\right\} \\
&+ \left\{B_2^z B_3^{-z} B_1^{-2z} + B_2 B_1^{-z} B_3^{-z} + B_2 B_3 B_1^{-2z}\right\} + \left\{B_1[B_2 B_3]^{-2z} + \mathbb{IM}_2(B_1, B_2, B_3^z)\right\} \\
&= \left[E_1 + E_2 + E_3 + E_4 + E_5 + E_6 + E_7 + E_8 + E_9\right](B_1, B_2, B_3)
\end{aligned}
$$

where:

$$
\begin{array}{lll}
E_1(B_1, B_2, B_3) = B_1^z \left[B_2 B_3^{-z}\right]^{-2z} & E_2(B_1, B_2, B_3) = B_1 \left[B_2 B_3^{-z}\right]^{-z} & E_3(B_1, B_2, B_3) = B_3^z \left[B_2 B_1^{-2z}\right]^{-z} \\
E_4(B_1, B_2, B_3) = B_2 B_3 B_1^{-2z} & E_5(B_1, B_2, B_3) = B_2^z B_3^{-z} B_1^{-2z} & E_6(B_1, B_2, B_3) = B_2 B_1^{-z} B_3^{-z} \\
E_7(B_1, B_2, B_3) = B_2 B_3 B_1^{-2z} & E_8(B_1, B_2, B_3) = B_1[B_2 B_3]^{-2z} & E_9(B_1, B_2, B_3) = \mathbb{IM}_2(B_1, B_2, B_3^z)
\end{array}
$$

Equation (85) will be evaluated twice, in the first evaluation, substituting in $B_1 = \frac{\partial A_1}{\partial x}$, $B_2 = \frac{\partial A_2}{\partial x}$, $B_3 = A_3$, in the second evaluation, we substitute in $B_1 = \frac{\partial A_1}{\partial x}$, $B_3 = A_2$, $B_2 = \frac{\partial A_3}{\partial x}$. Then

the 2 evaluations will be summed together to have: $\Pi_z(\frac{\partial A_1}{\partial x}, \frac{\partial A_2}{\partial x}, A_3) + \Pi_z(\frac{\partial A_1}{\partial x}, A_2, \frac{\partial A_3}{\partial x})$. With straightforward algebra, it's easy to see:

$$E_1\left(\frac{\partial A_1}{\partial x}, \frac{\partial A_2}{\partial x}, A_3\right) + E_1\left(\frac{\partial A_1}{\partial x}, A_2, \frac{\partial A_3}{\partial x}\right) = A_1^{x+z}\left[A_2 A_3^{-z}\right]^{x-2z}$$

$$E_2\left(\frac{\partial A_1}{\partial x}, \frac{\partial A_2}{\partial x}, A_3\right) + E_2\left(\frac{\partial A_1}{\partial x}, A_2, \frac{\partial A_3}{\partial x}\right) = A_1^{x}\left[A_2 A_3^{-z}\right]^{x-z}$$

$$\begin{aligned} &E_3\left(\frac{\partial A_1}{\partial x}, \frac{\partial A_2}{\partial x}, A_3\right) + E_3\left(\frac{\partial A_1}{\partial x}, A_2, \frac{\partial A_3}{\partial x}\right) \\ &= A_1^{x-2z}\left[A_3^{z} A_2^{-z}\right]^{x} - A_3^{x+z}\left[A_1^{x-z} A_2^{-z}\right]^{-z} - A_3^{z}\left[A_1^{x-z} A_2^{x-z}\right]^{-z} \end{aligned}$$

$$E_4\left(\frac{\partial A_1}{\partial x}, \frac{\partial A_2}{\partial x}, A_3\right) + E_4\left(\frac{\partial A_1}{\partial x}, A_2, \frac{\partial A_3}{\partial x}\right) = \left[A_2 A_3\right]^{x} A_1^{x-2z}$$

$$E_5\left(\frac{\partial A_1}{\partial x}, \frac{\partial A_2}{\partial x}, A_3\right) + E_5\left(\frac{\partial A_1}{\partial x}, A_2, \frac{\partial A_3}{\partial x}\right) = \left[A_2^{z} A_3^{-z}\right]^{x} A_1^{x-2z}$$

$$E_6\left(\frac{\partial A_1}{\partial x}, \frac{\partial A_2}{\partial x}, A_3\right) + E_6\left(\frac{\partial A_1}{\partial x}, A_2, \frac{\partial A_3}{\partial x}\right) = A_1^{x-z}\left[A_2 A_3^{-z}\right]^{x}$$

$$E_7\left(\frac{\partial A_1}{\partial x}, \frac{\partial A_2}{\partial x}, A_3\right) + E_7\left(\frac{\partial A_1}{\partial x}, A_2, \frac{\partial A_3}{\partial x}\right) = \left[A_2 A_3\right]^{x} A_1^{x-2z}$$

$$E_8\left(\frac{\partial A_1}{\partial x}, \frac{\partial A_2}{\partial x}, A_3\right) + E_8\left(\frac{\partial A_1}{\partial x}, A_2, \frac{\partial A_3}{\partial x}\right) = A_1^{x}\left[A_2 A_3\right]^{x-2z}$$

$$E_9\left(\frac{\partial A_1}{\partial x}, \frac{\partial A_2}{\partial x}, A_3\right) + E_9\left(\frac{\partial A_1}{\partial x}, A_2, \frac{\partial A_3}{\partial x}\right) = \mathbb{IM}_2(A_1^{x}, A_2, A_3^{x+z}) + \mathbb{IM}_2(A_1^{x}, A_2^{x}, A_3^{z})$$

In summary, we have:

$$\Pi_z(\frac{\partial A_1}{\partial x},\frac{\partial A_2}{\partial x},A_3)+\Pi_z(\frac{\partial A_1}{\partial x},A_2,\frac{\partial A_3}{\partial x})=\left(\begin{array}{c} f_1+f_2+f_3+f_4+f_5+f_6+f_7 \\ +f_8+f_9+f_{10}+f_{11}+f_{12} \end{array}\right)$$

where:

$$\begin{array}{ll} f_1(A_1,A_2,A_3)=A_1^{x+z}\left[A_2A_3^{-z}\right]^{x-2z} & f_2(A_1,A_2,A_3)=A_1^{x}\left[A_2A_3^{-z}\right]^{x-z} \\ f_3(A_1,A_2,A_3)=A_1^{x-2z}\left[A_3^{z}A_2^{-z}\right]^{x} & f_4(A_1,A_2,A_3)=-A_3^{x+z}\left[A_1^{x-z}A_2^{-z}\right]^{-z} \\ f_5(A_1,A_2,A_3)=-A_3^{z}\left[A_1^{x-z}A_2^{x-z}\right]^{-z} & f_6(A_1,A_2,A_3)=\left[A_2A_3\right]^{x}A_1^{x-2z} \\ f_7(A_1,A_2,A_3)=\left[A_2^{z}A_3^{-z}\right]^{x}A_1^{x-2z} & f_8(A_1,A_2,A_3)=A_1^{x-z}\left[A_2A_3^{-z}\right]^{x} \\ f_9(A_1,A_2,A_3)=\left[A_2A_3\right]^{x}A_1^{x-2z} & f_{10}(A_1,A_2,A_3)=A_1^{x}[A_2A_3]^{x-2z} \\ f_{11}(A_1,A_2,A_3)=\mathbb{IM}_2(A_1^{x},A_2,A_3^{x+z}) & f_{12}(A_1,A_2,A_3)=\mathbb{IM}_2(A_1^{x},A_2^{x},A_3^{z}) \end{array}$$

If we group the following 4 terms together, we have:

$$\left(f_3+f_6+f_7+f_9\right)(A_1,A_2,A_3)=A_1^{x-2z}\left[2A_2A_3+A_2^{z}A_3^{-z}+A_2^{-z}A_3^{z}\right]^{x}$$

The permutation sum of the expression above will be:

$$\begin{array}{r} 2A_1^{x-2z}\left[2A_2A_3+A_2^{z}A_3^{-z}+A_2^{-z}A_3^{z}\right]^{x} \\ +2A_2^{x-2z}\left[2A_3A_1+A_3^{z}A_1^{-z}+A_3^{-z}A_1^{z}\right]^{x} \\ +2A_3^{x-2z}\left[2A_1A_2+A_1^{z}A_2^{-z}+A_1^{-z}A_2^{z}\right]^{x} \end{array} \tag{86}$$

Let's look at f_1 and f_4, their permutation sum cancels with each other because of the following relations:

$$\begin{array}{l} f_1(A_1,A_2,A_3)+f_1(A_1,A_3,A_2)=\overrightarrow{(25)}=A_1^{x+z}\left[A_2^{-z}A_3^{-z}\right]^{x-z}=\overrightarrow{(21)}=-f_4(A_2,A_3,A_1)-f_4(A_3,A_2,A_1) \\ f_1(A_2,A_3,A_1)+f_1(A_2,A_1,A_3)=\overrightarrow{(25)}=A_2^{x+z}\left[A_3^{-z}A_1^{-z}\right]^{x-z}=\overrightarrow{(21)}=-f_4(A_3,A_1,A_2)-f_4(A_1,A_3,A_2) \\ f_1(A_3,A_1,A_2)+f_1(A_3,A_2,A_1)=\overrightarrow{(25)}=A_3^{x+z}\left[A_1^{-z}A_2^{-z}\right]^{x-z}=\overrightarrow{(21)}=-f_4(A_1,A_2,A_3)-f_4(A_2,A_1,A_3) \end{array}$$

We then consider the following sums:

$$\begin{array}{l} f_2(A_1,A_2,A_3)+f_2(A_1,A_3,A_2)=A_1^{x}\left[A_2A_3^{-z}\right]^{x-z}+A_1^{x}\left[A_3A_2^{-z}\right]^{x-z}=\overrightarrow{(25)}=A_1^{x}\left[A_2^{-z}A_3^{-z}\right]^{x} \\ f_2(A_2,A_3,A_1)+f_2(A_2,A_1,A_3)=\overrightarrow{(25)}=A_2^{x}\left[A_3^{-z}A_1^{-z}\right]^{x} \\ f_2(A_3,A_1,A_2)+f_2(A_3,A_2,A_1)=\overrightarrow{(25)}=A_3^{x}\left[A_1^{-z}A_2^{-z}\right]^{x} \end{array} \tag{87}$$

$$\begin{aligned}
f_{10}(A_1,A_2,A_3)+f_{10}(A_1,A_3,A_2) &= 2A_1^x[A_2A_3]^{x-2z}\\
f_{10}(A_2,A_3,A_1)+f_{10}(A_2,A_1,A_3) &= 2A_2^x[A_3A_1]^{x-2z}\\
f_{10}(A_3,A_1,A_2)+f_{10}(A_3,A_2,A_1) &= 2A_3^x[A_1A_2]^{x-2z}
\end{aligned} \tag{88}$$

$$\begin{aligned}
f_5(A_1,A_2,A_3)+f_5(A_2,A_1,A_3) &= -2A_3^z\left[A_1^{x-z}A_2^{x-z}\right]^{-z}\\
f_5(A_2,A_3,A_1)+f_5(A_3,A_2,A_1) &= -2A_1^z\left[A_2^{x-z}A_3^{x-z}\right]^{-z}\\
f_5(A_3,A_1,A_2)+f_5(A_1,A_3,A_2) &= -2A_2^z\left[A_3^{x-z}A_1^{x-z}\right]^{-z}
\end{aligned} \tag{89}$$

$$\begin{aligned}
f_8(A_1,A_2,A_3)+f_8(A_1,A_3,A_2) &= A_1^{x-z}\left[A_2A_3^{-z}+A_2^{-z}A_3\right]^x\\
f_8(A_2,A_3,A_1)+f_8(A_2,A_1,A_3) &= A_2^{x-z}\left[A_3A_1^{-z}+A_3^{-z}A_1\right]^x\\
f_8(A_3,A_1,A_2)+f_8(A_3,A_2,A_1) &= A_3^{x-z}\left[A_1A_2^{-z}+A_1^{-z}A_2\right]^x
\end{aligned} \tag{90}$$

Finally we put the last 2 terms (f_{11} and f_{12}) together, they look like the internal multiple integrals studied in Weglein et. al. 2003, and Shaw et. al. 2002.

$$\begin{aligned}
f_{11}(A_1,A_2,A_3)+f_{12}(A_1,A_2,A_3) &= \mathbb{IM}_2\left(A_1^x,A_2,A_3^{x+z}\right)+\mathbb{IM}_2\left(A_1^x,A_2^x,A_3^z\right)\\
f_{11}(A_1,A_3,A_2)+f_{12}(A_1,A_3,A_2) &= \mathbb{IM}_2\left(A_1^x,A_3,A_2^{x+z}\right)+\mathbb{IM}_2\left(A_1^x,A_3^x,A_2^z\right)\\
f_{11}(A_2,A_3,A_1)+f_{12}(A_2,A_3,A_1) &= \mathbb{IM}_2\left(A_2^x,A_3,A_1^{x+z}\right)+\mathbb{IM}_2\left(A_2^x,A_3^x,A_1^z\right)\\
f_{11}(A_2,A_1,A_3)+f_{12}(A_2,A_1,A_3) &= \mathbb{IM}_2\left(A_2^x,A_1,A_3^{x+z}\right)+\mathbb{IM}_2\left(A_2^x,A_1^x,A_3^z\right)\\
f_{11}(A_3,A_1,A_2)+f_{12}(A_3,A_1,A_2) &= \mathbb{IM}_2\left(A_3^x,A_1,A_2^{x+z}\right)+\mathbb{IM}_2\left(A_3^x,A_1^x,A_2^z\right)\\
f_{11}(A_3,A_2,A_1)+f_{12}(A_3,A_2,A_1) &= \mathbb{IM}_2\left(A_3^x,A_2,A_1^{x+z}\right)+\mathbb{IM}_2\left(A_3^x,A_2^x,A_1^z\right)
\end{aligned} \tag{91}$$

Finally we sum the terms in equations (86, 87, 88. 89, 90, 91) together to obtain the permutation sum of $16\mathcal{SC}_{3,2}^{\mathtt{left}}$. Remembering that fact that $\mathcal{SC}_{3,2}^{\mathtt{left}}$ is only half of $\mathcal{SC}_{3,2}$, we have:

$$\begin{aligned}
&\mathbb{SC}_{3,2}(A_1,A_2,A_3)=\frac{2}{16}\left(\mathtt{eq86}+\mathtt{eq87}+\mathtt{eq88}+\mathtt{eq89}+\mathtt{eq90}+\mathtt{eq91}\right)\\
&=\frac{1}{4}\begin{pmatrix} A_1^{x-2z}\left[2A_2A_3+A_2^zA_3^{-z}+A_2^{-z}A_3^z\right]^x\\ A_2^{x-2z}\left[2A_3A_1+A_3^zA_1^{-z}+A_3^{-z}A_1^z\right]^x\\ A_3^{x-2z}\left[2A_1A_2+A_1^zA_2^{-z}+A_1^{-z}A_2^z\right]^x\end{pmatrix}\\
&+\frac{1}{8}\begin{pmatrix} A_1^x\left[A_2^{-z}A_3^{-z}\right]^x\\ A_2^x\left[A_3^{-z}A_1^{-z}\right]^x\\ A_3^x\left[A_1^{-z}A_2^{-z}\right]^x\end{pmatrix}+\frac{1}{4}\begin{pmatrix} A_1^x[A_2A_3]^{x-2z}\\ A_2^x[A_3A_1]^{x-2z}\\ A_3^x[A_1A_2]^{x-2z}\end{pmatrix}-\frac{1}{4}\begin{pmatrix} A_3^z\left[A_1^{x-z}A_2^{x-z}\right]^{-z}\\ A_1^z\left[A_2^{x-z}A_3^{x-z}\right]^{-z}\\ A_2^z\left[A_3^{x-z}A_1^{x-z}\right]^{-z}\end{pmatrix}\\
&+\frac{1}{8}\begin{pmatrix} A_1^{x-z}\left[A_2A_3^{-z}+A_2^{-z}A_3\right]^x\\ A_2^{x-z}\left[A_3A_1^{-z}+A_3^{-z}A_1\right]^x\\ A_3^{x-z}\left[A_1A_2^{-z}+A_1^{-z}A_2\right]^x\end{pmatrix}+\frac{1}{8}\begin{pmatrix} \mathbb{IM}_2\left(A_1^x,A_2,A_3^{x+z}\right)+\mathbb{IM}_2\left(A_1^x,A_2^x,A_3^z\right)\\ \mathbb{IM}_2\left(A_1^x,A_3,A_2^{x+z}\right)+\mathbb{IM}_2\left(A_1^x,A_3^x,A_2^z\right)\\ \mathbb{IM}_2\left(A_2^x,A_3,A_1^{x+z}\right)+\mathbb{IM}_2\left(A_2^x,A_3^x,A_1^z\right)\\ \mathbb{IM}_2\left(A_2^x,A_1,A_3^{x+z}\right)+\mathbb{IM}_2\left(A_2^x,A_1^x,A_3^z\right)\\ \mathbb{IM}_2\left(A_3^x,A_1,A_2^{x+z}\right)+\mathbb{IM}_2\left(A_3^x,A_1^x,A_2^z\right)\\ \mathbb{IM}_2\left(A_3^x,A_2,A_1^{x+z}\right)+\mathbb{IM}_2\left(A_3^x,A_2^x,A_1^z\right)\end{pmatrix}
\end{aligned} \tag{92}$$

If among the 3 terms A_1, A_2, A_3, 2 of them are equal. We have:

$$\begin{aligned}\mathbb{SC}_{3,2}(A_1,A_1,A_2) &= \frac{1}{4}\begin{pmatrix} A_1^{x-2z}\left[2A_2A_1 + A_2^zA_1^{-z} + A_2^{-z}A_1^z\right]^x \\ A_2^{x-2z}\left[A_1A_1 + A_1^zA_1^{-z}\right]^x \end{pmatrix} \\ &+\frac{1}{16}\begin{pmatrix} 2A_1^x\left[A_1^{-z}A_2^{-z}\right]^x \\ A_2^x\left[A_1^{-z}A_1^{-z}\right]^x \end{pmatrix} + \frac{1}{8}\begin{pmatrix} 2A_1^x[A_1A_2]^{x-2z} \\ A_2^x[A_1A_1]^{x-2z} \end{pmatrix} - \frac{1}{8}\begin{pmatrix} A_2^z\left[A_1^{x-z}A_1^{x-z}\right]^{-z} \\ 2A_1^z\left[A_1^{x-z}A_2^{x-z}\right]^{-z} \end{pmatrix} \\ &+\frac{1}{8}\begin{pmatrix} A_1^{x-z}\left[A_1A_2^{-z} + A_1^{-z}A_2\right]^x \\ A_2^{x-z}\left[A_1A_1^{-z}\right]^x \end{pmatrix} + \frac{1}{16}\begin{pmatrix} \mathbb{IM}_2\left(A_1^x,A_1,A_2^{x+z}\right) + \mathbb{IM}_2\left(A_1^x,A_1^x,A_2^z\right) \\ \mathbb{IM}_2\left(A_1^x,A_2,A_1^{x+z}\right) + \mathbb{IM}_2\left(A_1^x,A_2^x,A_1^z\right) \\ \mathbb{IM}_2\left(A_2^x,A_1,A_1^{x+z}\right) + \mathbb{IM}_2\left(A_2^x,A_1^x,A_1^z\right) \end{pmatrix}\end{aligned} \tag{93}$$

If all three terms are the same $A_1 = A_2 = A_3 = A$, we have:

$$\begin{aligned}\mathbb{SC}_{3,2}(A,A,A) &= \frac{1}{4}A^{x-2z}\left[AA + A^zA^{-z}\right]^x + \frac{1}{16}A^x\left[A^{-z}A^{-z}\right]^x \\ &+\frac{1}{8}A^x[AA]^{x-2z} - \frac{1}{8}A^z\left[A^{x-z}A^{x-z}\right]^{-z} + \frac{1}{8}A^{x-z}\left[AA^{-z}\right]^x \\ &+\frac{1}{16}\mathbb{IM}_2\left(A^x,A,A^{x+z}\right) + \frac{1}{16}\mathbb{IM}_2\left(A^x,A^x,A^z\right)\end{aligned}$$

$$\begin{aligned}&= \frac{1}{4}A^{x-2z}\left[AA + A^zA^{-z}\right]^x + \frac{1}{16}A^x\left[A^{-z}A^{-z}\right]^x \\ &+\frac{1}{8}A^x[AA]^{x-2z} - \frac{1}{8}A^z\left[A^{x-z}A^{x-z}\right]^{-z} + \frac{1}{8}AA^{x-z}A^{x-z} + \frac{1}{16}A^x\left[A^{-z}A^{-z}\right]^x \\ &+\frac{1}{16}\mathbb{IM}_2\left(A^x,A,A^{x+z}\right) + \frac{1}{16}\mathbb{IM}_2\left(A^x,A^x,A^z\right)\end{aligned}$$

$$\begin{aligned}\mathbb{SC}_{3,2}(A,A,A) &= \frac{1}{4}A^{x-2z}\left[AA + A^zA^{-z}\right]^x + \frac{1}{8}A^x[AA]^{x-2z} \\ &-\frac{1}{8}A^z\left[A^{x-z}A^{x-z}\right]^{-z} + \frac{1}{8}AA^{x-z}A^{x-z} + \frac{1}{8}A^x\left[A^{-z}A^{-z}\right]^x \\ &+\frac{1}{16}\mathbb{IM}_2\left(A^x,A,A^{x+z}\right) + \frac{1}{16}\mathbb{IM}_2\left(A^x,A^x,A^z\right)\end{aligned} \tag{94}$$

Evaluation of $\mathcal{SC}_{3,3}$ and $\mathbb{SC}_{3,3}$

We then Fourier transform $\widetilde{\mathcal{SC}}_{3,3}$ (equation (80)) into (x,z) domain, and finish the x-wise integration as below:

$$\mathcal{SC}_{3,3}(x,z) = \frac{1}{2\pi}\int_{-\infty}^{\infty} dk_m e^{ik_m x}\widetilde{\mathcal{SC}}_{3,3}(k_m,z)$$

$$= \frac{2\pi}{256\pi^4}\int_{-\infty}^{\infty} dk_m e^{ik_m x}\int_{-\infty}^{\infty} dk_1\int_{-\infty}^{\infty} dk_2\int_{-\infty}^{\infty} dz_1\widetilde{A_1}(0.5k_m-k_1,z_1)\int_{-\infty}^{\infty} dz_2\widetilde{A_2}(k_1-k_2,z_2)$$

$$\times\int_{-\infty}^{\infty} dz_3\widetilde{A_3}(k_2+0.5k_m,z_3)\left(k_m^2+2(k_1^2+k_2^2)-\frac{(\varepsilon_1 a_1+\varepsilon_2 a_2)^2}{8}\right)\delta(\varepsilon_0+\varepsilon_1+\varepsilon_2)$$

$$= \frac{1}{128\pi^3}\int_{-\infty}^{\infty} dz_1\int_{-\infty}^{\infty} dz_2\int_{-\infty}^{\infty} dz_3\delta(\varepsilon_0+\varepsilon_1+\varepsilon_2)\left(\mathcal{I}_1-\frac{\varepsilon_1^2}{8}\mathcal{I}_2-\frac{\varepsilon_1\varepsilon_2}{4}\mathcal{I}_3-\frac{\varepsilon_2^2}{8}\mathcal{I}_4\right)$$

$$= \frac{1}{128\pi^3}\int_{-\infty}^{\infty} dz_1\int_{-\infty}^{\infty} dz_2\int_{-\infty}^{\infty} dz_3\delta(\varepsilon_0+\varepsilon_1+\varepsilon_2)\left(\mathcal{I}_1-\frac{|z_1-z_2|^2}{32}\mathcal{I}_2-\frac{|z_1-z_2|\,|z_2-z_3|}{16}\mathcal{I}_3-\frac{|z_2-z_3|^2}{32}\mathcal{I}_4\right)$$

where $\mathcal{I}_1$, $\mathcal{I}_2$, $\mathcal{I}_3$, and $\mathcal{I}_4$ are defined below by Fourier transform over k_m:

$$\mathcal{I}_1 = \int_{-\infty}^{\infty} dx_1 A_1(x_1,z_1)\int_{-\infty}^{\infty} dx_2 A_2(x_2,z_2)\int_{-\infty}^{\infty} dx_3 A_3(x_3,z_3)\int_{-\infty}^{\infty} dk_m e^{ik_m(x-0.5x_1-0.5x_3)}$$

$$\times\int_{-\infty}^{\infty} dk_1 e^{ik_1(x_1-x_2)}\int_{-\infty}^{\infty} dk_2 e^{ik_2(x_2-x_3)}\left(k_m^2+2k_1^2+2k_2^2\right)$$

`Using equation (127) we have`

$$= 16\pi^3\left\{\bar{A}_1{}^{2x}\bar{A}_2\bar{A}_3+\bar{A}_1\bar{A}_2{}^{2x}\bar{A}_3+\bar{A}_1\bar{A}_2\bar{A}_3{}^{2x}+\bar{A}_1{}^{x}\bar{A}_2{}^{x}\bar{A}_3+\bar{A}_1\bar{A}_2{}^{x}\bar{A}_3{}^{x}\right\}$$

$$\mathcal{I}_2 = \int_{-\infty}^{\infty} dx_1 A_1(x_1,z_1)\int_{-\infty}^{\infty} dx_2 A_2(x_2,z_2)\int_{-\infty}^{\infty} dx_3 A_3(x_3,z_3)\int_{-\infty}^{\infty} dk_m e^{ik_m(x-0.5x_1-0.5x_3)}$$

$$\times\int_{-\infty}^{\infty} dk_1 e^{ik_1(x_1-x_2)}\int_{-\infty}^{\infty} dk_2 e^{ik_2(x_2-x_3)}\left(k_m^2-4k_1^2\right)^2$$

`Using equation (128) we have`

$$= 128\pi^3\bar{A}_1{}^{2x}\left[\bar{A}_2\bar{A}_3\right]^{2x} = 128\pi^3\bar{A}_1{}^{2x}\left\{\bar{A}_2{}^{2x}\bar{A}_3+2\bar{A}_2{}^{x}\bar{A}_3{}^{x}+\bar{A}_2\bar{A}_3{}^{2x}\right\}$$

$$\mathcal{I}_3 = \int_{-\infty}^{\infty} dx_1 A_1(x_1,z_1) \int_{-\infty}^{\infty} dx_2 A_2(x_2,z_2) \int_{-\infty}^{\infty} dx_3 A_3(x_3,z_3) \int_{-\infty}^{\infty} dk_m e^{ik_m(x-0.5x_1-0.5x_3)}$$
$$\times \int_{-\infty}^{\infty} dk_1 e^{ik_1(x_1-x_2)} \int_{-\infty}^{\infty} dk_2 e^{ik_2(x_2-x_3)} \left(k_m^2-4k_1^2\right)\left(k_m^2-4k_2^2\right)$$

Using equation (129) we have

$$= 128\pi^3 \left\{ \bar{A}_1{}^{2x} \bar{A}_2 \bar{A}_3{}^{2x} + \bar{A}_1{}^{2x} \bar{A}_2{}^{x} \bar{A}_3{}^{x} + \bar{A}_1{}^{x} \bar{A}_2{}^{2x} \bar{A}_3{}^{x} + \bar{A}_1{}^{x} \bar{A}_2{}^{x} \bar{A}_3{}^{2x} \right\}$$

$$\mathcal{I}_4 = \int_{-\infty}^{\infty} dx_1 A_1(x_1,z_1) \int_{-\infty}^{\infty} dx_2 A_2(x_2,z_2) \int_{-\infty}^{\infty} dx_3 A_3(x_3,z_3) \int_{-\infty}^{\infty} dk_m e^{ik_m(x-0.5x_1-0.5x_3)}$$
$$\times \int_{-\infty}^{\infty} dk_1 e^{ik_1(x_1-x_2)} \int_{-\infty}^{\infty} dk_2 e^{ik_2(x_2-x_3)} \left(k_m^2-4k_2^2\right)^2$$

Using equation (130) we have

$$= 128\pi^3 \left[\bar{A}_1 \bar{A}_2\right]^{2x} \bar{A}_3{}^{2x} = 128\pi^3 \left\{ \bar{A}_1{}^{2x} \bar{A}_2 + 2\bar{A}_1{}^{x} \bar{A}_2{}^{x} + \bar{A}_1 \bar{A}_2{}^{2x} \right\} \bar{A}_3{}^{2x}$$

where $\bar{A}_1$, $\bar{A}_2$, and $\bar{A}_3$ are functions of x and defined by:

$$\begin{aligned} \bar{A}_1(x) &= A_1(x,z_1) \\ \bar{A}_2(x) &= A_2(x,z_2) \\ \bar{A}_3(x) &= A_3(x,z_3) \end{aligned} \tag{95}$$

We then finish the z-wise integration. Because $\mathcal{I}_1$, $\mathcal{I}_2$, $\mathcal{I}_3$, and $\mathcal{I}_4$ will be multiplied by different functions of z, and the product will be used as the integrand of the z-wise integral:

$$\frac{1}{128\pi^3} \int_{-\infty}^{\infty} dz_1 \int_{-\infty}^{\infty} dz_2 \int_{-\infty}^{\infty} dz_3 \delta(\varepsilon_0+\varepsilon_1+\varepsilon_2)$$

We'd better to consider these integrals differently.

First let's continue the integration of $\mathcal{I}_1$:

$$\frac{1}{128\pi^3} \int_{-\infty}^{\infty} dz_1 \int_{-\infty}^{\infty} dz_2 \int_{-\infty}^{\infty} dz_3 \delta(\varepsilon_0+\varepsilon_1+\varepsilon_2) \mathcal{I}_1$$
$$= \frac{1}{8} \int_{-\infty}^{\infty} dz_1 \int_{-\infty}^{\infty} dz_2 \int_{-\infty}^{\infty} dz_3 \delta(\varepsilon_0+\varepsilon_1+\varepsilon_2) \left[\begin{array}{c} \bar{A}_1{}^{2x} \bar{A}_2 \bar{A}_3 + \bar{A}_1 \bar{A}_2{}^{2x} \bar{A}_3 + \bar{A}_1 \bar{A}_2 \bar{A}_3{}^{2x} \\ +\bar{A}_1{}^{x} \bar{A}_2{}^{x} \bar{A}_3 + \bar{A}_1 \bar{A}_2{}^{x} \bar{A}_3{}^{x} \end{array} \right]$$

where $\bar{A}_1$, $\bar{A}_2$, and $\bar{A}_3$ are 3 functions of x and are defined in equation (95).

There are 5 terms in the $\mathcal{I}_1$, for the first term, $\bar{A}_1^{2x}\bar{A}_2\bar{A}_3$ is actually $\frac{\partial^2 A_1(x,z_1)}{\partial x^2}A_2(x,z_2)A_3(x,z_3)$. If we define: $\breve{A}_1(z_1) = \frac{\partial^2 A_1(x,z_1)}{\partial x^2}$, $\breve{A}_2(z_2) = A_2(x,z_2)$, $\breve{A}_3(z_3) = A_3(x,z_3)$, we can study the behavior of the z-wise integral without worrying about the irregularities in the x-direction. And the z-wise integral can be written as:

$$
\begin{aligned}
&\int_{-\infty}^{\infty} dz_1\breve{A}_1(z_1)\int_{-\infty}^{\infty} dz_2\breve{A}_2(z_2)\int_{-\infty}^{\infty} dz_3\breve{A}_3(z_3)\delta\left(\frac{z_1+z_3}{2}-z+\frac{|z_1-z_2|}{2}+\frac{|z_2-z_3|}{2}\right)\\
&=\int_{-\infty}^{\infty} dz_1\delta\left(z_1-z\right)\breve{A}_1(z_1)\int_{-\infty}^{z_1} dz_2\breve{A}_2(z_2)\int_{-\infty}^{z_2} dz_3\breve{A}_3(z_3)\\
&+\int_{-\infty}^{\infty} dz_3\delta\left(z_3-z\right)\breve{A}_3(z_3)\int_{-\infty}^{z_3} dz_2\breve{A}_2(z_2)\int_{-\infty}^{z_2} dz_1\breve{A}_1(z_1)\\
&+\int_{-\infty}^{\infty} dz_3\delta\left(z_2-z\right)\breve{A}_2(z_2)\left(\int_{-\infty}^{z_2} dz_1\breve{A}_1(z_1)\right)\left(\int_{-\infty}^{z_2} dz_3\breve{A}_3(z_3)\right)\\
&+\int_{-\infty}^{\infty} du\delta\left(u-z\right)\int_{-\infty}^{u} dz_3\breve{A}_3(z_3)\int_{-\infty}^{u} dz_1\breve{A}_1(z_1)\breve{A}_2(z_1+z_3-u)\\
&=\breve{A}_1\left[\breve{A}_2\breve{A}_3^{-z}\right]^{-z}+\breve{A}_3\left[\breve{A}_2\breve{A}_1^{-z}\right]^{-z}+\breve{A}_1^{-z}\breve{A}_2\breve{A}_3^{-z}+\mathbb{IM}_1(\breve{A}_3,\breve{A}_2,\breve{A}_1)
\end{aligned}
$$

The other 4 terms in $\mathcal{I}_1$ can be treated the same way, the z-wise integral is captured by the integral above. We only need to change the definition of $\breve{A}_1$, $\breve{A}_2$, $\breve{A}_3$.

Let's define 2 set of operators, the first set purely operate on x:

$$
\begin{aligned}
&\Pi_x^{(1)} = \Pi_x^{(1,1)} + \Pi_x^{(1,2)} + \Pi_x^{(1,3)} + \Pi_x^{(1,4)} + \Pi_x^{(1,5)}\\
&\Pi_x^{(1,2)} = \partial_{x1}\partial_{x1} \quad \Pi_x^{(1,2)} = \partial_{x2}\partial_{x2} \quad \Pi_x^{(1,3)} = \partial_{x3}\partial_{x3} \quad \Pi_x^{(1,4)} = \frac{1}{8}\partial_{x1}\partial_{x2} \quad \Pi_x^{(1,5)} = \partial_{x2}\partial_{x3}
\end{aligned}
$$

The input to the operators like $\Pi_x^{(1)}$ is actually the product of 3 terms, each of them is a function of x. Even though the order of terms of a product doesn't matter, but we define the operator in such a way that the order is important, to facilitate the process of finding where each term comes from.

For example, let's consider the product $f_1(x)f_2(x)f_3(x)$ of 3 functions of x, will be changed by the operator $\partial_{x1}\partial_{x2}$ as follows:

$$
\partial_{x1}\partial_{x2}\left[f_1(x)f_2(x)f_3(x)\right] = \frac{\partial f_1(x)}{\partial x}\frac{\partial f_2(x)}{\partial x}f_3(x)
$$

The output of the operators above will still be products, but to be considered as ordered as mentioned before. In the definition, the operators will change each factor, but not their relative order.

The output of the operators above will be input for the following z-wise operators. This time every of the 3 factors in the product will be considered as function of z. And the z-wise operators will be defined as:

$$\begin{aligned}
\Pi_z^{(1)} &= \Pi_z^{(1,1)} + \Pi_z^{(1,2)} + \Pi_z^{(1,3)} + \Pi_z^{(1,4)} \\
\Pi_z^{(1,1)}(A,B,C) &= A\left[BC^{-z}\right]^{-z} \\
\Pi_z^{(1,2)}(A,B,C) &= C\left[BA^{-z}\right]^{-z} \\
\Pi_z^{(1,3)}(A,B,C) &= A^{-z}BC^{-z} \\
\Pi_z^{(1,4)}(A,B,C) &= \mathbb{IM}_1(C,B,A)
\end{aligned}$$

Because the output of $\Pi_z^{(1)}$ is final result, we don't need to consider them as ordered. They are just ordinary integrals, partial derivatives, and products.

In this operator notation, the z-wise integration of $\mathcal{I}_1$ can be simply written as:

$$\frac{1}{128\pi^3}\int_{-\infty}^{\infty} dz_1 \int_{-\infty}^{\infty} dz_2 \int_{-\infty}^{\infty} dz_3 \delta(\varepsilon_0+\varepsilon_1+\varepsilon_2)\mathcal{I}_1 = \frac{1}{8}\Pi_z^{(1)}\Pi_x^{(1)}(A_1,A_2,A_3)$$

Let's use a table to promptly identify the result of the successive application of the x and z-wise operators.

$\breve{A}_1$	$\breve{A}_2$	$\breve{A}_3$	$\breve{A}_1\left[\breve{A}_2\breve{A}_3^{-z}\right]^{-z}$	$\breve{A}_3\left[\breve{A}_2\breve{A}_1^{-z}\right]^{-z}$	$\breve{A}_1^{-z}\breve{A}_2\breve{A}_3^{-z}$	$\mathbb{IM}_1(\breve{A}_3,\breve{A}_2,\breve{A}_1)$
A_1^{2x}	A_2	A_3	$\Pi_z^{(1,1)}\Pi_x^{(1,2)}$	$\Pi_z^{(1,2)}\Pi_x^{(1,2)}$	$\Pi_z^{(1,3)}\Pi_x^{(1,2)}$	$\Pi_z^{(1,4)}\Pi_x^{(1,2)}$
A_1	A_2^{2x}	A_3	$\Pi_z^{(1,1)}\Pi_x^{(1,2)}$	$\Pi_z^{(1,2)}\Pi_x^{(1,2)}$	$\Pi_z^{(1,3)}\Pi_x^{(1,2)}$	$\Pi_z^{(1,4)}\Pi_x^{(1,2)}$
A_1	A_2	A_3^{2x}	$\Pi_z^{(1,1)}\Pi_x^{(1,3)}$	$\Pi_z^{(1,2)}\Pi_x^{(1,3)}$	$\Pi_z^{(1,3)}\Pi_x^{(1,3)}$	$\Pi_z^{(1,4)}\Pi_x^{(1,3)}$
A_1^{x}	A_2^{x}	A_3	$\Pi_z^{(1,1)}\Pi_x^{(1,4)}$	$\Pi_z^{(1,2)}\Pi_x^{(1,4)}$	$\Pi_z^{(1,3)}\Pi_x^{(1,4)}$	$\Pi_z^{(1,4)}\Pi_x^{(1,4)}$
A_1	A_2^{x}	A_3^{x}	$\Pi_z^{(1,1)}\Pi_x^{(1,5)}$	$\Pi_z^{(1,2)}\Pi_x^{(1,5)}$	$\Pi_z^{(1,3)}\Pi_x^{(1,5)}$	$\Pi_z^{(1,4)}\Pi_x^{(1,5)}$

How to use the table above? For example, in this table $\Pi_z^{(1,1)}\Pi_x^{(1,1)}$ is located in the second row, the fourth column. In the second row, we have: $\breve{A}_1 = A_1^{2x}$, $\breve{A}_2 = A_2$, and $\breve{A}_3 = A_3$. And the topmost element of the fourth-row is $\breve{A}_1\left[\breve{A}_2\breve{A}_3^{-z}\right]^{-z}$, we can simply substitute in values of $\breve{A}_1$, $\breve{A}_2$, and $\breve{A}_3$ obtained before to have:

$$\begin{aligned}
\Pi_z^{(1,1)}\Pi_x^{(1,1)}(A_1,A_2,A_3) &= A_1^{2x}\left[A_2A_3^{-z}\right]^{-z} \\
\Pi_z^{(1,2)}\Pi_x^{(1,3)}(A_1,A_2,A_3) &= A_3^{2x}\left[A_2A_1^{-z}\right]^{-z} \\
\Pi_z^{(1,3)}\Pi_x^{(1,2)}(A_1,A_2,A_3) &= A_2^{2x}A_1^{-z}A_3^{-z}
\end{aligned}$$

Let's denote the permutation sum of $\Pi_z^{(1,1)}\Pi_x^{(1,1)}(A_1,A_2,A_3)$ as $\sum^{\odot}\Pi_z^{(1,1)}\Pi_x^{(1,1)}$, that is:

$$\begin{aligned}\sum^{\odot}\Pi_z^{(1,1)}\Pi_x^{(1,1)} &= \Pi_z^{(1,1)}\Pi_x^{(1,1)}(A_1,A_2,A_3)+\Pi_z^{(1,1)}\Pi_x^{(1,1)}(A_2,A_3,A_1)+\Pi_z^{(1,1)}\Pi_x^{(1,1)}(A_3,A_1,A_2)\\ &+\Pi_z^{(1,1)}\Pi_x^{(1,1)}(A_1,A_3,A_2)+\Pi_z^{(1,1)}\Pi_x^{(1,1)}(A_2,A_1,A_3)+\Pi_z^{(1,1)}\Pi_x^{(1,1)}(A_3,A_2,A_1)\end{aligned}$$

we have:

$$\sum^{\odot}\Pi_z^{(1,1)}\Pi_x^{(1,1)}=\sum^{\odot}\Pi_z^{(1,2)}\Pi_x^{(1,3)}=\frac{1}{2}\sum^{\odot}\Pi_z^{(1,3)}\Pi_x^{(1,2)}$$

and

$$\begin{aligned}&\sum^{\odot}\left(\Pi_z^{(1,1)}\Pi_x^{(1,1)}+\Pi_z^{(1,2)}\Pi_x^{(1,3)}=\Pi_z^{(1,3)}\Pi_x^{(1,2)}\right)\\ &=4\left(A_1^{2x}A_2^{-z}A_3^{-z}+A_2^{2x}A_3^{-z}A_1^{-z}+A_3^{2x}A_1^{-z}A_2^{-z}\right)\end{aligned}\tag{96}$$

Let's consider the following terms:

$$\begin{aligned}&\Pi_z^{(1,3)}\Pi_x^{(1,1)}(A_1,A_2,A_3)=A_1^{2x-z}A_2A_3^{-z}\\ =&\Pi_z^{(1,3)}\Pi_x^{(1,3)}(A_3,A_2,A_1)=A_2\left[A_1^{2x}A_3^{-z}\right]^{-z}+A_2\left[A_3A_1^{2x-z}\right]^{-z}\\ =&\Pi_z^{(1,1)}\Pi_x^{(1,2)}(A_2,A_1,A_3)+\Pi_z^{(1,1)}\Pi_x^{(1,3)}(A_2,A_3,A_1)=A_2\left[A_1^{2x}A_3^{-z}\right]^{-z}+A_2\left[A_3A_1^{2x-z}\right]^{-z}\\ =&\Pi_z^{(1,2)}\Pi_x^{(1,2)}(A_3,A_1,A_2)+\Pi_z^{(1,2)}\Pi_x^{(1,1)}(A_1,A_3,A_2)\end{aligned}$$

It's easy to find their permutation sums are the same:

$$\sum^{\odot}\Pi_z^{(1,3)}\Pi_x^{(1,1)}=\sum^{\odot}\Pi_z^{(1,3)}\Pi_x^{(1,3)}=\sum^{\odot}\Pi_z^{(1,1)}\Pi_x^{(1,2)}+\sum^{\odot}\Pi_z^{(1,1)}\Pi_x^{(1,3)}=\sum^{\odot}\Pi_z^{(1,2)}\Pi_x^{(1,2)}+\sum^{\odot}\Pi_z^{(1,2)}\Pi_x^{(1,1)},$$

and

$$\begin{aligned}&\sum^{\odot}\left(\Pi_z^{(1,3)}\Pi_x^{(1,1)}+\Pi_z^{(1,3)}\Pi_x^{(1,3)}+\Pi_z^{(1,1)}\Pi_x^{(1,2)}+\Pi_z^{(1,1)}\Pi_x^{(1,3)}+\Pi_z^{(1,2)}\Pi_x^{(1,2)}+\sum^{\odot}\Pi_z^{(1,2)}\Pi_x^{(1,1)}\right)\\ &=4\begin{pmatrix}A_1^{2x-z}A_2A_3^{-z}+A_2^{2x-z}A_3A_1^{-z}+A_3^{2x-z}A_1A_2^{-z}\\ A_1^{2x-z}A_3A_2^{-z}+A_3^{2x-z}A_2A_1^{-z}+A_2^{2x-z}A_1A_3^{-z}\end{pmatrix}\end{aligned}\tag{97}$$

Let's have a look at the following terms:

$$\Pi_z^{(1,1)}\Pi_x^{(1,5)}(A_1,A_2,A_3)+\Pi_z^{(1,2)}\Pi_x^{(1,4)}(A_2,A_3,A_1)=A_1\left[A_2^xA_3^{x-z}\right]^{-z}+A_1\left[A_3^xA_2^{x-z}\right]^{-z}=A_1A_2^{x-z}A_3^{x-z}$$
$$\Pi_z^{(1,1)}\Pi_x^{(1,4)}(A_1,A_2,A_3)=\Pi_z^{(1,2)}\Pi_x^{(1,5)}(A_3,A_2,A_1)=A_1^x\left[A_2^xA_3^{-z}\right]^{-z}=A_1^xA_2^{x-z}A_3^{-z}-A_1^x\left[A_2^{x-z}A_3\right]^{-z}$$
$$\Pi_z^{(1,3)}\Pi_x^{(1,4)}(A_1,A_2,A_3)=\Pi_z^{(1,3)}\Pi_x^{(1,5)}(A_3,A_2,A_1)=A_2^xA_1^{x-z}A_3^{-z}$$

The permutation sum of the terms above is:

$$\begin{aligned}
\sum^{\odot}\left(\Pi_z^{(1,1)}\Pi_x^{(1,5)}+\Pi_z^{(1,2)}\Pi_x^{(1,4)}\right)&=2\left(A_1A_2^{x-z}A_3^{x-z}+A_2A_3^{x-z}A_1^{x-z}+A_3A_1^{x-z}A_2^{x-z}\right)\\
\sum^{\odot}\left(\Pi_z^{(1,3)}\Pi_x^{(1,4)}+\Pi_z^{(1,3)}\Pi_x^{(1,5)}\right)&=2\begin{pmatrix}A_1^xA_2^{x-z}A_3^{-z}+A_2^xA_3^{x-z}A_1^{-z}+A_3^xA_1^{x-z}A_2^{-z}\\A_1^xA_3^{x-z}A_2^{-z}+A_2^xA_1^{x-z}A_3^{-z}+A_3^xA_2^{x-z}A_1^{-z}\end{pmatrix}\\
\sum^{\odot}\left(\Pi_z^{(1,1)}\Pi_x^{(1,4)}+\Pi_z^{(1,2)}\Pi_x^{(1,5)}\right)&=2\begin{pmatrix}A_1^x\left[A_2^xA_3^{-z}\right]^{-z}+A_2^x\left[A_3^xA_1^{-z}\right]^{-z}+A_3^x\left[A_1^xA_2^{-z}\right]^{-z}\\A_1^x\left[A_3^xA_2^{-z}\right]^{-z}+A_2^x\left[A_1^xA_3^{-z}\right]^{-z}+A_3^x\left[A_2^xA_1^{-z}\right]^{-z}\end{pmatrix}
\end{aligned}\tag{98}$$

Finally let's consider terms involving higher-lower-higher relation:

$$\begin{aligned}
\Pi_z^{(1,4)}\Pi_x^{(1,1)}(A_1,A_2,A_3)&=\Pi_z^{(1,4)}\Pi_x^{(1,3)}(A_3,A_2,A_1)=\mathbb{IM}_1\left(A_1^{2x},A_2,A_3\right)\\
\Pi_z^{(1,4)}\Pi_x^{(1,4)}(A_1,A_2,A_3)&=\Pi_z^{(1,4)}\Pi_x^{(1,5)}(A_3,A_2,A_1)=\mathbb{IM}_1\left(A_1^x,A_2^x,A_3\right)\\
\Pi_z^{(1,4)}\Pi_x^{(1,2)}(A_1,A_2,A_3)&=\mathbb{IM}_1\left(A_1,A_2^{2x},A_3\right)
\end{aligned}$$

It's easy to check the following relations:

$$\begin{aligned}
&\sum^{\odot}\Pi_z^{(1,4)}\Pi_x^{(1,1)}=\sum^{\odot}\Pi_z^{(1,4)}\Pi_x^{(1,3)}=\\
&\begin{pmatrix}\mathbb{IM}_1\left(A_1^{2x},A_2,A_3\right)+\mathbb{IM}_1\left(A_2^{2x},A_3,A_1\right)+\mathbb{IM}_1\left(A_3^{2x},A_1,A_2\right)\\\mathbb{IM}_1\left(A_1^{2x},A_3,A_2\right)+\mathbb{IM}_1\left(A_2^{2x},A_1,A_3\right)+\mathbb{IM}_1\left(A_3^{2x},A_2,A_1\right)\end{pmatrix}\\
&\sum^{\odot}\Pi_z^{(1,4)}\Pi_x^{(1,4)}=\sum^{\odot}\Pi_z^{(1,4)}\Pi_x^{(1,5)}\\
&\begin{pmatrix}\mathbb{IM}_1\left(A_1^x,A_2^x,A_3\right)+\mathbb{IM}_1\left(A_2^x,A_3^x,A_1\right),\mathbb{IM}_1\left(A_3^x,A_1^x,A_2\right)\\\mathbb{IM}_1\left(A_1^x,A_3^x,A_2\right)+\mathbb{IM}_1\left(A_2^x,A_1^x,A_3\right),\mathbb{IM}_1\left(A_3^x,A_2^x,A_1\right)\end{pmatrix}\\
&\sum^{\odot}\Pi_z^{(1,4)}\Pi_x^{(1,2)}=\\
&2\left(\mathbb{IM}_1\left(A_1,A_2^{2x},A_3\right)+\mathbb{IM}_1\left(A_2,A_3^{2x},A_1\right)+\mathbb{IM}_1\left(A_3,A_1^{2x},A_2\right)\right)
\end{aligned}$$

And naturally, we have:

$$
\begin{aligned}
&\sum^{\odot}\Pi_z^{(1,4)}\Pi_x^{(1,1)}+\sum^{\odot}\Pi_z^{(1,4)}\Pi_x^{(1,3)}+\sum^{\odot}\Pi_z^{(1,4)}\Pi_x^{(1,4)}+\sum^{\odot}\Pi_z^{(1,4)}\Pi_x^{(1,5)}+\sum^{\odot}\Pi_z^{(1,4)}\Pi_x^{(1,2)}\\
&=2\begin{pmatrix}\mathbb{IM}_1\left(A_1^{2x},A_2,A_3\right)+\mathbb{IM}_1\left(A_2^{2x},A_3,A_1\right)+\mathbb{IM}_1\left(A_3^{2x},A_1,A_2\right)\\ \mathbb{IM}_1\left(A_1^{2x},A_3,A_2\right)+\mathbb{IM}_1\left(A_2^{2x},A_1,A_3\right)+\mathbb{IM}_1\left(A_3^{2x},A_2,A_1\right)\end{pmatrix}\\
&+2\begin{pmatrix}\mathbb{IM}_1\left(A_1^{x},A_2^{x},A_3\right)+\mathbb{IM}_1\left(A_2^{x},A_3^{x},A_1\right),\mathbb{IM}_1\left(A_3^{x},A_1^{x},A_2\right)\\ \mathbb{IM}_1\left(A_1^{x},A_3^{x},A_2\right)+\mathbb{IM}_1\left(A_2^{x},A_1^{x},A_3\right),\mathbb{IM}_1\left(A_3^{x},A_2^{x},A_1\right)\end{pmatrix}\\
&+2\left(\mathbb{IM}_1\left(A_1,A_2^{2x},A_3\right)+\mathbb{IM}_1\left(A_2,A_3^{2x},A_1\right)+\mathbb{IM}_1\left(A_3,A_1^{2x},A_2\right)\right)
\end{aligned}
\tag{99}
$$

Summarizing the results obtained in equation (96, 97, 98, 99), we have:

$$
\begin{aligned}
&\frac{1}{128\pi^3}\int_{-\infty}^{\infty}dz_1\int_{-\infty}^{\infty}dz_2\int_{-\infty}^{\infty}dz_3\delta(\varepsilon_0+\varepsilon_1+\varepsilon_2)\mathcal{I}_1=\frac{1}{8}\Pi_z^{(1)}\Pi_x^{(1)}(A_1,A_2,A_3)\\
&=\frac{1}{2}\left(A_1^{2x}A_2^{-z}A_3^{-z}+A_2^{2x}A_3^{-z}A_1^{-z}+A_3^{2x}A_1^{-z}A_2^{-z}\right)\\
&+\frac{1}{2}\begin{pmatrix}A_1^{2x-z}A_2A_3^{-z}+A_2^{2x-z}A_3A_1^{-z}+A_3^{2x-z}A_1A_2^{-z}\\ A_1^{2x-z}A_3A_2^{-z}+A_3^{2x-z}A_2A_1^{-z}+A_2^{2x-z}A_1A_3^{-z}\end{pmatrix}\\
&+\frac{1}{4}\left(A_1A_2^{x-z}A_3^{x-z}+A_2A_3^{x-z}A_1^{x-z}+A_3A_1^{x-z}A_2^{x-z}\right)\\
&+\frac{1}{4}\begin{pmatrix}A_1^{x}A_2^{x-z}A_3^{-z}+A_2^{x}A_3^{x-z}A_1^{-z}+A_3^{x}A_1^{x-z}A_2^{-z}\\ A_1^{x}A_3^{x-z}A_2^{-z}+A_2^{x}A_1^{x-z}A_3^{-z}+A_3^{x}A_2^{x-z}A_1^{-z}\end{pmatrix}\\
&+\frac{1}{4}\begin{pmatrix}A_1^{x}\left[A_2^{x}A_3^{-z}\right]^{-z}+A_2^{x}\left[A_3^{x}A_1^{-z}\right]^{-z}+A_3^{x}\left[A_1^{x}A_2^{-z}\right]^{-z}\\ A_1^{x}\left[A_3^{x}A_2^{-z}\right]^{-z}+A_2^{x}\left[A_1^{x}A_3^{-z}\right]^{-z}+A_3^{x}\left[A_2^{x}A_1^{-z}\right]^{-z}\end{pmatrix}\\
&+\frac{1}{4}\begin{pmatrix}\mathbb{IM}_1\left(A_1^{2x},A_2,A_3\right)+\mathbb{IM}_1\left(A_2^{2x},A_3,A_1\right)+\mathbb{IM}_1\left(A_3^{2x},A_1,A_2\right)\\ \mathbb{IM}_1\left(A_1^{2x},A_3,A_2\right)+\mathbb{IM}_1\left(A_2^{2x},A_1,A_3\right)+\mathbb{IM}_1\left(A_3^{2x},A_2,A_1\right)\end{pmatrix}\\
&+\frac{1}{4}\begin{pmatrix}\mathbb{IM}_1\left(A_1^{x},A_2^{x},A_3\right)+\mathbb{IM}_1\left(A_2^{x},A_3^{x},A_1\right),\mathbb{IM}_1\left(A_3^{x},A_1^{x},A_2\right)\\ \mathbb{IM}_1\left(A_1^{x},A_3^{x},A_2\right)+\mathbb{IM}_1\left(A_2^{x},A_1^{x},A_3\right),\mathbb{IM}_1\left(A_3^{x},A_2^{x},A_1\right)\end{pmatrix}\\
&+\frac{1}{4}\left(\mathbb{IM}_1\left(A_1,A_2^{2x},A_3\right)+\mathbb{IM}_1\left(A_2,A_3^{2x},A_1\right)+\mathbb{IM}_1\left(A_3,A_1^{2x},A_2\right)\right)
\end{aligned}
\tag{100}
$$

If among the 3 terms, A_1, A_2, A_3, 2 of them are equal. Equation (100) can be written as:

$$\begin{aligned}\frac{1}{128\pi^3}\int \mathcal{I}_1 = &\frac{1}{4}\left(2A_1^{2x}A_1^{-z}A_2^{-z} + A_2^{2x}A_1^{-z}A_1^{-z}\right)\\ &+\frac{1}{2}\left(\ A_1^{2x-z}A_1A_2^{-z} + A_1^{2x-z}A_2A_1^{-z} + A_2^{2x-z}A_1A_1^{-z}\ \right)\\ &+\frac{1}{8}\left(2A_1A_1^{x-z}A_2^{x-z} + A_2A_1^{x-z}A_1^{x-z}\right)\\ &+\frac{1}{4}\left(\ A_1^{x}A_1^{x-z}A_2^{-z} + A_1^{x}A_2^{x-z}A_1^{-z} + A_2^{x}A_1^{x-z}A_1^{-z}\ \right)\\ &+\frac{1}{4}\left(\ A_1^{x}\left[A_1^{x}A_2^{-z}\right]^{-z} + A_1^{x}\left[A_2^{x}A_1^{-z}\right]^{-z} + A_2^{x}\left[A_1^{x}A_1^{-z}\right]^{-z}\ \right)\\ &+\frac{1}{4}\left(\ \mathbb{IM}_1\left(A_1^{2x},A_1,A_2\right) + \mathbb{IM}_1\left(A_1^{2x},A_2,A_1\right) + \mathbb{IM}_1\left(A_2^{2x},A_1,A_1\right)\ \right)\\ &+\frac{1}{4}\left(\ \mathbb{IM}_1\left(A_1^{x},A_1^{x},A_2\right) + \mathbb{IM}_1\left(A_1^{x},A_2^{x},A_1\right),\mathbb{IM}_1\left(A_2^{x},A_1^{x},A_1\right)\ \right)\\ &+\frac{1}{8}\left(2\mathbb{IM}_1\left(A_1,A_1^{2x},A_2\right) + \mathbb{IM}_1\left(A_1,A_2^{2x},A_1\right)\right)\end{aligned} \tag{101}$$

If all three terms are the same $A_1 = A_2 = A_3 = A$, we have:

$$\begin{aligned}\frac{1}{128\pi^3}\int \mathcal{I}_1 = &\frac{1}{4}A^{2x}A^{-z}A^{-z} + \frac{1}{2}A^{2x-z}AA^{-z} + \frac{1}{8}AA^{x-z}A^{x-z}\\ &+\frac{1}{4}A^{x}A^{x-z}A^{-z} + \frac{1}{4}A^{x}\left[A^{x}A^{-z}\right]^{-z} + \frac{1}{4}\mathbb{IM}_1\left(A^{2x},A,A\right)\\ &+\frac{1}{4}\mathbb{IM}_1\left(A^{x},A^{x},A\right) + \frac{1}{8}\mathbb{IM}_1\left(A,A^{2x},A\right)\end{aligned}$$

Rewrite $A^xA^{x-z}A^{-z}$ as $\frac{1}{2}A^x[A^{-z}A^{-z}]^x$, we have:

$$\begin{aligned}\frac{1}{128\pi^3}\int \mathcal{I}_1 = &\frac{1}{4}A^{2x}A^{-z}A^{-z} + \frac{1}{2}A^{2x-z}AA^{-z} + \frac{1}{8}AA^{x-z}A^{x-z}\\ &+\frac{1}{8}A^{x}\left[A^{-z}A^{-z}\right]^{x} + \frac{1}{4}A^{x}\left[A^{x}A^{-z}\right]^{-z} + \frac{1}{4}\mathbb{IM}_1\left(A^{2x},A,A\right)\\ &+\frac{1}{4}\mathbb{IM}_1\left(A^{x},A^{x},A\right) + \frac{1}{8}\mathbb{IM}_1\left(A,A^{2x},A\right)\end{aligned} \tag{102}$$

Let's check the second x-wise integral:

$$\mathcal{I}_2 = 128\pi^3\bar{A}_1{}^{2x}\left[\bar{A}_2\bar{A}_3\right]^{2x} = 128\pi^3\bar{A}_1{}^{2x}\left\{\bar{A}_2{}^{2x}\bar{A}_3 + 2\bar{A}_2{}^{x}\bar{A}_3{}^{x} + \bar{A}_2\bar{A}_3{}^{2x}\right\}$$

where $\bar{A}_1$, $\bar{A}_2$, and $\bar{A}_3$ are 3 functions of x and are defined in equation (95).

It will be input into the following z-wise integral:

$$\frac{1}{128\pi^3}\int_{-\infty}^{\infty}dz_1\int_{-\infty}^{\infty}dz_2\int_{-\infty}^{\infty}dz_3\delta(\varepsilon_0+\varepsilon_1+\varepsilon_2)\frac{-1}{32}\left|z_1-z_2\right|^2\mathcal{I}_2$$
$$=-\frac{1}{32}\int_{-\infty}^{\infty}dz_1\int_{-\infty}^{\infty}dz_2\int_{-\infty}^{\infty}dz_3\delta(\varepsilon_0+\varepsilon_1+\varepsilon_2)\left|z_1-z_2\right|^2\left[\ \bar{A}_1{}^{2x}\bar{A}_2{}^{2x}\bar{A}_3+2\bar{A}_1{}^{2x}\bar{A}_2{}^{x}\bar{A}_3{}^{x}+\bar{A}_1{}^{2x}\bar{A}_2\bar{A}_3{}^{2x}\ \right]$$

Just like the case discussed for integration over $\mathcal{I}_1$, the z-wise integration over $\mathcal{I}_2$ will be look like:

$$\int_{-\infty}^{\infty}dz_1\breve{A}_1(z_1)\int_{-\infty}^{\infty}dz_2\breve{A}_2(z_2)\int_{-\infty}^{\infty}dz_3\breve{A}_3(z_3)\left(z_1-z_2\right)^2\delta\left(\frac{z_1+z_3}{2}-z+\frac{\left|z_1-z_2\right|}{2}+\frac{\left|z_2-z_3\right|}{2}\right)$$
$$=\int_{-\infty}^{\infty}dz_1\delta\left(z_1-z\right)\breve{A}_1(z_1)\int_{-\infty}^{z_1}dz_2\left(z_1-z_2\right)^2\breve{A}_2(z_2)\int_{-\infty}^{z_2}dz_3\breve{A}_3(z_3)$$
$$+\int_{-\infty}^{\infty}dz_3\delta\left(z_3-z\right)\breve{A}_3(z_3)\int_{-\infty}^{z_3}dz_2\breve{A}_2(z_2)\int_{-\infty}^{z_2}dz_1\left(z_1-z_2\right)^2\breve{A}_1(z_1)$$
$$+\int_{-\infty}^{\infty}dz_3\delta\left(z_2-z\right)\breve{A}_2(z_2)\left(\int_{-\infty}^{z_2}dz_1\left(z_1-z_2\right)^2\breve{A}_1(z_1)\right)\left(\int_{-\infty}^{z_2}dz_3\breve{A}_3(z_3)\right)$$
$$+\int_{-\infty}^{\infty}du\delta\left(u-z\right)\int_{-\infty}^{u}dz_3\left(u-z_3\right)^2\breve{A}_3(z_3)\int_{-\infty}^{u}dz_1\breve{A}_1(z_1)\breve{A}_2(z_1+z_3-u)$$
$$=\breve{A}_1\left[\breve{A}_2\breve{A}_3^{-z}\right]^{-3z}+\breve{A}_3\left[\breve{A}_2\breve{A}_1^{-3z}\right]^{-z}+\breve{A}_1^{-3z}\breve{A}_2\breve{A}_3^{-z}+\mathbb{IM}_3(\breve{A}_3,\breve{A}_2,\breve{A}_1)$$

Just as before, let's define 2 set operations:

$$\Pi_x^{(2)}=\Pi_x^{(2,1)}+\Pi_x^{(2,2)}+\Pi_x^{(2,3)}$$
$$\Pi_x^{(2,1)}=\partial_{x1}\partial_{x1}\partial_{x2}\partial_{x2}\qquad\Pi_x^{(2,2)}=2\partial_{x1}\partial_{x1}\partial_{x2}\partial_{x3}\qquad\Pi_x^{(2,3)}=\partial_{x1}\partial_{x1}\partial_{x3}\partial_{x3}$$
$$\Pi_z^{(2)}=\Pi_z^{(2,1)}+\Pi_z^{(2,2)}+\Pi_z^{(2,3)}+\Pi_z^{(2,4)}$$
$$\Pi_z^{(2,1)}(A,B,C)=A\left[BC^{-z}\right]^{-3z}\qquad\Pi_z^{(2,2)}(A,B,C)=C\left[BA^{-z}\right]^{-3z}$$
$$\Pi_z^{(2,3)}(A,B,C)=A^{-3z}BC^{-z}\qquad\Pi_z^{(2,4)}(A,B,C)=\mathbb{IM}_3(A,B,C)$$

Expressed by operators above, the z-wise integral over $\mathcal{I}_2$ is $\Pi_z^{(2)}\Pi_x^{(2)}$. We can use a table to clearly denote the result of successive application of those x- and z-wise operators:

fac	$\breve{A}_1$	$\breve{A}_2$	$\breve{A}_3$	$\breve{A}_1\left[\breve{A}_2\breve{A}_3^{-z}\right]^{3z}$	$\breve{A}_3\left[\breve{A}_2\breve{A}_1^{-3z}\right]^{-z}$	$\breve{A}_1^{-3z}\breve{A}_2\breve{A}_3^{-z}$	$\mathbb{IM}_3(\breve{A}_1,\breve{A}_2,\breve{A}_3)$
	A_1^{2x}	A_2^{2x}	A_3	$\Pi_z^{(2,1)}\Pi_x^{(2,1)}$	$\Pi_z^{(2,2)}\Pi_x^{(2,1)}$	$\Pi_z^{(2,3)}\Pi_x^{(2,1)}$	$\Pi_z^{(2,4)}\Pi_x^{(2,1)}$
2	A_1^{2x}	A_2^{x}	A_3^{x}	$\Pi_z^{(2,1)}\Pi_x^{(2,2)}$	$\Pi_z^{(2,2)}\Pi_x^{(2,2)}$	$\Pi_z^{(2,3)}\Pi_x^{(2,2)}$	$\Pi_z^{(2,4)}\Pi_x^{(2,2)}$
	A_1^{2x}	A_2	A_3^{2x}	$\Pi_z^{(2,1)}\Pi_x^{(2,3)}$	$\Pi_z^{(2,2)}\Pi_x^{(2,3)}$	$\Pi_z^{(2,3)}\Pi_x^{(2,3)}$	$\Pi_z^{(2,4)}\Pi_x^{(2,3)}$

Because of the following relations:

$$\Pi_z^{(2,1)}\Pi_z^{(2,1)}(A_1,A_2,A_3)+\Pi_z^{(2,1)}\Pi_z^{(2,3)}(A_1,A_3,A_2)=A_1^{2x}\left[A_2^{2x}A_3^{-z}\right]^{-3z}+A_1^{2x}\left[A_3A_2^{2x-z}\right]^{-3z}$$
$$=\overrightarrow{(25)}=A_1^{2x}\left[A_2^{2x-z}A_3^{-z}\right]^{-2z}$$
$$\Pi_z^{(2,1)}\Pi_z^{(2,1)}(A_1,A_3,A_2)+\Pi_z^{(2,1)}\Pi_z^{(2,3)}(A_1,A_2,A_3)=A_1^{2x}\left[A_3^{2x}A_2^{-z}\right]^{-3z}+A_1^{2x}\left[A_2A_3^{2x-z}\right]^{-3z}$$
$$=\overrightarrow{(25)}=A_1^{2x}\left[A_3^{2x-z}A_2^{-z}\right]^{-2z}$$
$$\Pi_z^{(2,1)}\Pi_z^{(2,2)}(A_1,A_2,A_3)+\Pi_z^{(2,1)}\Pi_z^{(2,2)}(A_1,A_3,A_2)=2A_1^{2x}\left[A_2^{x}A_3^{x-z}\right]^{-3z}+2A_1^{2x}\left[A_3^{x}A_2^{x-z}\right]^{-3z}$$
$$=\overrightarrow{(25)}=2A_1^{2x}\left[A_2^{x-z}A_3^{x-z}\right]^{-2z}$$
$$A_1^{2x}\left[A_2^{2x-z}A_3^{-z}\right]^{-2z}+2A_1^{2x}\left[A_2^{x-z}A_3^{x-z}\right]^{-2z}+A_1^{2x}\left[A_3^{2x-z}A_2^{-z}\right]^{-2z}=\overrightarrow{(21)}=A_1^{2x}\left[A_2^{-z}A_3^{-z}\right]^{2x-2z}$$

We have:

$$\begin{aligned}&\sum^{\odot}\Pi_z^{(2,1)}\Pi_x^{(2,1)}(A_1,A_2,A_3)+\sum^{\odot}\Pi_z^{(2,1)}\Pi_x^{(2,1)}(A_1,A_2,A_3)+\sum^{\odot}\Pi_z^{(2,1)}\Pi_x^{(2,1)}(A_1,A_2,A_3)\\ =&A_1^{2x}\left[A_2^{-z}A_3^{-z}\right]^{2x-2z}+A_2^{2x}\left[A_3^{-z}A_1^{-z}\right]^{2x-2z}+A_3^{2x}\left[A_1^{-z}A_2^{-z}\right]^{2x-2z}\end{aligned}\tag{103}$$

Let's look at the following terms:

$$\Pi_z^{(2,2)}\Pi_x^{(2,1)}(A_1,A_2,A_3)=A_3\left[A_2^{2x}A_3^{2x-3z}\right]^{-z}=A_3A_2^{2x-z}A_1^{2x-3z}-A_3\left[A_2^{2x-z}A_1^{2x-2z}\right]^{-z}$$
$$\Pi_z^{(2,2)}\Pi_x^{(2,2)}(A_1,A_2,A_3)=2A_3^{x}A_2^{x-z}A_1^{2x-3z}-2A_3^{x}\left[A_2^{x-z}A_1^{2x-2z}\right]^{-z}$$
$$\Pi_z^{(2,2)}\Pi_x^{(2,3)}(A_1,A_2,A_3)=A_3^{2x}A_2^{-z}A_1^{2x-3z}-A_3^{2x}\left[A_2^{-z}A_1^{2x-2z}\right]^{-z}$$

Let's group all 3 first terms after the last 3 "=" sign, and denote the result by a function $f_1(A_1,A_2,A_3)$. And the remaining part is denoted as $f_2(A_1,A_2,A_3)$. The reason for this breakup is trying to make the integrals and derivatives distributed as balanced as possible.

$$f_1(A_1,A_2,A_3)=A_3A_2^{2x-z}A_1^{2x-3z}+2A_3^{x}A_2^{x-z}A_1^{2x-3z}+A_3^{2x}A_2^{-z}A_1^{2x-3z}=A_1^{2x-3z}\left[A_3A_2^{-z}\right]^{2x}$$
$$f_2(A_1,A_2,A_3)=-A_3\left[A_2^{2x-z}A_1^{2x-2z}\right]^{-z}-2A_3^{x}\left[A_2^{x-z}A_1^{2x-2z}\right]^{-z}-A_3^{2x}\left[A_2^{-z}A_1^{2x-2z}\right]^{-z}$$
$$\Pi_z^{(2,2)}\left[\Pi_x^{(2,1)}+\Pi_x^{(2,2)}+\Pi_x^{(2,3)}\right](A_1,A_2,A_3)=f_1(A_1,A_2,A_3)+f_2(A_1,A_2,A_3)$$

And $f_1(A_1,A_2,A_3)$ is equivalent to the following:

$$\Pi_z^{(2,3)}\left[\Pi_x^{(2,1)}+\Pi_x^{(2,2)}+\Pi_x^{(2,3)}\right](A_1,A_3,A_2)=A_1^{2x-3z}\left[A_3A_2^{-z}\right]^{2x}$$

So their permutation sums are actually the same:

$$\begin{aligned}&\sum^{\odot}\left[\Pi_z^{(2,3)}\Pi_x^{(2,1)}+\Pi_z^{(2,3)}\Pi_x^{(2,2)}+\Pi_z^{(2,3)}\Pi_x^{(2,3)}+f_1\right](A_1,A_2,A_3)\\&=2\begin{pmatrix}A_1^{2x-3z}\left[A_3A_2^{-z}\right]^{2x}+A_2^{2x-3z}\left[A_1A_3^{-z}\right]^{2x}+A_3^{2x-3z}\left[A_2A_1^{-z}\right]^{2x}\\A_1^{2x-3z}\left[A_2A_3^{-z}\right]^{2x}+A_2^{2x-3z}\left[A_3A_1^{-z}\right]^{2x}+A_3^{2x-3z}\left[A_1A_2^{-z}\right]^{2x}\end{pmatrix}\end{aligned}\tag{104}$$

We summarize the permutation sum of f_2 as follows.

$$\begin{aligned}\sum^{\odot}f_2=&-\left(A_1A_2^{2x-2z}A_3^{2x-2z}+A_2A_3^{2x-2z}A_1^{2x-2z}+A_3A_1^{2x-2z}A_2^{2x-2z}\right)\\&-2\begin{pmatrix}A_1^{x}\left[A_2^{x-z}A_3^{2x-2z}\right]^{-z}+A_2^{x}\left[A_3^{x-z}A_1^{2x-2z}\right]^{-z}+A_3^{x}\left[A_1^{x-z}A_2^{2x-2z}\right]^{-z}\\A_1^{x}\left[A_3^{x-z}A_2^{2x-2z}\right]^{-z}+A_2^{x}\left[A_1^{x-z}A_3^{2x-2z}\right]^{-z}+A_3^{x}\left[A_2^{x-z}A_1^{2x-2z}\right]^{-z}\end{pmatrix}\\&-\begin{pmatrix}A_1^{2x}\left[A_2^{-z}A_3^{2x-2z}\right]^{-z}+A_2^{2x}\left[A_3^{-z}A_1^{2x-2z}\right]^{-z}+A_3^{2x}\left[A_1^{-z}A_2^{2x-2z}\right]^{-z}\\A_1^{2x}\left[A_3^{-z}A_2^{2x-2z}\right]^{-z}+A_2^{2x}\left[A_1^{-z}A_3^{2x-2z}\right]^{-z}+A_3^{2x}\left[A_2^{-z}A_1^{2x-2z}\right]^{-z}\end{pmatrix}\end{aligned}\tag{105}$$

Finally let's look at the portion which lower-higher-lower relation relations between adjacent scatters:

$$\begin{aligned}&\Pi_z^{(2,4)}\left[\Pi_x^{(2,1)}+\Pi_x^{(2,2)}+\Pi_x^{(2,3)}\right](A_1,A_2,A_3)\\&=\mathbb{IM}_3\left(A_1^{2x},A_2^{2x},A_3\right)+2\mathbb{IM}_3\left(A_1^{2x},A_2^{x},A_3^{x}\right)+\mathbb{IM}_3\left(A_1^{2x},A_2,A_3^{2x}\right)\\&=\mathbb{IM}_{3X}\left(A_1,A_2,A_3\right)\end{aligned}$$

The last step in the equations above move the x-wise operations inside the z-wise integral. In summary, their permutation sum can be written as:

$$\sum^{\odot}\Pi_z^{(2,4)}\left[\Pi_x^{(2,1)}+\Pi_x^{(2,2)}+\Pi_x^{(2,3)}\right]=\begin{pmatrix}\mathbb{IM}_{3X}\left(A_1,A_2,A_3\right)+\mathbb{IM}_{3X}\left(A_2,A_3,A_1\right)\\\mathbb{IM}_{3X}\left(A_3,A_1,A_2\right)+\mathbb{IM}_{3X}\left(A_1,A_3,A_2\right)\\\mathbb{IM}_{3X}\left(A_2,A_1,A_3\right)+\mathbb{IM}_{3X}\left(A_3,A_2,A_1\right)\end{pmatrix}\tag{106}$$

Finally we sum the terms in equations (103, 104, 105, 106) together to obtain the permutation sum of -32 times the z-wise integral over $\mathcal{I}_2$. Because the permutation sum of the z-wise integral over $\mathcal{I}_4$ is actually equivalent to that of $\mathcal{I}_2$ (this fact will be proved shortly after), we can simply express their sum by multiplying a factor of 2:

$$
\begin{aligned}
&\frac{1}{128\pi^3}\int_{-\infty}^{\infty}dz_1\int_{-\infty}^{\infty}dz_2\int_{-\infty}^{\infty}dz_3\left(-\frac{(z_1-z_2)^2}{32}\mathcal{I}_2-\frac{(z_2-z_3)^2}{32}\mathcal{I}_4\right)\\
=&-\frac{1}{16}\left(\mathsf{eq103}+\mathsf{eq104}+\mathsf{eq105}+\mathsf{eq106}\right)\\
=&-\frac{1}{16}\left(A_1^{2x}\left[A_2^{-z}A_3^{-z}\right]^{2x-2z}+A_2^{2x}\left[A_3^{-z}A_1^{-z}\right]^{2x-2z}+A_3^{2x}\left[A_1^{-z}A_2^{-z}\right]^{2x-2z}\right)\\
&-\frac{1}{8}\begin{pmatrix}A_1^{2x-3z}\left[A_3A_2^{-z}\right]^{2x}+A_2^{2x-3z}\left[A_1A_3^{-z}\right]^{2x}+A_3^{2x-3z}\left[A_2A_1^{-z}\right]^{2x}\\A_1^{2x-3z}\left[A_2A_3^{-z}\right]^{2x}+A_2^{2x-3z}\left[A_3A_1^{-z}\right]^{2x}+A_3^{2x-3z}\left[A_1A_2^{-z}\right]^{2x}\end{pmatrix}\\
&+\frac{1}{16}\left(A_1A_2^{2x-2z}A_3^{2x-2z}+A_2A_3^{2x-2z}A_1^{2x-2z}+A_3A_1^{2x-2z}A_2^{2x-2z}\right)\\
&+\frac{1}{8}\begin{pmatrix}A_1^{x}\left[A_2^{x-z}A_3^{2x-2z}\right]^{-z}+A_2^{x}\left[A_3^{x-z}A_1^{2x-2z}\right]^{-z}+A_3^{x}\left[A_1^{x-z}A_2^{2x-2z}\right]^{-z}\\A_1^{x}\left[A_3^{x-z}A_2^{2x-2z}\right]^{-z}+A_2^{x}\left[A_1^{x-z}A_3^{2x-2z}\right]^{-z}+A_3^{x}\left[A_2^{x-z}A_1^{2x-2z}\right]^{-z}\end{pmatrix}\\
&+\frac{1}{16}\begin{pmatrix}A_1^{2x}\left[A_2^{-z}A_3^{2x-2z}\right]^{-z}+A_2^{2x}\left[A_3^{-z}A_1^{2x-2z}\right]^{-z}+A_3^{2x}\left[A_1^{-z}A_2^{2x-2z}\right]^{-z}\\A_1^{2x}\left[A_3^{-z}A_2^{2x-2z}\right]^{-z}+A_2^{2x}\left[A_1^{-z}A_3^{2x-2z}\right]^{-z}+A_3^{2x}\left[A_2^{-z}A_1^{2x-2z}\right]^{-z}\end{pmatrix}\\
&-\frac{1}{16}\begin{pmatrix}\mathbb{IM}_{3X}\left(A_1,A_2,A_3\right)+\mathbb{IM}_{3X}\left(A_2,A_3,A_1\right)\\\mathbb{IM}_{3X}\left(A_3,A_1,A_2\right)+\mathbb{IM}_{3X}\left(A_1,A_3,A_2\right)\\\mathbb{IM}_{3X}\left(A_2,A_1,A_3\right)+\mathbb{IM}_{3X}\left(A_3,A_2,A_1\right)\end{pmatrix}
\end{aligned}
\tag{107}
$$

If among these three scatters: A_1, A_2, A_3, there are only 2 distinct ones. We have:

$$
\begin{aligned}
&\frac{1}{128\pi^3}\int_{-\infty}^{\infty}dz_1\int_{-\infty}^{\infty}dz_2\int_{-\infty}^{\infty}dz_3\left(-\frac{(z_1-z_2)^2}{32}\mathcal{I}_2-\frac{(z_2-z_3)^2}{32}\mathcal{I}_4\right)\\
=&-\frac{1}{32}\left(2A_1^{2x}\left[A_1^{-z}A_2^{-z}\right]^{2x-2z}+A_2^{2x}\left[A_1^{-z}A_1^{-z}\right]^{2x-2z}\right)\\
&-\frac{1}{8}\begin{pmatrix}A_1^{2x-3z}\left[A_2A_1^{-z}\right]^{2x}+A_1^{2x-3z}\left[A_1A_2^{-z}\right]^{2x}+A_2^{2x-3z}\left[A_1A_1^{-z}\right]^{2x}\end{pmatrix}\\
&+\frac{1}{32}\left(2A_1A_1^{2x-2z}A_2^{2x-2z}+A_2A_1^{2x-2z}A_1^{2x-2z}\right)\\
&+\frac{1}{8}\begin{pmatrix}A_1^{x}\left[A_1^{x-z}A_2^{2x-2z}\right]^{-z}+A_1^{x}\left[A_2^{x-z}A_1^{2x-2z}\right]^{-z}+A_2^{x}\left[A_1^{x-z}A_1^{2x-2z}\right]^{-z}\end{pmatrix}\\
&+\frac{1}{16}\begin{pmatrix}2A_1^{2x}\left[A_1^{-z}A_2^{2x-2z}\right]^{-z}+A_2^{2x}\left[A_1^{-z}A_1^{2x-2z}\right]^{-z}\end{pmatrix}\\
&-\frac{1}{16}\begin{pmatrix}\mathbb{IM}_{3X}\left(A_1,A_1,A_2\right)+\mathbb{IM}_{3X}\left(A_1,A_2,A_1\right)+\mathbb{IM}_{3X}\left(A_2,A_1,A_1\right)\end{pmatrix}
\end{aligned}
\tag{108}
$$

If all 3 scatters are identical: $A_1=A_2=A_3=A$, we have:

$$\begin{aligned}
&\frac{1}{128\pi^3}\int_{-\infty}^{\infty}dz_1\int_{-\infty}^{\infty}dz_2\int_{-\infty}^{\infty}dz_3\left(-\frac{(z_1-z_2)^2}{32}\mathcal{I}_2-\frac{(z_2-z_3)^2}{32}\mathcal{I}_4\right)\\
&=-\frac{1}{32}A^{2x}\left[A^{-z}A^{-z}\right]^{2x-2z}-\frac{1}{8}A^{2x-3z}\left[AA^{-z}\right]^{2x}+\frac{1}{32}AA^{2x-2z}A^{2x-2z}\\
&\quad+\frac{1}{8}A^{x}\left[A^{x-z}A^{2x-2z}\right]^{-z}+\frac{1}{16}A^{2x}\left[A^{-z}A^{2x-2z}\right]^{-z}-\frac{1}{16}\mathbb{IM}_{3X}\left(A,A,A\right)
\end{aligned}\tag{109}$$

Let's check the fourth x-wise integral:

$$\mathcal{I}_4=128\pi^3\left[\bar{A}_1\bar{A}_2\right]^{2x}\bar{A}_3{}^{2x}=128\pi^3\left\{\bar{A}_1{}^{2x}\bar{A}_2+2\bar{A}_1{}^{x}\bar{A}_2{}^{x}+\bar{A}_1\bar{A}_2{}^{2x}\right\}\bar{A}_3{}^{2x}$$

where $\bar{A}_1$, $\bar{A}_2$, and $\bar{A}_3$ are 3 functions of x and are defined in equation (95).

The integration result over $\mathcal{I}_4$ is actually identical to that of $\mathcal{I}_2$ (with different arguments). This means that their permutation sums are the same. The proof is as follows. This time let's explicitly consider $\mathcal{I}_4$ as a function of (A_1,A_2,A_3).

$$\begin{aligned}
&\int_{-\infty}^{\infty}dz_1\int_{-\infty}^{\infty}dz_2\int_{-\infty}^{\infty}dz_3\delta\left(\varepsilon_0+\varepsilon_1+\varepsilon_2\right)\mathcal{I}_4(A_1,A_2,A_3)\\
&=\int_{-\infty}^{\infty}dz_1\int_{-\infty}^{\infty}dz_2\int_{-\infty}^{\infty}dz_3\delta\left(\frac{z_1+z_3}{2}-z+\frac{|z_1-z_2|}{2}+\frac{|z_2-z_3|}{2}\right)\\
&\quad\times\int_{-\infty}^{\infty}dx_1A_1(x_1,z_1)\int_{-\infty}^{\infty}dx_2A_2(x_2,z_2)\int_{-\infty}^{\infty}dx_3A_3(x_3,z_3)\int_{-\infty}^{\infty}dk_m e^{ik_m(x-0.5x_1-0.5x_3)}\\
&\quad\times\int_{-\infty}^{\infty}dk_1e^{ik_1(x_1-x_2)}\int_{-\infty}^{\infty}dk_2e^{ik_2(x_2-x_3)}\left(k_m^2-4k_2^2\right)^2
\end{aligned}$$

Let's define the following change of variables: $k_1'=-k_2$ $k_2'=-k_1$, $x_1=x_3'$, $x_2=x_2'$, $x_3=x_1'$, $z_2'=z_2$, $z_1'=z_3$, $z_3'=z_1$, we can change the integration above into:

$$\begin{aligned}
&=\int_{-\infty}^{\infty}dz_1'\int_{-\infty}^{\infty}dz_2'\int_{-\infty}^{\infty}dz_3'\delta\left(\frac{z_1'+z_3'}{2}-z+\frac{|z_1'-z_2'|}{2}+\frac{|z_2'-z_3'|}{2}\right)\\
&\quad\times\int_{-\infty}^{\infty}dx_1'A_3(x_1',z_1')\int_{-\infty}^{\infty}dx_2'A_2(x_2',z_2')\int_{-\infty}^{\infty}dx_3'A_1(x_3',z_3')\int_{-\infty}^{\infty}dk_m e^{ik_m(x-0.5x_1'-0.5x_3')}\\
&\quad\times\int_{-\infty}^{\infty}dk_2'e^{ik_2'(x_2'-x_3')}\int_{-\infty}^{\infty}dk_1'e^{ik_1'(x_1'-x_2')}\left(k_m^2-4k_1'^2\right)^2
\end{aligned}$$

Please notice that all the integration variables with prime sign, because all this integration variables are dummy, we get the same expression if we remove the primes from them.

$$
\begin{aligned}
&= \int_{-\infty}^{\infty} dz_1 \int_{-\infty}^{\infty} dz_2 \int_{-\infty}^{\infty} dz_3 \delta\left(\frac{z_1+z_3}{2} - z + \frac{|z_1-z_2|}{2} + \frac{|z_2-z_3|}{2}\right) \\
&\quad \times \int_{-\infty}^{\infty} dx_1 A_3(x_1,z_1) \int_{-\infty}^{\infty} dx_2 A_2(x_2,z_2) \int_{-\infty}^{\infty} dx_3 A_1(x_3,z_3) \int_{-\infty}^{\infty} dk_m e^{ik_m(x-0.5x_1-0.5x_3)} \\
&\quad \times \int_{-\infty}^{\infty} dk_2 e^{ik_2(x_2-x_3)} \int_{-\infty}^{\infty} dk_1 e^{ik_1(x_1-x_2)} \left(k_m^2 - 4k_1^2\right)^2 \\
&= \int_{-\infty}^{\infty} dz_1 \int_{-\infty}^{\infty} dz_2 \int_{-\infty}^{\infty} dz_3 \delta\left(\varepsilon_0+\varepsilon_1+\varepsilon_2\right) \mathcal{I}_2(A_3,A_2,A_1)
\end{aligned}
$$

Finally let's consider the third x-wise integral:

$$
\mathcal{I}_3 = 128\pi^3 \left\{ \bar{A}_1^{\,2x} \bar{A}_2 \bar{A}_3^{\,2x} + \bar{A}_1^{\,2x} \bar{A}_2^{\,x} \bar{A}_3^{\,x} + \bar{A}_1^{\,x} \bar{A}_2^{\,2x} \bar{A}_3^{\,x} + \bar{A}_1^{\,x} \bar{A}_2^{\,x} \bar{A}_3^{\,2x} \right\}
$$

where $\bar{A}_1$, $\bar{A}_2$, and $\bar{A}_3$ are 3 functions of x and are defined in equation (95).

It will be input into the following z-wise integral:

$$
\begin{aligned}
&\frac{1}{128\pi^3} \int_{-\infty}^{\infty} dz_1 \int_{-\infty}^{\infty} dz_2 \int_{-\infty}^{\infty} dz_3 \delta(\varepsilon_0+\varepsilon_1+\varepsilon_2) \frac{-1}{16} |z_1-z_2| \, |z_2-z_3| \, \mathcal{I}_3 \\
&= -\frac{1}{16} \int_{-\infty}^{\infty} dz_1 \int_{-\infty}^{\infty} dz_2 \int_{-\infty}^{\infty} dz_3 \delta(\varepsilon_0+\varepsilon_1+\varepsilon_2) \, |z_1-z_2| \, |z_2-z_3| \\
&\quad \times \left[\bar{A}_1^{\,2x} \bar{A}_2 \bar{A}_3^{\,2x} + \bar{A}_1^{\,2x} \bar{A}_2^{\,x} \bar{A}_3^{\,x} + \bar{A}_1^{\,x} \bar{A}_2^{\,2x} \bar{A}_3^{\,x} + \bar{A}_1^{\,x} \bar{A}_2^{\,x} \bar{A}_3^{\,2x} \right]
\end{aligned}
$$

It's corresponding z-wise integral looks like:

$$
\begin{aligned}
&\int_{-\infty}^{\infty} dz_1 \breve{A}_1(z_1) \int_{-\infty}^{\infty} dz_2 \breve{A}_2(z_2) \int_{-\infty}^{\infty} dz_3 \breve{A}_3(z_3) |z_1 - z_2||z_2 - z_3| \delta(\varepsilon_0 + \varepsilon_1 + \varepsilon_2) \\
&= \int_{-\infty}^{\infty} dz_1 \delta(z_1 - z) \breve{A}_1(z_1) \int_{-\infty}^{z_1} dz_2 (z_1 - z_2) \breve{A}_2(z_2) \int_{-\infty}^{z_2} dz_3 (z_2 - z_3) \breve{A}_3(z_3) \\
&+ \int_{-\infty}^{\infty} dz_3 \delta(z_3 - z) \breve{A}_3(z_3) \int_{-\infty}^{z_3} dz_2 (z_3 - z_2) \breve{A}_2(z_2) \int_{-\infty}^{z_2} dz_1 (z_2 - z_1) \breve{A}_1(z_1) \\
&+ \int_{-\infty}^{\infty} dz_3 \delta(z_2 - z) \breve{A}_2(z_2) \left(\int_{-\infty}^{z_2} dz_1 (z_2 - z_1) \breve{A}_1(z_1) \right) \left(\int_{-\infty}^{z_2} dz_3 (z_2 - z_3) \breve{A}_3(z_3) \right) \\
&+ \int_{-\infty}^{\infty} du \delta(u - z) \int_{-\infty}^{u} dz_3 (u - z_3) \breve{A}_3(z_3) \int_{-\infty}^{u} dz_1 (u - z_1) \breve{A}_1(z_1) \breve{A}_2(z_1 + z_3 - u) \\
&= \breve{A}_1 \left[\breve{A}_2 \breve{A}_3^{-2z} \right]^{-2z} + \breve{A}_3 \left[\breve{A}_2 \breve{A}_1^{-2z} \right]^{-2z} + \breve{A}_1^{-2z} \breve{A}_2 \breve{A}_3^{-2z} + \mathbb{IM}_4(\breve{A}_3, \breve{A}_2, \breve{A}_1)
\end{aligned}
$$

Just like before, the integration can be summarized by 2 sets of operators:

$$
\begin{aligned}
&\Pi_x^{(3)} = \Pi_x^{(3,1)} + \Pi_x^{(3,2)} + \Pi_x^{(3,3)} + \Pi_x^{(3,4)} \\
&\Pi_x^{(3,1)} = \partial_{x1}\partial_{x1}\partial_{x3}\partial_{x3} \quad \Pi_x^{(3,2)} = \partial_{x1}\partial_{x1}\partial_{x2}\partial_{x3} \quad \Pi_x^{(3,3)} = \partial_{x1}\partial_{x2}\partial_{x2}\partial_{x3} \quad \Pi_x^{(3,4)} = \partial_{x1}\partial_{x2}\partial_{x3}\partial_{x3} \\
&\Pi_z^{(3)} = \Pi_z^{(3,1)} + \Pi_z^{(3,2)} + \Pi_z^{(3,3)} + \Pi_z^{(3,4)} \\
&\Pi_z^{(3,1)}(A,B,C) = A\left[BC^{-2z}\right]^{-2z} \quad \Pi_z^{(3,2)}(A,B,C) = C\left[BA^{-2z}\right]^{-2z} \\
&\Pi_z^{(3,3)}(A,B,C) = A^{-2z}BC^{-2z} \quad \Pi_z^{(3,4)}(A,B,C) = \mathbb{IM}_4(A,B,C)
\end{aligned}
$$

$\breve{A}_1$	$\breve{A}_2$	$\breve{A}_3$	$\breve{A}_1\left[\breve{A}_2\breve{A}_3^{-2z}\right]^{-2z}$	$\breve{A}_3\left[\breve{A}_2\breve{A}_1^{-2z}\right]^{-2z}$	$\breve{A}_1^{-2z}\breve{A}_2\breve{A}_3^{-2z}$	$\mathbb{IM}_4(\breve{A}_1,\breve{A}_2,\breve{A}_3)$
A_1^{2x}	A_2	A_3^{2x}	$\Pi_z^{(3,1)}\Pi_x^{(3,1)}$	$\Pi_z^{(3,2)}\Pi_x^{(3,1)}$	$\Pi_z^{(3,3)}\Pi_x^{(3,1)}$	$\Pi_z^{(3,4)}\Pi_x^{(3,1)}$
A_1^{2x}	A_2^{x}	A_3^{x}	$\Pi_z^{(3,1)}\Pi_x^{(3,2)}$	$\Pi_z^{(3,2)}\Pi_x^{(3,2)}$	$\Pi_z^{(3,3)}\Pi_x^{(3,2)}$	$\Pi_z^{(3,4)}\Pi_x^{(3,2)}$
A_1^{x}	A_2^{2x}	A_3^{x}	$\Pi_z^{(3,1)}\Pi_x^{(3,3)}$	$\Pi_z^{(3,2)}\Pi_x^{(3,3)}$	$\Pi_z^{(3,3)}\Pi_x^{(3,3)}$	$\Pi_z^{(3,4)}\Pi_x^{(3,3)}$
A_1^{x}	A_2^{x}	A_3^{2x}	$\Pi_z^{(3,1)}\Pi_x^{(3,4)}$	$\Pi_z^{(3,2)}\Pi_x^{(3,4)}$	$\Pi_z^{(3,3)}\Pi_x^{(3,4)}$	$\Pi_z^{(3,4)}\Pi_x^{(3,4)}$

With the help of the table above, it's easy to check:

$$
\begin{aligned}
\Pi_z^{(3,1)}\Pi_x^{(3,1)}(A_1,A_2,A_3) &= A_1^{2x}\left[A_2A_3^{2x-2z}\right]^{-2z} = \Pi_z^{(3,2)}\Pi_x^{(3,1)}(A_3,A_2,A_1) \\
\Pi_z^{(3,1)}\Pi_x^{(3,2)}(A_1,A_2,A_3) &= A_1^{2x}\left[A_2^{x}A_3^{x-2z}\right]^{-2z} = \Pi_z^{(3,2)}\Pi_x^{(3,4)}(A_3,A_2,A_1) \\
\Pi_z^{(3,1)}\Pi_x^{(3,3)}(A_1,A_2,A_3) &= A_1^{x}\left[A_2^{2x}A_3^{x-2z}\right]^{-2z} = \Pi_z^{(3,2)}\Pi_x^{(3,3)}(A_3,A_2,A_1) \\
\Pi_z^{(3,1)}\Pi_x^{(3,4)}(A_1,A_2,A_3) &= A_1^{x}\left[A_2^{x}A_3^{2x-2z}\right]^{-2z} = \Pi_z^{(3,2)}\Pi_x^{(3,2)}(A_3,A_2,A_1)
\end{aligned}
$$

¿From the relations above, it's easy to find that the following 2 permutation sums are equal:

$$\sum^{\odot} \Pi_z^{(3,1)} \left[\Pi_x^{(3,1)} + \Pi_x^{(3,2)} + \Pi_x^{(3,3)} + \Pi_x^{(3,4)}\right] = \sum^{\odot} \Pi_z^{(3,2)} \left[\Pi_x^{(3,1)} + \Pi_x^{(3,2)} + \Pi_x^{(3,3)} + \Pi_x^{(3,4)}\right]$$

and because:

$$\Pi_z^{(3,1)} \left[\Pi_x^{(3,1)} + \Pi_x^{(3,2)}\right](A_1, A_2, A_3) = A_1^{2x}\left[A_2 A_3^{x-2z}\right]^{x-2z}$$
$$\Pi_z^{(3,1)} \left[\Pi_x^{(3,3)} + \Pi_x^{(3,4)}\right](A_1, A_2, A_3) = A_1^{x}\left[A_2^{x} A_3^{x-2z}\right]^{x-2z}$$

We can group the permutation sum of the following terms as:

$$\begin{aligned}
&\sum^{\odot} \left[\Pi_z^{(3,1)} + \Pi_z^{(3,2)}\right] \left[\Pi_x^{(3,1)} + \Pi_x^{(3,2)} + \Pi_x^{(3,3)} + \Pi_x^{(3,4)}\right] \\
&= 2 \begin{pmatrix} A_1^{2x}\left[A_2 A_3^{x-2z}\right]^{x-2z} + A_2^{2x}\left[A_3 A_1^{x-2z}\right]^{x-2z} + A_3^{2x}\left[A_1 A_2^{x-2z}\right]^{x-2z} \\ A_1^{2x}\left[A_3 A_2^{x-2z}\right]^{x-2z} + A_2^{2x}\left[A_1 A_3^{x-2z}\right]^{x-2z} + A_3^{2x}\left[A_2 A_1^{x-2z}\right]^{x-2z} \end{pmatrix} \\
&+ 2 \begin{pmatrix} A_1^{x}\left[A_2^{x} A_3^{x-2z}\right]^{x-2z} + A_2^{x}\left[A_3^{x} A_1^{x-2z}\right]^{x-2z} + A_3^{x}\left[A_1^{x} A_2^{x-2z}\right]^{x-2z} \\ A_1^{x}\left[A_3^{x} A_2^{x-2z}\right]^{x-2z} + A_2^{x}\left[A_1^{x} A_3^{x-2z}\right]^{x-2z} + A_3^{x}\left[A_2^{x} A_1^{x-2z}\right]^{x-2z} \end{pmatrix}
\end{aligned} \tag{110}$$

In the high-low hierarchy, equation (110) summarizes 2 of them: $z_1 \geq z_2 \geq z_3$ $(l = 1)$, $z_1 \leq z_2 \leq z_3$ $(l = 4)$.

We then consider the following terms:

$$\Pi_z^{(3,3)}\Pi_x^{(3,1)}(A_1, A_2, A_3) + \Pi_z^{(3,3)}\Pi_x^{(3,2)}(A_1, A_2, A_3) = A_1^{2x-2z}\left[A_2 A_3^{x-2z}\right]^{x}$$
$$\Pi_z^{(3,3)}\Pi_x^{(3,3)}(A_1, A_2, A_3) + \Pi_z^{(3,3)}\Pi_x^{(3,4)}(A_1, A_2, A_3) = A_1^{x-2z}[A_2^{x} A_3^{x}]^{x}$$

The permutation sum of the terms above are:

$$\begin{aligned}
&\sum^{\odot} \Pi_z^{(3,3)} \left[\Pi_x^{(3,1)} + \Pi_x^{(3,2)} + \Pi_x^{(3,3)} + \Pi_x^{(3,4)}\right] \\
&= \begin{pmatrix} A_1^{2x-2z}\left[A_2 A_3^{x-2z}\right]^{x} + A_2^{2x-2z}\left[A_3 A_1^{x-2z}\right]^{x} + A_3^{2x-2z}\left[A_1 A_2^{x-2z}\right]^{x} \\ A_1^{2x-2z}\left[A_3 A_2^{x-2z}\right]^{x} + A_2^{2x-2z}\left[A_1 A_3^{x-2z}\right]^{x} + A_3^{2x-2z}\left[A_2 A_1^{x-2z}\right]^{x} \end{pmatrix} \\
&+ \begin{pmatrix} A_1^{x-2z}\left[A_2^{x} A_3^{x-2z}\right]^{x} + A_2^{x-2z}\left[A_3^{x} A_1^{x-2z}\right]^{x} + A_3^{x-2z}\left[A_1^{x} A_2^{x-2z}\right]^{x} \\ A_1^{x-2z}\left[A_3^{x} A_2^{x-2z}\right]^{x} + A_2^{x-2z}\left[A_1^{x} A_3^{x-2z}\right]^{x} + A_3^{x-2z}\left[A_2^{x} A_1^{x-2z}\right]^{x} \end{pmatrix}
\end{aligned} \tag{111}$$

In the high-low hierarchy, equation (111) summarizes the following: $z_1 \leq z_2 \geq z_3$ $(l = 3)$.

We now consider the terms in the high-low hierarchy, corresponding to the w-diagram.

$$\Pi_z^{(3,4)}\left[\Pi_x^{(3,1)}+\Pi_x^{(3,2)}\right]=\mathbb{IM}_4\left(A_1^{2x},A_2,A_3^{2x}\right)+\mathbb{IM}_4\left(A_1^{2x},A_2^{x},A_3^{x}\right)=\mathbb{IM}_{4X}\left(A_1^{x},A_2,A_3^{x}\right)$$
$$\Pi_z^{(3,4)}\left[\Pi_x^{(3,3)}+\Pi_x^{(3,4)}\right]=\mathbb{IM}_4\left(A_1^{x},A_2^{2x},A_3^{x}\right)+\mathbb{IM}_4\left(A_1^{x},A_2^{x},A_3^{2x}\right)=\mathbb{IM}_{4X}\left(A_1,A_2^{x},A_3^{x}\right)$$

The permutation sum of the terms above are:

$$\begin{aligned}&\sum^{\odot}\Pi_z^{(3,4)}\left[\Pi_x^{(3,1)}+\Pi_x^{(3,2)}+\Pi_x^{(3,3)}+\Pi_x^{(3,4)}\right]\\&=\begin{pmatrix}\mathbb{IM}_{4X}\left(A_1^{x},A_2,A_3^{x}\right)+\mathbb{IM}_{4X}\left(A_2^{x},A_3,A_1^{x}\right)+\mathbb{IM}_{4X}\left(A_3^{x},A_1,A_2^{x}\right)\\\mathbb{IM}_{4X}\left(A_1^{x},A_3,A_2^{x}\right)+\mathbb{IM}_{4X}\left(A_2^{x},A_1,A_3^{x}\right)+\mathbb{IM}_{4X}\left(A_3^{x},A_2,A_1^{x}\right)\end{pmatrix}\\&+\begin{pmatrix}\mathbb{IM}_{4X}\left(A_1,A_2^{x},A_3^{x}\right)+\mathbb{IM}_{4X}\left(A_2,A_3^{x},A_1^{x}\right)+\mathbb{IM}_{4X}\left(A_3,A_1^{x},A_2^{x}\right)\\\mathbb{IM}_{4X}\left(A_1,A_3^{x},A_2^{x}\right)+\mathbb{IM}_{4X}\left(A_2,A_1^{x},A_3^{x}\right)+\mathbb{IM}_{4X}\left(A_3,A_2^{x},A_1^{x}\right)\end{pmatrix}\end{aligned}\tag{112}$$

In the high-low hierarchy, equation (112) summarizes the following: $z_1\geq z_2\leq z_3$ $(l=2)$.

Finally we sum the terms in equations (110, 111, 112) together to obtain the permutation sum of -16 times the z-wise integral over $\mathcal{I}_3$. We have:

$$\begin{aligned}&\frac{1}{128\pi^3}\int_{-\infty}^{\infty}dz_1\int_{-\infty}^{\infty}dz_2\int_{-\infty}^{\infty}dz_3\left(-\frac{|z_1-z_2|\,|z_2-z_3|}{16}\right)\mathcal{I}_3=-\frac{1}{16}\left(\mathtt{eq110}+\mathtt{eq111}+\mathtt{eq112}\right)\\&=-\frac{1}{8}\begin{pmatrix}A_1^{2x}\left[A_2A_3^{x-2z}\right]^{x-2z}+A_2^{2x}\left[A_3A_1^{x-2z}\right]^{x-2z}+A_3^{2x}\left[A_1A_2^{x-2z}\right]^{x-2z}\\A_1^{2x}\left[A_3A_2^{x-2z}\right]^{x-2z}+A_2^{2x}\left[A_1A_3^{x-2z}\right]^{x-2z}+A_3^{2x}\left[A_2A_1^{x-2z}\right]^{x-2z}\end{pmatrix}\\&-\frac{1}{8}\begin{pmatrix}A_1^{x}\left[A_2^{x}A_3^{x-2z}\right]^{x-2z}+A_2^{x}\left[A_3^{x}A_1^{x-2z}\right]^{x-2z}+A_3^{x}\left[A_1^{x}A_2^{x-2z}\right]^{x-2z}\\A_1^{x}\left[A_3^{x}A_2^{x-2z}\right]^{x-2z}+A_2^{x}\left[A_1^{x}A_3^{x-2z}\right]^{x-2z}+A_3^{x}\left[A_2^{x}A_1^{x-2z}\right]^{x-2z}\end{pmatrix}\\&-\frac{1}{16}\begin{pmatrix}A_1^{2x-2z}\left[A_2A_3^{x-2z}\right]^{x}+A_2^{2x-2z}\left[A_3A_1^{x-2z}\right]^{x}+A_3^{2x-2z}\left[A_1A_2^{x-2z}\right]^{x}\\A_1^{2x-2z}\left[A_3A_2^{x-2z}\right]^{x}+A_2^{2x-2z}\left[A_1A_3^{x-2z}\right]^{x}+A_3^{2x-2z}\left[A_2A_1^{x-2z}\right]^{x}\end{pmatrix}\\&-\frac{1}{16}\begin{pmatrix}A_1^{x-2z}\left[A_2^{x}A_3^{x-2z}\right]^{x}+A_2^{x-2z}\left[A_3^{x}A_1^{x-2z}\right]^{x}+A_3^{x-2z}\left[A_1^{x}A_2^{x-2z}\right]^{x}\\A_1^{x-2z}\left[A_3^{x}A_2^{x-2z}\right]^{x}+A_2^{x-2z}\left[A_1^{x}A_3^{x-2z}\right]^{x}+A_3^{x-2z}\left[A_2^{x}A_1^{x-2z}\right]^{x}\end{pmatrix}\\&-\frac{1}{16}\begin{pmatrix}\mathbb{IM}_{4X}\left(A_1^{x},A_2,A_3^{x}\right)+\mathbb{IM}_{4X}\left(A_2^{x},A_3,A_1^{x}\right)+\mathbb{IM}_{4X}\left(A_3^{x},A_1,A_2^{x}\right)\\\mathbb{IM}_{4X}\left(A_1^{x},A_3,A_2^{x}\right)+\mathbb{IM}_{4X}\left(A_2^{x},A_1,A_3^{x}\right)+\mathbb{IM}_{4X}\left(A_3^{x},A_2,A_1^{x}\right)\end{pmatrix}\\&-\frac{1}{16}\begin{pmatrix}\mathbb{IM}_{4X}\left(A_1,A_2^{x},A_3^{x}\right)+\mathbb{IM}_{4X}\left(A_2,A_3^{x},A_1^{x}\right)+\mathbb{IM}_{4X}\left(A_3,A_1^{x},A_2^{x}\right)\\\mathbb{IM}_{4X}\left(A_1,A_3^{x},A_2^{x}\right)+\mathbb{IM}_{4X}\left(A_2,A_1^{x},A_3^{x}\right)+\mathbb{IM}_{4X}\left(A_3,A_2^{x},A_1^{x}\right)\end{pmatrix}\end{aligned}\tag{113}$$

If among the 3 scatters A_1, A_2, A_3, there are only 2 distinct ones. We have:

$$
\begin{aligned}
&\frac{1}{128\pi^3}\int_{-\infty}^{\infty}dz_1\int_{-\infty}^{\infty}dz_2\int_{-\infty}^{\infty}dz_3\left(-\frac{|z_1-z_2|\,|z_2-z_3|}{16}\right)\mathcal{I}_3\\
&=-\frac{1}{8}\left(\;A_1^{2x}\left[A_1A_2^{x-2z}\right]^{x-2z}+A_1^{2x}\left[A_2A_1^{x-2z}\right]^{x-2z}+A_2^{2x}\left[A_1A_1^{x-2z}\right]^{x-2z}\;\right)\\
&\quad-\frac{1}{8}\left(\;A_1^{x}\left[A_1^{x}A_2^{x-2z}\right]^{x-2z}+A_1^{x}\left[A_2^{x}A_1^{x-2z}\right]^{x-2z}+A_2^{x}\left[A_1^{x}A_1^{x-2z}\right]^{x-2z}\;\right)\\
&\quad-\frac{1}{16}\left(\;A_1^{2x-2z}\left[A_1A_2^{x-2z}\right]^{x}+A_1^{2x-2z}\left[A_2A_1^{x-2z}\right]^{x}+A_2^{2x-2z}\left[A_1A_1^{x-2z}\right]^{x}\;\right)\\
&\quad-\frac{1}{16}\left(\;A_1^{x-2z}\left[A_1^{x}A_2^{x-2z}\right]^{x}+A_1^{x-2z}\left[A_2^{x}A_1^{x-2z}\right]^{x}+A_2^{x-2z}\left[A_1^{x}A_1^{x-2z}\right]^{x}\;\right)\\
&\quad-\frac{1}{16}\left(\;\mathbb{IM}_{4X}\left(A_1^{x},A_1,A_2^{x}\right)+\mathbb{IM}_{4X}\left(A_1^{x},A_2,A_1^{x}\right)+\mathbb{IM}_{4X}\left(A_2^{x},A_1,A_1^{x}\right)\;\right)\\
&\quad-\frac{1}{16}\left(\;\mathbb{IM}_{4X}\left(A_1,A_1^{x},A_2^{x}\right)+\mathbb{IM}_{4X}\left(A_1,A_2^{x},A_1^{x}\right)+\mathbb{IM}_{4X}\left(A_2,A_1^{x},A_1^{x}\right)\;\right)
\end{aligned}
\tag{114}
$$

If all three scatters are identical: $A_1=A_2=A_3=A$, we have:

$$
\begin{aligned}
&\frac{1}{128\pi^3}\int_{-\infty}^{\infty}dz_1\int_{-\infty}^{\infty}dz_2\int_{-\infty}^{\infty}dz_3\left(-\frac{|z_1-z_2|\,|z_2-z_3|}{16}\right)\mathcal{I}_3\\
&=-\frac{1}{16}\left(\begin{array}{c}2A^{2x}\left[AA^{x-2z}\right]^{x-2z}+2A^{x}\left[A^{x}A^{x-2z}\right]^{x-2z}+A^{2x-2z}\left[AA^{x-2z}\right]^{x}\\ A^{x-2z}\left[A^{x}A^{x-2z}\right]^{x}+\mathbb{IM}_{4X}\left(A^{x},A,A^{x}\right)+\mathbb{IM}_{4X}\left(A,A^{x},A^{x}\right)\end{array}\right)
\end{aligned}
\tag{115}
$$

Let's summarize $\mathbb{SC}_3$ for the simplest case: $A_1=A_2=A_3=A$, that is, results from the following equations will be summed together: (84, 94, 102, 109, 115, 81).

$$
\begin{aligned}
&\mathbb{SC}_3(A,A,A)=-\frac{1}{8}A^{2z}A^{-z}A^{-z}-\frac{3}{4}A^{z}AA^{-z}-\frac{5}{16}A^{3}-\frac{1}{8}A^{z}\left[A^{2}\right]^{-z}-\frac{1}{16}\mathbb{IM}_1(A^{z},A,A^{z})\\
&+\frac{1}{4}A^{x-2z}\left[AA+A^{z}A^{-z}\right]^{x}+\frac{1}{8}A^{x}[AA]^{x-2z}-\frac{1}{8}A^{z}\left[A^{x-z}A^{x-z}\right]^{-z}\\
&+\frac{1}{4}AA^{x-z}A^{x-z}+\frac{1}{4}A^{x}\left[A^{-z}A^{-z}\right]^{x}+\frac{1}{16}\mathbb{IM}_2\left(A^{x},A,A^{x+z}\right)+\frac{1}{16}\mathbb{IM}_2\left(A^{x},A^{x},A^{z}\right)\\
&+\frac{1}{4}A^{2x}A^{-z}A^{-z}+\frac{1}{2}A^{2x-z}AA^{-z}\\
&+\frac{1}{4}A^{x}\left[A^{x}A^{-z}\right]^{-z}+\frac{1}{4}\mathbb{IM}_1\left(A^{2x},A,A\right)+\frac{1}{4}\mathbb{IM}_1\left(A^{x},A^{x},A\right)+\frac{1}{8}\mathbb{IM}_1\left(A,A^{2x},A\right)\\
&-\frac{1}{32}A^{2x}\left[A^{-z}A^{-z}\right]^{2x-2z}-\frac{1}{8}A^{2x-3z}\left[AA^{-z}\right]^{2x}+\frac{1}{32}AA^{2x-2z}A^{2x-2z}\\
&+\frac{1}{8}A^{x}\left[A^{x-z}A^{2x-2z}\right]^{-z}+\frac{1}{16}A^{2x}\left[A^{-z}A^{2x-2z}\right]^{-z}-\frac{1}{16}\mathbb{IM}_{3X}\left(A,A,A\right)\\
&-\frac{1}{8}\left[A^{x}\left\{A^{x-2z}\right\}^{2}\right]^{x}+\frac{1}{8}A^{x}\left[\left\{A^{x-z}\right\}^{2}\right]^{x-2z}-\frac{1}{16}A\left\{A^{2x-2z}\right\}^{2}-\frac{1}{8}A^{2x}\left[A^{-z}A^{2x-2z}\right]^{-z}\\
&+\frac{1}{16}A^{2x}\left[\left\{A^{-z}\right\}^{2}\right]^{2x-2z}+\mathbb{IM}_{4X}\left(A^{x},A,A^{x}\right)+\mathbb{IM}_{4X}\left(A,A^{x},A^{x}\right)
\end{aligned}
\tag{116}
$$

In the equation above, the fourth term of equation (102) and the third term of equation (109) are merged together because they are identical. Similarly, the fifth term of equation (102) is merged with the fourth term of equation (109) because their equivalence.

Appendix F: Derivation of α_3

The equation for α_3:

$$\alpha_3 = \mathbb{SC}_3(\alpha_1,\alpha_1,\alpha_1) + \mathbb{SC}_2(\alpha_1,\alpha_2)$$

First let's compute $\mathbb{SC}_3(\alpha_1,\alpha_1,\alpha_1)$ using equation (116) by simply substituting $A=\alpha_1$:

$$\begin{aligned}
\mathbb{SC}_3(\alpha_1,\alpha_1,\alpha_1) &= -\frac{1}{8}\alpha_1^{2z}\alpha_1^{-z}\alpha_1^{-z} - \frac{3}{4}\alpha_1^{z}\alpha_1\alpha_1^{-z} - \frac{5}{16}\alpha_1^3 - \frac{1}{8}\alpha_1^{z}\left[\alpha_1^2\right]^{-z} - \frac{1}{16}\mathbb{IM}_1(\alpha_1^z,\alpha_1,\alpha_1^z)\\
&+ \frac{1}{4}\alpha_1^{x-2z}\left[\alpha_1\alpha_1+\alpha_1^z\alpha_1^{-z}\right]^x + \frac{1}{8}\alpha_1^x[\alpha_1\alpha_1]^{x-2z} - \frac{1}{8}\alpha_1^z\left[\alpha_1^{x-z}\alpha_1^{x-z}\right]^{-z}\\
&+ \frac{1}{4}\alpha_1\alpha_1^{x-z}\alpha_1^{x-z} + \frac{1}{4}\alpha_1^x\left[\alpha_1^{-z}\alpha_1^{-z}\right]^x + \frac{1}{16}\mathbb{IM}_2\left(\alpha_1^x,\alpha_1,\alpha_1^{x+z}\right) + \frac{1}{16}\mathbb{IM}_2\left(\alpha_1^x,\alpha_1^x,\alpha_1^z\right)\\
&+ \frac{1}{4}\alpha_1^{2x}\alpha_1^{-z}\alpha_1^{-z} + \frac{1}{2}\alpha_1^{2x-z}\alpha_1\alpha_1^{-z}\\
&+ \frac{1}{4}\alpha_1^x\left[\alpha_1^x\alpha_1^{-z}\right]^{-z} + \frac{1}{4}\mathbb{IM}_1\left(\alpha_1^{2x},\alpha_1,\alpha_1\right) + \frac{1}{4}\mathbb{IM}_1\left(\alpha_1^x,\alpha_1^x,\alpha_1\right) + \frac{1}{8}\mathbb{IM}_1\left(\alpha_1,\alpha_1^{2x},\alpha_1\right)\\
&- \frac{1}{32}\alpha_1^{2x}\left[\alpha_1^{-z}\alpha_1^{-z}\right]^{2x-2z} - \frac{1}{8}\alpha_1^{2x-3z}\left[\alpha_1\alpha_1^{-z}\right]^{2x} + \frac{1}{32}\alpha_1\alpha_1^{2x-2z}\alpha_1^{2x-2z}\\
&+ \frac{1}{8}\alpha_1^x\left[\alpha_1^{x-z}\alpha_1^{2x-2z}\right]^{-z} + \frac{1}{16}\alpha_1^{2x}\left[\alpha_1^{-z}\alpha_1^{2x-2z}\right]^{-z} - \frac{1}{16}\mathbb{IM}_{3X}(\alpha_1,\alpha_1,\alpha_1)\\
&- \frac{1}{8}\left[\alpha_1^x\left\{\alpha_1^{x-2z}\right\}^2\right]^x + \frac{1}{8}\alpha_1^x\left[\left\{\alpha_1^{x-z}\right\}^2\right]^{x-2z} - \frac{1}{16}\alpha_1\left\{\alpha_1^{2x-2z}\right\}^2 - \frac{1}{8}\alpha_1^{2x}\left[\alpha_1^{-z}\alpha_1^{2x-2z}\right]^{-z}\\
&+ \frac{1}{16}\alpha_1^{2x}\left[\left\{\alpha_1^{-z}\right\}^2\right]^{2x-2z} + \mathbb{IM}_{4X}(\alpha_1^x,\alpha_1,\alpha_1^x) + \mathbb{IM}_{4X}(\alpha_1,\alpha_1^x,\alpha_1^x)
\end{aligned} \tag{117}$$

We then calculate $\mathbb{SC}_2(\alpha_1,\alpha_2)$, which can be calculated by equation (67) as:

$$\begin{aligned}
\mathbb{SC}_2(\alpha_1,\alpha_2) = &-\frac{1}{2}\left(2\alpha_1\alpha_2+\alpha_1^z\alpha_2^{-z}+\alpha_2^z\alpha_1^{-z}\right) + \frac{1}{2}\alpha_1^x\alpha_2^{x-2z} + \frac{1}{2}\alpha_2^x\alpha_1^{x-2z}\\
&+ 2\mathcal{SC}_{2,3,1}(\alpha_1,\alpha_2) + 2\mathcal{SC}_{2,3,1}(\alpha_2,\alpha_1)
\end{aligned} \tag{118}$$

Ignoring the last term in α_2, we have:

$$
\begin{aligned}
\alpha_2 &= -\frac{1}{2}\left\{\alpha_1^2 + \alpha_1^z\alpha_1^{-z}\right\} + \frac{1}{2}\alpha_1^x\alpha_1^{x-2z} = -\frac{1}{2}\left[\alpha_1\alpha_1^{-z}\right]^z + \frac{1}{2}\alpha_1^x\alpha_1^{x-2z}\\
\alpha_2^z &= -\frac{3}{2}\alpha_1\alpha_1^z - \frac{1}{2}\alpha_1^{2z}\alpha_1^{-z} + \frac{1}{2}\alpha_1^{x+z}\alpha_1^{x-2z} + \frac{1}{2}\alpha_1^x\alpha_1^{x-z}\\
\alpha_2^{-z} &= -\frac{1}{2}\alpha_1\alpha_1^{-z} + \frac{1}{2}\alpha_1^{x-z}\alpha_1^{x-2z} - \frac{1}{2}\left[\left\{\alpha_1^{x-z}\right\}^2\right]^{-z}\\
\alpha_2^x &= -\frac{1}{2}\left[\alpha_1^2 + \alpha_1^z\alpha_1^{-z}\right]^x + \frac{1}{2}\alpha_1^{2x}\alpha_1^{x-2z} + \frac{1}{2}\alpha_1^x\alpha_1^{2x-2z}\\
\alpha_2^{x-z} &= -\left[\alpha_1^x\alpha_1\right]^{-z} - \frac{1}{2}\left\{\alpha_1^x\alpha_1^{-z} - \left[\alpha_1^x\alpha_1\right]^{-z} + \alpha_1^{x-z}\alpha_1 - \left[\alpha_1^x\alpha_1\right]^{-z}\right\} + \frac{1}{2}\left[\alpha_1^x\alpha_1^{x-2z}\right]^{x-z}\\
&= -\frac{1}{2}\left\{\alpha_1^x\alpha_1^{-z} + \alpha_1^{x-z}\alpha_1\right\} + \frac{1}{2}\left[\alpha_1^x\alpha_1^{x-2z}\right]^{x-z}\\
\alpha_2^{x-2z} &= -\frac{1}{2}\alpha_1^{x-z}\alpha_1^{-z} + \frac{1}{2}\left[\alpha_1^x\alpha_1^{x-2z}\right]^{x-2z}\\
&= -\frac{1}{2}\alpha_1^{x-z}\alpha_1^{-z} + \frac{1}{2}\alpha_1^{2x-2z}\alpha_1^{x-2z} - \left[\alpha_1^{2x-z}\alpha_1^{x-z}\right]^{-2z}
\end{aligned}
$$

With results above, we can calculate various terms needed by equation (118) as follows:

$$
\begin{aligned}
-\alpha_2\alpha_1 &= \frac{1}{2}\alpha_1^z\alpha_1\alpha_1^{-z} + \frac{1}{2}\alpha_1^3 - \frac{1}{2}\alpha_1^x\alpha_1\alpha_1^{x-2z}\\
-\frac{1}{2}\alpha_2^z\alpha_1^{-z} &= \frac{3}{4}\alpha_1^z\alpha_1\alpha_1^{-z} + \frac{1}{4}\alpha_1^{2z}\left\{\alpha_1^{-z}\right\}^2 - \frac{1}{4}\alpha_1^{x+z}\alpha_1^{-z}\alpha_1^{x-2z} - \frac{1}{4}\alpha_1^x\alpha_1^{x-z}\alpha_1^{-z}\\
-\frac{1}{2}\alpha_2^{-z}\alpha_1^z &= \frac{1}{4}\alpha_1^z\alpha_1\alpha_1^{-z} - \frac{1}{4}\alpha_1^z\alpha_1^{x-z}\alpha_1^{x-2z} + \frac{1}{4}\alpha_1^z\left[\left\{\alpha_1^{x-z}\right\}^2\right]^{-z}\\
\frac{1}{2}\alpha_2^x\alpha_1^{x-2z} &= -\frac{1}{4}\left[\alpha_1^2 + \alpha_1^z\alpha_1^{-z}\right]^x\alpha_1^{x-2z} + \frac{1}{4}\alpha_1^{2x}\alpha_1^{x-2z}\alpha_1^{x-2z} + \frac{1}{4}\alpha_1^x\alpha_1^{2x-2z}\alpha_1^{x-2z}\\
\frac{1}{2}\alpha_1^x\alpha_2^{x-2z} &= -\frac{1}{4}\alpha_1^x\alpha_1^{x-z}\alpha_1^{-z} + \frac{1}{4}\alpha_1^x\alpha_1^{2x-2z}\alpha_1^{x-2z} - \frac{1}{2}\alpha_1^x\left[\alpha_1^{2x-z}\alpha_1^{x-z}\right]^{-2z}
\end{aligned}
$$

For short, let use $E_{m,n}$ denote the n-th expression in the right-hand-side of m-th equation. We can group the terms in the equation above as follows.

$$
\begin{aligned}
&E_{1,2} = \frac{1}{2}\alpha_1^3 \qquad E_{2,2} = \frac{1}{4}\alpha_1^{2z}\left\{\alpha_1^{-z}\right\}^2 \qquad E_{1,1} + E_{2,1} + E_{3,1} = \frac{3}{2}\alpha_1^z\alpha_1\alpha_1^{-z}\\
&E_{1,3} + E_{2,3} + E_{3,2} + E_{4,1} = -\frac{1}{2}\left[\alpha_1^2 + \alpha_1^z\alpha_1^{-z}\right]^x\alpha_1^{x-2z} \qquad E_{3,3} = \frac{1}{4}\alpha_1^z\left[\left\{\alpha_1^{x-z}\right\}^2\right]^{-z}\\
&E_{2,4} + E_{5,1} = -\frac{1}{4}\alpha_1^x\left[\left\{\alpha_1^{-z}\right\}^2\right]^x \qquad E_{4,2} + E_{4,3} + E_{5,2} = \frac{1}{4}\left[\alpha_1^x\left\{\alpha_1^{x-2z}\right\}^2\right]^x\\
&E_{5,3} = -\frac{1}{4}\alpha_1^x\left[\left\{\alpha_1^{x-z}\right\}^2\right]^{x-2z}
\end{aligned}
$$

$$
\begin{aligned}
\mathbb{SC}_2\left(\alpha_1,\alpha_1,\alpha_2\right) = &\frac{1}{2}\alpha_1^3 + \frac{1}{4}\alpha_1^{2z}\left\{\alpha_1^{-z}\right\}^2 + \frac{3}{2}\alpha_1^z\alpha_1\alpha_1^{-z}\\
&- \frac{1}{2}\left[\alpha_1^2 + \alpha_1^z\alpha_1^{-z}\right]^x\alpha_1^{x-2z} + \frac{1}{4}\alpha_1^z\left[\left\{\alpha_1^{x-z}\right\}^2\right]^{-z} - \frac{1}{4}\alpha_1^x\left[\left\{\alpha_1^{-z}\right\}^2\right]^x\\
&+ \frac{1}{4}\left[\alpha_1^x\left\{\alpha_1^{x-2z}\right\}^2\right]^x - \frac{1}{4}\alpha_1^x\left[\left\{\alpha_1^{x-z}\right\}^2\right]^{x-2z}
\end{aligned}
\tag{119}
$$

In the derivation above, we use:

$$\alpha_1^x \alpha_1^{x-z} \alpha_1^{-z} = \frac{1}{2} \alpha_1^x \left[\left\{ \alpha_1^{-z} \right\}^2 \right]^x \qquad \alpha_1^x \left[\alpha_1^{2x-z} \alpha_1^{x-z} \right]^{-2z} = \frac{1}{2} \alpha_1^x \left[\left\{ \alpha_1^{x-z} \right\}^2 \right]^{x-2z}$$

Appendix G: Derivation of partial α_4

Complete expression for α_4 can be found in equation (36), here only the most significant portion of $\mathbb{SC}_3(\alpha_1,\alpha_1,\alpha_2)$, $\mathbb{SC}_2(\alpha_1,\alpha_3)$, and $\mathbb{SC}(\alpha_2,\alpha_2)$ are included in the derivation. These derivations show the advantage of solving scattering equations in a general way.

The more significant portion of $\mathbb{SC}_3(\alpha_1,\alpha_1,\alpha_2)$ can be solved by applying $A_1=\alpha_1$, $A_2=\alpha_2$ in equation (83).

$$\mathbb{SC}_{3,1}(\alpha_1,\alpha_1,\alpha_2) = -\frac{1}{8}\left\{\begin{array}{l} 2\alpha_1^{2z}\alpha_1^{-z}\alpha_2^{-z} \\ \alpha_1^{-z}\alpha_1^{-z}\alpha_2^{2z}\end{array}\right\} - \frac{3}{4}\cdot\left\{\begin{array}{l} \alpha_1^{z}\alpha_1\alpha_2^{-z} \\ \alpha_1^{z}\alpha_1^{-z}\alpha_2 \\ \alpha_1\alpha_1^{-z}\alpha_2^{z}\end{array}\right\} - \frac{15}{16}\cdot\alpha_1\alpha_1\alpha_2$$
$$-\frac{1}{8}\cdot\left\{\begin{array}{l} 2\alpha_1^{z}[\alpha_1\alpha_2]^{-z} \\ \alpha_2^{z}[\alpha_1\alpha_1]^{-z}\end{array}\right\} - \frac{1}{16}\cdot\left\{\begin{array}{l} 2\mathbb{IM}_1(\alpha_1^z,\alpha_1,\alpha_2^z) \\ \mathbb{IM}_1(\alpha_1^z,\alpha_2,\alpha_1^z)\end{array}\right\}$$

First let's review some results from before (in α_2, only the more significant portion is included here):

$$\alpha_2 = -\frac{1}{2}\left(\alpha_1^2+\alpha_1^z\alpha_1^{-z}\right) = -\frac{1}{2}\left[\alpha_1\alpha_1^{-z}\right]^z \qquad \alpha_2^{-z} = -\frac{1}{2}\alpha_1\alpha_1^{-z}$$
$$\alpha_2^z = -\frac{1}{2}\left(3\alpha_1^z\alpha_1+\alpha_1^{2z}\alpha_1^{-z}\right)$$
$$\alpha_2^{2z} = -\frac{1}{2}\left(\alpha_1^{3z}\alpha_1^{-z}+4\alpha_1^{2z}\alpha_1+3\left\{\alpha_1^z\right\}^2\right)$$
$$[\alpha_1\alpha_2]^{-z} = -\frac{1}{2}\left[\alpha_1\left[\alpha_1\alpha_1^{-z}\right]^z\right]^{-z} = -\frac{1}{2}\alpha_1^2\alpha_1^{-z}+\frac{1}{2}\left[\alpha_1^z\alpha_1\alpha_1^{-z}\right]^{-z} = -\frac{1}{4}\left\{\alpha_1^2\alpha_1^{-z}+\left[\alpha_1^3\right]^{-z}\right\}$$

With simple algebra, we can calculate various terms in $\mathbb{SC}_{3,1}(\alpha_1,\alpha_1,\alpha_2)$.

$$-\frac{1}{4}\alpha_1^{2z}\alpha_1^{-z}\alpha_2^{-z} = \frac{1}{8}\alpha_1^{2z}\alpha_1\left\{\alpha_1^{-z}\right\}^2$$
$$-\frac{1}{8}\alpha_2^{2z}\left\{\alpha_1^{-z}\right\}^2 = \frac{1}{16}\alpha_1^{3z}\left\{\alpha_1^{-z}\right\}^3+\frac{1}{4}\alpha_1^{2z}\alpha_1\left\{\alpha_1^{-z}\right\}^2+\frac{3}{16}\left\{\alpha_1^z\alpha_1^{-z}\right\}^2$$
$$-\frac{3}{4}\alpha_1^z\alpha_1^{-z}\alpha_2 = \frac{3}{8}\alpha_1^z\alpha_1^2\alpha_1^{-z}+\frac{3}{8}\left\{\alpha_1^z\alpha_1^{-z}\right\}^2$$
$$-\frac{3}{4}\alpha_1\alpha_1^z\alpha_2^{-z} = \frac{3}{8}\alpha_1^z\alpha_1^2\alpha_1^{-z}$$
$$-\frac{3}{4}\alpha_1\alpha_1^{-z}\alpha_2^z = \frac{9}{8}\alpha_1^z\alpha_1^2\alpha_1^{-z}+\frac{3}{8}\alpha_1^{2z}\alpha_1\left\{\alpha_1^{-z}\right\}^2$$
$$-\frac{15}{16}\alpha_1^2\alpha_2 = \frac{15}{32}\alpha_1^4+\frac{15}{32}\alpha_1^z\alpha_1^2\alpha_1^{-z}$$
$$-\frac{1}{4}\alpha_1^z[\alpha_1\alpha_2]^{-z} = \frac{1}{16}\alpha_1^z\alpha_1^2\alpha_1^{-z}+\frac{1}{16}\alpha_1^z\left[\alpha_1^3\right]^{-z}$$
$$-\frac{1}{8}\alpha_2^z\left[\alpha_1^2\right]^{-z} = \frac{3}{16}\alpha_1^z\alpha_1\left[\alpha_1^2\right]^{-z}+\frac{1}{16}\alpha_1^{2z}\alpha_1^{-z}\left[\alpha_1^2\right]^{-z}$$
$$\texttt{Other} = -\frac{1}{16}\mathbb{IM}_1(\alpha_1^z,\alpha_2,\alpha_1^z)-\frac{1}{8}\cdot\mathbb{IM}(\alpha_1^z,\alpha_1,\alpha_2^z)$$

For the conciseness of notation, let's use $E_{m,n}$ to denote the n-th expression in the m-th row in the equation above. We can group terms as follows:

$$E_{6,1} = \frac{15}{32}\alpha_1^4 \qquad E_{2,1} = \frac{1}{16}\alpha_1^{3z}\left\{\alpha_1^{-z}\right\}^3 \qquad E_{1,1}+E_{2,2}+E_{5,2} = \frac{3}{4}\alpha_1\alpha_1^{2z}\left\{\alpha_1^{-z}\right\}^2$$
$$E_{3,1}+E_{4,1}+E_{5,1}+E_{6,2}+E_{7,1} = \frac{77}{32}\alpha_1^2\alpha_1^z\alpha_1^{-z} \qquad E_{2,3}+E_{3,2} = \frac{9}{16}\left\{\alpha_1^z\alpha_1^{-z}\right\}^2$$
$$E_{7,2} = \frac{1}{16}\alpha_1^z\left[\alpha_1^3\right]^{-z} \qquad E_{8,1} = \frac{3}{16}\alpha_1^z\alpha_1\left[\alpha_1^2\right]^{-z} \qquad E_{8,2} = \frac{1}{16}\alpha_1^{2z}\alpha_1^{-z}\left[\alpha_1^2\right]^{-z}$$

In summary, we have:

$$\begin{aligned}&\mathbb{SC}_{3,1}(\alpha_1,\alpha_1,\alpha_2) = \\ &\frac{15}{32}\alpha_1^4 + \frac{1}{16}\alpha_1^{3z}\left\{\alpha_1^{-z}\right\}^3 + \frac{3}{4}\alpha_1\alpha_1^{2z}\left\{\alpha_1^{-z}\right\}^2 + \frac{77}{32}\alpha_1^2\alpha_1^z\alpha_1^{-z} \\ &\frac{9}{16}\left\{\alpha_1^z\alpha_1^{-z}\right\}^2 + \frac{1}{16}\alpha_1^z\left[\alpha_1^3\right]^{-z} + \frac{3}{16}\alpha_1^z\alpha_1\left[\alpha_1^2\right]^{-z} + \frac{1}{16}\alpha_1^{2z}\alpha_1^{-z}\left[\alpha_1^2\right]^{-z} \\ &-\frac{1}{16}\mathbb{IM}_1(\alpha_1^z,\alpha_2,\alpha_1^z) - \frac{1}{8}\mathbb{IM}_1(\alpha_1^z,\alpha_1,\alpha_2^z)\end{aligned}$$

Simpler term $\mathbb{SC}_{2,1}(\alpha_2,\alpha_2)$ is calculated very concisely below (still, only the more significant portion of α_2 is considered). Substituting $A = A = \alpha_2$ into equation (68), omitting all terms after the first term, we have:

$$\begin{aligned}&\mathbb{SC}_{2,1}(\alpha_2,\alpha_2) = -\frac{\alpha_2^2+\alpha_2^z\alpha_2^{-z}}{2} \\ &= -\frac{1}{8}\alpha_1^4 - \frac{1}{4}\alpha_1^z\alpha_1^2\alpha_1^{-z} - \frac{1}{8}\left\{\alpha_1^z\alpha_1^{-z}\right\}^2 - \frac{3}{8}\alpha_1^z\alpha_1^2\alpha_1^{-z} - \frac{1}{8}\alpha_1^{2z}\alpha_1\left\{\alpha_1^{-z}\right\}^2 - \frac{1}{8}\alpha_1^4 \\ &= -\frac{5}{8}\alpha_1^z\alpha_1^2\alpha_1^{-z} - \frac{1}{8}\left\{\alpha_1^z\alpha_1^{-z}\right\}^2 - \frac{1}{8}\alpha_1^{2z}\alpha_1\left\{\alpha_1^{-z}\right\}^2\end{aligned}$$

We then calculating: $\mathbb{SC}_{2,1}(\alpha_1,\alpha_3)$ by substituting $A_1 = \alpha_1$, $A_2 = \alpha_2$ into equation (67), omitting all terms other than the first term, we have:

$$\mathbb{SC}_{2,1}(\alpha_1,\alpha_3) = -\alpha_1\alpha_3 - \frac{1}{2}\left\{\alpha_1^z\alpha_3^{-z} + \alpha_1^{-z}\alpha_3^z\right\}$$

We then calculate various expressions needed by the equation above:

$$\begin{aligned}
\alpha_3 =& \frac{3}{16}\alpha_1^3 + \frac{1}{8}\alpha_1^{2z}\left\{\alpha_1^{-z}\right\}^2 + \frac{3}{4}\alpha_1^z\alpha_1\alpha_1^{-z} - \frac{1}{8}\alpha_1^z\left[\alpha_1^2\right]^{-z} - \frac{1}{16}\mathbb{IM}_1(\alpha_1^z,\alpha_1,\alpha_1^z)\\
\alpha_3^z =& \frac{9}{16}\alpha_1^z\alpha_1^2 + \frac{1}{8}\alpha_1^{2z}\left\{\alpha_1^{-z}\right\}^2 + \frac{1}{4}\alpha_1^{2z}\alpha_1\alpha_1^{-z} + \frac{3}{4}\alpha_1^{2z}\alpha_1\alpha_1^{-z} + \frac{3}{4}\left\{\alpha_1^z\right\}^2\alpha_1^{-z} + \frac{3}{4}\alpha_1^z\alpha_1^2\\
& - \frac{1}{8}\alpha_1^{2z}\left[\alpha_1^2\right]^{-z} - \frac{1}{8}\alpha_1^z\alpha_1^2 - \frac{1}{16}\alpha_1^z[\alpha_1^z\alpha_1]^{-z} - \frac{1}{16}\alpha_1^z[\alpha_1^z\alpha_1]^{-z} + \frac{1}{16}\mathbb{IM}_1(\alpha_1^z,\alpha_1^z,\alpha_1^z)\\
=& \frac{1}{8}\alpha_1^{3z}\left\{\alpha_1^{-z}\right\}^2 + \frac{9}{8}\alpha_1^z\alpha_1^2 + \alpha_1^{2z}\alpha_1\alpha_1^{-z} - \frac{1}{8}\alpha_1^{2z}\left[\alpha_1^2\right]^{-z} + \frac{3}{4}\left\{\alpha_1^z\right\}^2\alpha_1^{-z}\\
& + \frac{1}{16}\mathbb{IM}_1(\alpha_1^z,\alpha_1^z,\alpha_1^z)
\end{aligned}$$

$$\left[\mathbb{SC}_{2,1}(\alpha_1,\alpha_2)\right]^{-z} = -\frac{1}{2}\left(\alpha_1\alpha_2^{-z} + \alpha_1^{-z}\alpha_2\right) = \frac{1}{4}\left(2\alpha_1^2\alpha_1^{-z} + \alpha_1^z\left\{\alpha_1^{-z}\right\}^2\right)$$

$$\begin{aligned}
\left[\mathbb{SC}_{3,1}(\alpha_1,\alpha_1,\alpha_1)\right]^{-z} &= -\frac{4}{16}\left[\alpha_1\left[\alpha_1\alpha_1^{-z}\right]^{-z}\right]^z - \frac{1}{16}\frac{\partial}{\partial z}\mathbb{IM}_1(\alpha_1,\alpha_1,\alpha_1)\\
&= -\frac{1}{8}\left[\alpha_1\left\{\alpha_1^{-z}\right\}^2\right]^z - \frac{1}{16}\alpha_1\left[\alpha_1^2\right]^{-z} - \frac{1}{16}\alpha_1\left[\alpha_1^2\right]^{-z} + \frac{1}{16}\mathbb{IM}_1(\alpha_1,\alpha_1^z,\alpha_1)\\
&= -\frac{1}{8}\alpha_1^z\left\{\alpha_1^{-z}\right\}^2 - \frac{1}{4}\alpha_1^2\alpha_1^{-z} - \frac{1}{8}\alpha_1\left[\alpha_1^2\right]^{-z} + \frac{1}{16}\mathbb{IM}_1(\alpha_1,\alpha_1^z,\alpha_1)
\end{aligned}$$

$$\begin{aligned}
\alpha_3^{-z} &= \left[\mathbb{SC}_{2,1}(\alpha_1,\alpha_2)\right]^{-z} + \left[\mathbb{SC}_{3,1}(\alpha_1,\alpha_1,\alpha_1)\right]^{-z}\\
&= \left[\alpha_{1+2} + \alpha_{2+1}\right]^{-z} + \alpha_{1\cdot1\cdot1}^{-z}\\
&= \frac{1}{8}\alpha_1^z\left\{\alpha_1^{-z}\right\}^2 + \frac{1}{4}\alpha_1^2\alpha_1^{-z} - \frac{1}{8}\alpha_1\left[\alpha_1^2\right]^{-z} + \frac{1}{16}\mathbb{IM}_1(\alpha_1,\alpha_1^z,\alpha_1)
\end{aligned}$$

$$\begin{aligned}
&\mathbb{SC}_{2,1}(\alpha_1,\alpha_3) = -\alpha_1\alpha_3 - \frac{1}{2}\left\{\alpha_1^z\alpha_3^{-z} + \alpha_1^{-z}\alpha_3^z\right\}\\
=& -\frac{3}{16}\alpha_1^4 - \frac{1}{8}\alpha_1^{2z}\alpha_1\left\{\alpha_1^{-z}\right\}^2 - \frac{3}{4}\alpha_1^z\alpha_1^2\alpha_1^{-z} + \frac{1}{8}\alpha_1^z\alpha_1\left[\alpha_1^2\right]^{-z} + \frac{1}{16}\alpha_1\mathbb{IM}_1(\alpha_1^z,\alpha_1,\alpha_1^z)\\
& - \frac{1}{16}\left\{\alpha_1^z\alpha_1^{-z}\right\}^2 - \frac{1}{8}\alpha_1^z\alpha_1^2\alpha_1^{-z} + \frac{1}{16}\alpha_1^z\alpha_1\left[\alpha_1^2\right]^{-z} - \frac{1}{32}\alpha_1^z\mathbb{IM}_1(\alpha_1,\alpha_1^z,\alpha_1)\\
& - \frac{1}{16}\alpha_1^{3z}\left\{\alpha_1^{-z}\right\}^3 - \frac{9}{16}\alpha_1^z\alpha_1^2\alpha_1^{-z} - \frac{1}{2}\alpha_1^{2z}\alpha_1\left\{\alpha_1^{-z}\right\}^2 + \frac{1}{16}\alpha_1^{2z}\left[\alpha_1^2\right]^{-z}\alpha_1^{-z} - \frac{3}{8}\left\{\alpha_1^z\alpha_1^{-z}\right\}^2\\
& - \frac{1}{32}\alpha_1^{-z}\mathbb{IM}_1(\alpha_1^z,\alpha_1^z,\alpha_1^z)\\
=& -\frac{3}{16}\alpha_1^4 - \frac{1}{16}\alpha_1^{3z}\left\{\alpha_1^{-z}\right\}^3 + \frac{3}{32}\left[\alpha_1^2\right]^z\left[\alpha_1^2\right]^{-z} - \frac{5}{8}\alpha_1^{2z}\alpha_1\left\{\alpha_1^{-z}\right\}^2 - \frac{23}{16}\alpha_1^z\alpha_1^2\alpha_1^{-z}\\
& - \frac{7}{16}\left\{\alpha_1^z\alpha_1^{-z}\right\}^2 + \frac{1}{16}\alpha_1^{2z}\left[\alpha_1^2\right]^{-z}\alpha_1^{-z} + \frac{1}{16}\alpha_1\mathbb{IM}_1(\alpha_1^z,\alpha_1,\alpha_1^z)\\
& - \frac{1}{32}\alpha_1^z\mathbb{IM}_1(\alpha_1,\alpha_1^z,\alpha_1) - \frac{1}{32}\alpha_1^{-z}\mathbb{IM}_1(\alpha_1^z,\alpha_1^z,\alpha_1^z)
\end{aligned}$$

In the derivation above, we use: $\alpha_1^z \alpha_1 \left[\alpha_1^2\right]^{-z} = 0.5 \left[\alpha_1^2\right]^z \left[\alpha_1^2\right]^{-z}$. We can also summarize to have:

$$\begin{aligned}
&\mathbb{SC}_{2,1}(\alpha_2, \alpha_2) + \mathbb{SC}_{2,1}(\alpha_1, \alpha_3) \\
=& -\frac{5}{16}\alpha_1^4 - \frac{1}{16}\alpha_1^{3z}\left\{\alpha_1^{-z}\right\}^3 + \frac{3}{32}\left[\alpha_1^2\right]^z\left[\alpha_1^2\right]^{-z} - \frac{3}{4}\alpha_1^{2z}\alpha_1\left\{\alpha_1^{-z}\right\}^2 - \frac{33}{16}\alpha_1^z\alpha_1^2\alpha_1^{-z} \\
&- \frac{9}{16}\left\{\alpha_1^z\alpha_1^{-z}\right\}^2 + \frac{1}{16}\alpha_1^{2z}\left[\alpha_1^2\right]^{-z}\alpha_1^{-z} + \frac{1}{16}\alpha_1\mathbb{IM}_1(\alpha_1^z, \alpha_1, \alpha_1^z) \\
&- \frac{1}{32}\alpha_1^z\mathbb{IM}_1(\alpha_1, \alpha_1^z, \alpha_1) - \frac{1}{32}\alpha_1^{-z}\mathbb{IM}_1(\alpha_1^z, \alpha_1^z, \alpha_1^z)
\end{aligned}$$

We summarize a step further to have:

$$\begin{aligned}
&\mathbb{SC}_{3,1}(\alpha_1, \alpha_1, \alpha_2) + \mathbb{SC}_{2,1}(\alpha_2, \alpha_2) + \mathbb{SC}_{2,1}(\alpha_1, \alpha_3) \\
&= \frac{5}{32}\alpha_1^4 + \frac{11}{32}\alpha_1^z\alpha_1^2\alpha_1^{-z} + \frac{1}{16}\alpha_1^z\left[\alpha_1^3\right]^{-z} + \frac{3}{16}\left[\alpha_1^2\right]^z\left[\alpha_1^2\right]^{-z} + \frac{1}{8}\alpha_1^{2z}\alpha_1^{-z}\left[\alpha_1^2\right]^{-z} \\
&- \frac{1}{16}\mathbb{IM}_1(\alpha_1^z, \alpha_2, \alpha_1^z) - \frac{1}{8}\mathbb{IM}_1(\alpha_1^z, \alpha_1, \alpha_2^z) + \frac{1}{16}\alpha_1\mathbb{IM}_1(\alpha_1^z, \alpha_1, \alpha_1^z) \\
&- \frac{1}{32}\alpha_1^z\mathbb{IM}_1(\alpha_1, \alpha_1^z, \alpha_1) - \frac{1}{32}\alpha_1^{-z}\mathbb{IM}_1(\alpha_1^z, \alpha_1^z, \alpha_1^z)
\end{aligned}$$

Appendix H: Issues in the derivation of closed-forms

In the more un-collapsed notation, one piece of α can be inverted as :

$$\widetilde{\mathcal{SC}}\left(\alpha_{j_1},\alpha_{j_2},\cdots,\alpha_{j_n}\right)=\frac{1}{2^{3n-2}\pi^n}\int\limits_{-\infty}^{\infty}dk_1\int\limits_{-\infty}^{\infty}dk_2\cdots\int\limits_{-\infty}^{\infty}dk_{n-1}$$
$$\times\int\limits_{-\infty}^{\infty}dz_1\widetilde{\alpha}_{j_1}(0.5k_m-k_1,z_1)\int\limits_{-\infty}^{\infty}dz_2\widetilde{\alpha}_{j_2}(k_1-k_2,z_2)\cdot\cdot$$
$$\times\int\limits_{-\infty}^{\infty}dz_n\widetilde{\alpha}_{j_n}(k_{n-1}+0.5k_m,z_n)\widetilde{\gamma}_n(k_m,k_1,\cdots,k_{n-1};\varepsilon_0,\cdots,\varepsilon_{n-1})$$

Generally speaking, if there are n scatters in the expression of a term in the inverse scattering series, the distribution used in the (k_m,z) domain is:

$$\begin{aligned}&\widetilde{\gamma}_n(k_m,k_1,\cdots,k_{n-1};\varepsilon_0,\cdots,\varepsilon_{n-1})\\&=-\int\limits_{-\infty}^{\infty}dk_z(-i)^{n-1}\frac{\left[k_z^2+k_m^2\right]^{n-1}}{u_1\cdots u_{n-1}}e^{i[\varepsilon_0k_z+\varepsilon_1u_1+\cdots+\varepsilon_{n-1}u_{n-1}]}\\&=-\int\limits_{-\infty}^{\infty}dk_z(-i)^{n-1}\frac{\left[k_z^2+k_m^2\right]^{n-1}}{u_1\cdots u_{n-1}}e^{i\triangle\psi}e^{i[\varepsilon_0+\varepsilon_1+\cdots+\varepsilon_{n-1}]k_z},\end{aligned}\tag{120}$$

where various variables are defined as follows :

$$\begin{aligned}&\varepsilon_0=0.5(z_1+z_n)-z,\qquad \varepsilon_j=0.5|z_j-z_{j+1}|\\&u_j=\mathrm{sgn}(k_z)\sqrt{k_z^2+a_n}\qquad\qquad a_j=k_z^2-4k_j^2\\&\triangle\psi=\varepsilon_1(u_1-k_z)+\cdots+\varepsilon_{n-1}(u_{n-1}-k_z)\\&(j=1,2,3,\cdots,n-1)\end{aligned}$$

We can further Fourier transform it from wave-number domain to space domain:

$$\begin{aligned}&\gamma_n\left(x-b_0,b_1,\cdots,b_{n-1};\varepsilon_0,\varepsilon_1,\cdots,\varepsilon_{n-1}\right)\\&=\frac{1}{(2\pi)^n}\int\limits_{-\infty}^{\infty}dk_me^{ik_m(x-b_0)}\int\limits_{-\infty}^{\infty}dk_1e^{ik_1b_1}\cdots\int\limits_{-\infty}^{\infty}dk_{n-1}e^{ik_{n-1}b_{n-1}}\widetilde{\gamma}_n\end{aligned}\tag{121}$$

where several new variables are introduced :

$$b_0=0.5(x_1+x_n),\qquad b_j=x_j-x_{j+1}\qquad\qquad(j=1,2,3,\cdots,n-1)$$

If we approximate $\widetilde{\gamma}_n$ by it's most singular parts, that is:

$$\widetilde{\gamma}_n\approx\widetilde{\gamma}_n^{1D}=\left[\frac{d^{n-1}\delta(u)}{du^{n-1}}\right]_{u=\varepsilon_0+\varepsilon_1+\cdots+\varepsilon_n}$$

where $\widetilde{\gamma}_n^{1D}$ is the most singular part of $\widetilde{\gamma}_n$. Please notice that $\widetilde{\gamma}_n^{1D}$ is not a function of k_m, k_1, $\cdots$, k_{n-1}. So if we substitute in γ_n^{1D} into equation (121), we will obtain a bunch of δ-functions,

$$\begin{aligned}
&\varepsilon = \varepsilon_0 + \varepsilon_1 + \cdots + \varepsilon_{n-1} \\
&\widetilde{\gamma}_n^{1D}\left(x - b_0, b_1, \cdots, b_{n-1}; \varepsilon_0, \varepsilon_1, \cdots, \varepsilon_{n-1}\right) = (2\pi)^n \delta^{(n)}(\varepsilon) \times \delta(\overrightarrow{x}) \\
&\delta(\overrightarrow{x}) = \delta(x - 0.5(x_1 + x_n))\delta(x_1 - x_2) \cdots \delta(x_{n-1} - x_n)
\end{aligned} \tag{122}$$

Let's consider the effects of applying $\delta(\overrightarrow{x})$ into integral of the form $\int_{-\infty}^{\infty} dx_1 f_1(x_1) \int_{-\infty}^{\infty} dx_2 f_2(x_2) \cdot \cdot \cdot \int_{-\infty}^{\infty} dx_n f_n(x_n)$. The sifting property of δ-function will give us an extremely simply answer: $f_1(x) f_2(x) \cdots f_n(x)$. The multiple integral reduced to simple multiplications. This simplification will convert the scattered information in the Fourier land into a concentrated information in the x-domain. And in this most singular term, x and z are perfectly decoupled, so the drastic change happened in k_m and x doesn't change the operation in z at all. As a result, $\widetilde{\gamma}_n^{1D}$ will produce results identical to what had been shown in Simon's 2002 and 2003 reports, only an extra variable x is added.

¿From the analysis above, it's easy to figure out the leading-order imaging subseries if only the most singular part of the distribution is considered:

$$\alpha^{LOIS}(x, z) = \alpha_1 \left(x \ , \ z - 0.5 \int_0^z du \alpha_1(x, u) \right) \tag{123}$$

Other singular terms, i.e, which are less singular than the most singular part, also display amazing concentration in x, but they need partial derivatives of the form $\partial/\partial x$, $\partial^2/\partial x^2$, $\partial^2/(\partial x \partial z)$, $\cdots$, which can be physically interpreted as the Taylor series expansion of $\alpha(x, z)$ in terms of $\alpha_1(x, z)$, will be included in the future work.

Appendix I: Several Fourier integrals for the second order equation

We present here several useful integrals in α_2 derivation. In this section, f and g are arbitrary functions or distributions. $\widetilde{f}$ and $\widetilde{g}$ are their corresponding Fourier transform. The equation (124) is used to transform the multi-D imaging and inversion terms in α_2 from (k_m, z) domain to (x, z) domain.

$$
\begin{aligned}
&\frac{1}{2\pi}\int_{-\infty}^{\infty} dk_1 \int_{-\infty}^{\infty} dk_m e^{ik_m x}\widetilde{f}(0.5k_m - k_1)\widetilde{g}(0.5k_m + k_1)\\
=&\frac{1}{2\pi}\int_{-\infty}^{\infty} dk_1 \int_{-\infty}^{\infty} dk_m e^{ik_m x}\int_{-\infty}^{\infty} dx_1 f(x_1)e^{-i(0.5k_m-k_1)x_1}\int_{-\infty}^{\infty} dx_2 g(x_2)e^{-i(0.5k_m+k_1)x_2}\\
=&\frac{1}{2\pi}\int_{-\infty}^{\infty} dk_1 \int_{-\infty}^{\infty} dx_1 f(x_1)e^{ik_1x_1}\int_{-\infty}^{\infty} dx_2 g(x_2)e^{-ik_1x_2}\int_{-\infty}^{\infty} dk_m e^{ik_m(x-0.5x_1-0.5x_2)}\\
=&\int_{-\infty}^{\infty} dk_1 \int_{-\infty}^{\infty} dx_1 f(x_1)e^{ik_1x_1}\int_{-\infty}^{\infty} dx_2 g(x_2)e^{-ik_1x_2}\delta(x-0.5x_1-0.5x_2)\\
=&2\int_{-\infty}^{\infty} dk_1 \int_{-\infty}^{\infty} dx_1 f(x_1)e^{ik_1x_1}\int_{-\infty}^{\infty} dx_2 g(x_2)e^{-ik_1x_2}\delta(x_1+x_2-2x)\\
=&2\int_{-\infty}^{\infty} dk_1 \int_{-\infty}^{\infty} dx_1 f(x_1)e^{ik_1x_1}g(2x-x_1)e^{-ik_1(2x-x_1)}\\
=&2\int_{-\infty}^{\infty} dx_1 f(x_1)g(2x-x_1)\int_{-\infty}^{\infty} dk_1 e^{-i2k_1(x-x_1)}\\
=&4\pi\int_{-\infty}^{\infty} dx_1 f(x_1)g(2x-x_1)\delta(2(x-x_1))\\
=&2\pi\int_{-\infty}^{\infty} dx_1 f(x_1)g(2x-x_1)\delta(x-x_1) \quad = \quad 2\pi f(x)g(x)
\end{aligned}
$$

$$
\int_{-\infty}^{\infty} dk_1 \int_{-\infty}^{\infty} dk_m e^{ik_m x}\widetilde{f}(0.5k_m - k_1)\widetilde{g}(0.5k_m + k_1) = \quad 4\pi^2 f(x)g(x) \tag{124}
$$

The equation (125) is used to transform the the remaining singular terms in α_2 from (k_m, z) domain

to (x, z) domain.

$$\begin{aligned}
&\frac{1}{2\pi}\int_{-\infty}^{\infty} dk_1 \int_{-\infty}^{\infty} dk_m e^{ik_m x}(k_m^2 - 4k_1^2)\widetilde{f}(0.5k_m - k_1)\widetilde{g}(0.5k_m + k_1)\\
=&\frac{1}{2\pi}\int_{-\infty}^{\infty} dk_1 \int_{-\infty}^{\infty} dk_m e^{ik_m x}(k_m^2 - 4k_1^2) \int_{-\infty}^{\infty} dx_1 f(x_1)e^{-i(0.5k_m - k_1)x_1} \int_{-\infty}^{\infty} dx_2 g(x_2)e^{-i(0.5k_m + k_1)x_2}\\
=&\frac{1}{2\pi}\int_{-\infty}^{\infty} dk_1 \int_{-\infty}^{\infty} dx_1 f(x_1)e^{ik_1 x_1} \int_{-\infty}^{\infty} dx_2 g(x_2)e^{-ik_1 x_2} \int_{-\infty}^{\infty} dk_m e^{ik_m(x - 0.5x_1 + 0.5x_2)}(k_m^2 - 4k_1^2)
\end{aligned}$$

If we define $u = 0.5x_1 + 0.5x_2 - x$, then the expression above can be expressed as:

$$\begin{aligned}
&= -\frac{1}{2\pi}\int_{-\infty}^{\infty} dk_1 \int_{-\infty}^{\infty} dx_1 f(x_1)e^{ik_1 x_1} \int_{-\infty}^{\infty} dx_2 g(x_2)e^{-ik_1 x_2}(2\pi)\left(\delta''(u) + 4k_1^2\delta(u)\right)\\
&= -8\int_{-\infty}^{\infty} dk_1 \int_{-\infty}^{\infty} dx_1 f(x_1)e^{ik_1 x_1} \int_{-\infty}^{\infty} dx_2 g(x_2)e^{-ik_1 x_2}\left(\delta''(2u) + k_1^2\delta(2u)\right)\\
&= -8\int_{-\infty}^{\infty} dx_1 f(x_1) \int_{-\infty}^{\infty} dk_1 e^{i2k_1(x_1 - x)}\left[g''(2x - x_1) + 2ik_1 g'(2x - x_1))\right]\\
&= -8\int_{-\infty}^{\infty} dx_1 f(x_1)\left[g''(2x - x_1)(2\pi)\delta(2x - 2x_1) + g'(2x - x_1)(2\pi) \times 2\delta'(2x - 2x_1))\right]\\
&= -8\int_{-\infty}^{\infty} dx_1 f(x_1)\left[g''(2x - x_1)\frac{(2\pi)}{2}\delta(x - x_1) + g'(2x - x_1)\frac{(4\pi)}{4}\delta'(x - x_1))\right]\\
&= -8\pi\int_{-\infty}^{\infty} dx_1 f(x_1)\left[g''(2x - x_1)\delta(x - x_1) + g'(2x - x_1)\delta'(x - x_1))\right]\\
&= -8\pi\int_{-\infty}^{\infty} dx_1 f(x_1)g''(2x - x_1)\delta(x - x_1) \; - \; 8\pi\int_{-\infty}^{\infty} dx_1 f(x_1)g'(2x - x_1)\delta'(x - x_1)\\
&= -8\pi f(x)g''(x) \; - \; 8\pi\left\{f'(x_1)g'(2x - x_1) - f(x_1)g''(2x - x_1)\right\}_{x_1 = x}\\
&= -8\pi f'(x)g'(x)
\end{aligned}$$

$$\frac{1}{2\pi}\int_{-\infty}^{\infty} dk_1 \int_{-\infty}^{\infty} dk_m e^{ik_m x}(k_m^2 - 4k_1^2)\widetilde{f}(0.5k_m - k_1)\widetilde{g}(0.5k_m + k_1) = -8\pi \times f'(x)g'(x) \qquad (125)$$

Derivation of equation (125) using different method.

$$\frac{1}{2\pi}\int_{-\infty}^{\infty}dk_1\int_{-\infty}^{\infty}dx_1 f(x_1)e^{ik_1x_1}\int_{-\infty}^{\infty}dx_2 g(x_2)e^{-ik_1x_2}\int_{-\infty}^{\infty}dk_m e^{ik_m(x-0.5x_1-0.5x_2)}(k_m^2-4k_1^2)$$
$$=\frac{1}{2\pi}\int_{-\infty}^{\infty}dx_1 f(x_1)\int_{-\infty}^{\infty}dx_2 g(x_2)\int_{-\infty}^{\infty}dk_1 e^{ik_1(x_1-x_2)}\int_{-\infty}^{\infty}dk_m e^{ik_m(x-0.5x_1-0.5x_2)}(k_m^2-4k_1^2)$$

Let's define $b_0=0.5(x_1+x_2)$, $b_1=x_1-x_2$, we have: $x_1=b_0+0.5b_1$, and $x_2=b_0-0.5b_1$. And we calculate the 2 innermost integral in the equation above as:

$$\int_{-\infty}^{\infty}dk_1 e^{ik_1b_1}\int_{-\infty}^{\infty}dk_m e^{ik_m(x-b_0)}(k_m^2-4k_1^2)=-(2\pi)\int_{-\infty}^{\infty}dk_1 e^{-ik_1b_1}\left[\delta''(x-b_0)+4\delta(x-b_0)\right]$$
$$=-4\pi^2\left[\delta''(x-b_0)\delta(b_1)-4\delta(x-b_0)\delta''(b_1)\right]$$

We can equivalently express the left hand side of equation (125) as:

$$=-2\pi\int_{-\infty}^{\infty}dx_1 f(x_1)\int_{-\infty}^{\infty}dx_2 g(x_2)\left[\delta''(x-b_0)\delta(b_1)-4\delta(x-b_0)\delta''(b_1)\right]$$
$$=-2\pi\int_{-\infty}^{\infty}db_0\int_{-\infty}^{\infty}db_1 f(b_0+0.5b_1)g(b_0-0.5b_1)\left[\delta''(x-b_0)\delta(b_1)-4\delta(x-b_0)\delta''(b_1)\right]$$
$$=-2\pi\int_{-\infty}^{\infty}db_0\delta''(x-b_0)\int_{-\infty}^{\infty}db_1 f(b_0+0.5b_1)g(b_0-0.5b_1)\delta(b_1)$$
$$+8\pi\int_{-\infty}^{\infty}db_0\delta(x-b_0)\int_{-\infty}^{\infty}db_1 f(b_0+0.5b_1)g(b_0-0.5b_1)\delta''(b_1)$$
$$=-2\pi\int_{-\infty}^{\infty}db_0\delta''(x-b_0)f(b_0)g(b_0)$$
$$+8\pi\int_{-\infty}^{\infty}db_0\delta(x-b_0)\frac{f''(b_0)g(b_0)-2f'(b_0)g'(b_0)+f(b_0)g''(b_0)}{4}$$
$$=-8\pi\times f'(x)g'(x).$$

Appendix J: Several Fourier integrals for the third order equation

We present here several useful integrals in α_3 derivation. In this section, f_1, f_2, and f_3 are arbitrary functions or distributions. $\widetilde{f_1}$, $\widetilde{f_2}$ and $\widetilde{f_3}$ are their corresponding Fourier transform. The equation (126) is used to transform the multi-D imaging and inversion terms in α_3 from (k_m, z) domain to (x, z) domain. In this appendix, let's define $b_0 = 0.5(x_1 + x_3)$, $b_1 = x_1 - x_2$ and $b_2 = x_2 - x_3$. We have: $x_1 = b_0 + 0.5b_1 + 0.5b_2$, $x_2 = b_0 - 0.5b_1 + 0.5b_2$, $x_3 = b_0 - 0.5b_1 - 0.5b_2$.

$$\begin{aligned}
&\frac{1}{2\pi}\int_{-\infty}^{\infty} dx_1 f_1(x_1)\int_{-\infty}^{\infty} dx_2 f_2(x_2)\int_{-\infty}^{\infty} dx_3 f_3(x_3)\int_{-\infty}^{\infty} dk_1 e^{ik_1(x_1-x_2)}\int_{-\infty}^{\infty} dk_2 e^{ik_2(x_2-x_3)}\\
&\qquad\times\int_{-\infty}^{\infty} dk_m\left[\rho_1 a_1+\rho_2 a_2\right] e^{ik_m(x-0.5x_1-0.5x_3)}\\
=&\frac{1}{2\pi}\int_{-\infty}^{\infty} dx_1 f_1(x_1)\int_{-\infty}^{\infty} dx_2 f_2(x_2)\int_{-\infty}^{\infty} dx_3 f_3(x_3)\delta(x_1-x_2)\delta(x_2-x_3)\delta(x-0.5x_1-0.5x_3)\\
=&\frac{1}{2\pi}\int_{-\infty}^{\infty} dx_1 f_1(x_1)\int_{-\infty}^{\infty} dx_2 f_2(x_2)\int_{-\infty}^{\infty} dx_3 f_3(x_3)\int_{-\infty}^{\infty} dk_1 e^{-ik_1(x_1-x_2)}\int_{-\infty}^{\infty} dk_2 e^{-ik_2(x_2-x_3)}\\
&\qquad\times\int_{-\infty}^{\infty} dk_m\left[\rho_1 a_1+\rho_2 a_2\right] e^{-ik_m(x-0.5x_1-0.5x_3)}\\
=&\frac{1}{2\pi}\int_{-\infty}^{\infty} db_0\int_{-\infty}^{\infty} db_1\int_{-\infty}^{\infty} db_2 f_1(b_0+0.5b_1+0.5b_2) f_2(b_0-0.5b_1+0.5b_2) f_3(b_0-0.5b_1-0.5b_2)\\
&\qquad\times\int_{-\infty}^{\infty} dk_1 e^{-ik_1 b_1}\int_{-\infty}^{\infty} dk_2 e^{-ik_2 b_2}\int_{-\infty}^{\infty} dk_m\left[\rho_1 a_1+\rho_2 a_2\right] e^{-ik_m(x-b_3)}\\
=&-\int_{-\infty}^{\infty} db_0\int_{-\infty}^{\infty} db_1\int_{-\infty}^{\infty} db_2 f_1(b_0+0.5b_1+0.5b_2) f_2(b_0-0.5b_1+0.5b_2) f_3(b_0-0.5b_1-0.5b_2)\\
&\qquad\times\int_{-\infty}^{\infty} dk_1 e^{-ik_1 b_1}\int_{-\infty}^{\infty} dk_2 e^{-ik_2 b_2}\left[(\rho_1+\rho_2)\delta''(x-b_0)+4(\rho_1 k_1^2+\rho_2 k_2^2)\delta(x-b_0)\right]\\
=&-2\pi\int_{-\infty}^{\infty} db_0\int_{-\infty}^{\infty} db_1\int_{-\infty}^{\infty} db_2 f_1(b_0+0.5b_1+0.5b_2) f_2(b_0-0.5b_1+0.5b_2) f_3(b_0-0.5b_1-0.5b_2)\\
&\qquad\times\int_{-\infty}^{\infty} dk_1 e^{-ik_1 b_1}\left[(\rho_1+\rho_2)\delta''(x-b_0)\delta(b_2)+4(\rho_1 k_1^2\delta(x-b_0)\delta(b_2)-\rho_2\delta(x-b_0)\delta''(b_2))\right]
\end{aligned}$$

$$
\begin{aligned}
&= -4\pi^2 \int_{-\infty}^{\infty} db_0 \int_{-\infty}^{\infty} db_1 \int_{-\infty}^{\infty} db_2 f_1(b_0+0.5b_1+0.5b_2) f_2(b_0-0.5b_1+0.5b_2) f_3(b_0-0.5b_1-0.5b_2) \\
&\quad \times \left[(\rho_1+\rho_2)\delta''(x-b_0)\delta(b_1)\delta(b_2) - 4\rho_1\delta(x-b_0)\delta''(b_1)\delta(b_2) - 4\rho_2\delta(x-b_0)\delta(b_1)\delta''(b_2)\right] \\
&\quad = -4\pi^2(I_1+I_2+I3)
\end{aligned}
$$

$$
\begin{aligned}
I_1 =& (\rho_1+\rho_2) \int_{-\infty}^{\infty} db_0 \int_{-\infty}^{\infty} db_1 \int_{-\infty}^{\infty} db_2 f_1(b_0+0.5b_1+0.5b_2) f_2(b_0-0.5b_1+0.5b_2) f_3(b_0-0.5b_1-0.5b_2) \\
&\times \delta''(x-b_0)\delta(b_1)\delta(b_2) \\
=& (\rho_1+\rho_2) \int_{-\infty}^{\infty} db_0 \delta''(x-b_0) \int_{-\infty}^{\infty} db_1 \delta(b_1) \\
&\times \int_{-\infty}^{\infty} db_2 f_1(b_0+0.5b_1+0.5b_2) f_2(b_0-0.5b_1+0.5b_2) f_3(b_0-0.5b_1-0.5b_2)\delta(b_2) \\
=& (\rho_1+\rho_2) \int_{-\infty}^{\infty} db_0 \delta''(x-b_0) \int_{-\infty}^{\infty} db_1 \delta(b_1) f_1(b_0+0.5b_1) f_2(b_0-0.5b_1) f_3(b_0-0.5b_1) \\
=& (\rho_1+\rho_2) \int_{-\infty}^{\infty} db_0 \delta''(x-b_0) f_1(b_0) f_2(b_0) f_3(b_0) \\
=& (\rho_1+\rho_2) \frac{\partial(f_1(x)f_2(x)f_3(x))}{\partial x} \\
=& (\rho_1+\rho_2)\left[f_1''(x)f_2(x)f_3(x) + f_1(x)f_2''(x)f_3(x) + f_1(x)f_2(x)f_3''(x)\right] \\
&+ 2(\rho_1+\rho_2)\left[f_1'(x)f_2'(x)f_3(x) + f_1'(x)f_2(x)f_3'(x) + f_1(x)f_2'(x)f_3'(x)\right]
\end{aligned}
$$

$$
\begin{aligned}
I_2 &= 4\rho_1 \int_{-\infty}^{\infty} db_1 \delta''(b_1) \int_{-\infty}^{\infty} db_0 \delta(x-b_0) \\
&\quad \times \int_{-\infty}^{\infty} db_2 f_1(b_0+0.5b_1+0.5b_2) f_2(b_0-0.5b_1+0.5b_2) f_3(b_0-0.5b_1-0.5b_2)\delta(b_2) \\
&= 4\rho_1 \int_{-\infty}^{\infty} db_1 \delta''(b_1) f_1(x+0.5b_1) f_2(x-0.5b_1) f_3(x-0.5b_1) \\
&= \rho_1\left[f_1''(x)f_2(x)f_3(x) + f_1(x)f_2''(x)f_3(x) + f_1(x)f_2(x)f_3''(x)\right] \\
&\quad + 2\rho_1\left[-f_1'(x)f_2'(x)f_3(x) - f_1'(x)f_2(x)f_3'(x) + f_1(x)f_2'(x)f_3'(x)\right]
\end{aligned}
$$

$$
\begin{aligned}
I_3 =& 4\rho_2 \int_{-\infty}^{\infty} db_0 \delta(x-b_0) \int_{-\infty}^{\infty} db_1 \delta(b_1) \\
& \times \int_{-\infty}^{\infty} db_2 f_1(b_0+0.5b_1+0.5b_2) f_2(b_0-0.5b_1+0.5b_2) f_3(b_0-0.5b_1-0.5b_2) \delta''(b_2) \\
=& 4\rho_2 \int_{-\infty}^{\infty} db_2 \delta''(b_2) f_1(x+0.5b_2) f_2(x+0.5b_2) f_3(x-0.5b_2) \\
=& \rho_2 \left[f_1''(x) f_2(x) f_3(x) + f_1(x) f_2''(x) f_3(x) + f_1(x) f_2(x) f_3''(x) \right] \\
& + 2\rho_2 \left[f_1'(x) f_2'(x) f_3(x) - f_1'(x) f_2(x) f_3'(x) - f_1(x) f_2'(x) f_3'(x) \right] \\
& I_1 + I_2 + I_3 = -4 \left\{ \rho_1 f_1'(x) \left[f_2(x) f_3(x) \right]' + \rho_2 f_3'(x) \left[f_1(x) f_2(x) \right]' \right\}
\end{aligned}
$$

$$
\begin{aligned}
& \int_{-\infty}^{\infty} dx_1 f_1(x_1) \int_{-\infty}^{\infty} dx_2 f_2(x_2) \int_{-\infty}^{\infty} dx_3 f_3(x_3) \int_{-\infty}^{\infty} dk_1 e^{-ik_1(x_1-x_2)} \int_{-\infty}^{\infty} dk_2 e^{-ik_2(x_2-x_3)} \\
& \quad \times \int_{-\infty}^{\infty} dk_m \left[\rho_1 a_1 + \rho_2 a_2 \right] e^{-ik_m(x-0.5x_1-0.5x_3)} \\
& = -32\pi^3 \left\{ \rho_1 f_1'(x) \left[f_2(x) f_3(x) \right]' + \rho_2 f_3'(x) \left[f_1(x) f_2(x) \right]' \right\}
\end{aligned} \tag{126}
$$

The following integrals will be used to simplify the last singular term in α_3.

$$
\begin{aligned}
& \int_{-\infty}^{\infty} dx_1 f_1(x_1) \int_{-\infty}^{\infty} dx_2 f_2(x_2) \int_{-\infty}^{\infty} dx_3 f_3(x_3) \int_{-\infty}^{\infty} dk_m e^{ik_m(x-0.5x_1-0.5x_3)} \\
& \quad \times \int_{-\infty}^{\infty} dk_1 e^{ik_1(x_1-x_2)} \int_{-\infty}^{\infty} dk_2 e^{ik_2(x_2-x_3)} \left(k_m^2 + 2k_1^2 + 2k_2^2 \right)
\end{aligned}
$$

In the equation below, all the functions have the same argument (x), for compactness, this argument is omitted.

$$
\begin{aligned}
\cdots =& \frac{1}{4} \left(4f_1'' f_2 f_3 + 4f_1 f_2'' f_3 + 4f_1 f_2 f_3'' + 8f_1' f_2' f_3 + 8f_1' f_2 f_3' + 8f_1 f_2' f_3' \right) \\
& + \frac{1}{4} \left(2f_1'' f_2 f_3 + 2f_1 f_2'' f_3 + 2f_1 f_2 f_3'' - 4f_1' f_2' f_3 - 4f_1' f_2 f_3' + 4f_1 f_2' f_3' \right) \\
& + \frac{1}{4} \left(2f_1'' f_2 f_3 + 2f_1 f_2'' f_3 + 2f_1 f_2 f_3'' + 4f_1' f_2' f_3 - 4f_1' f_2 f_3' - 4f_1 f_2' f_3' \right) \\
=& 2f_1'' f_2 f_3 + 2f_1 f_2'' f_3 + 2f_1 f_2 f_3'' + 2f_1' f_2' f_3 + 2f_1 f_2' f_3'
\end{aligned}
$$

So we have:

$$\begin{aligned}&\int_{-\infty}^{\infty} dx_1 f_1(x_1) \int_{-\infty}^{\infty} dx_2 f_2(x_2) \int_{-\infty}^{\infty} dx_3 f_3(x_3) \int_{-\infty}^{\infty} dk_m e^{ik_m(x-0.5x_1-0.5x_3)} \\ &\qquad \times \int_{-\infty}^{\infty} dk_1 e^{ik_1(x_1-x_2)} \int_{-\infty}^{\infty} dk_2 e^{ik_2(x_2-x_3)} \left(k_m^2+2k_1^2+2k_2^2\right) \\ =&16\pi^2 \left\{f_1'' f_2 f_3 + f_1 f_2'' f_3 + f_1 f_2 f_3'' + f_1' f_2' f_3 + f_1 f_2' f_3'\right\}\end{aligned} \tag{127}$$

We next calculate the following integral. We give the relatively simple final answer here. We provide the framework of proof immediately after.

$$\begin{aligned}&\int_{-\infty}^{\infty} dx_1 f_1(x_1) \int_{-\infty}^{\infty} dx_2 f_2(x_2) \int_{-\infty}^{\infty} dx_3 f_3(x_3) \int_{-\infty}^{\infty} dk_m e^{ik_m(x-0.5x_1-0.5x_3)} \\ &\qquad \times \int_{-\infty}^{\infty} dk_1 e^{ik_1(x_1-x_2)} \int_{-\infty}^{\infty} dk_2 e^{ik_2(x_2-x_3)} \left(k_m^2-4k_1^2\right)^2 \\ =&128\pi^3 f_1'' \left[f_2 f_3\right]''\end{aligned} \tag{128}$$

Here we provide the framework of the proof of the equation (128): integral above involve lots of terms, but in the end all the terms containing derivatives higher than the second order cancel with each other. We have a relative simple expression in the end.

$$\begin{aligned}=&f_1'''' f_2 f_3 + f_1 f_2'''' f_3 + f_1 f_2 f_3'''' + 4f_1''' f_2' f_3 + 4f_1''' f_2 f_3' + 4f_1' f_2''' f_3 + 4f_1' f_2 f_3''' + 4f_1 f_2''' f_3' \\ &+ 4f_1 f_2' f_3''' + 6f_1'' f_2'' f_3 + 6f_1'' f_2 f_3'' + 6f_1 f_2'' f_3'' + 12f_1'' f_2' f_3' + 12f_1' f_2'' f_3' + 12f_1' f_2' f_3'' \\ &- 2f_1'''' f_2 f_3 - 2f_1 f_2'''' f_3 - 2f_1 f_2 f_3'''' - 4f_1 f_2''' f_3' - 4f_1 f_2' f_3''' \\ &+ 4f_1'' f_2'' f_3 + 4f_1'' f_2 f_3'' - 12f_1 f_2'' f_3'' + 8f_1'' f_2' f_3' \\ &+ f_1'''' f_2 f_3 + f_1 f_2'''' f_3 + f_1 f_2 f_3'''' - 4f_1''' f_2' f_3 - 4f_1''' f_2 f_3' - 4f_1' f_2''' f_3 - 4f_1' f_2 f_3''' + 4f_1 f_2''' f_3' \\ &+ 4f_1 f_2' f_3''' + 6f_1'' f_2'' f_3 + 6f_1'' f_2 f_3'' + 6f_1 f_2'' f_3'' + 12f_1'' f_2' f_3' - 12f_1' f_2'' f_3' - 12f_1' f_2' f_3'' \\ =&16f_1'' f_2'' f_3 + 16f_1'' f_2 f_3'' + 32f_1'' f_2' f_3' \\ =&16f_1'' \left(f_2 f_3\right)''\end{aligned}$$

Now let's provide the answer for another integral. In the final answer, all functions should have the same argument (x), which is omitted to make it compact.

$$\begin{aligned}&\int_{-\infty}^{\infty} dx_1 f_1(x_1) \int_{-\infty}^{\infty} dx_2 f_2(x_2) \int_{-\infty}^{\infty} dx_3 f_3(x_3) \int_{-\infty}^{\infty} dk_m e^{ik_m(x-0.5x_1-0.5x_3)} \\ &\qquad \times \int_{-\infty}^{\infty} dk_1 e^{ik_1(x_1-x_2)} \int_{-\infty}^{\infty} dk_2 e^{ik_2(x_2-x_3)} \left(k_m^2-4k_1^2\right)\left(k_m^2-4k_2^2\right) \\ =&128\pi^3 \left(f_1'' f_2 f_3'' + f_1'' f_2' f_3' + f_1' f_2'' f_3' + f_1' f_2' f_3''\right)\end{aligned} \tag{129}$$

Just like the derivation process of the integral before equation (129), integrals involve high order derivatives of δ-function will give rise to lots of terms, but higher order terms cancels with each other, and we have a final expression relatively simple:

$$
\begin{aligned}
=&\frac{1}{16}\left(I_1+I_2+I_3+I_4\right)=16\left(f_1''f_2f_3''+f_1''f_2'f_3'+f_1'f_2''f_3'+f_1'f_2'f_3''\right)\\
I_1=&16f_1''''f_2f_3+16f_1f_2''''f_3+16f_1f_2f_3''''+64f_1'''f_2'f_3+64f_1'''f_2f_3'+64f_1'f_2'''f_3+\\
&64f_1'f_2f_3'''+64f_1f_2'''f_3'+64f_1f_2'f_3'''+96f_1''f_2''f_3+96f_1''f_2f_3''+96f_1f_2''f_3''+\\
&192f_1''f_2'f_3'+192f_1'f_2''f_3'+192f_1'f_2'f_3''\\
I_2=&-16f_1''''f_2f_3-16f_1f_2''''f_3-16f_1f_2f_3''''-64f_1f_2'''f_3'-\\
&64f_1f_2'f_3'''+32f_1''f_2''f_3+32f_1''f_2f_3''-96f_1f_2''f_3''+64f_1''f_2'f_3'\\
I_3=&-16f_1''''f_2f_3-16f_1f_2''''f_3-16f_1f_2f_3''''-64f_1'''f_2'f_3-64f_1'f_2'''f_3-\\
&96f_1''f_2''f_3+32f_1''f_2f_3''+32f_1f_2''f_3''+64f_1'f_2'f_3''\\
I_4=&16f_1''''f_2f_3+16f_1f_2''''f_3+16f_1f_2f_3''''-64f_1'''f_2f_3'-64f_1'f_2f_3'''-32f_1''f_2''f_3+\\
&96f_1''f_2f_3''-32f_1f_2''f_3''+64f_1'f_2''f_3'
\end{aligned}
$$

Finally comes the last equation utilized to simplify the α_3 terms.

$$
\begin{aligned}
&\int_{-\infty}^{\infty}dx_1f_1(x_1)\int_{-\infty}^{\infty}dx_2f_2(x_2)\int_{-\infty}^{\infty}dx_3f_3(x_3)\int_{-\infty}^{\infty}dk_me^{ik_m(x-0.5x_1-0.5x_3)}\\
&\qquad\times\int_{-\infty}^{\infty}dk_1e^{ik_1(x_1-x_2)}\int_{-\infty}^{\infty}dk_2e^{ik_2(x_2-x_3)}\left(k_m^2-4k_2^2\right)^2\\
=&128\pi^3\left[f_1(x)f_2(x)\right]''f_3''(x)
\end{aligned}
\tag{130}
$$

The seemingly simple equation (130) resulted from the cancellation of the following lengthy terms.

$$
\begin{aligned}
=&\frac{1}{16}\left(I_1+I_2+I_3\right)=16\left(f_1''f_2f_3''+f_1f_2''f_3''+f_1'f_2'f_3''\right)\\
I_1=&16f_1''''f_2f_3+16f_1f_2''''f_3+16f_1f_2f_3''''+64f_1'''f_2'f_3+64f_1'''f_2f_3'+64f_1'f_2'''f_3+\\
&64f_1'f_2f_3'''+64f_1f_2'''f_3'+64f_1f_2'f_3'''+96f_1''f_2''f_3+96f_1''f_2f_3''+96f_1f_2''f_3''+\\
&192f_1''f_2'f_3'+192f_1'f_2''f_3'+192f_1'f_2'f_3''\\
I_2=&-32f_1''''f_2f_3-32f_1f_2''''f_3-32f_1f_2f_3''''-128f_1'''f_2'f_3-128f_1'f_2'''f_3-\\
&192f_1''f_2''f_3+64f_1''f_2f_3''+64f_1f_2''f_3''+128f_1'f_2'f_3''\\
I_3=&16f_1''''f_2f_3+16f_1f_2''''f_3+16f_1f_2f_3''''+64f_1'''f_2'f_3-64f_1'''f_2f_3'+\\
&64f_1'f_2'''f_3-64f_1'f_2f_3'''-64f_1f_2'''f_3'-64f_1f_2'f_3'''+96f_1''f_2''f_3+96f_1''f_2f_3''+\\
&96f_1f_2''f_3''-192f_1''f_2'f_3'-192f_1'f_2''f_3'+192f_1'f_2'f_3''
\end{aligned}
$$

Reflector location using high-order inverse scattering series terms

Kristopher A. Innanen

Abstract

In considering the longer-term future of non-linear inverse scattering series based methods, there arises a need to characterize and progress beyond the limitations of leading-order methods for locating reflected primaries. To that end, a generating function that appears to adequately capture many of the terms associated with the imaging and inversion of primaries, including higher-order imaging terms (in contrast to the leading order terms discussed by Shaw et al., 2003), is presented. A categorization of terms based on higher vs. lower derivative orders is shown (as a one-dimensional version of the categorization developed in the appendices of Liu et al., 2005), to reproduce the "imaging" vs. "inversion" categorization. A simple numeric test is illustrated; a large contrast model is used to produce contrasting output from both leading order and higher order algorithms.

1 Introduction

The purpose of this note is to postulate a form for a subseries that involves itself with all processing objectives associated with the primaries of a recorded wave field; namely, imaging (or reflector location) and inversion (or target identification). As such, I make direct comparative statements between new mathematical inverse scattering series forms and the leading order imaging subseries (LOIS) of Shaw et al. (2003), and the so-called coupled, or simultaneous imaging and inversion subseries (SII) of Innanen et al. (2004). The goal is to develop methodologies that work well under conditions of large-contrast, in which significant levels of location error are noted at leading order.

The leading order imaging subseries, and coupled imaging and inversion subseries share the same subset of terms that locate the reflectors in depth, and as such both produce precisely the same reflector depth approximations. We more or less accept that there exist higher order terms that "complete the job" of reflector location, especially for models of high contrast. We see evidence of this even in the third order primary processing terms in the ISS:

$$\alpha_3(z) = \alpha_3^{(1)}(z) + \alpha_3^{(2)}(z) + \alpha_3^{(3)}(z) + \alpha_3^{(4)}(z), \tag{1}$$

where

$$\begin{aligned}
\alpha_3^{(1)}(z) &= \frac{1}{8}\alpha_1''(z)\left(\int_0^z \alpha_1(z')dz'\right)^2, \\
\alpha_3^{(2)}(z) &= \frac{3}{16}\alpha_1^3(z), \\
\alpha_3^{(3)}(z) &= \frac{3}{4}\alpha_1(z)\alpha_1'(z)\int_0^z \alpha_1(z')dz', \\
\alpha_3^{(4)}(z) &= -\frac{1}{8}\alpha_1'(z)\int_0^z \alpha_1^2(z')dz'.
\end{aligned} \tag{2}$$

These expressions include the term $\alpha_3^{(4)}(z)$, which appears to be involved with higher order imaging (see appendix A). We are curious about any simple subseries that generates this and other, higher order terms, that do not appear in either LOIS or SII. The production and analysis of high order inverse scattering series primary terms is the subject of this note.

1.1 High-order processing in the context of M-OSRP research

Elsewhere in this report we document the progression, towards greater complexity, of the non-linear processing and inversion algorithms deriving from the inverse scattering series. The strategy always involves investigation of the simplest imaginable physical framework that admits the phenomenon under study. For instance, Liu et al. (2005) study multidimensional issues in the processing/imaging of primaries; this is accomplished by shedding all (otherwise important) complexities, such as multi-parameter elastic behavior, and investigating the facets of the 2D problem under the simplistic single-parameter acoustic wave propagation model. This is for the straightforward reason that isolating levels of added complexity has the impact of isolating behaviors of the inverse scattering series.

In this paper I consider the addition of high-order reflector location terms to computable and closed-form subseries; to initiate this study (visible in action in the latter examples of multi-dimensional imaging of Liu et al., 2005), in light of the above strategies, it is only necessary to work in a 1D single parameter acoustic framework.

2 High order coupled imaging and inversion

Consider the quantity

$$\alpha_{HOI}(z) = \sum_{n=0}^{\infty} \frac{(-1/2)^n}{n!} \frac{d^n}{dz^n} \left\{ \alpha_1(z) \left[\sum_{k=1}^{\infty} \frac{1}{4^{k-1}} \int_0^z \alpha_1^k(z')dz' \right]^n \right\}, \tag{3}$$

and its closed form companion

$$\alpha_{HOI}(z) = \int_{-\infty}^{\infty} e^{ikz} \left[\int_{\infty}^{\infty} e^{-ik\left[z' + \frac{1}{2}\int_0^{z'} \frac{\alpha_1(z'')}{1-\frac{1}{4}\alpha_1(z'')}dz''\right]} \alpha_1(z')dz' \right] dk, \tag{4}$$

the latter of which is based on the summation

$$\sum_{k=1}^{\infty} \frac{1}{4^{k-1}} \alpha_1^k(z') = \alpha_1(z') \sum_{k=0}^{\infty} \left(\frac{\alpha_1(z')}{4} \right)^k = \frac{\alpha_1(z')}{1 - \frac{1}{4}\alpha_1(z')} \tag{5}$$

as well as the SII summation from MOSRP03. This HOI quantity can be considered analytically using equation (3) and/or numerically using equation (4).

3 Expansions for low n, and the partitioning of tasks via regularity

Consider expansions of the HOI structure for several values of n; moreover, consider the arrangement of functions from the point of view of Liu et al. (2005) – by their regularity. The n'th term in $\alpha_{HOI}(z)$ is $\alpha_{HOI(n)}(z)$, where

$$\begin{aligned}\alpha_{HOI(n)}(z) &= \frac{(-1/2)^n}{n!}\frac{d^n}{dz^n}\left\{\alpha_1(z)\left[\sum_{k=1}^{\infty}\frac{1}{4^{k-1}}\int_0^z \alpha_1^k(z')dz'\right]^n\right\} \\ &= C_n\frac{d^n}{dz^n}M(z)L(z),\end{aligned} \tag{6}$$

and where we have set

$$\begin{aligned}C_n &= \frac{(-1/2)^n}{n!}, \\ M(z) &= \alpha_1(z), \\ L(z) &= \left[\sum_{k=1}^{\infty}\frac{1}{4^{k-1}}\int_0^z \alpha_1^k(z')dz'\right]^n.\end{aligned} \tag{7}$$

That is, we have broken the generating function up into two bits, $M(z)$ being *More* discontinuous, or irregular, and $L(z)$ being *Less* discontinuous. This is based on the idea that $\alpha_1(z)$ has discontinuities in it – we usually consider them to be Heaviside-like steps – and since $L(z)$ involves the integral of $\alpha_1(z)$, it is by definition one order *Less* discontinuous[1] than M. With these definitions, and using the chain rule for the n'th derivative, equation (6) can be written

$$\alpha_{HOI(n)}(z) = C_n\left(\sum_{i=0}^{n}\frac{n!}{i!(n-i)!}M^{(n-i)}L^{(i)}\right), \tag{8}$$

where the superscript (i) is the i'th derivative with respect to z. Inspection indicates that at $i=0$ we will have the most discontinuous part of the HOI subseries for that n, since it involves the highest order derivative acting on the more discontinuous component M:

$$\begin{aligned}\alpha_{HOI(n)}(z)|_{i=0} &= C_n\left(M^{(n)}L^{(0)}\right) \\ &= C_n\alpha_1^{(n)}(z)\left[\sum_{k=1}^{\infty}\frac{1}{4^{k-1}}\int_0^z \alpha_1^k(z')dz'\right]^n \\ \alpha_{HOI(n)}(z)|_{i=0,k=1} &= C_n\alpha_1^{(n)}(z)\left[\int_0^z \alpha_1(z')dz'\right]^n,\end{aligned} \tag{9}$$

[1] This assumes that the exponentiation of a discontinuous function does not alter its regularity. We make assumptions kind of like this all the time, e.g. $H^2(z-z_0) = H(z-z_0)$.

the last result coming from the case $k = 1$ (at which HOI becomes the simultaneous imaging and inversion subseries SII, and the n'th LOIS term has been generated). This indicates that picking out the most discontinuous part of HOI at any n, i.e. $i = 0$, produces the terms most involved with imaging. The complement to this idea can be tested by considering the least discontinuous part at $i = n$, and for $k = 1$, and (for simplicity's sake) at second order, $n = 1$:

$$\begin{aligned}
\alpha_{HOI(n)}(z)|_{i=n} &= C_n \left(M^{(0)} L^{(n)} \right) \\
&= C_n \alpha_1(z) \left\{ \left[\sum_{k=1}^{\infty} \frac{1}{4^{k-1}} \int_0^z \alpha_1^k(z')dz' \right]^n \right\}^{(n)} \\
\alpha_{HOI(n)}(z)|_{i=n,k=1} &= C_n \alpha_1(z) \left\{ \int_0^z \alpha_1(z')dz' \right\}^{(1)} \\
&= -\frac{1}{2}\alpha_1^2(z).
\end{aligned} \tag{10}$$

This suggests that the least discontinuous part of HOI picks out the terms most involved with inversion.

Some points:

1. This consideration of regularity is how Liu et al. (2005) distinguish imaging vs. inversion terms in the more complicated 2D arena. The idea is that the most discontinuous, or singular, portions of the n'th term are involved with imaging, and least involved with inversion.
2. For any n (and fixed $k = 1$, there is the LOIS (Shaw et al., 2003) term at the most singular point, and the inversion term at the least singular point, but also a range of intermediate terms.
3. Choosing fixed $k = 1$ reduces the problem to that of SII (Innanen et al., 2004) and/or LOIS, so we must look to $k > 1$ for contributions to higher order imaging, if they are there.
4. Since SII contains all $i = 1, n$ but was fixed at $k = 1$, and it is known to produce mixed task terms (i.e., imaging and inversion), but no higher order imaging, perhaps the indices i and k can distinguish between the meaning of intermediate terms, i.e. whether they correspond to mixed tasks, or to truly higher order processing.

Expansion for $n = [1, 2]$, $k = [1, 2]$

Some of these issues can be addressed by expanding for more values of k in equation (6), that is, using n rather than i as an index. Consider substituting the full expressions for M and L into the $n = 1$, $n = 2$ terms, and using $k = [0, 1, 2]$ contributions. Within $\alpha_{HOI(n)}(z)|_{n=1,k=[1,2]} + \alpha_{HOI(n)}(z)|_{n=2,k=[0,1]}$ are terms that are 2nd, 3rd, and higher order. Grouping the 2nd order terms produces

$$\alpha_{HOI}^{2nd}(z) = -\frac{1}{2}\alpha_1'(z) \left(\int_0^z \alpha_1(z')dz' \right) - \frac{1}{2}\alpha_1^2(z). \tag{11}$$

Further, grouping the 3rd order terms, we have

$$\begin{aligned}\alpha_{HOI}^{3rd}(z) =& \frac{1}{8}\alpha_1''(z)\left(\int_0^z \alpha_1(z')dz'\right)^2 + \frac{3}{4}\alpha_1'(z)\alpha_1(z)\int_0^z \alpha_1(z')dz' \\ &+\frac{1}{8}\alpha_1^3(z) - \frac{1}{8}\alpha_1'(z)\left(\int_0^z \alpha_1^2(z')dz'\right).\end{aligned} \tag{12}$$

This is a fairly satisfactory reproduction of the terms derived directly from the ISS equations; note, however, that this remains an approximation of the inversion subseries – the inversion term has a coefficient of 1/8 rather than 3/16.

4 Numeric example

As with closed-form SII, it is difficult to show analytically how it works (in contrast to LOIS). So a numeric example is used in this section to provide evidence that $\alpha_{HOI}(z)$ is a higher-order expression that couples imaging and inversion.

Figure 1 illustrates the difference between SII and HOI for a high-contrast example. There is a slight offset yet between amplitudes of α and α_{HOI}, but the approximation error of the reflector depth is clearly greatly reduced.

References

Innanen, K. A., Nita, B., and Weglein, A. B. "Investigating the Grouping of Inverse Scattering Series Terms: Simultaneous Imaging and Inversion I (Theory)." *M-OSRP Annual Report*, (2004)

Liu, F., Nita, B., Weglein, A. B., and Innanen, K. A. "Inverse scattering series for vertically and laterally varying media." *M-OSRP 03 Annual Report*, (2004).

Shaw, S. A., Weglein, A. B., Foster, D. J., Matson, K. H. and Keys, R. G. "Isolation of a Leading Order Depth Imaging Series and Analysis of its Convergence Properties." *M-OSRP 02*, (2003).

Shaw, S. A., "An inverse scattering series algorithm for depth imaging of reflection data from a layered acoustic medium with an unknown velocity model." *Ph.D. Thesis, University of Houston*, (2005).

Appendix A

In this appendix I put forth some circumstantial arguments as to the "higher-order imaging" nature of one of the third-order terms of the inverse scattering series (for normal incidence problems in a 1D single parameter acoustic medium), namely:

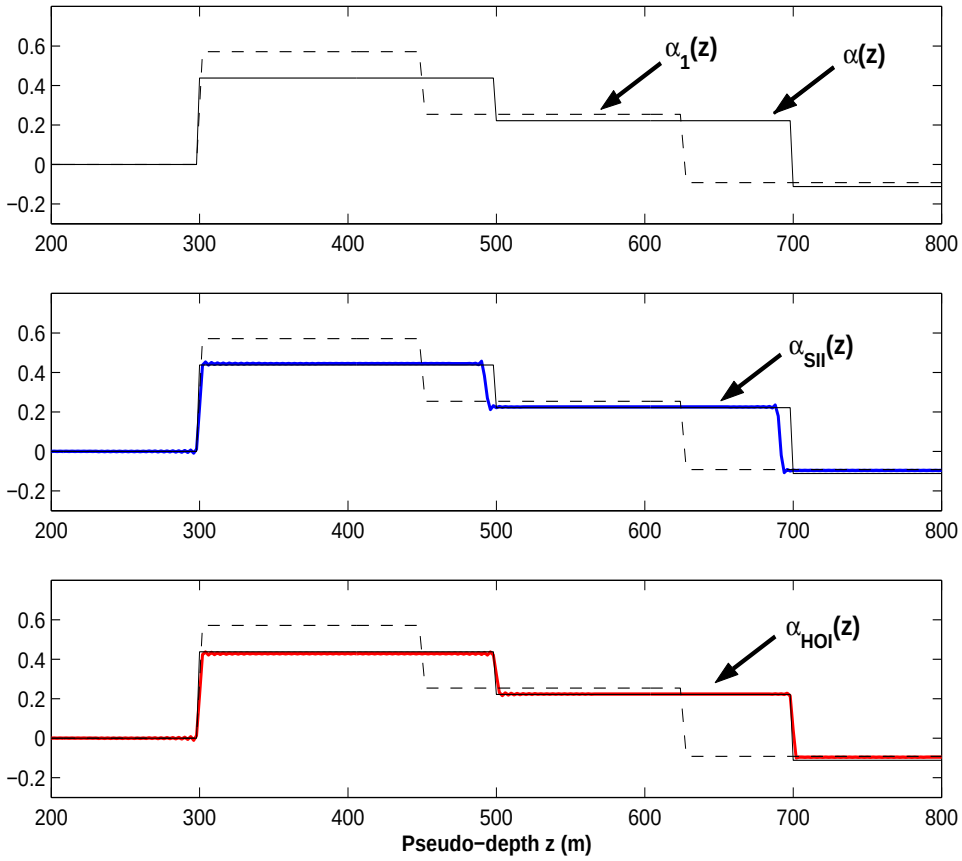

Figure 1: *Large contrast example illustrates the difference between SII and HOI. Top: true $\alpha(z)$ (solid) vs. $\alpha_1(z)$ (dashed). Middle: α_{SII} (blue) overlain on linear and true perturbations. Bottom: α_{HOI} (red) overlain on linear and true perturbations. The main difference is in increased reflector depth accuracy.*

$$\alpha_3^{(4)}(z) = -\frac{1}{8}\alpha_1'(z)\int_0^z \alpha_1^2(z')dz'. \tag{13}$$

Substituting

$$\begin{aligned}\alpha_1^2(z) &= \alpha_1(z)\alpha_1(z)\\ &= \alpha_1(z)\frac{d}{dz}\left(\int_0^z \alpha_1(z')dz'\right)\\ &= \frac{d}{dz}\left(\alpha_1(z)\int_0^z \alpha_1(z')dz'\right) - \alpha_1'(z)\int_0^z \alpha_1(z')dz'\end{aligned} \tag{14}$$

into equation (13) produces

$$\begin{aligned}\alpha_3^{(4)}(z) = &-\frac{1}{8}\alpha_1'(z)\alpha_1(z)\int_0^z \alpha_1(z')dz' \\ &+\frac{1}{4}\alpha_1'(z)\int_0^z\left[-\frac{1}{2}\alpha_1'(z')\int_0^{z'}\alpha_1(z'')dz''\right]dz'.\end{aligned} \tag{15}$$

This term, therefore, may be split into two parts. The first, of the form $\alpha_1'\alpha_1\int_0^z\alpha_1$, alters the coefficient of one of the other third-order terms ($\alpha_3^{(3)}$ in equation 1). The second operates in an interesting way: it is a second-order imaging operator,

$$\alpha_1'(z')\int_0^{z'}F(z'')dz'',$$

acting on a second-order imaging quantity:

$$F(z) = -\frac{1}{2}\alpha_1'(z)\int_0^z\alpha_1(z')dz',$$

to form an overall third-order quantity. This is qualitatively suggestive that a higher-order reflector locator, or "mover", constitutes part of this term.

On acoustic reciprocity theorems and the construction of transmission response from reflection data

Bogdan G. Nita and Arthur B. Weglein

Abstract

Seismic exploration methods rely mainly on reflection data to determine the structure and characteristics of the subsurface. However, procedures exist to perform imaging and inversion using either entirely transmission data, i.e. VSP, or a combination of transmition and reflection data. In addition, newly developed inverse scattering methods for imaging without an adequate velocity model suggest that transmission data is required for developing a model type independent algorithm (see Weglein et al. (28)). Recently, there has been an increasing interest in procedures for constructing the transmitted wavefield (as opposed to measuring it) from recorded reflection data. In this paper we review the method of determining the amplitude and the phase of the transmission response from recorded seismic data based on reciprocity theorems.

1 Introduction

Inverse scattering series is presently the only direct non-linear inversion method which is capable of performing full inversion without adequate information about the unknown medium. Task specific methods for free-surface multiple elimination and internal multiple attenuation extracted from the full inverse scattering series have shown tremendeous capability and practical value (27). In addition, the two algorithms are model type independent, i.e. they perform with the same efficiency independent on the earth's model type, e.g. acoustic, elastic, inelastic, etc. Recently, a task specific subseries aimed at performing imaging, *i.e.* locating reflectors in space, has been identified and tested on analytical data for simple 1D-earth examples with encouraging results (see Shaw and Weglein (19) and Shaw et al. (20). Liu et al. (12) has very recently shown the first multidimensional acoustic examples of these methods for determining the horizontal and the vertical reflector location without knowing or determining the overburden velocity model. Weglein et al. (26) analyzed the possibility and requirements for a model type independent imaging algorithm. As some of the diagrams included in Shaw et al. (20), describing scattering interaction within the imaging subseries, imply that a model type independent algorithm would require both reflection and transmission data.

Most of the seismic exploration techniques involve collection and interpretation of reflection data to determine the earth structure and properties. However there are a few procedures which involve collecting and interpreting borehole VSP transmission data, independently or in addition to reflection data. In recent years, a promising method, based on reciprocity theorems, has been developed to construct the transmission response (rather than measure it) from recorded reflection data. Among the advantages we mention the relatively reduced cost of computing rather than collecting the data, and the resulting transmission data having similar characteristics (wavelet, with or without free surface multiples, no ghosts etc) with the input reflection data.

In this paper we present the method of constructing the transmission response from recorded reflection data based on acoustic reciprocity theorems. The paper is organized as follows. The first section discusses the decomposition of the two-way wavefields into pressure normalized and flux normalized one-way wavefields and their satisfying of the reciprocity principle. The second section presents the reciprocity theorems of convolution and correlation type for both two-way and one-way acoustic wavefields and focus our attention on the relationship between the reflection and the transmission responses in an acustic experiment with no free surface which allows the construction of the amplitude of the transmitted wavefield from reflection data. Section 4 then analyzes the construction of the phase properties from amplitude information for real minimum phase signals. Section 5 further investigates the properties of minimum phase wavefields and reflection coefficients and presents both time and frequency domains interpretations. Some conclusions are drawn in the last section. Finally we mention that, while we discuss mainly the acoustic case, the methods presented can be extended to the elastic case.

2 Pressure normalized and flux normalized one-way wavefields

Acoustic reciprocity is a fundamental property of the acoustic wave equation for the total wavefield which, in its most elementary form, states that the acoustic response does not change if the source and receiver are interchanged (17). Applications to seismic exploration were discussed, among others, by Fokkema and van den Berg (5). In many situations, e.g. migration/inversion, it is useful to decompose the total wavefield into up-going and down-going wavefields. This decomposition is not unique and the resulting one way propagators are no longer solutions to the acoustic wave equation and, hence, it is not obvious that they obey the reciprocity principle. In fact, whether or not the one-way Green's functions satisfy the acoustic reciprocity, depends on how the wavefield decomposition is performed. Two types of decompositions are used for different purposes in seismic applications, namely pressure normalized and flux normalized decompositions, with only the latter resulting in reciprocal up-going and down-going fields.

Flux normalized decompositions have been found for wavefields propagating through any inhomogeneous media (7), (8) and general reciprocity theorems for flux normalized one-way wavefields and propagators in arbitrarily inhomogeneous media have been derived (22). In this section, following Wapenaar (23), we present the pressure normalized and flux normalized decompositions and show that the amplitudes of the transmitted up-going and down-going wavefields through a horizontal interface in a simple 1.5D model, are different in the former and equal in the latter. This is an indication of the reciprocity principle being satisfied only by the flux normalized decomposition. We also note that neither of the two decompositions require information about the medium that the wavefield propagates through, but only about the medium where the wavefield is recorded in a particular seismic experiment.

In the space-frequency domain the pressure normalized down-going and up-going wavefields, P^+ and P^-can be written

$$\begin{pmatrix} P^+ \\ P^- \end{pmatrix} = \frac{1}{2} \begin{pmatrix} 1 & \left(\hat{H}_1^{-1}\omega\rho\,\cdot\right) \\ 1 & -\left(\hat{H}_1^{-1}\omega\rho\,\cdot\right) \end{pmatrix} \begin{pmatrix} P \\ V_z \end{pmatrix}, \tag{1}$$

where P and V_z are the acoustic pressure and the vertical component of particle velocity respectively, ω is the frequency, ρ the mass density and $\hat{H}_1$ is the square root operator for the pseudo-Helmholtz

operator $\hat{H}_2$, i.e. $\hat{H}_1\hat{H}_1 = \hat{H}_2$, with

$$\hat{H}_2 = \left(\frac{\omega}{c}\right)^2 + \rho\frac{\partial}{\partial x}\left(\frac{1}{\rho}\frac{\partial}{\partial x}\cdot\right) + \rho\frac{\partial}{\partial y}\left(\frac{1}{\rho}\frac{\partial}{\partial y}\cdot\right). \tag{2}$$

For 1D media this relation can be written in the wavenumber-frequency domain as

$$\begin{pmatrix} P^+ \\ P^- \end{pmatrix} = \frac{1}{2}\begin{pmatrix} 1 & \omega\rho/k_z \\ 1 & -\omega\rho/k_z \end{pmatrix}\begin{pmatrix} P \\ V_z \end{pmatrix}, \tag{3}$$

where k_z denotes the vertical wavenumber. Assuming the medium has an interface between two homogeneous half spaces, denoted below by 1 and 2, one can calculate the reflection and the transmission coefficients using continuity of P and V_z at that interface and find

$$R = \frac{\rho_2/k_{z,2} - \rho_1/k_{z,1}}{\rho_2/k_{z,2} + \rho_1/k_{z,1}} \tag{4}$$

and

$$T^+ = 1 + R, \qquad T^+ = 1 - R. \tag{5}$$

Notice that the up-going and down-going transmission coefficients are not equal and satisfy

$$T^+ = \frac{k_{z,1}}{k_{z,2}}\frac{\rho_2}{\rho_1}T^- \tag{6}$$

which shows that the reciprocity principle is not satisfied by the one-way wavefields obtained through this method.

The flux-normalized down-going and up-going wavefields, also denoted by P^+ and P^-, can be obtained as

$$\begin{pmatrix} P^+ \\ P^- \end{pmatrix} = \frac{1}{\sqrt{2}}\begin{pmatrix} \hat{\mathcal{H}}_1^{\frac{1}{2}}(\omega\rho)^{-\frac{1}{2}} & \hat{\mathcal{H}}_1^{-\frac{1}{2}}(\omega\rho)^{\frac{1}{2}} \\ \hat{\mathcal{H}}_1^{\frac{1}{2}}(\omega\rho)^{-\frac{1}{2}} & -\hat{\mathcal{H}}_1^{-\frac{1}{2}}(\omega\rho)^{\frac{1}{2}} \end{pmatrix}\begin{pmatrix} P \\ V_z \end{pmatrix} \tag{7}$$

where the pseudo-Helmholtz operator $\hat{H}_2$ was redefined as

$$\hat{\mathcal{H}}_2 = \rho^{-\frac{1}{2}}\left(\hat{H}_2\rho^{\frac{1}{2}}\cdot\right) \tag{8}$$

and the square root operator is defined in terms of $\hat{\mathcal{H}}_2$ to satisfy $\hat{\mathcal{H}}_1\hat{\mathcal{H}}_1 = \hat{\mathcal{H}}_2$. Note that $\hat{\mathcal{H}}_2$ can be written as

$$\hat{\mathcal{H}}_2 = \left(\frac{\omega}{c'}\right)^2 + \frac{\partial^2}{\partial x^2} + \frac{\partial^2}{\partial y^2} \tag{9}$$

with

$$\left(\frac{\omega}{c'}\right)^2 = \left(\frac{\omega}{c}\right)^2 - \frac{3\left(\left(\frac{\partial\rho}{\partial x}\right)^2 + \left(\frac{\partial\rho}{\partial y}\right)^2\right)}{4\rho^2} + \frac{\frac{\partial^2\rho}{\partial^2 x} + \frac{\partial^2\rho}{\partial^2 y}}{2\rho}. \tag{10}$$

For a 1D media this relation can be written in the wavenumber-frequency domain as

$$\begin{pmatrix} P^+ \\ P^- \end{pmatrix} = \frac{1}{\sqrt{2}}\begin{pmatrix} \sqrt{\frac{k_z}{\omega\rho}} & \sqrt{\frac{\omega\rho}{k_z}} \\ \sqrt{\frac{k_z}{\omega\rho}} & -\sqrt{\frac{\omega\rho}{k_z}} \end{pmatrix}\begin{pmatrix} P \\ V_z \end{pmatrix}. \tag{11}$$

As before, the reflection and transmission coefficients can be calculated to find

$$R = \frac{\rho_2/k_{z,2} - \rho_1/k_{z,1}}{\rho_2/k_{z,2} + \rho_1/k_{z,1}} \tag{12}$$

and

$$T^+ = T^- = \sqrt{1 - R^2} \tag{13}$$

which is an indication that, in this decomposition, the reciprocity principle is satisfied.

Notice that both pressure normalized and flux-normalized decomposition procedures/operators, in expressions (1) and (7), require information only about the medium where data (P and V_z on a measurement surface) is recorded.

3 Reciprocity theorems

The initial method for deriving symmetry relations for reflection and transmission responses was to find 'propagation invariants' for the 3D inhomogeneous acoustic and elastic media, see e.g. (6), (9), (21). For acoustic media such an invariant is given, in the space-frequency domain, by

$$\int\limits_{z=const.} d^2\mathbf{x} \left\{ P_A V_{z,B} - V_{z,A} P_B \right\} \tag{14}$$

where the integral is performed over an arbitrary horizontal surface defined by $z = const.$, P and V_z are, as before, the acoustic pressure and vertical component of particle velocity respectively, and A and B represent two independent acoustic states. The notion of invariant refers to the fact that this quantity remains the same at any depth as long as the medium between the two depths does not contain any sources, i.e.

$$\int\limits_{z_M=const.} d^2\mathbf{x} \left\{ P_A V_{z,B} - V_{z,A} P_B \right\} = \int\limits_{z_m=const.} d^2\mathbf{x} \left\{ P_A V_{z,B} - V_{z,A} P_B \right\} \tag{15}$$

for any source-free region between depths z_M and z_m.

In addition to expression (15), which represents a special case of reciprocity theorems of the convolution-type, we can also have reciprocity theorems of the correlation-type (see e.g. (2), (5)) from which we find similarly

$$\int\limits_{z_M=const.} d^2\mathbf{x} \left\{ P_A^* V_{z,B} + V_{z,A}^* P_B \right\} = \int\limits_{z_m=const.} d^2\mathbf{x} \left\{ P_A^* V_{z,B} + V_{z,A}^* P_B \right\} \tag{16}$$

where * denotes complex conjugation. Unlike equation (15) which is valid for both lossless and dissipative media, equation (16) is only valid for lossless media (see e.g. (25)).

Notice that both relations (15) and (16) are written for the full two-way wavefields. However, to relate reflection and transmission responses in a seismic experiment, similar equations are needed for one-way wavefields. Reciprocity theorems for one-way wavefields have been derived by Wapenaar

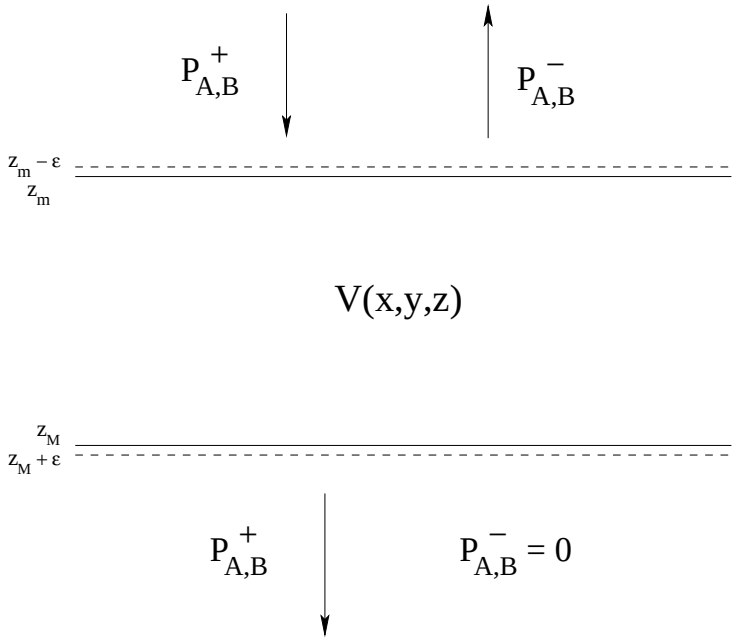

Figure 1: *The choice of acoustic states in an experiment without free surface and corresponding up-going and down-going wavefields*

and Grimbergen (22). They can also be divided into reciprocity theorems of the convolution type, for which we can write analogous to equation (15)

$$\int\limits_{z_M=const.} d^2\mathbf{x}\left\{P_A^+ P_B^- - P_A^- P_B^+\right\} = \int\limits_{z_m=const.} d^2\mathbf{x}\left\{P_A^+ P_B^- - P_A^- P_B^+\right\} \tag{17}$$

and reciprocity theorems of the correlation type, analogous to equation (16),

$$\int\limits_{z_M=const.} d^2\mathbf{x}\left\{(P_A^+)^* P_B^+ - (P_A^-)^* P_B^-\right\} = \int\limits_{z_m=const.} d^2\mathbf{x}\left\{(P_A^+)^* P_B^+ - (P_A^-)^* P_B^-\right\} \tag{18}$$

where P^+ and P^- are flux normalized down-going and up-going wavefields respectively. Equation (17) holds for primary and multiply reflected waves, including evanescent modes, in 3D lossless or dissipative inhomogeneous media. Equation (18) is less general and it can be viewed as an approximation since it assumes that the medium is lossless and that evanescent wavemodes can be neglected.

The two states A and B can be chosen in different ways for deriving relations between reflection and transmission responses (for a comprehensive description see (25)). In this paper we will concentrate specifically on the case that leads to the reconstruction of the transmission response from reflection data. For this purpose we choose both states A and B to represent experiments with the source located at depth $z_m - \epsilon$ in a homogeneous half space (see Figure 1). The space coordinates of these sources are denoted by $\mathbf{x}_A$ and $\mathbf{x}_B$. The inhomogeneity $V(x, y, z)$ is located between depths z_m and z_M and the space beyond $z_M + \epsilon$ is again a homogeneous space. A receiver located at the same depth as the source with coordinates $\mathbf{x}$ would record the reflection response $R(\mathbf{x}, \mathbf{x}_A, \omega)$ while

a receiver located deeper than z_M would record the transmition response $T(\mathbf{x}, \mathbf{x}_A, \omega)$. To obtain a relationship between the reflection and transmission responses R and T we are going to use the one-way reciprocity theorem of the correlation type, equation (17). For that we notice that, with the states A and B defined as above, we have the following. At depth z_m

$$P^+_{A,B}(\mathbf{x}, \mathbf{x}_{A,B}, \omega) = \delta(x - x_{A,B})\delta(y - y_{A,B})s_{A,B}(\omega) \tag{19}$$

$$P^-_{A,B}(\mathbf{x}, \mathbf{x}_{A,B}, \omega) = R(\mathbf{x}, \mathbf{x}_{A,B}, \omega)s_{A,B}(\omega) \tag{20}$$

where s represents the source signature. At depth z_M

$$P^+_{A,B}(\mathbf{x}, \mathbf{x}_{A,B}, \omega) = T(\mathbf{x}, \mathbf{x}_{A,B}, \omega)s_{A,B}(\omega) \tag{21}$$

$$P^-_{A,B}(\mathbf{x}, \mathbf{x}_{A,B}, \omega) = 0. \tag{22}$$

Substituting these into equation (17) and dividing by $s^*_A(\omega)s_B(\omega)$ we find

$$\int_{z_M} d^2\mathbf{x}\, T^*(\mathbf{x}, \mathbf{x}_A, \omega)T(\mathbf{x}, \mathbf{x}_B, \omega) + \int_{z_m} d^2\mathbf{x}\, R^*(\mathbf{x}, \mathbf{x}_A, \omega)R(\mathbf{x}, \mathbf{x}_B, \omega) = \delta(\mathbf{x}_B - \mathbf{x}_A). \tag{23}$$

This relation provides amplitude information about the transmitted data from recorded reflection data and viceversa. However all the phase information is lost in this process and there is no unique way to recover it from this relation alone. Reconstructing the phase from the amplitude for a signal would require additional information which is sometimes provided by the minimum phase condition which will be discussed in the following sections. This property of the recorded wavefield depends on the medium that the wave propagates through and, in general, it is not satisfied. In other words, even when the source wavelet used in a seismic experiment is minimum phase, the interaction with complex subsurface structures changes the phase properties of the wavefield resulting in a non-minimum phase signal to be recorded on the measurement surface. Bostock (3) points out some of the cases in which the wavefield preserves the minimum phase namely for pre-critical intramodal free surface reverberations and transmitted P-waves in weak to moderate contrast stratification with small horizontal wavenumbers. However, for general acoustic and elastic media and wavefield propagation with arbitrary horizontal wavenumber, the recorded signal will have a mixed phase character.

For 1D media Wapenaar et al. (24) describes the procedure of reconstructing the transmission response from reflection data. The reconstruction implicitly uses the fact that the transmission response for a 1D acoustic media is minimum phase and hence its full phase can be reconstructed. In the following sections, we will discuss the definition and some of the properties of minimum phase property and show how the reconstruction of the phase from amplitude information only is possible for this type of signals.

4 Reconstructing the phase properties from amplitude information for real signals

In this section we present the mathematical description of causal and minimum phase signals and their equivalent representations in the frequency domain. We will denote by $f(t)$ an arbitrary time

domain function and by $F(\omega)$ its Fourier transform representation. The two functions f and F are related by

$$F(\omega) = \int_{-\infty}^{\infty} e^{i\omega t} f(t) dt, \tag{24}$$

and

$$f(t) = \frac{1}{2\pi} \int_{-\infty}^{\infty} e^{-i\omega t} F(\omega) d\omega. \tag{25}$$

A sufficient condition for the Fourier transform of $f(t)$ to exist and satisfy equation (25) is for $f(t)$ to be absolutely integrable, i.e.

$$\int_{-\infty}^{\infty} |f(t)| dt < \infty. \tag{26}$$

In this section we will assume that this relation holds for the function f. Its Fourier transform, $F(\omega)$, is usually a complex function

$$F(\omega) = X(\omega) + iY(\omega), \tag{27}$$

with X and Y real functions which generally are independent of one another. However there are special cases in which the two functions are related and these relations imply specific restrictions on the original function $f(t)$.

The function $f(t)$ is called causal if $f(t) = 0$ for $t < 0$. This is a time-domain property which is equivalent to saying that the Fourier transform F contains no poles in the upper half complex ω-plane (see e.g. (16)) and hence it is analytic in that domain. A little more subtle equivalent condition is that the real and imaginary parts of $F(\omega)$ are related through the Hilbert transform (these relations are sometimes called Kramers-Kronig causality conditions see e.g. (10))

$$X(\omega) = -\frac{1}{\pi} \int_{-\infty}^{\infty} \frac{Y(y)}{\omega - y} dy \tag{28}$$

$$Y(\omega) = \frac{1}{\pi} \int_{-\infty}^{\infty} \frac{X(x)}{\omega - x} dx. \tag{29}$$

The conclusion is that a causal signal can be fully constructed from the real or the imaginary parts of its Fourier transform only.

Next we want to study the reconstruction of the phase of the signal (and hence the reconstruction of the full signal) from its measured amplitude. Notice that we can write the function $F(\omega)$ as

$$F(\omega) = R(\omega) e^{i\phi(\omega)} \tag{30}$$

where $R(\omega) = \sqrt{X^2(\omega) + Y^2(\omega)}$ and $\phi(\omega) = arctan\left[\frac{Y(\omega)}{X(\omega)}\right]$. When $F(\omega)$ does not contain any zeros in the upper half complex ω-plane we can rewrite (see e.g. (16))

$$F(\omega) = e^{\rho(\omega) + i\phi(\omega)} \tag{31}$$

where $R(\omega) = e^{\rho(\omega)}$ or $\rho(\omega) = \ln[R(\omega)]$ After applying natural logarithm, ln, on both sides of the equation, we find

$$\ln[F(\omega)] = \rho(\omega) + i\phi(\omega). \tag{32}$$

The conditions that F is analytic and that it does not contain any zeros in the upper half plane, ensure that $\ln[F(\omega)]$ is analytic in the upper half plane and hence $\rho(\omega)$ and $\phi(\omega)$ are related through the Hilbert transform relations (28) and (29). In other words, when both conditions are satisfied, i.e. F has no poles and no zeros in the upper half plane, the phase $\phi(\omega)$ can be constructed from the amplitude $R(\omega)$. The second condition is called the minimum phase-shift or simply the minimum phase condition.

5 Minimum phase in time and frequency domains

In this section we go over the descriptions of minimum phase signals in both time and frequency domains and their different interpretations.

We saw in the previous section that the signal $F(\omega)$ is called minimum phase if it does not contain any zeros in the upper half of the complex frequency plane (see also (16)). This condition insures that the inverse of F, $F^{-1}(\omega)$, does not have any poles in the same upper half complex frequency plane and hence its inverse Fourier transform is a causal signal itself. Any zero in the upper half complex frequency plane creates phase shifts in the time domain function when the frequency is varied from $-\infty$ to $+\infty$, as it is, for example, when performing an inverse Fourier transform. In particular, it was shown by Lyon (13) that passing beneath a zero of F located in the upper half complex frequency plane creates a phase shift of $(-\pi)$. One can also show, see e.g. (11), that as the frequency is varied from $+\infty$ to 0, a non-minimum phase function experiences a greater positive phase shift than a minimum phase function with the same magnitude.

Time domain descriptions of minimum phase signals are also useful and have been obtained by Eisner (4). The description involves the output energy of the system defined as

$$E_f = \int_{-\infty}^{T} |f(t)|^2 dt. \tag{33}$$

If we define $h(t)$ to be $f(t)$ convolved with an all-pass and causal function $p(t)$, i.e. $h(t) = f(t) * p(t)$, then one can show that

$$E_f \geqslant E_h \tag{34}$$

or, in other words, any multiplication by a causal all-pass function has the effect of decreasing the energy that has arrived up to time T. The implications are that the response energy of a minimum phase signal integrated up to time T is greater than that of a non-minimum phase signal with the same frequency domain magnitude. In other words, a minimum phase signal has more energy concentrated at early times than any other signal sharing its spectrum (see also (18)).

Minimum phase condition for the normal incidence reflection coefficient of an object immersed in a homogeneous medium has been studied by McDaniel (14), (15). He shows, based on the time domain interpretation of the minimum phase condition given above, that such an object would have the property of reflecting the acoustic energy faster than an object with the same magnitude

of reflection coefficient but with a non-minimum phase property. Furthermore, a minimum phase medium would be one in which the perfect velocity transfer condition would hold, i.e. the wave that enters the medium and the one that exists the medium would have the same propagation speed. For the seismic case this is true for any intramodal PP and SS normal incidence reflections. More general situations, i.e. angle dependent reflection/transmission coefficients and reflection coefficients of converted waves, are presently under investigation.

6 Conclusions

In this paper we have discussed a method of constructing the transmission response of a 3D acoustic medium from recorded reflection data. We have shown that, after the free surface effects (ghosts and multiples) have been removed the reciprocity theorem of the correlation type relates the amplitude of the reflection data with the amplitude of the transmission response. The phase however is not uniquely recoverable from this relation and additional information is required to construct it. This information is sometimes provided by the minimum phase condition which has also been described from different points of view and in both time and frequency domain. Some open questions remain, for example what is the connection between non-minimum phase reflection data and the constructed minimum phase transmission data and can these two types of data can be used together in an imaging algorithm; or, in the case the reflection data is transformed to minimum phase before using reciprocity, how much of imaging can be achieved with this transformed data. These question and others will be further investigated in future research.

Acknowledgments

This work was partially supported by NSF-CMG award number DMS-0327778. The support of M-OSRP sponsors is also gratefully acknowledged.

References

[1] K. Aki, P. G. Richards (1980), *Quantitative Seismology,* W. H. Freeman and Company, San Francisco.

[2] N. N. Bojarski (1983), *Generalized reaction principles and reciprocity theorems for the wave equations and the relationship between the time-advanced and time-retarded fields*, J. Acoust. Soc. Am., **74**, pp. 281-285.

[3] M. Bostock (2004), *Green's functions, source signatures, and the normalization of teleseismic wave fields*, Journal of Geophysical Research B: Solid Earth 109, no.3, pp. B03303 1-15.

[4] E. Eisner (1984), *Minimum phase for continuous time and discrete time functions*, Geophys. Prospect, **32**, pp. 533-541.

[5] J. T. Fokkema and P. M. van den Berg (1993), *Seismic applications of acoustic reciprocity*, Elsevier Science Publ. Co., Inc.

[6] A. J. Haines (1988), *Multi-source, multi-receiver synthetic seismograms for laterally heterogeneous media using F-K domain propagators*, Geophys. J. Int., **95**, pp. 237-260.

[7] M. V. de Hoop (1992), *Directional decomposition of transient acoustic wavefields*, PhD thesis, Delft Univ. of Tech.

[8] M. V. de Hoop (1996), *Generalization of the Bremmer coupling series*, J. Math. Phys., **37**, pp. 3246-3282.

[9] B. L. N. Kennett, K. Koketsu, A. J. Haines (1990), *Propagation invariants, reflection and transmission in anisotropic, laterally heterogeneous media*, Geophys. J. Int., **103**, pp. 95-101.

[10] T. W. Korner (1993), *Fourier Analysis*, Cambridge University Press.

[11] B. C. Kuo (1991), *Automated Control Systems*, 6th ed., Prentice Hall, Englewood Cliffs, New Jersey.

[12] F. Liu, B. G. Nita, A. B. Weglein, K. H. Innanen (2005), *Inverse scattering series for vertically and laterally varying media*, in preparation.

[13] R. H. Lyon (1986), *Statistics of phase and magnitude of structural transfer functions*, in Random Vibrations - Status and Recent Developments, Studies in Applied Mechanics, edited by I. Elishakoff and R. H. Lyon, Elsevier, Amsterdam, pp. 201-208.

[14] J. G. McDaniel (1999), *Applications of the causality condition to one-dimensional acoustic reflection problems*, J. Acoust. Soc. Amer. **105** (5), pp. 2710-2716.

[15] J. G. McDaniel, C. L. Clarke (2001), *Interpretation and identification of minimum phase reflection coefficients*, J. Acoust. Soc. Amer. **110** (6), pp. 3003-3010.

[16] A. Papoulis (1962), *The Fourier integral and its applications*, Electronic Science Series, McGraw-Hill, New York.

[17] J. W. S. Rayleigh (1878), *The theory of sound*, Dover Publications Inc. (reprinted 1945).

[18] E. A. Robinson, S. Treitel (1980), *Geophysical Signal Analysis*, Prentice Hall, Englewood Cliffs, New Jersey.

[19] S. A. Shaw, A. B. Weglein (2003), *Imaging seismic reflection data at the correct depth without specifying an accurate velocity model: initial numerical examples of an inverse scattering subseries*, in Frontiers of remote sensing information processing, C.H. Chen (ed.), World scientific publishing co.

[20] S. A. Shaw, A. B. Weglein, D. J. Foster, K. H. Matson, R. G. Keys (2004), *Isolation of a leading order depth imaging series and analysis of its convergence properties*, J. Seis. Expl. 13 (2), pp. 99-120.

[21] H. Takenaka, B. L. N. Kennett, K. Koketsu (1993), *The integral operator representation of propagation invariants for elastic waves in irregularly layered media*, Wave Motion, **17**, pp. 299-317.

[22] K. Wapenaar and J. L. T. Grimbergen (1996), *Reciprocity theorems for one way wavefields*, Geophys. J. Int., **127**, pp. 169-177.

[23] K. Wapenaar (1998), *Reciprocity properties of one way propagators*, Geophysics, **63**, no. 4, pp. 1795-1798.

[24] K. Wapenaar, D. Draganov, J. Thorbecke (2003), *Relations between codas in reflection and transmission data and their applications in seismic imaging*, in ed. Uchida, T., 6th Ann. Int. Mtg., Soc. Explor. Geophys. of Japan, Expanded Abstracts, pp. 152-159.

[25] K. Wapenaar, J. Thorbecke, D. Draganov (2004), *Relations between reflection and transmission responses of three-dimensional inhomogeneous media*, Geophys. J. Int., **156**, pp. 179-194.

[26] A. B. Weglein, K. H. Matson, D. J. Foster, P. M. Carvalho, D. Corrigan, S. A. Shaw, *Imaging and inversion at depth without a velocity model: theory, concepts and initial evaluation*, SEG Expanded Abstracts, 70^{th} Annual Meeting of the Society for Exploration Geophysicists, Calgary, Canada.

[27] A. B. Weglein, F. V. Araujo, P. M. Carvalho, R. H. Stolt, K. H. Matson, R. Coates, D. Corrigan, D. J. Foster, S. A. Shaw, H. Zhang (2003), *Inverse scattering series and seismic exploration*, Topical Review Inverse Problems, 19, pp. R27-R83.

[28] A. B. Weglein, B. G. Nita, K. A. Innanen, F. Liu, S. Shaw, H. Zhang, G. Pavlis, C. Fan (2005), *Inverse scattering model type independent imaging: initial concepts and analysis*, invited paper for Special Issue of Geophysics on Seismic Interferometry, Daylight Imaging and Time-Reversal, Editors Kees Wapenaar and Deyan Draganov (Delft University of Technology), Johan O.A. Robertsson (WesternGeco Oslo Technology Center) in preparation. preparation.

Non-linear construction of a Q-compensation operator directly from measured reflection data

Kristopher A. Innanen and Arthur B. Weglein

Abstract

We continue to pursue a resolution to the conjecture of Innanen and Weglein (2003), that the mechanisms embodied in the erstwhile imaging or reflector location subseries, will act on a suitably determined *attenuated* linear inverse to perform Q-compensation without ever knowing or determining Q. In this paper we demonstrate the conceptual and (albeit simplistic) practical viability of this idea. This is accomplished through (1) the computation (from only the data and a homogeneous, non-attenuating Green's function) of a linear inverse that is *complex*, by virtue of viscous impedance contrasts; and (2) substitution of this linear inverse into a subseries postulated to be for the construction of a Q-compensation operator. A final integral, bringing this expression into the physical domain, is approximated. The results indicate a definitive correction of the smoothing effects of the unknown attenuation factors in the medium. We comment on the direction of future research.

1 Introduction

Innanen and Weglein (2003) have remarked that the form of the forward scattering series, given an acoustic reference medium and an absorptive-dispersive actual medium, indicates that a subseries of the inverse scattering series might be found that would work to compensate for all propagation effects, including absorption and dispersion compensation. This postulated subseries would share many mathematical qualities with the imaging subseries of Shaw (2005), amongst which are (1) actively engaging the data non-linearly, such that (2) no accurate (or existing) prior estimate of medium parameters are required. In other words, non-linear Q-compensation directly in terms of measured reflection data, without prior knowledge of Q.

Instances of successful application of the inverse scattering series (Weglein et al., 2003) have relied heavily on the linear inverse as input to higher order terms. In light of this, Innanen and Weglein (2004) describe the linearized inversion of the absorptive/dispersive case, finding in particular that the problem may be cast to extract the linear acoustic-absorptive-dispersive model *if* the associated complex/frequency dependent reflectivity was detectable in the data record. The nature of the non-linear operations for Q-compensation, and the computation of the linear input to these operations having been explored to a degree, we next consider what amounts to the non-linear construction of a Q-compensation operator, given an acoustic, non-attenuating homogeneous reference medium and reflected wave field data.

In this paper we demonstrate the conceptual and numerical viability of such a construction. We discuss (1) the computation (from only the data and a homogeneous, non-attenuating Green's function) of a linear inverse that is complex, by virtue of viscous impedance contrasts; and (2) substitution of this linear inverse into a subseries postulated to be for the construction of a Q-compensation operator. We review the inverse scattering subseries identified as being involved

with the correction of propagation-based, or, glibly, durational, effects in a measured wave field; we furthermore review the mathematical traits of an operator that has the numerical wherewithal to accomplish the un-smoothing required for Q-compensation. A simple 1D normal-incidence seismic reflection experiment is used to demonstrate how data, attenuated and altered in phase and amplitude by complex impedance contrasts, may effect to non-linearly interact with itself to produce just such an operator. Several numerical examples involving a layered attenuating medium are illustrated; clear evidence of compensation is visible, as is marked effects of the "leading-order" nature of this non-linear procedure.

1.1 Q issues in the context of M-OSRP research

The research described in this paper continues in the strategic vein at M-OSRP of isolating issues of added complexity. In other words, if Q (in this case) is the *only* parameter of consequence in the chosen model, then all of the complexity arising in the non-linear machinations of the forward and inverse scattering series that follow are immediately identifiable as being due to, or being required because of, Q.

In this year's annual report we see a variety of enhancements to the complexity of the model in our developing non-linear methods: moving a one parameter acoustic imaging algorithm from 1D to 2D (Liu et al., 2004) but not adding parameters; moving a target identification algorithm from one acoustic to two acoustic and three elastic parameters, but not adding dimensions (Zhang and Weglein, 2005). A real world application will be a combination of all these generalizations, and a synthesis of this research will accommodate them, once the items to be synthesized are understood in isolation. It is important to view each element of this research effort both on its own and in light of its sister projects.

The development of this paper envisions a "data-in, data-out" type of final algorithm. The theory, as with all current descriptions of primary-processing algorithms within the scope of the inverse scattering series, most often involves the linear inverse, presently, in this paper, designated $\beta_1(z)$ and considered in the pseudo-depth domain. The linear inverse is directly computed from the "input data", and the "output data" is computed directly from the result of the non-linear operations upon $\beta_1(z)$, namely $\beta_{LOQC}(z)$. Schematically, we will consider

$$\begin{aligned} &D_{in}(\omega) \rightarrow \beta_1(z) \quad \text{linear,} \\ &\beta_1(z) \rightarrow \beta_{LOQC}(z) \quad \text{non-linear,} \\ &\beta_{LOQC}(z) \rightarrow D_{out}(\omega) \quad \text{linear.} \end{aligned} \tag{1}$$

2 Review

The postulate of Innanen and Weglein (2003) is that the inverse scattering series mechanisms so far used as a means to locate reflectors in depth, from data amplitudes and a simple homogeneous reference medium only, are doing this task, and only this task, because in the problems chosen, *misplacement of reflectors* is the only durational "effect of propagation" to be corrected for. If we are faced with a further effect, like attenuation, then similar subseries forms, similar mechanisms, will be by assumption involved with its correction.

Portions of the inverse scattering series that concern themselves with the processing and inversion of reflected primaries have been identified (Weglein et al., 2003) by generating the inverse scattering series entire, in which into the Born series representation of a scattered wave field $\psi_{\mathbf{s}}$ (in terms of a Green's operator $\mathbf{G_0}$ and scattering operator $\mathbf{V}$)

$$\psi_{\mathbf{s}} = \mathbf{G_0 V G_0} + \mathbf{G_0 V G_0 V G_0} + ..., \tag{2}$$

is substituted a series representation of $\mathbf{V}$ in increasing orders in the measured scattered field. This leads to a prescription for the order-by-order solution for $\mathbf{V}$. In a 1D constant density acoustic medium, $\mathbf{V}$ may be replaced by a wavespeed perturbation $\alpha(z) = 1 - c_0^2/c^2(z)$, and solved for as $\alpha = \alpha_1 + \alpha_2 + \alpha_3 + ...$ Task-specific analysis and algorithm development then involves separating this series into components that are deemed to be significant in the context of seismic processing objectives. We next review one of these components.

2.1 Direct non-linear imaging

First we review the leading order imaging subseries of Shaw (2005). With the linear inverse $\alpha_1(z)$ having been computed directly in terms of the data amplitudes as described in the above reference, we compute an imaged output $\alpha_{LI}(z)$ whose discontinuities are correctly re-located in depth with no change in amplitude (i.e., no beyond-linear parameter estimation) from input to output.

$$\begin{aligned}
\alpha_{LI}(z) &= \sum_{n=0}^{\infty} \frac{(-1/2)^n}{n!} \alpha_1^{(n)}(z) \left[\int_0^z \alpha_1(z')dz' \right]^n \\
&= \int_{-\infty}^{\infty} e^{ikz} \sum_{n=0}^{\infty} \frac{1}{n!} \left(\frac{ik}{2} \int_0^z \alpha_1(z')dz' \right)^n \alpha_1(k)dk \\
&= \int_{-\infty}^{\infty} e^{ik\left[z - \frac{1}{2}\int_0^z \alpha_1(z')dz'\right]} \alpha_1(k)dk \\
&= \alpha_1 \left(z - \frac{1}{2} \int_0^z \alpha_1(z')dz' \right).
\end{aligned} \tag{3}$$

Should α_1 be complex instead of fully real, the last step is brought into question because a complex α_1 affects the convergence of the integral. We avoid this in what follows by working always with the second-to-last expression above, namely:

$$\alpha_{LI}(z) = \int_{-\infty}^{\infty} e^{ik\left[z - \frac{1}{2}\int_0^z \alpha_1(z')dz'\right]} \alpha_1(k)dk, \tag{4}$$

and working to form numerically stable approximations of the integrand.

2.2 Ill-conditioned "un-smoothing" problems

We next consider ill-conditioned deconvolution, which is a class of problems that includes *Q-compensation with known Q* (e.g., Song and Innanen, 2002). It will be useful to be able to recognize

the mathematical traits of such a problem in this note. Consider first a general forward convolution problem of the form:

$$d_{\Delta T}(z) = M_{\Delta T}(z) * d_0(z) = \int_{-\infty}^{\infty} M_{\Delta T}(z - z')d_0(z')dz', \tag{5}$$

where $d_{\Delta T}$ is the distribution in z of a variable parameterized by ΔT (e.g., the spatial distribution of temperature in a rod after time ΔT); d_0 is an input variable (e.g., the spatial distribution of temperature in the rod at time zero), and $M_{\Delta T}$ relates the two. Let us consider an integrable kernel, that obeys

$$\int_{-\infty}^{\infty} |M_{\Delta T}(k)|^2 dk < \infty, \tag{6}$$

in the domain conjugate to z; to satisfy this $M(k)$ must not increase as $k \to \infty$. In a problem with a diffusive component, like heat flow, continuation of potential fields, and absorptive-dispersive propagation, these kernels in fact decay, often rapidly. The inverse problem, in which we deconvolve this function, assuming we know it, from $d_{\Delta T}$ (e.g., to reconstruct the original temperature distribution in the rod), is then expressible as:

$$d_0(z) = M_{\Delta T}^{-1}(z) * d_{\Delta T}(z) = \frac{1}{2\pi} \int_{-\infty}^{\infty} e^{ikz} \frac{d_{\Delta T}(k)}{M_{\Delta T}(k)} dk, \tag{7}$$

since a convolution problem is inverted by spectral division in the conjugate (k) domain. The reciprocal of a function that we have determined to be decaying with k will obviously be increasing with k. The wavenumber components of the operator $1/M_{\Delta T}(k)$, i.e. its singular values, increase with increasing wavenumber. This is characteristic of problems involving the removal of smoothing effects – large wavenumbers have been preferentially suppressed, so to recover the original signal they must be preferentially magnified. The condition number, or ratio of largest to smallest singular values of such an operator is generally very large, leading to the categorization of $1/M_{\Delta T}(k)$ as ill-conditioned. All instances of absorption-compensation fall into this category: the well-known sensitivity to incoherent noise of the method is due to this characteristic. Seeing a form like that of equation (7) appear in our analysis of a potential Q compensation via the inverse scattering series (ISS) would be encouraging and permit comparative statements to be made.

2.3 Complex data and complex linear perturbations

We consider seismic data that has arisen due to interactions of an incident field with complex impedance contrasts. For this note, consider reference and non-reference dispersion relations

$$k = \frac{\omega}{c_0}, \quad K_n = \frac{\omega}{c_0}\left(1 + \frac{i}{2Q_n}\right), \tag{8}$$

that is a 1D normal incidence experimental framework, where deviations from reference involve contrasts in Q only, and in which the Q model chosen is a simple friction model (e.g., Aki and Richards, 2002) involving no dispersion. In this case the requisite perturbation operator $V = k^2 - K^2$ will contain variations in a single parameter, and have both real and imaginary components. We consider the perturbation

$$k^2\beta(z) = 1 - \frac{K^2(z)}{k^2} = k^2\left(\frac{i}{2Q(z)} - \frac{1}{4Q^2(z)}\right). \tag{9}$$

Reflection coefficients $R_n = (K_{n-1} - K_n)/(K_{n-1} + K_n)$ resulting from interactions with contrasts in this medium are complex, and the associated data are imprinted in its phase and amplitude by these impedance contrasts. We, for the time being, make the assumption that (whatever model one has chosen) the phase/amplitude imprinting of R_n within the data record is sufficient to reconstruct the "complex data" that $R_n \in \mathcal{C}$ implies.

The mathematics of the linear absorptive/dispersive inverse relationship reveals that in the presence of complex data D, the complexity is directly transferred to estimated parameter distribution. Solving the single parameter 1D normal incidence linear inverse problem (with a causal 1D acoustic constant density Green's function G_0 characterized by wavespeed c_0, a plane incident wave ψ_0, and scattered wave field data D), given by

$$D(z_g|z_s;\omega) = \int_{-\infty}^{\infty} G_0(z_g|z';\omega)k^2\beta_1(z')\psi_0(z'|z_s;\omega)dz', \tag{10}$$

for the linear component of a perturbation in Q only (i.e. in which the medium has wavespeed c_0 everywhere), we have

$$\beta_1(z) = 4\int_0^z D(z')dz', \qquad \beta_1, D \in \mathcal{C}. \tag{11}$$

The linear inverse $\beta_1(z)$ will act as input to the Q-compensation mechanisms of the inverse scattering series.

3 Leading order Q-compensation

The similarity of the mathematics of the inverse scattering series terms for processing primaries in the presence and/or absence of complex V_1 means that we can follow exactly the manipulations of Shaw, and write down a candidate set of terms:

$$\begin{aligned}\beta_{LOQC}(z) &= \sum_{n=0}^{\infty} \frac{(-1/2)^n}{n!}\beta_1^{(n)}(z)\left(\int_0^z \beta_1(z')dz'\right)^n. \\ &= \int_{-\infty}^{\infty} e^{ik\left[z-\frac{1}{2}\int_0^z \beta_1(z')dz'\right]}\beta_1(k)dk,\end{aligned} \tag{12}$$

following equation (4) in the second step.

The conjecture of Innanen and Weglein leads us to look to this relationship as the first step to understanding how the ISS might operate to correct for the attenuative effects of Q without ever determining Q itself. We may make some preliminary comments about the form of this summed subseries to that end.

1. Equation (12) operates without knowing or determining non-reference parameters. The only input is β_1, which is computed directly from the data and reference Green's operators.

2. Since events in the data record from an experiment with $1/Q \neq 0$ are smoothed, so too will $\beta_1(z)$ be smoothed, since the two quantities are related by an integral. The objective of a Q compensation subseries must be to unsmooth $\beta_1(z)$, boosting its large-wavenumber components appropriately.

3. Equation (12) has the ability, at least mechanically, to reinstate decayed large wavenumber signal components. Notice that if $\beta_1 \in \mathcal{C}$, the exponential operator acting on $\beta_1(k)$ has a component similar to the ill-conditioned $1/M_{\Delta T}(k)$ of equation (7).

4. This summed subseries boosts large wavenumber components of $\beta_1(k)$, in computing the output at a given z. It does so using an operator that, rather than relying on a known distribution of Q values (as in standard Q compensation) contains the cumulative (integrated) complex linear perturbation down to that z. This implies a Q processing framework, in which nonlinear communication between data events interrogates the amplitudes of the data for complex, Q-corrective information.

In this paper we will rely on numerical tests of equation (12) to validate this last statement.

4 Numeric examples

Here I illustrate some numerical tests of the algorithm implied by equation (12). Representing the complex linear inverse as $\beta_1 = \beta_{1R} + i\beta_{1I}$, we approximate the operator in equation (12) by

$$e^{ik\left[z-\frac{1}{2}\int_0^z \beta_1(z')dz'\right]} \approx e^{ik\left[z-\frac{1}{2}\int_0^z \beta_{R1}(z')dz'\right]} \left(W_g(k) e^{\frac{k}{2}\int_0^z \beta_{I1}(z')dz'}\right), \tag{13}$$

truncating the highest wavenumber components with a shouldered gate function W_g, that is defined to be a boxcar function convolved with a Gaussian, normalized to unit height. This function may be altered using the width of the gate and the variance of the Gaussian as appropriate given an estimate of ambient noise level, etc. For the current effort, in which no noise is included, the cutoff is kept very high, excluding only the largest singular values of the operator.

Figure 1a contains an example data set associated with a 1D normal incidence experiment, in which waves propagate everywhere with $c_0 = 1500$m/s, and contrasts are permitted in Q only. The reference medium is non-attenuative. Figure 1b illustrates the associated $\beta_1(z)$. The smoothing and attenuation of the lower interfaces is clear. Figure 1c illustrates the derivative of $\beta_1(z)$ plotted against the first derivative of its non-attenuated companion (i.e. what we would like β_1 to be transformed into after compensation).

Figures 2, 3 and 4 illustrate the effect of the LOQC series on the three events that have experienced attenuation.

A significant level of Q-compensation is noticeable within these events. The 'leading order' nature of the subseries is also noticeable, however, in the differences yet present between the LOQC results and the 'perfect' benchmark.

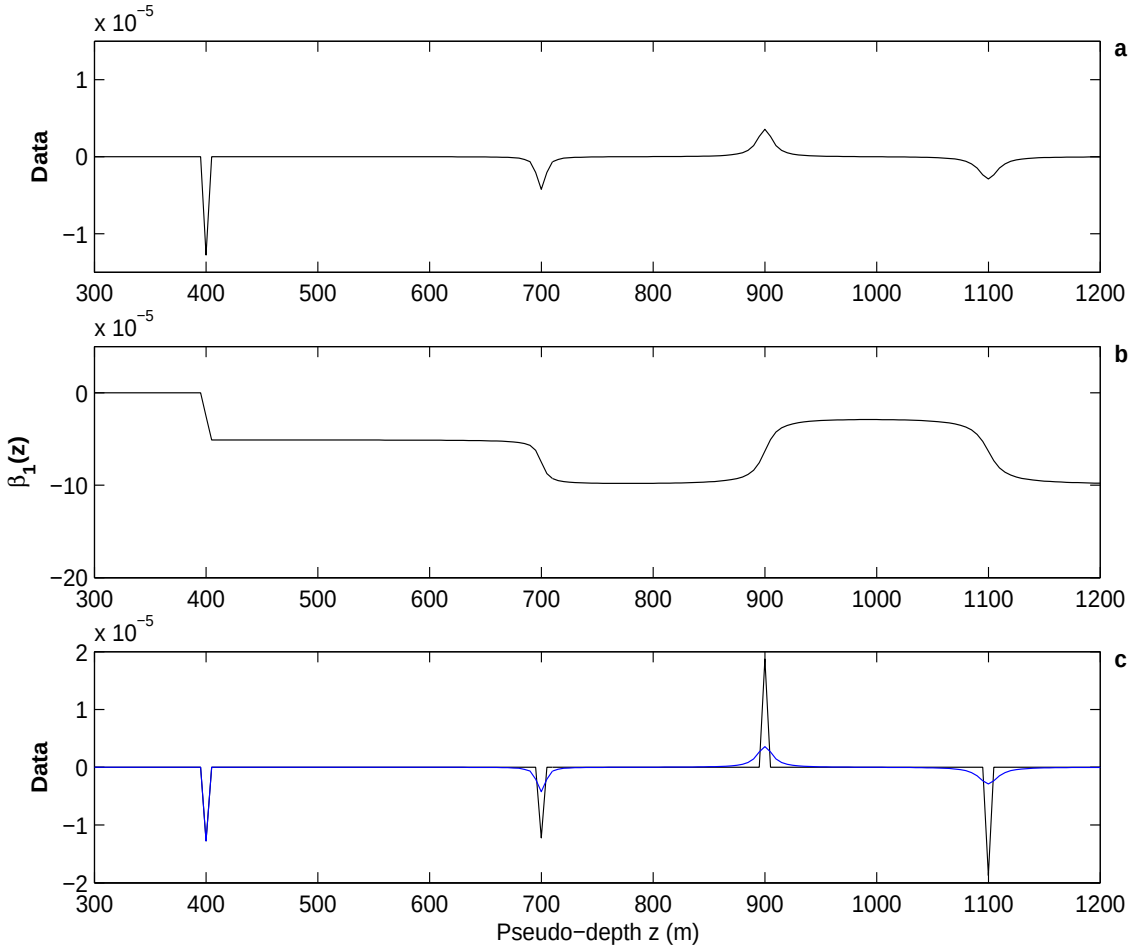

Figure 1: *Input data and linear inverse example. (a) Input data from 4-layer example: lower three events are strongly attenuated by layer Q. (b) Imaginary component of the linear inverse $\beta_1(z)$: reconstructed contrasts are smoothed as linear inversion with acoustic reference attempts no Q compensation. (c) Input data (blue) plotted against corresponding data with attenuation exactly removed (black): the goal of Q compensation will be to make the blue signal resemble the black signal as closely as possible. Using ISS methods this will be attempted with no knowledge or determination of the layer Q values.*

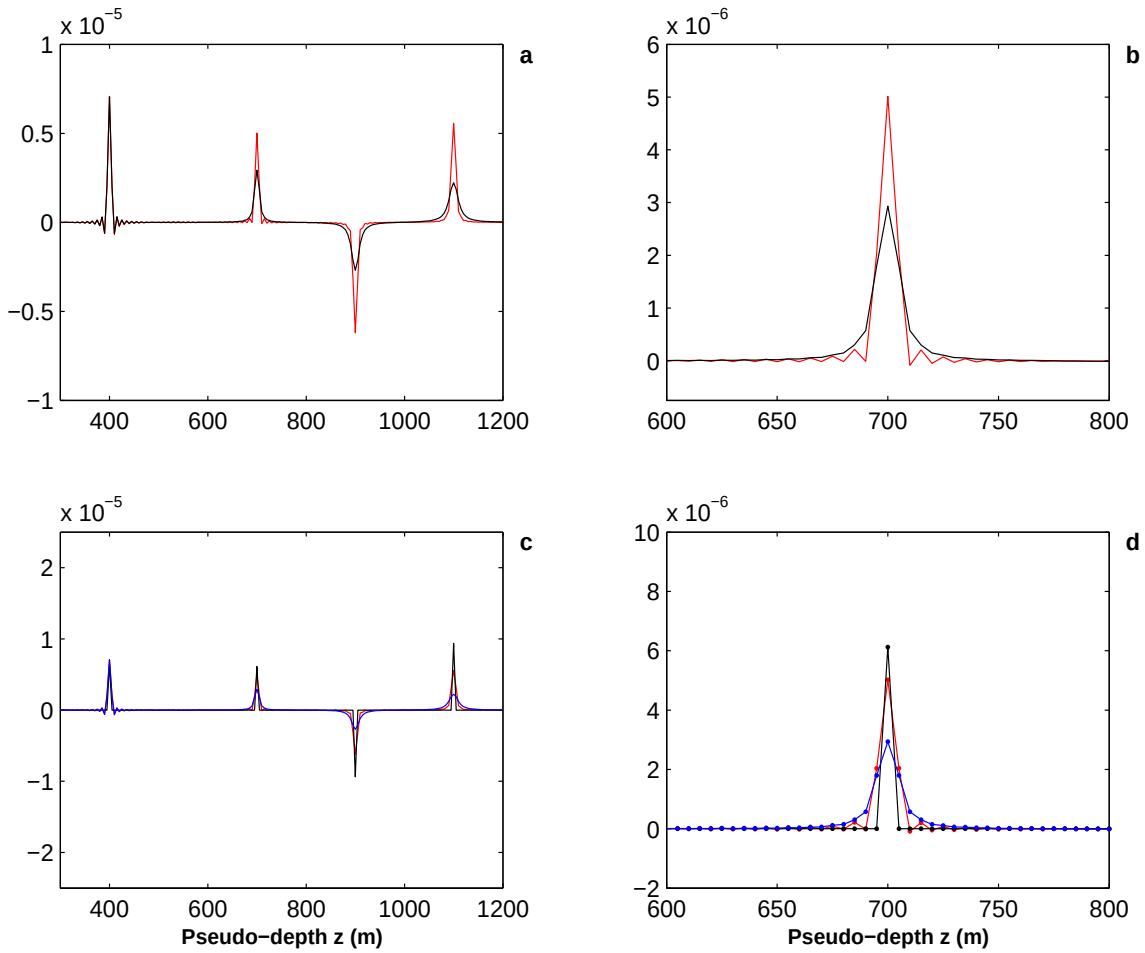

Figure 2: *Leading order Q compensation example. (a) Attenuated data record (black) plotted against* $0.25 \times \beta'_{LOQC}(z)$*, i.e. the Q compensated result transformed into data space (red); (b) detail of* (a) *at first event; (c) data record (blue) vs. un-attenuated data (black) vs. LOQC result (red); (d) detail of* (c) *at first event. A strong level of correction is noted: the difference between black and red in* (d) *illustrates the leading-order nature of this algorithm.*

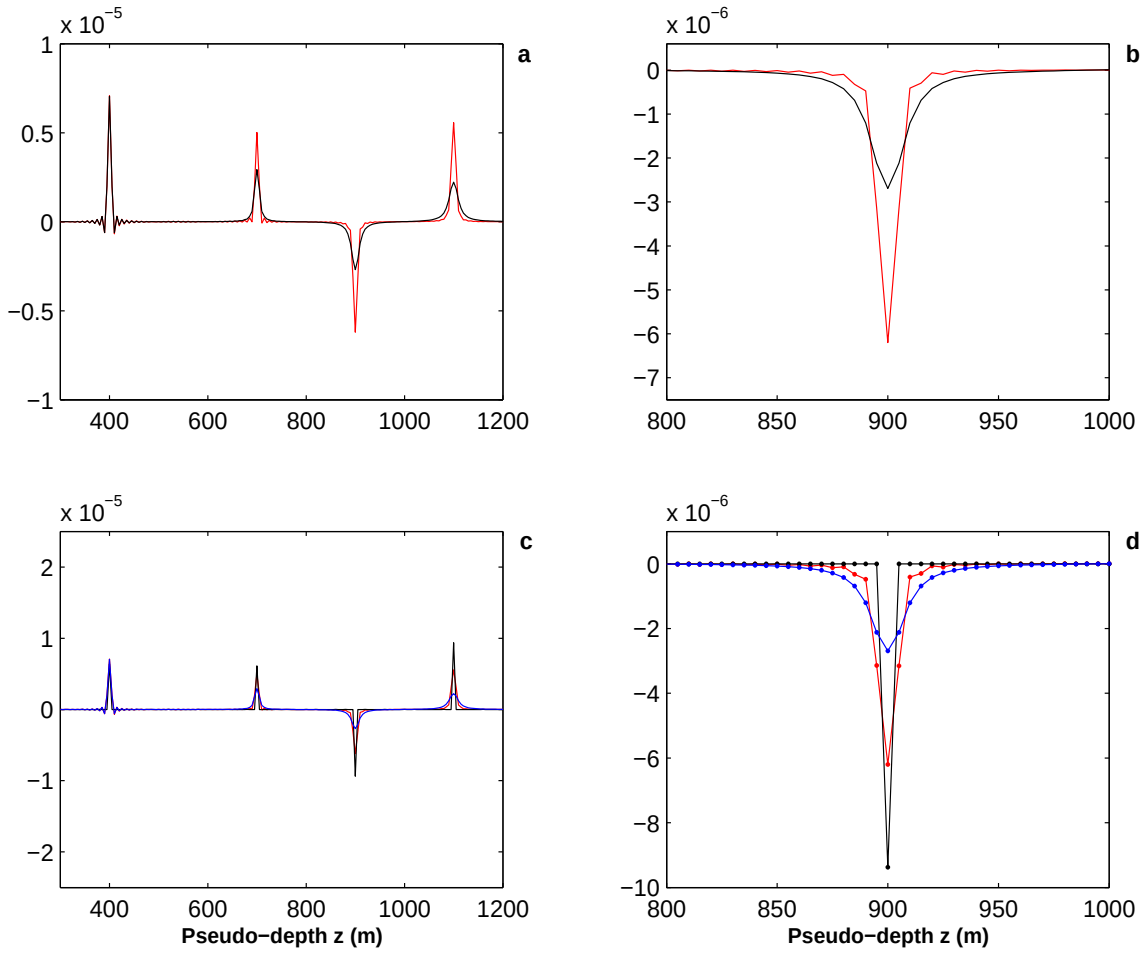

Figure 3: *Leading order Q compensation example. (a) Attenuated data record (black) plotted against* $0.25 \times \beta'_{LOQC}(z)$*, i.e. the Q compensated result transformed into data space (red); (b) detail of* (a) *at second event; (c) data record (blue) vs. un-attenuated data (black) vs. LOQC result (red); (d) detail of* (c) *at second event. A strong level of correction is noted: the difference between black and red in* (d) *illustrates the leading-order nature of this algorithm.*

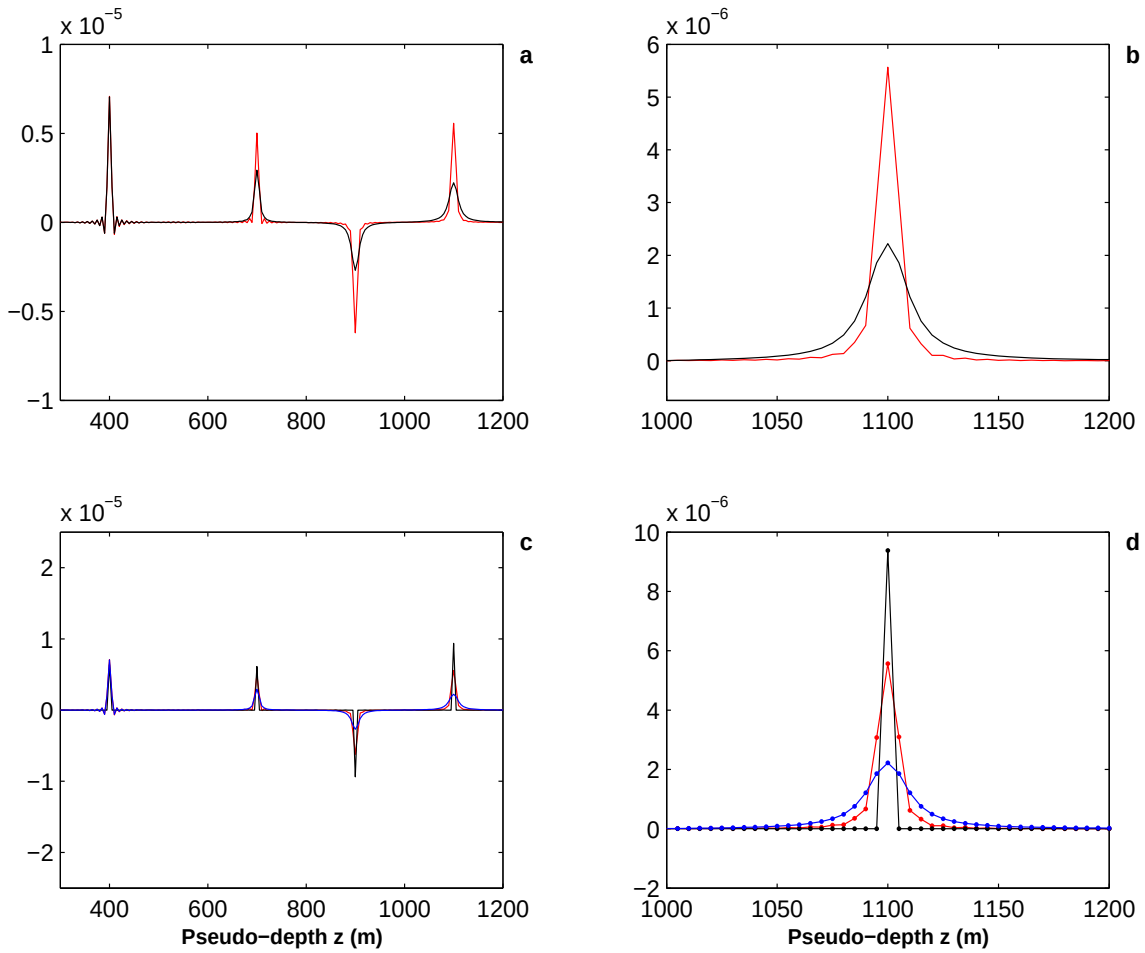

Figure 4: *Leading order Q compensation example. (a) Attenuated data record (black) plotted against* $0.25 \times \beta'_{LOQC}(z)$*, i.e. the Q compensated result transformed into data space (red); (b) detail of* (a) *at third event; (c) data record (blue) vs. un-attenuated data (black) vs. LOQC result (red); (d) detail of* (c) *at third event. A strong level of correction is noted: the difference between black and red in* (d) *illustrates the leading-order nature of this algorithm.*

5 Conclusions

We have presented a mechanism for, and some preliminary numerical tests of, the non-linear construction of a Q compensation operator directly in terms of an attenuated data set.

The aims and plans for development of these ideas and algorithms are as follows. First, the underlying theory involves fully 3D media: ideally, the development of the Q-compensation operator will fully realize this multidimensional potential. To that end, the lessons gleaned from the multidimensional form of the imaging subseries, which, as we have noted, are driven by the same mathematical mechanisms as those which construct the Q operator, will be applicable here (Liu et al., 2004). Secondly, the "leading-order" nature of this operator construction is visible in the accuracy, or completeness, of the compensation, at lower contrasts than in the case of the imaging or reflector location incarnation of the series. This suggests that the greatest efficacy may stem from the development of the high-order imaging terms as applied to this problem.

Finally, a gulf exists between this current development and a form that genuinely fits into the "Q-compensation" idiom (e.g. Hargreaves and Calvert, 1991; Song and Innanen, 2002). This is because at present it is rudimentary in its ability to act as a data $\rightarrow$ data mapping. Ultimately, the same level of effectiveness that currently exists in the free-surface multiple elimination and internal multiple attenuation methods is sought: in particular, (to as great an extent as possible) that a model-type independent algorithm, acting directly on an input data set, outputs, directly, a Q-compensated data set.

6 Acknowledgments

The authors gratefully acknowledge the support of the sponsors and personnel of M-OSRP (University of Houston) and CDSST (University of British Columbia).

References

[Aki, 2002] Aki, K. and Richards, P. G., Quantitative Seismology, 2002: *University Science Books*, (2002): 2nd Ed.

[Hargreaves and Calvert, 1991] Hargreaves, N. D. and Calvert, A. J., Inverse Q-filtering by Fourier transform, 1991: Geophysics **56**, 519–527.

[Innanen and Weglein, 2003] Innanen, K. A. and Weglein, A. B., Construction of Absorptive/Dispersive Wave Fields with the Forward Scattering Series, 2003: Journal of Seismic Exploration, **12**, 259–282.

[Innanen and Weglein, 2004] Innanen, K. A. and Weglein, A. B., Linear inversion for absorptive/dispersive medium parameters, 2004: Proceedings of the Society of Explorational Geophysicists/Denver 2004 International Exposition and 74th Annual Meeting.

[Liu et al., 2004] Liu, F., Nita, B., Weglein, A. B., and Innanen, K. A., Inverse scattering series for vertically and laterally varying media, 2004: *M-OSRP 04 Annual Report*.

[Shaw, 2005] Shaw, S. A., An inverse scattering series algorithm for depth imaging of reflection data from a layered acoustic medium with an unknown velocity model, 2005: Ph.D. Thesis, University of Houston.

[Song and Innanen, 2002] Song, S. G. and Innanen, K. A., Multiresolution modeling and wavefield reconstruction in attenuating media, 2002: Geophysics **67**, 1192–1201.

[Weglein, 2003] Weglein, A. B., Araujo, F. A., Carvalho, P. M., Stolt, R. H., Matson, K. H., Coates, R., Foster, D. J., Shaw, S. A., and Zhang, H., Topical Review: Inverse-scattering Series and Seismic Exploration, 2003: Inverse Problems, **19**, R27–R83.

[Zhang and Weglein, 2005] Zhang, H., and Weglein, A. B., Topical Review: Inverse-scattering Series and Seismic Exploration, 2005: *M-OSRP04 Annual Report.*

The inverse scattering series for tasks associated with primaries: Depth imaging and direct non-linear inversion of 1D variable velocity and density acoustic media

Haiyan Zhang and Arthur B. Weglein

Abstract

This paper presents the first analysis, and direct depth imaging and inversion algorithms for tasks associated with primaries for a variable velocity and density acoustic medium. The method derives from the inverse scattering series, and hence assumes the actual subsurface properties governing the propagation of waves is neither known nor determined. In this first foray into the multi-parameter inverse series, we simplify the analysis by assuming earth properties are to only vary in depth, and the required data is a shot record. The depth imaging algorithm without the velocity first decides if the input velocity is adequate, and if adequate conventional migration is prescribed. If the data decides the verdict on the velocity is inadequate it acts to remove the incorrect image and constructs the correct one, without knowing or determining the velocity. Other terms in the algorithm are identified as performing non-linear direct AVO, and once again, allow the data self determination of overburden velocity adequacy, and acts accordingly to improve upon linear estimates of property changes. The role of velocity is clarified, as central and all-important in location, in that only an incorrect velocity causes a depth imaging response from the series, independent of how you parameterize the acoustic problem, or what error other properties might suffer. Benefit of non-linear direct inversion is demonstrated over linear standard procedure, for a set of examples using analytic and numerical techniques. The common problem of linear "leaking" between linear property change predictions is also addressed by the series, and located and analyzed in this paper.

1 Introduction

The ultimate objective of inverse problems is to determine medium and target properties from measurements external to the object under investigation. At the very first moment of problem definition, there is an immediate requirement and unavoidable expectation, that the model type of the medium be specified. In that step of model type specification, the number and type of parameters and dimension of spatial variation of those parameters are given, and carefully prescribed, and in that way you provide the inverse problem with clarity and meaning. Among the different model types used in exploration seismology are, e.g., acoustic, elastic, heterogeneous, anisotropic, and anelastic, and perhaps most important, the dimension of variability of the properties associated with these model types. One would reasonably expect that the details of methods and algorithms for inversion objectives, and any tasks associated with achieving those ultimate objectives, would overall and each separately depend upon that starting assumption on model type. However, the ultimate objective of seismic inversion has never been achieved in a straight ahead single step manner directly from the seismic data, and that lack of success has not been due to a lack of computer power. The indirect model matching procedures have that computer power problem, especially in

the applications to a multi-dimensional complex earth, where it is rare to have a reasonable proximal starting model. Those complex ill-defined geologic circumstances are the biggest impediments and challenges to current exploration and production seismic effectiveness.

The only direct multi-dimensional inversion procedure for seismic application, the inverse scattering series (ISS), does not require a proximal starting model and only assumes reference medium information. Of course, the whole inverse series has very limited application (Matson, 1997). What makes ISS powerful is the so-called task isolated subseries which is a subset of the whole series that acts like only one task is performed for that subset (Weglein et al., 2003). All of these subseries act in a certain sequence so that the total seismic data can be processed accordingly. The order of processing is (1) free surface multiple removal (2) internal multiple removal (3) imaging and (4) inversion. The free surface multiple removal and internal multiple attenuation subseries have been presented by Weglein et al. (1997). Those two multiple procedures are model type independent, i.e., they work for acoustic, elastic and anelastic medium. Taking internal multiples from attenuation to elimination is being studied. The task specific subseries associated with primaries (i.e., for imaging and inversion) have been progressed too (Weglein et al., 2002, Innanen, 2003, Shaw et al., 2003, Liu et al., 2005 and Shaw, 2005). Compared with model type independent multiple removal procedures, there is a full expectation that tasks and algorithms associated with primaries will have a closer interest in model type. For example, there is no way to even imagine that medium property identification can take place without reference to a specific model type. Tasks and issues associated with structural determination, without knowing the medium, are also vastly different depending on the dimension of variation number of velocities that are required for imaging. Hence, a staged approach and isolation of tasks philosophy is essential in this yet tougher neighborhood, and even more in demand for seeking insights and then practical algorithms for these more complicated and daunting objectives. We adopt the staged and isolation of issues approach for primaries. The isolated task achievement plan can often spin-off incomplete but useful intermediate objectives. The test and standard is not necessarily how complete the method is but rather how does it compare to, and improve upon, current best practice.

The stages within the strategy for primaries are as follows: (1) 1D earth, with one parameter, velocity as a function of depth, and a normal incidence wave, (2) 1D earth with one parameter subsurface and offset data, one shot record; (3) 2D earth with one parameter, velocity, varying in x and z, and a suite of shot records; (4) 1D acoustic earth with two parameters varying, velocity and density, one propagation velocity, and one shot record of PP data, and (5) 1D elastic earth, two elastic isotropic parameters and density, and two wave speeds, for P and S waves, and PP, PS, SP, and SS shot records data collected. This paper takes the first step of direct non-linear inversion methodology, and task isolation and specifically for tasks associated with primaries, into a world of more that one property changing, stage (4). The model is acoustic and a second paper in this set generalizes this for the elastic case. We take these steps and learn to navigate through this complexity and steer it towards useful and powerful algorithms.

In this paper, for the first time, a two-parameter direct non-linear inversion solution is obtained for 1D acoustic media 2D experiment. From this solution, the tasks for imaging-only and inversion-only terms are separated successfully. Tests with analytic data indicate significant added value, beyond linear estimates, in terms of both the proximity to actual value and the increased range of angles over which the improved estimates are useful.

A closed form of the inversion terms for one interface case is also obtained. This closed form would

be very useful in predicting the precritical data using the postcritical data.

We also found a special parameter Δc ($\Delta c = c - c_0$), i.e., P-velocity change across an interface. Its born inversion $(\Delta c)_1$ always has the right sign. That is, the sign of $(\Delta c)_1$ is same as that of Δc. After exchanging the parameters, we got another form of the non-linear solution. There would be no leakage correction at all in this solution. And it obviously indicates that the imaging terms care only about velocity changes. The mislocation is due to the wrong velocity. This is suggestive of possible generalization to multi-D medium, also of possible model type independent imaging which only depends on velocity changes.

The paper has the following structure: Section 2 is a brief introduction to the inverse scattering series. In section 3 we show the derivation in detail and then derive the closed form followed by numerical tests. Last section contains further discussions about the special parameters and conclusions.

2 Inverse scattering series

Consider the basic wave equations (Weglein et al., 2003)

$$LG = \delta, \tag{1}$$

$$L_0 G_0 = \delta, \tag{2}$$

where L and L_0 are respectively the differential operators that describe wave propagation in the actual and reference medium, and G and G_0 are the corresponding Green's functions.

We define the perturbation $V = L_0 - L$ (Weglein et al., 2002). The Lippmann- Schwinger equation,

$$G = G_0 + G_0 V G, \tag{3}$$

relates G, G_0 and V (see, e.g., Taylor, 1972). Iterating this equation back into itself generates the Born series

$$G = G_0 + G_0 V G_0 + G_0 V G_0 V G_0 + \cdots . \tag{4}$$

Then the scattered field $\psi_s \equiv G - G_0$ can be written as

$$\begin{aligned} \psi_s &= G_0 V G_0 + G_0 V G_0 V G_0 + \cdots \\ &= (\psi_s)_1 + (\psi_s)_2 + \cdots , \end{aligned} \tag{5}$$

where $(\psi_s)_n$ is the portion of ψ_s that is n^{th} order in V. The measured values of ψ_s are the data, D, where

$$D = (\psi_s)_{ms} = (\psi_s)_{\text{on the measurement surface}}.$$

Expanding V as a series in orders of D (Weglein et al., 1997)

$$V = V_1 + V_2 + \cdots , \tag{6}$$

then substituting (6) into (5) and evaluating (5) on the measurement surface yields

$$D = [G_0(V_1 + V_2 + \cdots)G_0]_{ms} + [G_0(V_1 + V_2 + \cdots)G_0(V_1 + V_2 + \cdots)G_0]_{ms} + \cdots . \tag{7}$$

Setting terms of equal order in the data equal, leads to the equations that determine V_1, V_2, ... directly from D and G_0.

$$D = [G_0 V_1 G_0]_{ms}, \tag{8}$$

$$0 = [G_0 V_2 G_0]_{ms} + [G_0 V_1 G_0 V_1 G_0]_{ms}, \tag{9}$$

$$\begin{aligned} 0 =& [G_0 V_3 G_0]_{ms} + [G_0 V_1 G_0 V_2 G_0]_{ms} + [G_0 V_2 G_0 V_1 G_0]_{ms} \\ &+ [G_0 V_1 G_0 V_1 G_0 V_1 G_0]_{ms}, \end{aligned} \tag{10}$$

$$\vdots$$

Equations (8)–(10) calculate V_1, V_2, ..., and hence achieve full inversion for V (see eq. (6)) from the recorded data D (with free surface and internal multiples) and the Green's function of the reference medium G_0.

3 Derivation of α_1, β_1 and α_2, β_2

To illustrate task (4), we will consider a 1D acoustic two-parameter earth model (e.g. bulk modulus and density or velocity and density). We start with the 3D acoustic wave equations in the actual and reference medium (Clayton and Stolt, 1981, Weglein et al., 1997)

$$\left[\frac{\omega^2}{K(\mathbf{r})} + \nabla \cdot \frac{1}{\rho(\mathbf{r})}\nabla\right] G(\mathbf{r}, \mathbf{r}_s; \omega) = \delta(\mathbf{r} - \mathbf{r}_s), \tag{11}$$

$$\left[\frac{\omega^2}{K_0(\mathbf{r})} + \nabla \cdot \frac{1}{\rho_0(\mathbf{r})}\nabla\right] G_0(\mathbf{r}, \mathbf{r}_s; \omega) = \delta(\mathbf{r} - \mathbf{r}_s), \tag{12}$$

where $G(\mathbf{r}, \mathbf{r}_s; \omega)$ and $G_0(\mathbf{r}, \mathbf{r}_s; \omega)$ are respectively the free-space causal Green's operators that describe wave propagation in the actual and reference medium. $K = c^2\rho$, is P-bulk modulus, c is P-wave velocity and ρ is the density. Those quantities with subscript "0" are for the reference medium, and, those without the subscript are for the actual medium. Then the perturbation is

$$V = L_0 - L = \frac{\omega^2 \alpha}{K_0} + \nabla \cdot \frac{\beta}{\rho_0}\nabla, \tag{13}$$

where $\alpha = 1 - \frac{K_0}{K}$, $\beta = 1 - \frac{\rho_0}{\rho}$. Assuming both ρ_0 and c_0 are constants, eq. (12) becomes

$$\left(\frac{\omega^2}{c_0^2} + \nabla^2\right) G_0(\mathbf{r}, \mathbf{r}_s; \omega) = \rho_0 \delta(\mathbf{r} - \mathbf{r}_s), \tag{14}$$

and for the 1-D case, the perturbation V has the following form

$$V(z, \nabla) = \frac{\omega^2 \alpha(z)}{K_0} + \frac{1}{\rho_0}\beta(z\frac{\partial^2}{\partial x^2} + \frac{1}{\rho_0}\frac{\partial}{\partial z}\beta(z)\frac{\partial}{\partial z}. \tag{15}$$

We expand $V(z, \nabla)$, $\alpha(z)$ and $\beta(z)$ respectively as

$$V(z, \nabla) = V_1(z, \nabla) + V_2(z, \nabla) + \cdots, \tag{16}$$

$$\alpha(z) = \alpha_1(z) + \alpha_2(z) + \cdots, \tag{17}$$

$$\beta(z) = \beta_1(z) + \beta_2(z) + \cdots. \tag{18}$$

Then we have

$$V_1(z,\nabla) = \frac{\omega^2\alpha_1(z)}{K_0} + \frac{1}{\rho_0}\beta_1(z)\frac{\partial^2}{\partial x^2} + \frac{1}{\rho_0}\frac{\partial}{\partial z}\beta_1(z)\frac{\partial}{\partial z}, \tag{19}$$

$$V_2(z,\nabla) = \frac{\omega^2\alpha_2(z)}{K_0} + \frac{1}{\rho_0}\beta_2(z)\frac{\partial^2}{\partial x^2} + \frac{1}{\rho_0}\frac{\partial}{\partial z}\beta_2(z)\frac{\partial}{\partial z}, \tag{20}$$

$$\vdots$$

Substituting (19) into (8), we can get the linear solution for α_1 and β_1 in frequency domain

$$\widetilde{D}(q_g,\theta,z_g,z_s) = -\frac{\rho_0}{4}e^{-iq_g(z_s+z_g)}\left[\frac{1}{\cos^2\theta}\widetilde{\alpha_1}(-2q_g) + (1-\tan^2\theta)\widetilde{\beta}_1(-2q_g)\right], \tag{21}$$

where the subscripts s and g denote source and receiver quantities respectively, and q_g, θ and $k = \omega/c_0$ shown in Figure 1, have the following relations (Matson, 1997)

$$q_g = q_s = k\cos\theta,$$

$$k_g = k_s = k\sin\theta.$$

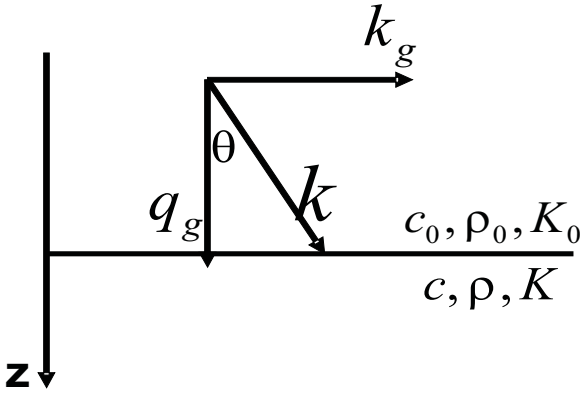

Figure 1: *The relationship between q_g, k_g and θ.*

Similarly, substituting (20) into (9), we can get the solution for $\alpha_2(z)$ and $\beta_2(z)$ as a function of $\alpha_1(z)$ and $\beta_1(z)$

$$\begin{aligned}\frac{1}{\cos^2\theta}\alpha_2(z) + (1-\tan^2\theta)\beta_2(z) = &-\frac{1}{2\cos^4\theta}\alpha_1^2(z) - \frac{1}{2}(1+\tan^4\theta)\beta_1^2(z) + \frac{\tan^2\theta}{\cos^2\theta}\alpha_1(z)\beta_1(z)\\ &- \frac{1}{2\cos^4\theta}\alpha_1'(z)\int_0^z dz'[\alpha_1(z') - \beta_1(z')]\\ &+ \frac{1}{2}(\tan^4\theta - 1)\beta_1'(z)\int_0^z dz'[\alpha_1(z') - \beta_1(z')],\end{aligned} \tag{22}$$

where $\alpha_1'(z) = \frac{\mathrm{d}\alpha_1(z)}{\mathrm{dz}}$, $\beta_1'(z) = \frac{\mathrm{d}\beta_1(z)}{\mathrm{dz}}$.

We have obtained the first two parameter direct non-linear inversion of 1D acoustic media for a 2D experiment. As shown in (21) and (22), given two different angles θ, we can determine α_1, β_1 and then α_2, β_2. For a single-interface example, we can also show that only the first three terms on the right hand side contribute to amplitude correction, while the last two terms perform imaging in depth since they will be zero after the integration across the interface. Therefore, in this solution, the tasks for imaging-only and inversion-only terms are separated successfully. If another choice of free parameter other than θ (e.g., ω or k_h) was selected, then the functional form between the data and the first order perturbation changes. Furthermore, the relationship between the first and second order perturbation is then also different, and new analysis would be required for the purpose of identifying specific task separated terms. In our experience, the choice of θ as free parameter (for a 1D medium) is particularly well suited for allowing a task separated identification of terms in the inverse series. Details about the significance of this solution will be presented in the following sections.

4 A special case: one interface model

In this section, we derive a closed form for the inversion terms. From this closed form, we can easily get the same results as those in eq. (21) and (22). We also show some numerical tests using analytic data. From the numerical results, we see how the corresponding non-linear terms contribute to the relative changes in the P-wave bulk modulus $\left(\alpha = \frac{\Delta K}{K}\right)$, density $\left(\beta = \frac{\Delta \rho}{\rho}\right)$, impedance $\left(\frac{\Delta I}{I}\right)$ and velocity $\left(\frac{\Delta c}{c}\right)$ respectively.

4.1 Closed form for the inversion terms

4.1.1 Incident angle not greater than critical angle, i.e. $\theta \leq \theta_c$

For a single interface example, the reflection coefficient has the following form (Keys, 1989)

$$R(\theta) = \frac{(\rho_1/\rho_0)(c_1/c_0)\sqrt{1-\sin^2\theta} - \sqrt{1-(c_1^2/c_0^2)\sin^2\theta}}{(\rho_1/\rho_0)(c_1/c_0)\sqrt{1-\sin^2\theta} + \sqrt{1-(c_1^2/c_0^2)\sin^2\theta}}. \tag{23}$$

Also, from the definitions of α and β we have

$$\alpha = 1 - \frac{K_0}{K_1} = 1 - \frac{\rho_0 c_0^2}{\rho_1 c_1^2},$$

and

$$\beta = 1 - \frac{\rho_0}{\rho_1}.$$

After adding 1 on both sides of (23), we can get

$$1 + R(\theta) = \frac{2\cos\theta}{\cos\theta + (\rho_0/\rho_1)\sqrt{(c_0^2/c_1^2) - \sin^2\theta}}. \tag{24}$$

Then, using the definitions of α and β, after some mathematics, (24) becomes

$$\frac{4R(\theta)}{\left(1+R(\theta)\right)^2} = \frac{\alpha}{\cos^2\theta} + (1-\tan^2\theta)\beta - \frac{\alpha\beta}{\cos^2\theta} + \beta^2\tan^2\theta, \tag{25}$$

which is the closed form we derived for two parameter case.

4.1.2 Incident angle greater than critical angle, i.e. $\theta > \theta_c$

For $\theta > \theta_c$, (23) becomes

$$R(\theta) = \frac{(\rho_1/\rho_0)(c_1/c_0)\sqrt{1-\sin^2\theta} - i\sqrt{(c_1^2/c_0^2)\sin^2\theta - 1}}{(\rho_1/\rho_0)(c_1/c_0)\sqrt{1-\sin^2\theta} + i\sqrt{(c_1^2/c_0^2)\sin^2\theta - 1}}. \tag{26}$$

Then, (24) becomes

$$1 + R(\theta) = \frac{2\cos\theta}{\cos\theta + i\,(\rho_0/\rho_1)\,\sqrt{\sin^2\theta - \left(c_0^2/c_1^2\right)}}, \tag{27}$$

which leads to the same closed form as (25)

$$\frac{4R(\theta)}{\left(1+R(\theta)\right)^2} = \frac{\alpha}{\cos^2\theta} + (1-\tan^2\theta)\beta - \frac{\alpha\beta}{\cos^2\theta} + \beta^2\tan^2\theta.$$

As we see, this closed form is valid for all incident angles. Therefore, the precritical angle data should be able to be predicted using the postcritical angle data.

In addition, for normal incidence ($\theta = 0$) and constant density ($\beta = 0$) media, the closed form (25) will be reduced to

$$\alpha = \frac{4R}{\left(1+R\right)^2}. \tag{28}$$

This represents the relationship between α and R for one parameter 1D acoustic constant density medium and 1D normal incidence obtained in (Innanen, 2003). In this case, α becomes $1 - c_0^2/c_1^2$ and R becomes $(c_1 - c_0)\,/\,(c_1 + c_0)$.

4.1.3 Derivation of the inversion terms from the closed form

From the closed form (25), using the Taylor expansion

$$\frac{1}{\left(1+R(\theta)\right)^2} = \left[1 - R(\theta) + R^2(\theta) - \ldots\right]^2$$

on the left hand side, and setting the terms of equal order in the data equal, we have

$$\frac{\alpha_1}{\cos^2\theta} + (1-\tan^2\theta)\beta_1 = 4R(\theta), \tag{29}$$

$$\frac{\alpha_2}{\cos^2\theta} + (1-\tan^2\theta)\beta_2 = -\frac{1}{2}\frac{\alpha_1^2}{\cos^4\theta} - \frac{1}{2}(1+\tan^4\theta)\beta_1^2 + \frac{\tan^2\theta}{\cos^2\theta}\alpha_1\beta_1. \tag{30}$$

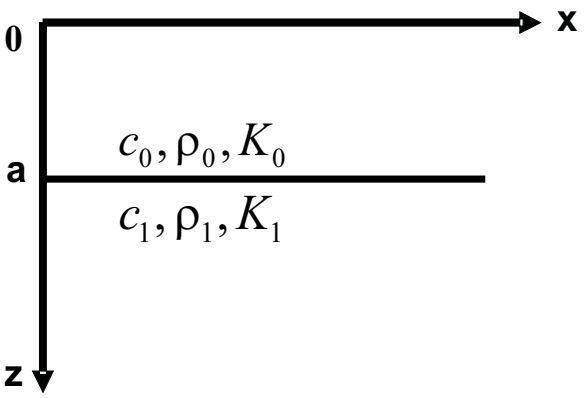

Figure 2: *1D one interface acoustic model.*

Specifically, for the one interface example (in Figure 2), we assume the interface surface is at $z = a$, and suppose $z_s = z_g = 0$.

Using perfect data (Clayton and Stolt, 1981, Weglein et al., 1986)

$$\widetilde{D}(q_g, \theta) = \rho_0 R(\theta) \frac{e^{2iq_g a}}{4\pi i q_g}, \tag{31}$$

and substituting (31) into (21), after Fourier transformation over $2q_g$, for $z > a$ and fixed θ, we get

$$\frac{1}{\cos^2\theta}\alpha_1(z) + (1 - \tan^2\theta)\beta_1(z) = 4R(\theta)H(z - a). \tag{32}$$

Also, the non-linear solution (22) will reduce to

$$\begin{aligned}\frac{1}{\cos^2\theta}\alpha_2(z) + (1 - \tan^2\theta)\beta_2(z) = &- \frac{1}{2\cos^4\theta}\alpha_1^2(z) - \frac{1}{2}(1 + \tan^4\theta)\beta_1^2(z) \\ &+ \frac{\tan^2\theta}{\cos^2\theta}\alpha_1(z)\beta_1(z),\end{aligned} \tag{33}$$

The two equations (32) and (33) agree with (29) and (30) respectively.

4.2 Numerical test

From (32), choosing two different angles to solve for α_1 and β_1

$$\beta_1(\theta_1, \theta_2) = 4\frac{R(\theta_1)\cos^2\theta_1 - R(\theta_2)\cos^2\theta_2}{\cos(2\theta_1) - \cos(2\theta_2)}, \tag{34}$$

$$\alpha_1(\theta_1, \theta_2) = \beta_1(\theta_1, \theta_2) + 4\frac{R(\theta_1) - R(\theta_2)}{\tan^2\theta_1 - \tan^2\theta_2}. \tag{35}$$

Similarly, from (33), given two different angles we can solve for α_2 and β_2 in terms of α_1 and β_1

$$\begin{aligned}\beta_2(\theta_1, \theta_2) = \Bigg[&-\frac{1}{2}\alpha_1^2\left(\frac{1}{\cos^2\theta_1} - \frac{1}{\cos^2\theta_2}\right) + \alpha_1\beta_1\left(\tan^2\theta_1 - \tan^2\theta_2\right) - \frac{1}{2}\beta_1^2 \\ &\times \left(\cos^2\theta_1 - \cos^2\theta_2 + \frac{\sin^4\theta_1}{\cos^2\theta_1} - \frac{\sin^4\theta_2}{\cos^2\theta_2}\right)\Bigg] / \left[\cos(2\theta_1) - \cos(2\theta_2)\right],\end{aligned} \tag{36}$$

$$\alpha_2(\theta_1,\theta_2) = \beta_2(\theta_1,\theta_2) + \left[-\frac{1}{2}\alpha_1^2\left(\frac{1}{\cos^4\theta_1} - \frac{1}{\cos^4\theta_2}\right) + \alpha_1\beta_1\left(\frac{\tan^2\theta_1}{\cos^2\theta_1} - \frac{\tan^2\theta_2}{\cos^2\theta_2}\right) - \frac{1}{2}\beta_1^2\left(\tan^4\theta_1 - \tan^4\theta_2\right)\right] / \left(\tan^2\theta_1 - \tan^2\theta_2\right). \quad (37)$$

Where α_1 and β_1 in (36) and (37) denote $\alpha_1(\theta_1,\theta_2)$ and $\beta_1(\theta_1,\theta_2)$ respectively.

For a specific model, $\rho_0 = 1.0g/cm^3$, $\rho_1 = 1.1g/cm^3$, $c_0 = 1500m/s$ and $c_1 = 1700m/s$. In the following figures, we gave the results for the relative changes in the P-wave bulk modulus $\left(\alpha = \frac{\Delta K}{K}\right)$, density $\left(\beta = \frac{\Delta\rho}{\rho}\right)$, impedance $\left(\frac{\Delta I}{I}\right)$ and velocity $\left(\frac{\Delta c}{c}\right)$ corresponding to different pairs of θ_1 and θ_2.

From Figure 3, we can see that when we add α_2 to α_1, the result is much closer to the exact value of α. Furthermore, the result is better behaved, i.e., the plot surface becomes flatter, over a larger range of precritical angles. Similarly, from Figure 4, we can also see the results of $\beta_1+\beta_2$ are much better than those of β_1. In addition, we can see that the sign of β_1 is wrong at some angles, while, the results for $\beta_1+\beta_2$ always have the right sign. So after including β_2, we would correct the sign of the density, which is very important in the earth identification. And also the results of $\frac{\Delta I}{I}$ (see Figure 5) and $\frac{\Delta c}{c}$ (see Figure 6) are much closer to their exact values respectively compared to the linear results.

Especially, we notice that the values of $\left(\frac{\Delta c}{c}\right)_1$ are always greater than zero, that is, the sign of $(\Delta c)_1$ is always positive, which is same as that of the exact value Δc. We will further discuss this in the next section.

5 Special parameters for linear inversion

As we mentioned before, in general, since the relationship between data and target property changes is non-linear, linear inversion will produce errors in target property prediction. When one actual property change is zero, the linear prediction of the change can be non-zero. Also, when the actual change is positive, the predicted linear approximation can be negative. There is a special parameter for linear inversion of acoustic media, that never suffers the latter problem.

From (23) we can see when $c_0 = c_1$, the reflection coefficient is independent of θ, then from the linear form (35), we have

$$\left(\frac{\Delta c}{c}\right)_1 = \frac{1}{2}(\alpha_1 - \beta_1) = 0 \text{ when } \Delta c = 0,$$

i.e., when $\Delta c = 0$, $(\Delta c)_1 = 0$. This generalizes to when $\Delta c > 0$, then $(\Delta c)_1 > 0$, or when $\Delta c < 0$, then $(\Delta c)_1 < 0$, as well. This can be shown mathematically (See Appendix B for details).

Therefore, we can, firstly, get the right sign of relative change in P-wave velocity from the linear inversion $(\Delta c)_1$, then, get more accurate amplitude when we include non-linear terms.

We also note that when the velocity doesn't change across an interface, i.e., $c_0 = c_1$, looking at the integrand of imaging terms $\alpha_1 - \beta_1$ (see (22)), the image doesn't move because $\alpha_1 - \beta_1 = 0$ in this

situation. We can see this more explicitly when we change the two parameters α and β to $\frac{\Delta c}{c}$ and β. Using the two relationships below (See details in Appendix A)

$$\left(\frac{\Delta c}{c}\right)_1 = \frac{1}{2}(\alpha_1 - \beta_1),$$

and

$$\left(\frac{\Delta c}{c}\right)_2 = \frac{1}{2}\left[\frac{1}{4}(\alpha_1 + \beta_1)^2 - \beta_1^2 + (\alpha_2 - \beta_2)\right],$$

we can rewrite (22) as

$$\begin{aligned}\frac{1}{\cos^2\theta}\left(\frac{\Delta c}{c}\right)_2(z) + \beta_2(z) =& \frac{\cos^2\theta - 2}{2\cos^4\theta}\left(\frac{\Delta c}{c}\right)_1^2(z) - \frac{1}{2}\beta_1^2(z) \\ &- \frac{1}{\cos^4\theta}\left(\frac{\Delta c}{c}\right)_1'(z)\int_0^z dz'\left(\frac{\Delta c}{c}\right)_1 \\ &- \frac{1}{\cos^2\theta}\beta_1'(z)\int_0^z dz'\left(\frac{\Delta c}{c}\right)_1. \end{aligned} \tag{38}$$

This equation tells us many interesting things. One is that there is no leakage correction at all in this expression. The other is that, when we look at the integrand $\left(\frac{\Delta c}{c}\right)_1$ of the imaging terms, it indicates obviously that if we have the right velocity, the imaging terms will automatically be zero even without doing any integration. Otherwise, if we don't have the right velocity, these imaging terms would be used to move the interface closer to the right location from the wrong location. The conclusion is that the depth imaging terms depend only on the velocity errors.

6 Conclusion

Including terms beyond linear in earth property identification subseries provides added value. Although the model we used in the numerical test is simple, equ. (21) and (22) also work for larger contrast and complex targets. The inverse scattering series is a direct inversion procedure which inverts data independent of the properties of the target, without assumptions such as smooth geometry or small contrast. This work is a major step towards the realism for target identification. The numerical results are encouraging and this work will be extended to study the elastic case using three parameters (see, e.g., Boyse, 1986, Boyse and Keller, 1986).

Acknowledgements

We thank all sponsors of M-OSRP and we are grateful that D. Foster, R. Keys and R. Stolt are working with us on this project. The first author would also like to thank Bogdan Nita and Simon Shaw for valuable discussions.

Appendix A

The following is the derivation of $\left(\frac{\Delta c}{c}\right)_1$, $\left(\frac{\Delta c}{c}\right)_2$, $\left(\frac{\Delta I}{I}\right)_1$ and $\left(\frac{\Delta I}{I}\right)_2$ in terms of α_1, β_1 and α_2, β_2. Where $\Delta c = c - c_0$, $\Delta I = I - I_0$, $\Delta K = K - K_0$ and $\Delta\rho = \rho - \rho_0$.

Since $K = c^2\rho$, then we have

$$(c - \Delta c)^2 = \frac{K - \Delta K}{\rho - \Delta\rho}.$$

Divided by c^2, the equation above will become

$$2\left(\frac{\Delta c}{c}\right) - \left(\frac{\Delta c}{c}\right)^2 = \frac{\frac{\Delta K}{K} - \frac{\Delta\rho}{\rho}}{1 - \frac{\Delta\rho}{\rho}}.$$

Remember that $\alpha = \frac{\Delta K}{K}$ and $\beta = \frac{\Delta\rho}{\rho}$, the above equation can be rewritten as

$$2\left(\frac{\Delta c}{c}\right) - \left(\frac{\Delta c}{c}\right)^2 = \frac{\alpha - \beta}{1 - \beta}.$$

Then we have

$$2\left(\frac{\Delta c}{c}\right) - \left(\frac{\Delta c}{c}\right)^2 = (\alpha - \beta)(1 + \beta + \beta^2 + \cdots), \tag{39}$$

where the series expansion is valid for $|\beta| < 1$.

Similar to (17) and (18), we expand $\frac{\Delta c}{c}$ as

$$\left(\frac{\Delta c}{c}\right) = \left(\frac{\Delta c}{c}\right)_1 + \left(\frac{\Delta c}{c}\right)_2 + \cdots. \tag{40}$$

Then substitute (40), (17) and (18) into (39), and set those terms of equal order equal on both sides of (39), we will get

$$\left(\frac{\Delta c}{c}\right)_1 = \frac{1}{2}(\alpha_1 - \beta_1), \tag{41}$$

and

$$\left(\frac{\Delta c}{c}\right)_2 = \frac{1}{2}\left[\frac{1}{4}(\alpha_1 + \beta_1)^2 - \beta_1^2 + (\alpha_2 - \beta_2)\right]. \tag{42}$$

Similarly, using $I = c\rho$, we'll have

$$(I - \Delta I)^2 = (K - \Delta K)(\rho - \Delta\rho).$$

Divided by I^2, the equation above will become

$$2\left(\frac{\Delta I}{I}\right) - \left(\frac{\Delta I}{I}\right)^2 = \alpha + \beta - \alpha\beta. \tag{43}$$

We expand $\frac{\Delta I}{I}$ as

$$\left(\frac{\Delta I}{I}\right) = \left(\frac{\Delta I}{I}\right)_1 + \left(\frac{\Delta I}{I}\right)_2 + \cdots. \tag{44}$$

Then substitute (44), (17) and (18) into (43), and set those terms of equal order equal on both sides of (43), we will get

$$\left(\frac{\Delta I}{I}\right)_1 = \frac{1}{2}(\alpha_1 + \beta_1), \tag{45}$$

and

$$\left(\frac{\Delta I}{I}\right)_2 = \frac{1}{2}\left[\frac{1}{4}(\alpha_1 - \beta_1)^2 + (\alpha_2 + \beta_2)\right]. \tag{46}$$

Appendix B

For the single interface example, from (35), we have

$$\left(\frac{\Delta c}{c}\right)_1 = 2\frac{R(\theta_1) - R(\theta_2)}{\tan^2\theta_1 - \tan^2\theta_2}.$$

The reflection coefficient is

$$R(\theta) = \frac{(\rho_1/\rho_0)(c_1/c_0)\sqrt{1-\sin^2\theta} - \sqrt{1-(c_1^2/c_0^2)\sin^2\theta}}{(\rho_1/\rho_0)(c_1/c_0)\sqrt{1-\sin^2\theta} + \sqrt{1-(c_1^2/c_0^2)\sin^2\theta}}.$$

Let

$$A(\theta) = (\rho_1/\rho_0)(c_1/c_0)\sqrt{1-\sin^2\theta},$$
$$B(\theta) = \sqrt{1-(c_1^2/c_0^2)\sin^2\theta}.$$

Then

$$R(\theta_1) - R(\theta_2) = 2\frac{A(\theta_1)B(\theta_2) - B(\theta_1)A(\theta_2)}{[A(\theta_1) + B(\theta_1)]\,[A(\theta_2) + B(\theta_2)]},$$

where the denominator is greater than zero. The numerator is

$$\begin{aligned} 2\,[A(\theta_1)B(\theta_2) - B(\theta_1)A(\theta_2)] =& 2(\rho_1/\rho_0)(c_1/c_0)\left[\sqrt{1-\sin^2\theta_1}\sqrt{1-(c_1^2/c_0^2)\sin^2\theta_2}\right. \\ & \left. -\sqrt{1-\sin^2\theta_2}\sqrt{1-(c_1^2/c_0^2)\sin^2\theta_1}\right]. \end{aligned}$$

Now, we let

$$C = \sqrt{1-\sin^2\theta_1}\sqrt{1-(c_1^2/c_0^2)\sin^2\theta_2},$$
$$D = \sqrt{1-\sin^2\theta_2}\sqrt{1-(c_1^2/c_0^2)\sin^2\theta_1}.$$

Then,

$$C^2 - D^2 = \left(\frac{c_1^2}{c_0^2} - 1\right)(sin^2\theta_1 - sin^2\theta_2).$$

When $c_1 > c_0$ and $\theta_1 > \theta_2$, we have (Noticed that both C and D are positive.)

$$\left(\frac{c_1^2}{c_0^2} - 1\right)(sin^2\theta_1 - sin^2\theta_2) > 0,$$

so

$$R(\theta_1) - R(\theta_2) > 0;$$

Similarly, when $c_1 < c_0$ and $\theta_1 > \theta_2$, we have

$$\left(\frac{c_1^2}{c_0^2} - 1\right)(sin^2\theta_1 - sin^2\theta_2) < 0,$$

so

$$R(\theta_1) - R(\theta_2) < 0.$$

Remembering that $\left(\frac{\Delta c}{c}\right)_1 = 2\frac{R(\theta_1)-R(\theta_2)}{\tan^2\theta_1 - \tan^2\theta_2}$. So for $c_1 > c_0$, $(\Delta c)_1 > 0$ and for $c_1 < c_0$, $(\Delta c)_1 < 0$.

References

1. Boyse W E 1986 *Wave propagation and inversion in slightly inhomogeneous media* p 40
2. Boyse W E and Keller J B 1986 Inverse elastic scattering in three dimensions *J. Acoust. Soc. Am.* **79** 215–218
3. Clayton R W and Stolt R H 1981 A Born-WKBJ inversion method for acoustic reflection data for attenuating multiples in seismic reflection data *Geophysics* **46** 1559–1567
4. Innanen K A 2003 "Methods for the Treatment of Acoustic and Absorptive/Dispersive Wave Field Measurements." *Ph.D. Thesis, University of British Columbia.*
5. Keys R G 1989 Polarity reversals in reflections from layered media *Geophysics* **54** 900–905
6. Liu F, Weglein A B, Innanen K A and Nita B G 2005 Multi-dimensional depth imaging without an adequate velocity model, in preparation
7. Matson K H 1997 An inverse scattering series method for attenuating elastic multiples from multicomponent land and ocean bottom seismic data *Ph.D. thesis* University of British Columbia p 18
8. Shaw S A, Weglein A B, Foster D J, Matson K H and Keys R G 2003 Isolation of a leading order depth imaging series and analysis of its convergence properties, in preparation
9. Shaw S A 2005 "An inverse scattering series algorithm for depth imaging of reflection data from a layered acoustic medium with an unknown velocity model" *Ph.D. thesis* University of Houston
10. Taylor J R 1972 *Scattering theory: the quantum theory of nonrelativistic collisions* (John Wiley & Sons, Inc.) p 133
11. Weglein A B, Violette P B and Keho T H 1986 Using multiparameter Born theory to obtain certain exact multiparameter inversion goals *Geophysics* **51** 1069–1074
12. Weglein A B, Gasparotto F A, Carvalho P M and Stolt R H 1997 An inverse-scattering series method for attenuating multiples in seismic reflection data *Geophysics* **62** 1975–1989

13. Weglein A B, Foster D J, Matson K H, Shaw S A, Carvalho P M and Corrigan D 2002 Predicting the correct spatial location of reflectors without knowing or determining the precise medium and wave velocity: initial concept, algorithm and analytic and numerical example *J. Seism. Explor.* **10** 367–382

14. Weglein A B, Araújo F V, Carvalho P M, Stolt R H, Matson K H, Coates R, Corrigan D, Foster D J, Shaw S A and Zhang H 2003 Inverse scattering series and seismic exploration *Inverse Problem* **19** R27–R83

General References

15. Smith G C and Gidlow P M 1987 Weighted stacking for rock property estimation and detection of gas *Geophysical Prospecting* **35** 993–1014

16. Stolt R H 1992 (invited paper) *Geophysical Inversion* (Editors, J. B. Bednar, et al.) SIAM, Philadelphia, p 3–19

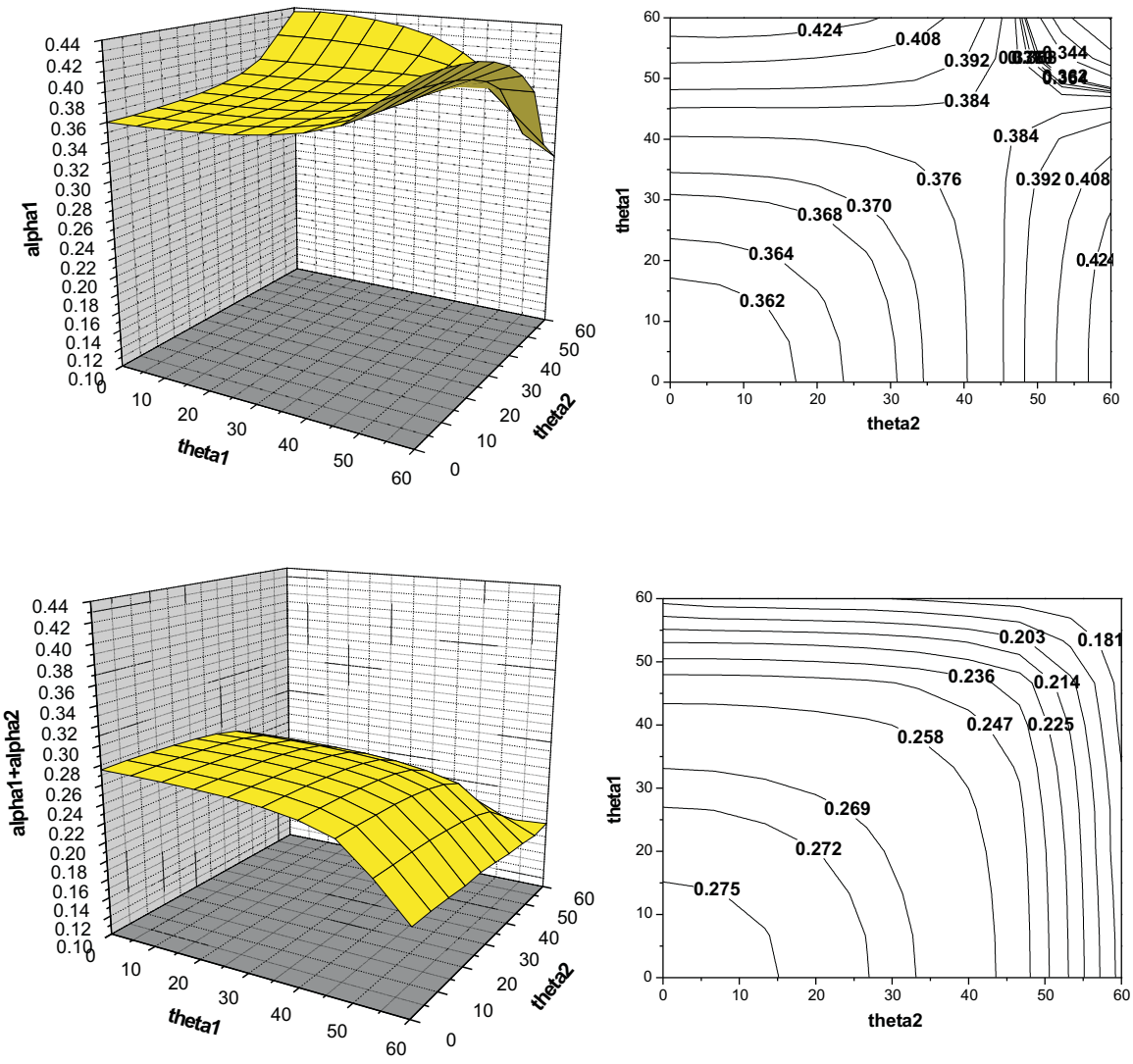

Figure 3: α_1 *(top) and* $\alpha_1 + \alpha_2$ *(bottom) displayed as a function of two different angles. The graphs on the right are the corresponding contour plots of the graphs on the left. In this example, the exact value of* α *is 0.292.*

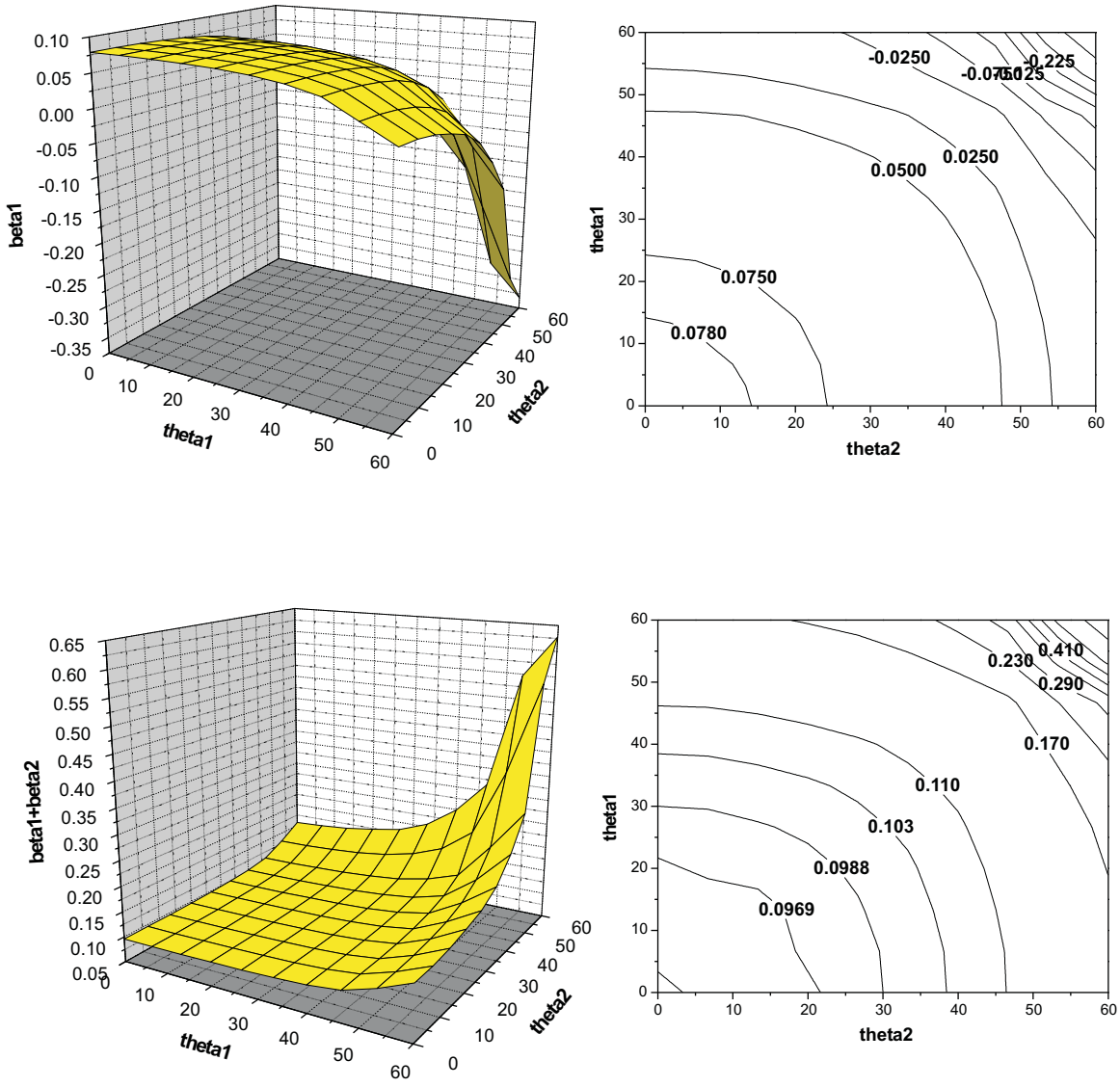

Figure 4: β_1 *(top) and* $\beta_1 + \beta_2$ *(bottom). In this example, the exact value of* β *is 0.09.*

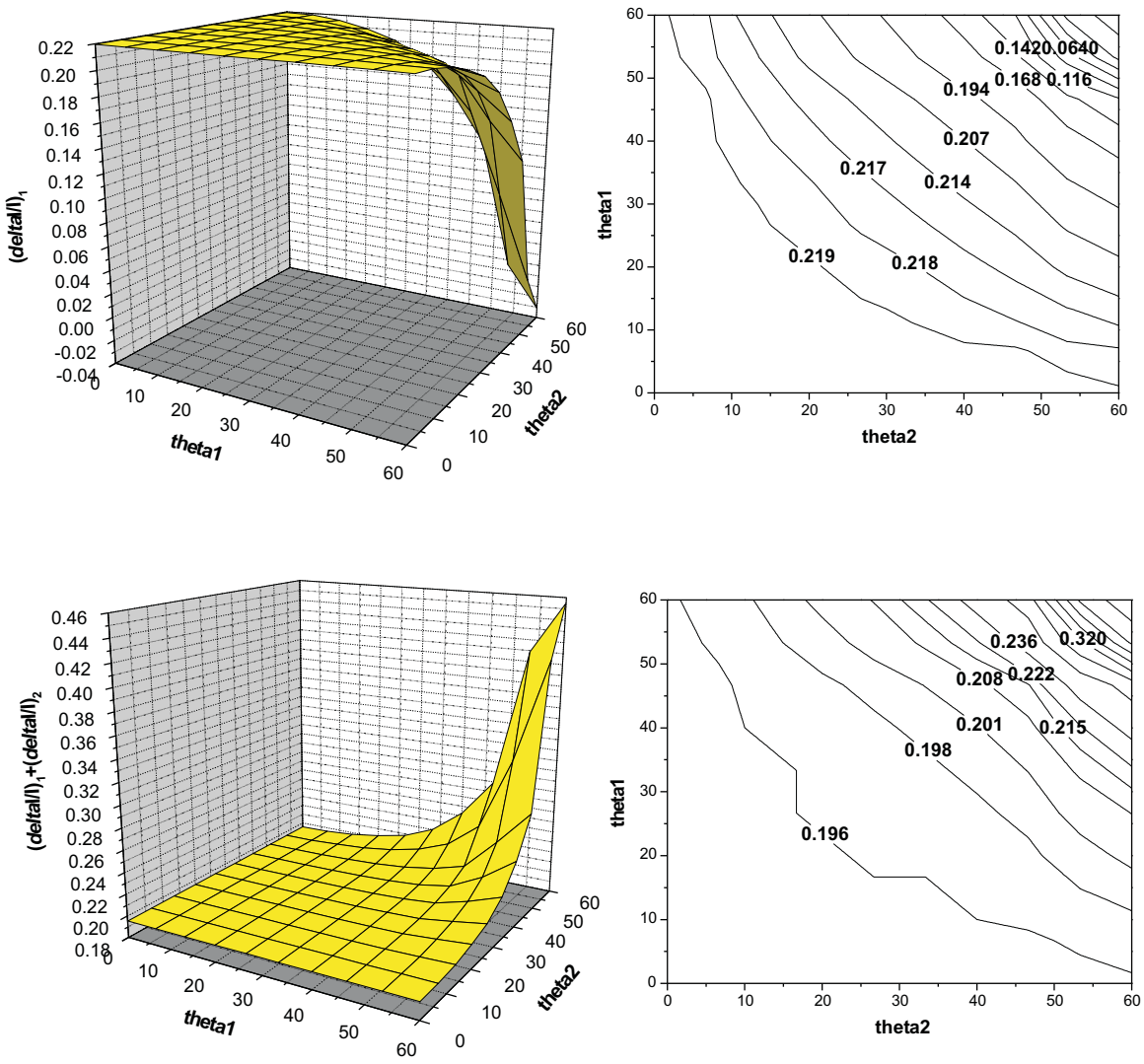

Figure 5: *Linear approximation to relative change in impedance (see details in Appendix A)* $\left(\frac{\Delta I}{I}\right)_1 = \frac{1}{2}(\alpha_1 + \beta_1)$ *(top). Sum of linear and first non-linear terms* $\left(\frac{\Delta I}{I}\right)_1 + \left(\frac{\Delta I}{I}\right)_2 = \left(\frac{\Delta I}{I}\right)_1 + \frac{1}{2}\left[\frac{1}{4}(\alpha_1 - \beta_1)^2 + (\alpha_2 + \beta_2)\right]$ *(bottom). In this example, the exact value of* $\frac{\Delta I}{I}$ *is 0.198.*

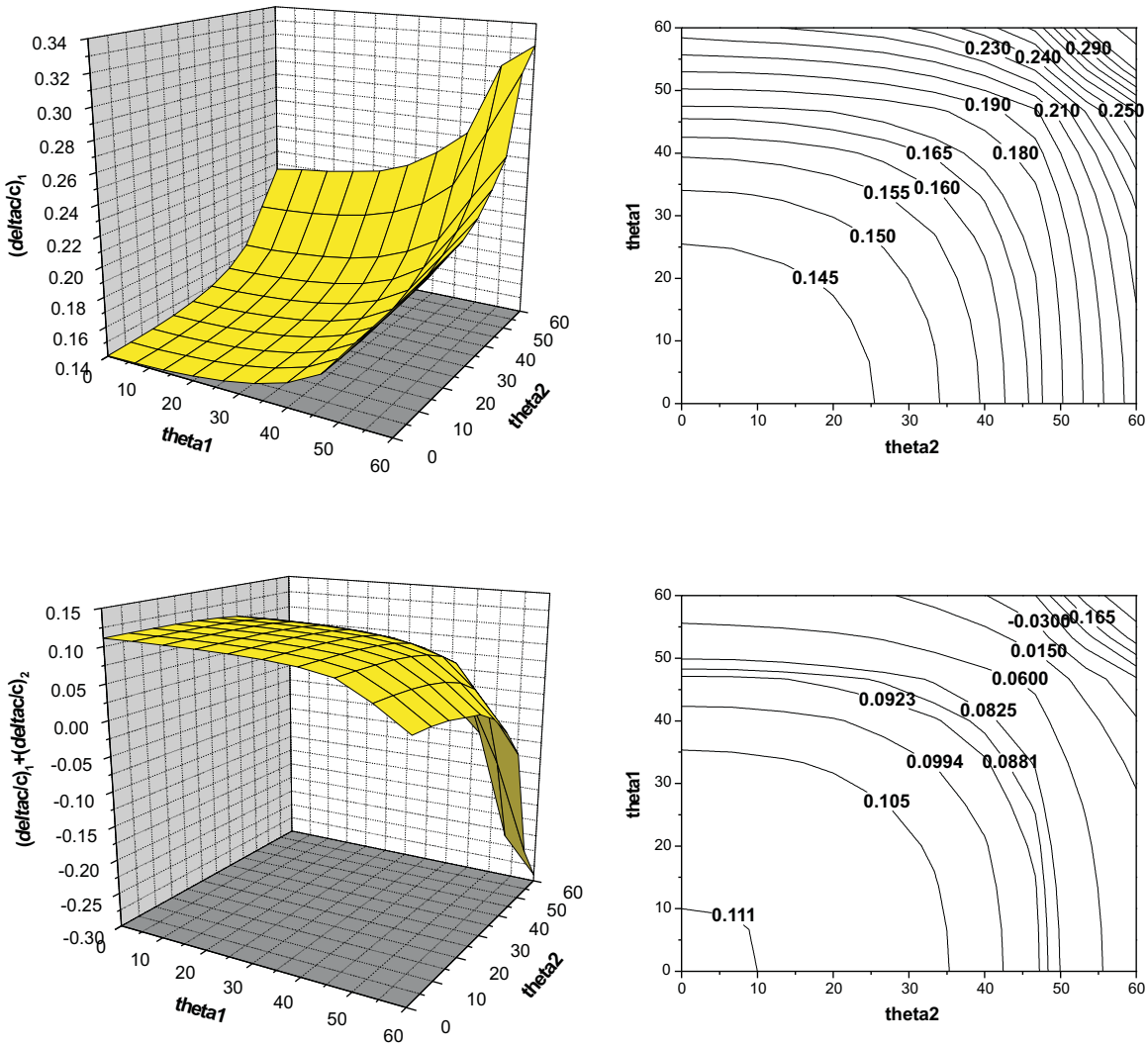

Figure 6: *Linear approximation to relative change in velocity (see details in Appendix A)* $\left(\frac{\Delta c}{c}\right)_1 = \frac{1}{2}(\alpha_1 - \beta_1)$ *(top). Sum of linear and first non-linear terms* $\left(\frac{\Delta c}{c}\right)_1 + \left(\frac{\Delta c}{c}\right)_2 = \left(\frac{\Delta c}{c}\right)_1 + \frac{1}{2}\left[\frac{1}{4}(\alpha_1 + \beta_1)^2 - \beta_1^2 + (\alpha_2 - \beta_2)\right]$ *(bottom). In this example, the exact value of* $\frac{\Delta c}{c}$ *is 0.118.*

Velocity independent depth imaging and non-linear direct target identification for 1D elastic media: testing and evaluation for application to non-linear AVO, using only PP data

Haiyan Zhang, Arthur B. Weglein and Robert G. Keys*
* ExxonMobil and Adjunct Professor, Physics Dept., M-OSRP, UH

Abstract

In this paper, we present the first velocity independent depth imaging and non-linear direct target identification method and algorithm for 1D elastic media from the inverse scattering series (ISS). The terms for moving mislocated reflectors are separated from amplitude analysis terms. The non-linear direct elastic inversion method requires that PP, PS, SP and SS data as input. We show how PP data can be used to approximately synthesize the PS, SP and SS data. We show that in all cases where this synthesis is reasonably accurate, the subsequent non-linear inversion provides added value over linear and that situation represents three out of four cases examined. Even in the one case where the approximate data synthesis is far from accurate, some mild value is derived from non-linear prediction results in comparison with linear estimates. In the four cases where at least one of the synthesized data is reasonable, then improved estimates are reported in comparison to linear methods. We can reasonably infer that with actual PP, PS, SP and SS data collected, all four cases will be of added value when compared to linear inverse procedures. In several cases linear inversion predicted the wrong sign for changes in density. The non-linear prediction has the correct sign in each case. The method is direct with neither a model matching nor cost function minimization.

1 Introduction

The objective of seismic exploration is to predict the location and properties of the hydrocarbon resources in the earth (i.e. imaging and inversion) using recorded seismic data. However, there is a large variety of seismic events in the recorded data while only one kind is regarded as signal by the imaging and inversion procedures: primaries. The rest of the data is considered noise. That means a series of preprocessing operations need to be performed on the seismic data before imaging and inversion in order to remove the unwanted noise. The operations include wavelet estimation, deghosting, free surface multiple removal and internal multiple removal. In M-OSRP projects, with the exception of wavelet estimation (Guo et al., 2004) and deghosting (Zhang and Weglein, 2004), algorithms which are derived from Green's theorem, the rest of the tasks are performed by only one tool: the inverse scattering series (ISS).

The original inverse scattering series research aimed at task (1), free surface multiple removal and (2), internal multiple removal, was developed and applied successfully in 2D and 3D field data (Weglein et al., 1997 and Weglein et al., 2003). The next step is the processing of primaries. Beginning with 2001, we started to look at the tasks that work on primaries, which include task (3), depth imaging and task (4), parameter estimation. We started by analyzing a one parameter 1D acoustic constant density medium and 1D normal incidence (Weglein et al., 2002, Innanen,

2003, Shaw et al., 2003 and Shaw, 2005). The extension to a one parameter 2D acoustic medium is studied by Liu et al. (2005). In this paper we made a major step towards realism for target identification by extending the earlier work on non-linear inversion of 2D acoustic data for a two parameter 1D medium (Zhang and Weglein, 2003) to three parameter 1D elastic medium. This is the first step of direct non-linear inversion from acoustic to elastic – a more realistic world. We take these steps in 1D to allow the best chance to use analytic data to do the numerical tests and hence understand our workings within a 1D world. It would be very useful, as a framework and insights, for launching to the next more realistic step – the multi-parameter and multi-D medium. However, more realism is more complicated with more issues involved. Following the task separation strategy, we ask the question what kind of tasks should we expect in this more complex, elastic, setting? In acoustic case, for example, there is only one velocity (P wave velocity) involved and there is only one mislocation. The imaging terms only need to move the one mislocation to the correct location. When we extend our previous work on two parameter acoustic case to present three parameter elastic case, there will be four mislocations because of the two reference velocities (P wave velocity and S velocity). Therefore, for the non-linear elastic inversion, there will be more tasks need to be achieved. For example, the "four mislocations", which come from linear inversion, need to be moved to one correct location.

It is important to point out that the above four tasks we mentioned are not direct applications of the whole inverse scattering series (ISS), which has very limited application (Matson, 1997). Instead, each task is performed by a task specific subseries which is a subset of the whole series that acts as though only one specific task, and no other, existed (Weglein et al., 2003). What makes this task specific subseries method attractive is that each subseries has less to achieve and hence better convergence properties than the full series. As in the case of the full series, a task oriented subseries only requires data and information about a reference medium; no information about the subsurface is ever required. This characteristic is especially useful when the current methods (like velocity dependent migration or imaging) fail due to inadequate information about the subsurface in complex geometry and complex medium.

So, why are we trying to use non-linear inversion? This is because the character (i.e., the amplitude and phase) of the reflected data events, depends on the properties of the medium that the wave travelled through and the contrast in properties across reflectors. The reflection process (e.g., the reflection coefficient for 1D normal incidence acoustic model) has a non-linear dependence on any property change at the reflector, and depends on the incident angle and also the geometry of the reflector which can be, e.g., horizontal, dipping, curved, corrugated and diffractive. Current state of the art seismic analysis techniques typically assume a simple linear relationship between the reflection coefficient and changes in properties, and a simple horizontal reflector geometry. Those assumptions are often violated in practice and can cause serious misinterpretations and erroneous predictions which would affect the drilling decisions.

In this report we will use the direct non-linear inversion method for estimation of material property changes that avoids small property change assumptions, or model-matching procedures, or assumes a simple target geometry. To date, this is the only candidate method with this more realistic, more physically complete, and, hence more reliable prediction capability and potential. In this report, the first non-linear inversion term for three parameter 1D elastic medium is presented. In theory, it is impossible to perform exact inversion without all four components of data. However, as you can find in the following numerical tests for four models, very good inversion results can still be achieved even when only PP data measurements are available. This means that we could perform

elastic inversion only using pressure measurements, i.e. towed streamer data. The numerical test results show that, for most of the models we used, this particular non-linear approach (only use PP data as input) provides useful results especially in correcting the sign of the densities obtained from linear inversion.

In the following we will first briefly review the theory of ISS and then present the derivations for non-linear inversion when only PP data is available. Numerical tests are performed for four models. Finally we'll present some concluding remarks.

2 Background for 2D elastic inversion

In this section we consider the inversion problem in two dimensions for an elastic medium.

2.1 In the displacement space

We begin with some basic equations in the displacement space (Matson, 1997):

$$L\mathbf{u} = \mathbf{f}, \tag{1}$$

$$L_0\mathbf{u} = \mathbf{f}, \tag{2}$$

$$LG = \mathbf{I}, \tag{3}$$

$$L_0G_0 = \mathbf{I}, \tag{4}$$

where L and L_0 are the differential operators that describe the wave propagation in the actual and reference medium, respectively, $\mathbf{u}$ and $\mathbf{f}$ are the corresponding displacement and source terms, respectively, and G and G_0 are the corresponding Green operators for the actual and reference medium.

Defining the perturbation $V = L_0 - L$, the Lippmann- Schwinger equation for the elastic media in the displacement space is

$$G = G_0 + G_0VG. \tag{5}$$

Iterating this equation back into itself generates the Born series

$$G = G_0 + G_0VG_0 + G_0VG_0VG_0 + \cdots . \tag{6}$$

We define the data D as the measured values of the scattered wave field. Then, on the measurement surface, we have

$$D = G_0 V G_0 + G_0 V G_0 V G_0 + \cdots . \tag{7}$$

Expanding V as a series in orders of D (Weglein et al., 1997), we have

$$V = V_1 + V_2 + V_3 + \cdots . \tag{8}$$

Substituting Eq. (8) into Eq. (7), evaluating Eq. (7), and setting terms of equal order in the data equal, we get the equations that determine V_1, V_2, ... from D and G_0.

$$D = G_0 V_1 G_0, \tag{9}$$

$$0 = G_0 V_2 G_0 + G_0 V_1 G_0 V_1 G_0, \tag{10}$$

$$\vdots$$

In the actual medium, the 2-D elastic wave equation is (Weglein and Stolt, 1992)

$$L\mathbf{u} \equiv \left[\rho\omega^2 \begin{pmatrix} 1 & 0 \\ 0 & 1 \end{pmatrix} + \begin{pmatrix} \partial_1\gamma\partial_1 + \partial_2\mu\partial_2 & \partial_1(\gamma - 2\mu)\partial_2 + \partial_2\mu\partial_1 \\ \partial_2(\gamma - 2\mu)\partial_1 + \partial_1\mu\partial_2 & \partial_2\gamma\partial_2 + \partial_1\mu\partial_1 \end{pmatrix}\right] \begin{bmatrix} u_1 \\ u_2 \end{bmatrix} = \mathbf{f}, \tag{11}$$

where

$\mathbf{u} = \begin{bmatrix} u_1 \\ u_2 \end{bmatrix}$ = displacement,

ρ = density,

γ = bulk modulus ($\equiv \rho\alpha^2$ where α = P velocity),

μ = shear modulus ($\equiv \rho\beta^2$ where β = S velocity),

ω = temporal frequency (angular), and

$\mathbf{f}$ is the source term.

For constant $(\rho, \gamma, \mu) = (\rho_0, \gamma_0, \mu_0)$, $(\alpha, \beta) = (\alpha_0, \beta_0)$, the operator L becomes

$$L_0 \equiv \left[\rho_0\omega^2 \begin{pmatrix} 1 & 0 \\ 0 & 1 \end{pmatrix} + \begin{pmatrix} \gamma_0\partial_1^2 + \mu_0\partial_2^2 & (\gamma_0 - \mu_0)\partial_1\partial_2 \\ (\gamma_0 - \mu_0)\partial_1\partial_2 & \mu_0\partial_1^2 + \gamma_0\partial_2^2 \end{pmatrix}\right]. \tag{12}$$

Then,

$$
\begin{aligned}
V \equiv & L_0 - L \\
= & -\rho_0 \begin{bmatrix} a_\rho\omega^2 + \alpha_0^2\partial_1 a_\gamma \partial_1 + \beta_0^2 \partial_2 a_\mu \partial_2 & \partial_1(\alpha_0^2 a_\gamma - 2\beta_0^2 a_\mu)\partial_2 + \beta_0^2\partial_2 a_\mu \partial_1 \\ \partial_2(\alpha_0^2 a_\gamma - 2\beta_0^2 a_\mu)\partial_1 + \beta_0^2 \partial_1 a_\mu \partial_2 & a_\rho\omega^2 + \alpha_0^2 \partial_2 a_\gamma \partial_2 + \beta_0^2 \partial_1 a_\mu \partial_1 \end{bmatrix},
\end{aligned} \tag{13}
$$

where $a_\rho \equiv \frac{\rho}{\rho_0} - 1$, $a_\gamma \equiv \frac{\gamma}{\gamma_0} - 1$ and $a_\mu \equiv \frac{\mu}{\mu_0} - 1$. For a 1D earth (i.e. a_ρ, a_γ and a_μ are only functions of depth z), we have

$$
\begin{bmatrix} V^{11} & V^{12} \\ V^{21} & V^{22} \end{bmatrix} = -\rho_0 \begin{bmatrix} a_\rho\omega^2 + \alpha_0^2 a_\gamma \partial_1^2 + \beta_0^2 \partial_2 a_\mu \partial_2 & (\alpha_0^2 a_\gamma - 2\beta_0^2 a_\mu)\partial_1\partial_2 + \beta_0^2 \partial_2 a_\mu \partial_1 \\ \partial_2(\alpha_0^2 a_\gamma - 2\beta_0^2 a_\mu)\partial_1 + \beta_0^2 a_\mu \partial_1\partial_2 & a_\rho\omega^2 + \alpha_0^2 \partial_2 a_\gamma \partial_2 + \beta_0^2 a_\mu \partial_1^2 \end{bmatrix}. \tag{14}
$$

2.2 Transform to PS space

For convenience, we change the basis from $\mathbf{u} = \begin{bmatrix} u_1 \\ u_2 \end{bmatrix}$ to $\begin{pmatrix} \phi^P \\ \phi^S \end{pmatrix}$ to allow L_0 to be diagonal,

$$
\mathbf{\Phi} = \begin{pmatrix} \phi^P \\ \phi^S \end{pmatrix} = \begin{bmatrix} \gamma_0(\partial_1 u_1 + \partial_2 u_2) \\ \mu_0(\partial_1 u_2 - \partial_2 u_1) \end{bmatrix}, \tag{15}
$$

also, we have

$$
\begin{pmatrix} \phi^P \\ \phi^S \end{pmatrix} = \Gamma_0 \Pi \mathbf{u} = \begin{bmatrix} \gamma_0(\partial_1 u_1 + \partial_2 u_2) \\ \mu_0(\partial_1 u_2 - \partial_2 u_1) \end{bmatrix}, \tag{16}
$$

where $\Pi = \begin{pmatrix} \partial_1 & \partial_2 \\ -\partial_2 & \partial_1 \end{pmatrix}$, $\Gamma_0 = \begin{pmatrix} \gamma_0 & 0 \\ 0 & \mu_0 \end{pmatrix}$. In the reference medium, the operator L_0 will transform in the new basis via a transformation

$$
\hat{L}_0 \equiv \Pi L_0 \Pi^{-1} \Gamma_0^{-1} = \begin{pmatrix} \hat{L}_0^P & 0 \\ 0 & \hat{L}_0^S \end{pmatrix},
$$

where $\hat{L}_0$ is L_0 transformed to PS space, $\Pi^{-1} = \begin{pmatrix} \partial_1 & -\partial_2 \\ \partial_2 & \partial_1 \end{pmatrix} \nabla^{-2}$ is the inverse matrix of Π, $\hat{L}_0^P = \omega^2/\alpha_0^2 + \nabla^2$, $\hat{L}_0^S = \omega^2/\beta_0^2 + \nabla^2$, and

$$
\mathbf{F} = \Pi \mathbf{f} = \begin{pmatrix} F^P \\ F^S \end{pmatrix}. \tag{17}
$$

Then, in PS domain, Eq. (2) becomes,

$$
\begin{pmatrix} \hat{L}_0^P & 0 \\ 0 & \hat{L}_0^S \end{pmatrix} \begin{pmatrix} \phi^P \\ \phi^S \end{pmatrix} = \begin{pmatrix} F^P \\ F^S \end{pmatrix}. \tag{18}
$$

Since $G_0 \equiv L_0^{-1}$, let $\hat{G}_0^P = \left(\hat{L}_0^P\right)^{-1}$ and $\hat{G}_0^S = \left(\hat{L}_0^S\right)^{-1}$, then, displacement G_0 in PS domain becomes

$$\hat{G}_0 = \Gamma_0 \Pi G_0 \Pi^{-1} = \begin{pmatrix} \hat{G}_0^P & 0 \\ 0 & \hat{G}_0^S \end{pmatrix}. \tag{19}$$

So, in the reference medium, after transforming from the displacement domain to PS domain, both L_0 and G_0 become diagonal.

Multiplying Eq. (5) from the left by the operator $\Gamma_0\Pi$ and from the right by the operator Π^{-1}, and using Eq. (19),

$$\begin{aligned} \Gamma_0 \Pi G \Pi^{-1} &= \hat{G}_0 + \hat{G}_0 \left(\Pi V \Pi^{-1} \Gamma_0^{-1} \right) \Gamma_0 \Pi G \Pi^{-1} \\ &= \hat{G}_0 + \hat{G}_0 \hat{V} \hat{G}, \end{aligned} \tag{20}$$

where the displacement Green's operator G is transformed to the PS domain as

$$\hat{G} = \Gamma_0 \Pi G \Pi^{-1} = \begin{pmatrix} \hat{G}^{PP} & \hat{G}^{PS} \\ \hat{G}^{SP} & \hat{G}^{SS} \end{pmatrix}. \tag{21}$$

The perturbation V in the PS domain becomes

$$\hat{V} = \Pi V \Pi^{-1} \Gamma_0^{-1} = \begin{pmatrix} \hat{V}^{PP} & \hat{V}^{PS} \\ \hat{V}^{SP} & \hat{V}^{SS} \end{pmatrix}, \tag{22}$$

where, as before, the left superscripts of the matrices represent the type of measurement and the right ones are the source type.

Similarly, applying the PS transformation to the entire inverse series gives

$$\hat{V} = \hat{V}_1 + \hat{V}_2 + \hat{V}_3 + \cdots. \tag{23}$$

It follows, from Eqs. (20) and (23) that

$$\hat{D} = \hat{G}_0 \hat{V}_1 \hat{G}_0, \tag{24}$$

$$\hat{G}_0 \hat{V}_2 \hat{G}_0 = -\hat{G}_0 \hat{V}_1 \hat{G}_0 \hat{V}_1 \hat{G}_0, \tag{25}$$

$$\vdots$$

where $\hat{D} = \begin{pmatrix} \hat{D}^{PP} & \hat{D}^{PS} \\ \hat{D}^{SP} & \hat{D}^{SS} \end{pmatrix}$ are the data in the PS domain.

In the displacement space we have, for Eq. (1),

$$\mathbf{u} = G\mathbf{f}. \tag{26}$$

Then, in the PS domain, Eq. (26) becomes

$$\mathbf{\Phi} = \hat{G}\mathbf{F}. \tag{27}$$

On the measurement surface, we have

$$\hat{G} = \hat{G}_0 + \hat{G}_0 \hat{V}_1 \hat{G}_0. \tag{28}$$

We substitute Eq. (28) into Eq. (27), and rewrite Eq. (27) in matrix form:

$$\begin{pmatrix} \phi^P \\ \phi^S \end{pmatrix} = \begin{pmatrix} \hat{G}_0^P & 0 \\ 0 & \hat{G}_0^S \end{pmatrix} \begin{pmatrix} F^P \\ F^S \end{pmatrix} + \begin{pmatrix} \hat{G}_0^P & 0 \\ 0 & \hat{G}_0^S \end{pmatrix} \begin{pmatrix} \hat{V}_1^{PP} & \hat{V}_1^{PS} \\ \hat{V}_1^{SP} & \hat{V}_1^{SS} \end{pmatrix} \begin{pmatrix} \hat{G}_0^P & 0 \\ 0 & \hat{G}_0^S \end{pmatrix} \begin{pmatrix} F^P \\ F^S \end{pmatrix}. \tag{29}$$

This can be written as the following two equations

$$\phi^P = \hat{G}_0^P F^P + \hat{G}_0^P \hat{V}_1^{PP} \hat{G}_0^P F^P + \hat{G}_0^P \hat{V}_1^{PS} \hat{G}_0^S F^S, \tag{30}$$

$$\phi^S = \hat{G}_0^S F^S + \hat{G}_0^S \hat{V}_1^{SP} \hat{G}_0^P F^P + \hat{G}_0^S \hat{V}_1^{SS} \hat{G}_0^S F^S. \tag{31}$$

We can see, from the two equations above, that for homogeneous media, (no perturbation, $\hat{V}_1 = 0$), there are only direct P and S waves and that the two kind of waves are separated. However, for inhomogeneous media, these two kinds of waves will be mixed together. If only the P wave is incident, $F^P = 1$, $F^S = 0$, then the above two equations (30) and (31) are respectively reduced to

$$\phi^P = \hat{G}_0^P + \hat{G}_0^P \hat{V}_1^{PP} \hat{G}_0^P, \tag{32}$$

$$\phi^S = \hat{G}_0^S \hat{V}_1^{SP} \hat{G}_0^P. \tag{33}$$

Hence, in this case, there is only the direct P wave $\hat{G}_0^P$, and no direct wave S. But there are two kinds of scattered waves: one is the P-to-P wave $\hat{G}_0^P \hat{V}_1^{PP} \hat{G}_0^P$, and the other is the P-to-S wave $\hat{G}_0^S \hat{V}_1^{SP} \hat{G}_0^P$. For the acoustic case, only the P wave exists, and hence we only have one equation $\phi^P = \hat{G}_0^P + \hat{G}_0^P \hat{V}_1^{PP} \hat{G}_0^P$.

Similarly, if only the S wave is incident, $F^P = 0$, $F^S = 1$, and the two equations (30) and (31) are respectively reduced to

$$\phi^P = \hat{G}_0^P \hat{V}_1^{PS} \hat{G}_0^S, \tag{34}$$

$$\phi^S = \hat{G}_0^S + \hat{G}_0^S \hat{V}_1^{SS} \hat{G}_0^S. \tag{35}$$

In this case, there is only the direct S wave $\hat{G}_0^S$, and no direct wave P. There are also two kinds of scattered waves: one is the S-to-P wave $\hat{G}_0^P \hat{V}_1^{PS} \hat{G}_0^S$, the other is the S-to-S wave $\hat{G}_0^S \hat{V}_1^{SS} \hat{G}_0^S$.

3 Linear inversion of 1D elastic medium for 2D experiment

Writing Eq. (24) in matrix form

$$\begin{pmatrix} \hat{D}^{PP} & \hat{D}^{PS} \\ \hat{D}^{SP} & \hat{D}^{SS} \end{pmatrix} = \begin{pmatrix} \hat{G}_0^P & 0 \\ 0 & \hat{G}_0^S \end{pmatrix} \begin{pmatrix} \hat{V}_1^{PP} & \hat{V}_1^{PS} \\ \hat{V}_1^{SP} & \hat{V}_1^{SS} \end{pmatrix} \begin{pmatrix} \hat{G}_0^P & 0 \\ 0 & \hat{G}_0^S \end{pmatrix}, \tag{36}$$

leads to four equations

$$\hat{D}^{PP} = \hat{G}_0^P \hat{V}_1^{PP} \hat{G}_0^P, \tag{37}$$

$$\hat{D}^{PS} = \hat{G}_0^P \hat{V}_1^{PS} \hat{G}_0^S, \tag{38}$$

$$\hat{D}^{SP} = \hat{G}_0^S \hat{V}_1^{SP} \hat{G}_0^P, \tag{39}$$

$$\hat{D}^{SS} = \hat{G}_0^S \hat{V}_1^{SS} \hat{G}_0^S. \tag{40}$$

For $z_s = z_g = 0$, in the $(k_s, z_s; k_g, z_g; \omega)$ domain, we get

$$\widetilde{D}^{PP}(k_g, 0; -k_g, 0; \omega) = -\frac{1}{4}\left(1 - \frac{k_g^2}{\nu_g^2}\right)\widetilde{a}_\rho^{(1)}(-2\nu_g) - \frac{1}{4}\left(1 + \frac{k_g^2}{\nu_g^2}\right)\widetilde{a}_\gamma^{(1)}(-2\nu_g) + \frac{2k_g^2\beta_0^2}{(\nu_g^2 + k_g^2)\alpha_0^2}\widetilde{a}_\mu^{(1)}(-2\nu_g), \tag{41}$$

$$\widetilde{D}^{PS}(\nu_g, \eta_g) = -\frac{1}{4}\left(\frac{k_g}{\nu_g} + \frac{k_g}{\eta_g}\right)\widetilde{a}_\rho^{(1)}(-\nu_g - \eta_g) - \frac{\beta_0^2}{2\omega^2}k_g(\nu_g + \eta_g)\left(1 - \frac{k_g^2}{\nu_g\eta_g}\right)\widetilde{a}_\mu^{(1)}(-\nu_g - \eta_g), \tag{42}$$

$$\widetilde{D}^{SP}(\nu_g, \eta_g) = \frac{1}{4}\left(\frac{k_g}{\nu_g} + \frac{k_g}{\eta_g}\right)\widetilde{a}_\rho^{(1)}(-\nu_g - \eta_g) + \frac{\beta_0^2}{2\omega^2}k_g(\nu_g + \eta_g)\left(1 - \frac{k_g^2}{\nu_g\eta_g}\right)\widetilde{a}_\mu^{(1)}(-\nu_g - \eta_g), \tag{43}$$

$$\widetilde{D}^{SS}(k_g, \eta_g) = -\frac{1}{4}\left(1 - \frac{k_g^2}{\eta_g^2}\right)\widetilde{a}_\rho^{(1)}(-2\eta_g) - \left[\frac{\eta_g^2 + k_g^2}{4\eta_g^2} - \frac{2k_g^2}{\eta_g^2 + k_g^2}\right]\widetilde{a}_\mu^{(1)}(-2\eta_g), \tag{44}$$

where

$$\nu_g^2 + k_g^2 = \frac{\omega^2}{\alpha_0^2},$$

$$\eta_g^2 + k_g^2 = \frac{\omega^2}{\beta_0^2}.$$

Now, using $k_g^2/\nu_g^2 = \tan^2\theta$ and $k_g^2/(\nu_g^2 + k_g^2) = \sin^2\theta$, where θ is the P-wave incident angle (see Figure 1). Then, Eq. (41) becomes

$$\widetilde{D}^{PP}(\nu_g, \theta) = -\frac{1}{4}(1 - \tan^2\theta)\widetilde{a}_\rho^{(1)}(-2\nu_g) - \frac{1}{4}(1 + \tan^2\theta)\widetilde{a}_\gamma^{(1)}(-2\nu_g) + \frac{2\beta_0^2\sin^2\theta}{\alpha_0^2}\widetilde{a}_\mu^{(1)}(-2\nu_g). \tag{45}$$

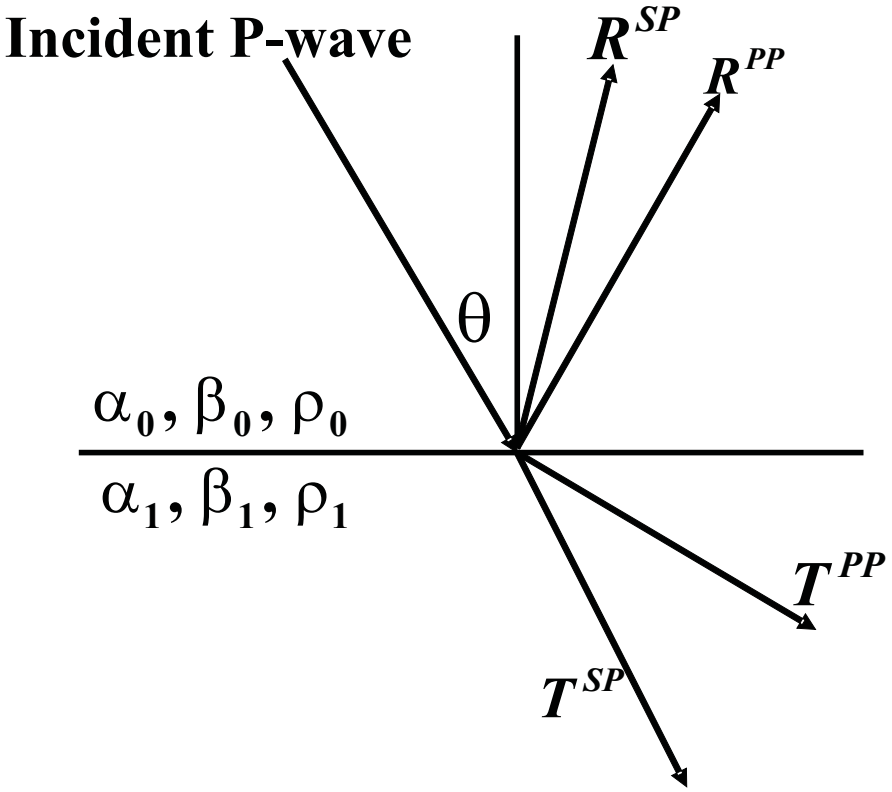

Figure 1: *Response of incident compressional wave on a planar elastic interface.* α_0, β_0 *and* ρ_0 *are the compressional wave velocity, shear wave velocity and density of the upper layer, respectively;* α_1, β_1 *and* ρ_1 *denote the compressional wave velocity, shear wave velocity and density of the lower layer.* R^{PP}, R^{SP}, T^{PP} *and* T^{SP} *denote the coefficients of the reflected compressional wave, the reflected shear wave, the transmitted compressional wave and the transmitted shear wave, respectively.*

4 Non-linear inversion of 1D elastic medium for 2D experiment

Writing Eq. (25) in matrix form:

$$\begin{aligned}&\begin{pmatrix}\hat{G}_0^P & 0\\ 0 & \hat{G}_0^S\end{pmatrix}\begin{pmatrix}\hat{V}_2^{PP} & \hat{V}_2^{PS}\\ \hat{V}_2^{SP} & \hat{V}_2^{SS}\end{pmatrix}\begin{pmatrix}\hat{G}_0^P & 0\\ 0 & \hat{G}_0^S\end{pmatrix}\\ &= -\begin{pmatrix}\hat{G}_0^P & 0\\ 0 & \hat{G}_0^S\end{pmatrix}\begin{pmatrix}\hat{V}_1^{PP} & \hat{V}_1^{PS}\\ \hat{V}_1^{SP} & \hat{V}_1^{SS}\end{pmatrix}\begin{pmatrix}\hat{G}_0^P & 0\\ 0 & \hat{G}_0^S\end{pmatrix}\begin{pmatrix}\hat{V}_1^{PP} & \hat{V}_1^{PS}\\ \hat{V}_1^{SP} & \hat{V}_1^{SS}\end{pmatrix}\begin{pmatrix}\hat{G}_0^P & 0\\ 0 & \hat{G}_0^S\end{pmatrix},\end{aligned} \tag{46}$$

leads to four equations

$$\hat{G}_0^P\hat{V}_2^{PP}\hat{G}_0^P = -\hat{G}_0^P\hat{V}_1^{PP}\hat{G}_0^P\hat{V}_1^{PP}\hat{G}_0^P - \hat{G}_0^P\hat{V}_1^{PS}\hat{G}_0^S\hat{V}_1^{SP}\hat{G}_0^P, \tag{47}$$

$$\hat{G}_0^P\hat{V}_2^{PS}\hat{G}_0^S = -\hat{G}_0^P\hat{V}_1^{PP}\hat{G}_0^P\hat{V}_1^{PS}\hat{G}_0^S - \hat{G}_0^P\hat{V}_1^{PS}\hat{G}_0^S\hat{V}_1^{SS}\hat{G}_0^S, \tag{48}$$

$$\hat{G}_0^S \hat{V}_2^{SP} \hat{G}_0^P = -\hat{G}_0^S \hat{V}_1^{SP} \hat{G}_0^P \hat{V}_1^{PP} \hat{G}_0^P - \hat{G}_0^S \hat{V}_1^{SS} \hat{G}_0^S \hat{V}_1^{SP} \hat{G}_0^P, \tag{49}$$

$$\hat{G}_0^S \hat{V}_2^{SS} \hat{G}_0^S = -\hat{G}_0^S \hat{V}_1^{SP} \hat{G}_0^P \hat{V}_1^{PS} \hat{G}_0^S - \hat{G}_0^S \hat{V}_1^{SS} \hat{G}_0^S \hat{V}_1^{SS} \hat{G}_0^S. \tag{50}$$

Because $\hat{V}_1^{PP}$ relates to $\hat{D}^{PP}$, $\hat{V}_1^{PS}$ relates to $\hat{D}^{PS}$, and so on, the four components of the data will be coupled for the non-linear elastic inversion. We cannot perform the direct non-linear inversion without knowing all components of the data.

As we stated before, when we extend our previous work on two parameter acoustic case to present three parameter elastic case, it is not just simply adding one more parameter, but there are more issues involved. Even for the linear case, the linear solutions we found (41), (42), (43) and (44), are much more complicated than those for the acoustic case. We would get four different sets of linear solution for the parameters from each component of the data respectively. Also, there would be four mislocations because of the two reference velocities (P wave velocity and S velocity). Since the theory is very complicated, we're trying to look for a particular non-linear approach–only use $\hat{D}^{PP}$ as input, to do the non-linear elastic inversion. This is also trying to answer one question: How much can we do if only given $\hat{D}^{PP}$? When we assume that we only use $\hat{D}^{PP}$ as input, we assume that $a_\rho^{(1)}$ obtained from $\hat{D}^{PS}$ is the same as those obtained from $\hat{D}^{PP}$ and $\hat{D}^{SP}$ and that $a_\mu^{(1)}$ obtained from $\hat{D}^{PS}$ is the same as those obtained from $\hat{D}^{PP}$ and $\hat{D}^{SP}$. Based on this assumption, we get the following second order (first term beyond linear) elastic inversion solution,

$$\begin{aligned}
&\left(1-\tan^2\theta\right) a_\rho^{(2)}(z) + \left(1+\tan^2\theta\right) a_\gamma^{(2)}(z) - 8b^2\sin^2\theta a_\mu^{(2)}(z) \\
=& -\frac{1}{2}\left(\tan^4\theta - 1\right)\left[a_\gamma^{(1)}(z)\right]^2 + \frac{\tan^2\theta}{\cos^2\theta} a_\gamma^{(1)}(z) a_\rho^{(1)}(z) \\
&+ \frac{1}{2}\left[\left(1-\tan^4\theta\right) - \left(\frac{1}{C}\right)\left(\frac{\alpha_0^2}{\beta_0^2}-1\right)\frac{\tan^2\theta}{\cos^2\theta}\right]\left[a_\rho^{(1)}(z)\right]^2 \\
&- 4b^2\left[\tan^2\theta - \left(\frac{1}{2C}\right)\left(\frac{\alpha_0^2}{\beta_0^2}-1\right)\tan^4\theta\right] a_\rho^{(1)}(z) a_\mu^{(1)}(z) \\
&+ 2b^4\left(\tan^2\theta - \frac{\alpha_0^2}{\beta_0^2}\right)\left[2\sin^2\theta - \frac{1}{C}\left(\frac{\alpha_0^2}{\beta_0^2}-1\right)\tan^2\theta\right]\left[a_\mu^{(1)}(z)\right]^2 \\
&- \frac{1}{2}\left(\frac{1}{\cos^4\theta}\right) a_\gamma^{(1)\prime}(z)\int_0^z dz'\left[a_\gamma^{(1)}\left(z'\right) - a_\rho^{(1)}\left(z'\right)\right] \\
&- \frac{1}{2}\left(1-\tan^4\theta\right) a_\rho^{(1)\prime}(z)\int_0^z dz'\left[a_\gamma^{(1)}\left(z'\right) - a_\rho^{(1)}\left(z'\right)\right] \\
&+ 4b^2\tan^2\theta a_\mu^{(1)\prime}(z)\int_0^z dz'\left[a_\gamma^{(1)}\left(z'\right) - a_\rho^{(1)}\left(z'\right)\right] \\
&+ \frac{1}{C}\left(\frac{\alpha_0^2}{\beta_0^2}-1\right)\tan^2\theta\left(\tan^2\theta - C\right) b^2\int_0^z dz' a_\mu^{(1)\prime}\left(\frac{(C-1)z'+2z}{(C+1)}\right) a_\rho^{(1)}\left(z'\right) H\left(z-z'\right) \\
&- \frac{2}{C}\left(\frac{\alpha_0^2}{\beta_0^2}-1\right)\tan^2\theta\left(\tan^2\theta - \frac{\alpha_0^2}{\beta_0^2}\right) b^4\int_0^z dz' a_\mu^{(1)\prime}\left(\frac{(C-1)z'+2z}{(C+1)}\right) a_\mu^{(1)}\left(z'\right) H\left(z-z'\right) \\
&+ \frac{1}{C}\left(\frac{\alpha_0^2}{\beta_0^2}-1\right)\tan^2\theta\left(\tan^2\theta + C\right) b^2\int_0^z dz' a_\mu^{(1)}\left(z'\right) a_\rho^{(1)\prime}\left(\frac{(C-1)z'+2z}{(C+1)}\right) H\left(z-z'\right) \\
&- \frac{1}{2C}\left(\frac{\alpha_0^2}{\beta_0^2}-1\right)\tan^2\theta\left(\tan^2\theta + 1\right)\int_0^z dz' a_\rho^{(1)}\left(z'\right) a_\rho^{(1)\prime}\left(\frac{(C-1)z'+2z}{(C+1)}\right) H\left(z-z'\right),
\end{aligned} \tag{51}$$

where $a_\rho^{(1)\prime}\left(\frac{(C-1)z'+2z}{(C+1)}\right) = d\left[a_\rho^{(1)}\left(\frac{(C-1)z'+2z}{(C+1)}\right)\right]/dz$, $b = \frac{\beta_0}{\alpha_0}$ and $C = \frac{\alpha_0}{\beta_0}\frac{\sqrt{1-\frac{\beta_0^2}{\alpha_0^2}\sin^2\theta}}{\sqrt{1-\sin^2\theta}} = \frac{1}{b}\frac{\sqrt{1-b^2\sin^2\theta}}{\sqrt{1-\sin^2\theta}}$.

The first five terms on the right side of the equation (51) are inversion terms, i.e. contribute to amplitude correction. The other terms on the right side of the equation are imaging terms. We can see that both inversion terms and imaging terms, especially the imaging terms, become much more complicated. Besides some similar terms in acoustic case, we have more terms here.

This is the first analysis of the non-linear elastic inversion. The question here is how well does this approximation work? In the following section, we see from the numerical tests that, remarkably, this approach works very well.

5 Numerical tests

For one interface 1D elastic medium case, as shown in Figure 1, the reflection R^{PP} coefficient has the following form (Foster et al., 1997)

$$R^{PP} = \frac{N}{D}. \tag{52}$$

Here we have

$$\begin{aligned} N = &-(1+2kx^2)^2 b\sqrt{1-c^2x^2}\sqrt{1-d^2x^2} - (1-a+2kx^2)^2 bcdx^2 \\ &+ (a-2kx^2)^2 cd\sqrt{1-x^2}\sqrt{1-b^2x^2} \\ &+ 4k^2x^2\sqrt{1-x^2}\sqrt{1-b^2x^2}\sqrt{1-c^2x^2}\sqrt{1-d^2x^2} - ad\sqrt{1-b^2x^2}\sqrt{1-c^2x^2} \\ &+ abc\sqrt{1-x^2}\sqrt{1-d^2x^2}. \end{aligned} \tag{53}$$

$$\begin{aligned} D = &(1+2kx^2)^2 b\sqrt{1-c^2x^2}\sqrt{1-d^2x^2} + (1-a+2kx^2)^2 bcdx^2 \\ &+ (a-2kx^2)^2 cd\sqrt{1-x^2}\sqrt{1-b^2x^2} \\ &+ 4k^2x^2\sqrt{1-x^2}\sqrt{1-b^2x^2}\sqrt{1-c^2x^2}\sqrt{1-d^2x^2} + ad\sqrt{1-b^2x^2}\sqrt{1-c^2x^2} \\ &+ abc\sqrt{1-x^2}\sqrt{1-d^2x^2}. \end{aligned} \tag{54}$$

$$a = \rho_1/\rho_0,\ b = \beta_0/\alpha_0,\ c = \alpha_1/\alpha_0,\ d = \beta_1/\alpha_0,\ k = ad^2 - b^2 \ and\ x = \sin\theta,$$

where the subscripts "0" and "1" denote the reference medium and actual medium respectively. Using perfect data (Clayton and Stolt, 1981, Weglein et al., 1986)

$$\widetilde{D}^{PP}(\nu_g,\theta) = -R^{PP}(\theta)\frac{e^{2i\nu_g a}}{4\pi i\nu_g}, \tag{55}$$

and substituting Eq.(55) into Eq.(45), Fourier transform Eq.(45) over $2\nu_g$, for $z > a$ and fixed θ, we have

$$(1-\tan^2\theta)a_\rho^{(1)}(z) + (1+\tan^2\theta)a_\gamma^{(1)}(z) - 8\frac{\beta_0^2}{\alpha_0^2}\sin^2\theta a_\mu^{(1)}(z) = 4R^{PP}(\theta)H(z-a). \tag{56}$$

In this paper, we used four models to do the numerical tests.

Model 1: shale (0.20 porosity) over oil sand (0.10 porosity).

$$\rho_0 = 2.32g/cm^3, \rho_1 = 2.46g/cm^3; \alpha_0 = 2627m/s, \alpha_1 = 4423m/s; \beta_0 = 1245m/s, \beta_1 = 2939m/s.$$

Model 2: shale over oil sand, 0.20 porosity.

$$\rho_0 = 2.32g/cm^3, \rho_1 = 2.27g/cm^3; \alpha_0 = 2627m/s, \alpha_1 = 3251m/s; \beta_0 = 1245m/s, \beta_1 = 2138m/s.$$

Model 3: shale (0.20 porosity) over oil sand (0.30 porosity).

$$\rho_0 = 2.32g/cm^3, \rho_1 = 2.08g/cm^3; \alpha_0 = 2627m/s, \alpha_1 = 2330m/s; \beta_0 = 1245m/s, \beta_1 = 1488m/s.$$

Model 4: oil sand over wet sand, 0.20 porosity.

$$\rho_0 = 2.27g/cm^3, \rho_1 = 2.32g/cm^3; \alpha_0 = 3251m/s, \alpha_1 = 3507m/s; \beta_0 = 2138m/s, \beta_1 = 2116m/s.$$

To test and compare methods, the top of sand reflection was modelled for oil sands with porosities of 10, 20, and 30%. The three models used the same shale overburden. An oil/water contact model was also constructed for the 20% porosity sand.

The high porosity model (30%) is typical of a weakly consolidated, shallow reservoir sand. Pore fluids have a large impact on the seismic response. Density, P-wave velocity, and the α/β ratio of the oil sand are lower than the density, P-wave velocity, and α/β ratio of the overlying shale. Consequently, there is a significant decrease in density and P-bulk modulus and an increase in shear modulus at the shale/oil sand interface.

The moderate porosity model (20%) represents deeper, more compacted reservoirs. Pore fluids have a large impact on seismic response, but the fluid effect is less than that of the high porosity case. The overlying shale has high density compared to the reservoir sand, but the P-wave velocity of the oil sand exceeds that of the shale. As a result, impedance contrast is reduced, and shear wave information becomes more important for detecting the reservoir.

The low porosity model (10%) represents a deep, consolidated reservoir sand. Pore fluids have little effect on the seismic response of the reservoir sand. It is difficult to distinguish oil sands from brine sands on the basis of seismic response. Impedance of the sand is higher than impedance of the shale.

The fourth model denotes an oil/water contact in a 20% porosity sand. At a fluid contact, both density and P-wave velocity increase in going from the oil zone into the wet zone. Because pore fluids have no effect on shear modulus, there is no change in shear modulus.

Using these four models, we can find the corresponding R^{PP} from Eq. (52). Then, choose three different angles θ_1, θ_2 and θ_3, we can get the linear solutions for $a_\rho^{(1)}$, $a_\gamma^{(1)}$ and $a_\mu^{(1)}$ from Eq. (56) , and then get the solutions for $a_\rho^{(2)}$, $a_\gamma^{(2)}$ and $a_\mu^{(2)}$ from equation (51).

There are two plots in each figure. The left ones are the results for the first order, while the right ones are the results for the first order plus the second order. The red line denotes the corresponding

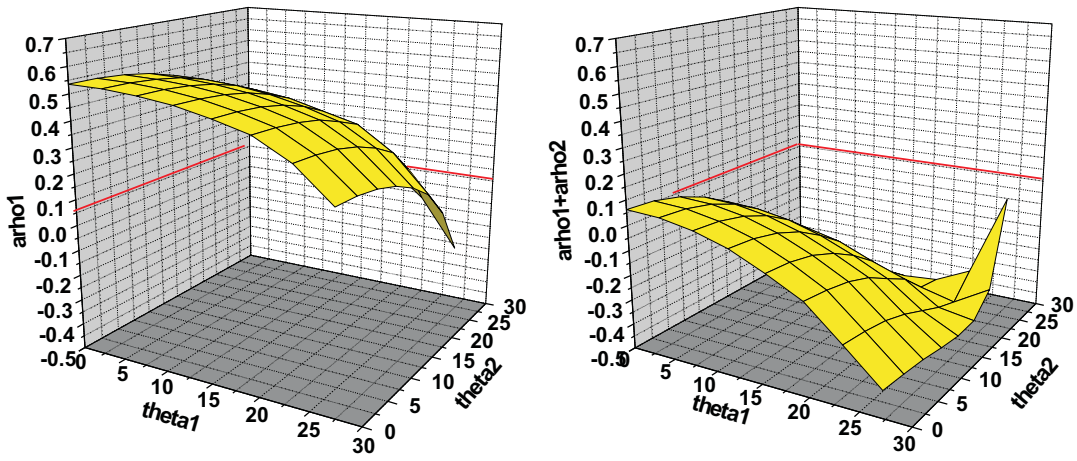

Figure 2: *Model 1: shale (0.20 porosity) over oil sand (0.10 porosity).* $\rho_0 = 2.32g/cm^3, \rho_1 = 2.46g/cm^3; \alpha_0 = 2627m/s, \alpha_1 = 4423m/s; \beta_0 = 1245m/s, \beta_1 = 2939m/s$. *For this model, the exact value of* a_ρ *is 0.06. The linear approximation* $a_\rho^{(1)}$ *(left) and the sum of linear and first non-linear* $a_\rho^{(1)} + a_\rho^{(2)}$ *(right).*

actual value. In the figures, we gave the results corresponding to different sets of angles θ_1 and θ_2. The third angle θ_3 is fixed as zero.

From the numerical results, we can see that all the second order provide improvements over the linear except for model four. When we add the second order to linear order, the results become much closer to the corresponding exact value and the surface become flatter. The most important thing is, for all of the four models, when we add the second order to first order, the sign of a_ρ is corrected. Like model four, (See Figure 11), $a_\rho^{(1)}$ becomes negative for some large angles. When we add $a_\rho^{(2)}$ to $a_\rho^{(1)}$, all of the results get the right sign.

For model three, (See Figure 10), the linear result $a_\mu^{(1)}$ is already very close to the exact value of a_μ. Although $a_\mu^{(1)} + a_\mu^{(2)}$ is still very close to the exact value, the surface looks a little further from the red line compared to the left plot.

We believe this is due to the use of $\hat{D}^{PP}$ only instead of all four components required by the procedure. We think the reason of the three out of the four models giving very good numerical results is that, there is at least one of the synthesized data (See figures 14 – 17) is reasonable for the three models. All of the "predicted" values in the figures 14 – 17, are predicted by the linear results from $\hat{D}^{PP}$. And the "actual" values are calculated from the Zoeppritz' equations.

6 Conclusion

This paper represents the first analysis of the non-linear elastic target location and identification and provides a user guide and useful lessons for these two non-linear tasks. In particular we show

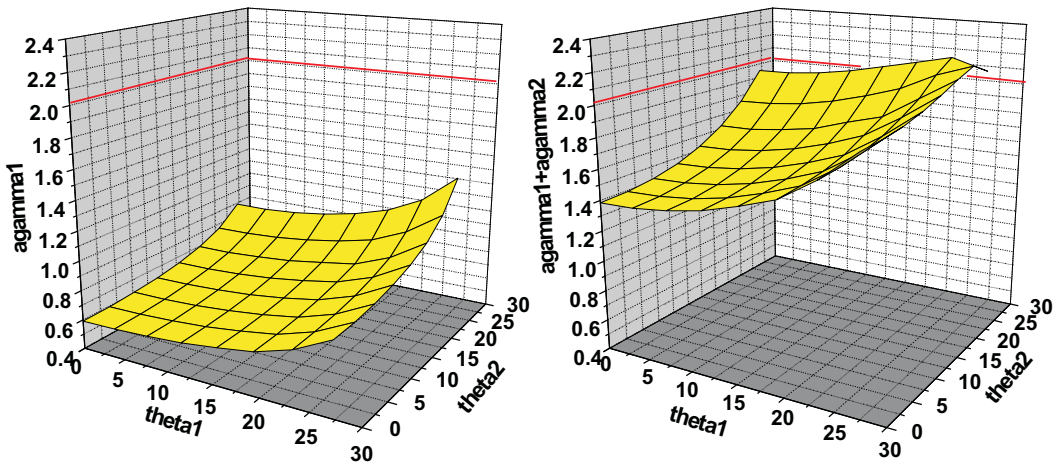

Figure 3: *Model 1: shale (0.20 porosity) over oil sand (0.10 porosity).* $\rho_0 = 2.32g/cm^3, \rho_1 = 2.46g/cm^3; \alpha_0 = 2627m/s, \alpha_1 = 4423m/s; \beta_0 = 1245m/s, \beta_1 = 2939m/s$. *For this model, the exact value of* a_γ *is 2.01. The linear approximation* $a_\gamma^{(1)}$ *(left) and the sum of linear and first non-linear* $a_\gamma^{(1)} + a_\gamma^{(2)}$ *(right).*

added value and improved capability for target identification provided by the first non-linear term in the inverse scattering inversion subseries. The theory itself needs all four components of the data, but in this first report on this project we analyzed an algorithm which inputs only $\hat{D}^{PP}$. Although $\hat{D}^{PP}$ can itself provide useful non-linear direct inversion results, the implication of this research is that further value would derive from actually measuring $\hat{D}^{PP}$, $\hat{D}^{PS}$, $\hat{D}^{SP}$ and $\hat{D}^{SS}$, as the method requires.

Acknowledgements

The M-OSRP sponsors are thanked for supporting this research. We are grateful to Douglas Foster for useful comments and suggestions. We appreciate the assistance of Kristopher Innanen, Bogdan Nita and Jingfeng Zhang in preparing this manuscript.

Appendix – correction of 2003 annual report

In the derivation for the second order inversion, some difficulties were encountered. Since we know the result of acoustic case from our earlier work (which started with the pressure wave equation), it would be helpful for us to start with the displacement space and reduce the elastic case to acoustic case, and finally, to compare those two acoustic results which have different starting points.

In the acoustic case, our earlier work (Weglein et al., 2003; Zhang and Weglein, 2003), if we start directly with the pressure wave equation and choose θ as the free parameter, α and β as the two

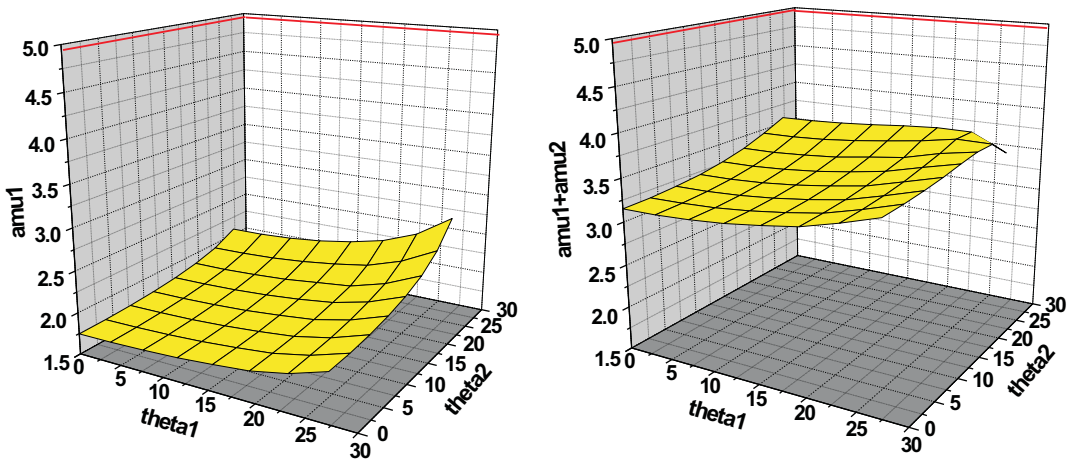

Figure 4: *Model 1: shale (0.20 porosity) over oil sand (0.10 porosity).* $\rho_0 = 2.32g/cm^3, \rho_1 = 2.46g/cm^3; \alpha_0 = 2627m/s, \alpha_1 = 4423m/s; \beta_0 = 1245m/s, \beta_1 = 2939m/s$. *For this model, the exact value of* a_μ *is 4.91. The linear approximation* $a_\mu^{(1)}$ *(left) and the sum of linear and first non-linear* $a_\mu^{(1)} + a_\mu^{(2)}$ *(right).*

material property parameters, we arrive at the following equation for the second order (first term beyond linear):

$$\begin{aligned}
&\frac{1}{\cos^2\theta}\alpha_2(z) + (1-\tan^2\theta)\beta_2(z) \\
=&-\frac{1}{2\cos^4\theta}\alpha_1^2(z) \\
&-\frac{1}{2}(1+\tan^4\theta)\beta_1^2(z) \\
&+\frac{\tan^2\theta}{\cos^2\theta}\alpha_1(z)\beta_1(z) \\
&-\frac{1}{2\cos^4\theta}\alpha_1'(z)\int_0^z dz'[\alpha_1(z') - \beta_1(z')] \\
&+\frac{1}{2}(\tan^4\theta - 1)\beta_1'(z)\int_0^z dz'[\alpha_1(z') - \beta_1(z')].
\end{aligned} \tag{57}$$

If we start with the displacement domain, as discussed, letting μ_0, β_0, μ, and $\beta = 0$ and choose θ as the free parameter, a_γ and a_ρ as the two material property parameters, the following solution

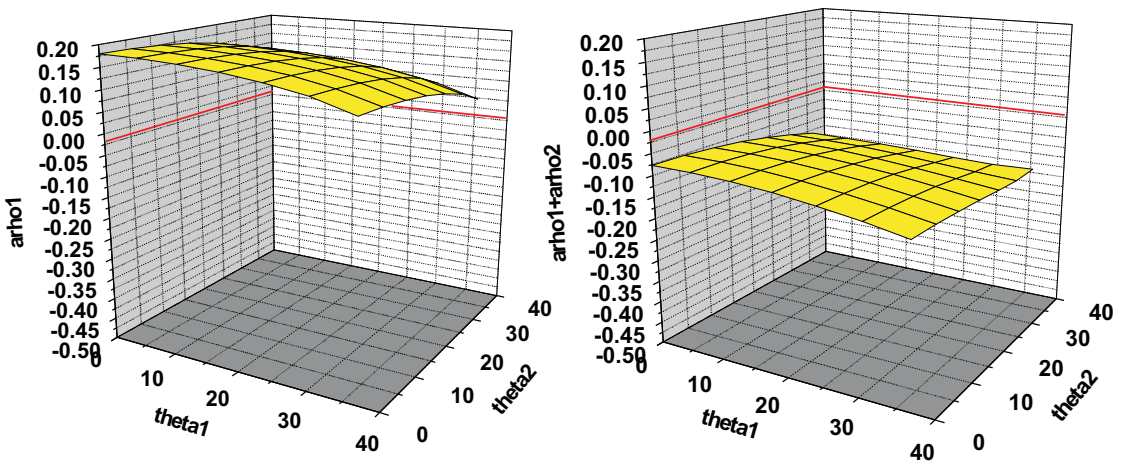

Figure 5: *Model 2: shale over oil sand, 0.20 porosity.* $\rho_0 = 2.32g/cm^3, \rho_1 = 2.27g/cm^3; \alpha_0 = 2627m/s, \alpha_1 = 3251m/s; \beta_0 = 1245m/s, \beta_1 = 2138m/s$. *For this model, the exact value of* a_ρ *is -0.022. The linear approximation* $a_\rho^{(1)}$ *(left) and the sum of linear and first non-linear* $a_\rho^{(1)} + a_\rho^{(2)}$ *(right).*

for second order is produced:

$$\begin{aligned}
&\frac{1}{\cos^2\theta} a_\gamma^{(2)}(z) + (1-\tan^2\theta) a_\rho^{(2)}(z) \\
=& -\frac{1}{2}(\tan^4\theta - 1) a_\gamma^{(1)^2}(z) \\
&-\frac{1}{2}\left(\frac{1}{\cos^4\theta} - 2\right) a_\rho^{(1)^2}(z) \\
&+\frac{\tan^2\theta}{\cos^2\theta} a_\gamma^{(1)}(z) a_\rho^{(1)}(z) \\
&-\frac{1}{2\cos^4\theta} a_\gamma^{(1)'}(z) \int_0^z dz' [a_\gamma^{(1)}(z') - a_\rho^{(1)}(z')] \\
&+\frac{1}{2}(\tan^4\theta - 1) a_\rho^{(1)'}(z) \int_0^z dz' [a_\gamma^{(1)}(z') - a_\rho^{(1)}(z')],
\end{aligned} \tag{58}$$

where the definition of θ is the same as that of Eq. (57), $a_\gamma^{(1)'} = \frac{da_\gamma^{(1)}}{dz}$ and $a_\rho^{(1)'} = \frac{da_\rho^{(1)}}{dz}$.

Next, we show that the two results Eq. (57) and Eq. (58) agree with each other.

Since $\alpha = 1 - \frac{\gamma_0}{\gamma}$, then

$$a_\gamma = \frac{\gamma}{\gamma_0} - 1 = \frac{\alpha}{1-\alpha} = \alpha + \alpha^2 + \alpha^3 + \cdots,$$

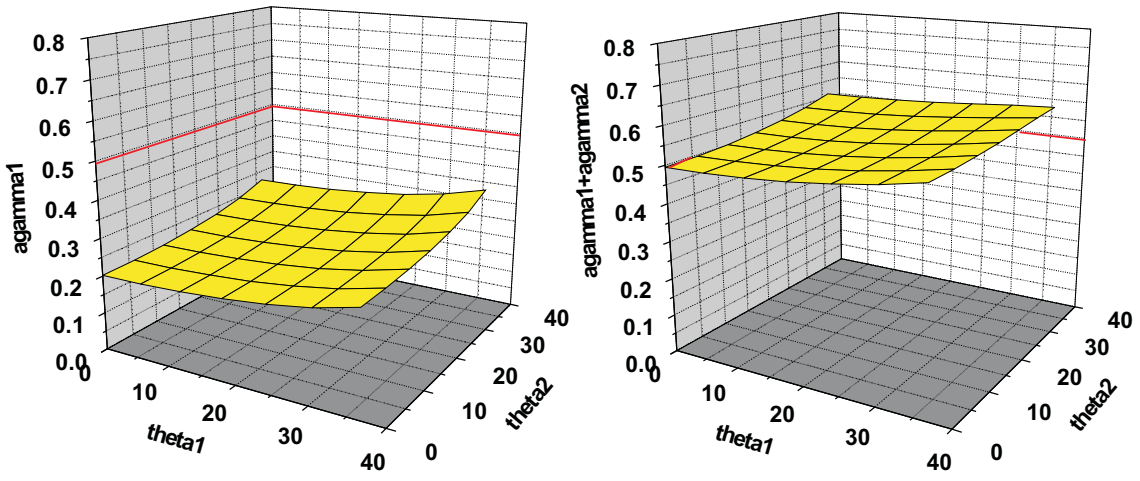

Figure 6: *Model 2: shale over oil sand, 0.20 porosity.* $\rho_0 = 2.32g/cm^3, \rho_1 = 2.27g/cm^3; \alpha_0 = 2627m/s, \alpha_1 = 3251m/s; \beta_0 = 1245m/s, \beta_1 = 2138m/s$. *For this model, the exact value of* a_γ *is 0.498. The linear approximation* $a_\gamma^{(1)}$ *(left) and the sum of linear and first non-linear* $a_\gamma^{(1)} + a_\gamma^{(2)}$ *(right).*

where the series expansion is valid for $|\alpha| < 1$. And then we have

$$a_\gamma^{(1)} = \alpha_1,$$

$$a_\gamma^{(2)} = \alpha_2 + \alpha_1^2,$$

$$\vdots$$

Similarly, since $\beta = 1 - \frac{\rho_0}{\rho}$, then

$$a_\rho = \frac{\rho}{\rho_0} - 1 = \frac{\beta}{1-\beta} = \beta + \beta^2 + \beta^3 + \cdots,$$

where the series expansion is valid for $|\beta| < 1$. And then we have

$$a_\rho^{(1)} = \beta_1,$$

$$a_\rho^{(2)} = \beta_2 + \beta_1^2,$$

$$\vdots$$

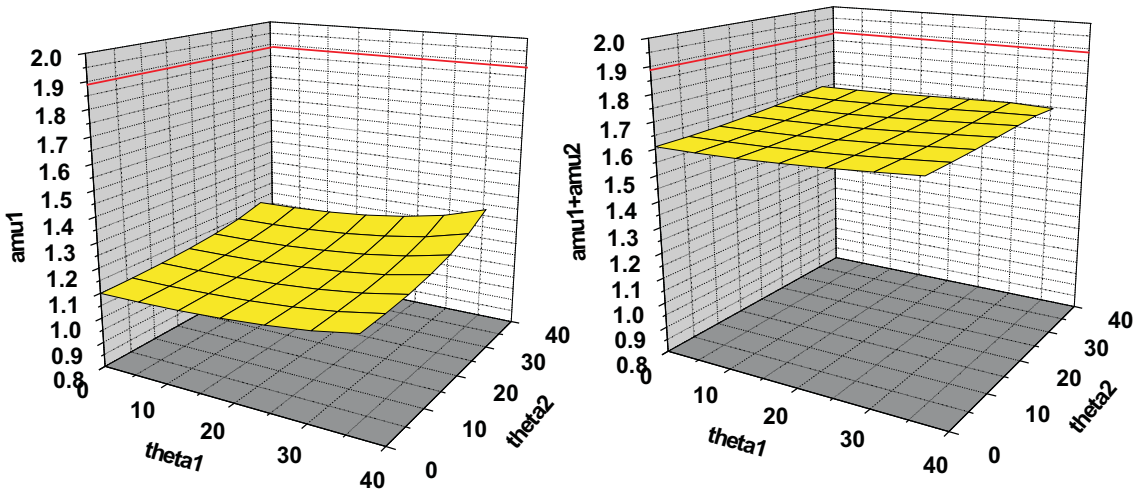

Figure 7: *Model 2: shale over oil sand, 0.20 porosity.* $\rho_0 = 2.32g/cm^3, \rho_1 = 2.27g/cm^3; \alpha_0 = 2627m/s, \alpha_1 = 3251m/s; \beta_0 = 1245m/s, \beta_1 = 2138m/s$. *For this model, the exact value of* a_μ *is 1.89. The linear approximation* $a_\mu^{(1)}$ *(left) and the sum of linear and first non-linear* $a_\mu^{(1)} + a_\mu^{(2)}$ *(right).*

Then, after some substitutions, Eq. (58) becomes

$$\begin{aligned}
&\frac{1}{\cos^2\theta}\alpha_2(z) + (1-\tan^2\theta)\beta_2(z) \\
=& -\frac{1}{2\cos^4\theta}\alpha_1^2(z) \\
&-\frac{1}{2}(1+\tan^4\theta)\beta_1^2(z) \\
&+\frac{\tan^2\theta}{\cos^2\theta}\alpha_1(z)\beta_1(z) \\
&-\frac{1}{2\cos^4\theta}\alpha_1'(z)\int_0^z dz'[\alpha_1(z') - \beta_1(z')] \\
&+\frac{1}{2}(\tan^4\theta - 1)\beta_1'(z)\int_0^z dz'[\alpha_1(z') - \beta_1(z')],
\end{aligned}$$

which is Eq. (57) exactly. Therefore Eq. (57) and Eq. (58) agree with each other.

The $A(z)$ term in the Eq. (51) of last year's annual report already been removed because we found a $-A(z)$ from one term which is considered mistakenly as zero when we reduce the elastic case to acoustic case.

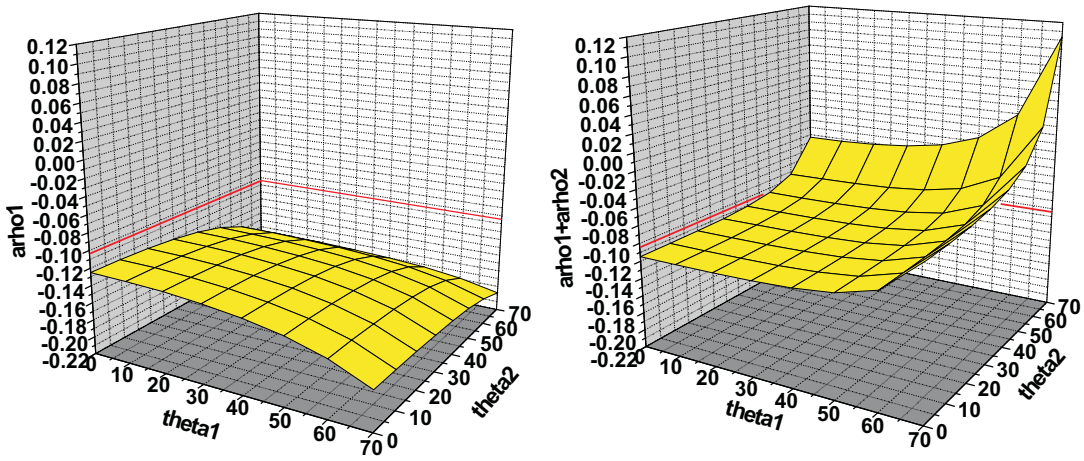

Figure 8: *Model 3: shale (0.20 porosity) over oil sand (0.30 porosity).* $\rho_0 = 2.32g/cm^3, \rho_1 = 2.08g/cm^3; \alpha_0 = 2627m/s, \alpha_1 = 2330m/s; \beta_0 = 1245m/s, \beta_1 = 1488m/s$. *For this model, the exact value of* a_ρ *is -0.103. The linear approximation* $a_\rho^{(1)}$ *(left) and the sum of linear and first non-linear* $a_\rho^{(1)} + a_\rho^{(2)}$ *(right).*

References

1. Guo Z, Tan T H and Weglein A B 2004 Wavelet estimation below towed streamer and ocean bottom cable data, *M-OSRP Annual Report*

2. Innanen K A 2003 "Methods for the Treatment of Acoustic and Absorptive/Dispersive Wave Field Measurements." *Ph.D. Thesis, University of British Columbia.*

3. Liu F, Weglein A B, Innanen K A and Nita B G 2005 Multi-dimensional depth imaging without an adequate velocity model, in preparation

4. Matson K H 1997 An inverse scattering series method for attenuating elastic multiples from multicomponent land and ocean bottom seismic data *Ph.D. thesis* University of British Columbia p 18

5. Shaw S A, Weglein A B, Foster D J, Matson K H and Keys R G 2003 Isolation of a Leading Order Depth Imaging Series and Analysis of its Convergence Properties. *M-OSRP Annual Report*

6. Shaw S A 2005 "An inverse scattering series algorithm for depth imaging of reflection data from a layered acoustic medium with an unknown velocity model" *Ph.D. thesis* University of Houston

7. Weglein A B and Stolt R H 1992 Notes on approaches on linear and non-linear migration-inversion, Personal Communication

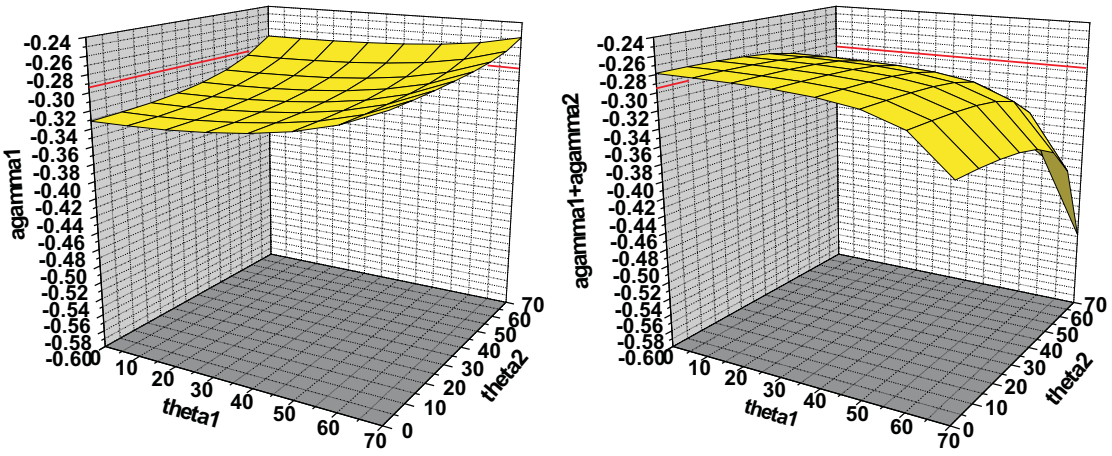

Figure 9: *Model 3: shale (0.20 porosity) over oil sand (0.30 porosity).* $\rho_0 = 2.32g/cm^3, \rho_1 = 2.08g/cm^3; \alpha_0 = 2627m/s, \alpha_1 = 2330m/s; \beta_0 = 1245m/s, \beta_1 = 1488m/s$. *For this model, the exact value of* a_γ *is -0.295. The linear approximation* $a_\gamma^{(1)}$ *(left) and the sum of linear and first non-linear* $a_\gamma^{(1)} + a_\gamma^{(2)}$ *(right).*

8. Weglein A B, Gasparotto F A, Carvalho P M and Stolt R H 1997 An inverse-scattering series method for attenuating multiples in seismic reflection data *Geophysics* **62** 1975–1989

9. Weglein A B, Foster D J, Matson K H, Shaw S A, Carvalho P M and Corrigan D 2002 Predicting the correct spatial location of reflectors without knowing or determining the precise medium and wave velocity: initial concept, algorithm and analytic and numerical example *J. Seism. Explor.* **10** 367–382

10. Weglein A B, Araújo F V, Carvalho P M, Stolt R H, Matson K H, Coates R, Corrigan D, Foster D J, Shaw S A and Zhang H 2003 Inverse scattering series and seismic exploration *Inverse Problem* **19** R27–R83

11. Zhang H and Weglein A B 2003 Target identification using the inverse scattering series; inversion of large contrast, variable velocity and density acoustic media, *M-OSRP Annual Report*

12. Zhang J and Weglein A B 2004 Deghosting of towed streamer and ocean bottom cable data, *M-OSRP Annual Report*

General References

13. Boyse W E 1986 *Wave propagation and inversion in slightly inhomogeneous media* p 40

14. Boyse W E and Keller J B 1986 Inverse elastic scattering in three dimensions *J. Acoust. Soc. Am.* **79** 215–218

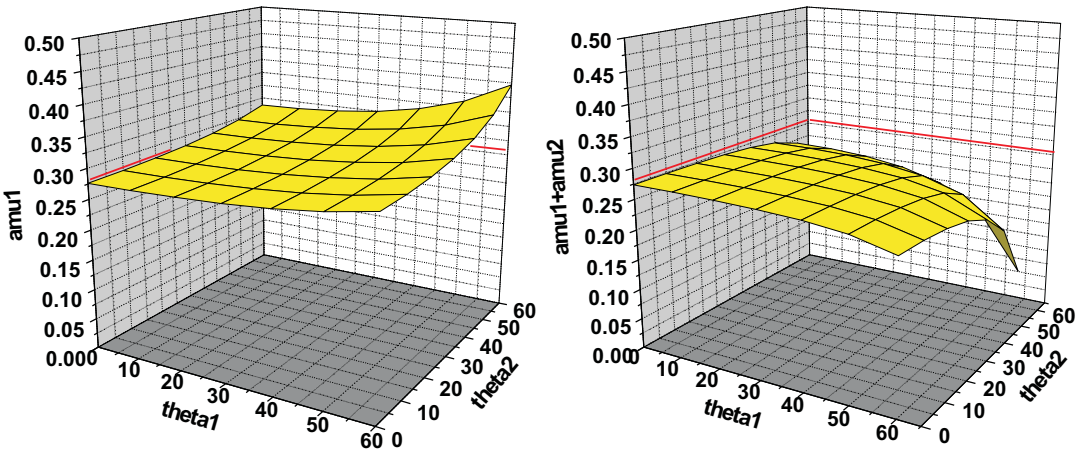

Figure 10: *Model 3: shale (0.20 porosity) over oil sand (0.30 porosity).* $\rho_0 = 2.32g/cm^3, \rho_1 = 2.08g/cm^3; \alpha_0 = 2627m/s, \alpha_1 = 2330m/s; \beta_0 = 1245m/s, \beta_1 = 1488m/s$. *For this model, the exact value of* a_μ *is 0.281. The linear approximation* $a_\mu^{(1)}$ *(left) and the sum of linear and first non-linear* $a_\mu^{(1)} + a_\mu^{(2)}$ *(right).*

15. Clayton R W and Stolt R H 1981 A Born-WKBJ inversion method for acoustic reflection data for attenuating multiples in seismic reflection data *Geophysics* **46** 1559–1567

16. Keys R G 1989 Polarity reversals in reflections from layered media *Geophysics* **54** 900–905

17. Shaw S A and Weglein A B 2004 A leading order imaging series for prestack data acquired over a laterally invariant acoustic medium. Part II: Analysis for data missing low frequencies, *M-OSRP Annual Report*

18. Taylor J R 1972 *Scattering theory: the quantum theory of nonrelativistic collisions* (John Wiley & Sons, Inc.) p 133

19. Weglein A B, Violette P B and Keho T H 1986 Using multiparameter Born theory to obtain certain exact multiparameter inversion goals *Geophysics* **51** 1069–1074

20. Weglein A B, Matson K H, Foster D J, Carvalho P M, Corrigan D and Shaw S A 2000 Imaging and inversion at depth without a velocity model: Theory, concepts and initial evaluation, In 70th Annual Internat. Mtg., Soc. Expl. Geophys., Expanded Abstracts, 1016-1019. Soc. Expl. Geophys.

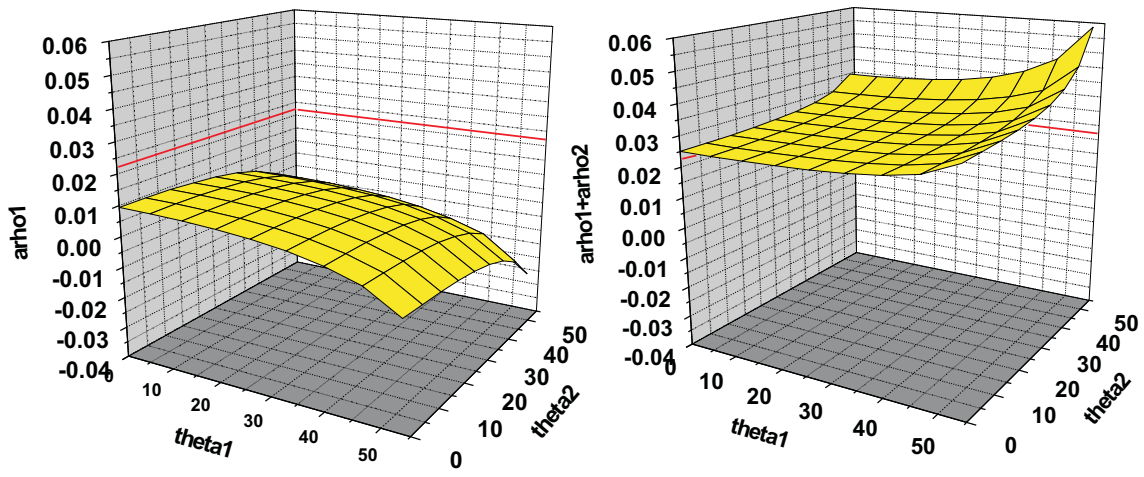

Figure 11: *Model 4: oil sand over wet sand, 0.20 porosity.* $\rho_0 = 2.27g/cm^3, \rho_1 = 2.32g/cm^3; \alpha_0 = 3251m/s, \alpha_1 = 3507m/s; \beta_0 = 2138m/s, \beta_1 = 2116m/s$. *For this model, the exact value of* a_ρ *is 0.022. The linear approximation* $a_\rho^{(1)}$ *(left) and the sum of linear and first non-linear* $a_\rho^{(1)} + a_\rho^{(2)}$ *(right).*

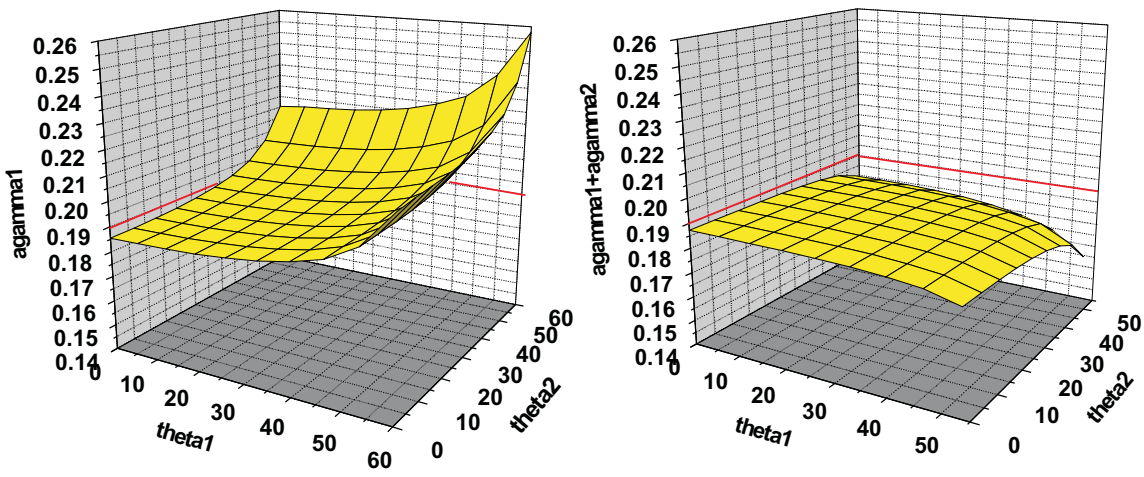

Figure 12: *Model 4: oil sand over wet sand, 0.20 porosity.* $\rho_0 = 2.27g/cm^3, \rho_1 = 2.32g/cm^3; \alpha_0 = 3251m/s, \alpha_1 = 3507m/s; \beta_0 = 2138m/s, \beta_1 = 2116m/s$. *For this model, the exact value of* a_γ *is 0.19. The linear approximation* $a_\gamma^{(1)}$ *(left) and the sum of linear and first non-linear* $a_\gamma^{(1)} + a_\gamma^{(2)}$ *(right).*

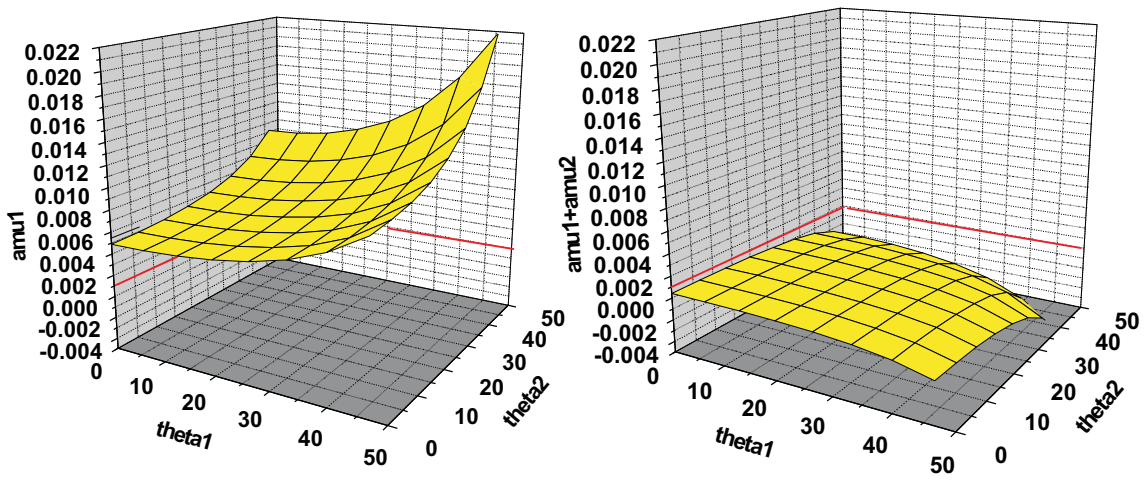

Figure 13: *Model 4: oil sand over wet sand, 0.20 porosity.* $\rho_0 = 2.27 g/cm^3, \rho_1 = 2.32 g/cm^3; \alpha_0 = 3251 m/s, \alpha_1 = 3507 m/s; \beta_0 = 2138 m/s, \beta_1 = 2116 m/s$. *For this model, the exact value of* a_μ *is 0.001. The linear approximation* $a_\mu^{(1)}$ *(left) and the sum of linear and first non-linear* $a_\mu^{(1)} + a_\mu^{(2)}$ *(right).*

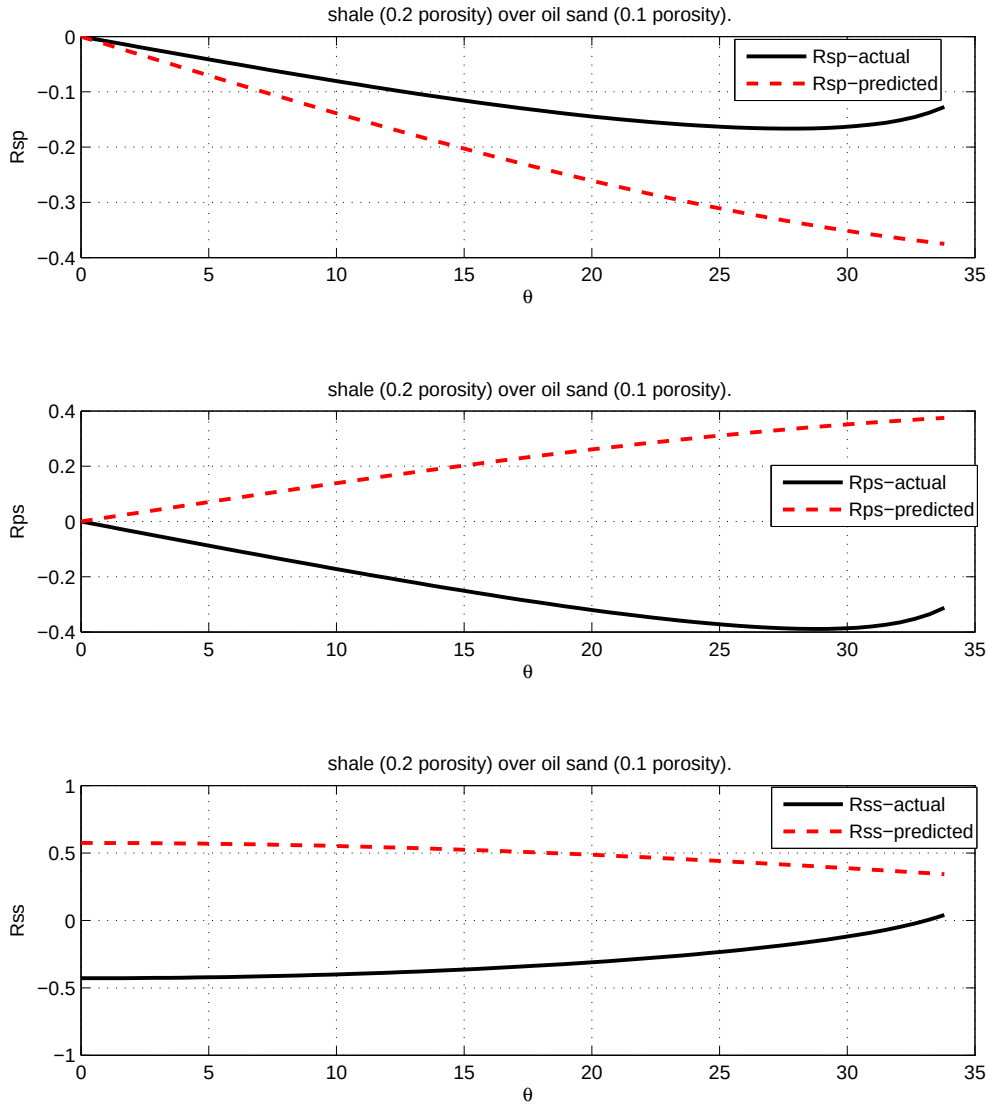

Figure 14: *The comparison between the synthesized values and the actual values of Rsp (top), Rps (middle) and Rss (bottom) for Model 1: shale (0.20 porosity) over oil sand (0.10 porosity).* $\rho_0 = 2.32g/cm^3, \rho_1 = 2.46g/cm^3; \alpha_0 = 2627m/s, \alpha_1 = 4423m/s; \beta_0 = 1245m/s, \beta_1 = 2939m/s.$

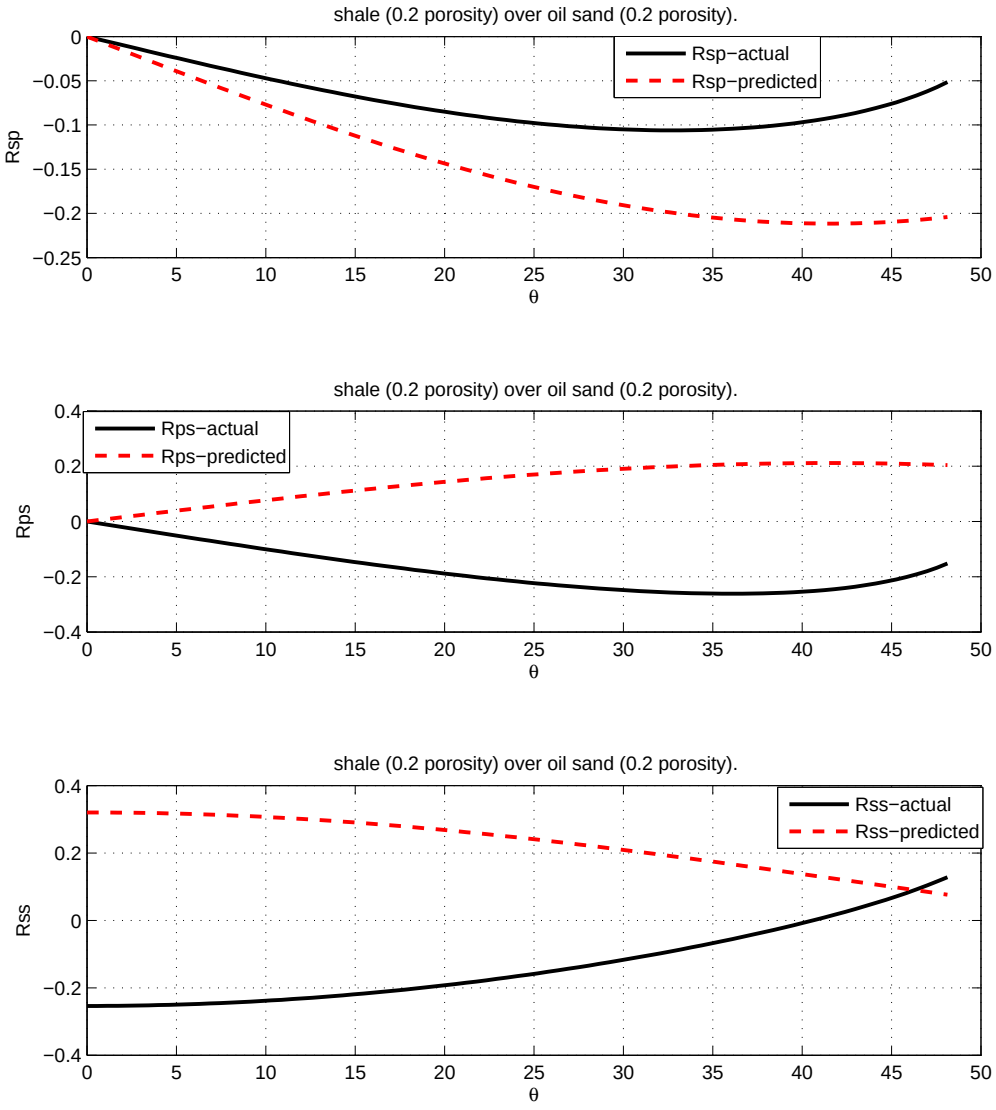

Figure 15: *The comparison between the synthesized values and the actual values of Rsp (top), Rps (middle) and Rss (bottom) for Model 2: shale over oil sand, 0.20 porosity.* $\rho_0 = 2.32g/cm^3, \rho_1 = 2.27g/cm^3; \alpha_0 = 2627m/s, \alpha_1 = 3251m/s; \beta_0 = 1245m/s, \beta_1 = 2138m/s.$

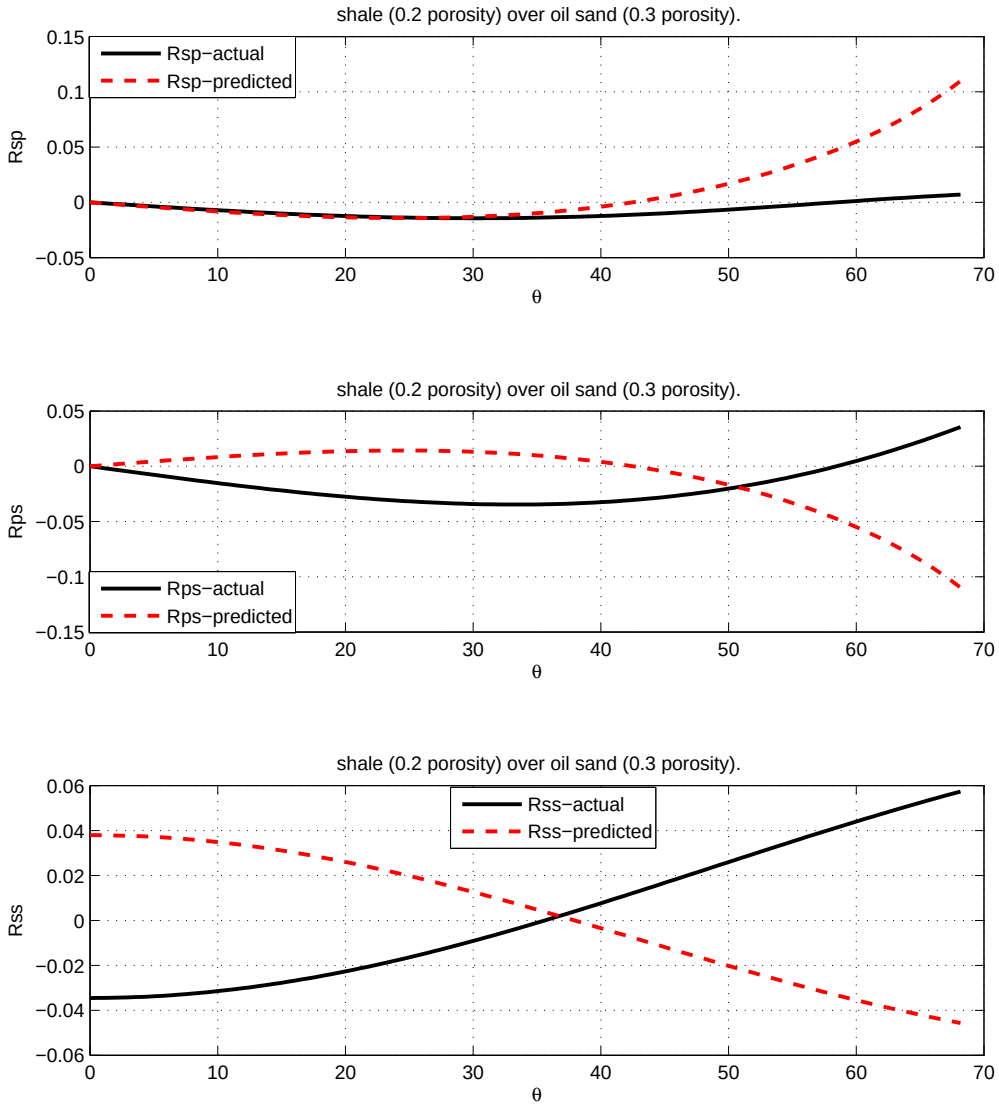

Figure 16: *The comparison between the synthesized values and the actual values of Rsp (top), Rps (middle) and Rss (bottom) for Model 3: shale (0.20 porosity) over oil sand (0.30 porosity).* $\rho_0 = 2.32g/cm^3, \rho_1 = 2.08g/cm^3; \alpha_0 = 2627m/s, \alpha_1 = 2330m/s; \beta_0 = 1245m/s, \beta_1 = 1488m/s.$

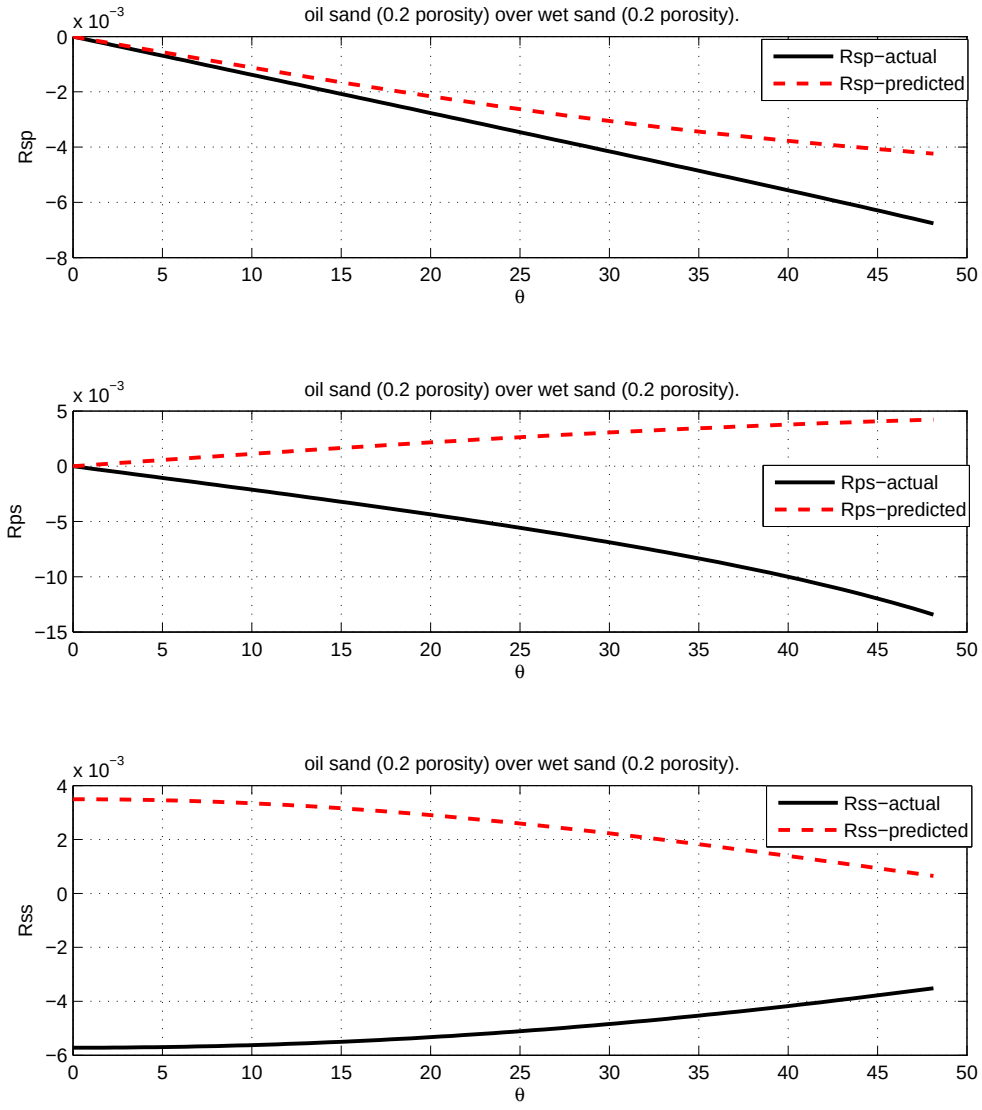

Figure 17: *The comparison between the synthesized values and the actual values of Rsp (top), Rps (middle) and Rss (bottom) for Model 4: oil sand over wet sand, 0.20 porosity.* $\rho_0 = 2.27g/cm^3, \rho_1 = 2.32g/cm^3; \alpha_0 = 3251m/s, \alpha_1 = 3507m/s; \beta_0 = 2138m/s, \beta_1 = 2116m/s.$